MASSACHUSETTS INSTITUTE OF TECHNOLOGY
LINCOLN LABORATORY
244 WOOD STREET
LEXINGTON, MA 02173-9108

Project Memorandum No. 47PM-OSR-0001 **Date** 10 January 1997

Subject: Quick-Look Analysis Results of Data Collected at OHMSETT During September 1996 Using a Ka-Band Radiometer to Estimate Oil Thickness

Author: T.J. Murphy and O.B. McMahon

Approved by : John Hunny

No distribution of this report shall be made to DTIC.

Transmittal outside the Department of Defense, other than initial distribution to DoD contractors, must have prior approval of the Lincoln Laboratory Program Manager.

No secondary distribution is authorized without prior written approval of the Lincoln Laboratory Program Manager.

This work is being performed under Air Force Contract No. F19628-95-C-0002.

LEXINGTON **MASSACHUSETTS**

Abstract

This report contains a "quick-look" analysis of the data collected at OHMSETT (the National Oil Response Test Facility) during joint tests using the Ka-Band Oil Spill Radiometric Measurement System and an IR imaging system. Radiometric brightness temperature versus measurement frequency plots are included for each of the "single-sweep" measurements; each time series measurement contains approximately 100 sweeps and will be analyzed for the final report. A detailed description of test activities is provided, as well as a comment concerning each brightness temperature versus measurement frequency plot. The results are also presented in tabular format. This document is intended to fulfill the requirement for a data summary within the 60-day post-test period.

1. Details Concerning the Test

The objective of this test was to obtain radiometric brightness temperature versus measurement frequency signatures simultaneously with an IR imaging system under a variety of calm water and wave conditions.

The Ka-Band Oil Spill Radiometric Measurement System, developed at Lincoln Laboratory, and an IR imaging system were used to collect oil thickness measurements at OHMSETT during September 1996. Targets of different oil types and thicknesses were measured during the day and night under selected wave conditions. Prior to each collection period, and when the operator noticed drifting in the receiver gain, the instrument was recalibrated using the hot/cold load procedure.

The instrument was used to collect data from targets consisting of diesel oil, crude oil, and mixtures of oil types that were readily available. Before measurements were collected over the oil targets, the radiometer operation was verified by measuring oil thicknesses in the calibrated test tank. A dry run was performed to co-locate the radiometer and IR camera aimpoint. Data sets were collected during two daytime and one nighttime operation.

The Ka-Band Oil Spill Radiometric Measurement System operates over 26 to 40 GHz, uses 12 receiver channels spaced at 1.1-GHz intervals, and each channel has a 250-MHz bandwidth. The system measures the radiometric temperature of the target; the result, presented to the instrument operator, is a plot of the 12 brightness temperature measurements versus measurement frequency. Estimates of oil thickness are performed by comparing the measured signature with a theoretical signature. The characteristic signature is a sinusoidal variation of radiometric brightness temperature versus frequency, with the frequency of oscillation of the brightness temperature increasing as thicker oil is measured.

The operator controls the recording of data to a file. Single measurement sweeps or a time series can be recorded. The data sets that were used for this postcollection analysis were single measurement sweeps.

Each data set is presented to an oil thickness estimation algorithm. The algorithm chooses the best fit of a theoretical prediction based on the result of comparing (1) a least mean squares (LMS) estimate, (2) a correlation-based estimate (CORR), and (3) an estimate based on the mean value and slope of the curve (MN/SL). A data analyst compares the algorithm result with the measured data and can choose to override the algorithm estimate with a curve that is a better fit to the data. These results are plotted and put in tabular form. The data analyst provides a comment concerning each plot of brightness temperature versus measurement frequency.

2. Equipment Checkout

Upon arrival at OHMSETT on 9 September 1996, the radiometer was set up on the main bridge. After the delivery of liquid nitrogen, the equipment was calibrated using the hot/cold load method. An oil type referred to as "Hydrocal" was available from the day (storage) tank on the bridge. This was the easiest oil to obtain for the on-site equipment checkout. The standard equipment checkout procedure uses the Lincoln Laboratory-fabricated "calibrated" test tank to measure various thicknesses (0 to 10-mm) of oil, in this case, Hydrocal. Table 1 summarizes the results of the postcollection data analysis; the shaded blocks indicate algorithm results (LMS, CORR, or MN/SL) that are close to or match the analyst's (visual) oil estimate. A comment is provided referring to the fit of the visual (analyst's choice) to the actual data.

8-9A0MM.DAT – This measurement, shown in Figure 1, was chosen as the water background reference.

Approximately 100 ml of oil was added to the tank; 100 ml of oil corresponds to a 1-mm oil film, assuming uniform coverage of the water surface. Oil coverage was described as patchy.

8-9A1MM.DAT – The algorithm result of 2.826 mm, shown in Figure 2, is a fair-to-good match to the measured data. The tank contained the volume of oil necessary to cover the surface of the water with 1 mm of oil; however, the actual coverage was patchy with approximately 50% of the surface area covered with oil.

Approximately 100 ml of oil was added to the tank. Oil coverage was again described as patchy.

8-9A2MM.DAT – The algorithm result of 3.000 mm, shown in Figure 3, is a fair match to the measured data. The tank contained the volume of oil necessary to cover the surface of the water with 2 mm of oil; however, the actual coverage was patchy with approximately 50% of the surface area covered with oil.

Approximately 100 ml of oil was added to the tank. Oil coverage was again described as patchy.

TABLE 1

Results of the 9 September 1996 Equipment Checkout Test

FILENAME	LMS	CORR	MN/SL	DECL	METHOD	VISUAL	COMMENT
8-9A0MM.DAT							Reference
8-9A1MM.DAT	2.825	2.975	2.825	2.825	LMS & MN/SL	2.825	Fair to good
8-9A2MM.DAT	6.275	3.000	2.725	6.725	LMS only	3.000	Fair
8-9A3MM.DAT	3.200	3.125	0.000	3.150	LMS & CORR	3.150	Fair (shape)
8-9A4MM.DAT	7.275	7.300	0.675	7.275	LMS & CORR	7.275	Good
8-9A5MM.DAT	4.975	8.125	2.400	4.975	LMS only	4.975	Fair to good
8-9B5MM.DAT	8.200	4.950	0.925	8.200	LMS only	4.950	Fair to good
8-9B6MM.DAT	6.050	2.875	2.375	2.875	CORR only	6.050	Poor
8-9A7MM.DAT	6.850	3.300	2.925	6.850	LMS only	6.850	Poor (shape)
8-9A8MM.DAT	7.950	7.950	2.300	7.950	LMS & CORR	7.950	Fair to good

8-9A3MM.DAT – The algorithm result of 3.150 mm, shown in Figure 4, is a fair-to-good match to the shape of the measured data. Based on their low values, it appears that the instrument gain has drifted.

Approximately 100 ml of oil was added to the tank. Oil had settled into a uniform thickness.

8-9A4MM.DAT – The algorithm result of 7.275 mm, shown in Figure 5, is a good match to the measured data. A plot of theoretical curves between 3.7 and 3.9 mm show similar characteristics in that there is a minimum near 30 GHz, and a maximum near 41 GHz, but the plots do not exhibit the same curvature characteristic and thus do not fit the measured data well.

Approximately 100 ml of oil was added to the tank.

8-9A5MM.DAT – The algorithm result of 4.975 mm, shown in Figure 6, is a fair-to-good match to the measured data.

A hot load calibration was performed.

8-9B5MM.DAT – The algorithm result of 4.950 mm, shown in Figure 7, is a fair-to-good match to the measured data.

Approximately 100 ml of oil was added to the tank. Oil coverage finally became uniform over the surface of the water.

8-9B6MM.DAT – The algorithm result of 6.050 mm, shown in Figure 8, is a poor match to the measured data. Based on the large amplitude variations, it appears that the gain of the instrument is drifting again.

Approximately 100 ml of oil was added to the tank.

8-9A7MM.DAT – The algorithm result of 6.850 mm, shown in Figure 9, is a somewhat poor match to the shape of the measured data plot.

Approximately 100 ml of oil was added to the tank.

8-9A8MM.DAT – The algorithm result of 7.950 mm, shown in Figure 10, is a fair-to-good match to the measured data.

The cause of the large variation in system gain was attributed to the heat buildup in the receiver electronics case. The instrument had not been used extensively in sunny conditions, and the solar heating of the electronics case created excess heat inside. A fan was installed. The equipment checkout continued on 10 September 1996 using the same calibrated test tank and oil type. Table 2 presents the results for this data collection.

There is a slight oil sheen on the surface of the water. The oil type used for this equipment checkout is Hydrocal.

910A0MM.DAT – The algorithm result of 0.500 mm, shown in Figure 11, is a good match to the measured data set.

910B0MM.DAT – The algorithm estimate of 3.250 mm is a poor match to the measured data set. A thinner estimate of 0.000 mm, hinted at by the MN/SL result and shown in Figure 12, is a good match.

910C0MM.DAT – This data set, shown in Figure 13, was chosen as the background water reference.

Approximately 100 ml of oil was added to the tank. Oil coverage was described as patchy, covering approximately 40% of the surface.

910A1MM.DAT – The algorithm estimate of 2.525 mm, shown in Figure 14, is a poor match to the measured data set.

910B1MM.DAT – The algorithm estimate of 2.575 mm, shown in Figure 15, is a fair match to the measured data.

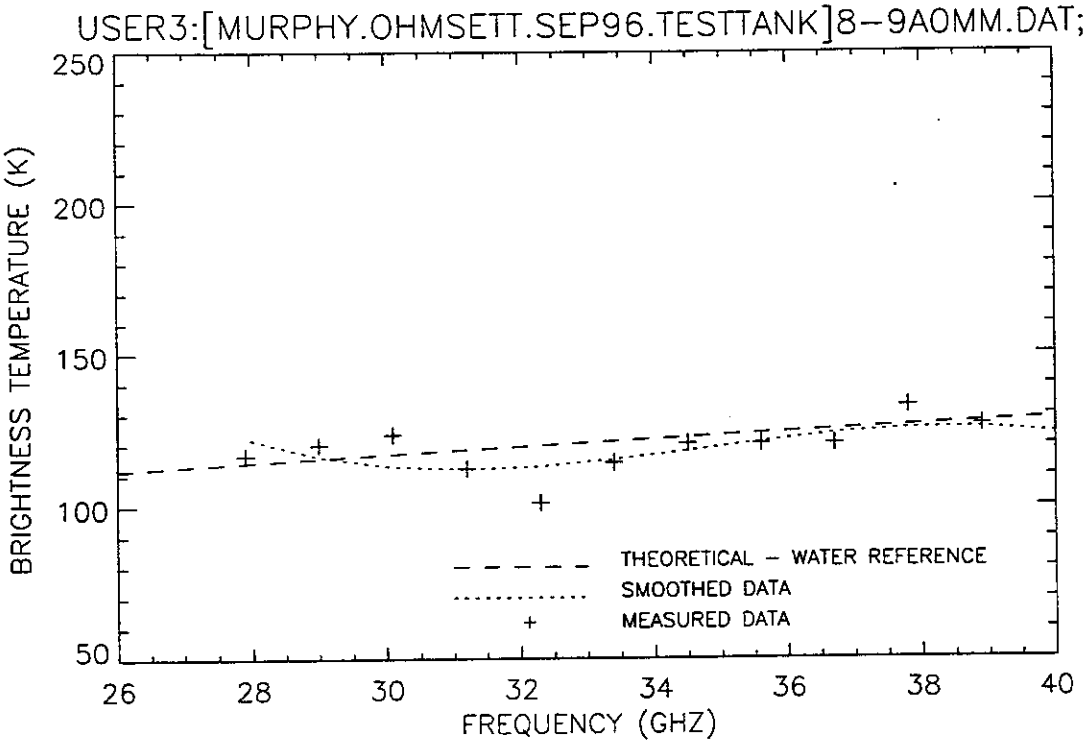

Figure 1. Plot of radiometric brightness temperature versus measurement frequency for water, equipment verification test, 9 September 1996.

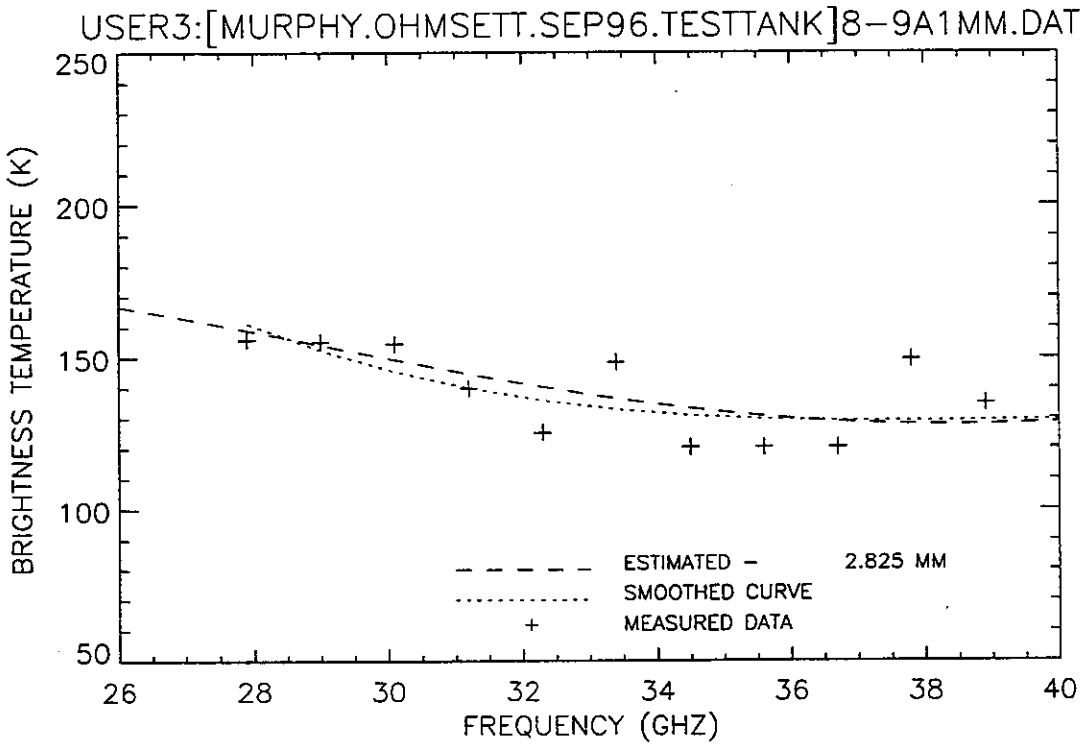

Figure 2. Plot of radiometric brightness temperature versus measurement frequency for 1-mm oil, equipment verification test, 9 September 199.

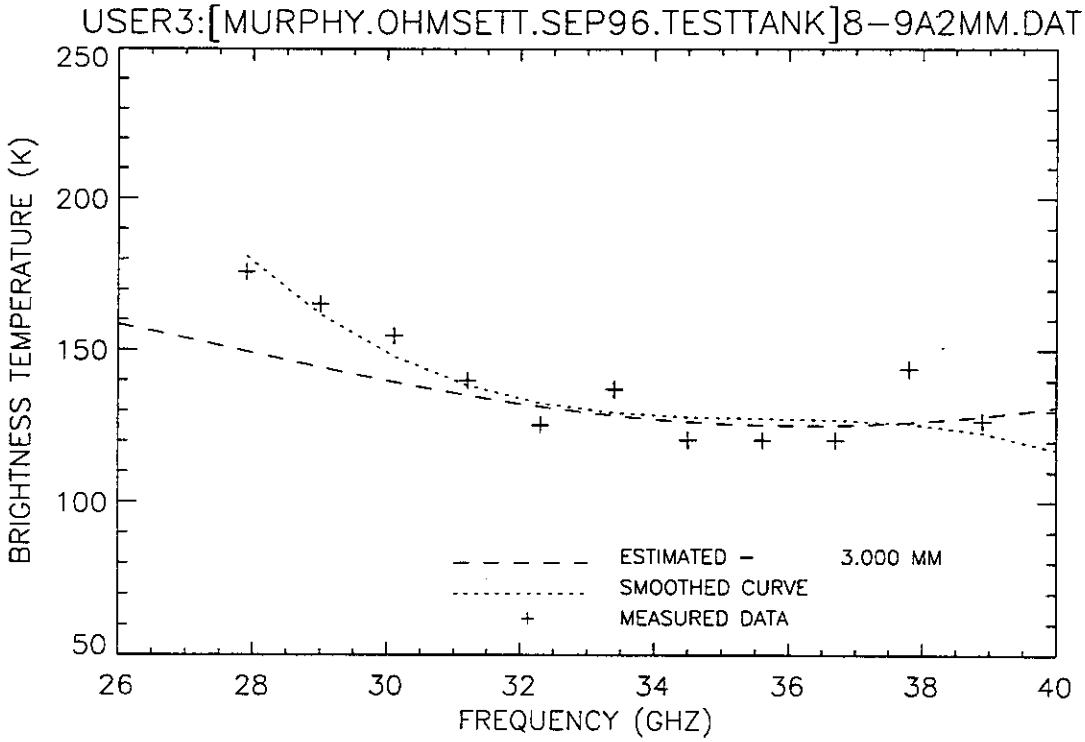

Figure 3. Plot of radiometric brightness temperature versus measurement frequency for 2-mm oil, equipment verification test, 9 September 1996.

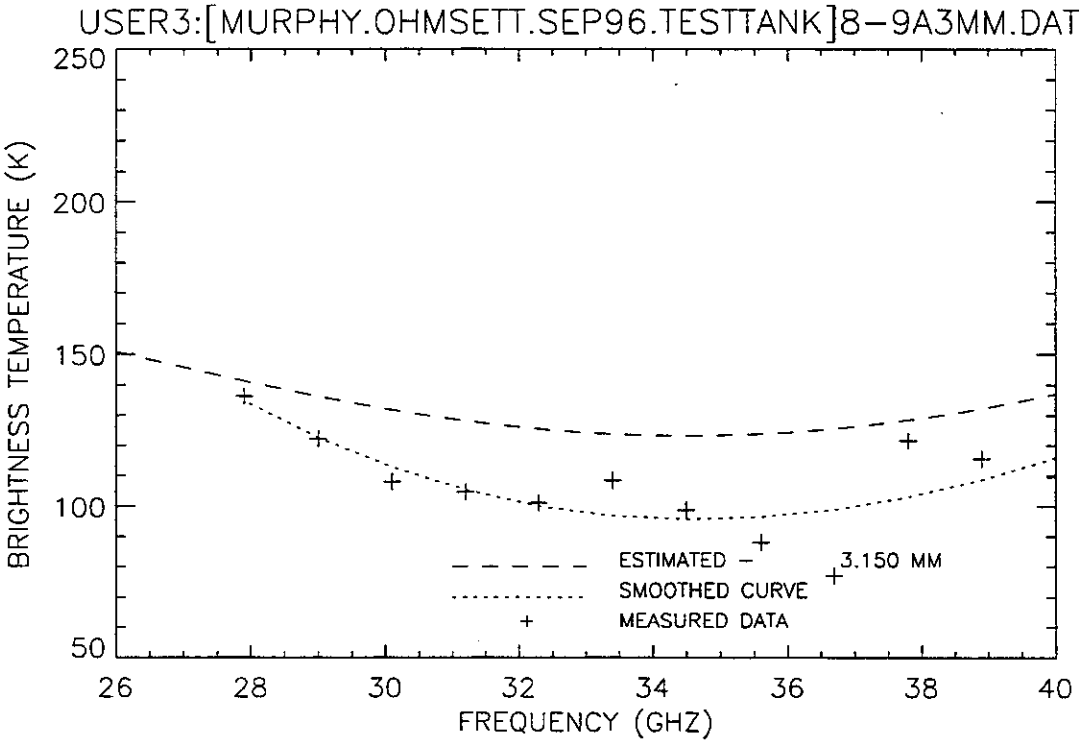

Figure 4. Plot of radiometric brightness temperature versus measurement frequency for 3-mm oil, equipment verification test, 9 September 1996.

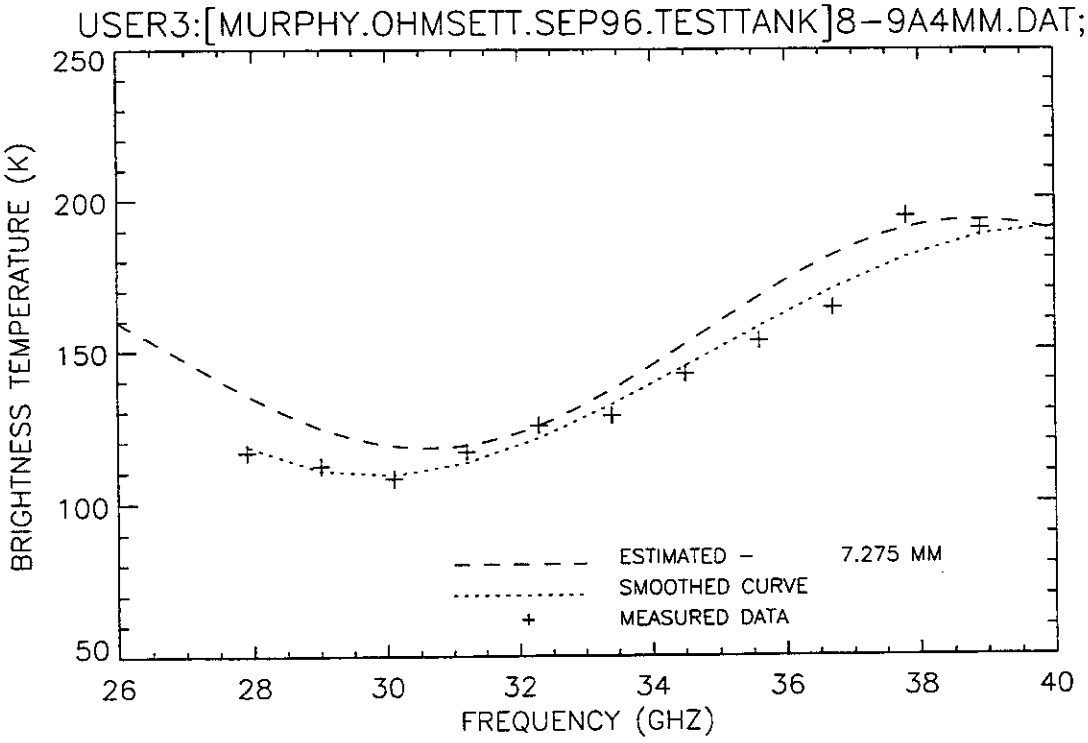

Figure 5. Plot of radiometric brightness temperature versus measurement frequency for 4-mm oil, equipment verification test, 9 September 1996.

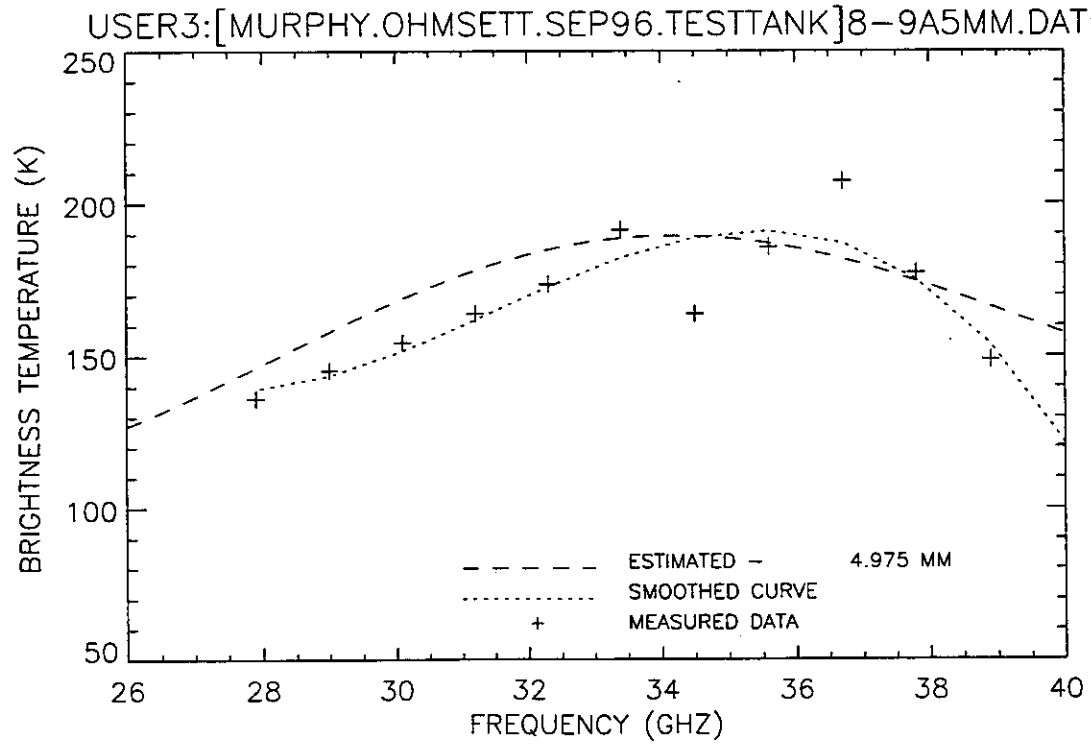

Figure 6. Plot of radiometric brightness temperature versus measurement frequency for 5-mm oil, equipment verification test, 9 September 1996, sweep A.

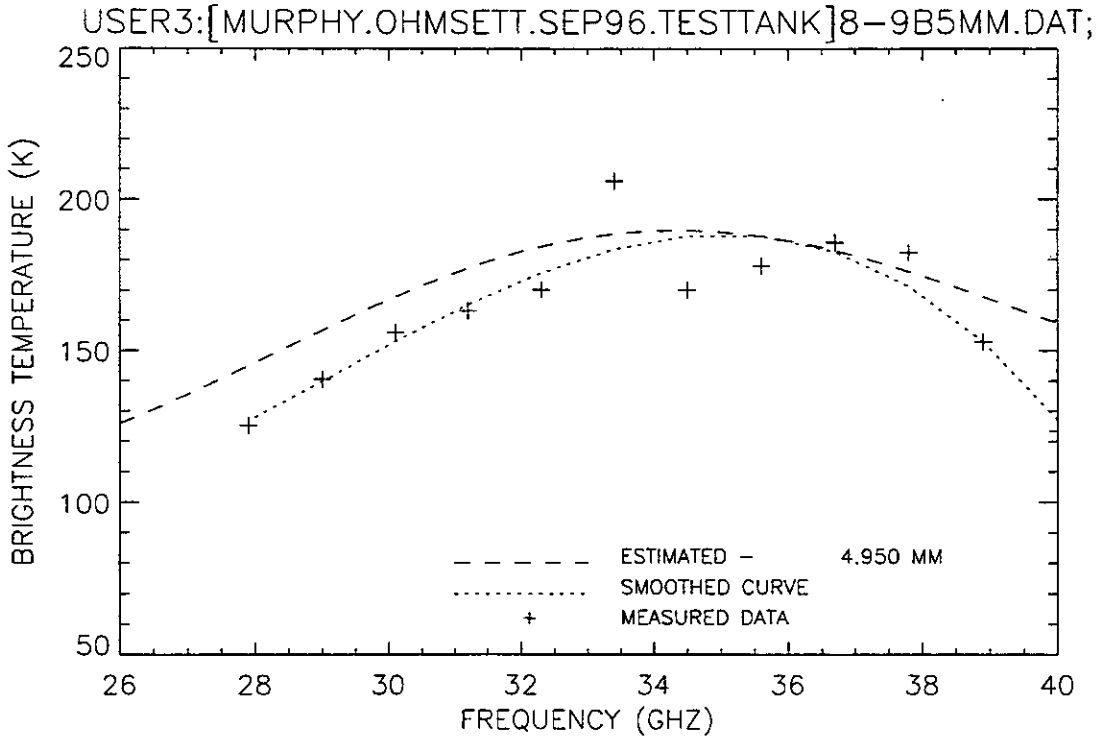

Figure 7. Plot of radiometric brightness temperature versus measurement frequency for 5-mm oil, equipment verification test, 9 September 1996, sweep B.

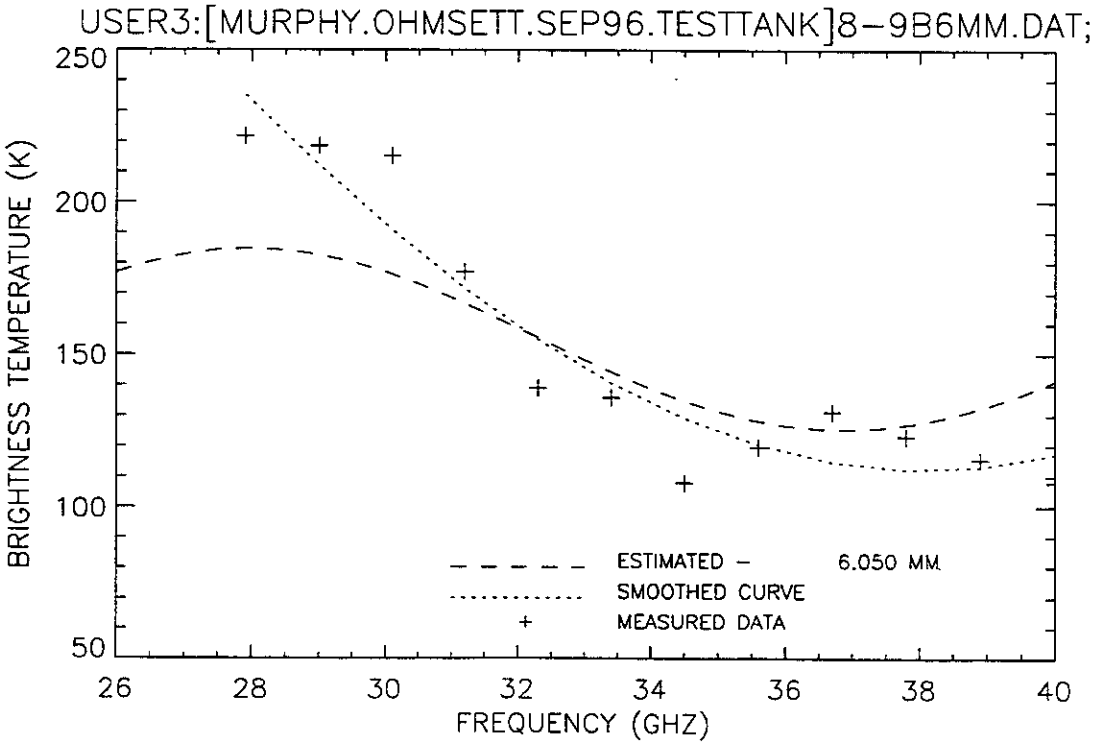

Figure 8. Plot of radiometric brightness temperature versus measurement frequency for 6-mm oil, equipment verification test, 9 September 1996.

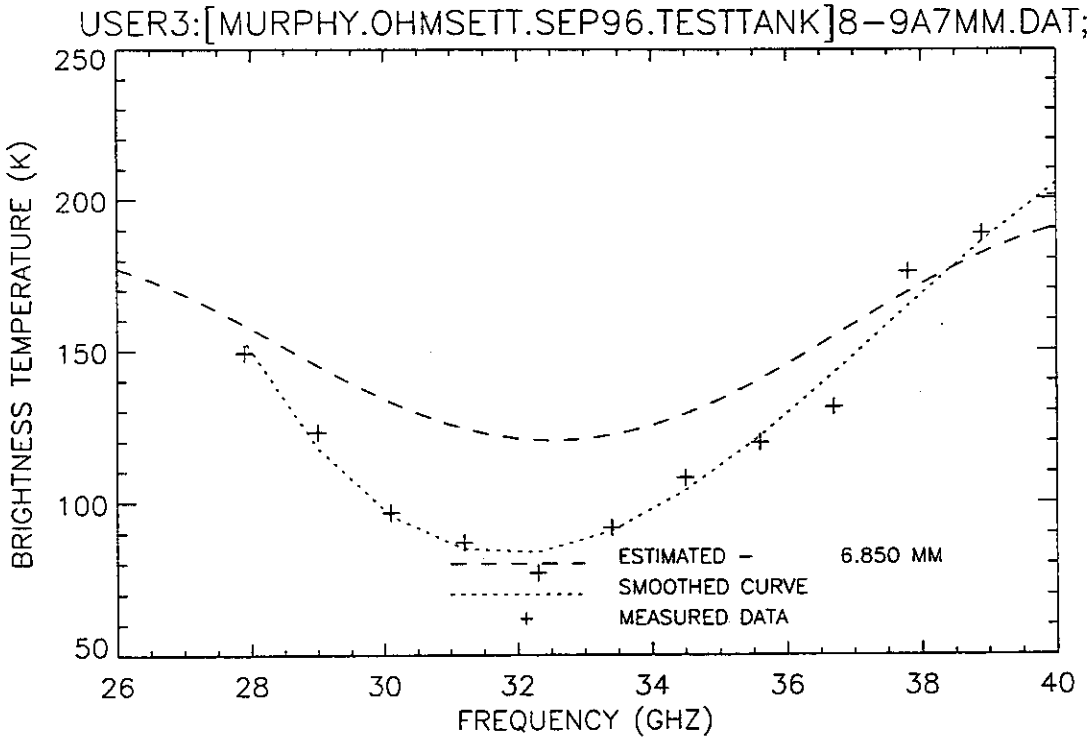

Figure 9. Plot of radiometric brightness temperature versus measurement frequency for 7-mm oil, equipment verification test, 9 September 1996.

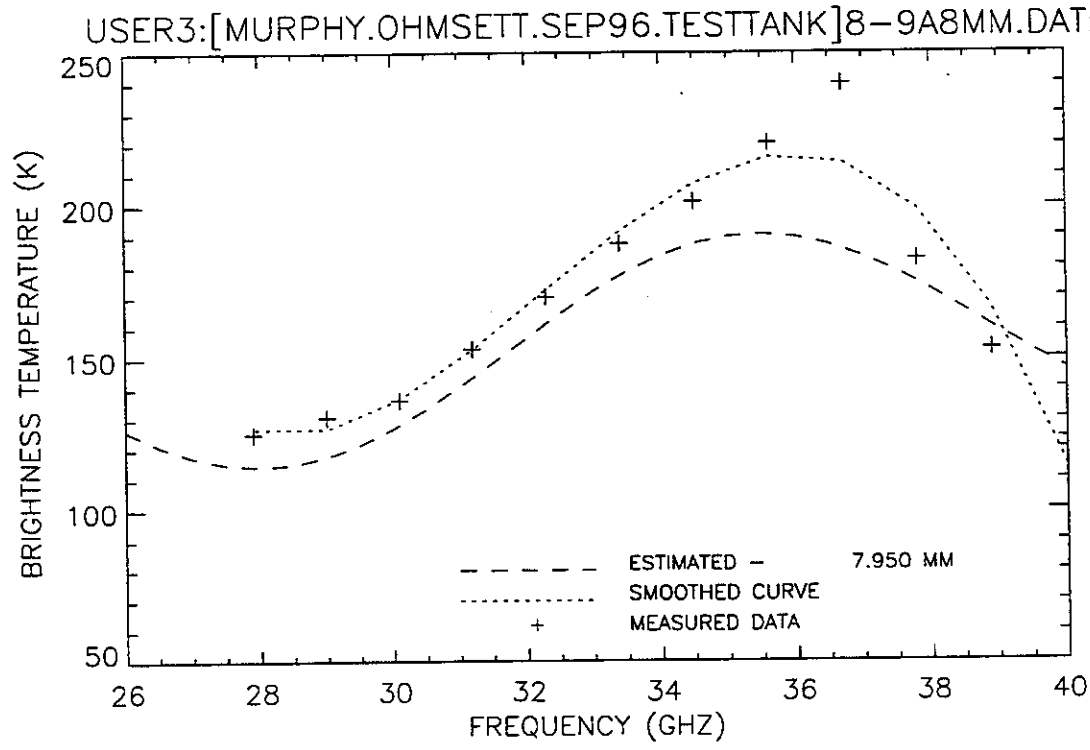

Figure 10. Plot of radiometric brightness temperature versus measurement frequency for 8-mm oil, equipment verification test, 9 September 1996.

TABLE 2

Results of the 10 September 1996 Equipment Checkout Test

FILENAME	LMS	CORR	MN/SL	DECL	METHOD	VISUAL	COMMENT
910C0MM.DAT							Reference
910A0MM.DAT	0.025	3.350	0.100	0.050	LMS & MN/SL	0.050	Good
910B0MM.DAT	3.300	3.225	0.300	3.250	LMS & CORR	0.000	Good
910A1MM.DAT	2.525	5.900	2.550	2.525	LMS & MN/SL	2.525	Good
910B1MM.DAT	2.575	2.850	2.575	2.575	LMS & MN/SL	2.575	Fair
910C1MM.DAT	2.475	2.975	2.500	2.475	LMS & MN/SL	2.475	Fair to good
910A2MM.DAT	2.225	2.675	2.250	2.225	LMS & MN/SL	2.225	Fair
910B2MM.DAT	2.450	2.650	2.450	2.450	LMS & MN/SL	2.450	Good
910C2MM.DAT	2.475	2.600	2.450	2.450	LMS & MN/SL	2.450	Good
910A3MM.DAT	2.925	3.075	2.975	2.950	LMS & MN/SL	2.950	Fair (shape)
910B3MM.DAT	2.925	3.075	3.000	3.025	MN/SL & CORR	3.025	Fair (shape)
910C3MM.DAT	3.175	6.325	0.525	3.175	LMS only	3.175	Fair
910D3MM.DAT	2.850	3.100	2.800	2.825	LMS & MN/SL	2.825	Fair
910A4MM.DAT	4.025	4.025	3.975	4.025	LMS & CORR	4.025	Fair to good
910B4MM.DAT	4.000	3.975	3.900	3.975	LMS & CORR	3.975	Fair
910C4MM.DAT	4.000	4.000	3.925	4.000	LMS & CORR	4.000	Fair
910A5MM.DAT	4.475	4.325	1.100	4.400	LMS & CORR	4.400	Fair (shape)
910B5MM.DAT	4.575	4.450	1.475	4.500	LMS & CORR	4.500	Fair (shape)
910C5MM.DAT	4.375	4.400	0.925	4.375	LMS & CORR	4.375	Fair (shape)
910A6MM.DAT	8.950	8.950	0.850	8.950	LMS & CORR	8.950	Good
910B6MM.DAT	8.925	8.950	3.975	8.925	LMS & CORR	8.925	Good to excellent
910C6MM.DAT	8.900	8.925	0.700	8.900	LMS & CORR	8.900	Good
910A7MM.DAT	6.625	3.275	2.650	6.625	LMS only	6.625	Good to excellent
910B7MM.DAT	6.625	3.300	0.600	3.300	CORR only	6.625	Good (shape)
910C7MM.DAT	3.100	3.250	3.050	3.075	LMS & MN/SL	6.600	Good (shape)
910A8MM.DAT	4.000	7.600	3.775	3.875	LMS & MN/SL	7.400	Good (shape)
910B8MM.DAT	7.450	7.450	0.775	7.450	LMS & CORR	7.450	Good (shape)
910C8MM.DAT	7.450	7.425	2.450	7.425	LMS & CORR	7.425	Good (shape)
910D8MM.DAT	7.450	7.425	2.450	7.425	LMS & CORR	7.425	Good (shape)
910A8XMM.DAT	8.375	1.625	3.800	1.625	CORR only	8.375	Fair (shape)
910B8XMM.DAT	8.425	1.650	3.925	8.425	LMS only	8.425	Fair (shape)

910C1MM.DAT – The algorithm estimate of 2.475 mm, shown in Figure 16, is a fair-to-good match to the measured data.

Approximately 100 ml of oil was added to the tank. Oil coverage was again described as patchy with 90% of the surface covered with oil.

910A2MM.DAT – The algorithm estimate of 2.225 mm, shown in Figure 17, is a fair-to-good match to the measured data.

910B2MM.DAT – The algorithm estimate of 2.450 mm, shown in Figure 18, is a good match to the measured data.

910C2MM.DAT – The algorithm estimate of 2.450 mm, shown in Figure 19, is a good match to the measured data points.

Approximately 100 ml of oil was added to the tank. Oil coverage was described as uniform. A hot load calibration was performed.

910A3MM.DAT – The algorithm estimate of 2.950 mm, shown in Figure 20, is a fair match to the shape of the measured data.

910B3MM.DAT – The algorithm estimate of 3.025 mm, shown in Figure 21, is a fair match to the shape of the measured data points.

910C3MM.DAT – The algorithm estimate of 3.175 mm, shown in Figure 22, is a fair match to the measured data.

A hot/cold load calibration was performed.

910D3MM.DAT – The algorithm estimate of 2.825 mm, shown in Figure 23, is a fair match to the measured data.

Approximately 100 ml of oil was added to the tank. Oil coverage was described as uniform. The instrument is again showing signs of gain drift.

910A4MM.DAT – The algorithm estimate of 4.025 mm, shown in Figure 24, is a fair-to-good match to the measured data.

910B4MM.DAT – The algorithm estimate of 3.975 mm, shown in Figure 25, is a fair match to the measured data.

910C4MM.DAT – The algorithm estimate of 4.000 mm, shown in Figure 26, is a fair match to the measured data.

Approximately 100 ml of oil was added to the tank. Oil coverage was described as uniform.

910A5MM.DAT – The algorithm estimate of 4.400 mm, shown in Figure 27, is a fair match to the shape of the measured data.

910B5MM.DAT – The algorithm estimate of 4.500 mm, shown in Figure 28, is a fair match to the shape of the measured data.

910C5MM.DAT – The algorithm estimate of 4.375 mm, shown in Figure 29, is a fair match to the shape of the measured data.

Approximately 100 ml of oil was added to the tank. Oil coverage was described as uniform.

910A6MM.DAT – The algorithm estimate of 8.950 mm, shown in Figure 30, is a good match to the measured data.

910B6MM.DAT – The algorithm estimate of 8.925 mm, shown in Figure 31, is a good-to-excellent match to the measured data.

910C6MM.DAT – The algorithm estimate of 8.900 mm, shown in Figure 32, is a good match to the measured data.

Approximately 100 ml of oil was added to the tank. Oil coverage was described as uniform.

910A7MM.DAT – The algorithm estimate of 6.625 mm, shown in Figure 33, is a good-to-excellent match to the measured data.

910B7MM.DAT – The algorithm estimate of 3.300 mm is a poor match to the measured data. The LMS only estimate of 6.625 mm, shown in Figure 34, results in a good shape match.

910C7MM.DAT – The algorithm estimate of 3.075 mm is a poor match to the measured data. This curve is similar in appearance to the 910B7MM.DAT measurement, therefore a thicker oil film was estimated. The estimate of 6.600 mm, shown in Figure 35, results in a good shape match to the data.

Approximately 100 ml of oil was added to the tank. Oil coverage was described as uniform. Again the instrument is showing signs of gain drift.

910A8MM.DAT – The algorithm estimate of 3.875 mm is a poor match to the measured data. The correlation-only estimate hints at a thicker estimate. An estimate of 7.400 mm, shown in Figure 36, results in a good shape match to the data.

910B8MM.DAT – The algorithm estimate of 7.450 mm, shown in Figure 37, is a good match to the shape of the measured data.

The operator noticed that the instrument gain had drifted and performed a new hot/cold load calibration.

910C8MM.DAT – The algorithm estimate of 7.425 mm, shown in Figure 38, is a good match to the shape of the measured data.

910D8MM.DAT – The algorithm estimate of 7.425 mm, shown in Figure 39, is a good match to the shape of the measured data.

Less than 100 ml of oil was added to the tank. Oil coverage was described as uniform.

910A8XMM.DAT – The algorithm estimate of 1.625 mm is a poor match to the measured data. The LMS-only estimate of 8.375 mm, shown in Figure 40, results in a fair match to the shape of the measured data.

910B8XMM.DAT – The algorithm estimate of 8.425 mm, shown in Figure 41, is a fair match to the shape of the measured data.

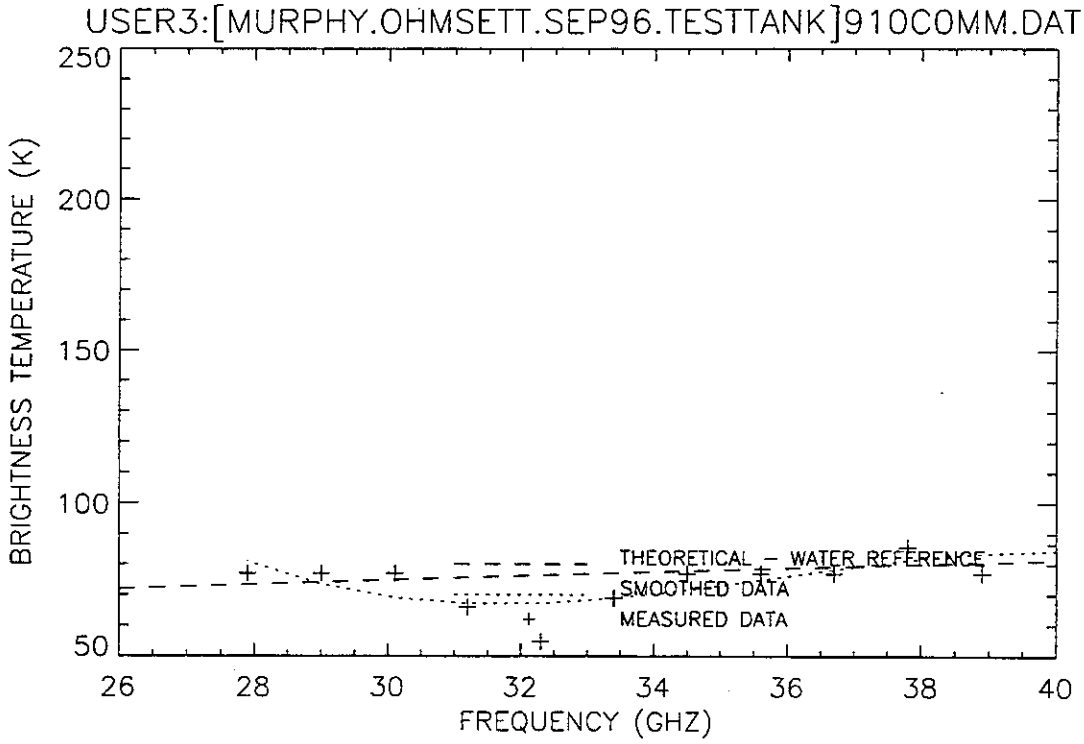

Figure 11. Plot of radiometric brightness temperature versus measurement frequency for water, equipment verification test, 10 September 1996.

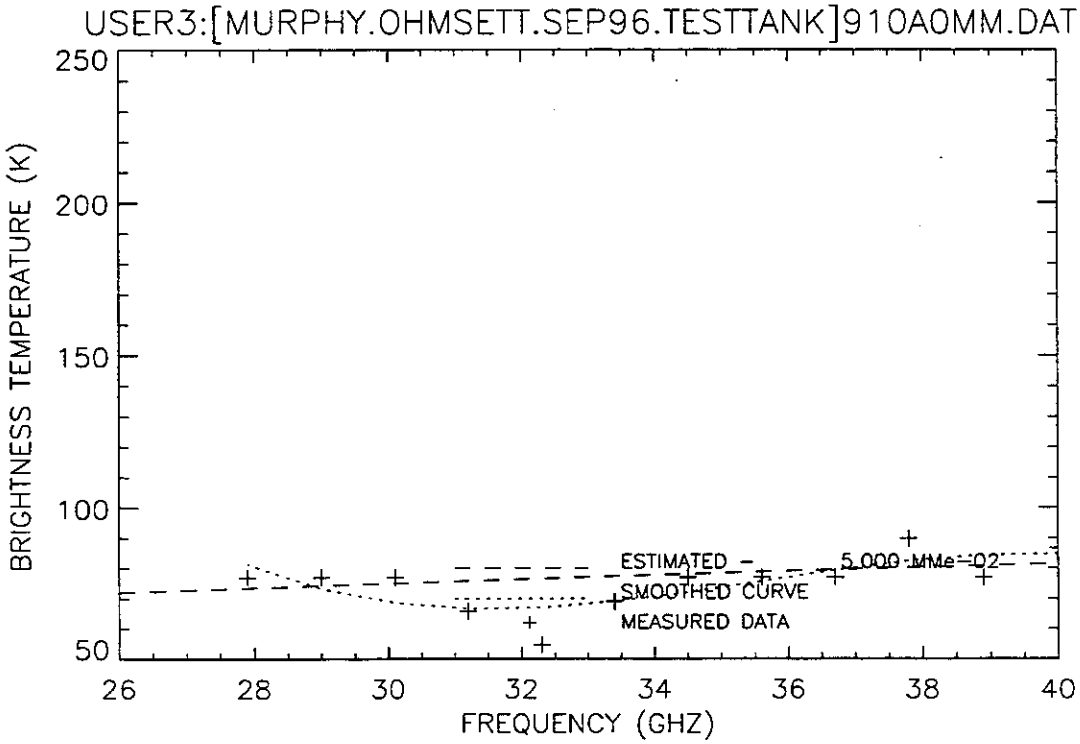

Figure 12. Plot of radiometric brightness temperature versus measurement frequency for water, equipment verification test, 10 September 1996, sweep A.

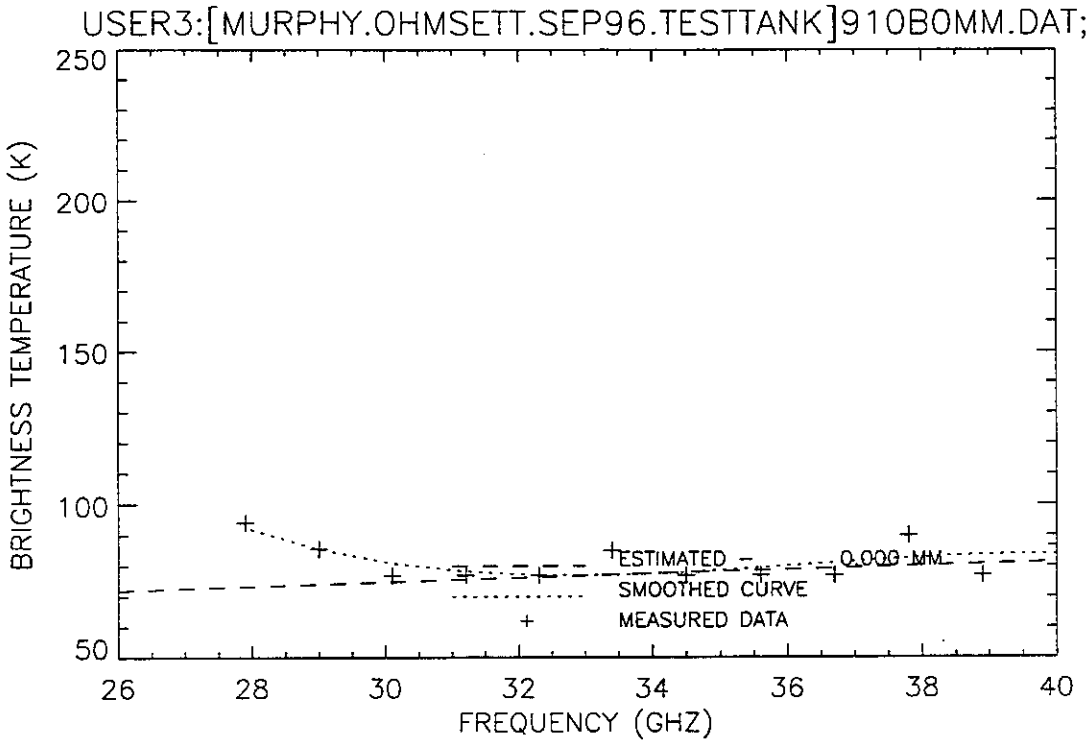

Figure 13. Plot of radiometric brightness temperature versus measurement frequency for water, equipment verification test, 10 September 1996, sweep B.

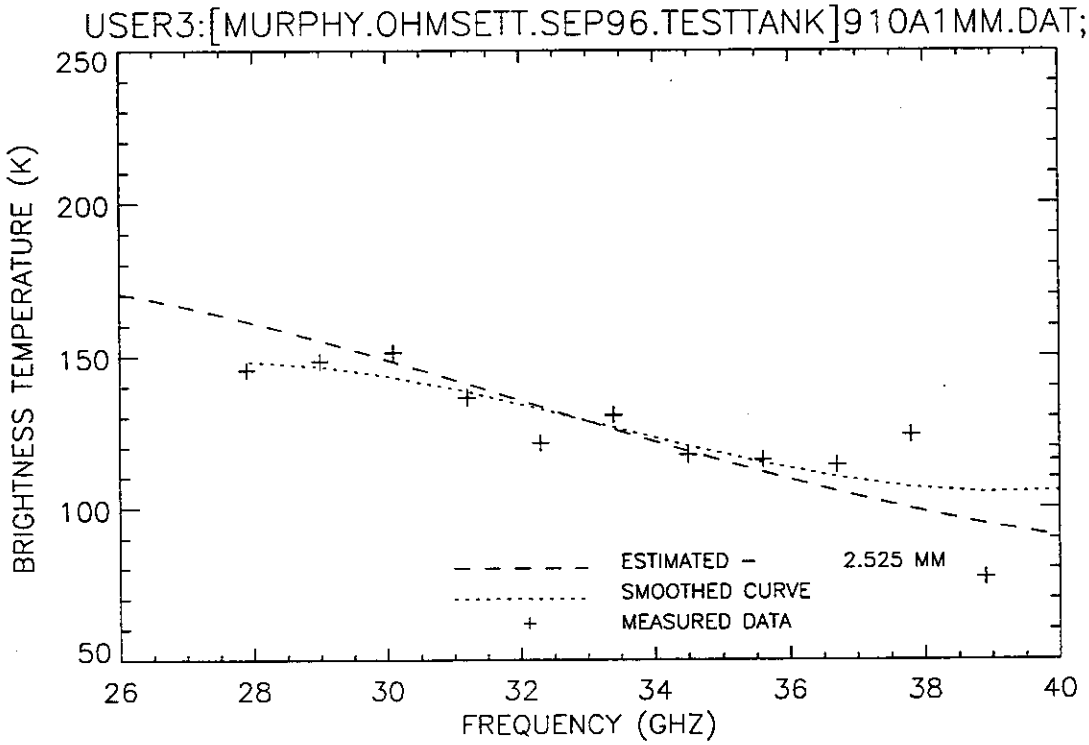

Figure 14. Plot of radiometric brightness temperature versus measurement frequency for 1-mm oil, equipment verification test, 10 September 1996, sweep A.

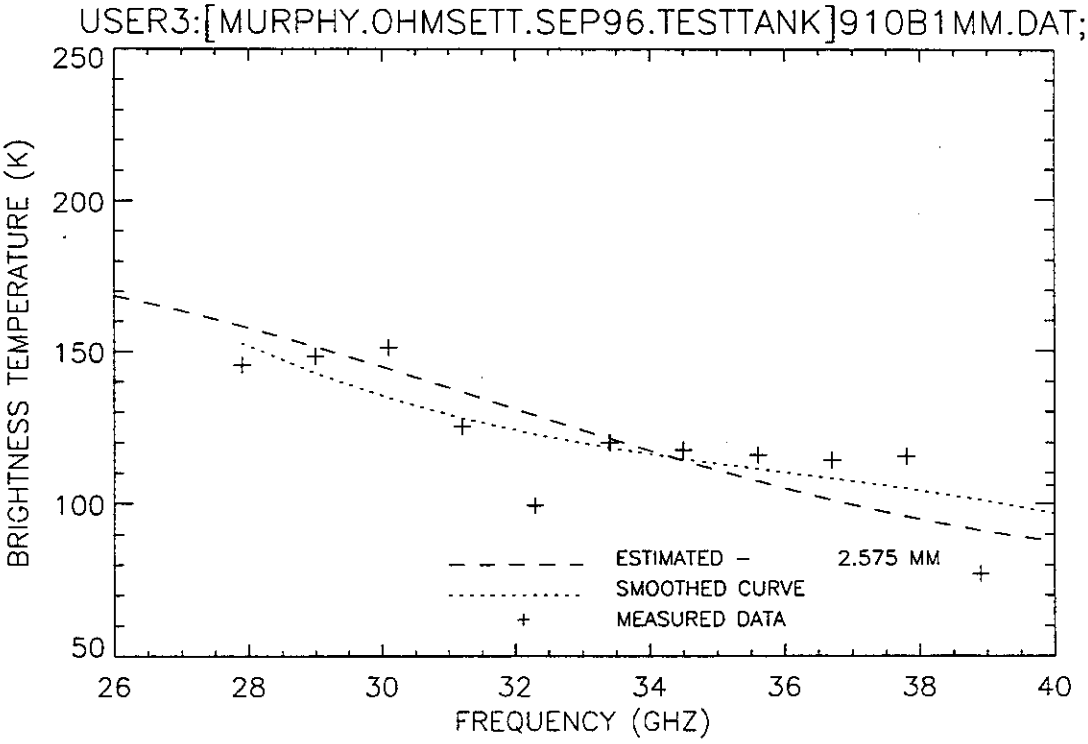

Figure 15. Plot of radiometric brightness temperature versus measurement frequency for 1-mm oil, equipment verification test, 10 September 1996, sweep B.

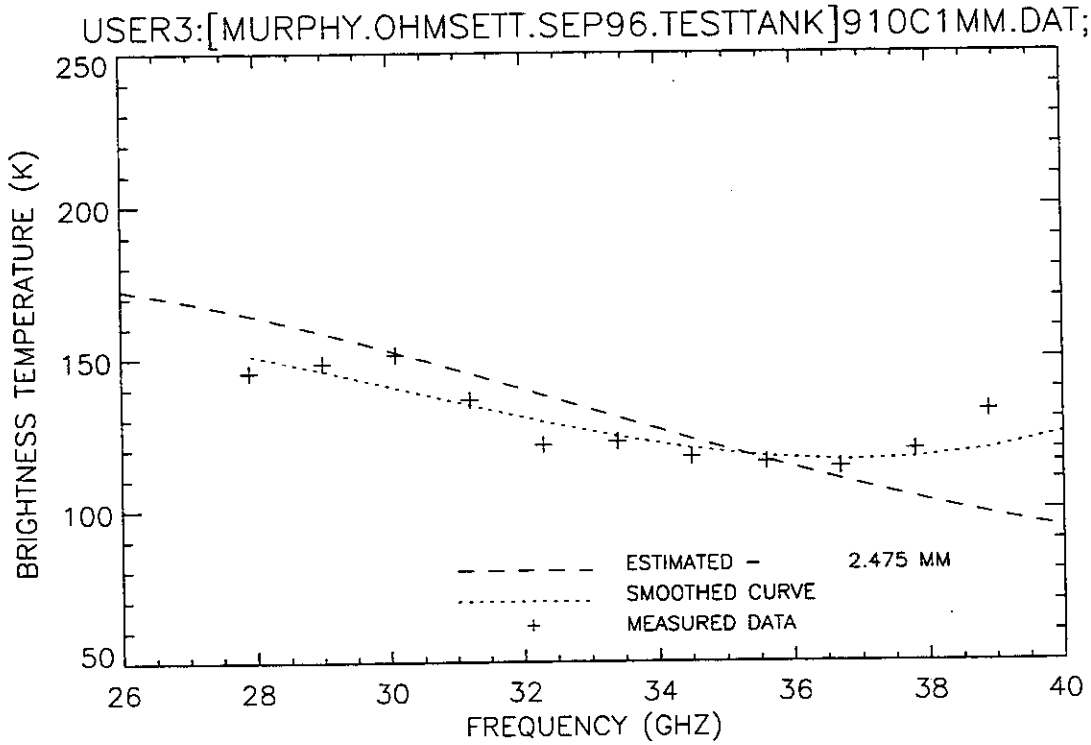

Figure 16. Plot of radiometric brightness temperature versus measurement frequency for 1-mm oil, equipment verification test, 10 September 1996, sweep C.

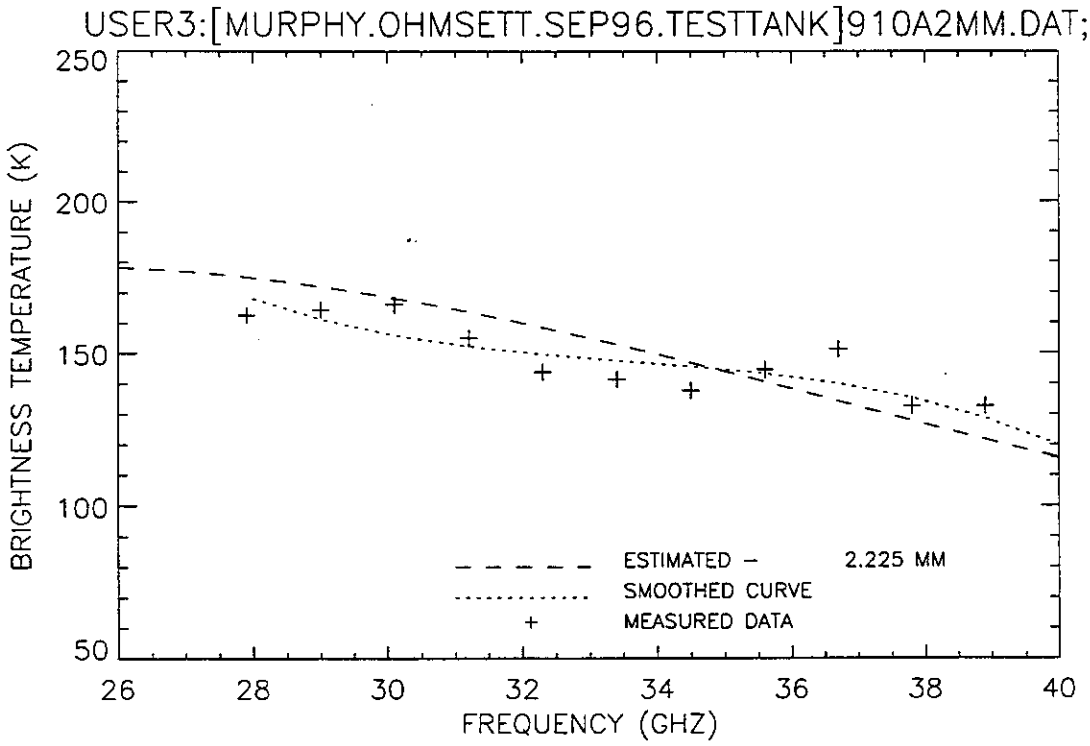

Figure 17. Plot of radiometric brightness temperature versus measurement frequency for 2-mm oil, equipment verification test, 10 September 1996, sweep A.

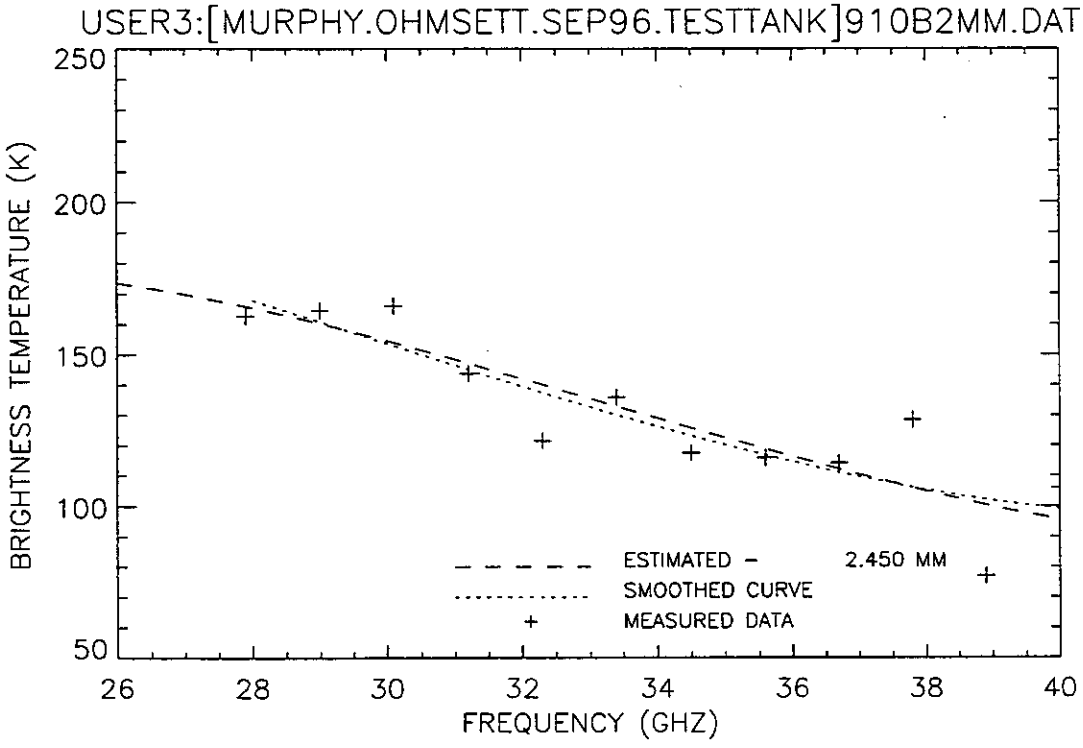

Figure 18. Plot of radiometric brightness temperature versus measurement frequency for 2-mm oil, equipment verification test, 10 September 1996, sweep B.

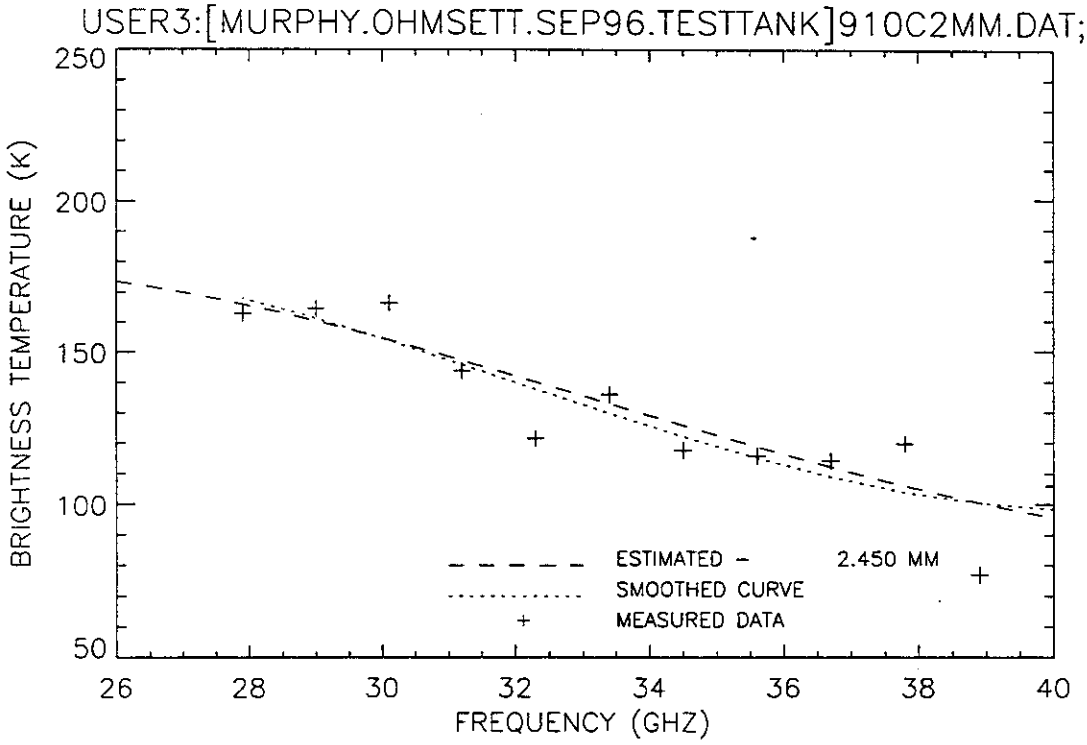

Figure 19. Plot of radiometric brightness temperature versus measurement frequency for 2-mm oil, equipment verification test, 10 September 1996, sweep C.

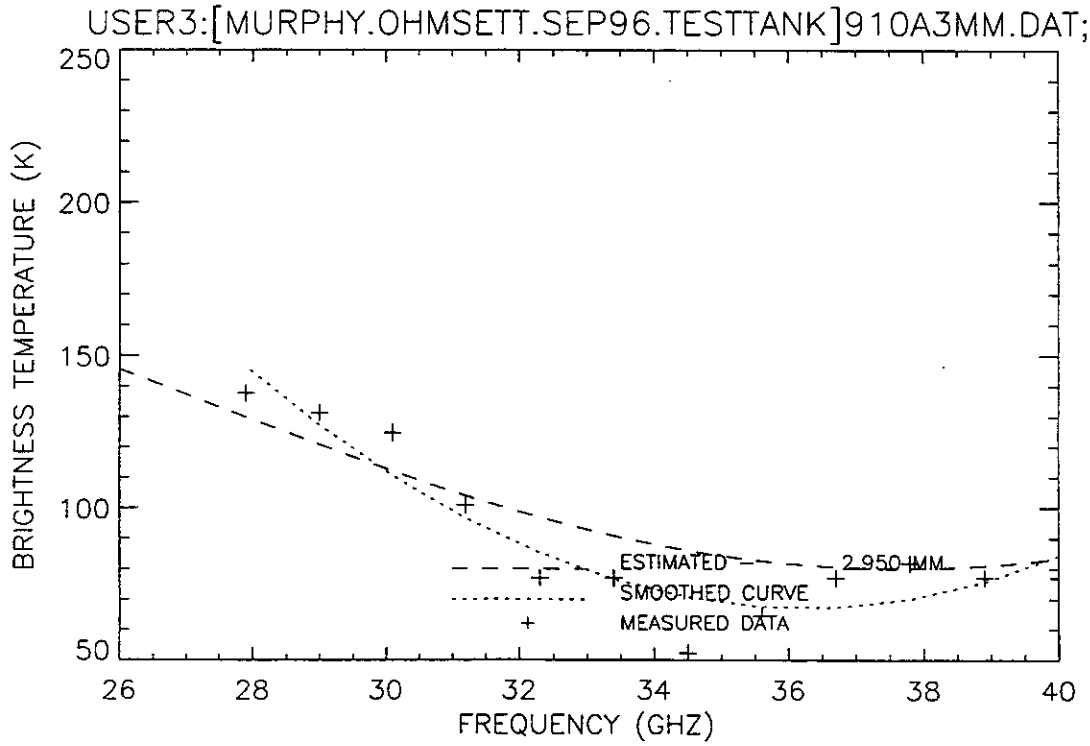

Figure 20. Plot of radiometric brightness temperature versus measurement frequency for 3-mm oil, equipment verification test, 10 September 1996, sweep A.

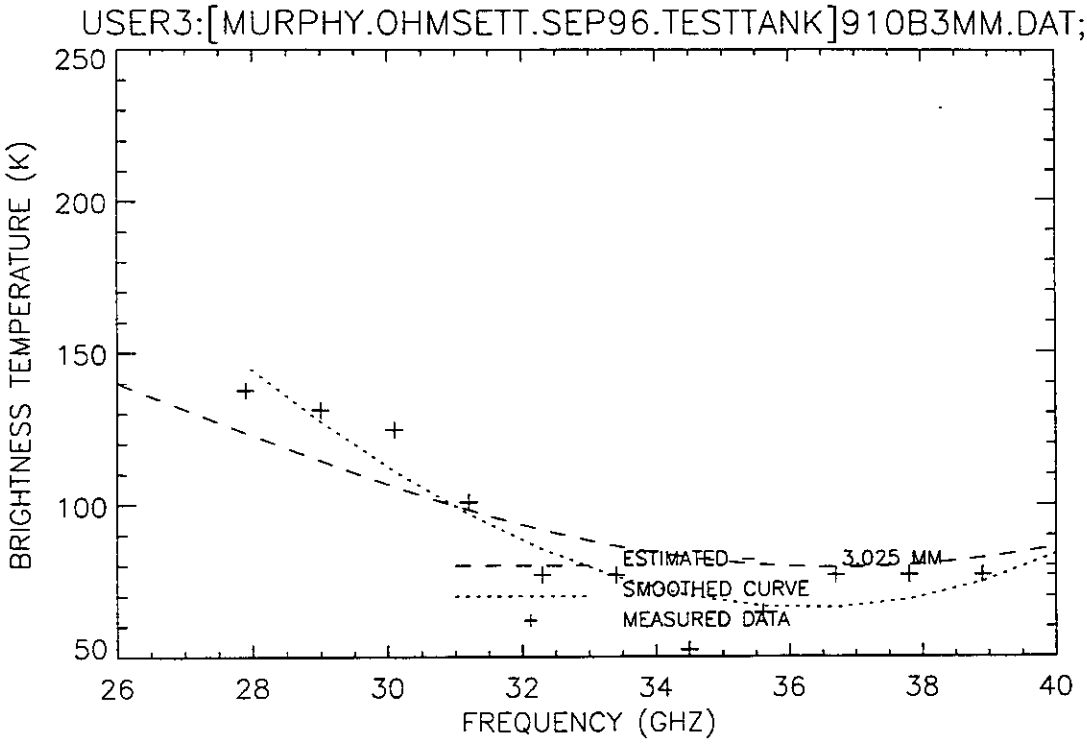

Figure 21. Plot of radiometric brightness temperature versus measurement frequency for 3-mm oil, equipment verification test, 10 September 1996, sweep B.

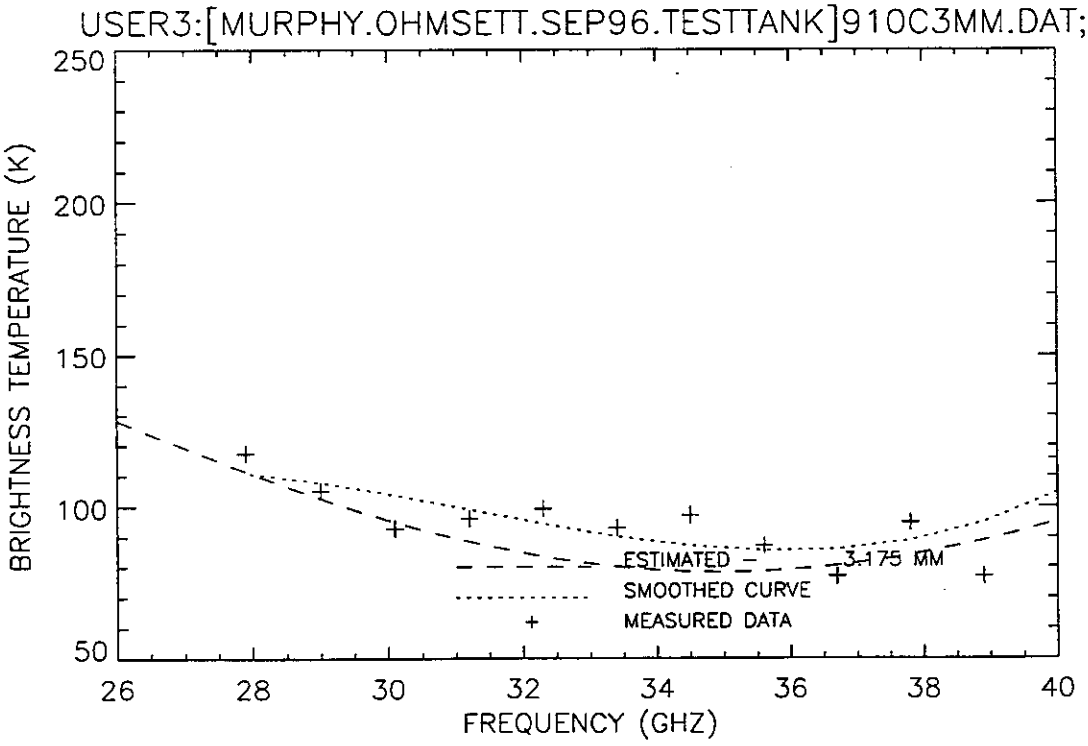

Figure 22. Plot of radiometric brightness temperature versus measurement frequency for 3-mm oil, equipment verification test, 10 September 1996, sweep C.

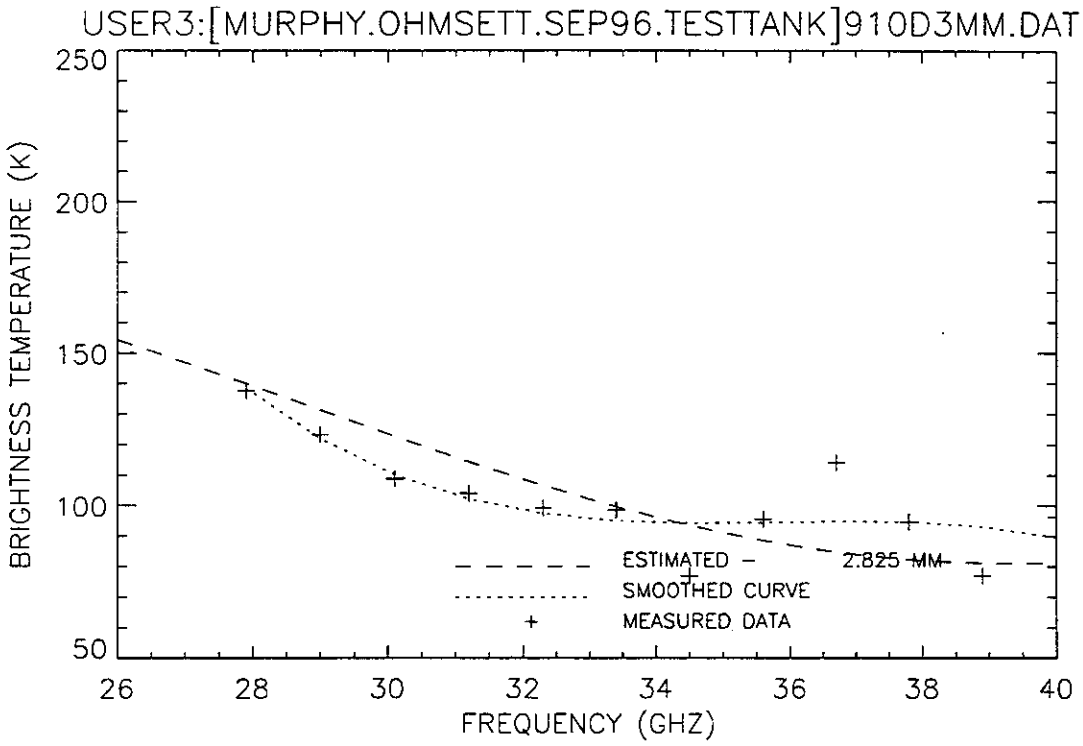

Figure 23. Plot of radiometric brightness temperature versus measurement frequency for 3-mm oil, equipment verification test, 10 September 1996, sweep D.

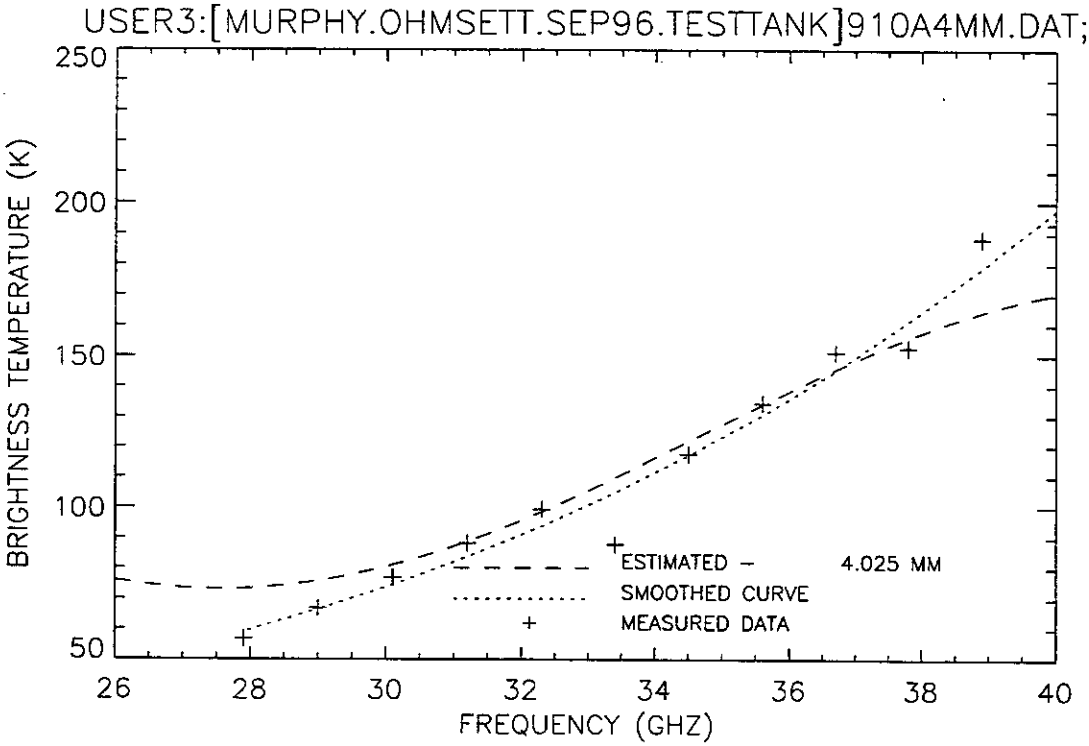

Figure 24. Plot of radiometric brightness temperature versus measurement frequency for 4-mm oil, equipment verification test, 10 September 1996, sweep A.

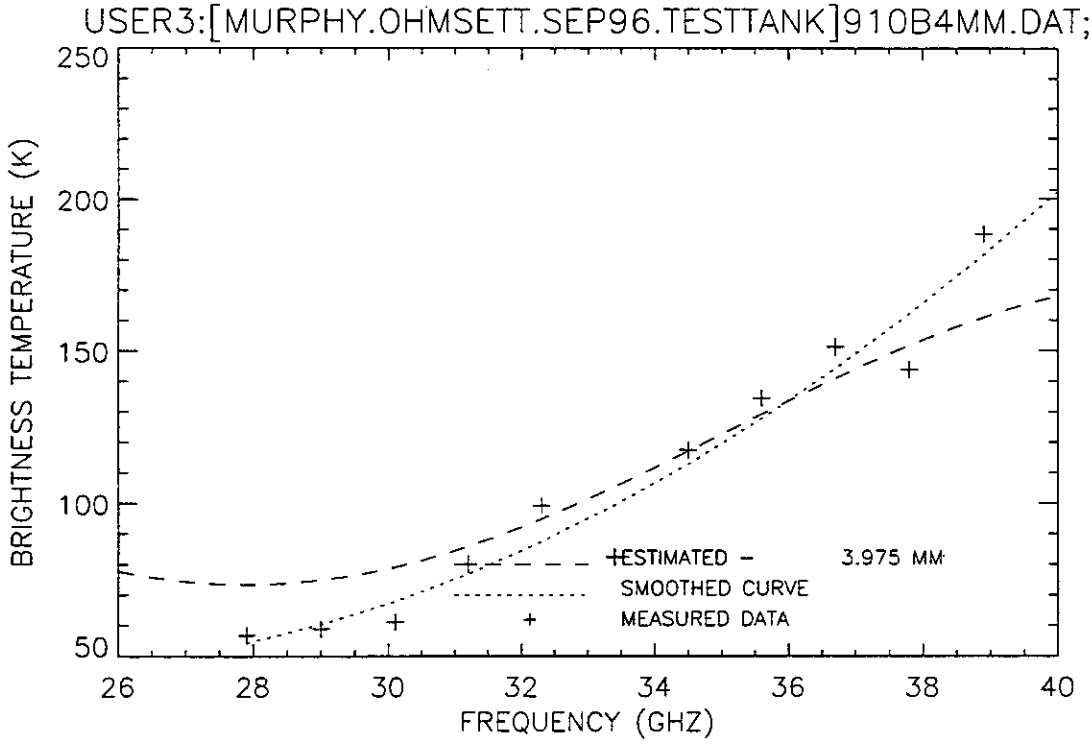

Figure 25. Plot of radiometric brightness temperature versus measurement frequency for 4-mm oil, equipment verification test, 10 September 1996, sweep B.

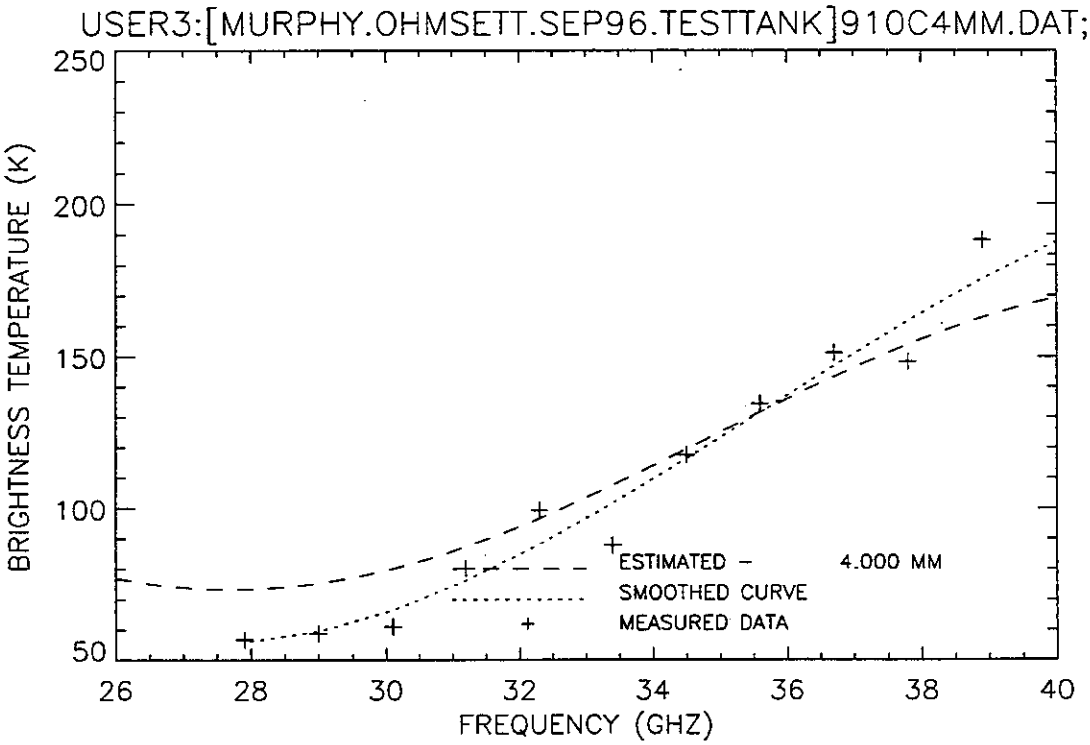

Figure 26. Plot of radiometric brightness temperature versus measurement frequency for 4-mm oil, equipment verification test, 10 September 1996, sweep C.

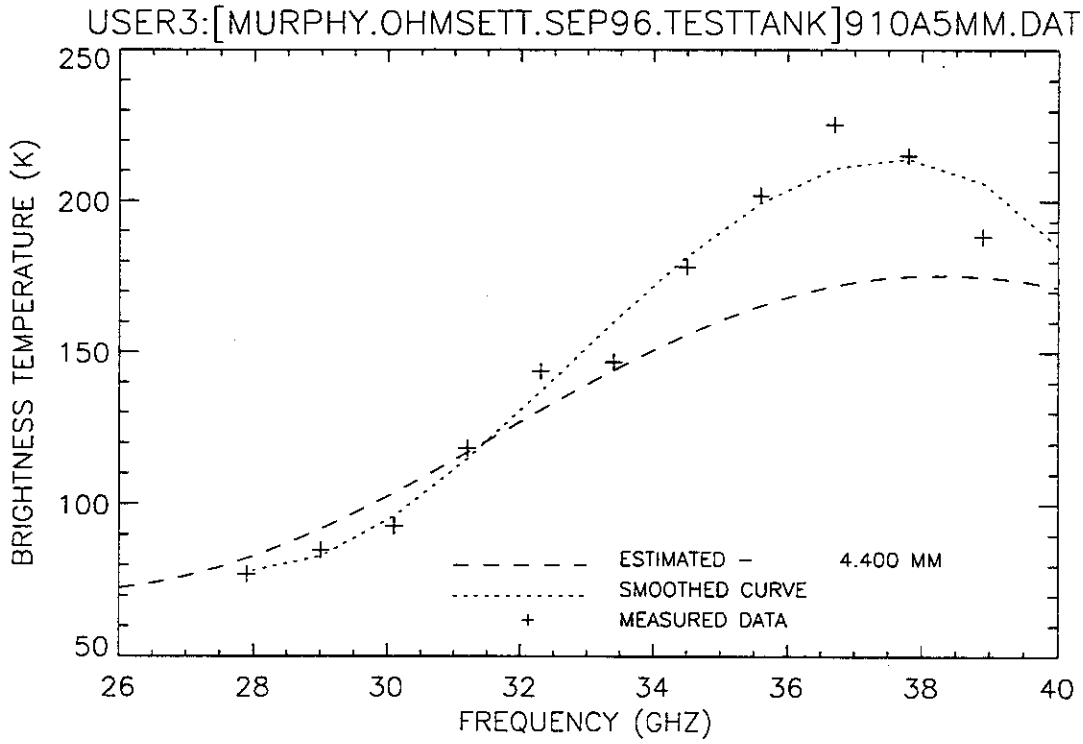

Figure 27. Plot of radiometric brightness temperature versus measurement frequency for 5-mm oil, equipment verification test, 10 September 1996, sweep A.

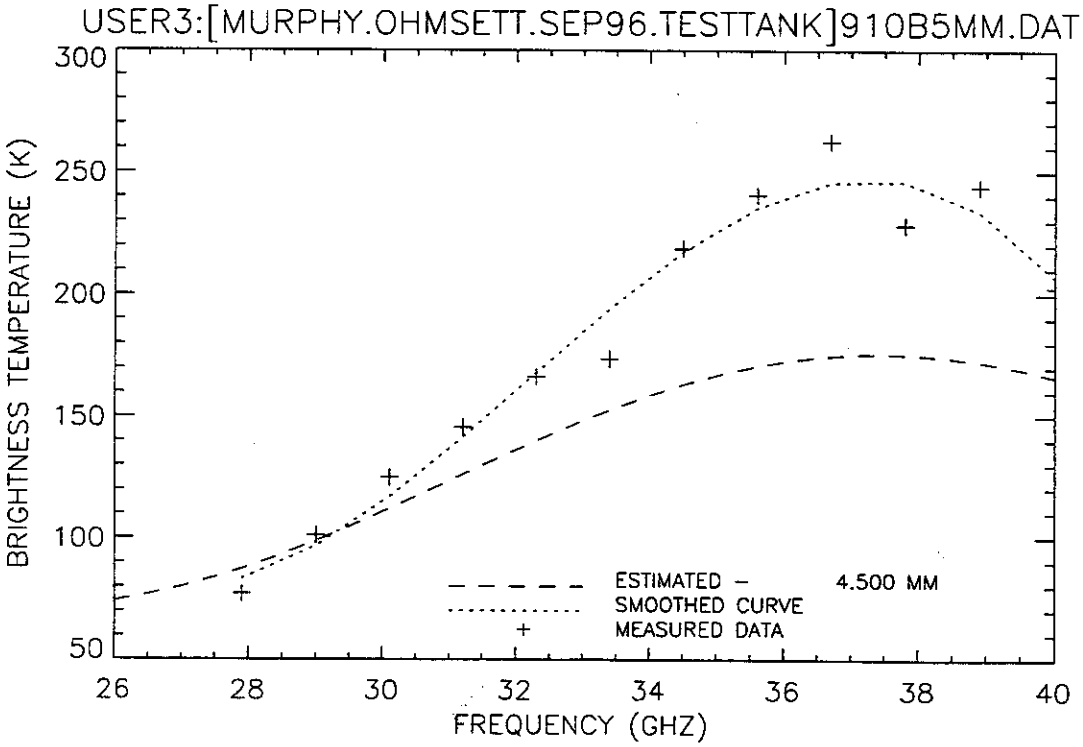

Figure 28. Plot of radiometric brightness temperature versus measurement frequency for 5-mm oil, equipment verification test, 10 September 1996, sweep B.

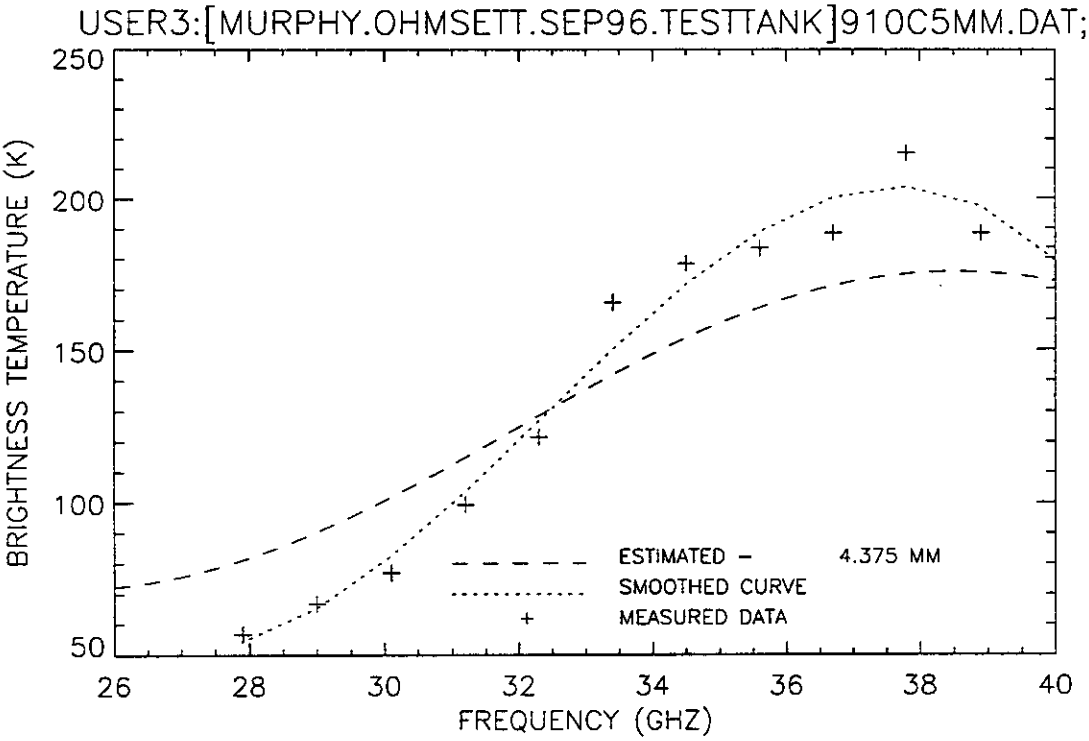

Figure 29. Plot of radiometric brightness temperature versus measurement frequency for 5-mm oil, equipment verification test, 10 September 1996, sweep C.

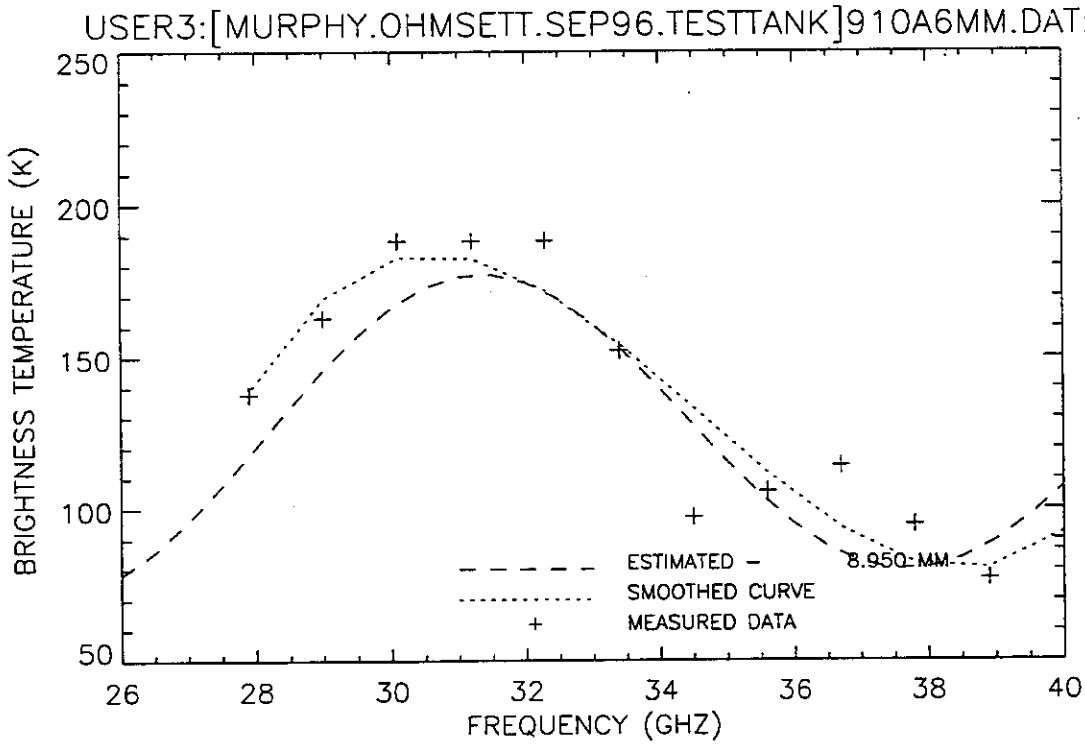

Figure 30. Plot of radiometric brightness temperature versus measurement frequency for 6-mm oil, equipment verification test, 10 September 1996, sweep A.

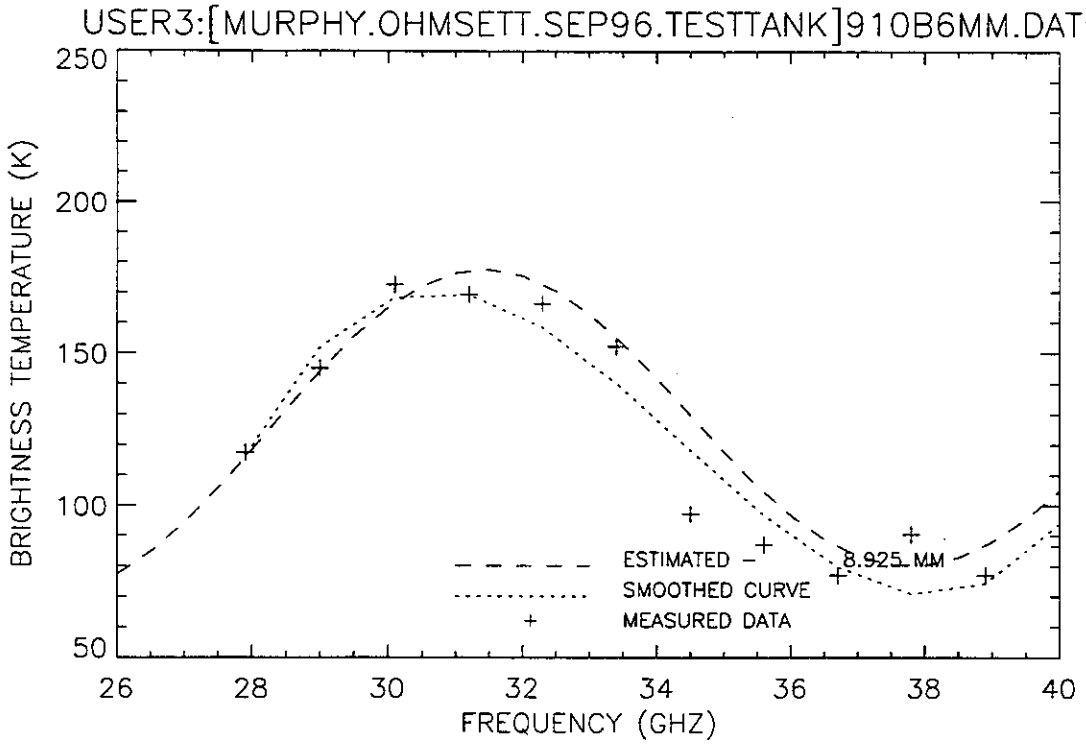

Figure 31. Plot of radiometric brightness temperature versus measurement frequency for 6-mm oil, equipment verification test, 10 September 1996, sweep B.

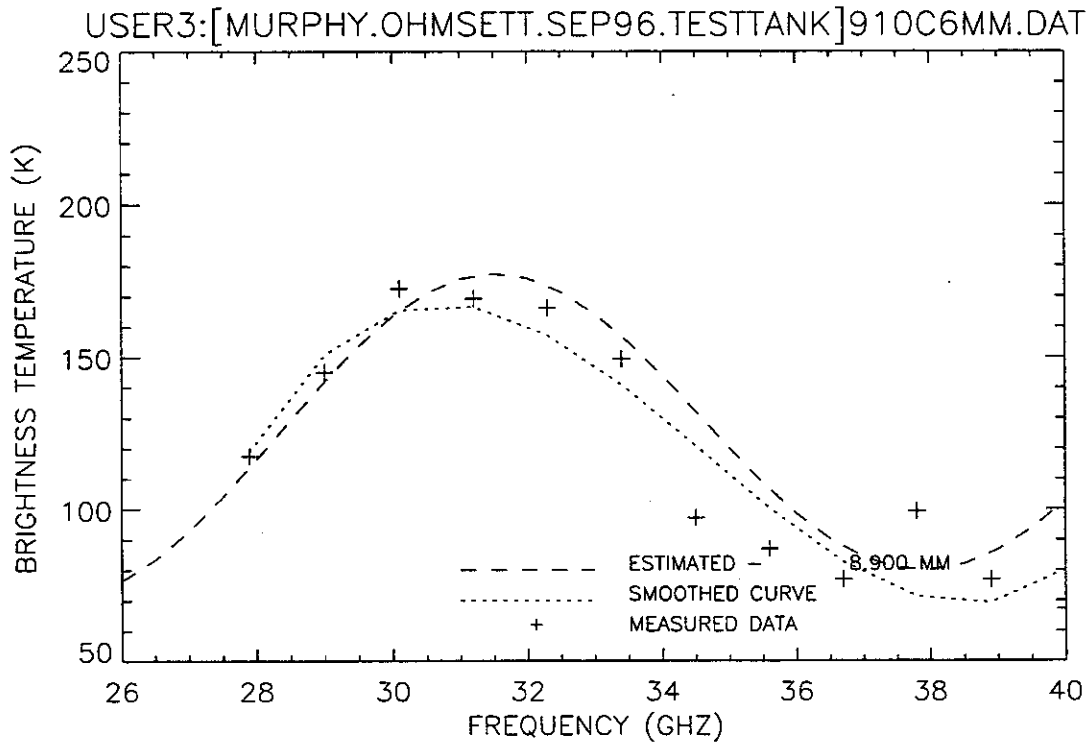

Figure 32. Plot of radiometric brightness temperature versus measurement frequency for 6-mm oil, equipment verification test, 10 September 1996, sweep C.

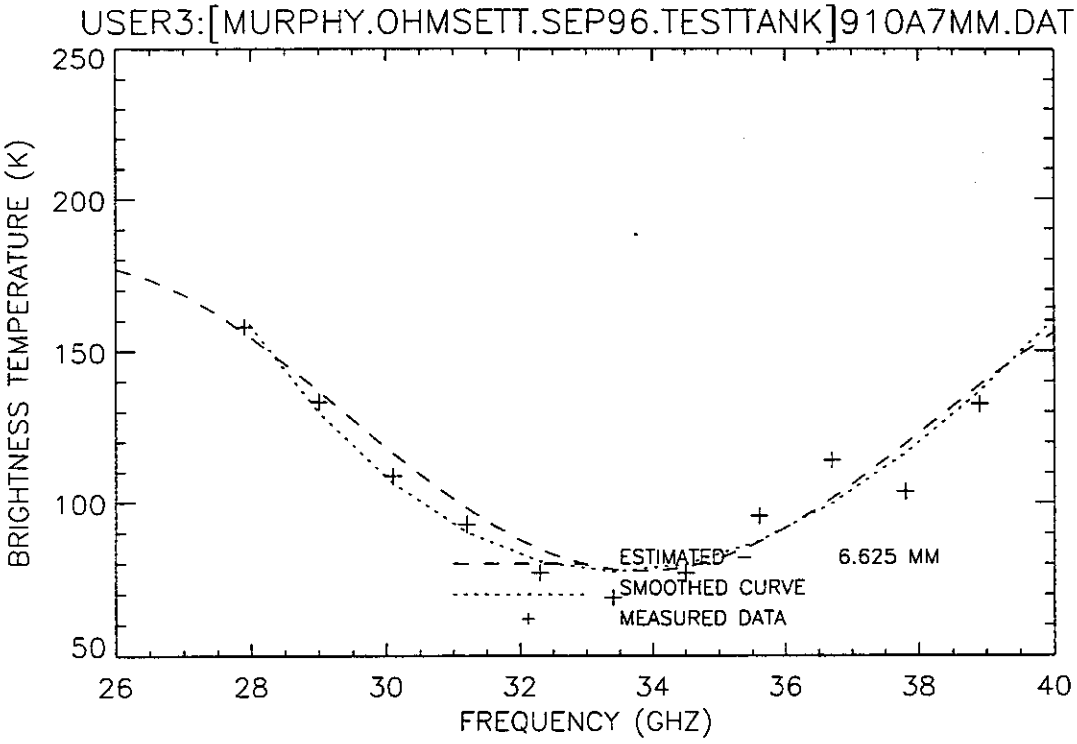

Figure 33. Plot of radiometric brightness temperature versus measurement frequency for 7-mm oil, equipment verification test, 10 September 1996, sweep A.

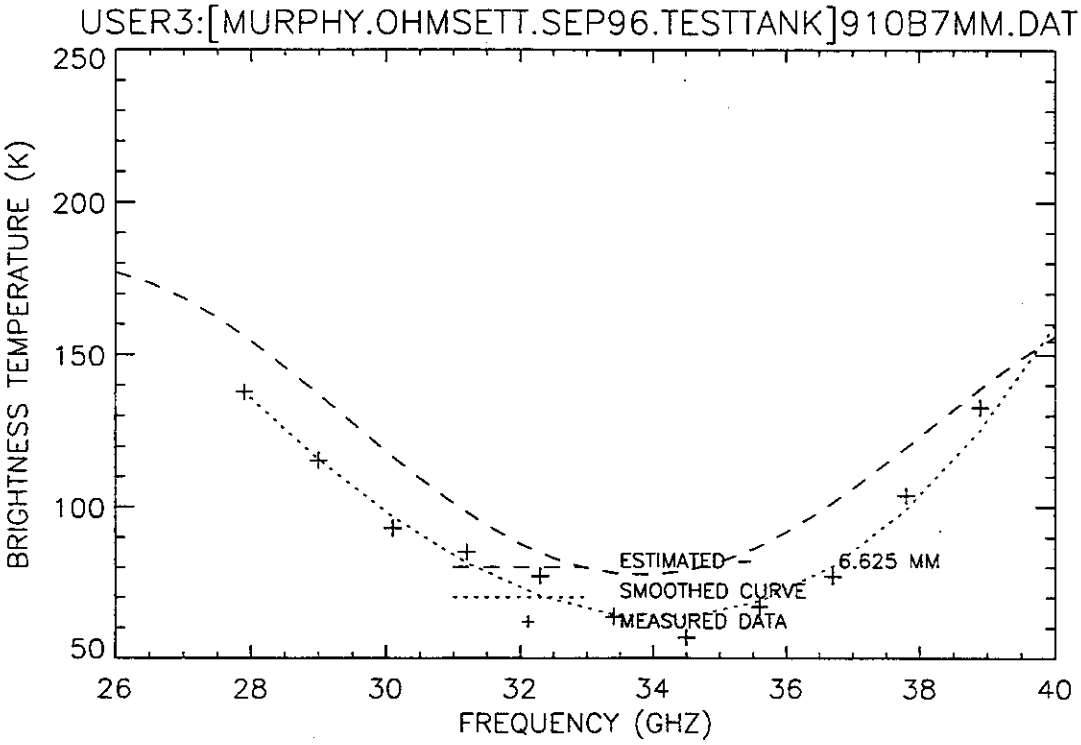

Figure 34. Plot of radiometric brightness temperature versus measurement frequency for 7-mm oil, equipment verification test, 10 September 1996, sweep B.

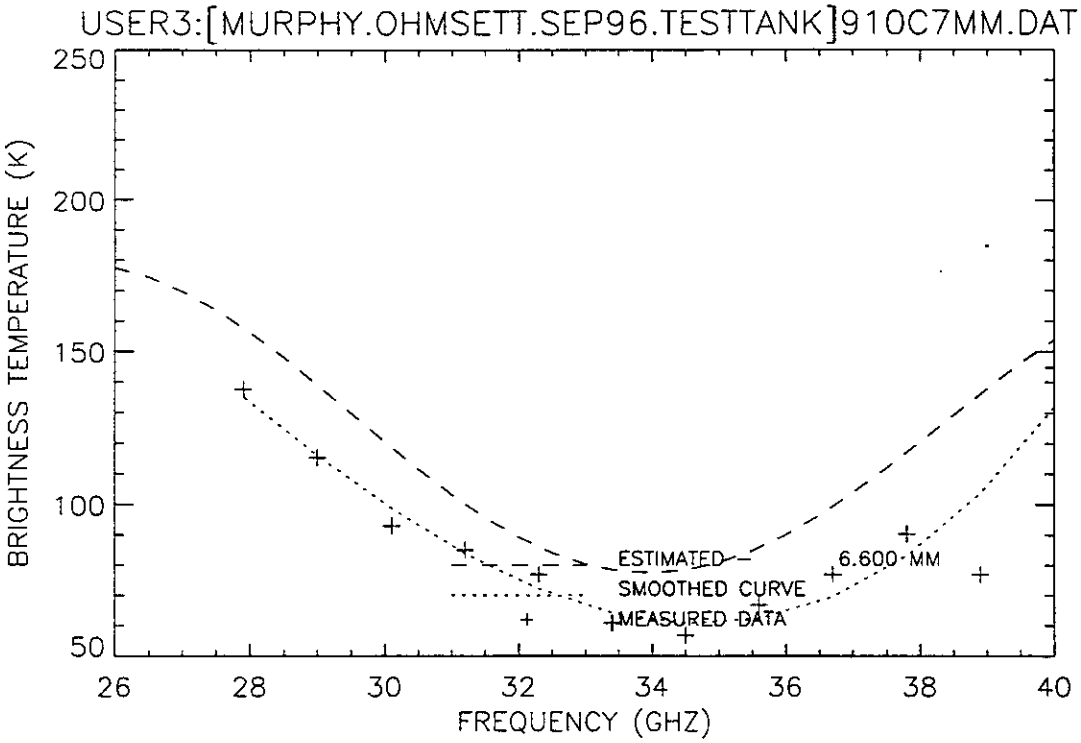

Figure 35. Plot of radiometric brightness temperature versus measurement frequency for 7-mm oil, equipment verification test, 10 September 1996, sweep C.

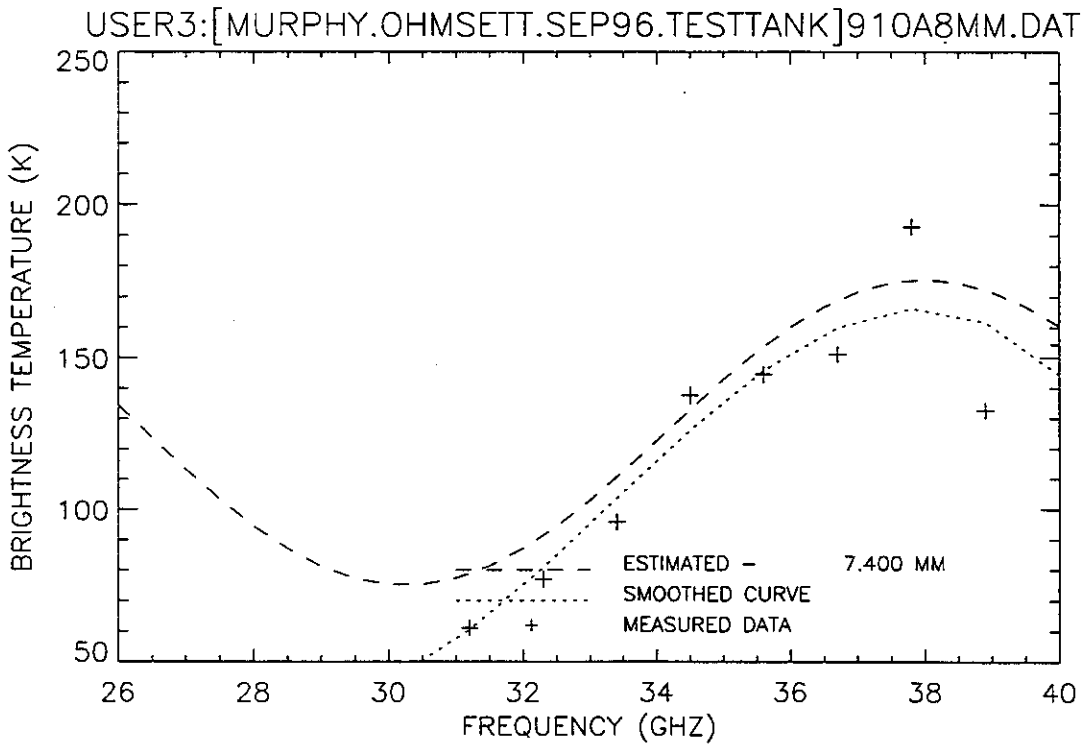

Figure 36. Plot of radiometric brightness temperature versus measurement frequency for 8-mm oil, equipment verification test, 10 September 1996, sweep A.

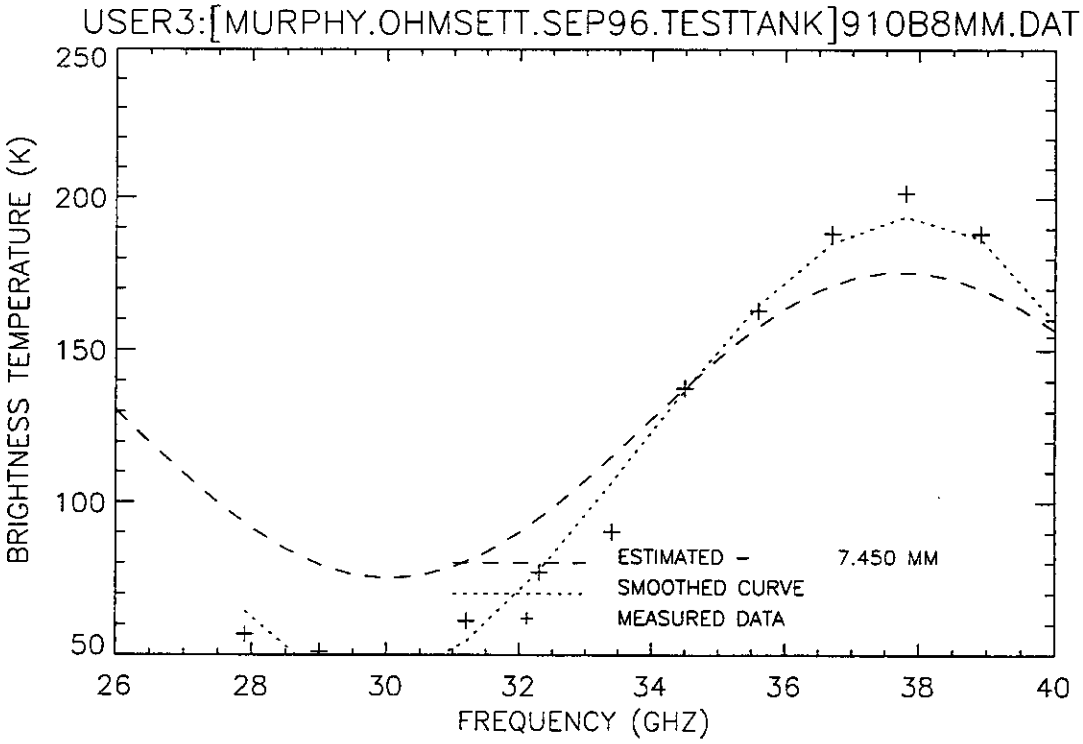

Figure 37. Plot of radiometric brightness temperature versus measurement frequency for 8-mm oil, equipment verification test, 10 September 1996, sweep B.

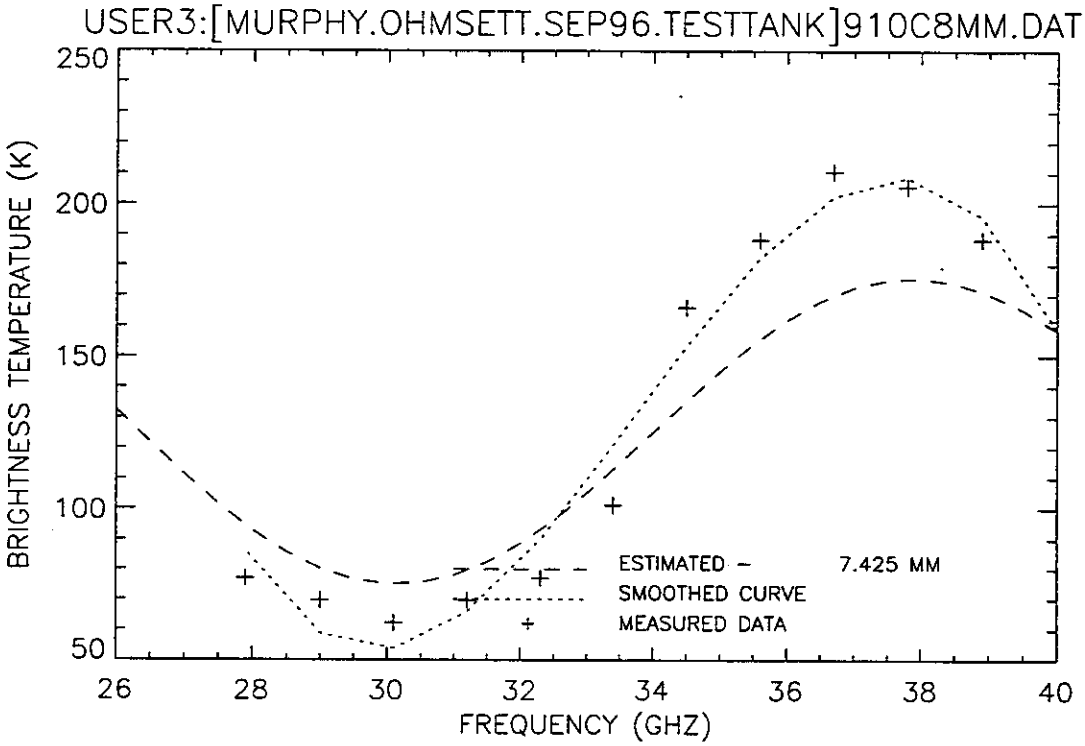

Figure 38. Plot of radiometric brightness temperature versus measurement frequency for 8-mm oil, equipment verification test, 10 September 1996, sweep C.

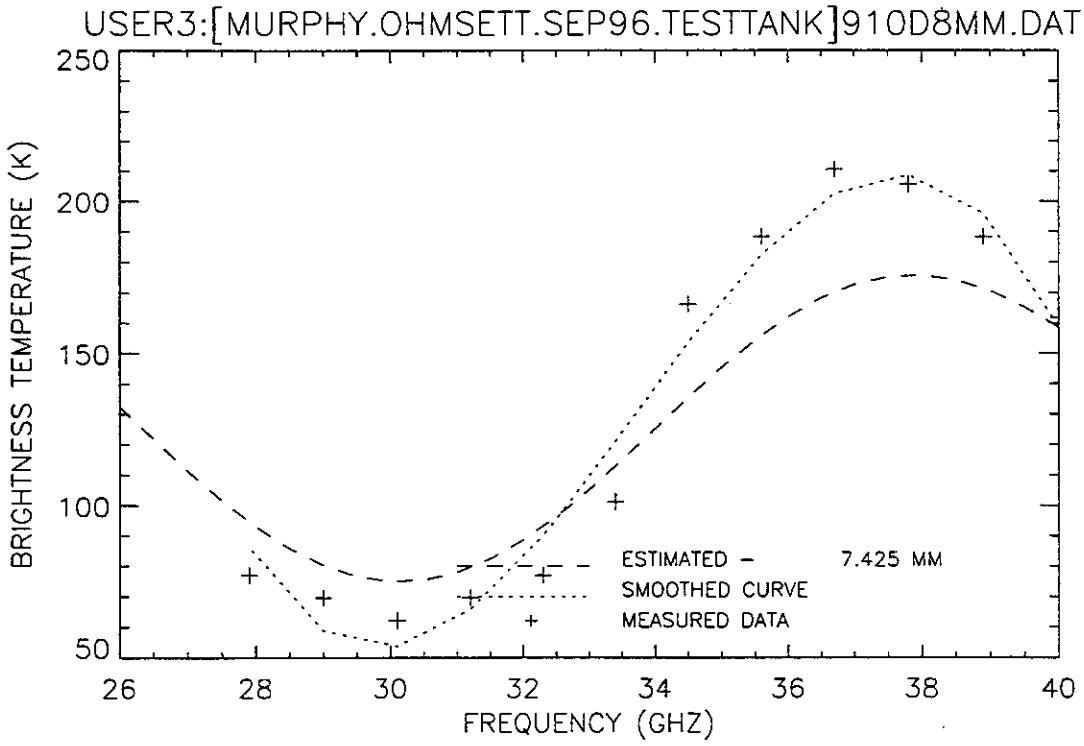

Figure 39. Plot of radiometric brightness temperature versus measurement frequency for 8-mm oil, equipment verification test, 10 September 1996, sweep D.

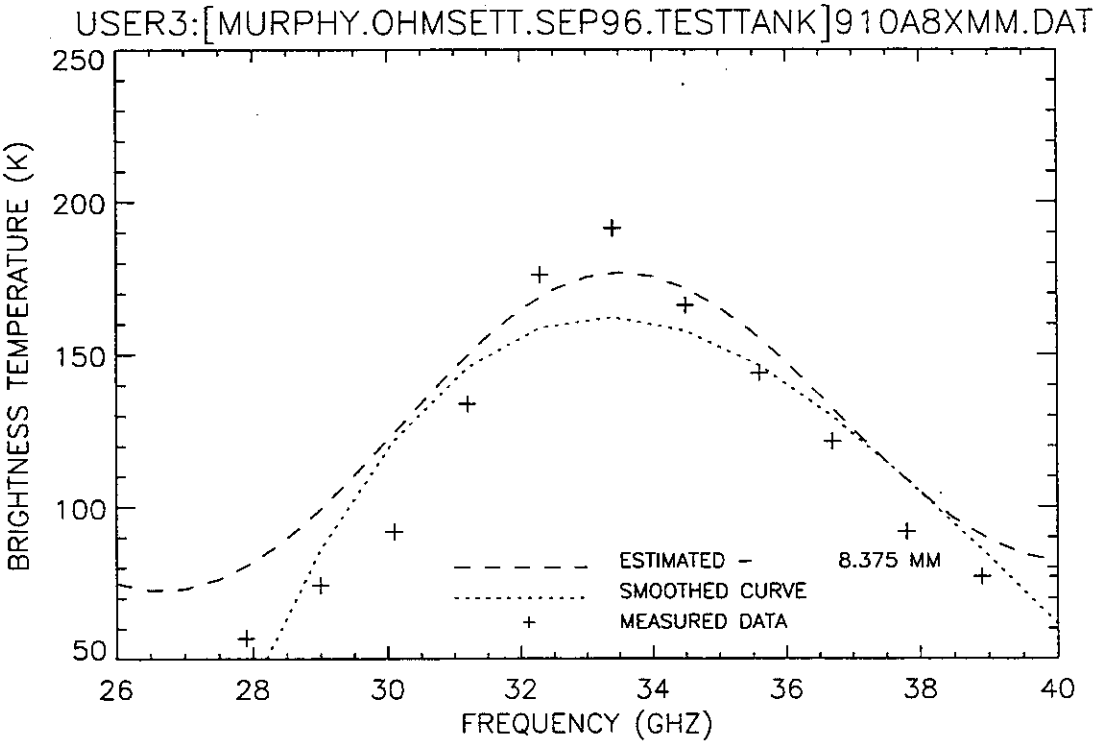

Figure 40. Plot of radiometric brightness temperature versus measurement frequency for 8-plus-mm oil, equipment verification test, 10 September 1996, sweep A.

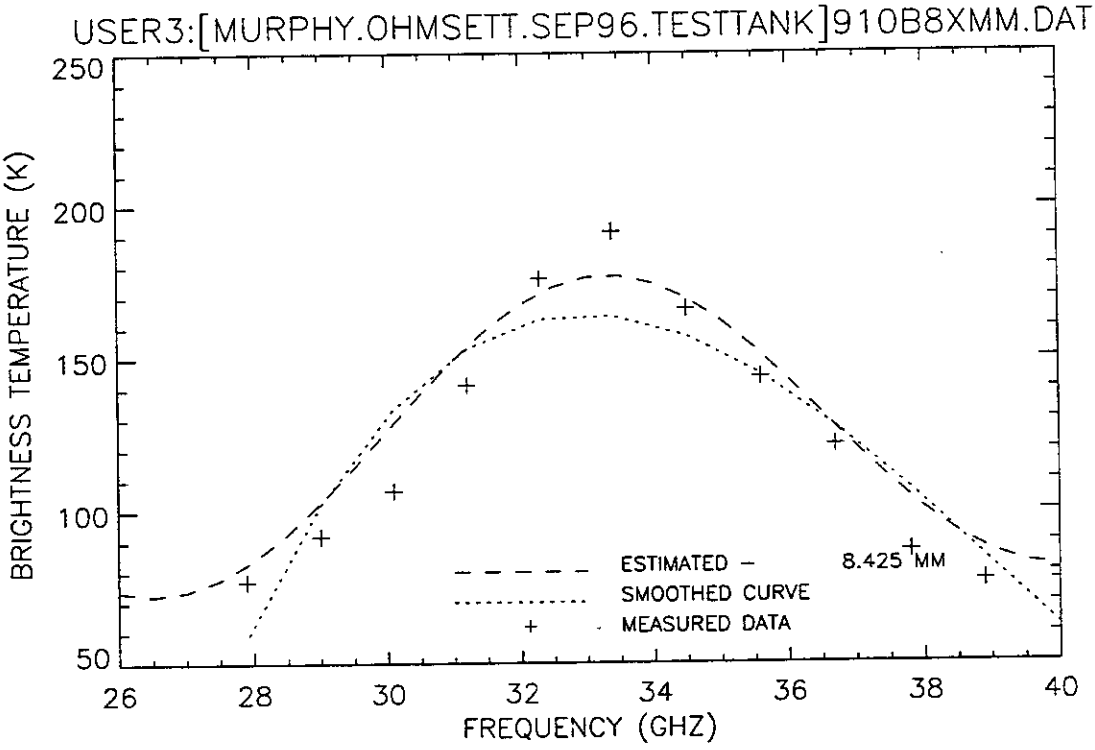

Figure 41. Plot of radiometric brightness temperature versus measurement frequency for 8-plus-mm oil, equipment verification test, 10 September 1996, sweep B.

3. Dry Run

The dry run test was intended to verify the ability of the radiometer and an IR system to collect co-located data and to practice the procedures for the collection of coincident data sets. To provide enough field of view (FOV) for the IR imaging camera to see the entire oil target, the camera was mounted on the high platform approximately 30 ft above the water. For the radiometer to remain out of the IR FOV, it was mounted on a scaffolding approximately 15 ft above the water.

Table 3 summarizes the results of the postcollection data analysis; the shaded blocks indicate algorithm results (LMS, CORR, MN/SL) that are close to or match the analyst's (visual) oil estimate. A comment is provided referring to the fit of the visual (analyst's choice) to the actual data.

The main bridge was moved to one of the southern oil targets to measure the center of the water reference pool. Visibly, this pool had a slight sheen indicating oil on the surface.

D00AWCA.DAT – This measurement, shown in Figure 42, was chosen as the water background reference.

D00BWCA.DAT – The algorithm result of 0.000 mm, shown in Figure 43, is a fair-to-good match to the measured data.

D00CWCA.DAT – The algorithm result of 0.025 mm, shown in Figure 44, is an excellent match to the measured data. D00DWCA.DAT – The algorithm result of 0.000 mm, shown in Figure 45, is a fair-to-good match to the measured data.

D00EWCA.DAT – The algorithm result of 0.250 mm, shown in Figure 46, is a good match to the measured data.

D00FWCA.DAT – The algorithm result of 0.050 mm, shown in Figure 47, is a good-to-excellent match to the measured data.

The main bridge was moved north to measure the center of a uniform 8.0-mm-thick diesel oil target.

TABLE 3

Results of the 10 September 1996 Dry Run Test

FILENAME	LMS	CORR	MN/SL	DECL	METHOD	VISUAL	COMMENT
D00AWCA.DAT							Reference
D00BWCA.DAT	0.000	1.400	0.000	0.000	LMS & MN/SL	0.000	Fair to good
D00CWCA.DAT	0.050	0.475	0.000	0.025	LMS & MN/SL	0.250	Excellent
D00DWCA.DAT	0.000	1.375	0.000	0.000	LMS & MN/SL	0.000	Fair to good
D00EWCA.DAT	0.275	1.550	0.250	0.250	LMS & MN/SL	0.250	Good
D00FWCA.DAT	0.075	3.725	0.050	0.050	LMS & MN/SL	0.050	Good to excellent
D20ADCA.DAT	2.050	3.100	2.125	2.075	LMS & MN/SL	2.075	Fair (mean)
D20AECA.DAT	2.375	3.125	2.400	2.375	LMS & MN/SL	2.375	Fair (mean)
D20AWFA.DAT	2.950	2.725	3.050	3.000	LMS & MN/SL	3.000	Good
D20BDCA.DAT	1.775	5.475	1.700	1.725	LMS & MN/SL	1.725	Good to excellent
D20BECA.DAT	2.175	2.700	2.200	2.175	LMS & MN/SL	2.175	Fair to good (mean)
D20BWFA.DAT	2.825	2.575	2.675	2.850	LMS & MN/SL	2.850	Good
D20CDCA.DAT	2.025	3.125	2.125	2.075	LMS & MN/SL	2.075	Good (mean)
D20CECA.DAT	2.075	2.775	2.100	2.075	LMS & MN/SL	2.075	Good
D20CWFA.DAT	2.900	5.775	2.975	2.925	LMS & MN/SL	2.925	Fair
D20DDCA.DAT	2.100	2.875	2.150	2.125	LMS & MN/SL	2.125	Fair to good (mean)
D20DECA.DAT	2.125	6.050	2.175	2.150	LMS & MN/SL	2.150	Good
D20DWFA.DAT	0.000	9.050	0.000	0.000	LMS & MN/SL	0.000	Poor - needs recalibration
D20EDCA.DAT	2.225	2.575	2.200	2.200	LMS & MN/SL	2.200	Good to excellent
D20EECA.DAT	2.075	2.925	2.150	2.100	LMS & MN/SL	2.100	Fair (mean)
D20FDCA.DAT	2.200	2.650	2.175	2.175	LMS & MN/SL	2.175	Good
D20FWFA.DAT	0.000	5.050	0.000	0.000	LMS & MN/SL	0.000	Poor - needs recalibration
D20GDCA.DAT	2.400	2.750	2.400	2.400	LMS & MN/SL	2.400	Good
D20GWFA.DAT	0.000	9.025	0.000	0.000	LMS & MN/SL	0.000	Poor - needs recalibration
D20HDCA.DAT	2.725	2.625	2.725	2.725	LMS & MN/SL	2.725	Good
D20HWFA.DAT	0.800	4.200	0.800	0.800	LMS & MN/SL	0.800	Excellent
D20JWFA.DAT	0.675	1.450	0.650	0.650	LMS & MN/SL	0.650	Good to excellent
D20KWFA.DAT	4.175	4.150	0.825	4.150	LMS & CORR	4.150	Good
D20LWFA.DAT	3.625	3.750	0.400	3.675	LMS & CORR	3.675	Good to excellent
D20MWFA.DAT	0.625	4.20	0.625	0.625	LMS & MN/SL	0.625	Good to excellent
D20NWFA.DAT	0.900	1.525	0.925	0.900	LMS & MN/SL	0.900	Fair
D20SDCA.DAT	2.575	2.975	2.575	2.575	LMS & MN/SL	2.575	Fair
D40AMCA.DAT	1.225	4.125	1.250	1.225	LMS & MN/SL	1.225	Fair to good
D40BMCA.DAT	4.525	4.075	1.150	4.075	CORR only	4.075	Good (shape)
D40CMCA.DAT	4.550	4.175	1.175	4.175	CORR only	4.175	Good (shape)
D40DMCA.DAT	1.050	4.100	1.050	1.050	LMS & MN/SL	1.050	Fair
D65ASCA.DAT	1.350	9.725	1.300	1.325	LMS & MN/SL	6.200	Poor (shape)
D65BSCA.DAT	1.825	9.625	1.500	1.825	LMS only	6.200	Poor (shape)
D65CSCA.DAT	1.375	9.725	1.325	1.350	LMS & MN/SL	6.200	Poor (shape)
D65DSCA.DAT	1.450	9.625	1.375	1.400	LMS & MN/SL	6.200	Poor (shape)
D80ADCA.DAT	2.200	9.325	1.100	2.200	LMS only	9.300	Fair (shape)
D80BDCA.DAT	9.125	9.050	0.975	9.075	LMS & CORR	9.075	Fair to good (shape)
D80CDCA.DAT	9.375	9.350	0.950	9.350	LMS & CORR	9.350	Good
D80DDCA.DAT	4.975	1.700	1.050	4.975	LMS only	4.975	Good

D80ADCA.DAT – The algorithm result of 2.200 mm is a poor match to the measured data. The measured data points indicate a much "warmer" background temperature estimate. An estimate of 9.300 mm, shown in Figure 48, is a fair shape match to the smoothed curve.

The operator observed that the measurement system gain had drifted and performed a V_{hot} calibration of the radiometer.

D80BDCA.DAT – The algorithm result of 9.075 mm, shown in Figure 49, is a fair-to-good match to the shape of the measured data plot.

D80CDCA.DAT – The algorithm result of 9.350 mm, shown in Figure 50, is a good match to the measured data.

D80DDCA.DAT – The algorithm result of 4.975 mm, shown in Figure 51, is a good match to the measured data. The measured data points seem a bit noisy. The on-site log indicates that the measurements over the pool vary between 8.5 and 9.5 mm, depending on the wind condition. Perhaps this data set was collected during a heavier gust, resulting in a thinner oil-on-water layer.

The main bridge was moved north to measure the center of a 6.5-mm uniform target of Sundex oil. During the movement of the main bridge, the operator recalibrated the V_{hot} temperature of the radiometer.

D65ASCA.DAT – The algorithm estimate of 1.325 mm is a poor match to the measured data set. An estimate of 6.200 mm, shown in Figure 52, is a good shape match but a poor overall temperature match. It is believed that the recalibration of the V_{hot} may have caused the overall shift in measured temperature.

D65BSCA.DAT – The algorithm estimate of 1.825 mm is a poor match to the measured data set. An estimate of 6.200 mm, shown in Figure 53, is a good shape match but a poor overall temperature match. It is believed that the recalibration of the V_{hot} may have caused the overall shift in measured temperature.

D65CSCA.DAT – The algorithm estimate of 1.325 mm is a poor match to the measured data set. An estimate of 6.200 mm, shown in Figure 54, is a good shape match but a

poor overall temperature match. It is believed that the recalibration of the V_{hot} may have caused the overall shift in measured temperature.

D65DSCA.DAT – The algorithm estimate of 1.400 mm is a poor match to the measured data set. An estimate of 6.200 mm, shown in Figure 55, is a good shape match but a poor overall temperature match. It is believed that the recalibration of the V_{hot} may have caused the overall shift in measured temperature.

The main bridge was moved north to the center of a "waste oil" target that had a nominal thickness of 2 mm. This target had swirly discolorations but overall had the appearance of oil, not the emulsion used during the October 1994 OHMSETT test.

D20AECA.DAT – The algorithm estimate of 2.375 mm, shown in Figure 56, is a fair match to the measured data points based on the mean value of the curve. The measured data set has a somewhat flat appearance similar to that seen for oil with bubbles on the surface or an emulsion with partial beam fill.

D20BECA.DAT – The algorithm estimate of 2.175 mm, shown in Figure 57, is a fair-to-good match to the measured data points based on the mean value of the curve. The measured data set has a somewhat flat appearance similar to that seen for oil with bubbles on the surface or an emulsion with partial beam fill.

D20CECA.DAT – The algorithm estimate of 2.075 mm, shown in Figure 58, is a good match to the measured data. The measured data set does not have as flat a curve as the previous measurements, although the 30- and 34-GHz points seem somewhat noisy.

D20DECA.DAT – The algorithm estimate of 2.150 mm, shown in Figure 59, is a good match to the measured data points.

D20EECA.DAT – The algorithm estimate of 2.100 mm, shown in Figure 60, is a fair match to the measured data points based on the mean value of the curve. The measured data set has a somewhat flat appearance similar to that seen for oil with bubbles on the surface or an emulsion with partial beam fill.

The main bridge was moved north to collect data from the center of a 4.0-mm oil target containing a mix of 50% diesel oil and 50% Sundex oil. The oil coverage appeared to be uniform in the target pool.

D40AMCA.DAT – The algorithm estimate of 1.225 mm is a fair-to-good match to the measured data points based on the mean value and positive slope characteristic of the curve. The correlation-only estimate of 4.125 mm, shown in Figure 61, matches the shape of the curve better but has a constant offset. The gain of the instrument may have drifted.

D40BMCA.DAT – The algorithm estimate of 4.075 mm, shown in Figure 62, is a good match to the measured data points based on the shape of the curve.

D40CMCA.DAT – The algorithm estimate of 4.175 mm, shown in Figure 63, is a good match to the measured data points based on the shape of the curve.

D40DMCA.DAT – The algorithm estimate of 1.050 mm, shown in Figure 64, is a fair match to the measured data points based on the mean value and positive slope characteristic of the curve. The correlation-only estimate of 4.100 mm might be the correct estimate; however, the curve shape does not have as good a match as seen in the previous examples.

The main bridge was moved north to the center of a 2-mm thick uniform diesel oil target. Based on the appearance (tint) of the dyed oil, thicker oil was present on the east side of the target and a thinner layer on the west.

D20ADCA.DAT – The algorithm estimate of 2.075 mm, shown in Figure 65, is a fair match to the measured data points based on the mean value of the curve. The measured data set has a somewhat flat appearance similar to that seen for oil with bubbles on the surface or an emulsion with partial beam fill.

D20BDCA.DAT – The algorithm estimate of 1.725 mm, shown in Figure 66, is a good-to-excellent match to the measured data points.

D20CDCA.DAT – The algorithm estimate of 2.075 mm, shown in Figure 67, is a good match to the measured data points based on the mean value of the curve. The measured data has a somewhat flat appearance similar to that seen for oil with bubbles on the surface or an emulsion with partial beam fill.

D20DDCA.DAT – The algorithm estimate of 2.125 mm, shown in Figure 68, is a fair-to-good match to the measured data points based on the mean value of the curve. The

measured data set has a somewhat flat appearance similar to that seen for oil with bubbles on the surface or an emulsion with partial beam fill.

The position of the radiometer was shifted so that measurements could be taken from the east side of the oil target pool.

D20EDCA.DAT – The algorithm estimate of 2.200 mm, shown in Figure 69, is a good-to-excellent match to the measured data points.

D20FDCA.DAT – The algorithm estimate of 2.175 mm, shown in Figure 70, is a good match to the measured data points.

D20GDCA.DAT – The algorithm estimate of 2.400 mm, shown in Figure 71, is a good match to the measured data points.

D20HDCA.DAT – The algorithm estimate of 2.725 mm, shown in Figure 72, is a good match to the measured data points.

The main bridge remained over the 2-mm diesel oil target with the radiometer shifted to measure the east side of the target pool. The next series of measurements were collected using the fans mounted on the south side of the main bridge to move the oil from the apparent thicker east side to the west side of the target pool. This first set of measurements was collected with the fans off from the same pool position as the D20EDCA.DAT to D20HDCA.DAT series.

D20AWCA.DAT – The algorithm estimate of 3.000 mm, shown in Figure 73, is a good match to the measured data points.

D20BWCA.DAT – The algorithm estimate of 2.850 mm, shown in Figure 74, is a good match to the measured data points.

D20CWCA.DAT – The algorithm estimate of 2.925 mm, shown in Figure 75, is a fair match to the measured data points.

The fans were turned on. The wind created by the fans pushed the oil to the west side of the target pool. The radiometer remained in the same position, measuring the east side of the pool that now contained only a slight sheen.

D20DWCA.DAT – The algorithm estimate of 0.000 mm, shown in Figure 76, is a poor match to the measured data points; however, if the background water temperature was adjusted so that a lower temperature could be used, then a good curve match could be found.

D20FWCA.DAT – The algorithm estimate of 0.000 mm, shown in Figure 77, is a poor match to the measured data points; however, if the background water temperature was adjusted so that a lower temperature could be used, then a good curve match could be found.

D20GWCA.DAT – The algorithm estimate of 0.000 mm, shown in Figure 78, is a poor match to the measured data points; however, if the background water temperature was adjusted so that a lower temperature could be used, then a good curve match could be found.

The radiometer was repositioned to collect measurements from the "edge" formed by the oil/water interface. This edge was somewhat west of the center of the target pool but moved east/west based on the aggregate wind speed and direction formed by the fans and the actual wind. The radiometer measurement position remained fixed during this set of measurements.

D20HWCA.DAT – The algorithm estimate of 0.800 mm, shown in Figure 79, is an excellent match to the measured data points.

D20JWCA.DAT – The algorithm estimate of 0.650 mm, shown in Figure 80, is a good-to-excellent match to the measured data points.

D20KWCA.DAT – The algorithm estimate of 4.150 mm, shown in Figure 81, is a good match to the measured data points.

D20LWCA.DAT – The algorithm estimate of 3.675 mm, shown in Figure 82, is a good-to-excellent match to the measured data points.

D20MWCA.DAT – The algorithm estimate of 0.625 mm, shown in Figure 83, is a good-to-excellent match to the measured data points.

D20NWCA.DAT – The algorithm estimate of 0.900 mm, shown in Figure 84, is a fair match to the measured data points based on the mean value. The data points exhibit a somewhat flat response over the measurement band similar to measurements with bubbles in the oil surface or a partial beam fill of emulsion.

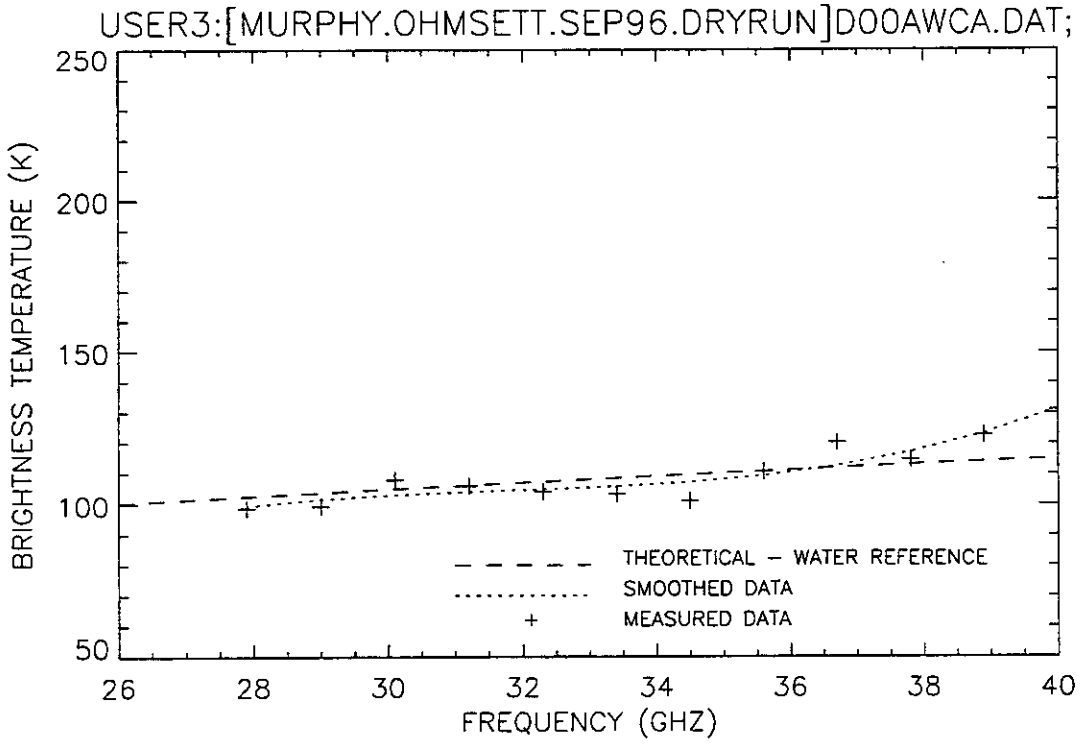

Figure 42. Plot of radiometric brightness temperature versus measurement frequency for water, dry run test, calm wave conditions, 10 September 1996, sweep A.

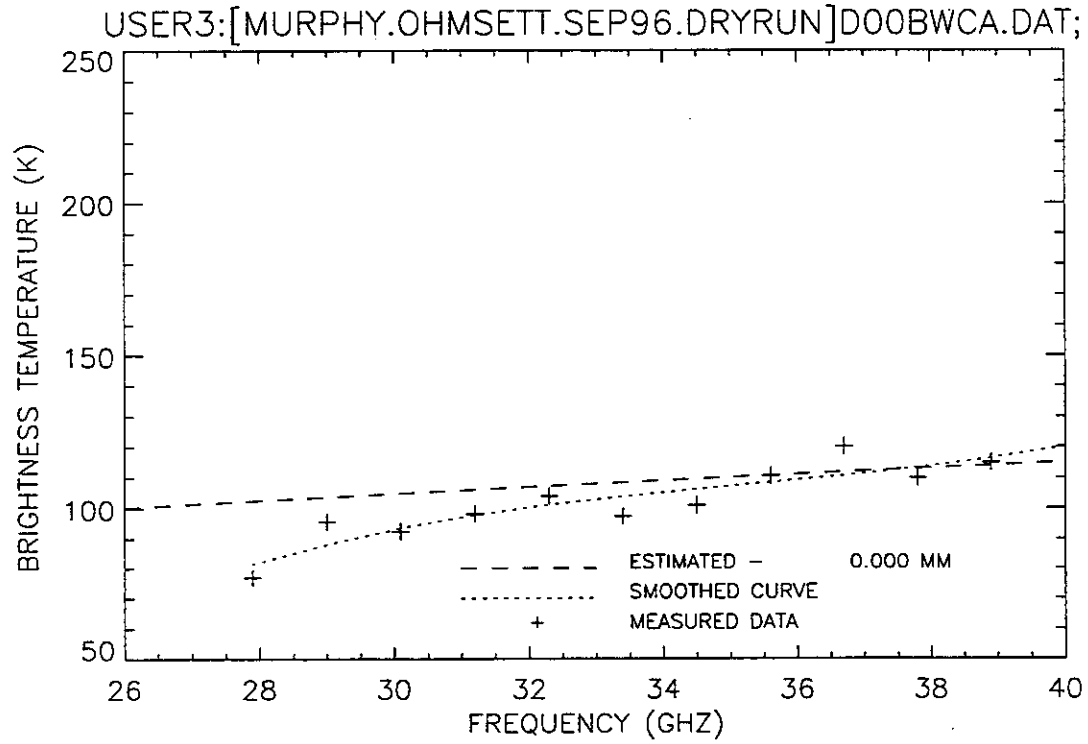

Figure 43. Plot of radiometric brightness temperature versus measurement frequency for water, dry run test, calm wave conditions, 10 September 1996, sweep B.

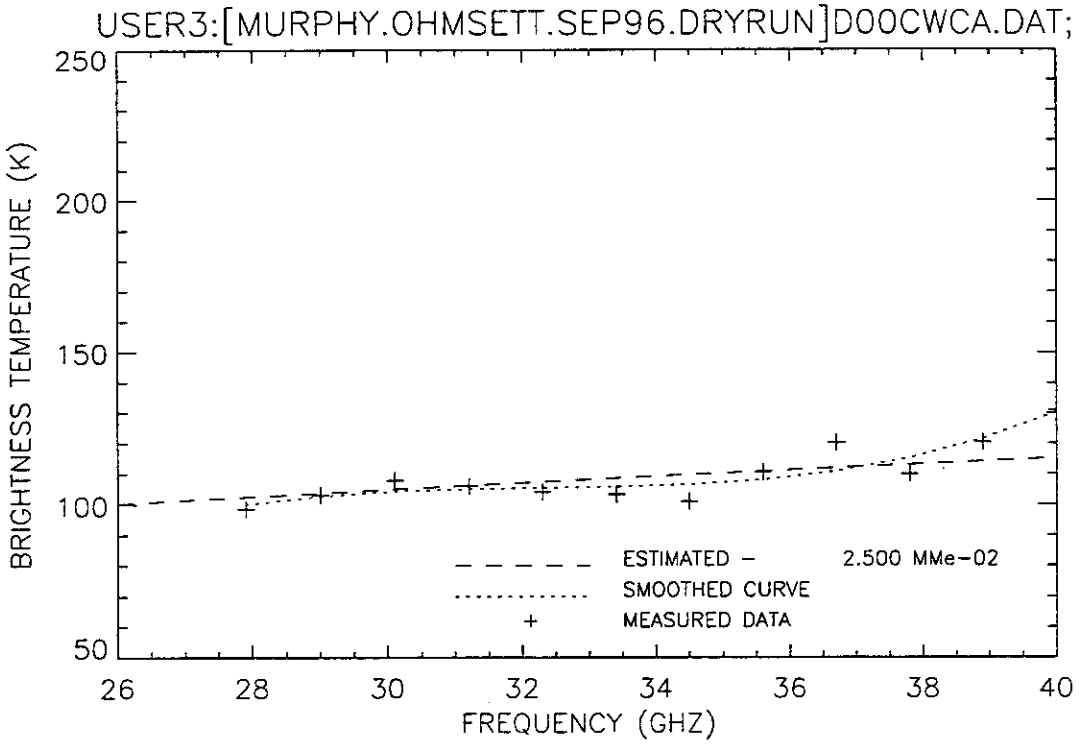

Figure 44. Plot of radiometric brightness temperature versus measurement frequency for water, dry run test, calm wave conditions, 10 September 1996, sweep C.

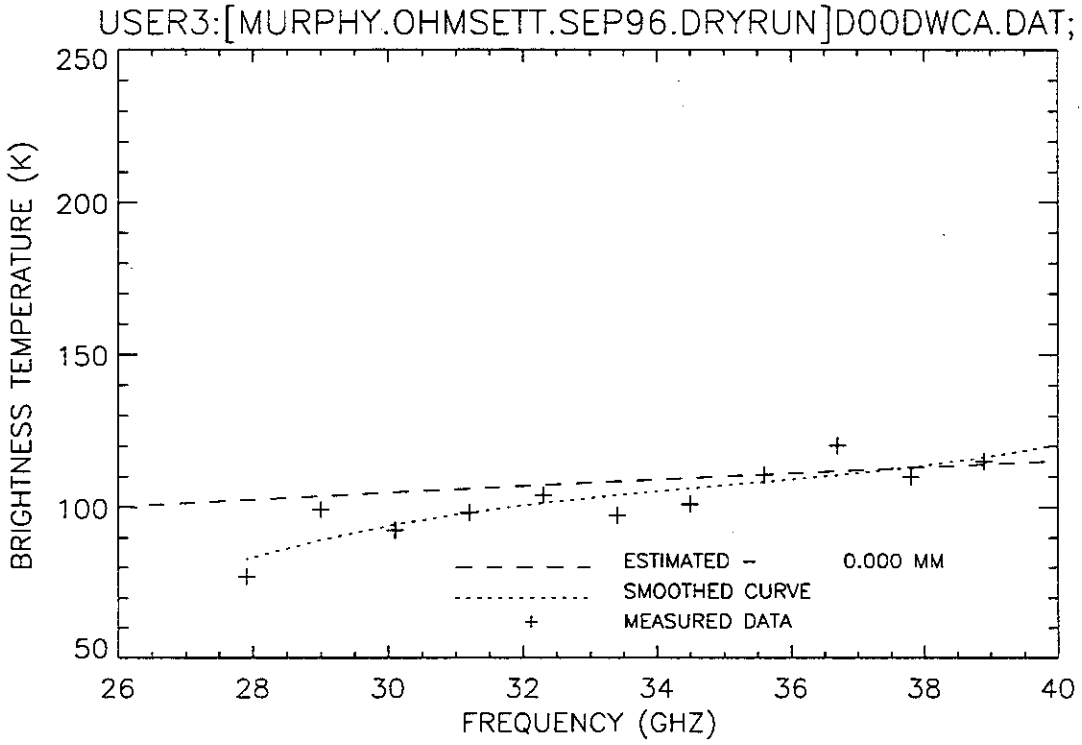

Figure 45. Plot of radiometric brightness temperature versus measurement frequency for water, dry run test, calm wave conditions, 10 September 1996, sweep D.

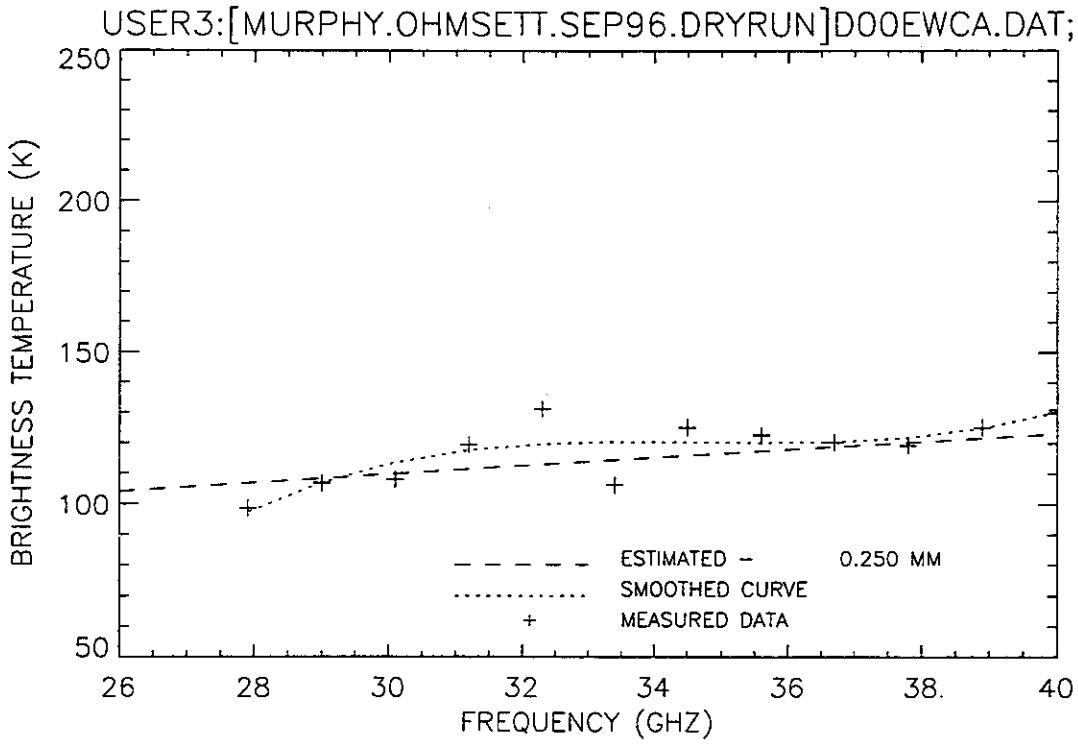

Figure 46. Plot of radiometric brightness temperature versus measurement frequency for water, dry run test, calm wave conditions, 10 September 1996, sweep E.

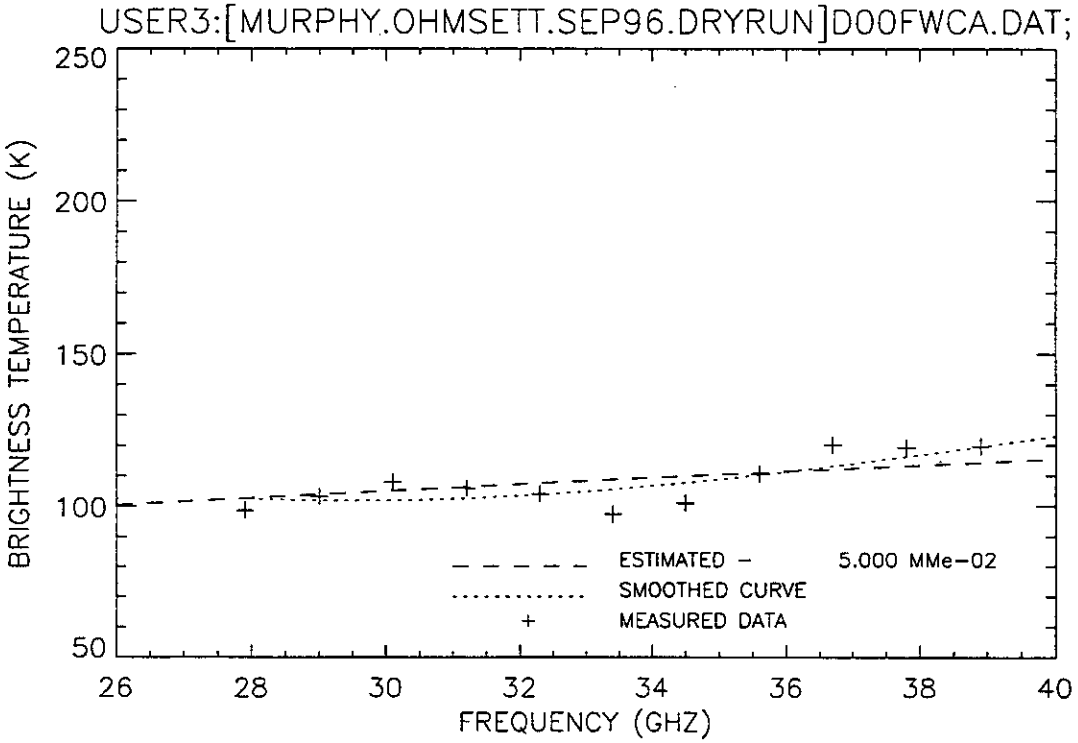

Figure 47. Plot of radiometric brightness temperature versus measurement frequency for water, dry run test, calm wave conditions, 10 September 1996, sweep F.

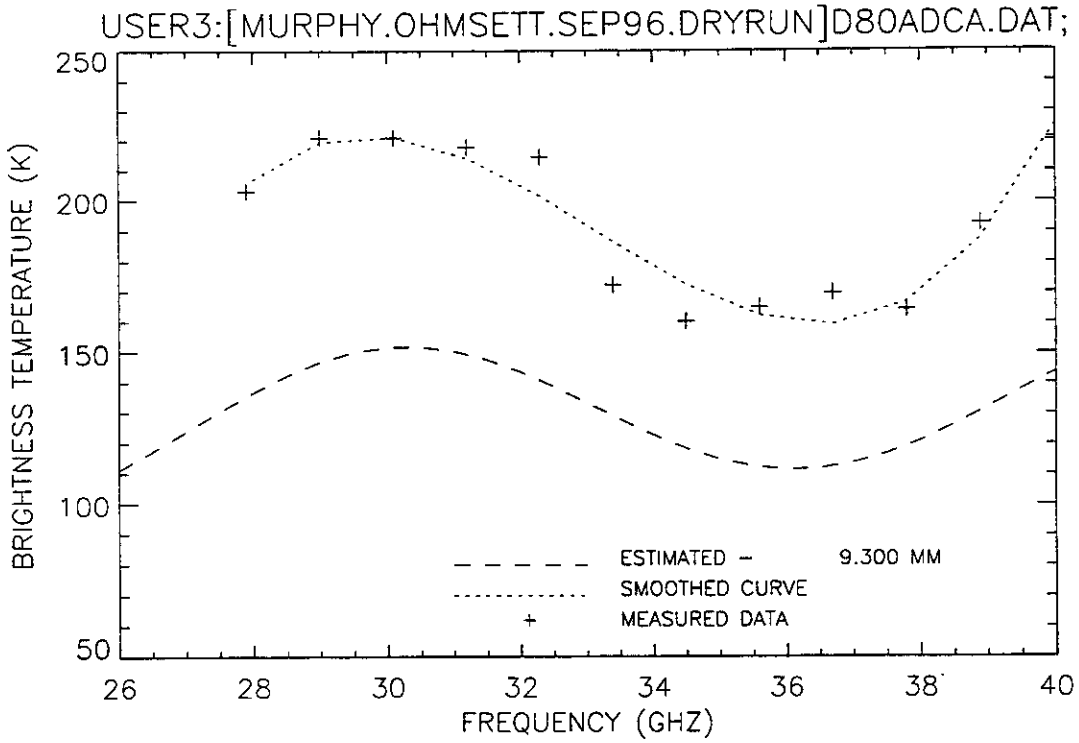

Figure 48. Plot of radiometric brightness temperature versus measurement frequency for 8-mm diesel oil, dry run test, calm wave conditions, 10 September 1996, sweep A.

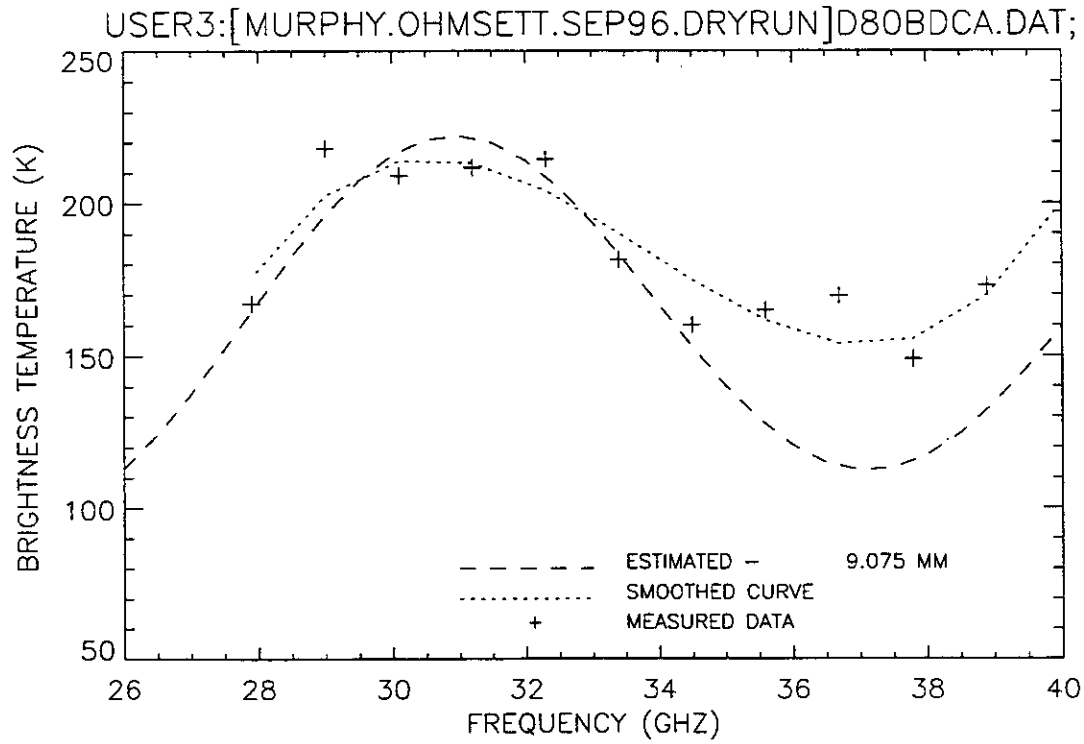

Figure 49. Plot of radiometric brightness temperature versus measurement frequency for 8-mm diesel oil, dry run test, calm wave conditions, 10 September 1996, sweep B.

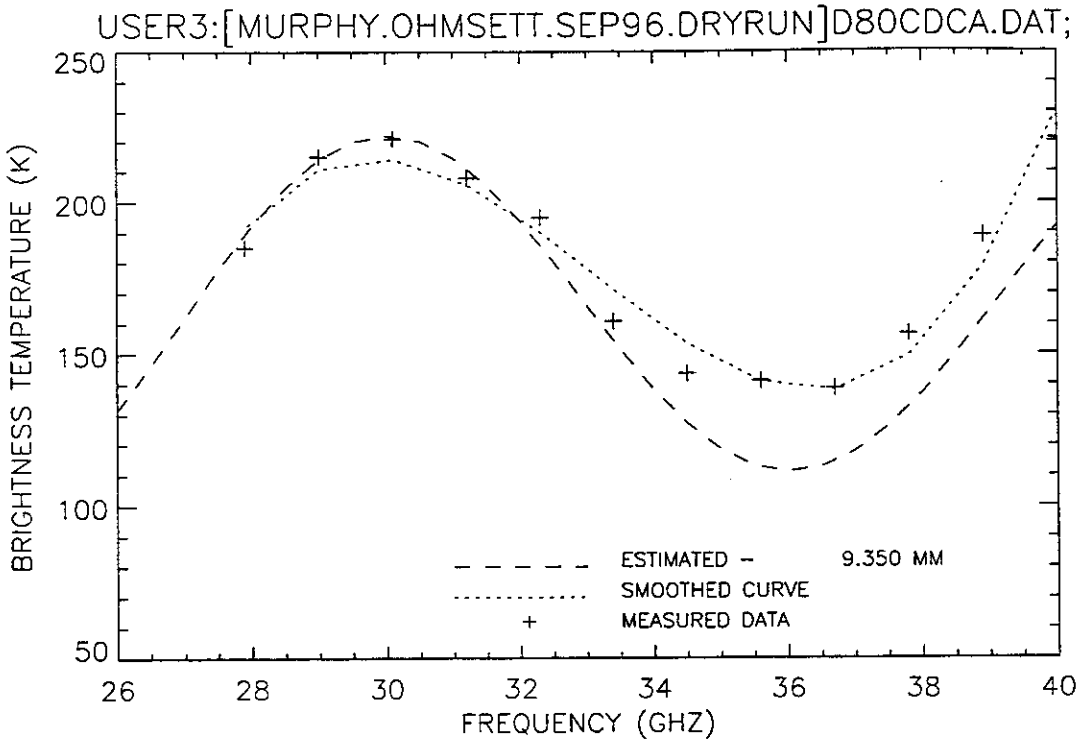

Figure 50. Plot of radiometric brightness temperature versus measurement frequency for 8-mm diesel oil, dry run test, calm wave conditions, 10 September 1996, sweep C.

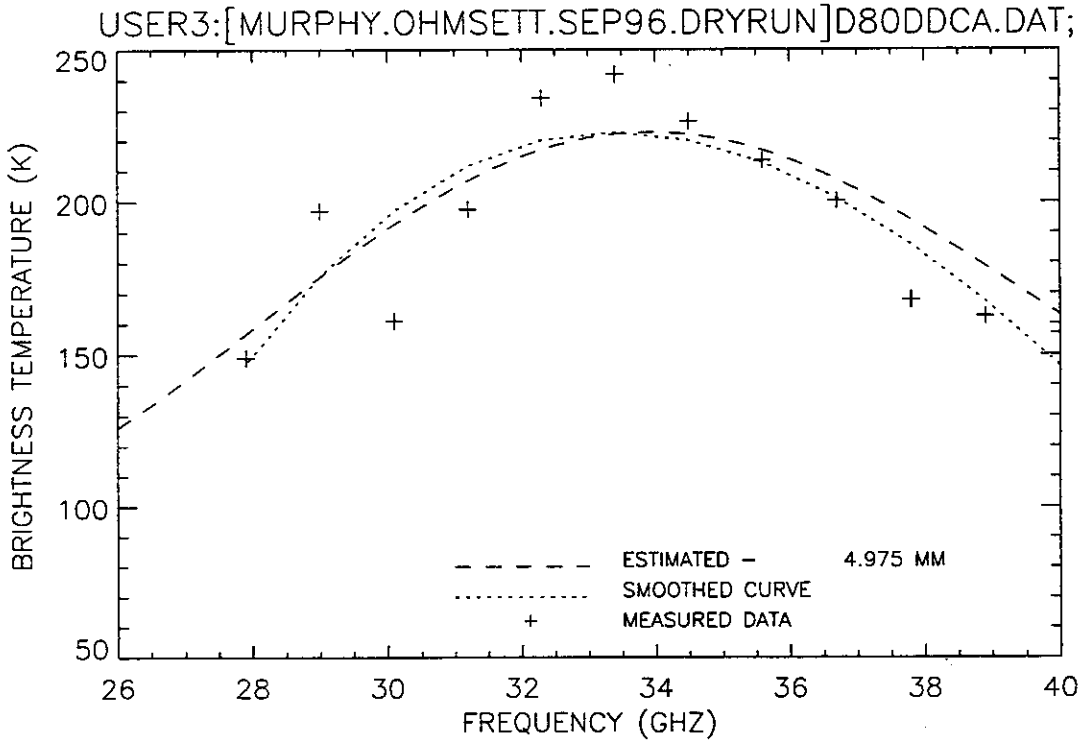

Figure 51. Plot of radiometric brightness temperature versus measurement frequency for 8-mm diesel oil, dry run test, calm wave conditions, 10 September 1996, sweep D.

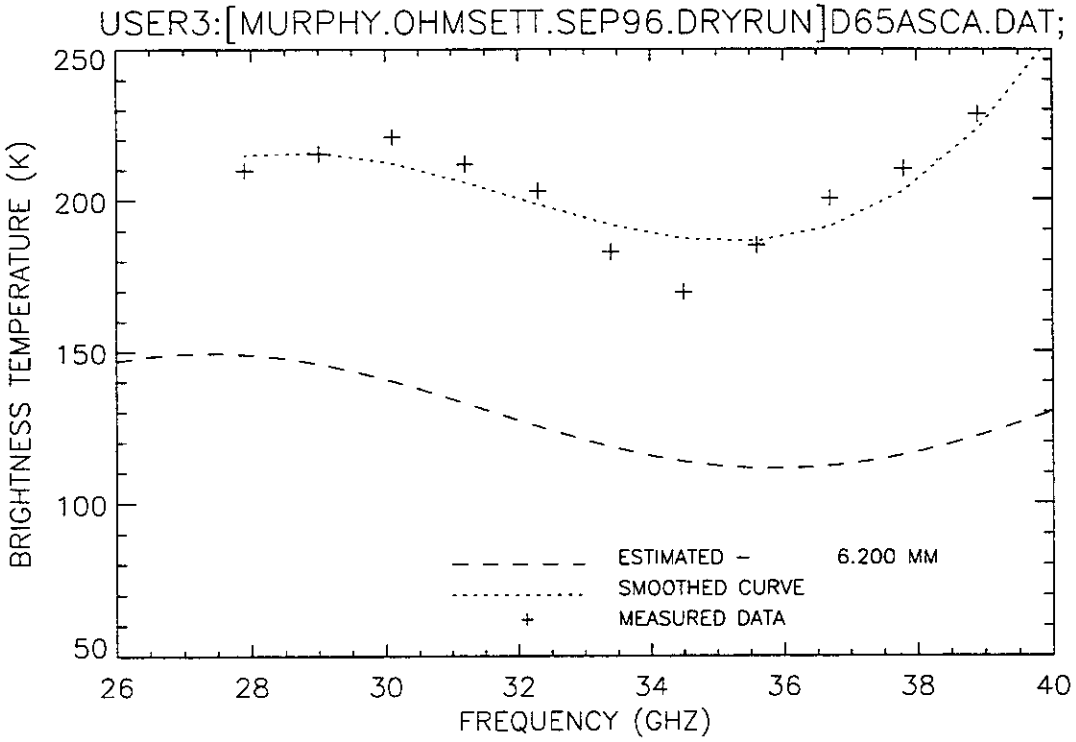

Figure 52. Plot of radiometric brightness temperature versus measurement frequency for 6.5-mm Sundex oil, dry run test, calm wave conditions, 10 September 1996, sweep A.

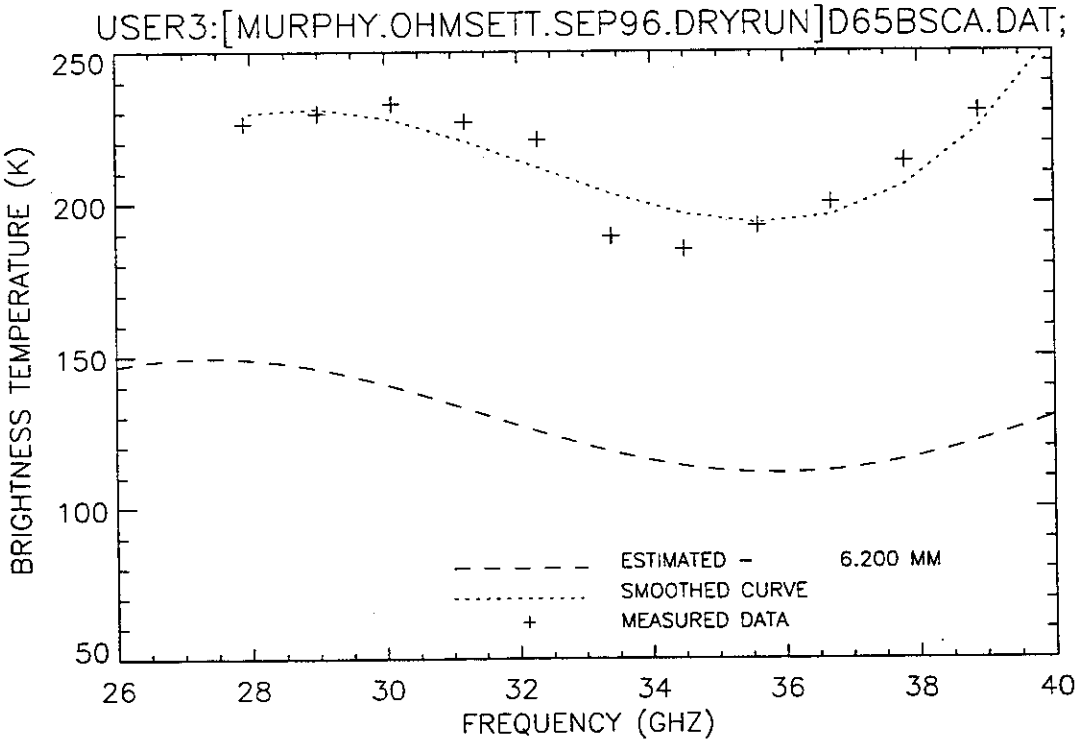

Figure 53. Plot of radiometric brightness temperature versus measurement frequency for 6.5-mm Sundex oil, dry run test, calm wave conditions, 10 September 1996, sweep B.

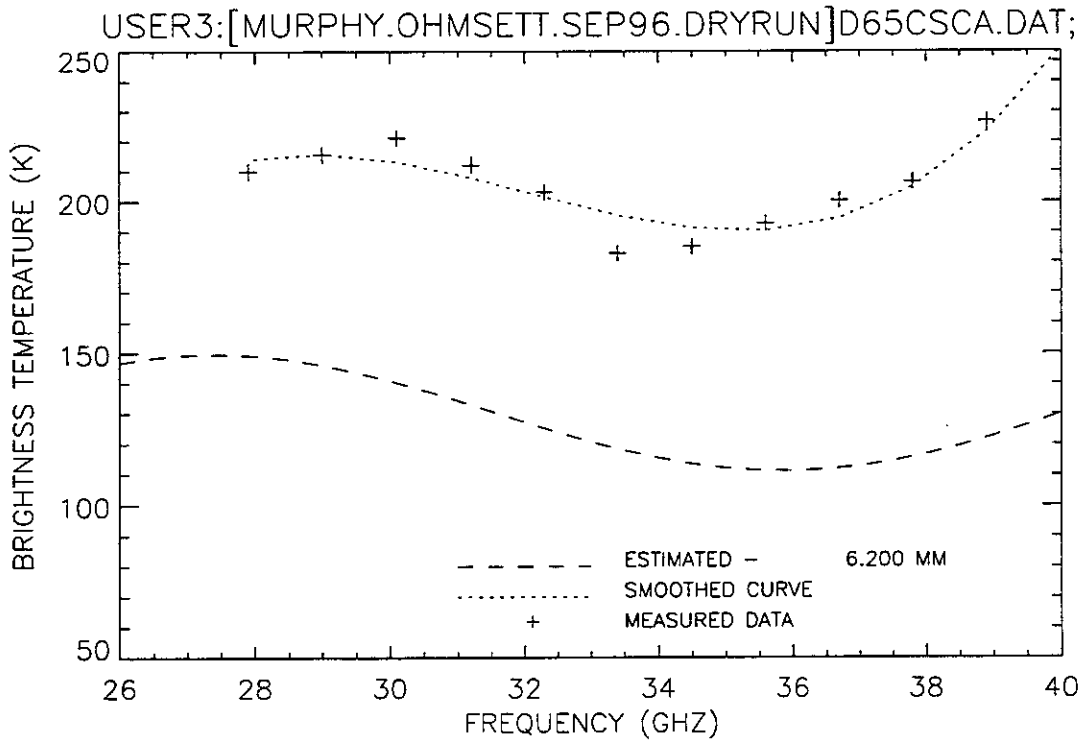

Figure 54. Plot of radiometric brightness temperature versus measurement frequency for 6.5-mm Sundex oil, dry run test, calm wave conditions, 10 September 1996, sweep C.

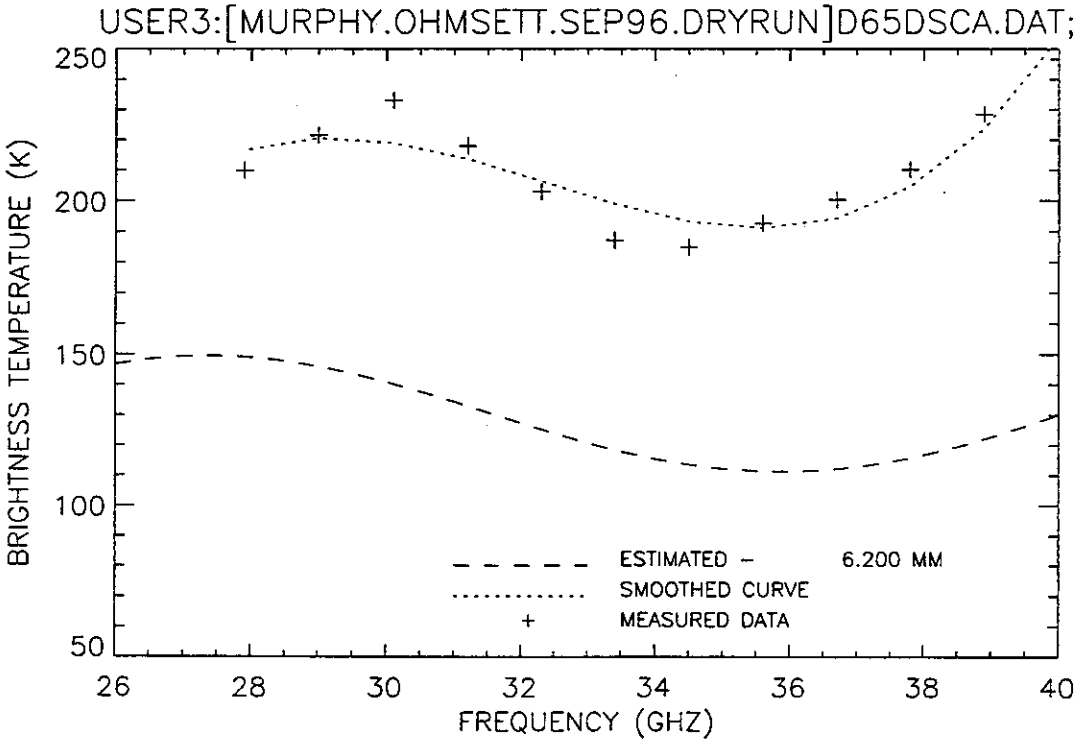

Figure 55. Plot of radiometric brightness temperature versus measurement frequency for 6.5-mm Sundex oil, dry run test, calm wave conditions, 10 September 1996, sweep D.

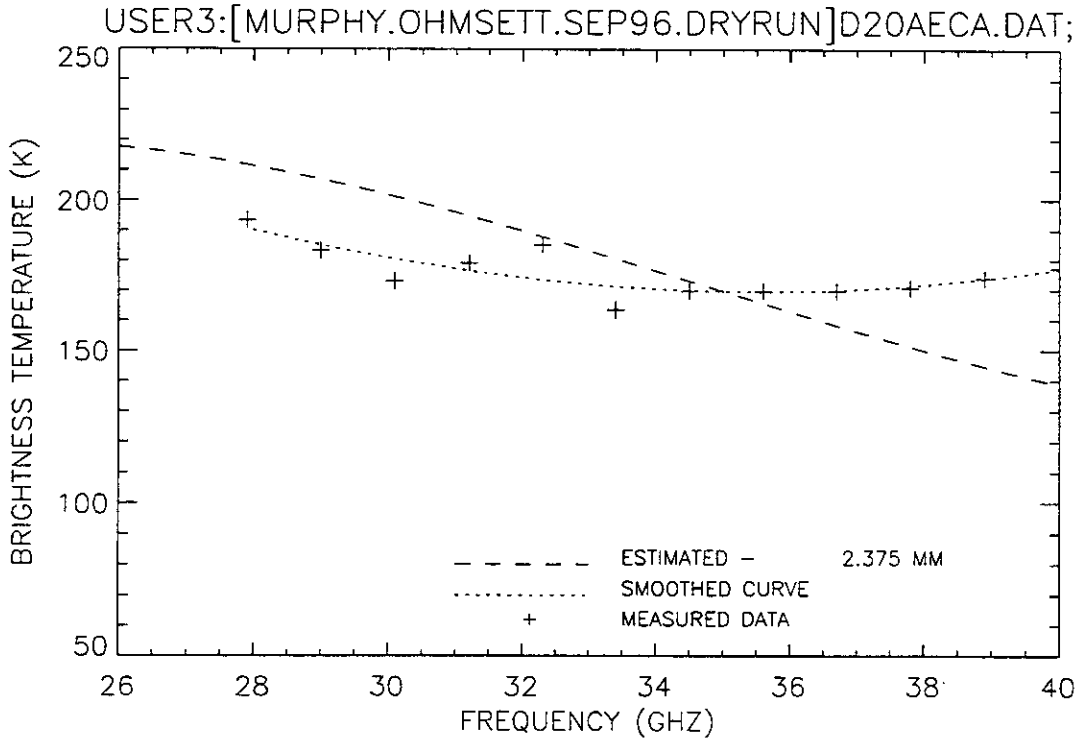

Figure 56. Plot of radiometric brightness temperature versus measurement frequency for 2-mm waste oil, dry run test, calm wave conditions, 10 September 1996, sweep A.

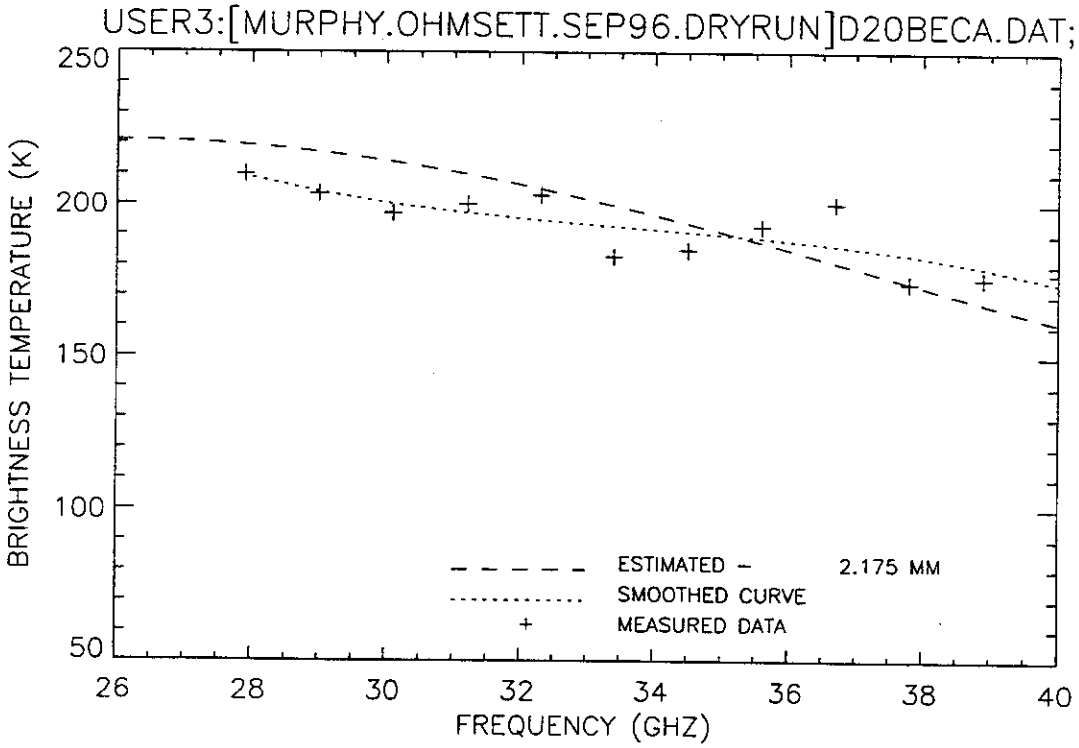

Figure 57. Plot of radiometric brightness temperature versus measurement frequency for 2-mm waste oil, dry run test, calm wave conditions, 10 September 1996, sweep B.

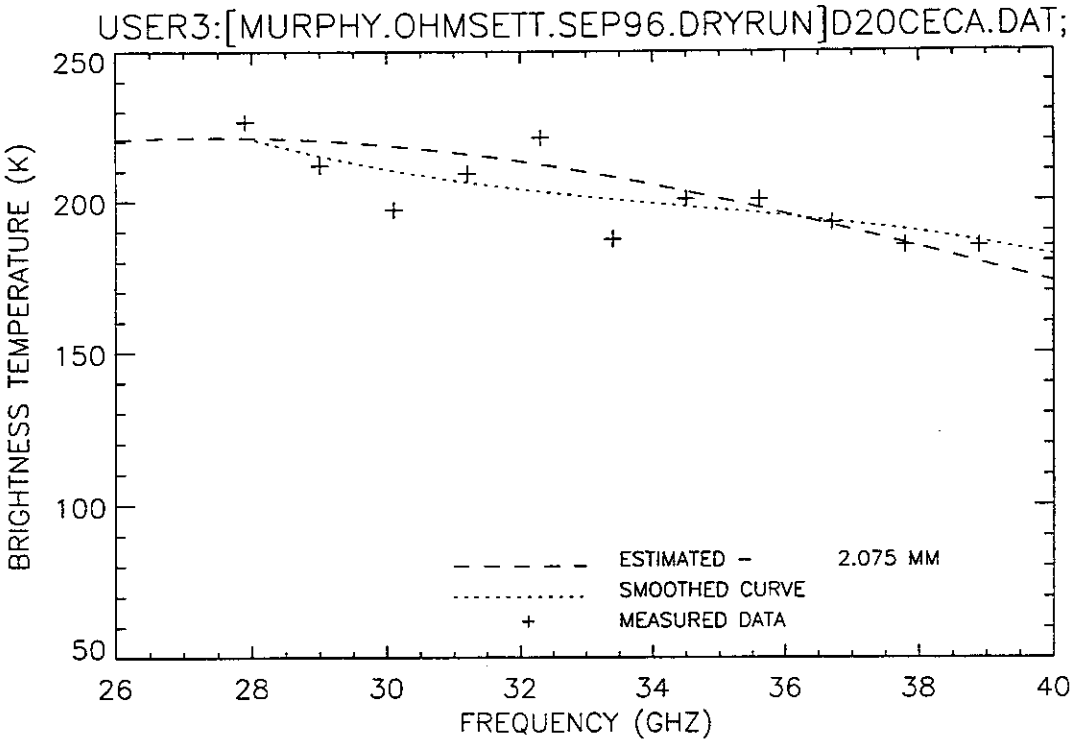

Figure 58. Plot of radiometric brightness temperature versus measurement frequency for 2-mm waste oil, dry run test, calm wave conditions, 10 September 1996, sweep C.

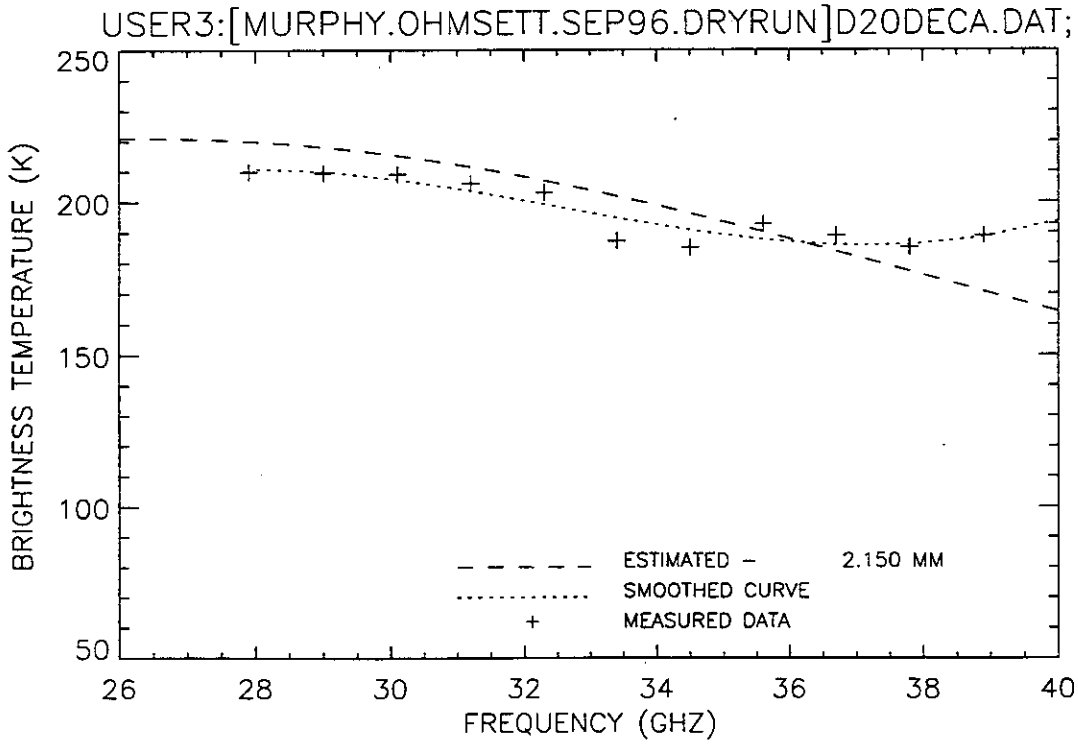

Figure 59. Plot of radiometric brightness temperature versus measurement frequency for 2-mm waste oil, dry run test, calm wave conditions, 10 September 1996, sweep D.

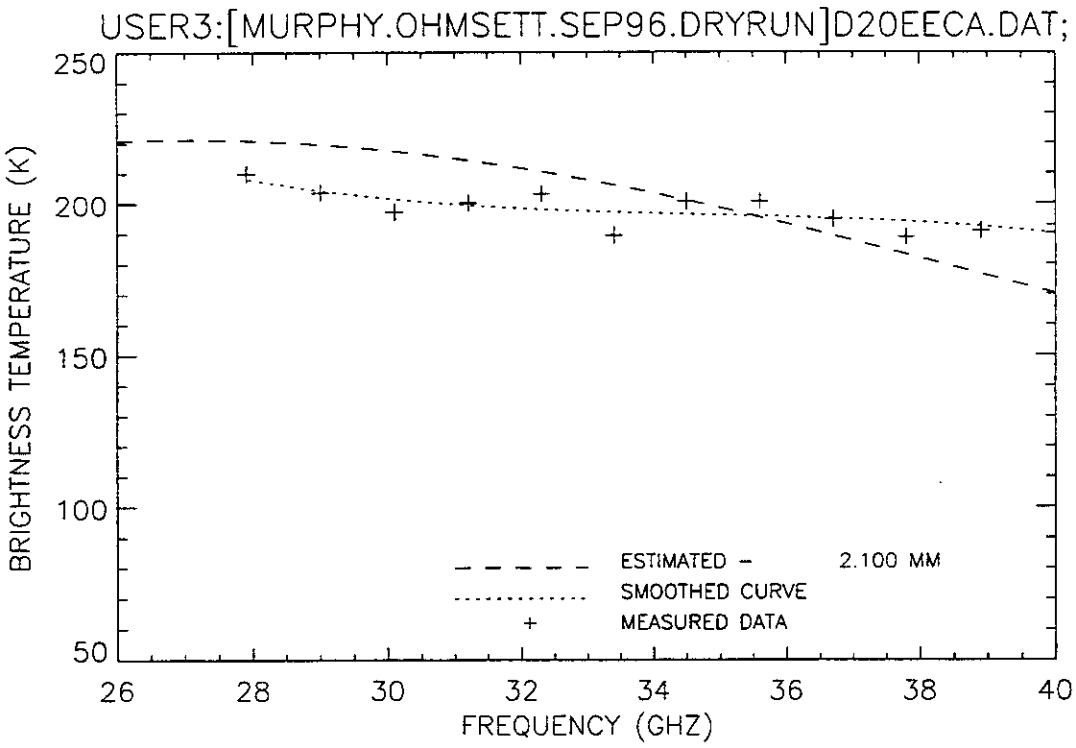

Figure 60. Plot of radiometric brightness temperature versus measurement frequency for 2-mm waste oil, dry run test, calm wave conditions, 10 September 1996, sweep E.

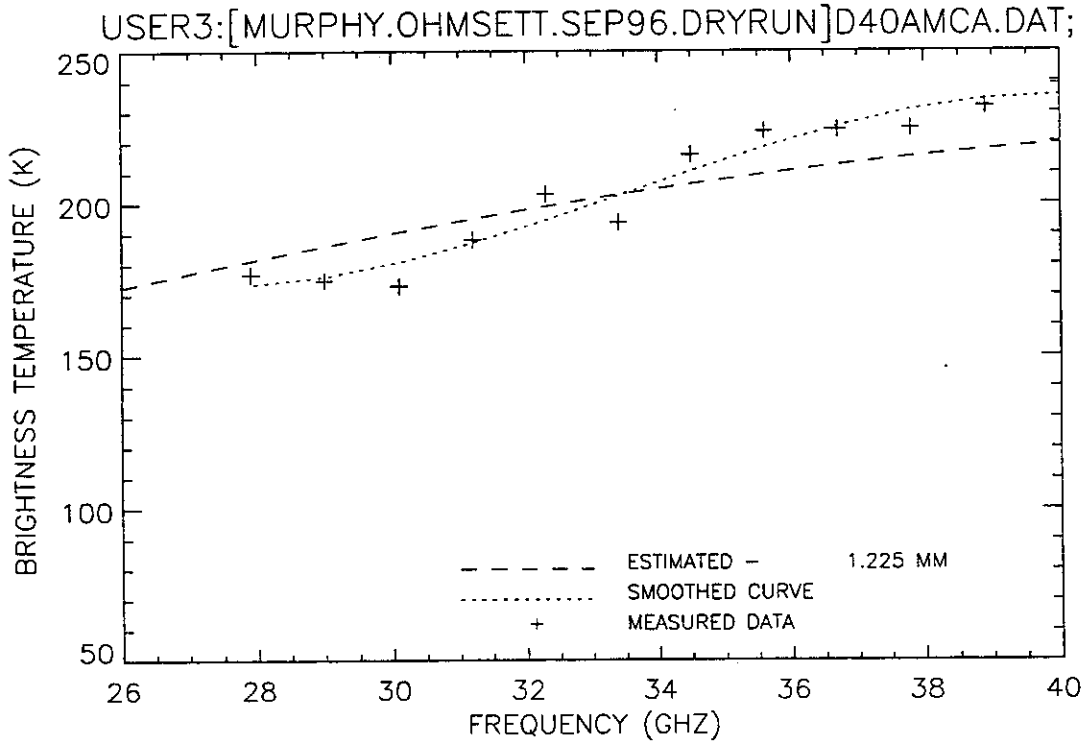

Figure 61. Plot of radiometric brightness temperature versus measurement frequency for 4.0 mm 50% mix of Sundex and diesel oil, dry run test, calm wave conditions, 10 September 1996, sweep A.

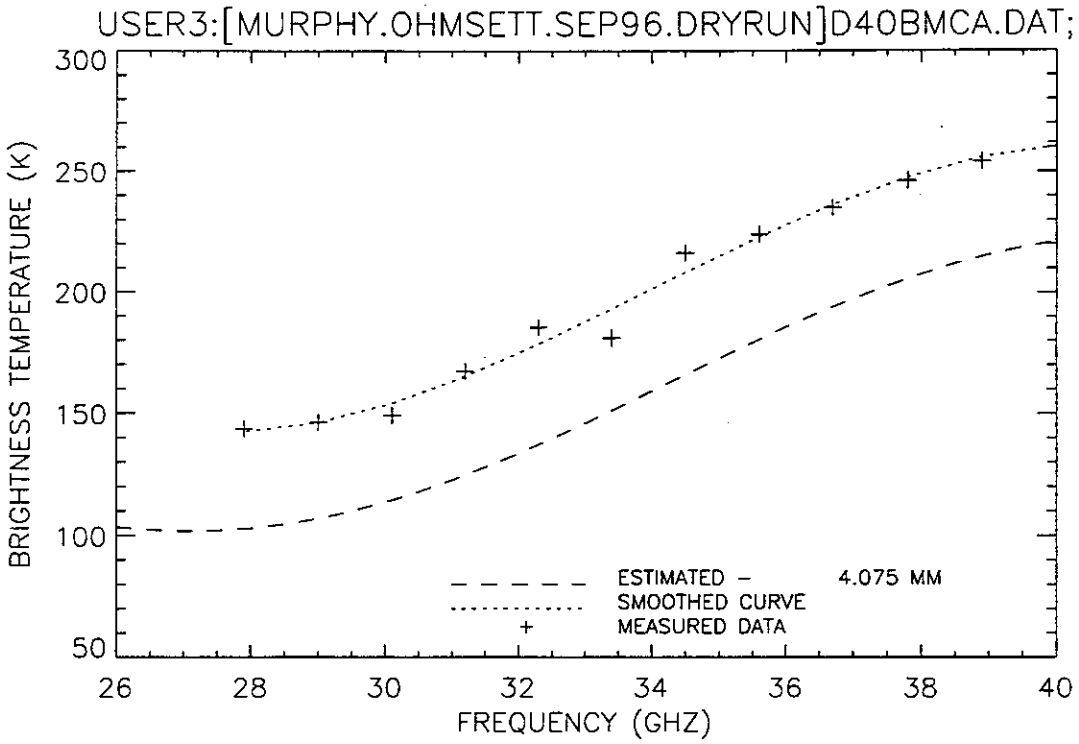

Figure 62. Plot of radiometric brightness temperature versus measurement frequency for 4.0 mm 50% mix of Sundex and diesel oil, dry run test, calm wave conditions, 10 September 1996, sweep B.

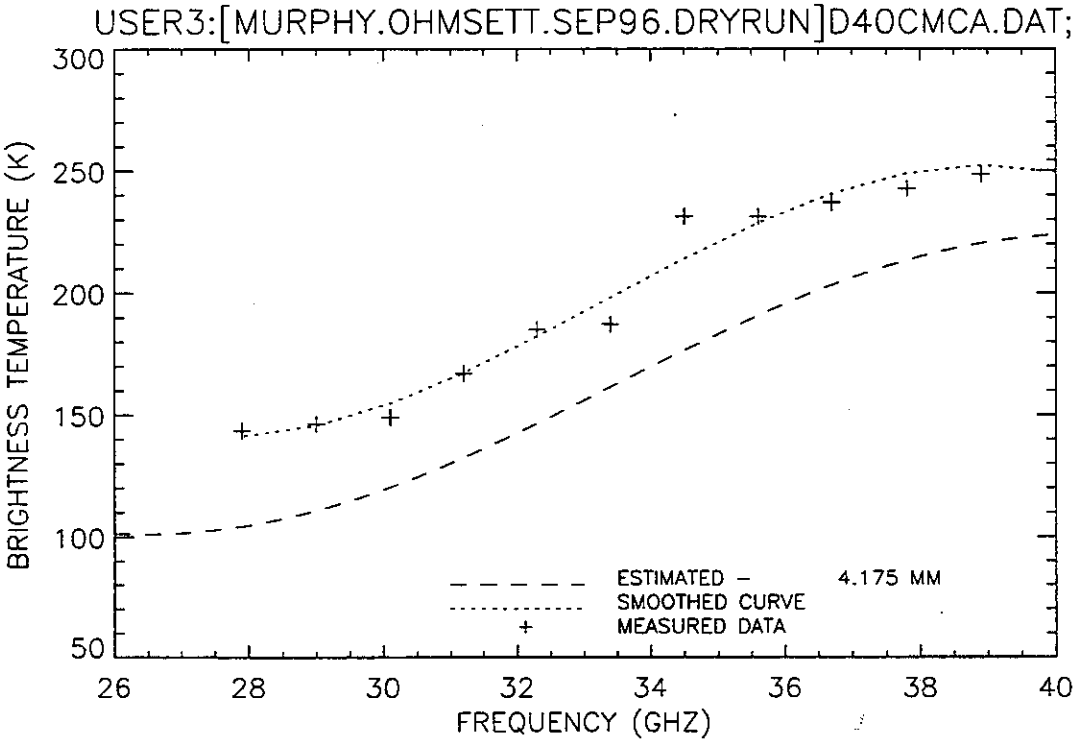

Figure 63. Plot of radiometric brightness temperature versus measurement frequency for 4.0 mm 50% mix of Sundex and diesel oil, dry run test, calm wave conditions, 10 September 1996, sweep C.

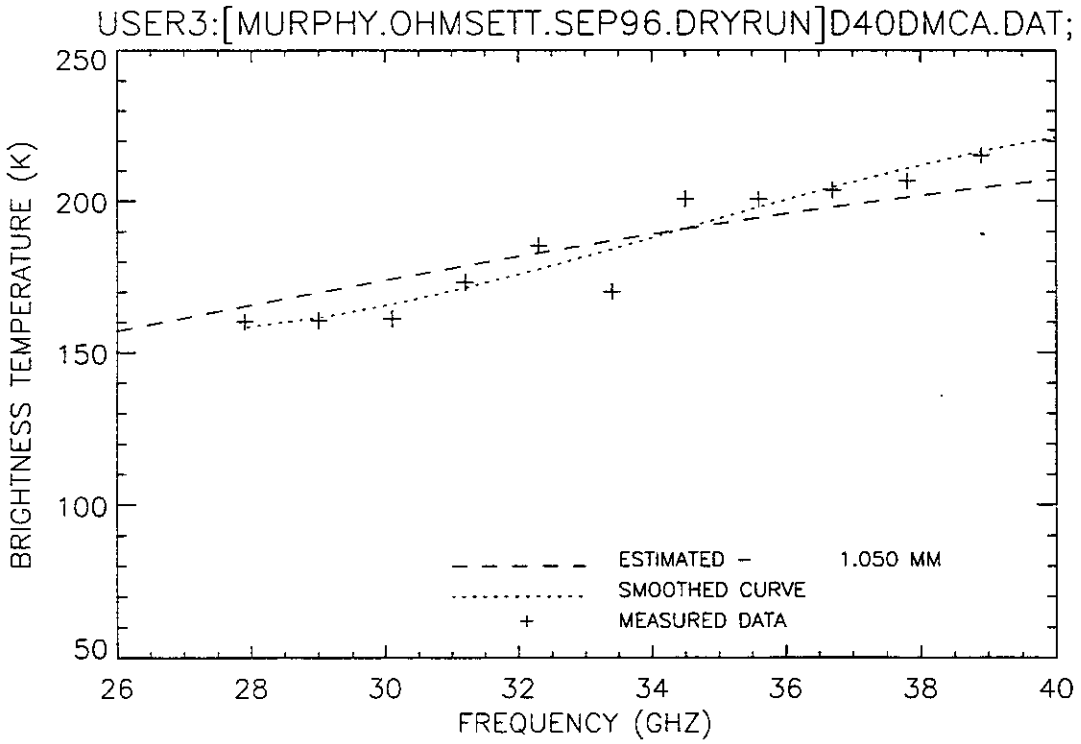

Figure 64. Plot of radiometric brightness temperature versus measurement frequency for 4.0 mm 50% mix of Sundex and diesel oil, dry run test, calm wave conditions, 10 September 1996, sweep D.

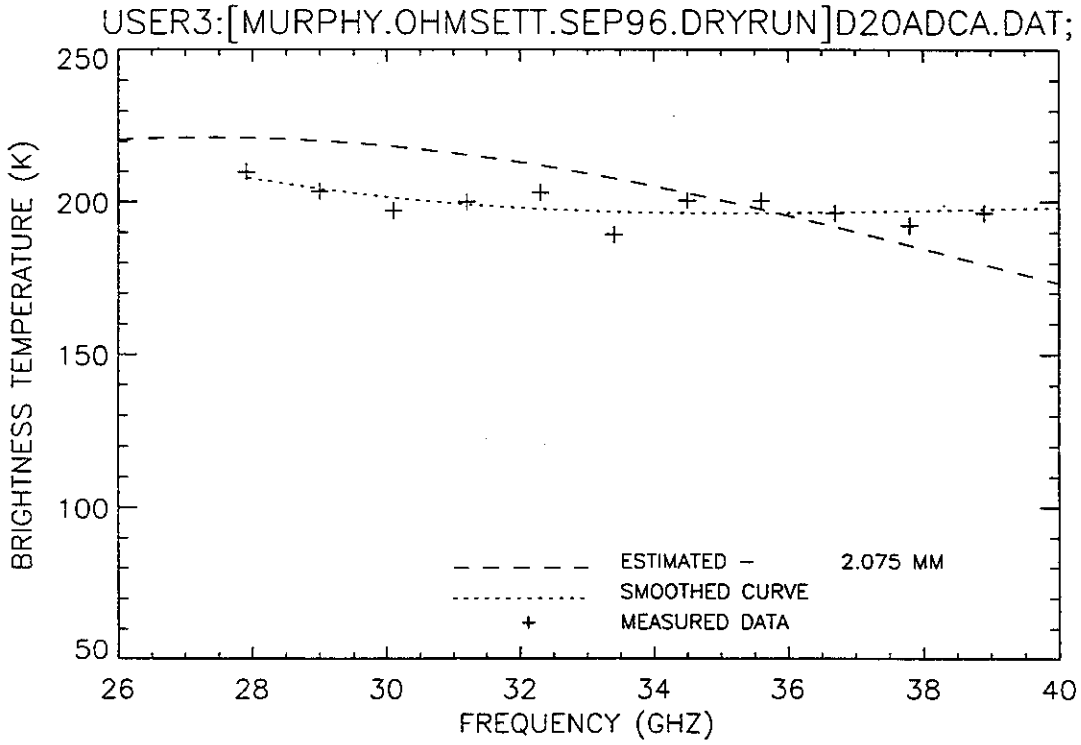

Figure 65. Plot of radiometric brightness temperature versus measurement frequency for 2-mm diesel oil, dry run test, calm wave conditions, 10 September 1996, sweep A.

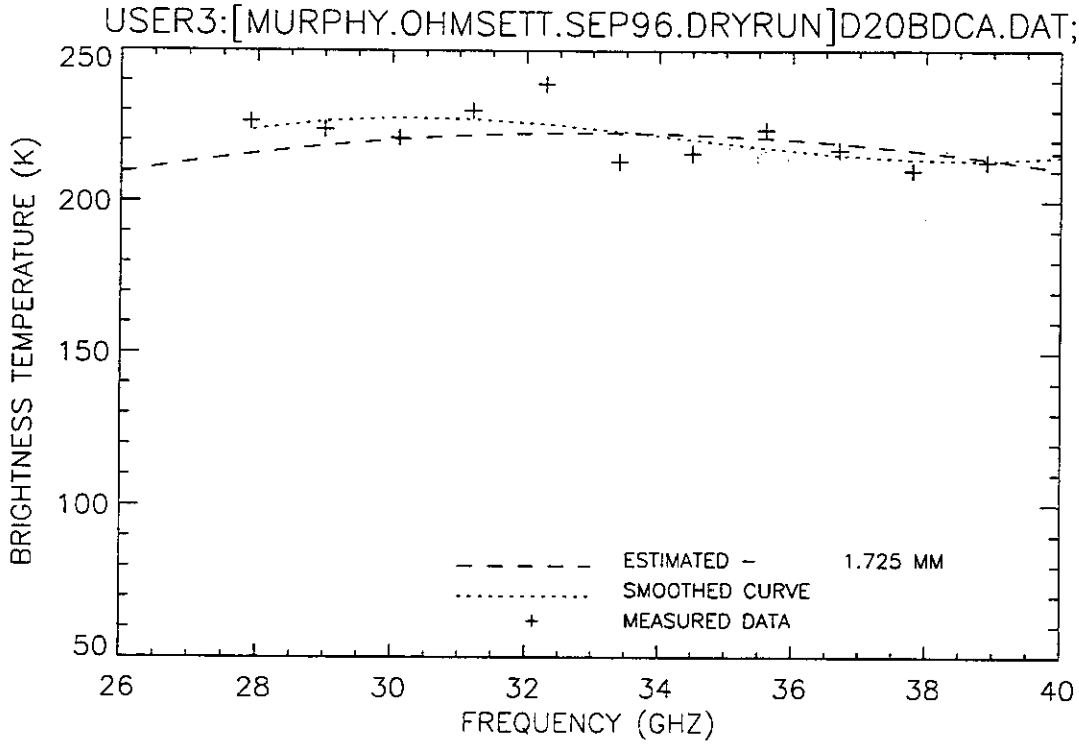

Figure 66. Plot of radiometric brightness temperature versus measurement frequency for 2-mm diesel oil, dry run test, calm wave conditions, 10 September 1996, sweep B.

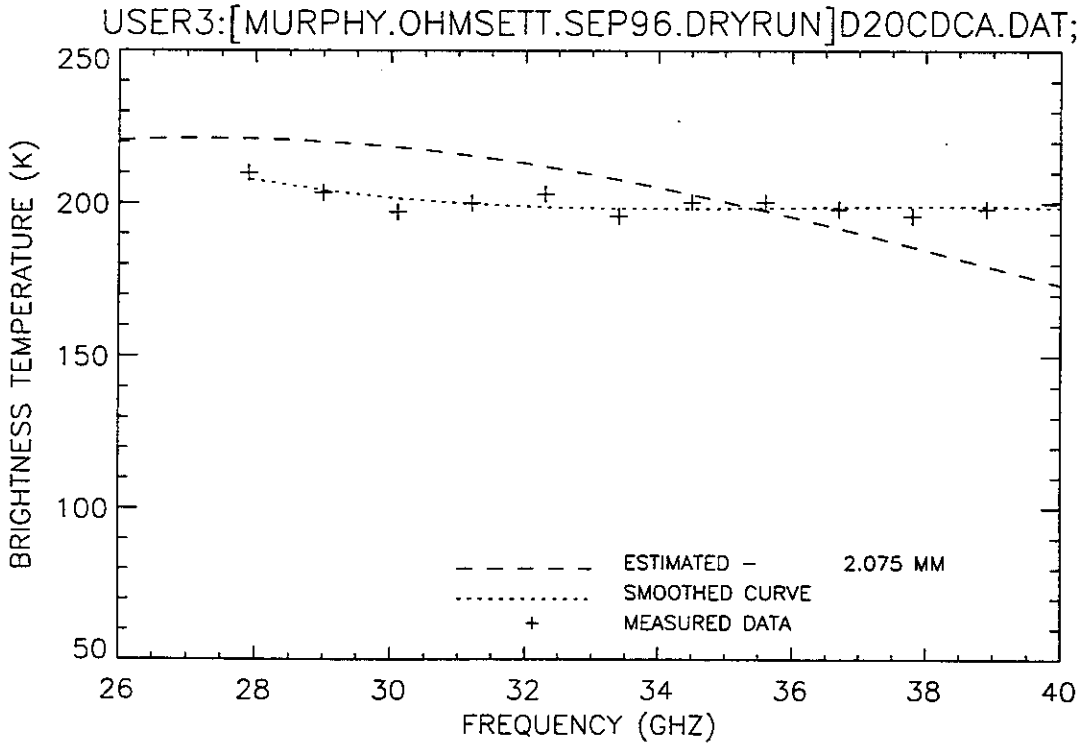

Figure 67. Plot of radiometric brightness temperature versus measurement frequency for 2-mm diesel oil, dry run test, calm wave conditions, 10 September 1996, sweep C.

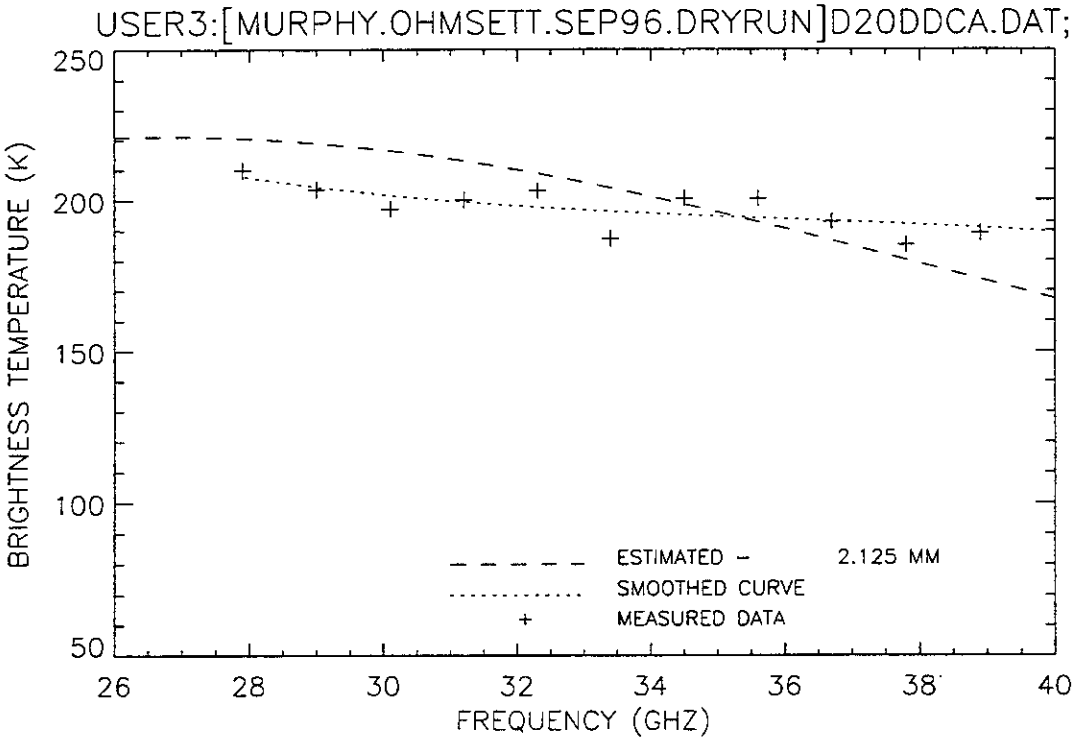

Figure 68. Plot of radiometric brightness temperature versus measurement frequency for 2-mm diesel oil, dry run test, calm wave conditions, 10 September 1996, sweep D.

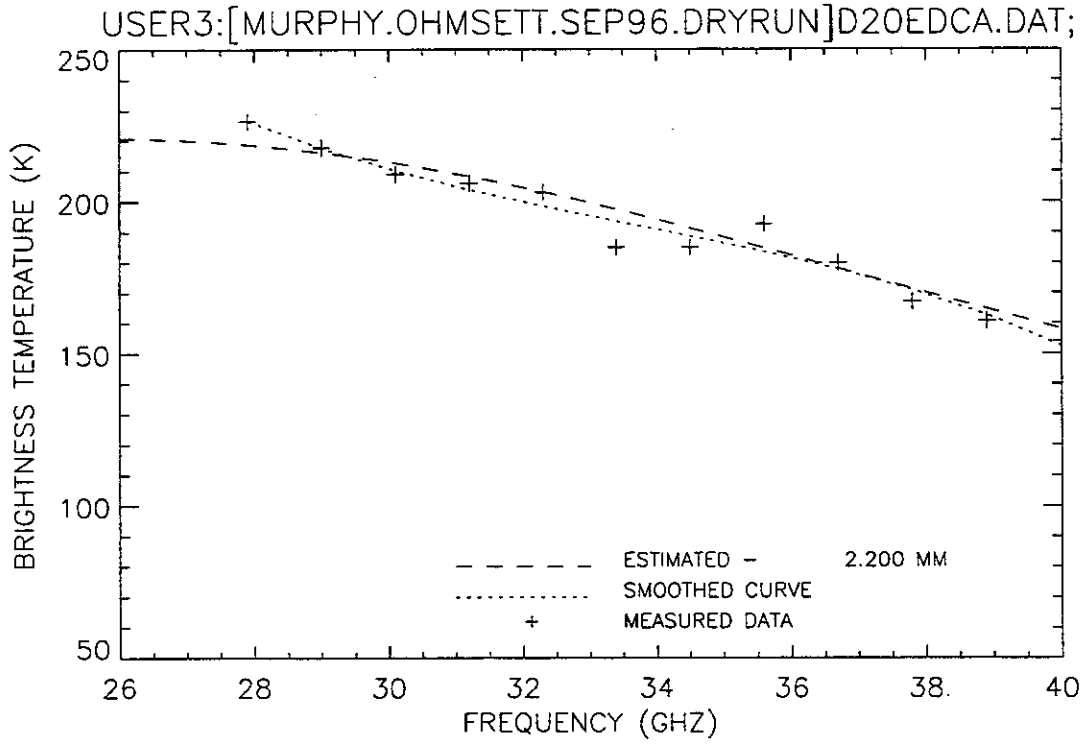

Figure 69. Plot of radiometric brightness temperature versus measurement frequency for 2-mm diesel oil, dry run test, calm wave conditions, 10 September 1996, sweep E.

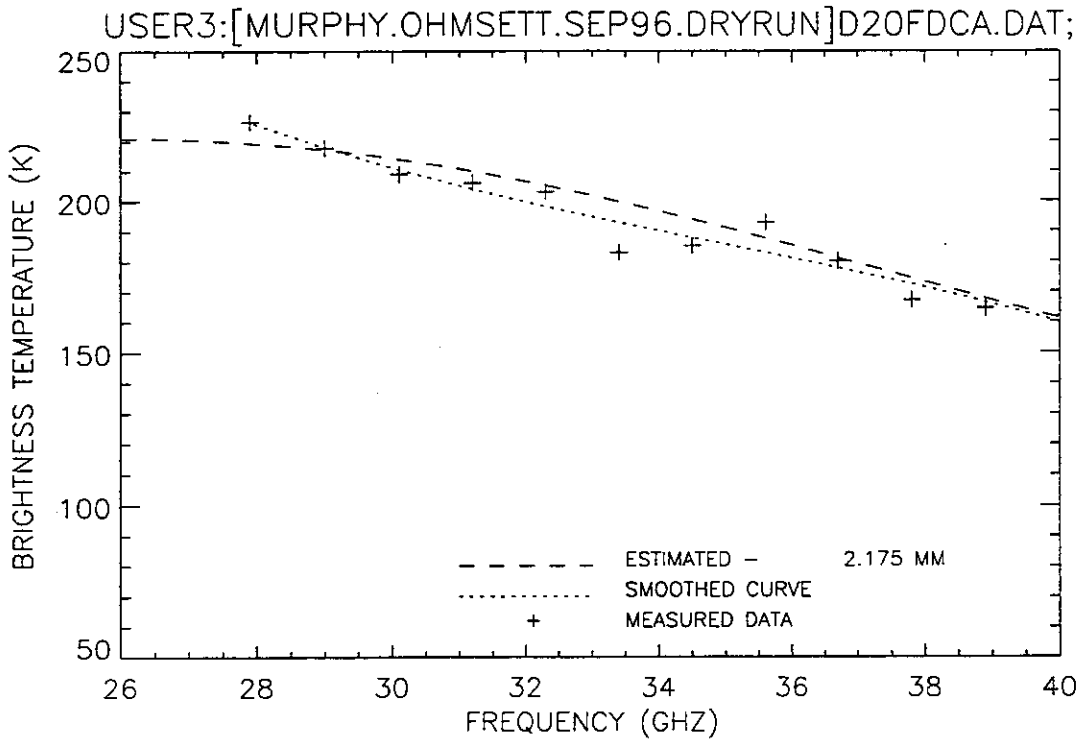

Figure 70. Plot of radiometric brightness temperature versus measurement frequency for 2-mm diesel oil, dry run test, calm wave conditions, 10 September 1996, sweep F.

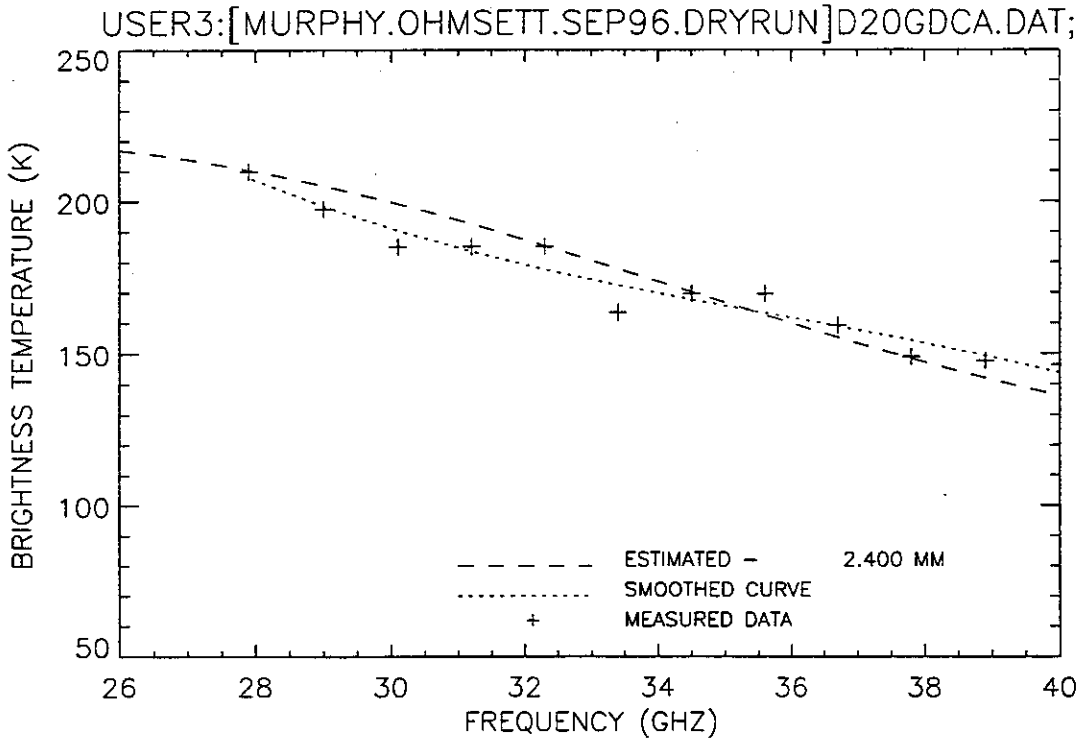

Figure 71. Plot of radiometric brightness temperature versus measurement frequency for 2-mm diesel oil, dry run test, calm wave conditions, 10 September 1996, sweep G.

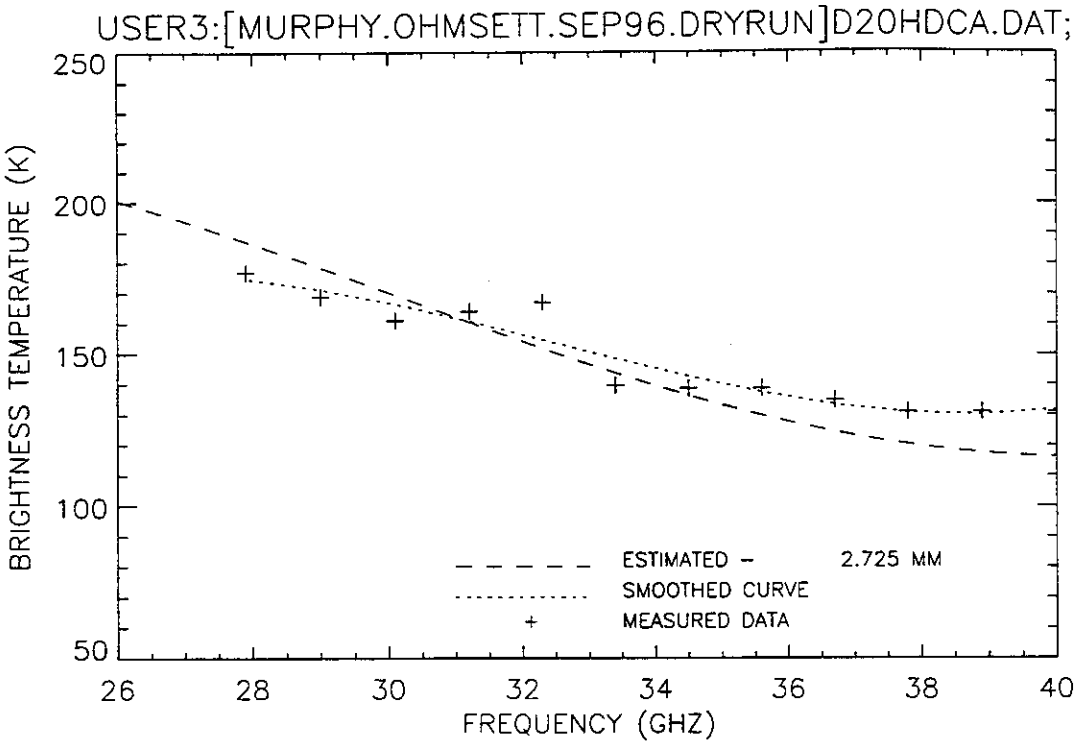

Figure 72. Plot of radiometric brightness temperature versus measurement frequency for 2-mm diesel oil, dry run test, calm wave conditions, 10 September 1996, sweep H.

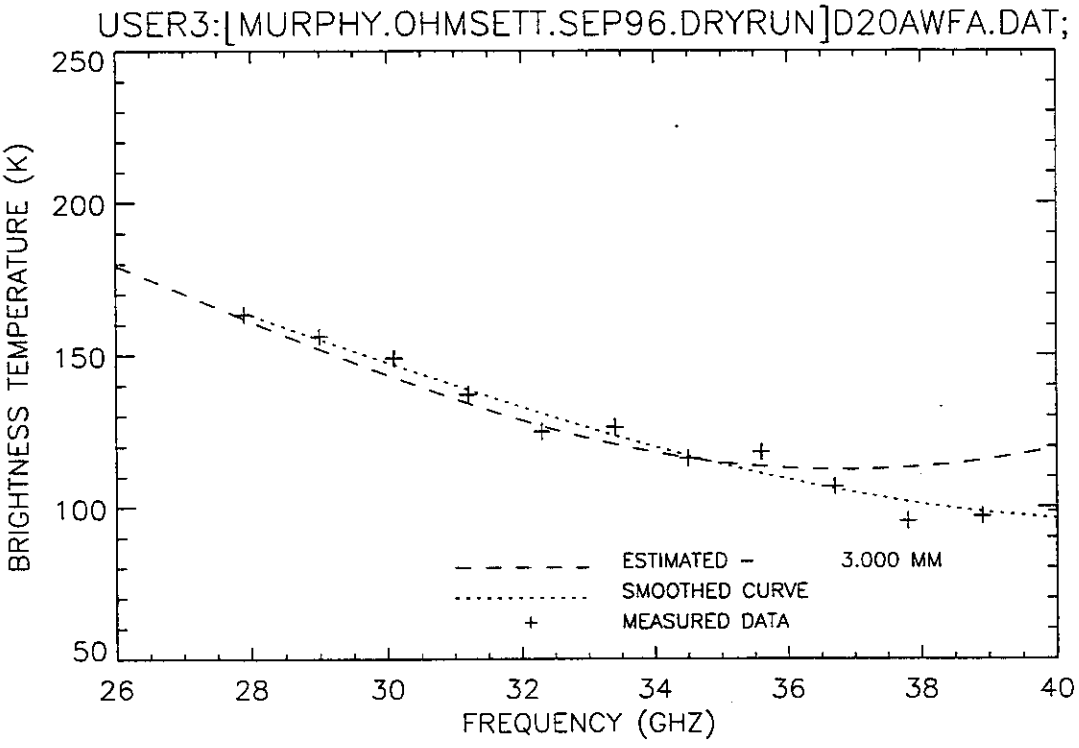

Figure 73. Plot of radiometric brightness temperature versus measurement frequency for 2-mm diesel oil, dry run test, calm wave conditions, prior to fan turn-on, 10 September 1996, sweep A.

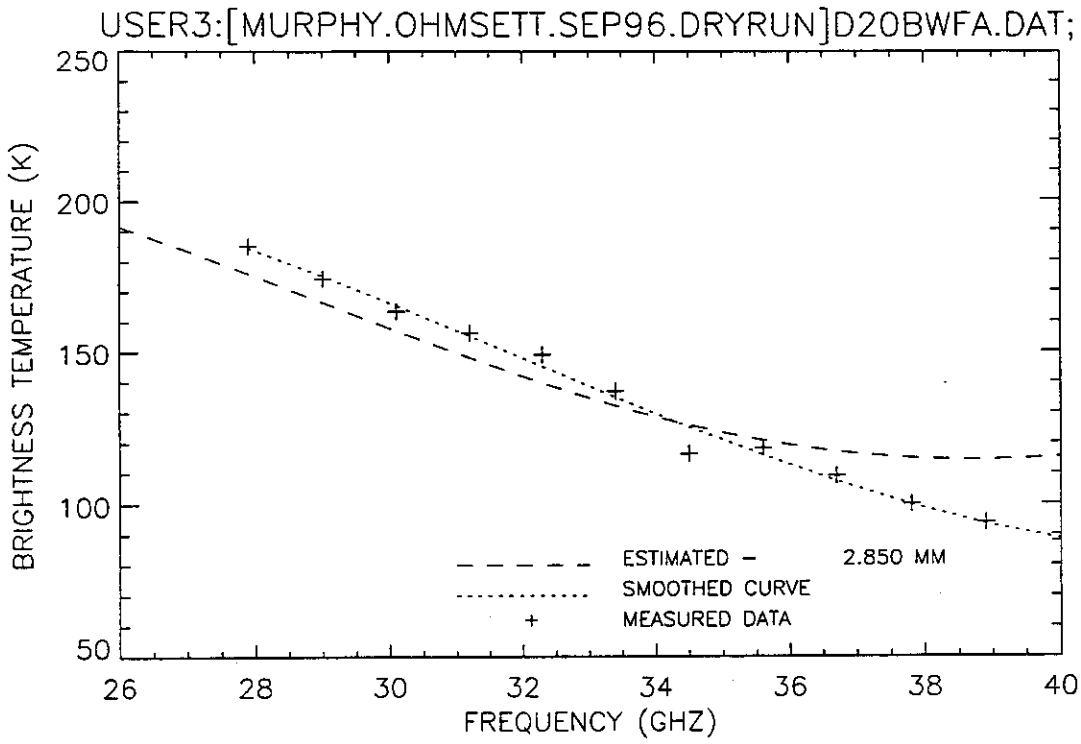

Figure 74. Plot of radiometric brightness temperature versus measurement frequency for 2-mm diesel oil, dry run test, calm wave conditions, prior to fan turn-on, 10 September 1996, sweep B.

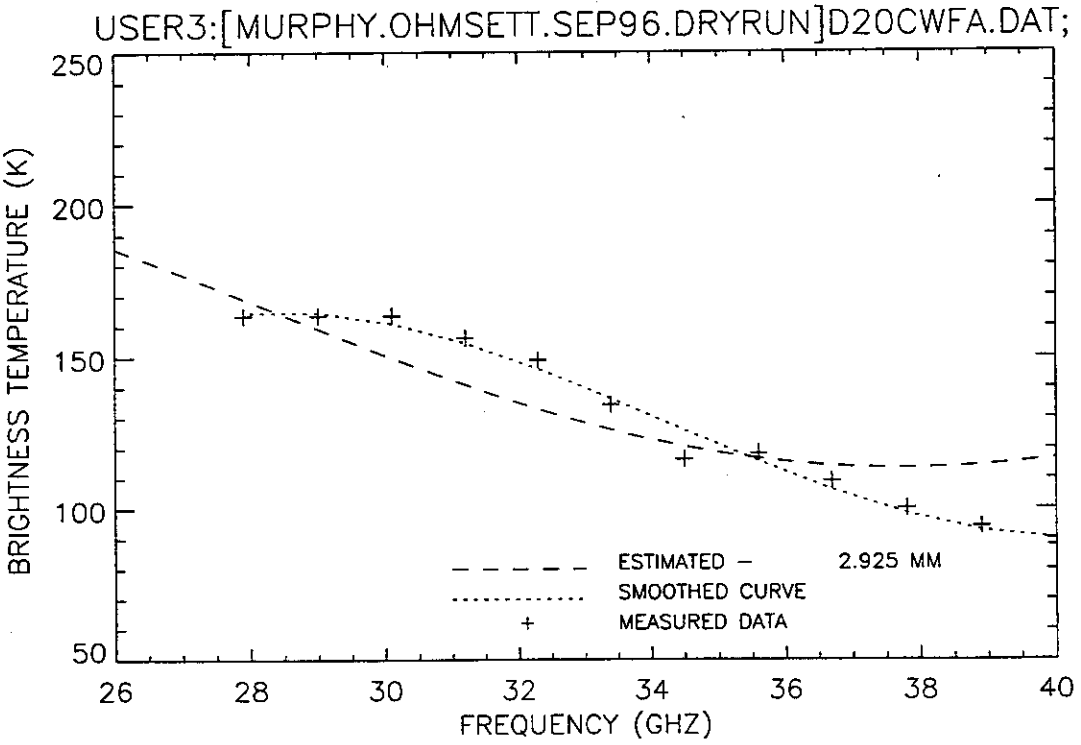

Figure 75. Plot of radiometric brightness temperature versus measurement frequency for 2-mm diesel oil, dry run test, calm wave conditions, prior to fan turn-on, 10 September 1996, sweep C.

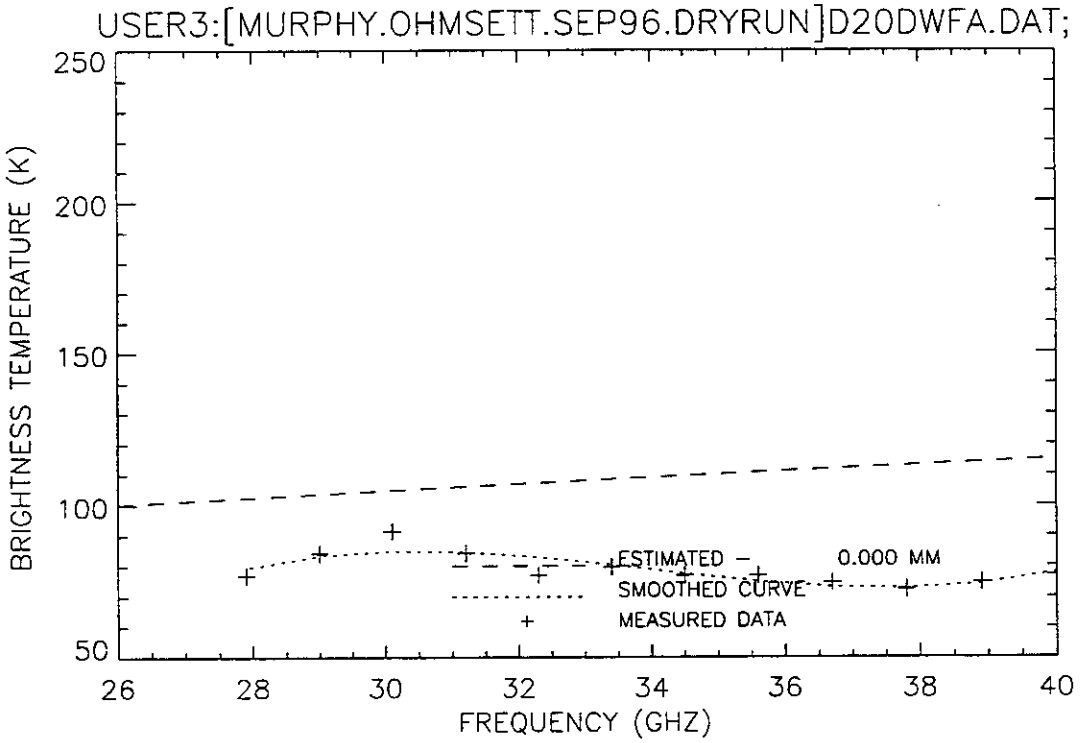

Figure 76. Plot of radiometric brightness temperature versus measurement frequency for 2-mm diesel oil, dry run test, calm wave conditions, after fan turn-on, 10 September 1996, sweep D.

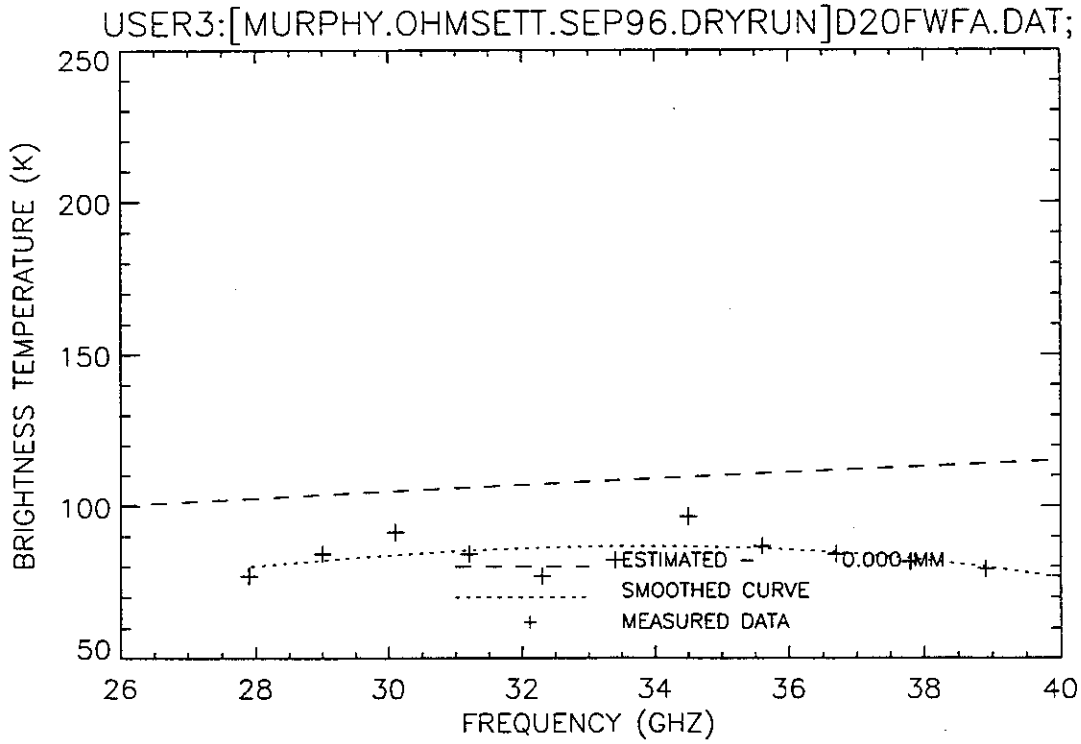

Figure 77. Plot of radiometric brightness temperature versus measurement frequency for 2-mm diesel oil, dry run test, calm wave conditions, after fan turn-on, 10 September 1996, sweep F.

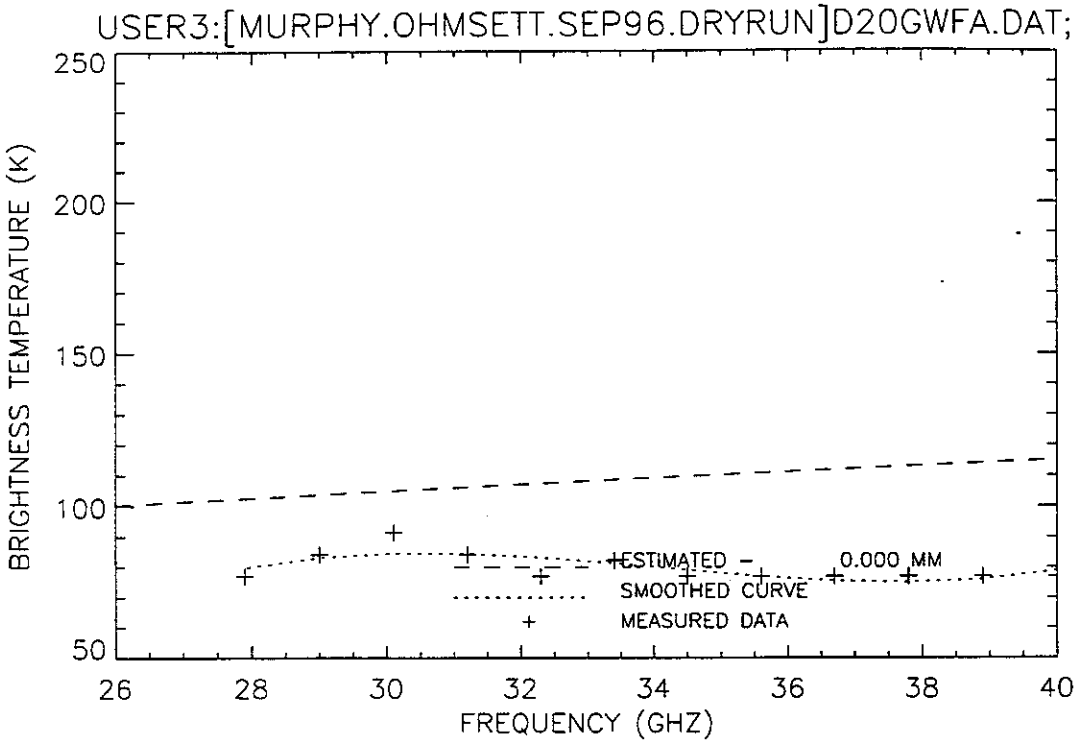

Figure 78. Plot of radiometric brightness temperature versus measurement frequency for 2-mm diesel oil, dry run test, calm wave conditions, after fan turn-on, 10 September 1996, sweep G.

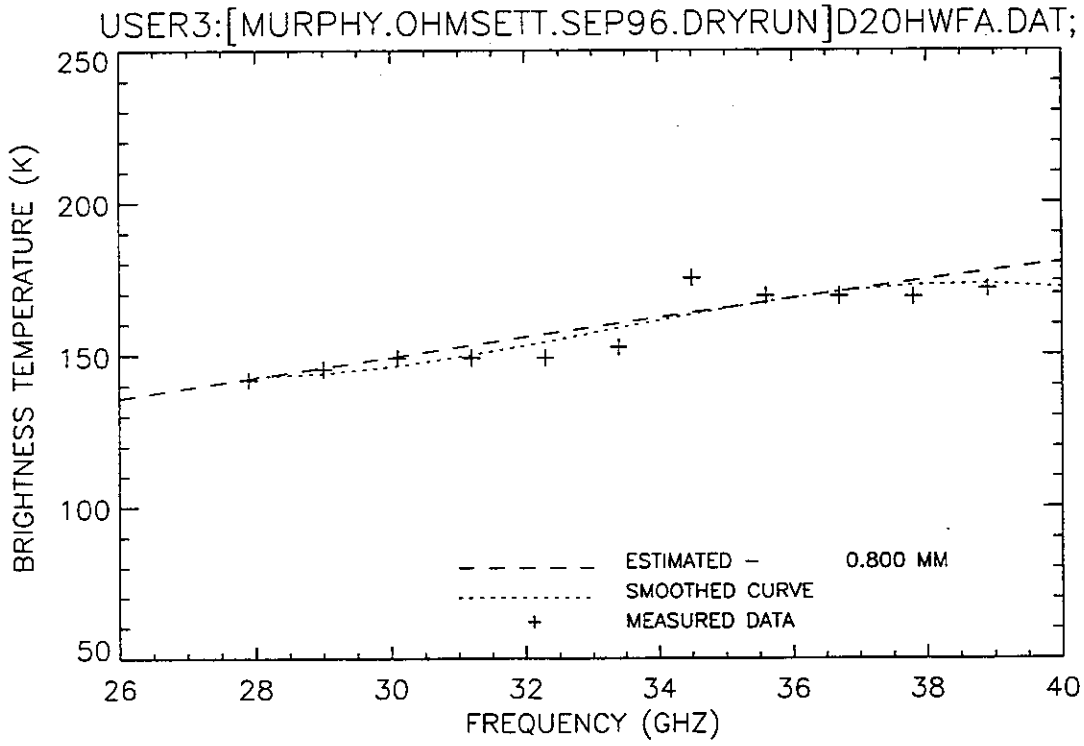

Figure 79. Plot of radiometric brightness temperature versus measurement frequency for 2-mm diesel oil, dry run test, calm wave conditions, after fan turn-on, 10 September 1996, sweep H.

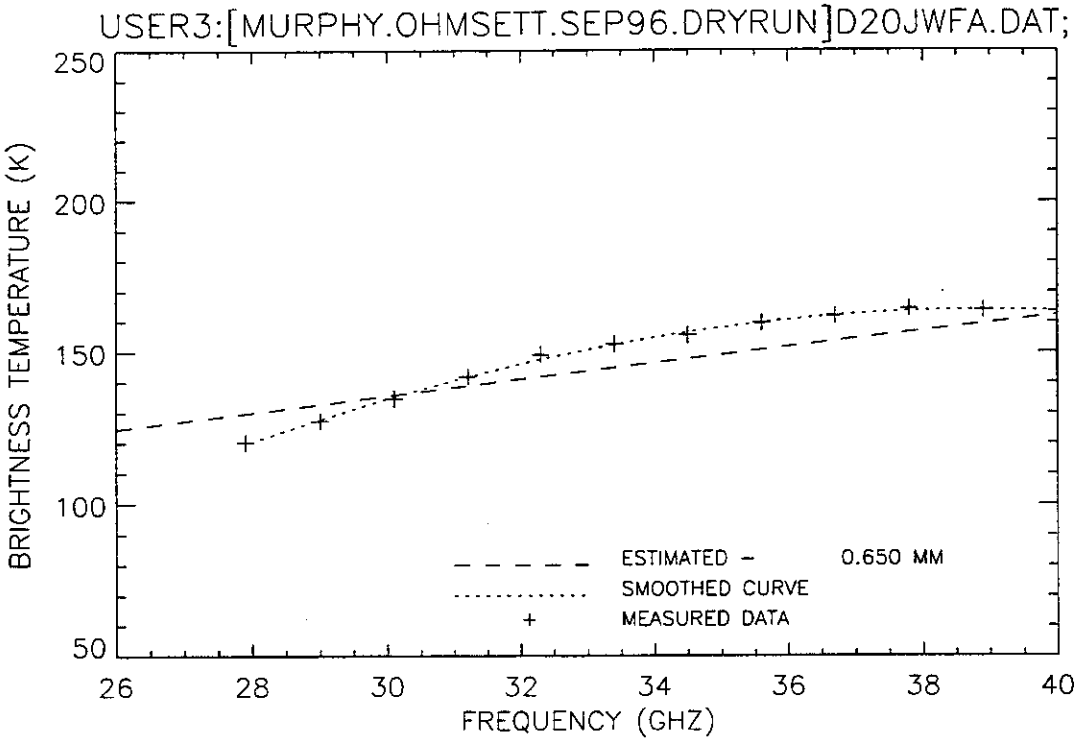

Figure 80. Plot of radiometric brightness temperature versus measurement frequency for 2-mm diesel oil, dry run test, calm wave conditions, after fan turn-on, 10 September 1996, sweep J.

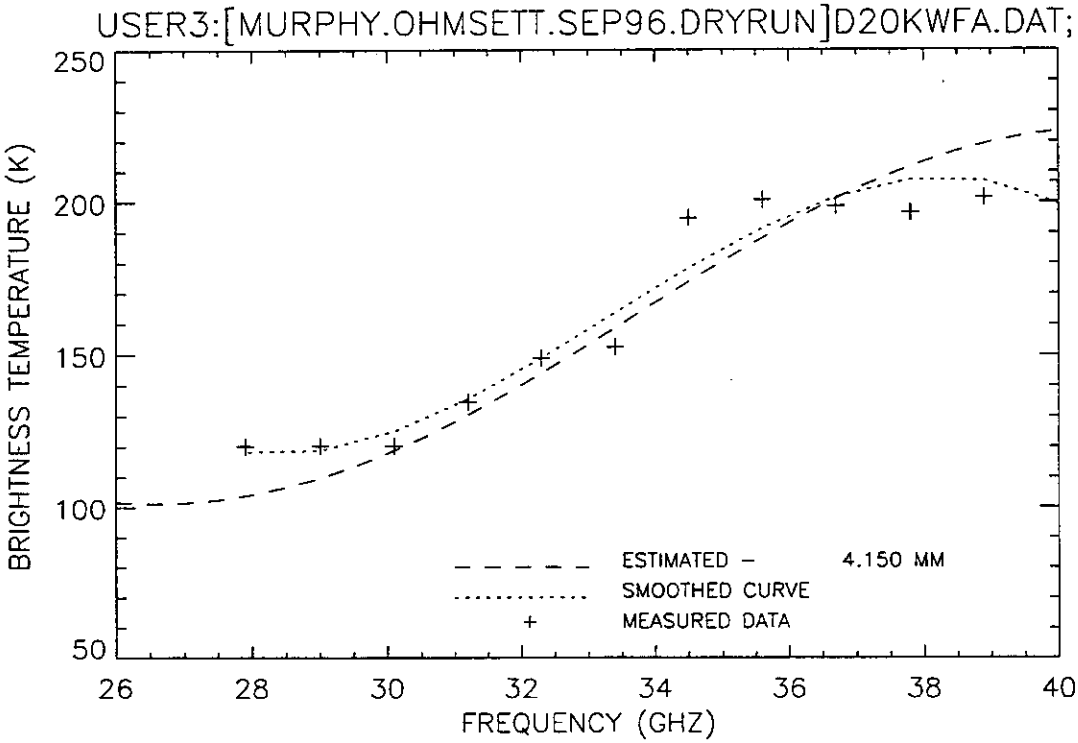

Figure 81. Plot of radiometric brightness temperature versus measurement frequency for 2-mm diesel oil, dry run test, calm wave conditions, after fan turn-on, 10 September 1996, sweep K.

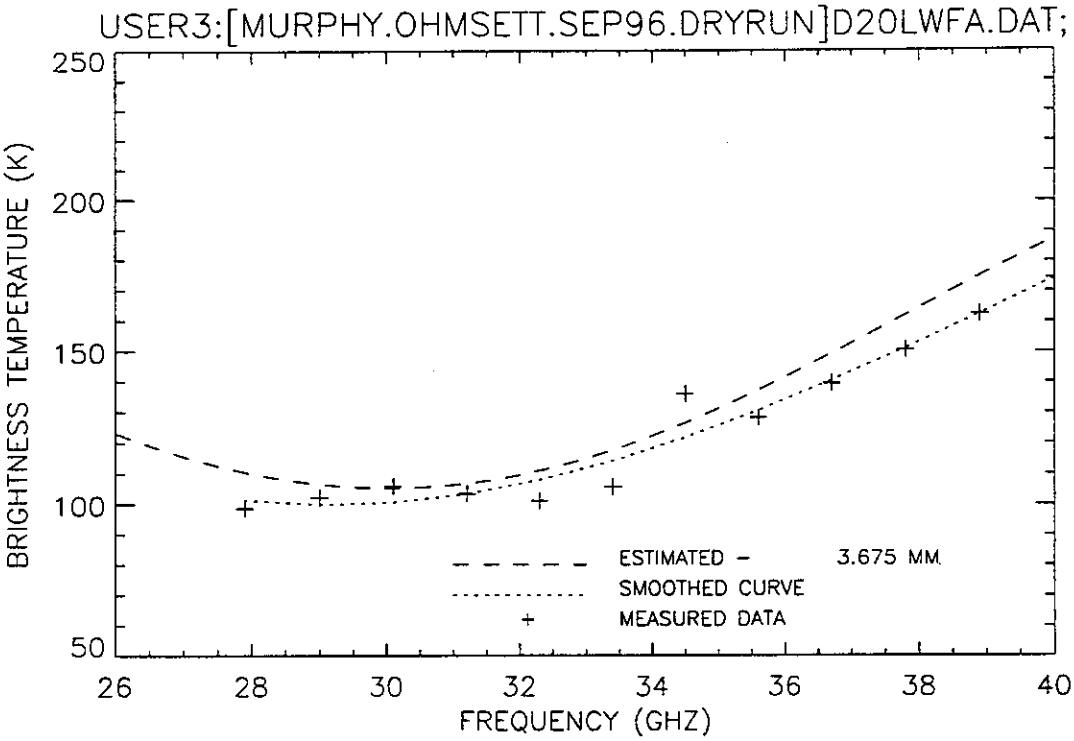

Figure 82. Plot of radiometric brightness temperature versus measurement frequency for 2-mm diesel oil, dry run test, calm wave conditions, after fan turn-on, 10 September 1996, sweep L.

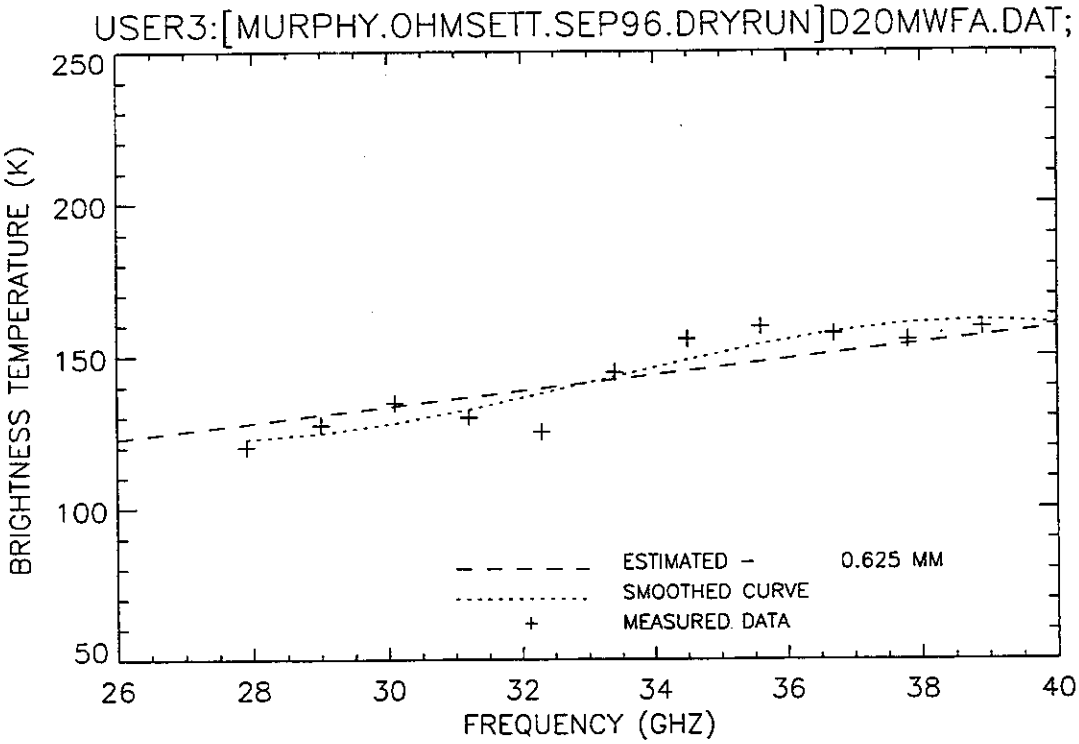

Figure 83. Plot of radiometric brightness temperature versus measurement frequency for 2-mm diesel oil, dry run test, calm wave conditions, after fan turn-on, 10 September 1996, sweep M.

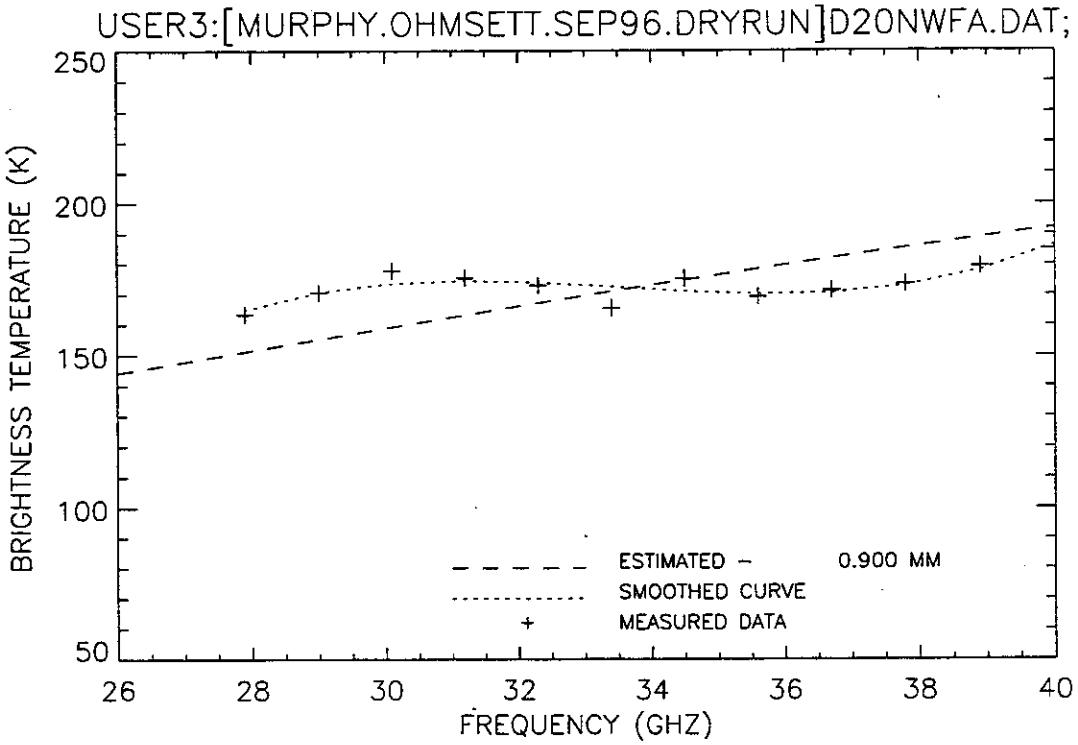

Figure 84. Plot of radiometric brightness temperature versus measurement frequency for 2-mm diesel oil, dry run test, calm wave conditions, after fan turn-on, 10 September 1996, sweep N.

4. Day 1 Tests
Diesel Oil, Calm Conditions

The plan for the day 1 tests was to measure diesel oil and crude oil targets. The crude oil had not arrived. The weather was not optimal for the test; a moderate wind was blowing that tended to herd the oil into a small sector of the containment boom. Because of the limited time available at the test facility, data collection proceeded without the crude oil and under less than optimal conditions.

Table 4 summarizes the results of the postcollection data analysis; the shaded blocks indicate algorithm results (LMS, CORR, MN/SL) that are close to or match the analyst's (visual) oil estimate. A comment is provided referring to the fit of the visual (analyst's choice) to the actual data.

The main bridge was moved to the cleanest-looking water target pool. The target pool had a visible sheen, so measurements were collected from an area that did not have a sheen but was outside the pool. The spot was approximately halfway between the water target and the 8-mm target, outside the pool's interconnecting lines. After an initial review of the data, the water reference file selected was that collected during the middle of the collection period because it seemed to be a better match to the data sets.

A100AWCA.DAT – The algorithm estimate of 0.100 mm, shown in Figure 85, is a fair-to-good match to the measured data. A slight sinusoidal variation in the data is observed. This characteristic appears to be in nearly all of the data collected on this day. Its cause is most likely due to the instrument calibration.

A100BWCA.DAT – The algorithm estimate of 0.125 mm, shown in Figure 86, is a fair-to-good match to the measured data.

A100CWCA.DAT – The algorithm estimate of 0.175 mm, shown in Figure 87, is a good match to the measured data.

A100DWCA.DAT – The algorithm estimate of 0.175 mm, shown in Figure 88, is a good match to the measured data.

The main bridge was moved to measure an area in the southeast portion of the 8-mm uniform diesel oil target pool.

TABLE 4

Results of the 11 September 1996 Day 1 Test

FILENAME	LMS	CORR	MN/SL	DECL	METHOD	VISUAL	COMMENT
A100ADCA.DAT							
A100AWCA.DAT	0.100	1.675	0.100	0.100	LMS & MN/SL	0.100	Fair to good
A100BDCA.DAT	0.450	1.700	0.475	0.450	LMS & MN/SL	0.450	Fair
A100BWCA.DAT	0.125	1.650	0.125	0.125	LMS & MN/SL	0.125	Fair to good
A100CDCA.DAT	0.475	8.800	0.475	0.475	LMS & MN/SL	0.475	Poor
A100CWCA.DAT	0.175	1.650	0.175	0.175	LMS & MN/SL	0.175	Good
A100DDCA.DAT	0.175	8.875	0.200	0.175	LMS & MN/SL	0.175	Poor to fair
A100DWCA.DAT	0.175	1.675	0.175	0.175	LMS & MN/SL	0.175	Good
A105ADCA.DAT	1.025	1.625	1.025	1.025	LMS & MN/SL	1.025	Fair to good (mean)
A105BDCA.DAT	0.975	4.575	0.975	0.975	LMS & MN/SL	0.975	Good to excellent
A105CDCA.DAT	1.000	1.625	1.000	1.000	LMS & MN/SL	1.000	Fair to good (mean)
A105DDCA.DAT	0.700	1.700	0.700	0.700	LMS & MN/SL	0.700	Fair (mean)
A105AECA.DAT	0.000	1.700	0.000	0.000	LMS & MN/SL	0.000	Poor to fair
A105FDCA.DAT	0.000	1.675	0.000	0.000	LMS & MN/SL	0.000	Poor
A105GDCA.DAT	0.000	8.950	0.000	0.000	LMS & MN/SL	0.000	Fair
A105HDCA.DAT	0.000	1.700	0.000	0.000	LMS & MN/SL	0.000	Poor
A105JDCA.DAT	5.125	1.700	1.025	5.125	LMS only	1.700	Inconclusive
A105KDCA.DAT	0.625	8.975	0.650	0.650	LMS & MN/SL	0.625	Fair (mean)
A105LDCA.DAT	0.375	8.975	0.400	0.375	LMS & MN/SL	0.375	Inconclusive
A105MDCA.DAT	0.725	8.975	0.750	0.725	LMS & MN/SL	0.725	Inconclusive
A110ADCA.DAT	1.625	1.675	1.675	1.675	CORR & MN/SL	1.675	Inconclusive
A110BDCA.DAT	1.675	1.700	1.675	1.675	LMS & MN/SL	1.675	Inconclusive
A110CDCA.DAT	1.750	5.150	1.675	1.700	LMS & MN/SL	1.700	Fair
A110DDCA.DAT	1.850	5.375	1.700	1.775	LMS & MN/SL	1.775	Poor to fair
A110EDCA.DAT	0.725	1.425	0.725	0.725	LMS & MN/SL	0.725	Good
A110FDCA.DAT	0.825	4.500	0.825	0.825	LMS & MN/SL	0.825	Fair to good
A110GDCA.DAT	0.800	1.550	0.800	0.800	LMS & MN/SL	0.800	Fair to good
A110HDCA.DAT	0.525	4.150	0.550	0.525	LMS & MN/SL	0.525	Fair
A120ADCA.DAT	3.000	2.725	3.125	3.050	LMS & MN/SL	3.050	Good
A120BDCA.DAT	2.825	5.825	2.900	2.850	LMS & MN/SL	5.800	Good (shape)
A120CDCA.DAT	2.850	5.900	2.900	2.875	LMS & MN/SL	2.875	Good
A120DDCA.DAT	2.975	5.650	0.525	2.975	LMS only	2.975	Poor to fair (shape)
A120EDCA.DAT	1.850	8.950	1.650	1.750	LMS & MN/SL	1.750	Fair (mean)
A120FDCA.DAT	2.125	5.425	1.200	2.125	LMS only	2.125	Good to excellent
A120GDCA.DAT	2.400	2.025	2.425	2.400	LMS & MN/SL	2.400	Good to excellent
A130ADCA.DAT	4.000	4.075	3.950	3.975	LMS & MN/SL	3.975	Good
A130BDCA.DAT	4.075	4.000	3.975	3.975	CORR & MN/SL	3.975	Fair to good
A130CDCA.DAT	4.150	1.275	0.775	4.150	LMS only	4.150	Fair
A130DDCA.DAT	3.875	4.150	3.875	3.875	LMS & MN/SL	3.875	Fair
A130EDCA.DAT	4.125	4.000	0.750	4.050	LMS & CORR	4.050	Fair
A130FDCA.DAT	4.425	4.300	1.020	4.350	LMS & CORR	4.350	Fair to good (shape)
A130GDCA.DAT	4.000	4.100	3.900	4.050	LMS & CORR	4.050	Good to excellent
A130SDCA.DAT	3.975	0.200	3.925	3.950	LMS & MN/SL	3.950	Fair (shape)
A180ADCA.DAT	1.225	7.475	2.175	1.225	LMS only	7.475	Good (shape)
A180BDCA.DAT	7.600	7.575	2.325	7.575	LMS & CORR	7.575	Good (shape)

TABLE 4 (Continued)

Results of the 11 September 1996 Day 1 Test

FILENAME	LMS	CORR	MN/SL	DECL	METHOD	VISUAL	COMMENT
A180CDCA.DAT	1.250	7.225	2.150	1.250	LMS only	7.500	Good (shape)
A180DDCA.DAT	1.050	7.750	2.350	1.050	LMS only	7.750	Good (shape)
A180EDCA.DAT	7.500	7.475	2.350	7.475	LMS & CORR	7.700	Good (shape)
A180FDCA.DAT	10.000	3.300	2.125	10.000	LMS only	10.000	Poor
A180GDCA.DAT	1.775	3.325	1.875	1.825	LMS & MN/SL	7.400	Fair (shape)
A180HDCA.DAT	1.200	7.425	2.200	1.200	LMS only	7.600	Good (shape)
A180JDCA.DAT	7.400	7.375	2.400	7.375	LMS & CORR	7.600	Good
A180KDCA.DAT	1.125	7.475	2.275	1.125	LMS only	7.600	Good (shape)
A180LDCA.DAT	8.050	8.075	2.475	8.050	LMS & CORR	8.050	Good
A1XXAMCA.DAT	0.600	1.575	3.825	0.600	LMS only	0.600	Fair
A1XXBMCA.DAT	0.675	1.625	0.700	0.675	LMS & MN/SL	0.675	Fair
A1XXCMCA.DAT	0.800	1.625	0.825	0.800	LMS & MN/SL	0.800	Fair to good
A1XXDMCA.DAT	1.025	8.950	1.025	1.025	LMS & MN/SL	1.025	Fair to good
A1XXEMCA.DAT	1.000	1.625	1.000	1.000	LMS & MN/SL	1.000	Fair
A1XXFMCA.DAT	1.025	1.650	1.025	1.025	LMS & MN/SL	1.025	Fair to good
A1XXGMCA.DAT	1.075	1.400	1.075	1.075	LMS & MN/SL	1.075	Good
A1XXHMCA.DAT	1.075	1.600	1.075	1.075	LMS & MN/SL	1.075	Good

A180ADCA.DAT – The algorithm estimate of 1.225 mm is a poor match to the measured data. If the correlation-only estimate of 7.475 mm shown in Figure 89 is used, a good match to the shape of the measured data is observed. The measured points appear warmer and of a slightly higher frequency than the theoretical prediction.

A180BDCA.DAT – The algorithm estimate of 7.575 mm, shown in Figure 90, is a good match to the shape of the measured data. The measured points appear to have a larger amplitude modulation and slightly higher frequency than the theoretical prediction. The 34- and 35-GHz data points appear to be noisy.

A180CDCA.DAT – The algorithm estimate of 1.250 mm is a poor match to the shape of the measured data. The correlation-only result of 7.225 mm, shown in Figure 91, is a better match; however an estimate of 7.500 mm results in the best shape match. The measured points appear to have a larger amplitude modulation and slightly higher frequency than the theoretical prediction. The 28-, 34-, and 35-GHz data points appear to be noisy.

A180DDCA.DAT – The algorithm estimate of 1.050 mm is a poor match to the shape of the measured data. The correlation-only estimate of 7.750 mm, shown in Figure 92,

results in a good shape match to the measured data. The 34- and 35-GHz data points appear to be noisy.

The radiometer position was shifted to measure an area in the southwest portion of the target pool.

A180EDCA.DAT – The algorithm estimate of 7.475 mm is a fair match to the shape of the measured data. However, if a slightly thicker estimate is used, namely 7.700 mm shown in Figure 93, the shape of the theoretical estimate matches the measured data better. The 34- and 35-GHz data points appear to be noisy.

A180FDCA.DAT – The algorithm estimate of 10.000 mm, shown in Figure 94, is a poor match to the measured data. The data points below 34 GHz compare favorably with the estimated curve. If the 34- and 35-GHz points are assumed to be high due to poor calibration or noise, the final three data points also compare favorably with the estimated curve.

A180GDCA.DAT – The algorithm estimate of 1.825 mm is a poor match to the shape of the measured data. None of the raw algorithm estimates give a reasonable result. The best match, shown in Figure 95, was found using an estimate of 7.400 mm. The 29- and 33-GHz data points appear to be noisy. The smoothed data curve seems to have a slightly higher frequency component than the estimated curve.

The main bridge was moved south so that data could be collected at the southernmost part of the target pool. At this point, the operator observed that the instrument's gain seemed to be drifting, so a new V_{HOT} calibration was performed during the bridge movement.

A180HDCA.DAT – The algorithm estimate of 1.200 mm is a poor match to the shape of the measured data. The correlation-only estimate of 7.425 mm is a fair match; however, the best match, shown in Figure 96, was obtained using an estimate of 7.600 mm. The 34- and 35-GHz data points appear to be noisy.

A180JDCA.DAT – The algorithm estimate of 7.375 mm is a fair match to the measured data. A better match, shown in Figure 97, was found using an estimate of 7.600 mm. The 34- and 35-GHz data points appear to be noisy.

A180KDCA.DAT – The algorithm estimate of 1.125 mm is a poor match to the shape of the measured data. The correlation-only estimate of 7.474 mm resulted in a fair

match. A better match, shown in Figure 98, was found using an estimate of 7.600 mm. The 34- and 35-GHz data points appear to be noisy.

A180LDCA.DAT – The algorithm estimate of 8.050 mm, shown in Figure 99, is a good match to the shape of the measured data. The oscillation frequency of the measured data appears to be slightly higher than the theoretical estimate.

The main bridge was moved north to collect data from the center of the 3-mm uniform diesel oil target.

A130ADCA.DAT – The algorithm estimate of 3.975 mm, shown in Figure 100, is a good match to the measured data.

A130BDCA.DAT – The algorithm estimate of 3.975 mm, shown in Figure 101, is a fair-to-good match to the measured data.

A130CDCA.DAT – The algorithm estimate of 4.150 mm, shown in Figure 102, is a fair match to the measured data.

A130DDCA.DAT – The algorithm estimate of 3.875 mm, shown in Figure 103, is a fair match to the measured data.

The main bridge was moved south to collect data from a new spot in the center of the southern portion of the target pool.

A130EDCA.DAT – The algorithm estimate of 4.050 mm, shown in Figure 104, is a fair match to the measured data.

A130FDCA.DAT – The algorithm estimate of 4.350 mm, shown in Figure 105, is a fair-to-good match to the measured data curve.

A130GDCA.DAT – The algorithm estimate of 4.050 mm, shown in Figure 106, is a good-to-excellent match to the measured data.

The main bridge was moved north to the northeast portion of the 2-mm diesel oil target. A visible gradient had formed across the pool, with the thickest oil in its northeast portion.

A120ADCA.DAT – The algorithm estimate of 3.050 mm, shown in Figure 107, is a good match to the measured data.

A120BDCA.DAT – The algorithm estimate of 2.850 mm is a fair match to the shape of the measured data curve; however, it was found that an estimate of 5.800 mm, shown in Figure 108, had a shape that was a better match. The estimate has an overall higher temperature than the measured points.

A120CDCA.DAT – The algorithm estimate of 2.875 mm, shown in Figure 109, is a good match to the measured data.

A120DDCA.DAT – The algorithm estimate of 2.975 mm, shown in Figure 110, is a poor-to-fair match to the measured data. The measured data points seem to indicate a slight sinusoidal variation.

The main bridge was moved south, and the radiometer position shifted to measure the southwest portion of the oil target. It was believed that this portion had a thinner oil film.

A120EDCA.DAT – The algorithm estimate of 1.750 mm, shown in Figure 111, is a fair match to the measured data based on the mean curve values. The measured data points have a slight sinusoidal variation.

A120FDCA.DAT – The algorithm estimate of 2.135 mm, shown in Figure 112, is a good-to-excellent match to the measured data.

A120GDCA.DAT – The algorithm estimate of 2.400 mm, shown in Figure 113, is a good-to-excellent match to the measured data.

The main bridge was moved north to collect data from the northwest sector of the 1-mm diesel oil target. A visible gradient had formed, with this sector appearing to contain the thickest oil.

A110ADCA.DAT – The algorithm estimate of 1.675 mm, shown in Figure 114, is a poor match to the measured data. Three data points match; however the remaining points are above the theoretical estimate, with the curve exhibiting a shape that is not recognizable. The result is inconclusive.

A110BDCA.DAT – The algorithm estimate of 1.675 mm, shown in Figure 115, is a poor match to the measured data. All the measured points are above the theoretical estimate, with the curve exhibiting a shape that is not recognizable. The result is inconclusive.

A110CDCA.DAT – The algorithm estimate of 1.700 mm, shown in Figure 116, is a fair match to the measured data. The smoothed curve exhibits a shape that is not recognizable; however, the mean temperature of the curve is a good match to the estimate.

A110DDCA.DAT – The algorithm estimate of 1.775 mm, shown in Figure 117, is a poor-to-fair match to the measured data. The smoothed curve exhibits a shape that is not recognizable; however, the mean temperature of the curve is a good match to the estimate.

The main bridge was moved a few feet south, and the containment area was moved a few feet east. Measurements were taken from the southwest sector of the oil target, which was presumably a thinner oil film.

A110EDCA.DAT – The algorithm estimate of 0.725 mm, shown in Figure 118, is a good match to the measured data.

A110FDCA.DAT – The algorithm estimate of 0.825 mm, shown in Figure 119, is a fair-to-good match to the measured data.

A110GDCA.DAT – The algorithm estimate of 0.800 mm, shown in Figure 120, is a fair-to-good match to the measured data.

A110HDCA.DAT – The algorithm estimate of 0.525 mm, shown in Figure 121, is a fair match to the measured data.

The main bridge was moved north to the 0.5-mm diesel oil target. The oil on the eastern side was visibly thicker than the oil on the western side. Some small isolated areas appeared to have no oil coverage. Measurements were collected from the eastern (thicker) side.

A105ADCA.DAT – The algorithm estimate of 1.025 mm, shown in Figure 122, is a fair-to-good match to the measured data. A slight sinusoidal variation is observed.

A105BDCA.DAT – The algorithm estimate of 0.975 mm, shown in Figure 123, is a good-to-excellent match to the measured data.

A105ADCA.DAT – The algorithm estimate of 1.000 mm, shown in Figure 124, is a fair-to-good match to the measured data. A slight sinusoidal variation is observed.

The main bridge was moved south and the radiometer repositioned to measure the western side (thinner area) of the target pool.

A105DDCA.DAT – The algorithm estimate of 0.700 mm, shown in Figure 125, is a fair match to the measured data. A sinusoidal variation is observed.

A105EDCA.DAT – The algorithm estimate of 0.000 mm, shown in Figure 126, is a poor-to-fair match to the measured data. A slight sinusoidal variation is observed. The mean value of the measurement is below the reference water temperature, indicating instrument gain drift.

A105FDCA.DAT – The algorithm estimate of 0.000 mm, shown in Figure 127, is a poor match to the measured data. A slight sinusoidal variation is observed. The mean value of the measurement is below the reference water temperature, indicating instrument gain drifted.

A105GDCA.DAT – The algorithm estimate of 0.000 mm, shown in Figure 128, is a fair match to the measured data. A slight sinusoidal variation is observed.

A105HDCA.DAT – The algorithm estimate of 0.000 mm, shown in Figure 129, is a poor match to the measured data. A slight sinusoidal variation is observed. The mean value of the measurement is below the reference water temperature, indicating instrument gain drifted.

The radiometer position was shifted to measure data from the extreme southeast sector of the target pool. The wind had shifted the thickest oil to this sector of the target pool. Also contained in this measurement area is a sizable patch of scum (discolored oil).

A105JDCA.DAT – The algorithm estimate of 5.125 mm is a poor match to the measured data. The correlation-only estimate of 1.700 mm, shown in Figure 130, is also a poor match. A slight sinusoidal variation is observed. The result is inconclusive.

A105KDCA.DAT – The algorithm estimate of 0.625 mm, shown in Figure 131, is a fair match to the measured data. A slight sinusoidal variation is observed.

A105LDCA.DAT – The algorithm estimate of 0.375 mm, shown in Figure 132, is a poor match to the measured data. A slight sinusoidal variation is observed. The result is inconclusive.

A105MDCA.DAT – The algorithm estimate of 0.725 mm, shown in Figure 133, is a poor match to the measured data. A sinusoidal variation is observed. The result is inconclusive.

The main bridge was moved south to the water-only target. Measurements were taken from its center.

A100ADCA.DAT – This data set, shown in Figure 134, was chosen to be the water background reference.

A100BDCA.DAT – The algorithm estimate of 0.450 mm, shown in Figure 135, is a fair match to the measured data.

A100CDCA.DAT – The algorithm estimate of 0.475 mm, shown in Figure 136, is a poor match to the measured data. A sinusoidal variation is observed.

A100DDCA.DAT – The algorithm estimate of 0.175 mm, shown in Figure 137, is a poor-to-fair match to the measured data. A sinusoidal variation is observed.

The main bridge was moved south to measure a target of unknown thickness composed of Hydrocal and diesel. The target had a moussey-looking patch, and a dark (presumably thick oil) patch all surrounded by a thinner oil film. The radiometer position was shifted to measure the thinner oil surrounding the dark patch.

A1XXAMCA.DAT – The algorithm estimate of 0.600 mm, shown in Figure 138, is a fair match to the measured data.

A1XXBMCA.DAT – The algorithm estimate of 0.675 mm, shown in Figure 139, is a fair match to the measured data.

A1XXCMCA.DAT – The algorithm estimate of 0.800 mm, shown in Figure 140, is a fair-to-good match to the measured data.

The radiometer position was shifted to measure the dark patch of oil.

A1XXDMCA.DAT – The algorithm estimate of 1.025 mm, shown in Figure 141, is a fair-to-good match to the measured data.

A1XXEMCA.DAT – The algorithm estimate of 1.000 mm, shown in Figure 142, is a fair match to the measured data.

A1XXFMCA.DAT – The algorithm estimate of 1.025 mm, shown in Figure 143, is a fair-to-good match to the measured data.

The radiometer position was shifted to measure the moussey oil patch.

A1XXGMCA.DAT – The algorithm estimate of 1.075 mm, shown in Figure 144, is a good match to the measured data.

A1XXHMCA.DAT – The algorithm estimate of 1.075 mm, shown in Figure 145, is a good match to the measured data.

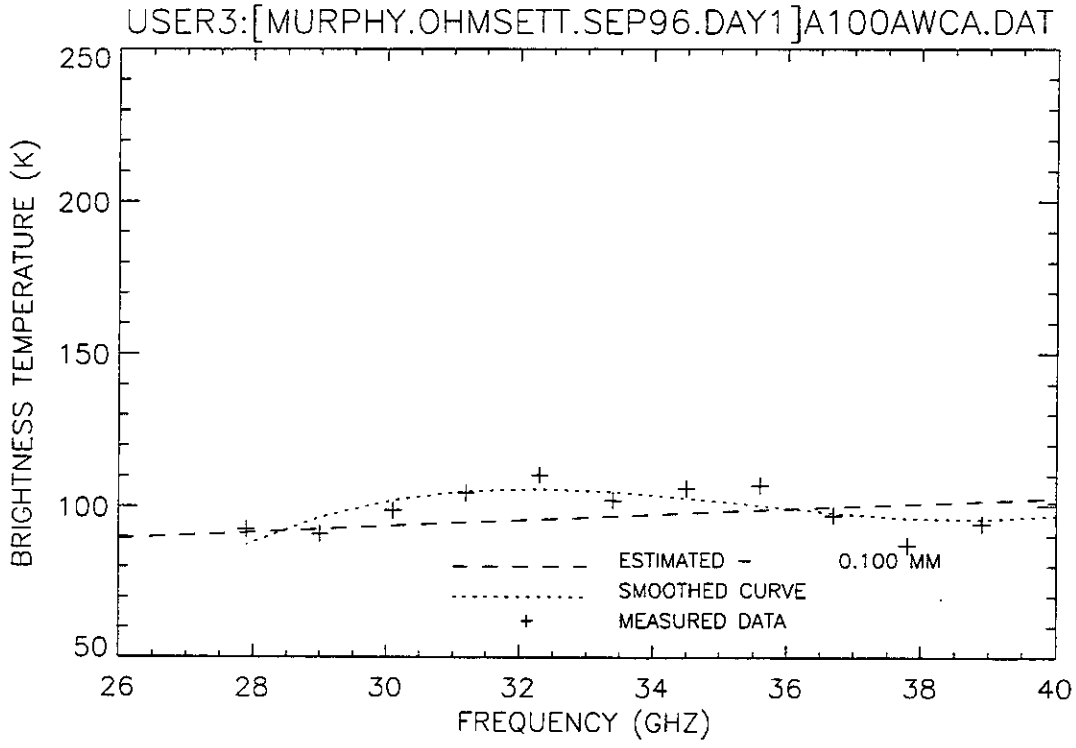

Figure 85. Plot of radiometric brightness temperature versus measurement frequency for water, day 1 test, calm wave conditions, 11 September 1996, sweep A.

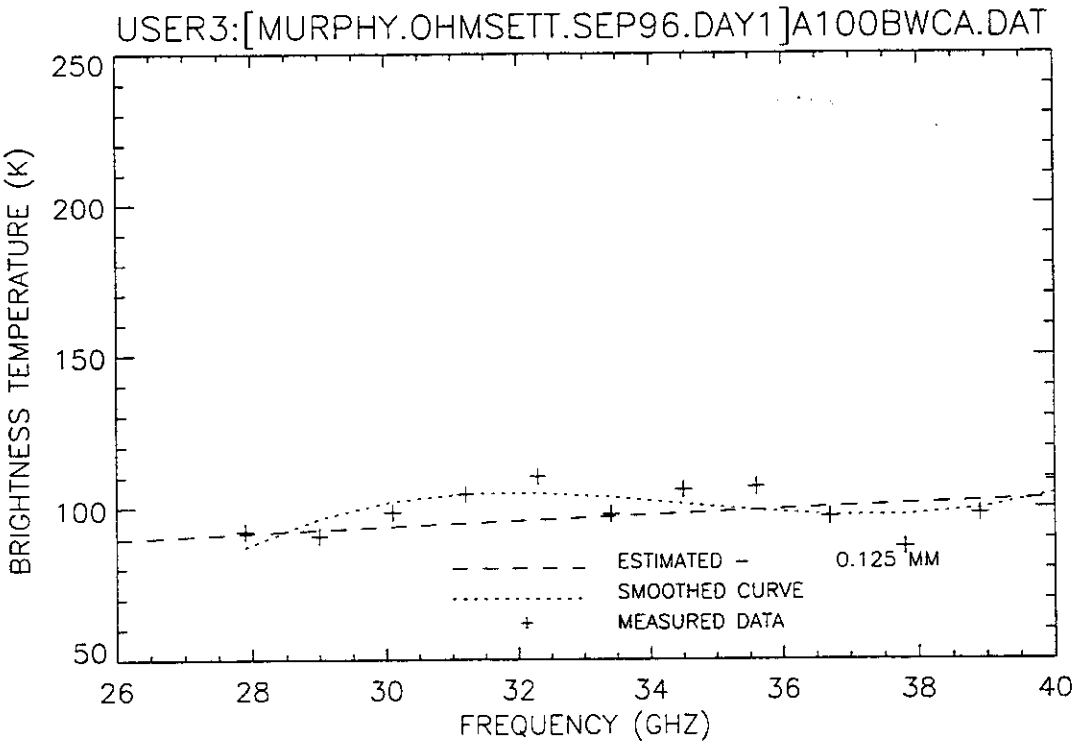

Figure 86. Plot of radiometric brightness temperature versus measurement frequency for water, day 1 test, calm wave conditions, 11 September 1996, sweep B.

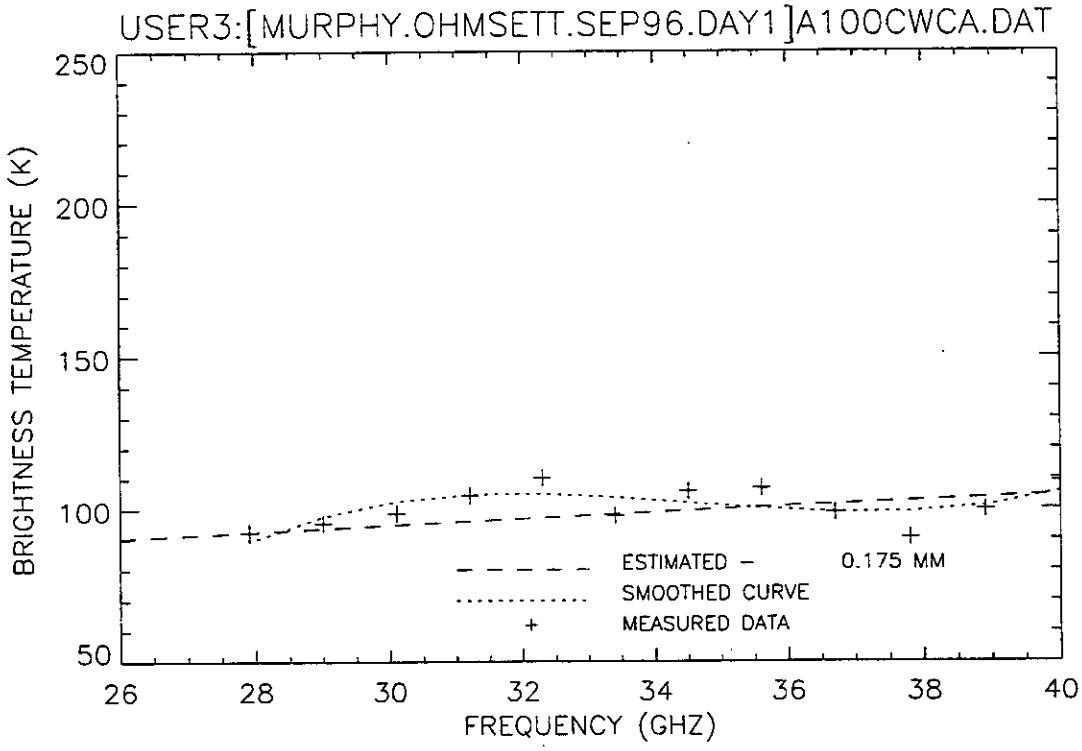

Figure 87. Plot of radiometric brightness temperature versus measurement frequency for water, day 1 test, calm wave conditions, 11 September 1996, sweep C.

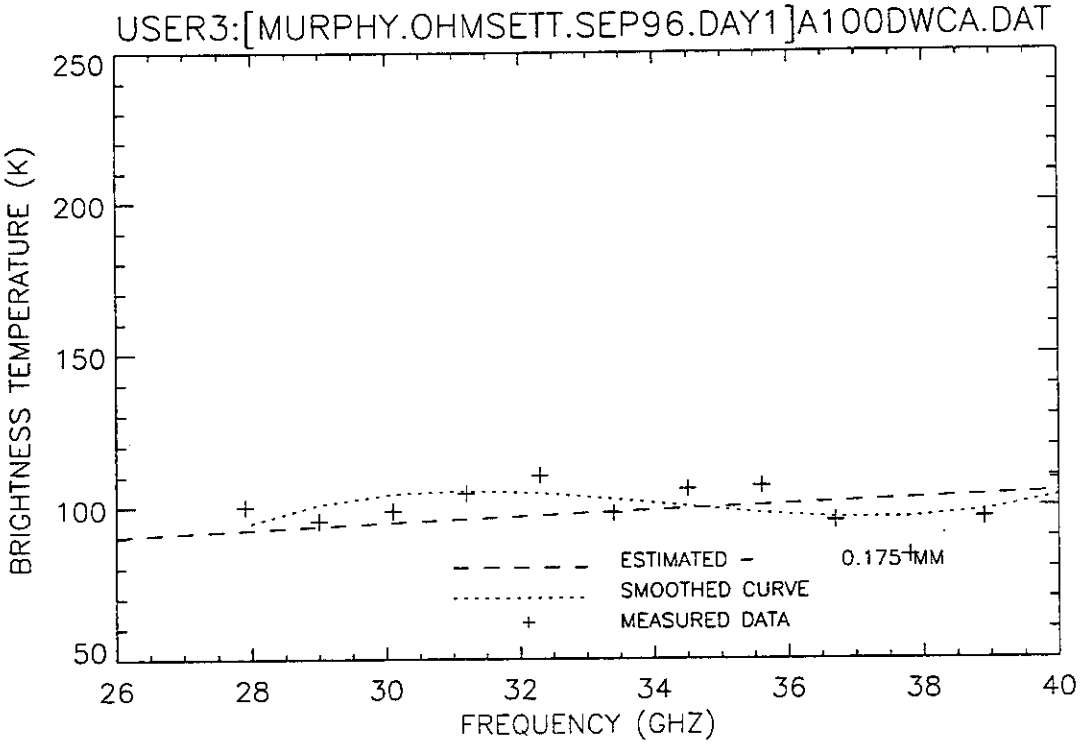

Figure 88. Plot of radiometric brightness temperature versus measurement frequency for water, day 1 test, calm wave conditions, 11 September 1996, sweep D.

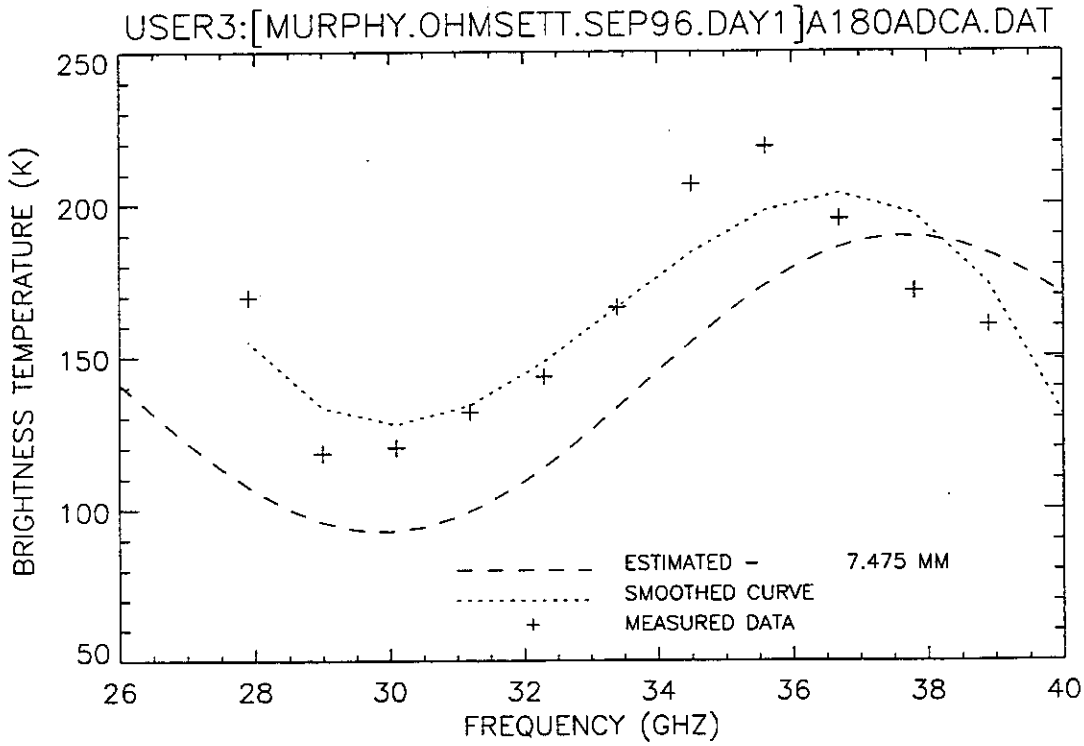

Figure 89. Plot of radiometric brightness temperature versus measurement frequency for 8-mm diesel oil, day 1 test, calm wave conditions, 11 September 1996, sweep A.

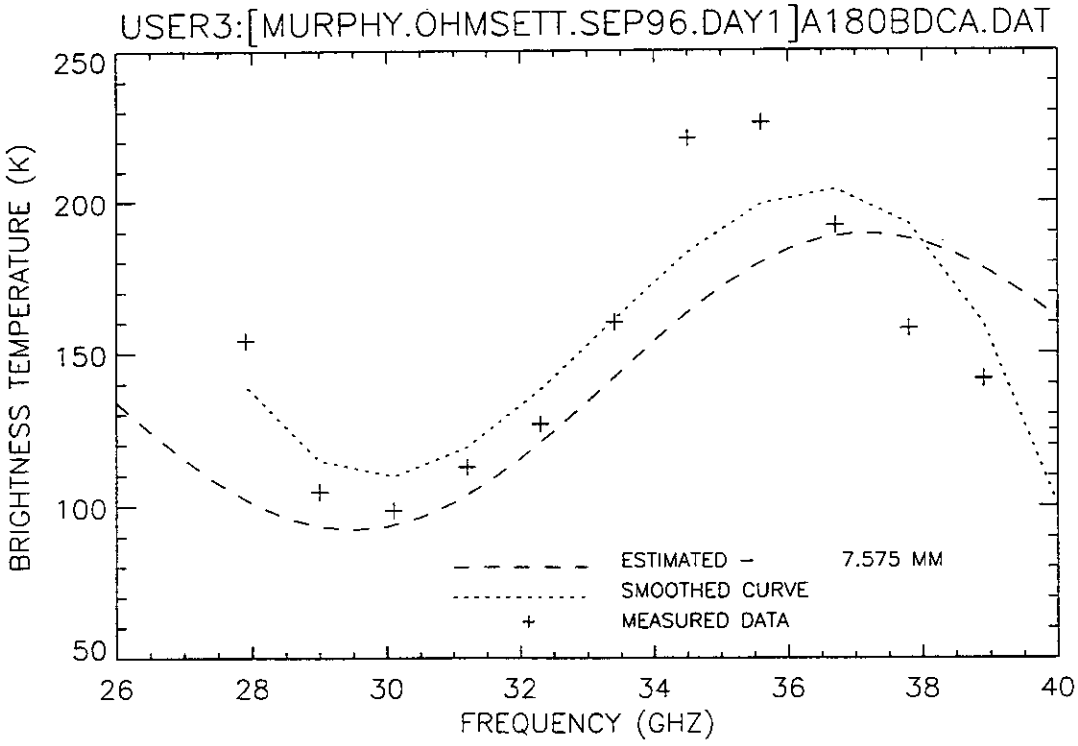

Figure 90. Plot of radiometric brightness temperature versus measurement frequency for 8-mm diesel oil, day 1 test, calm wave conditions, 11 September 1996, sweep B.

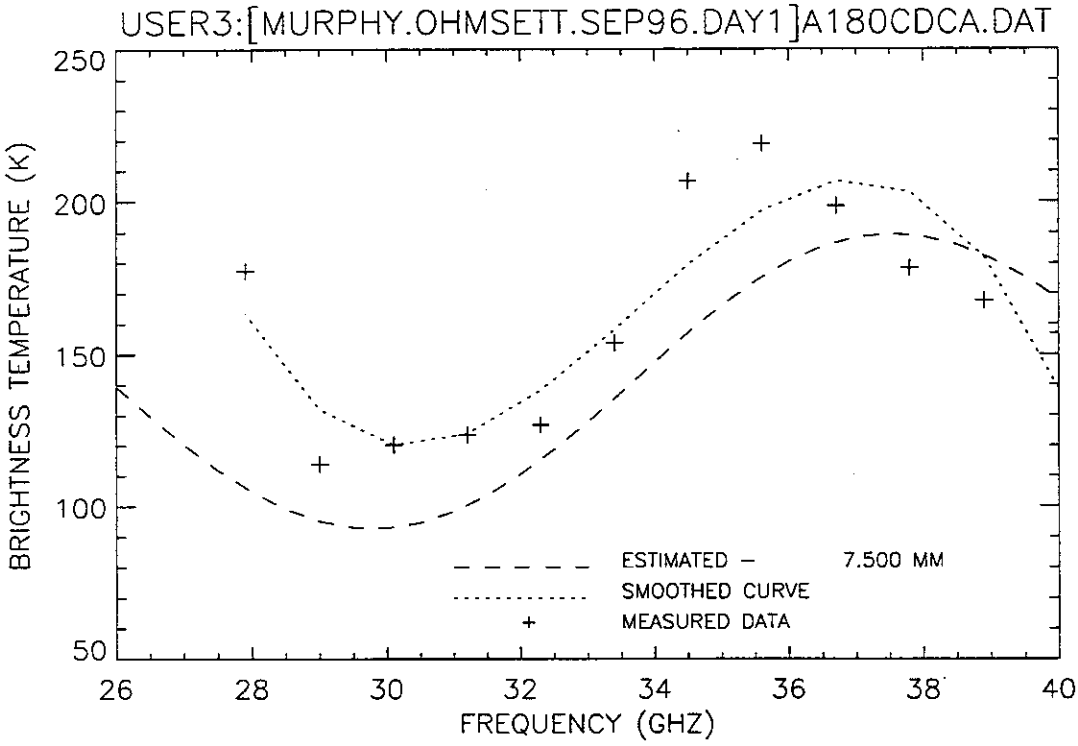

Figure 91. Plot of radiometric brightness temperature versus measurement frequency for 8-mm diesel oil, day 1 test, calm wave conditions, 11 September 1996, sweep C.

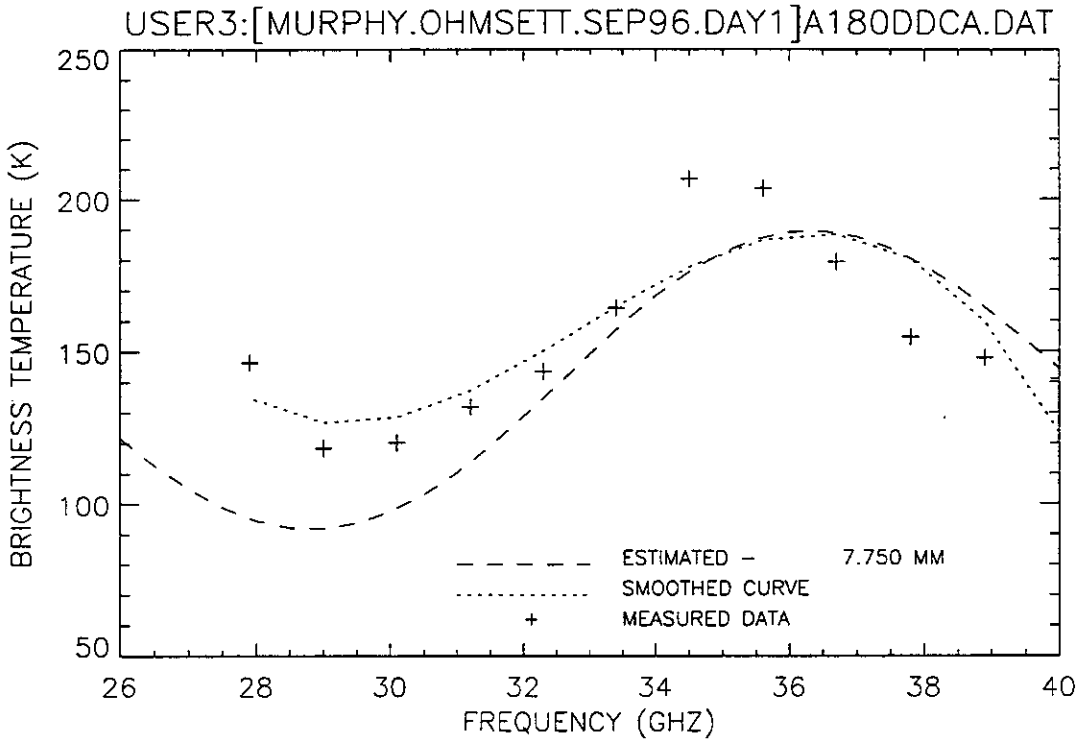

Figure 92. Plot of radiometric brightness temperature versus measurement frequency for 8-mm diesel oil, day 1 test, calm wave conditions, 11 September 1996, sweep D.

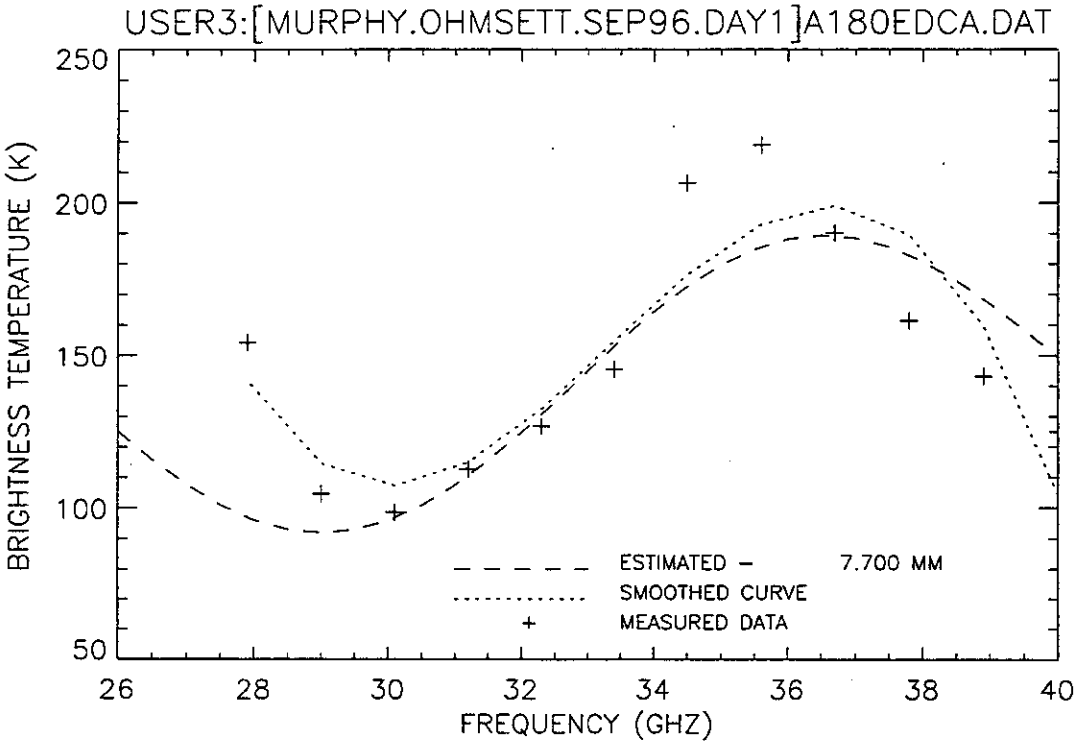

Figure 93. Plot of radiometric brightness temperature versus measurement frequency for 8-mm diesel oil, day 1 test, calm wave conditions, 11 September 1996, sweep E.

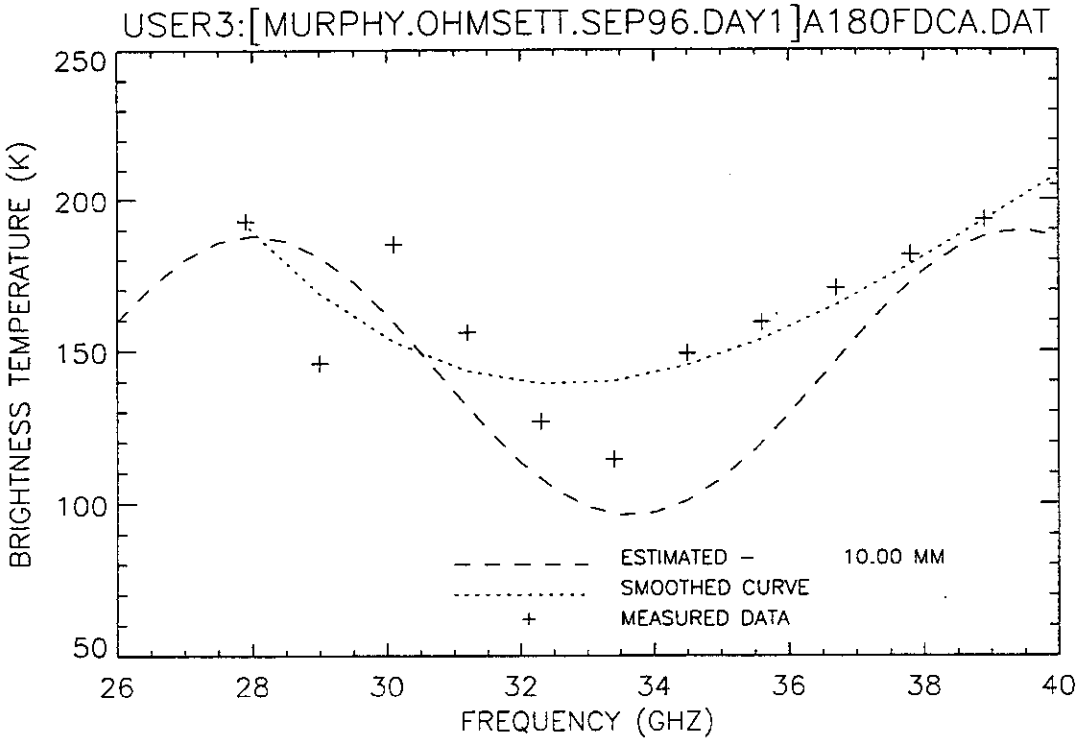

Figure 94. Plot of radiometric brightness temperature versus measurement frequency for 8-mm diesel oil, day 1 test, calm wave conditions, 11 September 1996, sweep F.

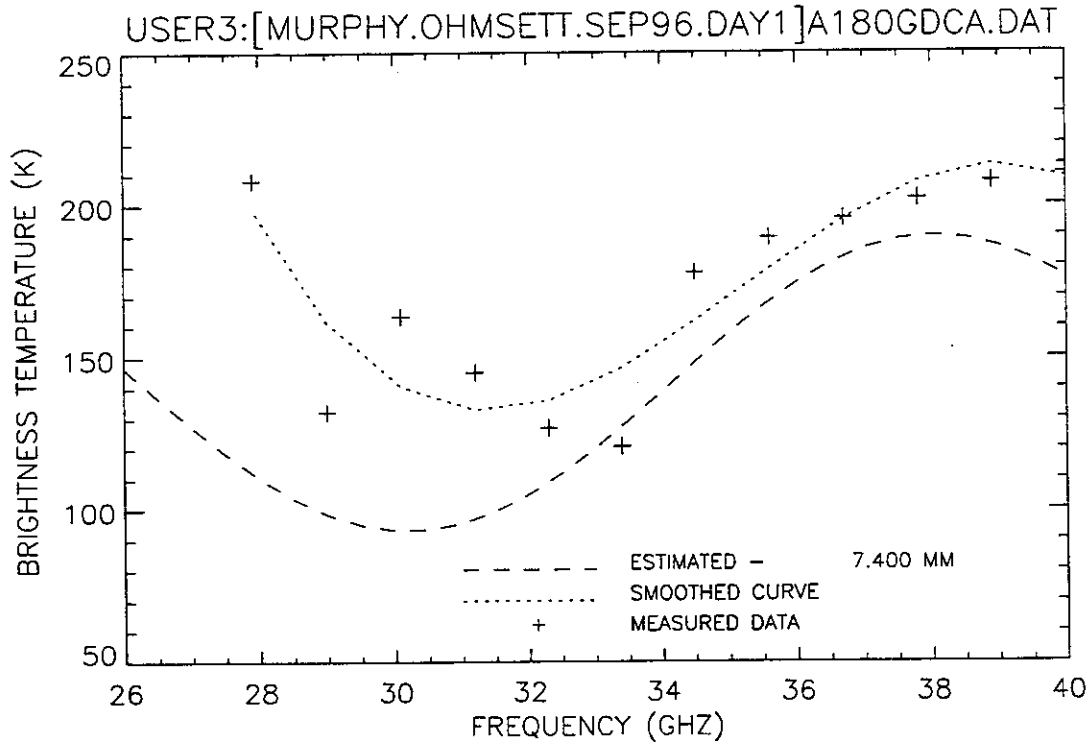

Figure 95. Plot of radiometric brightness temperature versus measurement frequency for 8-mm diesel oil, day 1 test, calm wave conditions, 11 September 1996, sweep G.

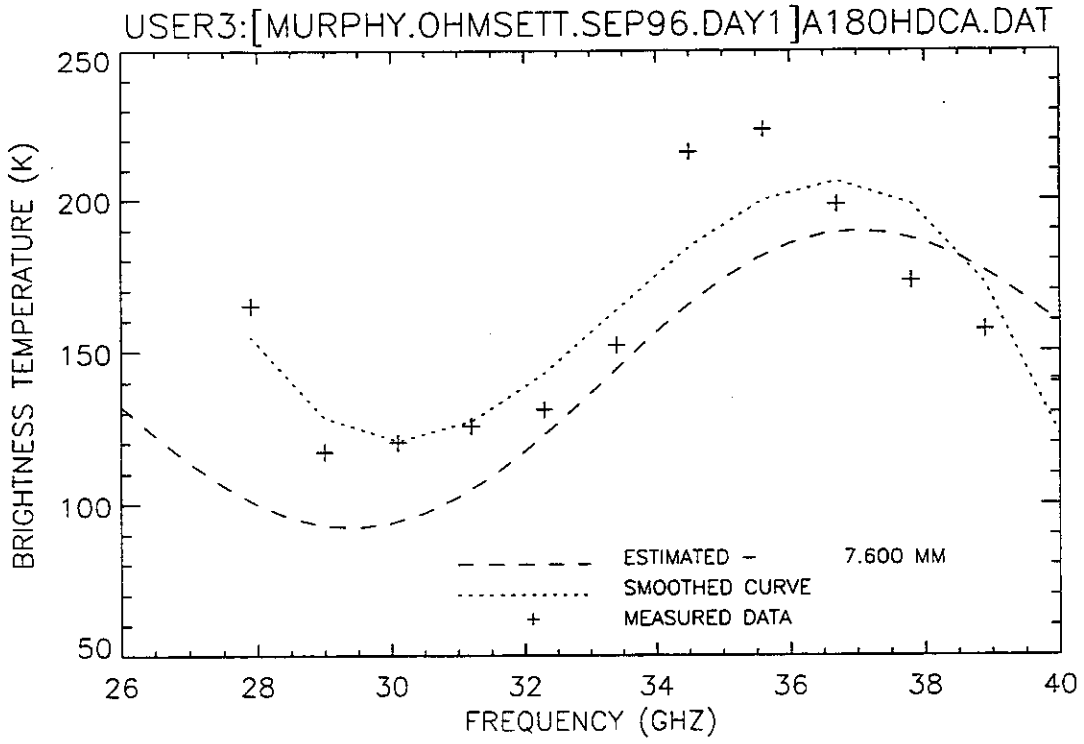

Figure 96. Plot of radiometric brightness temperature versus measurement frequency for 8-mm diesel oil, day 1 test, calm wave conditions, 11 September 1996, sweep H.

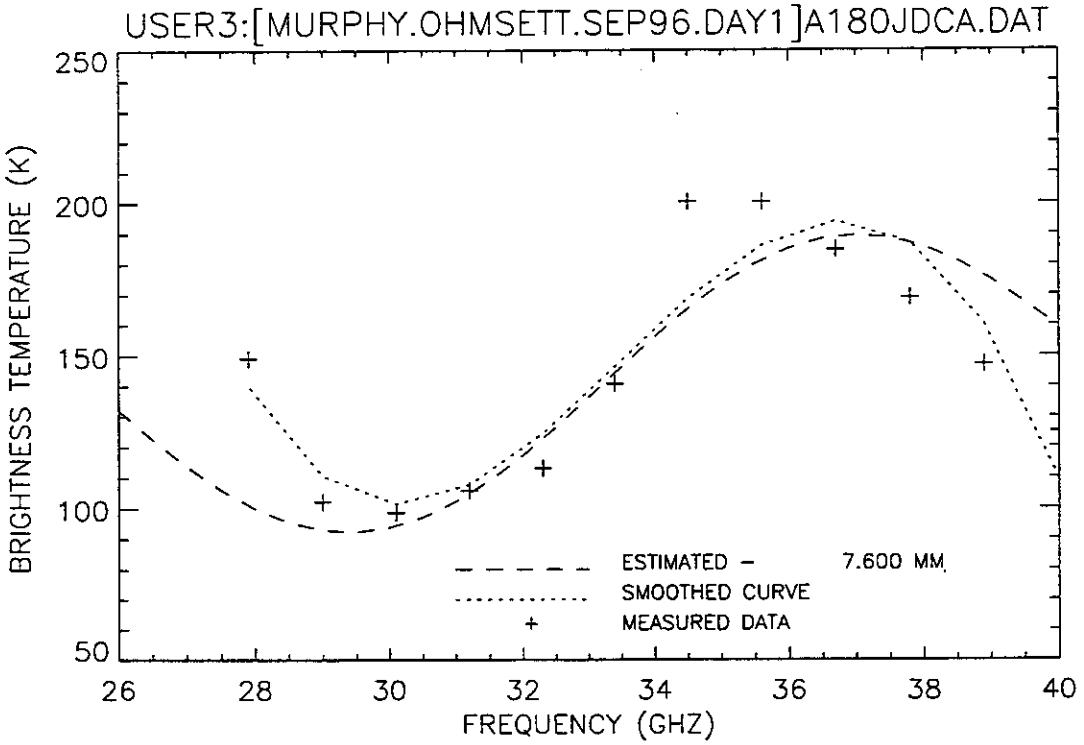

Figure 97. Plot of radiometric brightness temperature versus measurement frequency for 8-mm diesel oil, day 1 test, calm wave conditions, 11 September 1996, sweep J.

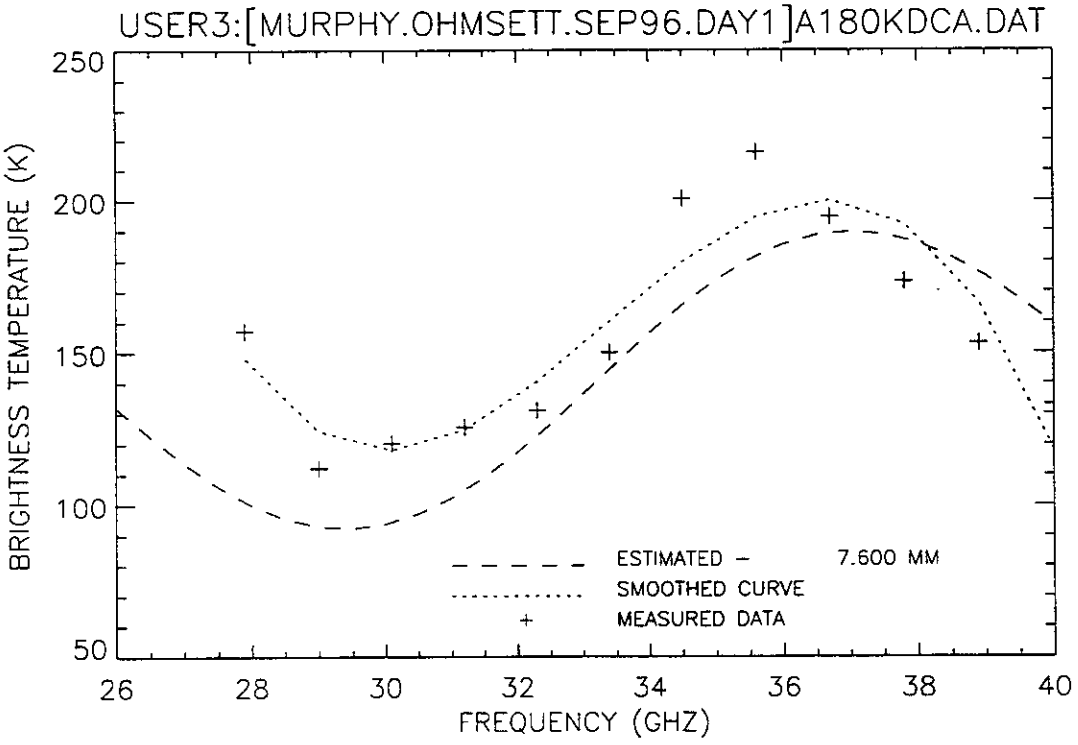

Figure 98. Plot of radiometric brightness temperature versus measurement frequency for 8-mm diesel oil, day 1 test, calm wave conditions, 11 September 1996, sweep K.

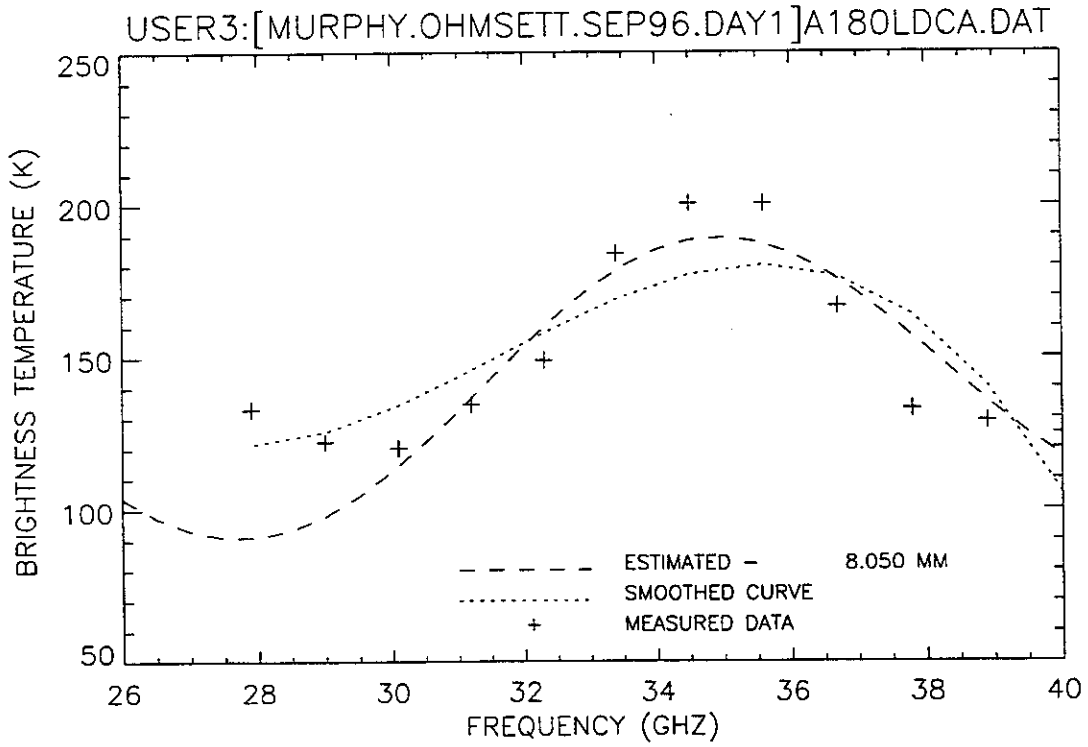

Figure 99. Plot of radiometric brightness temperature versus measurement frequency for 8-mm diesel oil, day 1 test, calm wave conditions, 11 September 1996, sweep L.

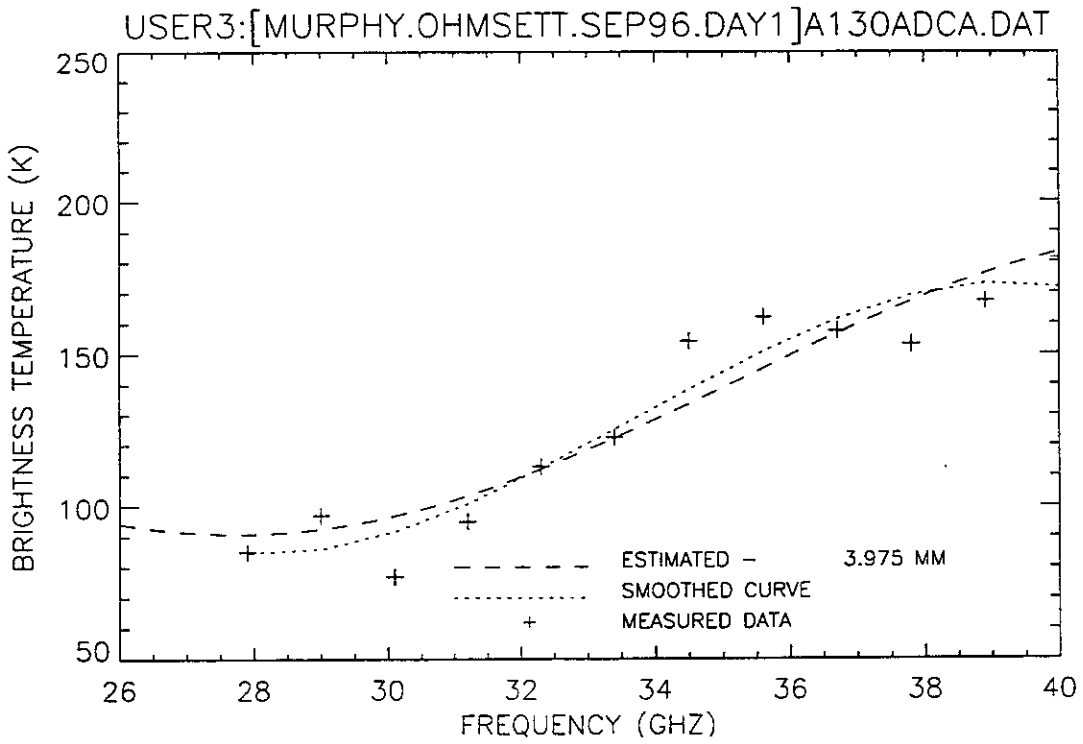

Figure 100. Plot of radiometric brightness temperature versus measurement frequency for 3-mm diesel oil, day 1 test, calm wave conditions, 11 September 1996, sweep A.

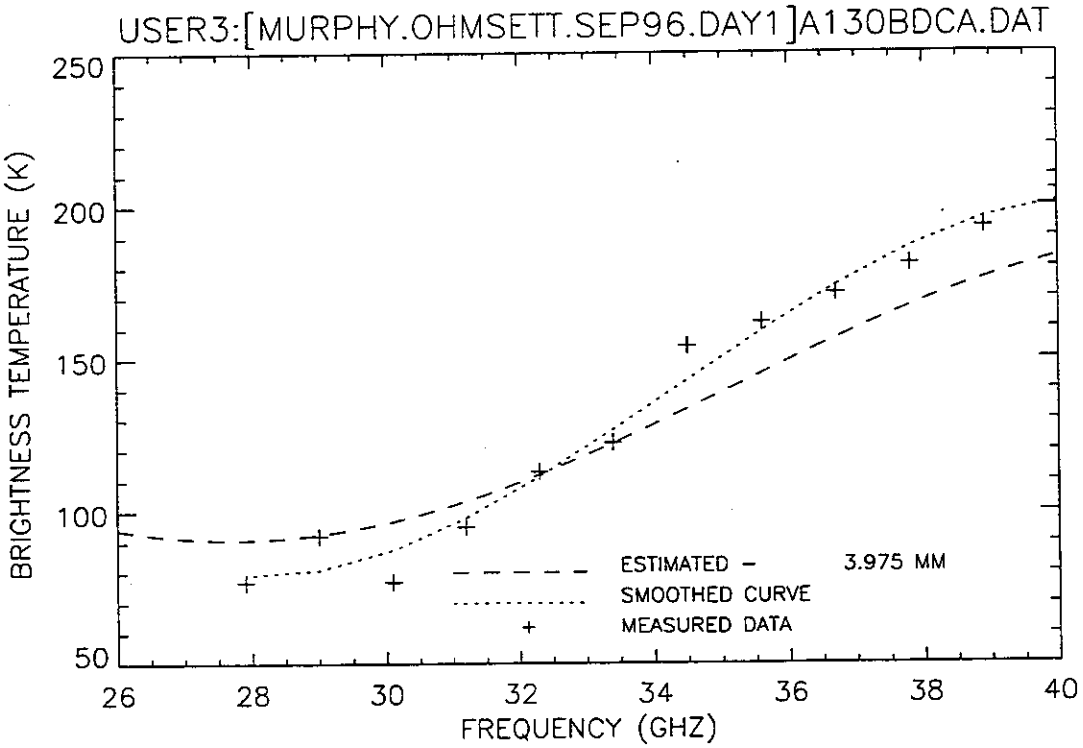

Figure 101. Plot of radiometric brightness temperature versus measurement frequency for 3-mm diesel oil, day 1 test, calm wave conditions, 11 September 1996, sweep B.

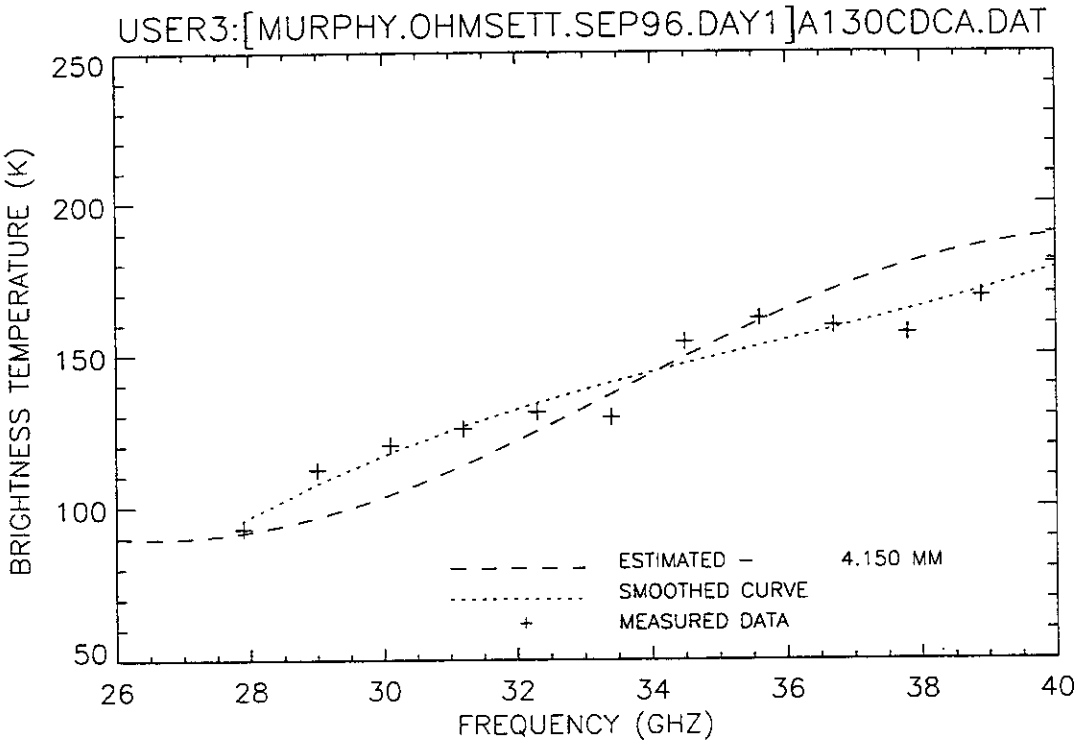

Figure 102. Plot of radiometric brightness temperature versus measurement frequency for 3-mm diesel oil, day 1 test, calm wave conditions, 11 September 1996, sweep C.

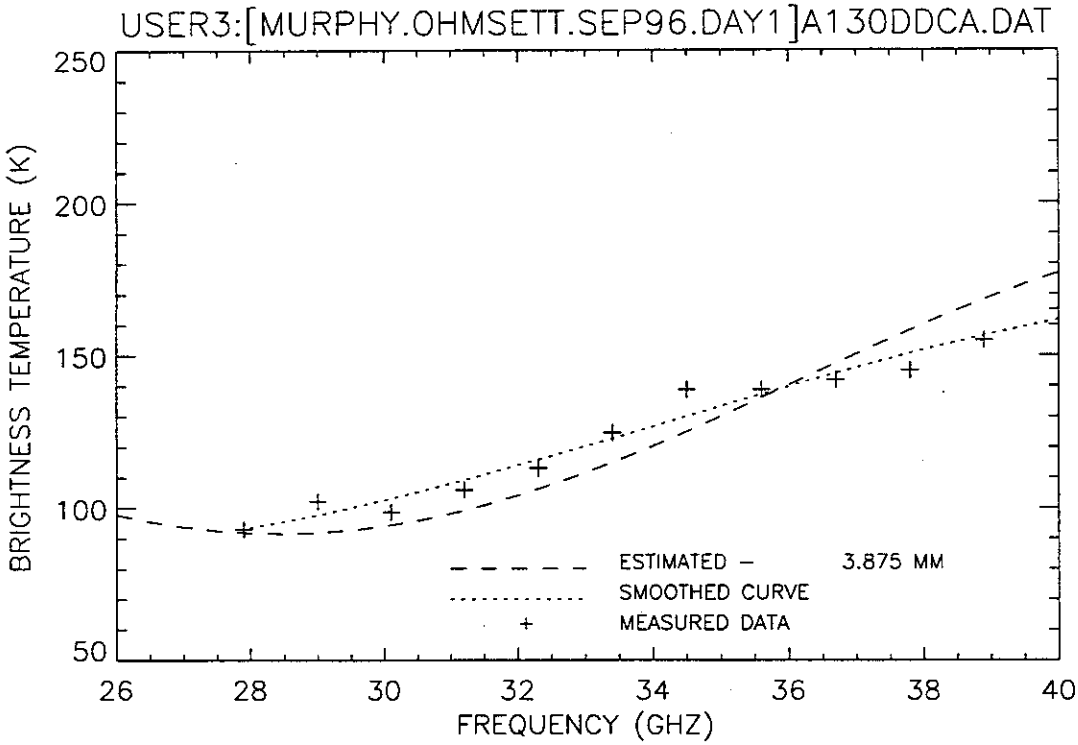

Figure 103. Plot of radiometric brightness temperature versus measurement frequency for 3-mm diesel oil, day 1 test, calm wave conditions, 11 September 1996, sweep D.

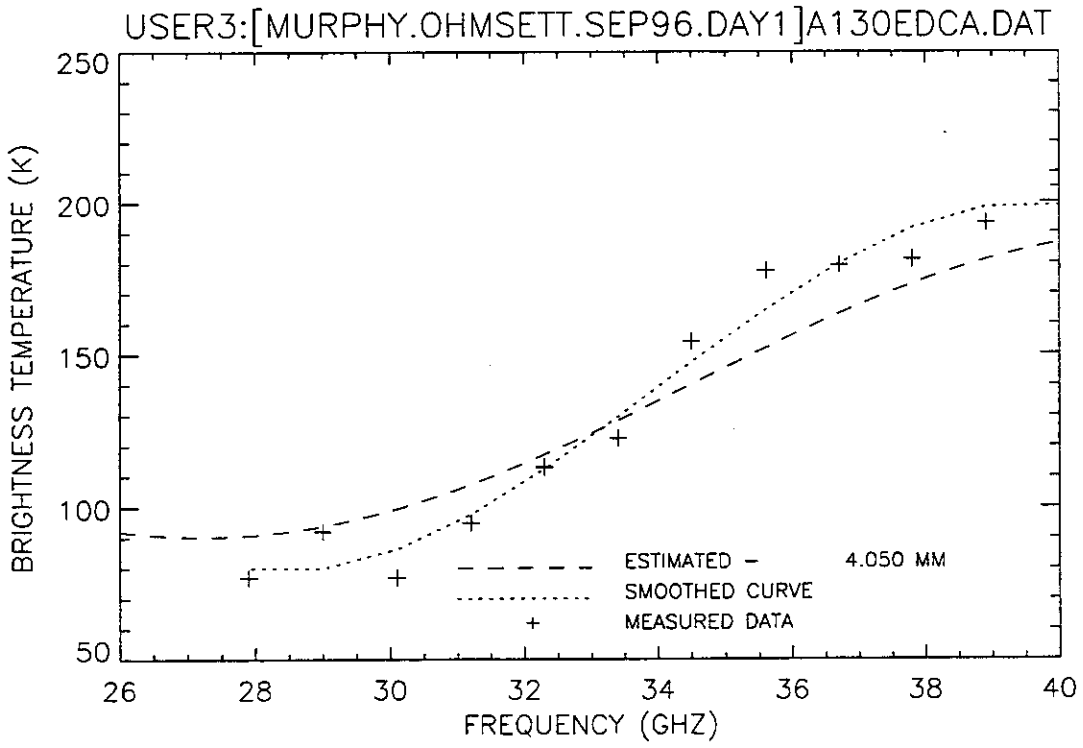

Figure 104. Plot of radiometric brightness temperature versus measurement frequency for 3-mm diesel oil, day 1 test, calm wave conditions, 11 September 1996, sweep E.

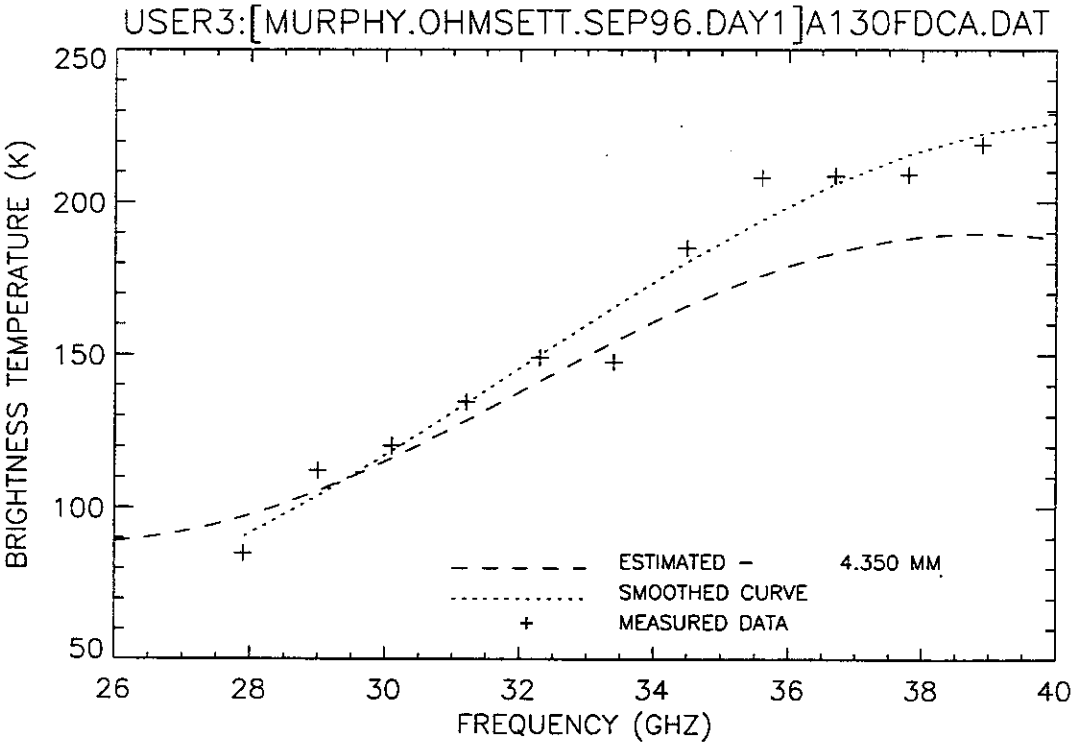

Figure 105. Plot of radiometric brightness temperature versus measurement frequency for 3-mm diesel oil, day 1 test, calm wave conditions, 11 September 1996, sweep F.

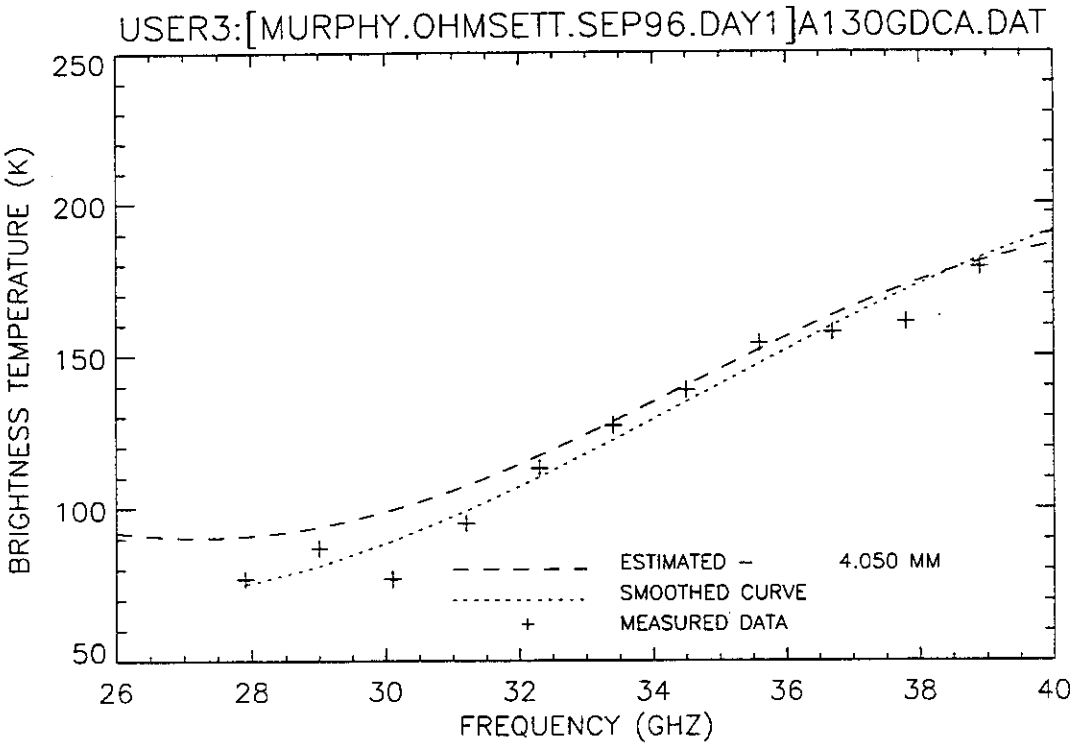

Figure 106. Plot of radiometric brightness temperature versus measurement frequency for 3-mm diesel oil, day 1 test, calm wave conditions, 11 September 1996, sweep G.

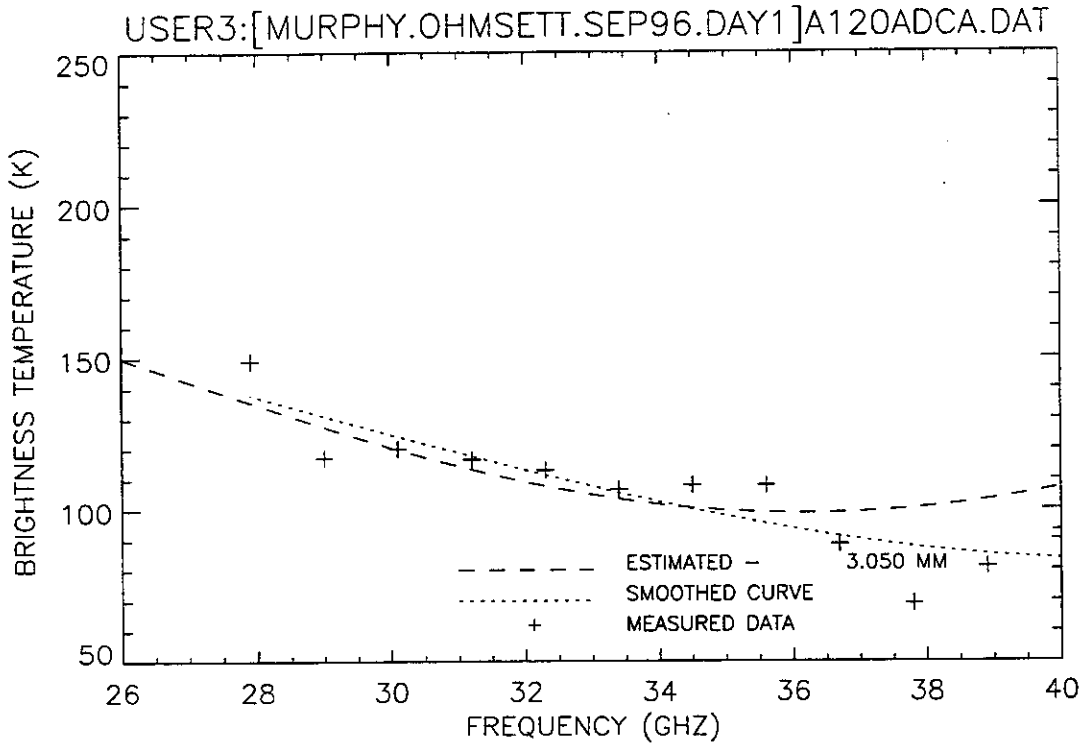

Figure 107. Plot of radiometric brightness temperature versus measurement frequency for 2-mm diesel oil, day 1 test, calm wave conditions, 11 September 1996, sweep A.

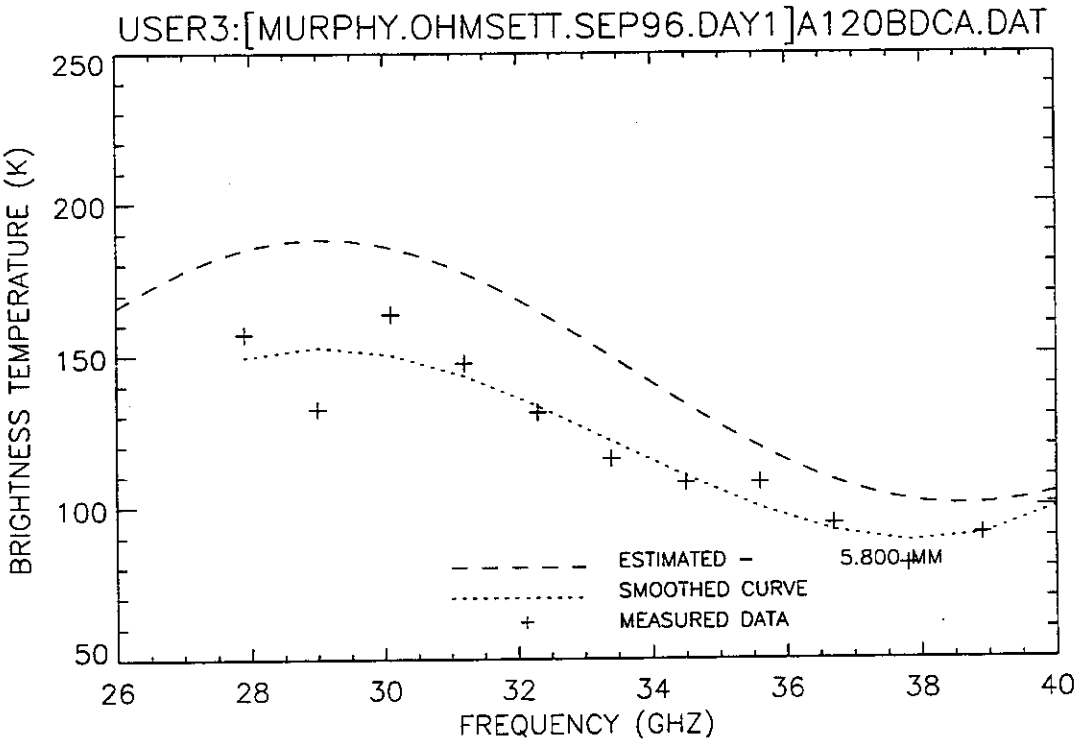

Figure 108. Plot of radiometric brightness temperature versus measurement frequency for 2-mm diesel oil, day 1 test, calm wave conditions, 11 September 1996, sweep B.

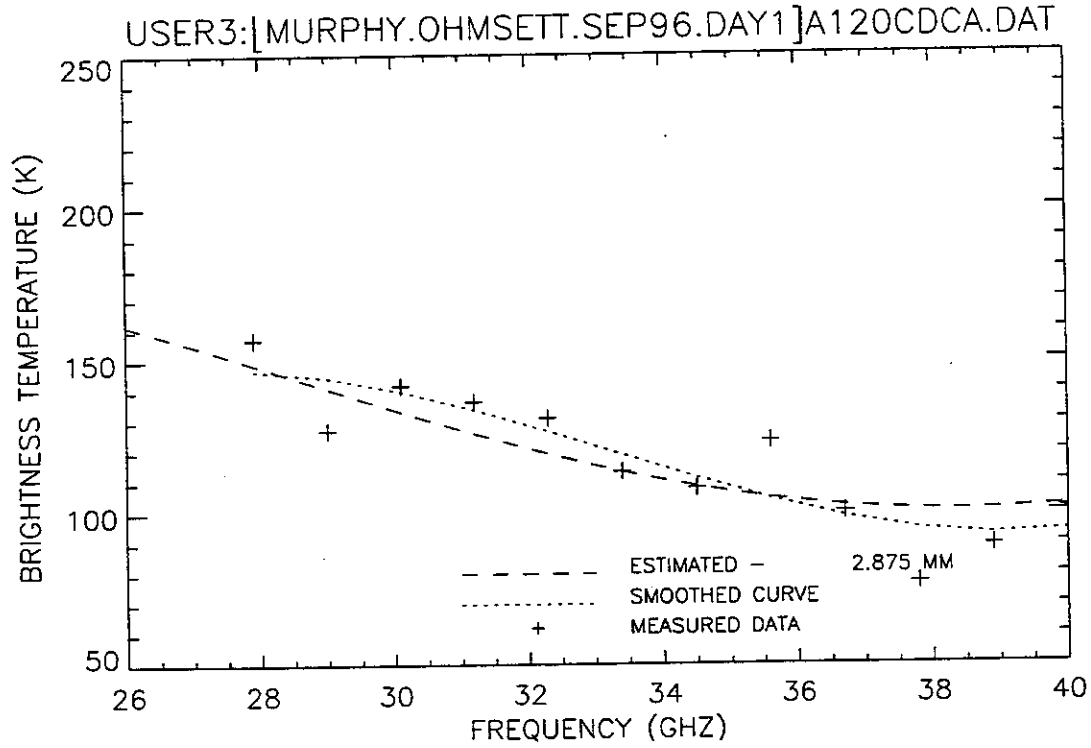

Figure 109. Plot of radiometric brightness temperature versus measurement frequency for 2-mm diesel oil, day 1 test, calm wave conditions, 11 September 1996, sweep C.

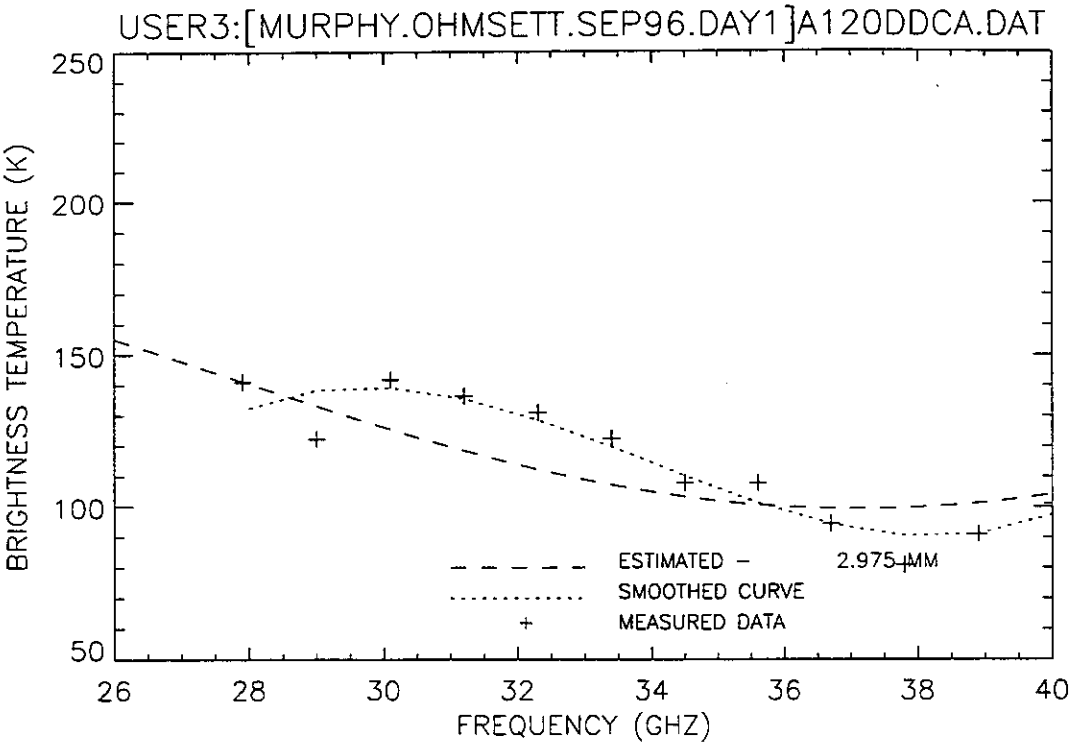

Figure 110. Plot of radiometric brightness temperature versus measurement frequency for 2-mm diesel oil, day 1 test, calm wave conditions, 11 September 1996, sweep D.

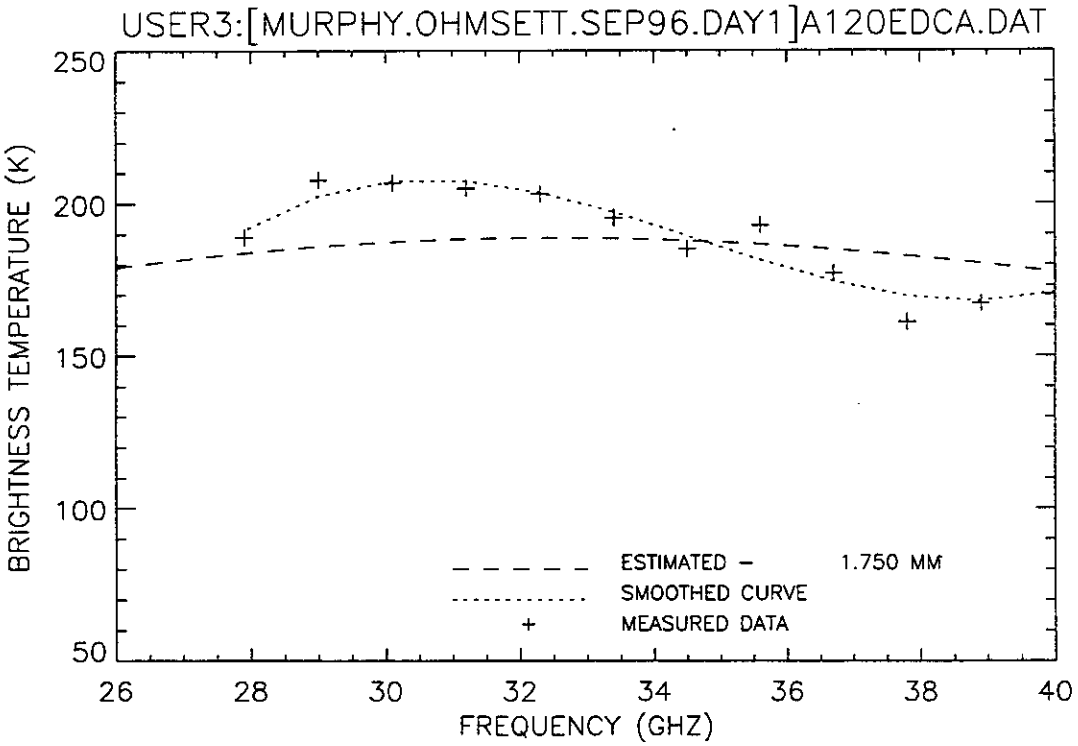

Figure 111. Plot of radiometric brightness temperature versus measurement frequency for 2-mm diesel oil, day 1 test, calm wave conditions, 11 September 1996, sweep E.

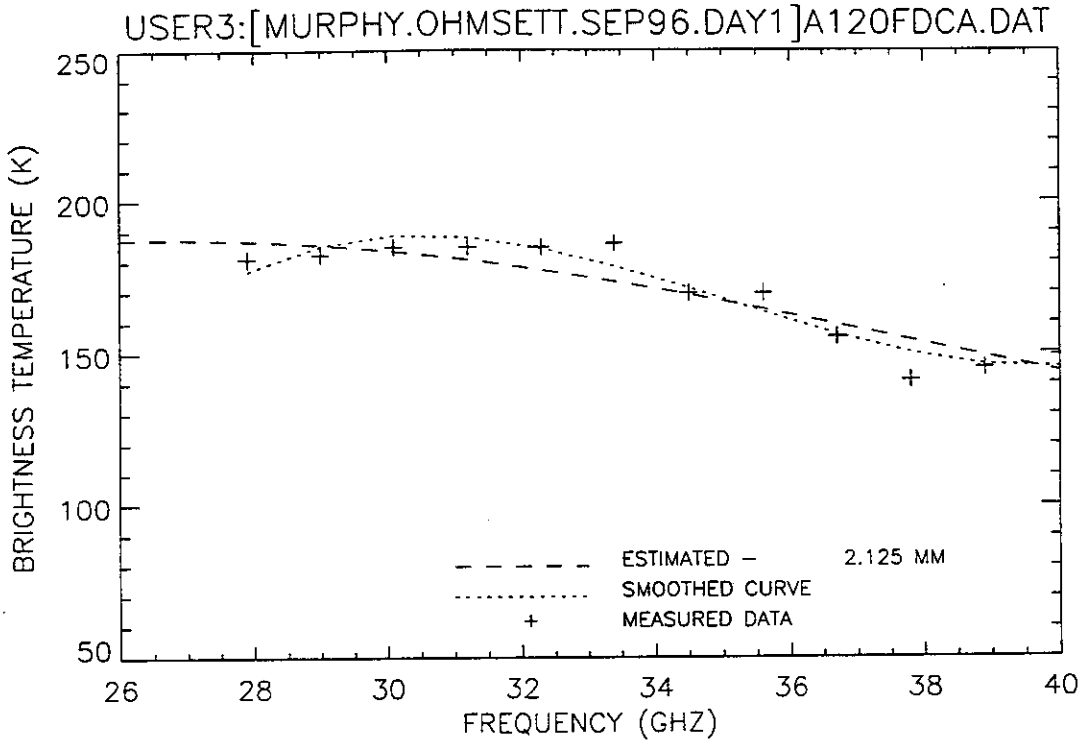

Figure 112. Plot of radiometric brightness temperature versus measurement frequency for 2-mm diesel oil, day 1 test, calm wave conditions, 11 September 1996, sweep F.

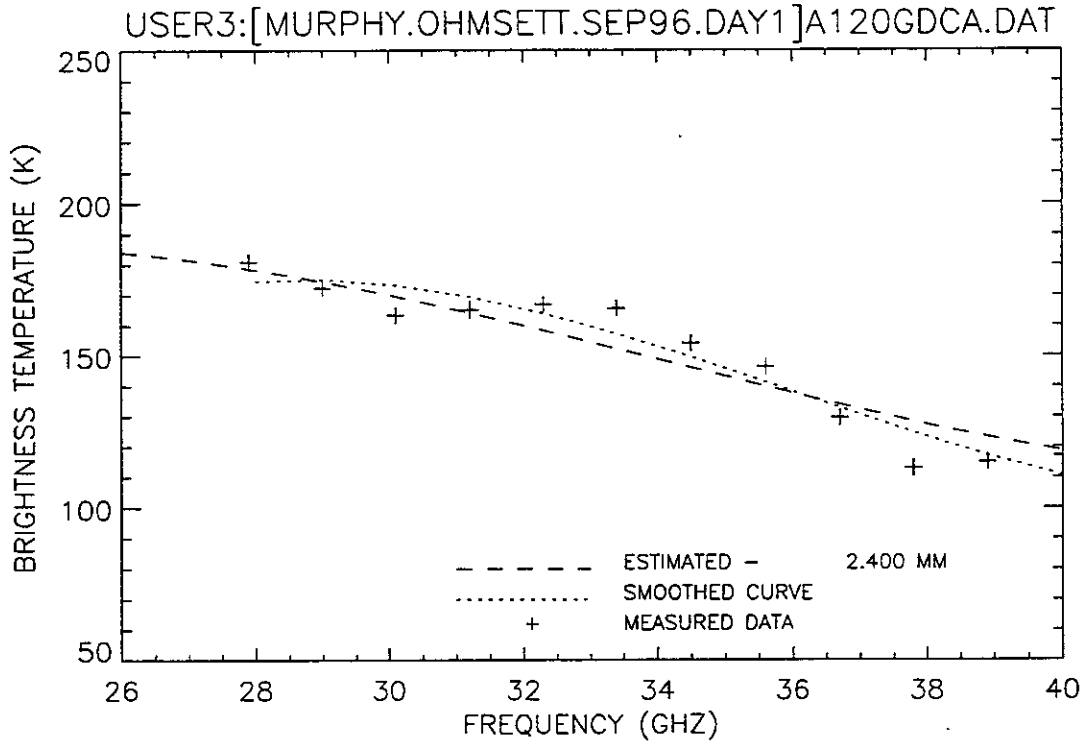

Figure 113. Plot of radiometric brightness temperature versus measurement frequency for 2-mm diesel oil, day 1 test, calm wave conditions, 11 September 1996, sweep G.

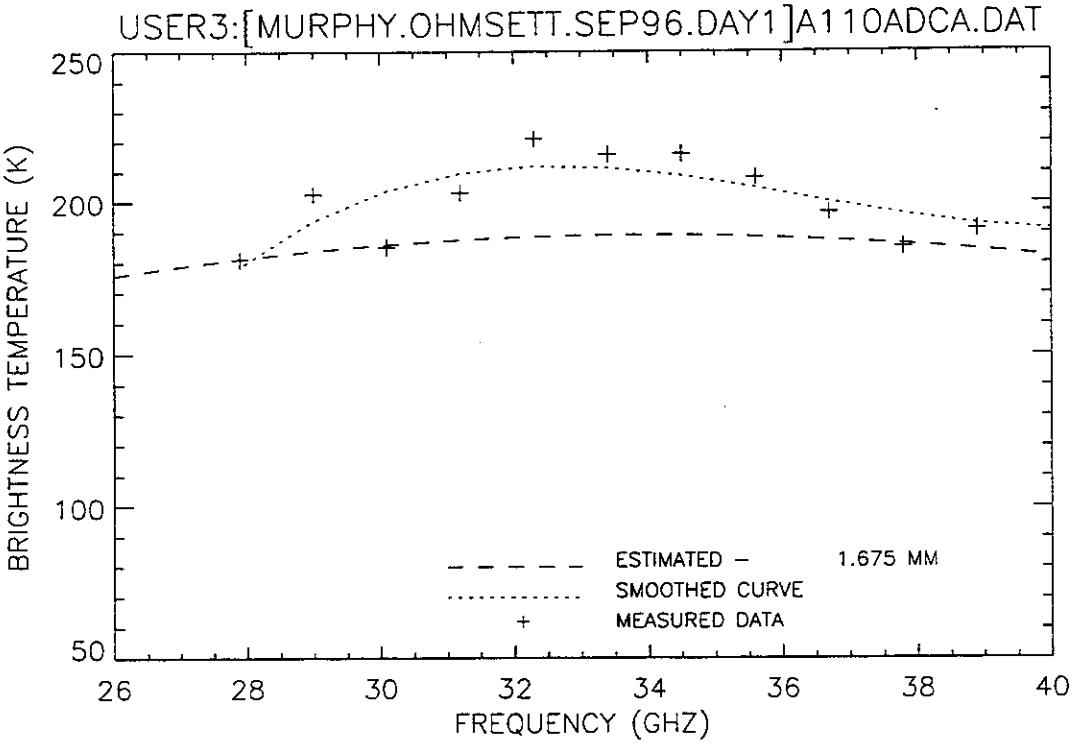

Figure 114. Plot of radiometric brightness temperature versus measurement frequency for 1-mm diesel oil, day 1 test, calm wave conditions, 11 September 1996, sweep A.

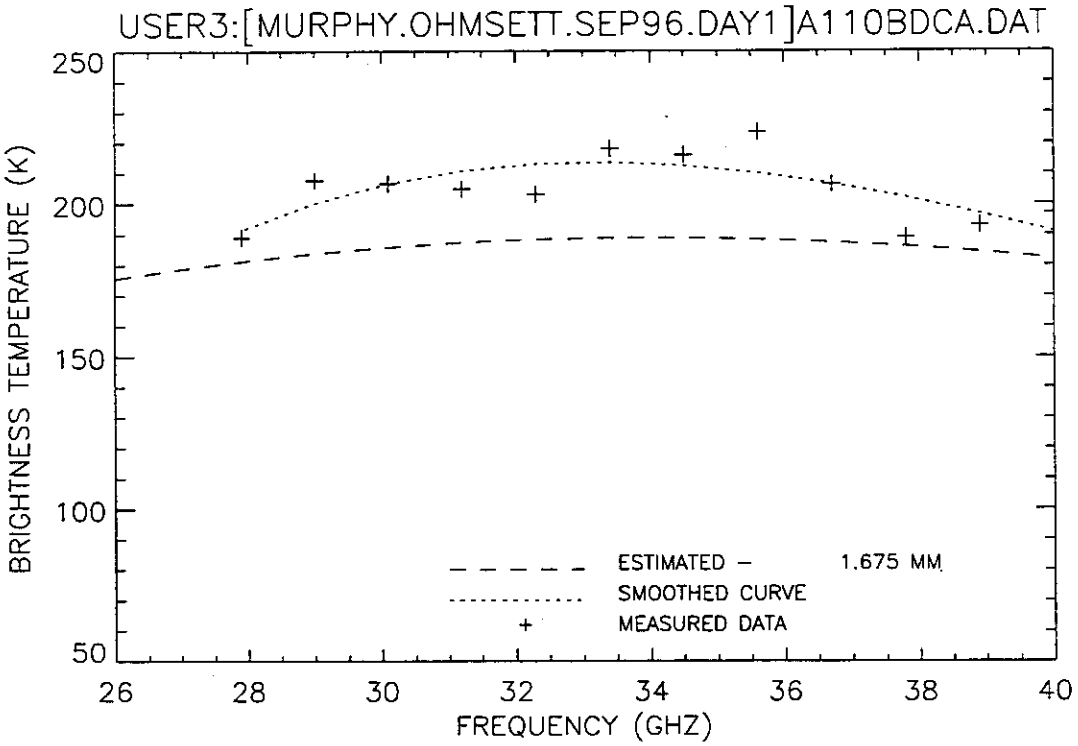

Figure 115. Plot of radiometric brightness temperature versus measurement frequency for 1-mm diesel oil, day 1 test, calm wave conditions, 11 September 1996, sweep B.

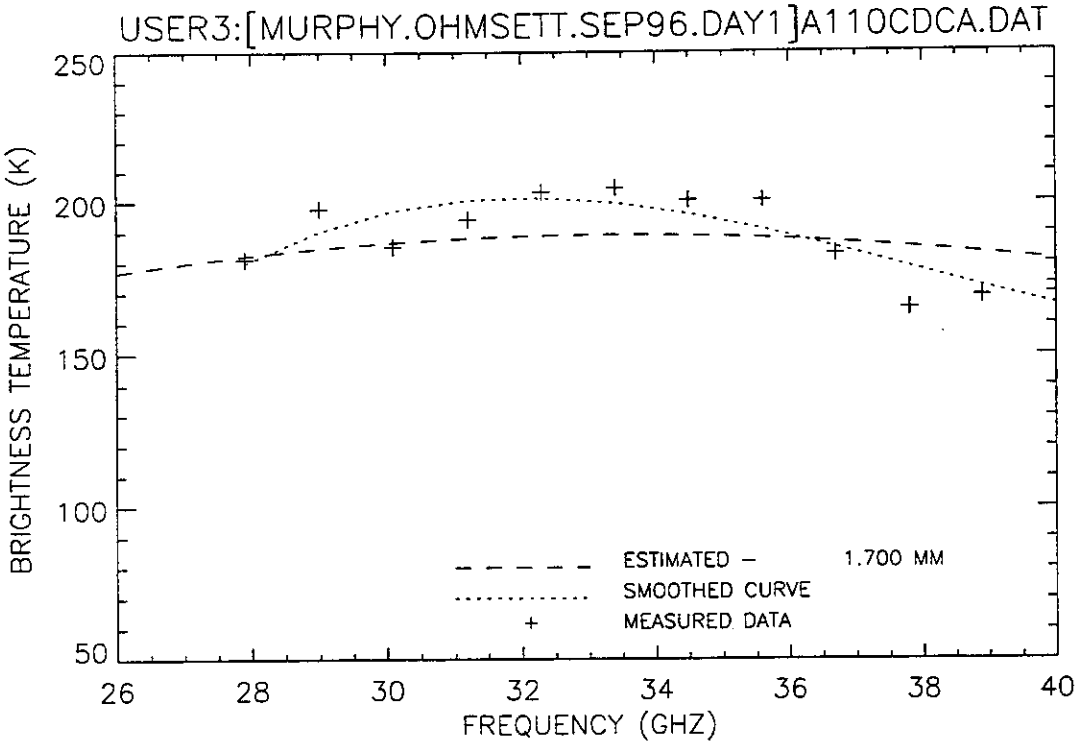

Figure 116. Plot of radiometric brightness temperature versus measurement frequency for 1-mm diesel oil, day 1 test, calm wave conditions, 11 September 1996, sweep C.

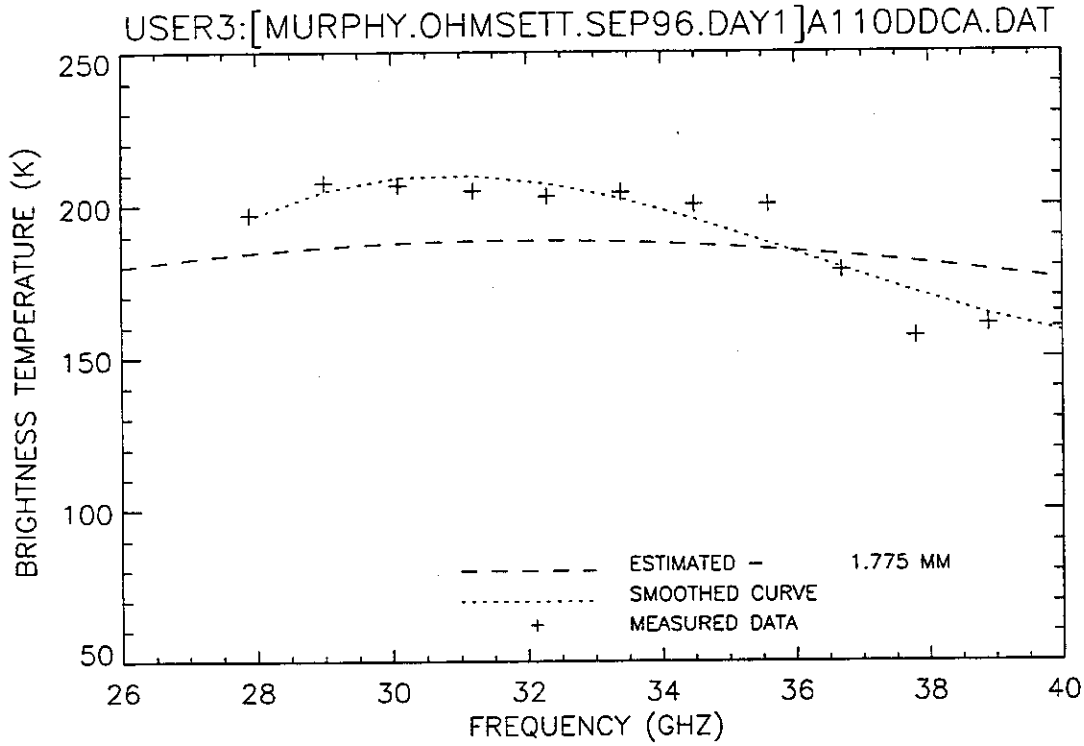

Figure 117. Plot of radiometric brightness temperature versus measurement frequency for 1-mm diesel oil, day 1 test, calm wave conditions, 11 September 1996, sweep D.

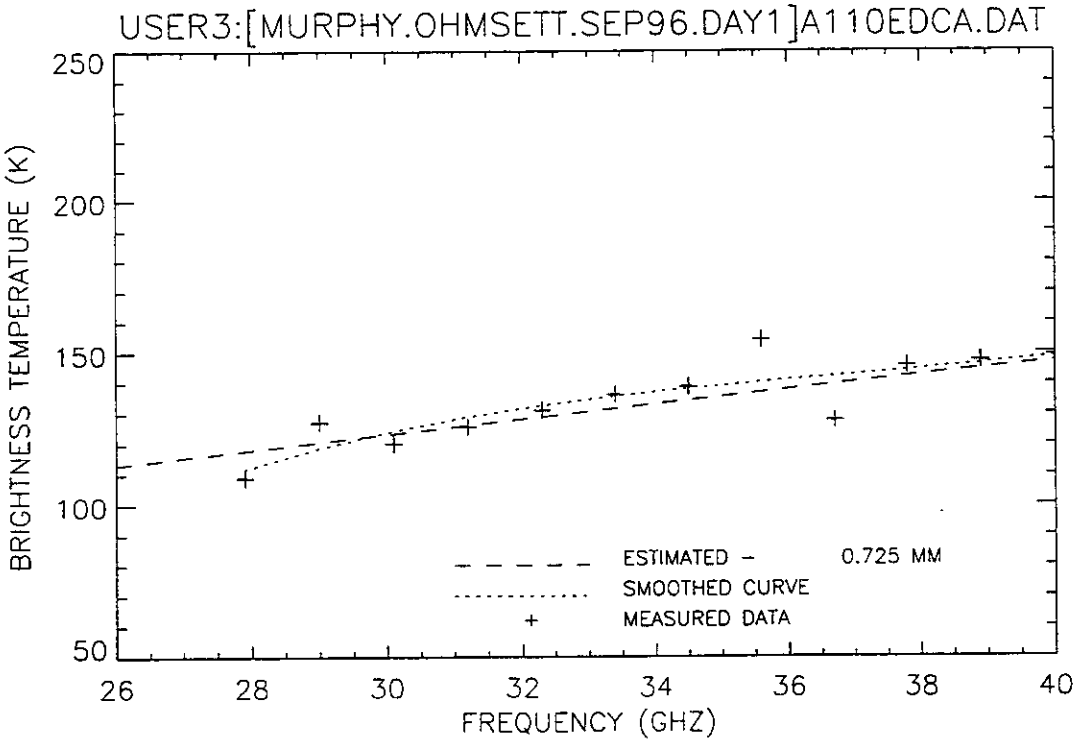

Figure 118. Plot of radiometric brightness temperature versus measurement frequency for 1-mm diesel oil, day 1 test, calm wave conditions, 11 September 1996, sweep E.

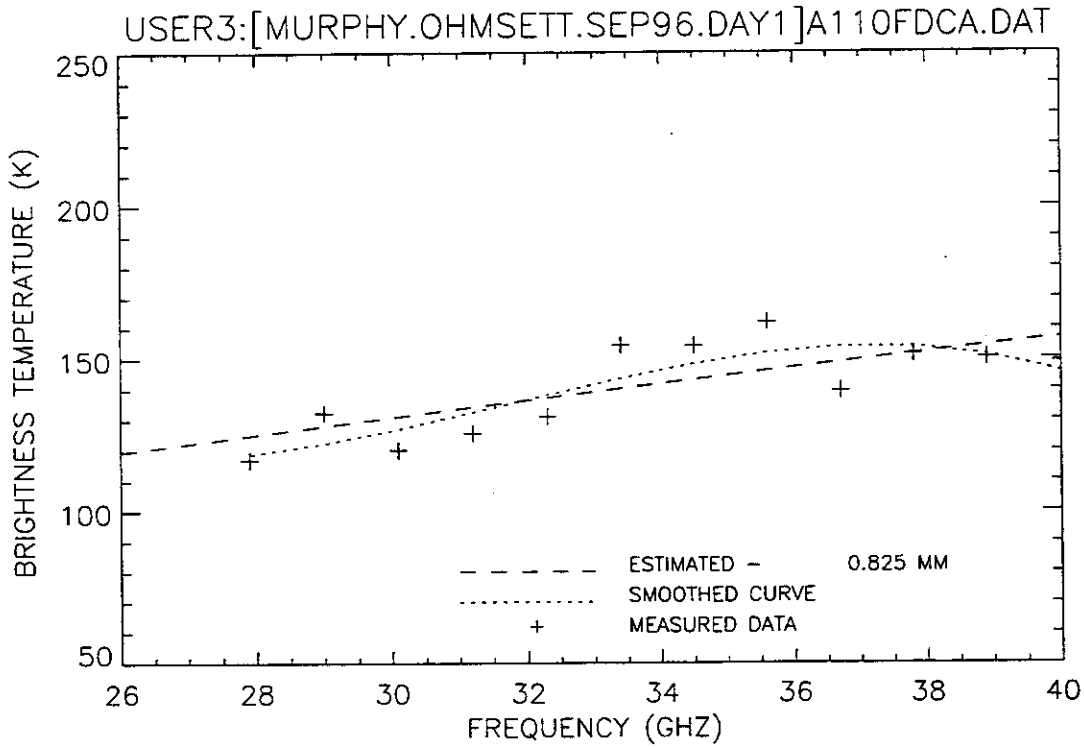

Figure 119. Plot of radiometric brightness temperature versus measurement frequency for 1-mm diesel oil, day 1 test, calm wave conditions, 11 September 1996, sweep F.

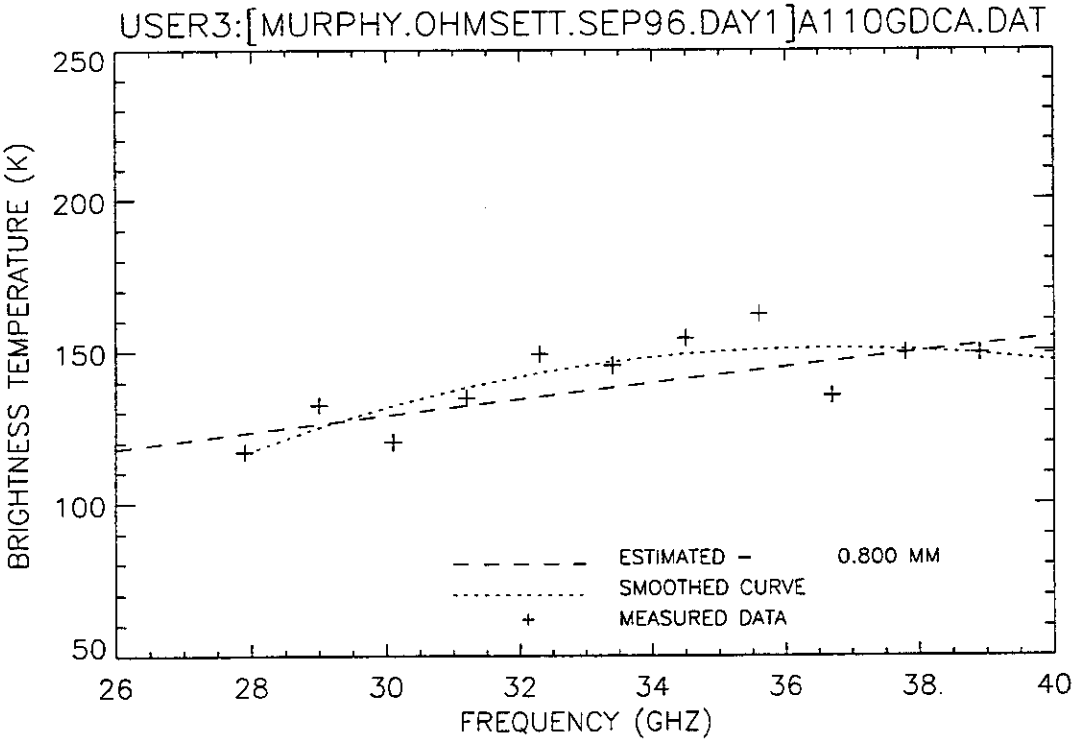

Figure 120. Plot of radiometric brightness temperature versus measurement frequency for 1-mm diesel oil, day 1 test, calm wave conditions, 11 September 1996, sweep G.

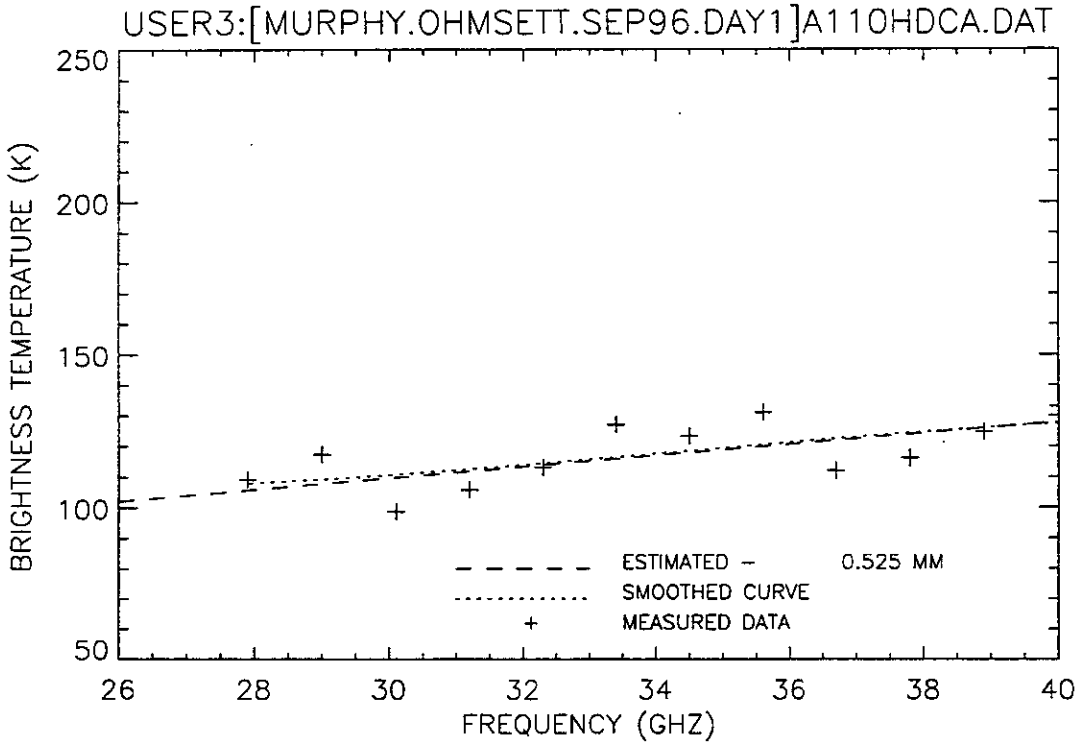

Figure 121. Plot of radiometric brightness temperature versus measurement frequency for 1-mm diesel oil, day 1 test, calm wave conditions, 11 September 1996, sweep H.

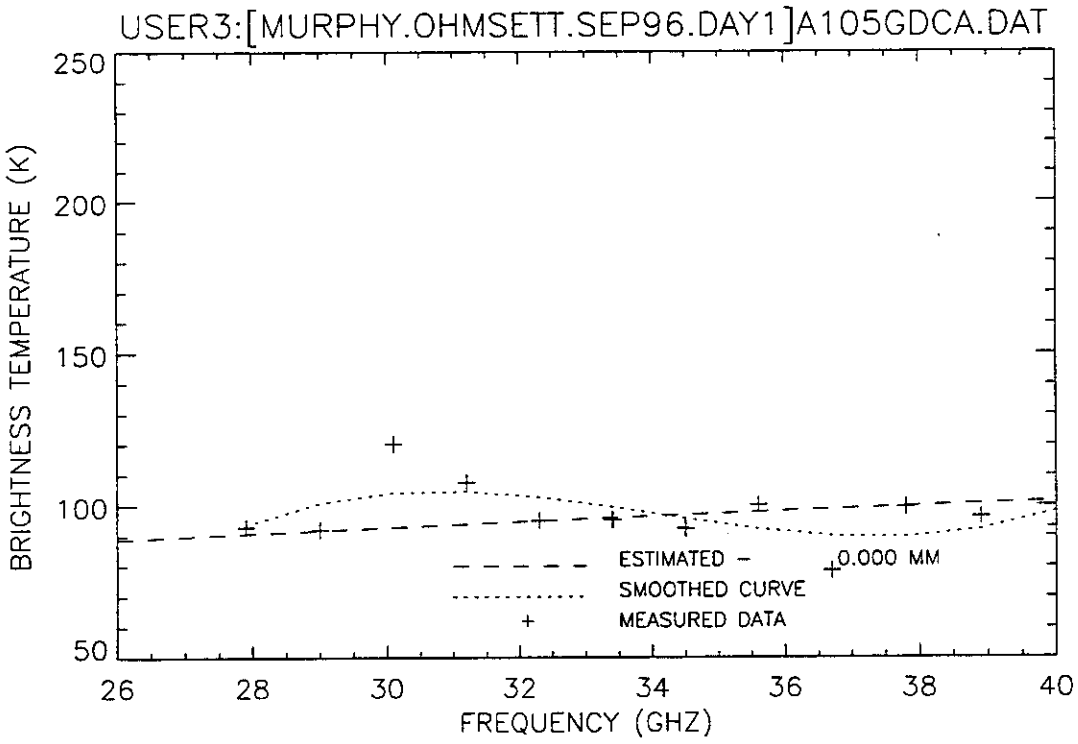

Figure 128. Plot of radiometric brightness temperature versus measurement frequency for 0.5-mm diesel oil, day 1 test, calm wave conditions, 11 September 1996, sweep G.

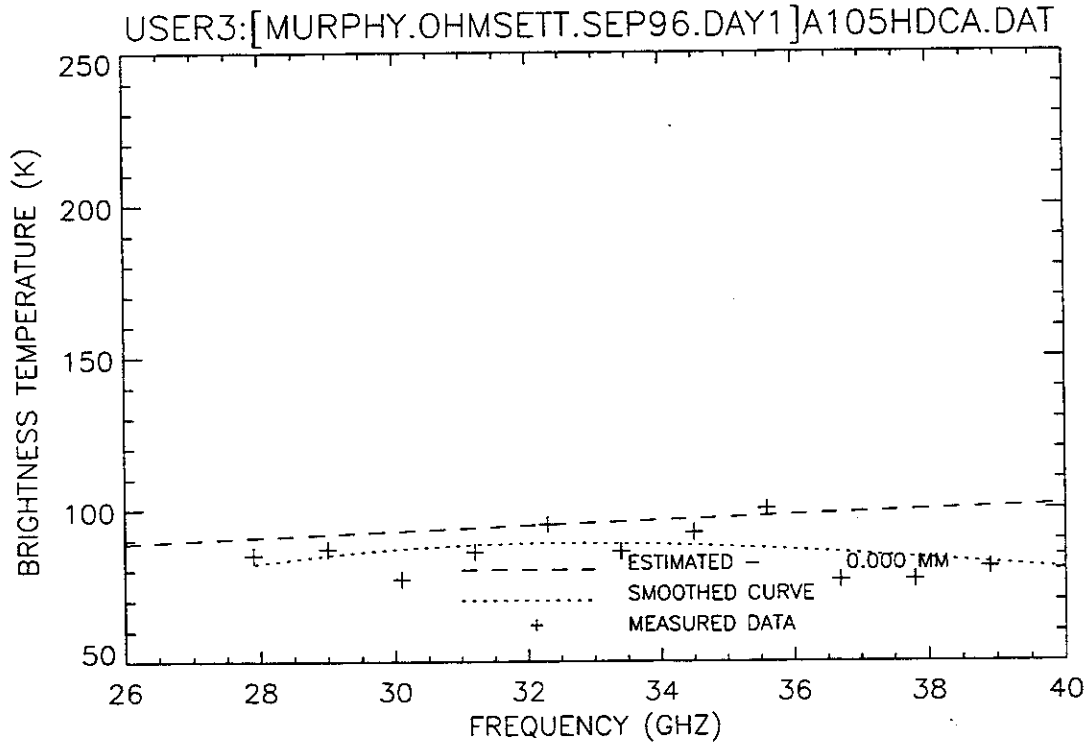

Figure 129. Plot of radiometric brightness temperature versus measurement frequency for 0.5-mm diesel oil, day 1 test, calm wave conditions, 11 September 1996, sweep H.

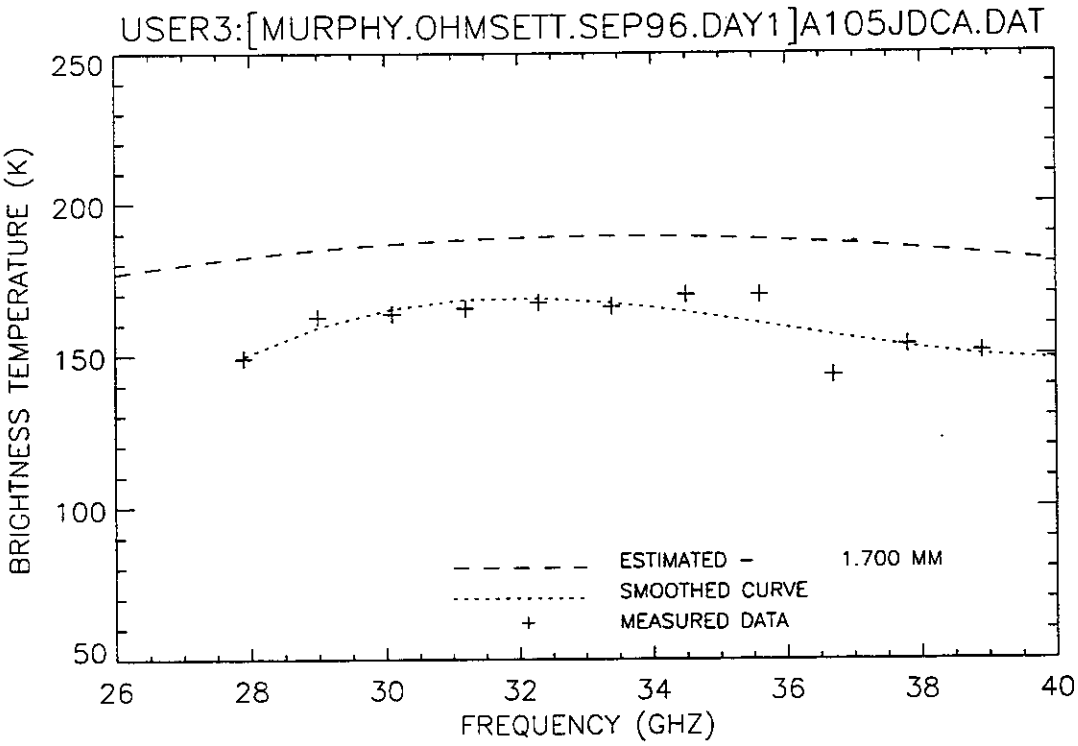

Figure 130. Plot of radiometric brightness temperature versus measurement frequency for 0.5-mm diesel oil, day 1 test, calm wave conditions, 11 September 1996, sweep J.

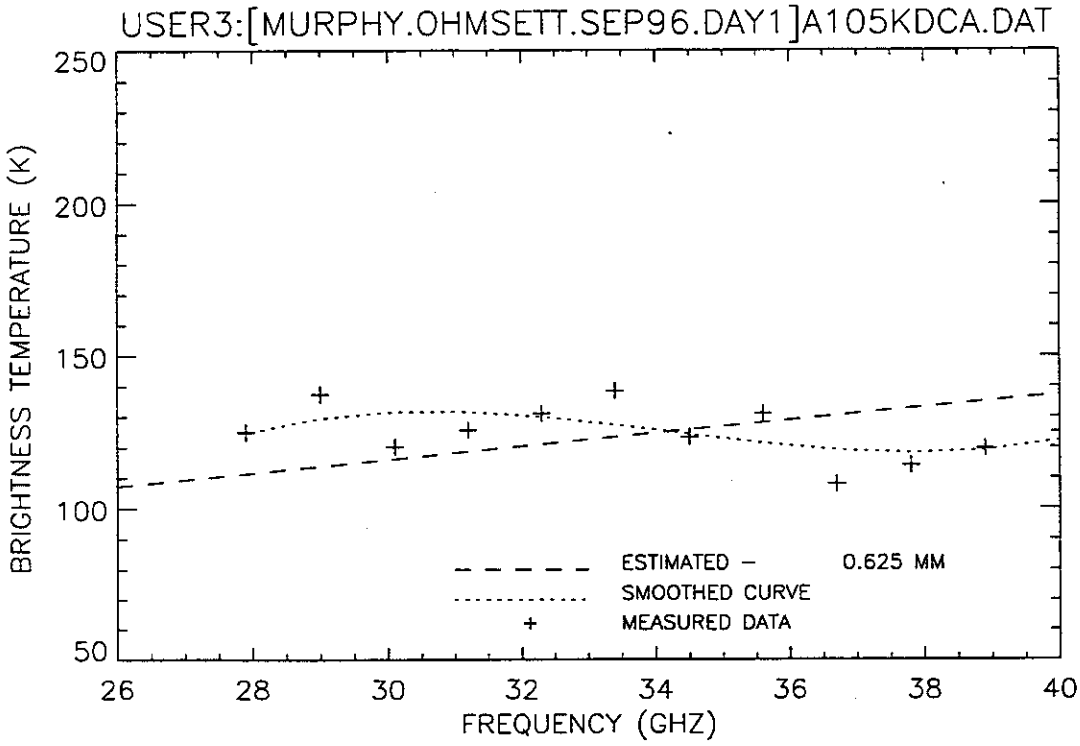

Figure 131. Plot of radiometric brightness temperature versus measurement frequency for 0.5-mm diesel oil, day 1 test, calm wave conditions, 11 September 1996, sweep K.

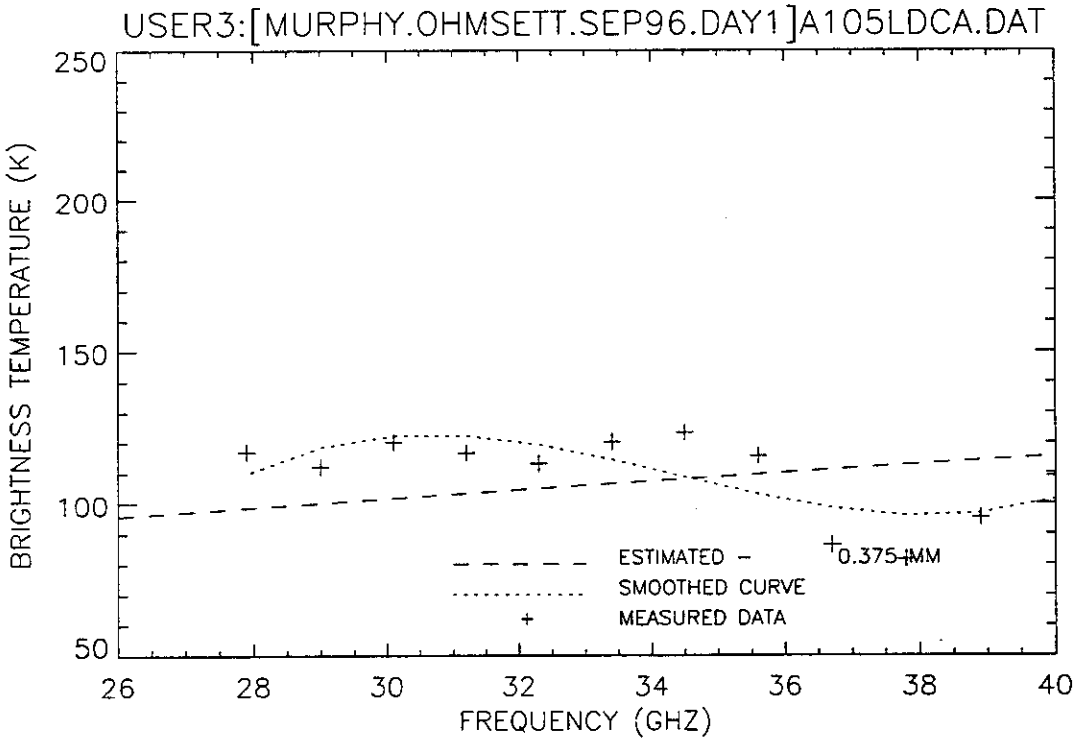

Figure 132. Plot of radiometric brightness temperature versus measurement frequency for 0.5-mm diesel oil, day 1 test, calm wave conditions, 11 September 1996, sweep L.

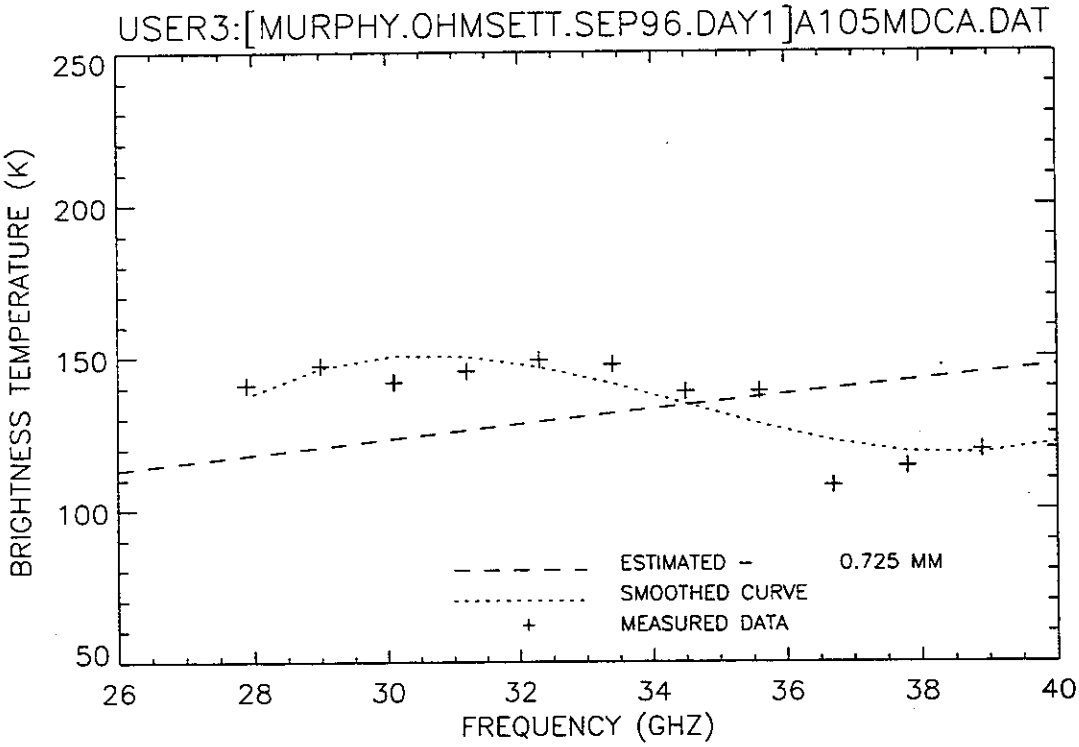

Figure 133. Plot of radiometric brightness temperature versus measurement frequency for 0.5-mm diesel oil, day 1 test, calm wave conditions, 11 September 1996, sweep M.

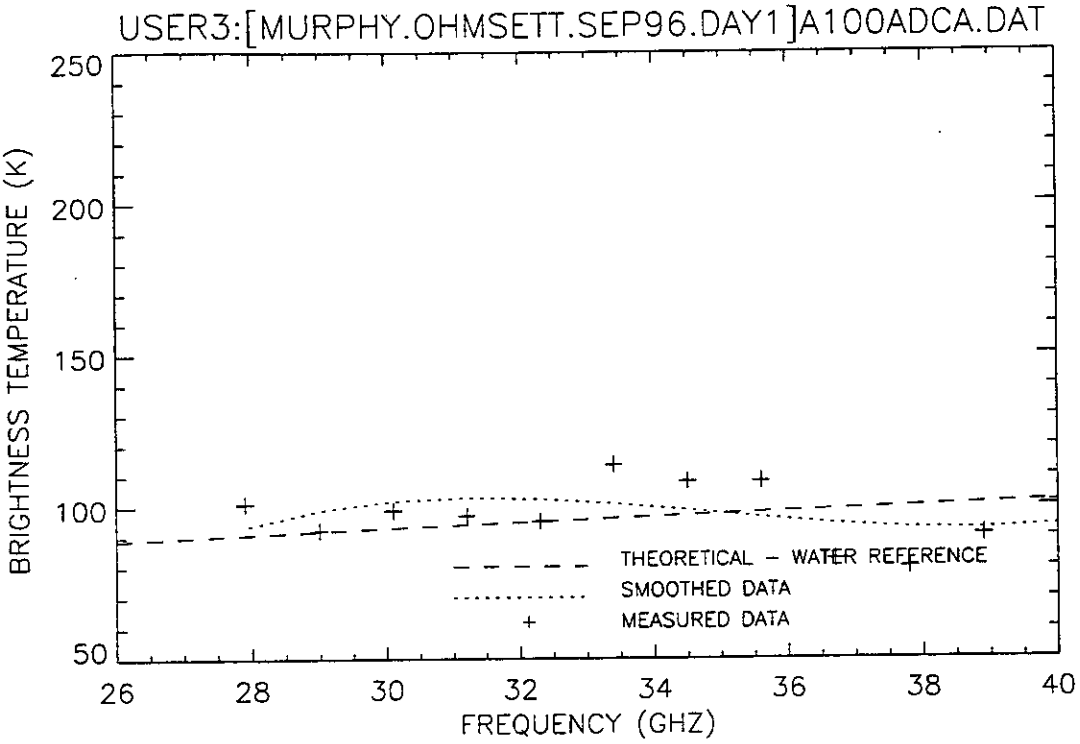

Figure 134. Plot of radiometric brightness temperature versus measurement frequency for water, day 1 test, calm wave conditions, 11 September 1996, sweep A.

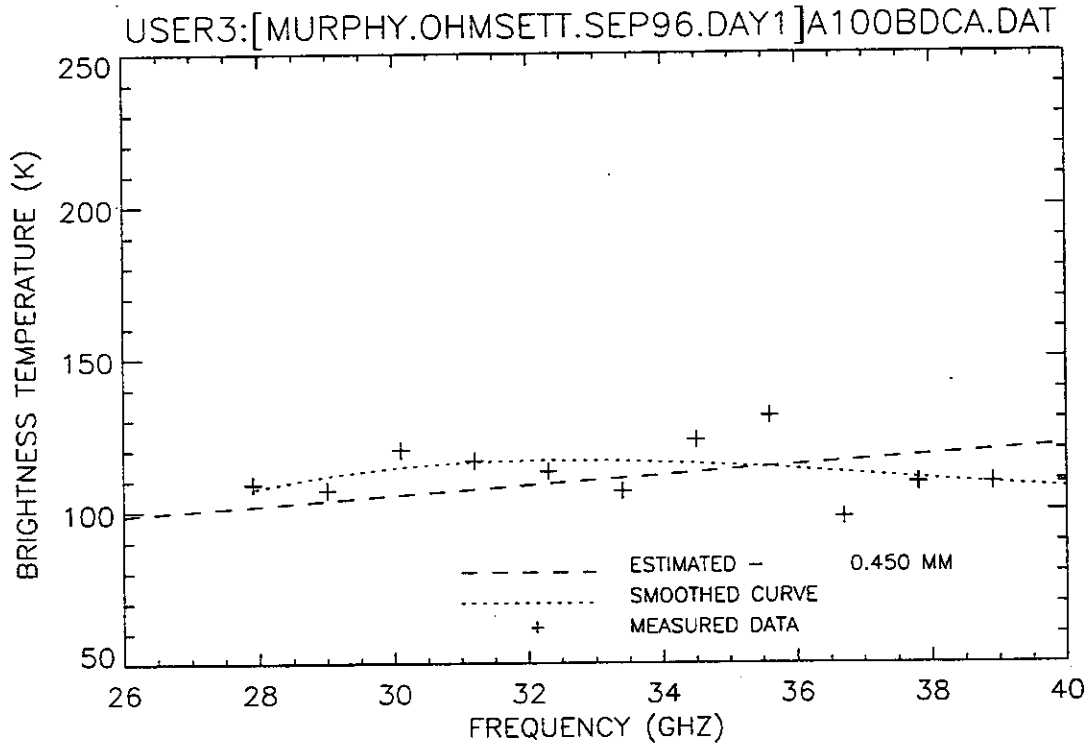

Figure 135. Plot of radiometric brightness temperature versus measurement frequency for water, day 1 test, calm wave conditions, 11 September 1996, sweep B.

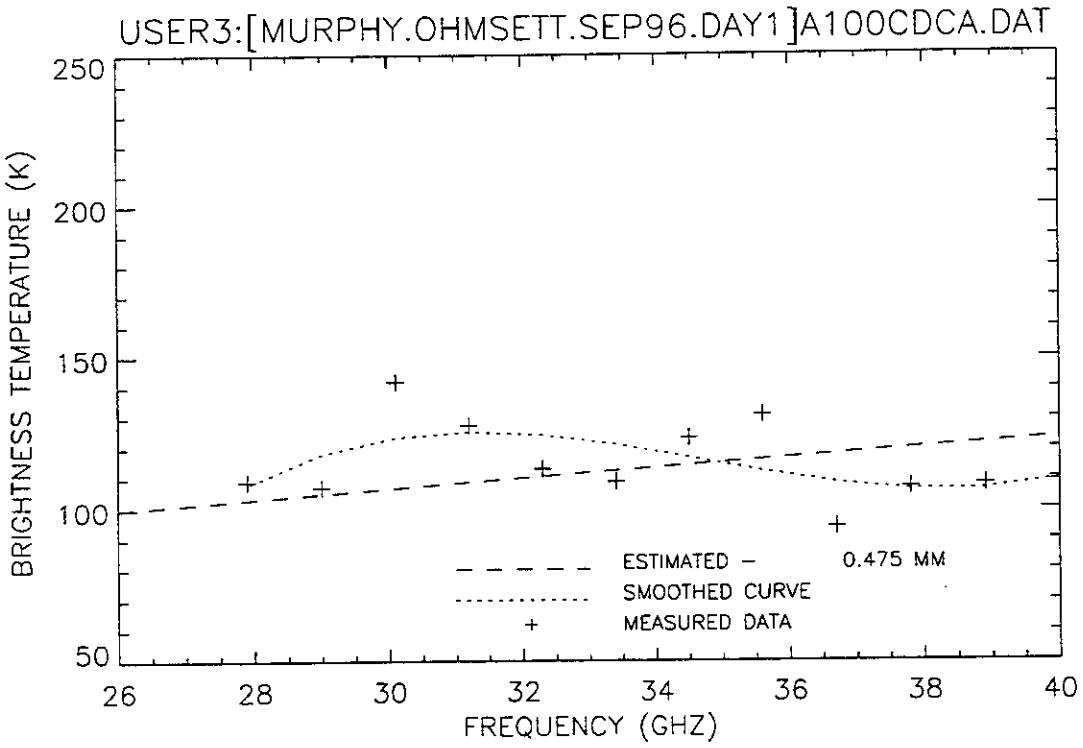

Figure 136. Plot of radiometric brightness temperature versus measurement frequency for water, day 1 test, calm wave conditions, 11 September 1996, sweep C.

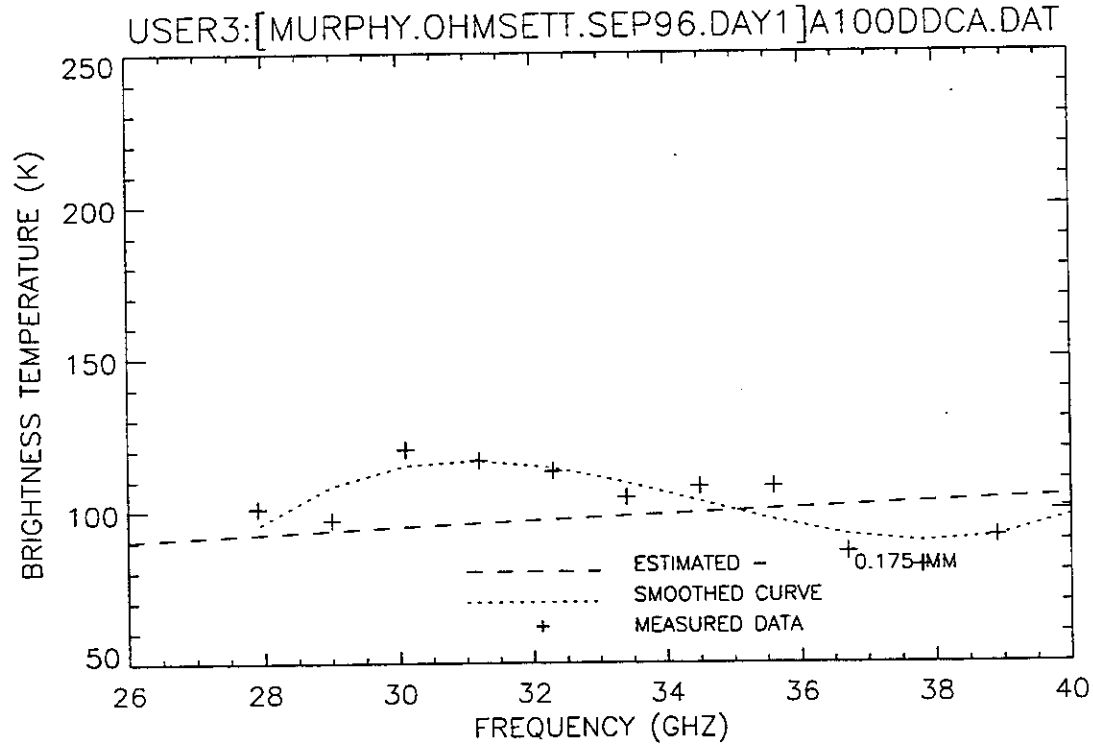

Figure 137. Plot of radiometric brightness temperature versus measurement frequency for water, day 1 test, calm wave conditions, 11 September 1996, sweep D.

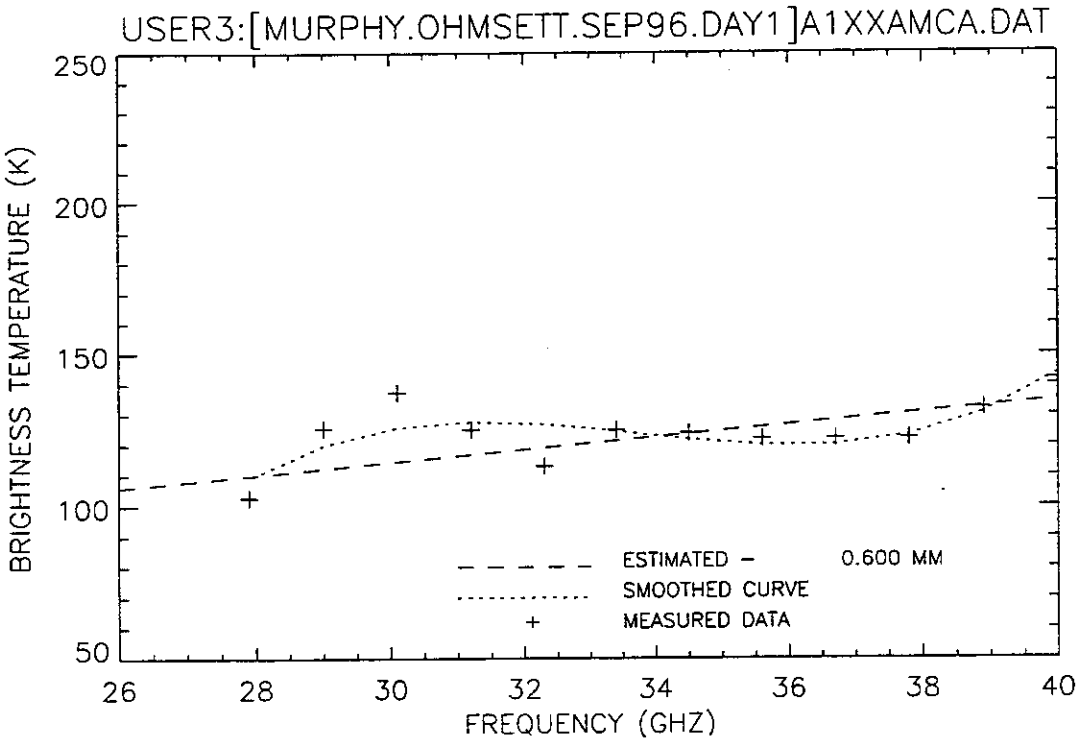

Figure 138. Plot of radiometric brightness temperature versus measurement frequency for an unknown thickness of diesel and Hydrocal oils, day 1 test, calm wave conditions, 11 September 1996, sweep A.

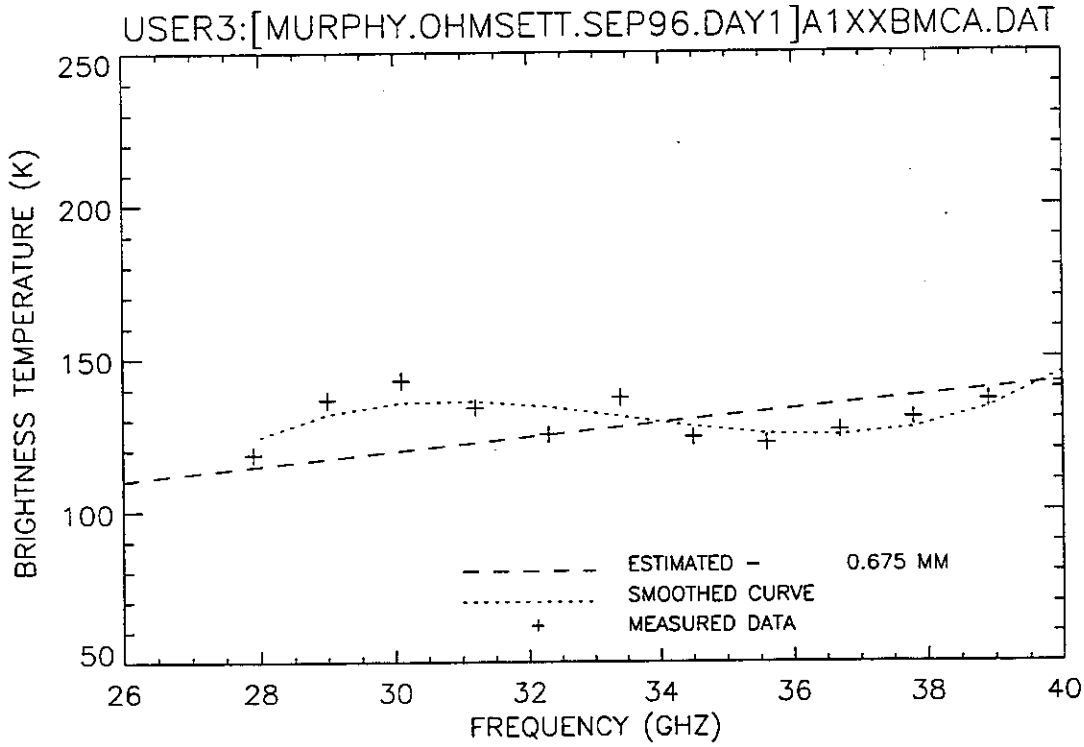

Figure 139. Plot of radiometric brightness temperature versus measurement frequency for an unknown thickness of diesel and Hydrocal oils, day 1 test, calm wave conditions, 11 September 1996, sweep B.

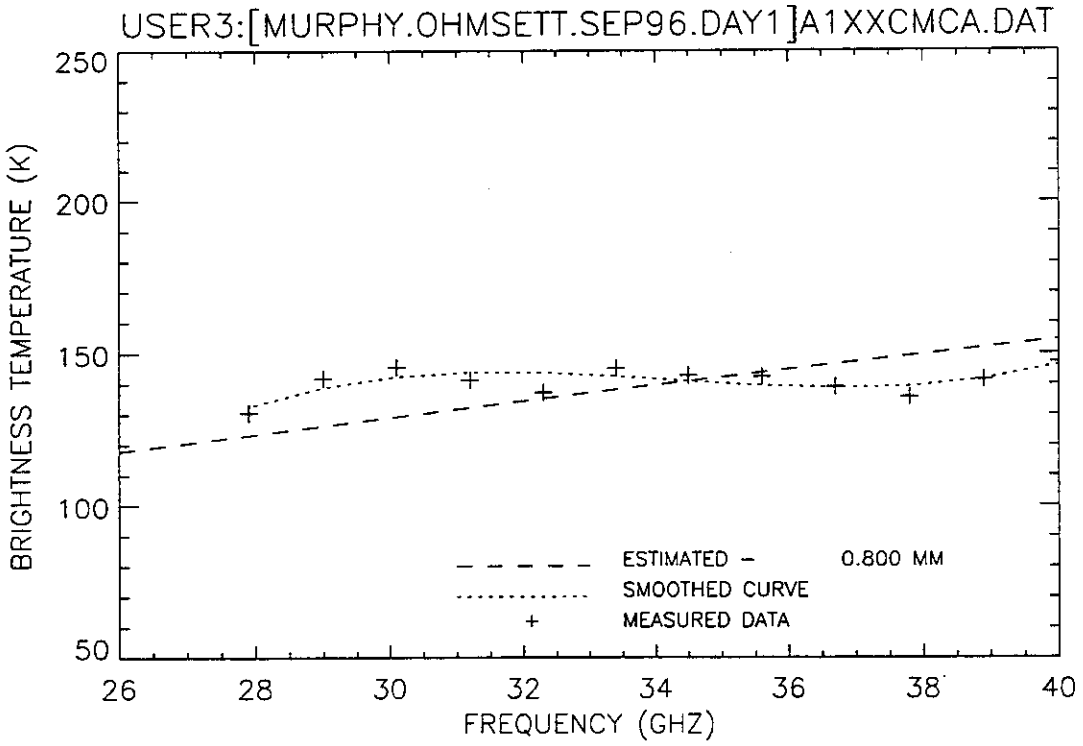

Figure 140. Plot of radiometric brightness temperature versus measurement frequency for an unknown thickness of diesel and Hydrocal oils, day 1 test, calm wave conditions, 11 September 1996, sweep C.

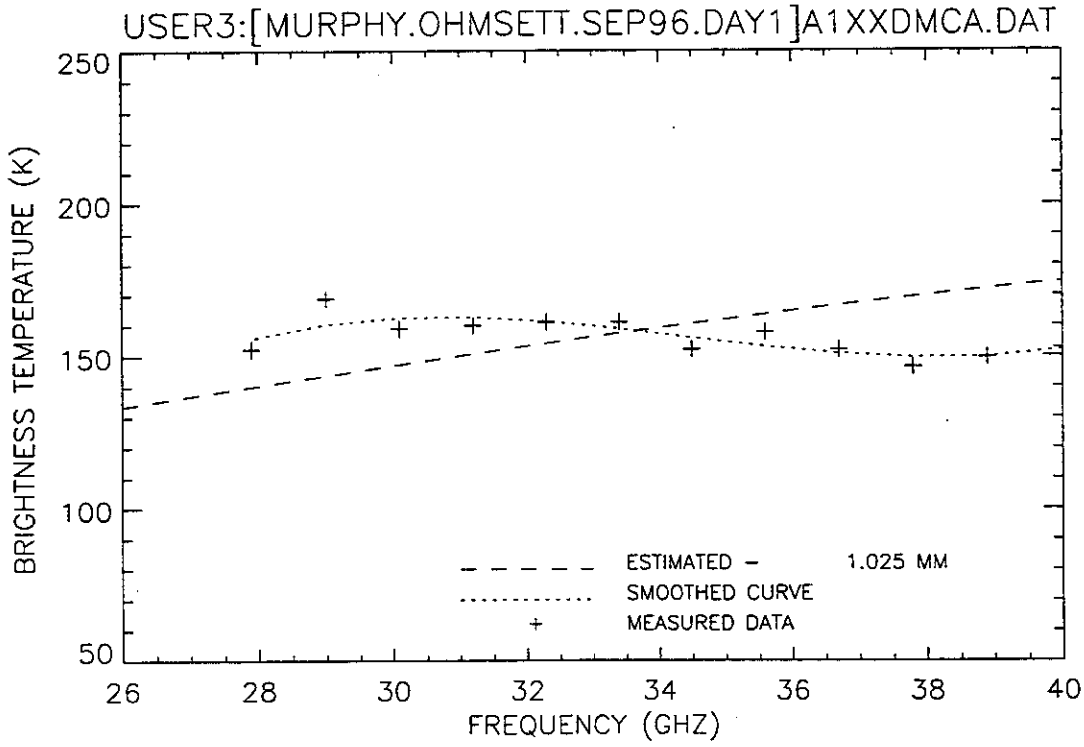

Figure 141. Plot of radiometric brightness temperature versus measurement frequency for an unknown thickness of diesel and Hydrocal oils, day 1 test, calm wave conditions, 11 September 1996, sweep D.

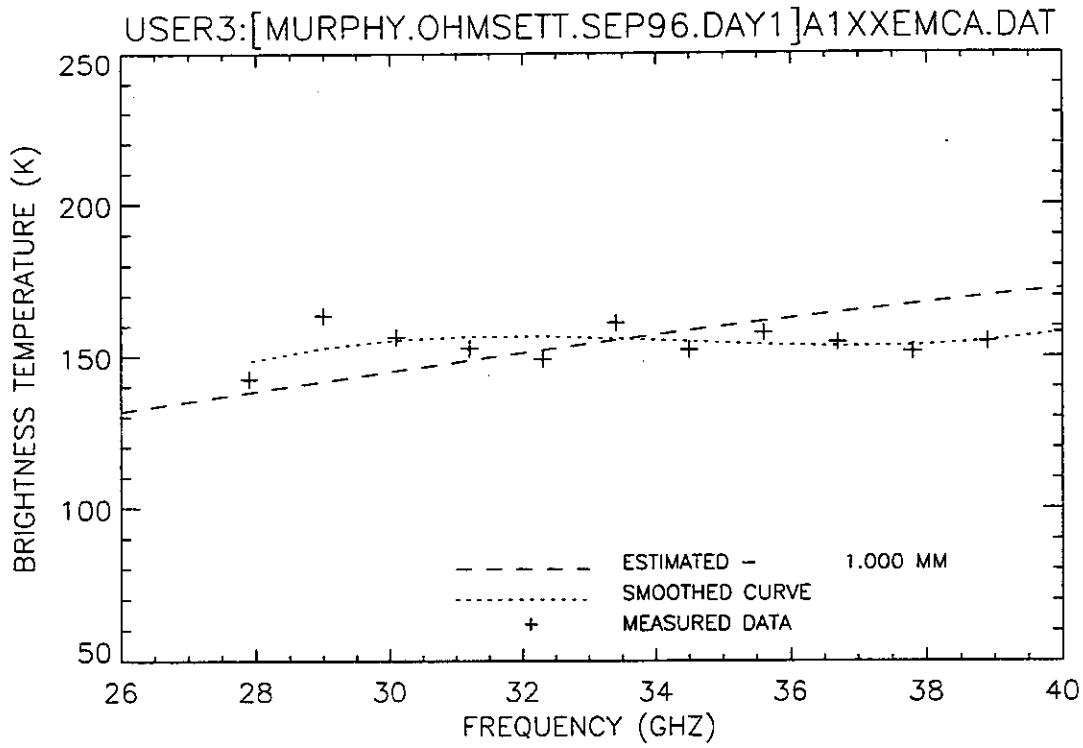

Figure 142. Plot of radiometric brightness temperature versus measurement frequency for an unknown thickness of diesel and Hydrocal oils, day 1 test, calm wave conditions, 11 September 1996, sweep E.

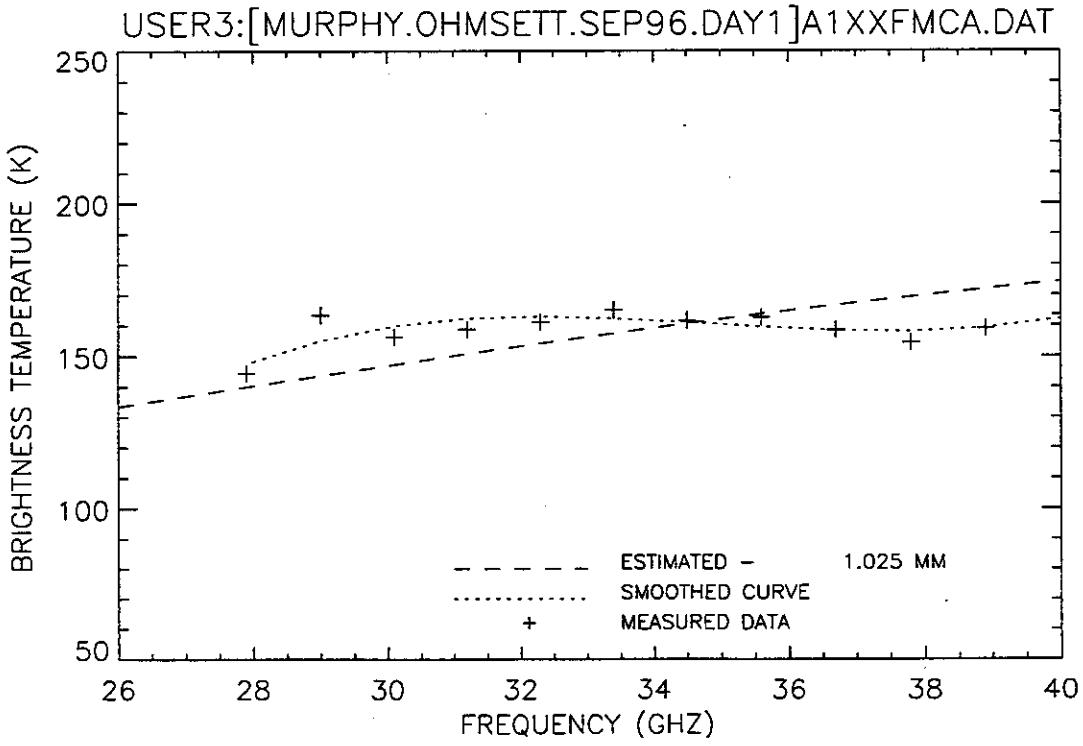

Figure 143. Plot of radiometric brightness temperature versus measurement frequency for an unknown thickness of diesel and Hydrocal oils, day 1 test, calm wave conditions, 11 September 1996, sweep F.

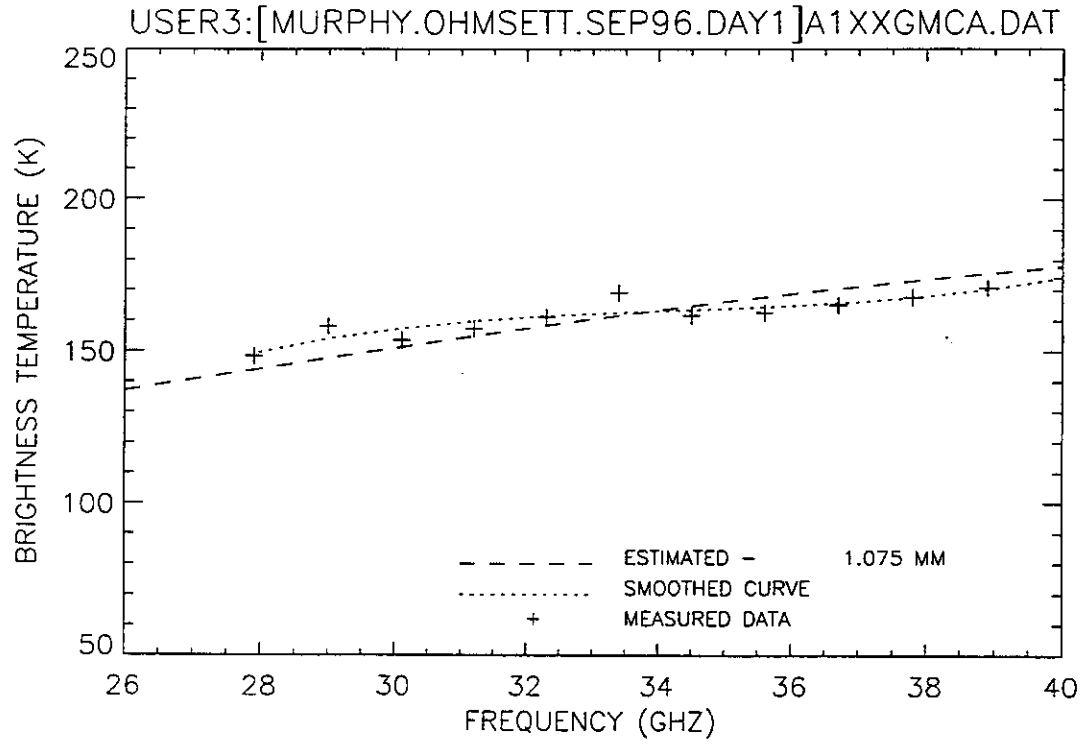

Figure 144. Plot of radiometric brightness temperature versus measurement frequency for an unknown thickness of diesel and Hydrocal oils, day 1 test, calm wave conditions, 11 September 1996, sweep G.

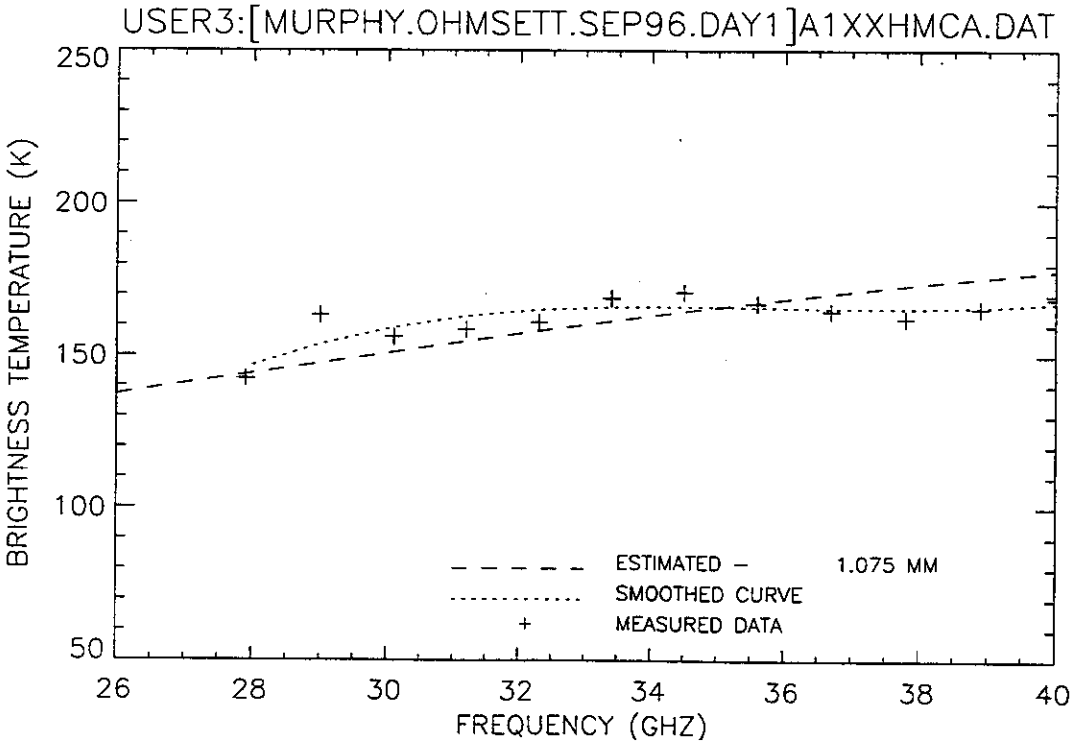

Figure 145. Plot of radiometric brightness temperature versus measurement frequency for an unknown thickness of diesel and Hydrocal oils, day 1 test, calm wave conditions, 11 September 1996, sweep H.

5. Night Test
Diesel and Crude Oil, Calm Wave Conditions

The same diesel oil targets from the day 1 test were used for the night test. The crude oil had been received, and the targets were laid out. Again, the conditions were not optimal; moderate wind and rain were expected. The collection continued because of the limited time available for using the facility.

Table 5 summarizes the results of the postcollection data analysis; the shaded blocks indicate algorithm results (LMS, CORR, MN/SL) that are close to or match the analyst's (visual) oil estimate. A comment is provided referring to the fit of the visual (analyst's choice) to the actual data.

The OHMSETT main bridge was moved to one of the southern oil targets to measure the center of the water reference pool. During the day, this pool had a slight sheen, indicating oil on the surface.

N100AWCA.DAT – The algorithm result of 0.000 mm, shown in Figure 146, is a poor match to the measured data, which are significantly lower than the estimated curve due to using the N100EWCA.DAT as the water reference.

A new hot/cold calibration was performed because the operator noticed that the instrument gain was drifting.

N100BWCA.DAT – The algorithm result of 0.000 mm, shown in Figure 147, is a poor-to-fair match to the measured data. Note that the measured data curve is closer to the estimate than the N100AWCA.DAT result, which is due to the recalibration of the radiometer.

N100CWCA.DAT – The algorithm result of 0.000 mm, shown in Figure 148, is a good-to-excellent match to the measured data.

N100DWCA.DAT – The algorithm result of 0.000 mm, shown in Figure 149, is a good-to-excellent match to the measured data. Note the slight sinusoid apparent in the measured data curve.

N100EWCA.DAT – This measurement, shown in Figure 150, was chosen as the water background reference. Note the slight sinusoid apparent in the measured curve.

TABLE 5

Results of the 12 September 1996 Night Test

FILENAME	LMS	CORR	MN/SL	DECL	METHOD	VISUAL	COMMENT
N100EWCA.DAT							Reference
N100AWCA.DAT	0.000	3.250	0.000	0.000	LMS & MN/SL	0.000	Poor
N100BWCA.DAT	0.000	7.100	0.000	0.000	LMS & MN/SL	0.000	Poor to fair
N100CWCA.DAT	0.000	3.625	0.025	0.000	LMS & MN/SL	0.000	Good to excellent
N100DWCA.DAT	0.000	0.225	0.000	0.000	LMS & MN/SL	0.000	Good to excellent
N105ACCA.DAT	0.525	0.475	3.725	0.500	LMS & CORR	0.500	Good
N105ADCA.DAT	0.675	7.050	0.675	0.675	LMS & MN/SL	0.675	Good
N105BCCA.DAT	0.550	3.825	0.525	0.525	LMS & MN/SL	0.525	Good
N105BDCA.DAT	0.550	9.300	0.550	0.550	LMS & MN/SL	0.550	Fair
N105CCCA.DAT	0.525	0.475	0.525	0.525	LMS & MN/SL	0.525	Good to excellent
N105CDCA.DAT	0.575	7.275	0.600	0.575	LMS & MN/SL	0.575	Good to excellent
N105DCCA.DAT	0.575	0.450	3.775	0.500	LMS & CORR	0.500	Good
N105DDCA.DAT	0.600	7.400	0.600	0.600	LMS & MN/SL	0.600	Good to excellent
N105ECCA.DAT	0.875	3.950	0.875	0.875	LMS & MN/SL	0.875	Fair to good
N105EDCA.DAT	0.000	1.400	0.000	0.000	LMS & MN/SL	0.000	Good to excellent
N105FCCA.DAT	0.875	3.975	0.875	0.875	LMS & MN/SL	0.850	Fair to good
N105FDCA.DAT	0.000	9.625	0.000	0.000	LMS & MN/SL	0.000	Good to excellent
N105GCCA.DAT	0.825	4.050	0.850	0.850	LMS & MN/SL	0.825	Fair to good
N105GDCA.DAT	0.275	3.825	0.275	0.275	LMS & MN/SL	0.275	Good to excellent
N110ACCA.DAT	1.475	1.325	1.650	1.400	LMS & CORR	1.400	Fair
N110ADCA.DAT	0.700	7.250	0.700	0.700	LMS & MN/SL	0.700	Fair
N110BCCA.DAT	1.475	1.475	1.575	1.475	LMS & CORR	1.475	Good
N110BDCA.DAT	0.725	7.275	0.725	0.725	LMS & MN/SL	0.725	Fair to good
N110CCCA.DAT	1.375	0.225	1.450	1.400	LMS & MN/SL	1.400	Good
N110CDCA.DAT	0.700	3.700	0.700	0.700	LMS & MN/SL	0.700	Fair to good
N110DCCA.DAT	1.425	1.000	1.500	1.450	LMS & MN/SL	1.450	Good
N110DDCA.DAT	0.750	3.700	0.725	0.725	LMS & MN/SL	0.725	Fair to good
N110ECCA.DAT	2.125	2.150	2.200	2.125	LMS & CORR	2.215	Fair
N110EDCA.DAT	0.400	3.975	0.375	0.375	LMS & MN/SL	0.375	Fair
N110FCCA.DAT	2.250	5.675	1.075	2.250	LMS only	2.250	Fair
N110FDCA.DAT	0.425	3.925	0.400	0.400	LMS & MN/SL	0.400	Fair to good
N110GCCA.DAT	2.175	1.850	2.250	2.200	LMS & MN/SL	2.200	Fair to good
N110GDCA.DAT	0.375	3.875	0.350	0.350	LMS & MN/SL	0.350	Fair to good
N110HCCA.DAT	1.400	0.450	1.550	1.475	LMS & MN/SL	1.475	Fair
N110HDCA.DAT	0.350	3.875	0.300	0.325	LMS & MN/SL	0.325	Fair to good
N110JCCA.DAT	1.400	0.475	1.575	1.475	LMS & MN/SL	1.475	Fair
N110KCCA.DAT	1.450	0.500	1.625	1.525	LMS & MN/SL	1.525	Fair
N110LCCA.DAT	1.475	1.175	1.650	1.550	LMS & MN/SL	1.550	Fair
N120ADCA.DAT	2.325	2.750	2.325	2.325	LMS & MN/SL	2.325	Excellent
N120ADDA.DAT	3.400	6.925	0.500	3.400	LMS only	3.400	Excellent
N120BDCA.DAT	2.425	2.750	2.425	2.425	LMS & MN/SL	2.425	Excellent
N120BDDA.DAT	3.375	6.925	3.325	3.500	LMS & MN/SL	3.350	Excellent
N120CDCA.DAT	2.250	2.700	2.225	2.225	LMS & MN/SL	2.225	Excellent
N120CDDA.DAT	3.425	3.425	0.450	3.425	LMS & CORR	3.425	Excellent
N120DDCA.DAT	2.150	2.775	2.125	2.125	LMS & MN/SL	2.125	Excellent

TABLE 5 (Continued)

Results of the 12 September 1996 Night Test

FILENAME	LMS	CORR	MN/SL	DECL	METHOD	VISUAL	COMMENT
N120DDDA.DAT	0.555	7.200	0.550	0.550	LMS & MN/SL	0.550	Good to excellent
N120EDCA.DAT	1.975	2.350	2.000	1.975	LMS & MN/SL	1.975	Good to excellent
N120EDDA.DAT	3.900	4.275	3.800	3.850	LMS & MN/SL	3.850	Good
N120FDCA.DAT	1.950	2.175	2.000	1.975	LMS & MN/SL	1.975	Good to excellent
N120FDDA.DAT	3.900	4.125	3.775	3.825	LMS & MN/SL	3.825	Good
N120GDCA.DAT	1.850	2.625	1.925	1.875	LMS & MN/SL	1.875	Good to excellent
N120GDDA.DAT	3.900	4.275	3.800	3.850	LMS & MN/SL	3.850	Good to excellent
N120HDCA.DAT	1.450	4.275	1.600	1.525	LMS & MN/SL	1.525	Fair to good
N120HDDA.DAT	3.925	4.425	0.650	3.925	LMS only	3.925	Fair
N120JDCA.DAT	1.500	4.300	1.650	1.575	LMS & MN/SL	1.575	Fair
N120JDDA.DAT	0.700	3.725	0.700	0.700	LMS & MN/SL	0.700	Good to excellent
N120KDCA.DAT	1.500	4.400	1.650	1.575	LMS & MN/SL	1.575	Fair
N120KDDA.DAT	0.550	7.400	0.550	0.550	LMS & MN/SL	0.550	Good to excellent
N120LDCA.DAT	1.400	4.225	1.550	1.475	LMS & MN/SL	1.475	Poor to fair
N120LDDA.DAT	0.450	3.950	3.500	0.450	LMS only	0.450	Excellent
N130ACCA.DAT	3.750	3.775	0.400	3.750	LMS & CORR	3.750	Good
N130ADCA.DAT	4.725	4.425	0.825	4.350	LMS & CORR	4.350	Good to excellent
N130ADFA.DAT	0.950	0.450	0.950	0.950	LMS & MN/SL	0.950	Good
N130BCCA.DAT	3.775	3.750	3.575	3.750	LMS & CORR	3.750	Good
N130BDCA.DAT	0.825	4.450	0.800	0.800	LMS & MN/SL	0.800	Good
N130BDFA.DAT	1.000	9.575	1.000	1.000	LMS & MN/SL	1.000	Fair to good
N130CCCA.DAT	3.625	3.675	0.250	3.650	LMS & CORR	3.650	Good
N130CDCA.DAT	7.800	4.550	0.825	7.800	LMS only	4.550	Good (shape)
N130CDFA.DAT	0.950	0.200	0.950	0.950	LMS & MN/SL	0.950	Good to excellent
N130DCCA.DAT	3.850	3.825	3.650	3.825	LMS & CORR	3.825	Good
N130DDCA.DAT	4.375	4.550	0.850	4.450	LMS & CORR	4.450	Good
N130DDFA.DAT	1.000	1.150	1.000	1.000	LMS & MN/SL	1.000	Excellent
N130ECCA.DAT	3.225	3.175	0.200	3.200	LMS & CORR	3.200	Good
N130EDCA.DAT	0.875	1.375	0.900	0.875	LMS & MN/SL	0.875	Good
N130EDFA.DAT	4.100	3.775	0.825	4.100	LMS only	4.100	Good
N130FCCA.DAT	3.125	3.075	3.225	3.100	LMS & CORR	3.100	Excellent
N130FDCA.DAT	0.875	9.175	0.900	0.875	LMS & MN/SL	0.875	Fair
N130FDFA.DAT	0.825	9.575	0.825	0.825	LMS & MN/SL	0.825	Fair
N130GCCA.DAT	3.150	3.175	3.175	3.175	LMS & CORR	3.175	Excellent
N130GDCA.DAT	0.900	1.400	0.925	0.900	LMS & MN/SL	0.900	Good to excellent
N130FGFA.DAT	4.250	3.925	0.900	4.250	LMS only	4.250	Good to excellent
N130HCCA.DAT	3.225	3.200	3.275	3.200	LMS & CORR	3.200	Excellent
N130HDCA.DAT	2.850	9.425	0.700	2.850	LMS only	2.850	Fair to good
N130HDFA.DAT	4.775	1.600	0.975	4.775	LMS only	4.775	Fair to good
N130JDCA.DAT	0.750	9.425	0.775	0.750	LMS & MN/SL	0.750	Fair (mean)
N130JDFA.DAT	4.400	4.350	0.925	4.375	LMS & CORR	4.375	Excellent
N130KDCA.DAT	3.200	3.300	0.650	3.250	LMS & CORR	3.325	Good to excellent
N130KDFA.DAT	3.925	3.900	3.900	3.900	LMS & MN/SL	3.900	Good to excellent
N130LDCA.DAT	3.450	3.400	0.600	3.425	LMS & CORR	3.425	Good to excellent
N130MDCA.DAT	3.550	3.525	3.550	3.550	LMS & MN/SL	3.550	Excellent
N130NDCA.DAT	3.650	3.600	3.625	3.600	LMS & CORR	3.600	Excellent

TABLE 5 (Continued)

Results of the 12 September 1996 Night Test

FILENAME	LMS	CORR	MN/SL	DECL	METHOD	VISUAL	COMMENT
N180ACCA.DAT	9.425	9.350	1.075	9.375	LMS & CORR	9.375	Good to excellent
N180ADCA.DAT	6.950	3.325	2.250	6.950	LMS only	7.200	Good (shape)
N180BCCA.DAT	8.575	1.675	0.800	8.575	LMS only	8.575	Good to excellent
N180BDCA.DAT	7.450	7.425	2.475	7.425	LMS & CORR	7.425	Good (shape)
N180CCCA.DAT	8.925	8.900	0.875	8.900	LMS & CORR	8.900	Good
N180CDCA.DAT	10.000	3.325	2.275	10.000	LMS only	10.000	Good
N180DCCA.DAT	8.300	1.675	0.825	1.675	CORR only	8.300	Fair to good
N180DDCA.DAT	7.150	7.150	2.475	7.150	LMS & CORR	7.500	Good to excellent
N180ECCA.DAT	10.000	3.350	2.150	10.000	LMS only	10.000	Fair to good
N180EDCA.DAT	7.425	7.425	2.500	7.425	LMS & CORR	7.425	Good
N180FCCA.DAT	8.950	8.900	0.925	8.925	LMS & CORR	8.925	Good
N180FDCA.DAT	10.000	3.300	2.225	10.000	LMS only	10.000	Fair to good
N180GCCA.DAT	7.325	7.275	1.000	7.300	LMS & CORR	7.300	Good
N180GDCA.DAT	10.000	3.300	2.200	3.300	CORR only	10.000	Good
N180HCCA.DAT	6.950	3.400	0.900	3.400	CORR only	6.950	Good to excellent
N180HDCA.DAT	10.000	3.300	2.250	3.300	CORR only	10.000	Good
N180JCCA.DAT	7.200	7.125	1.000	7.150	LMS & CORR	7.150	Fair to good
N180JDCA.DAT	7.200	7.225	2.450	7.200	LMS & CORR	7.500	Good
N180KCCA.DAT	7.100	3.475	0.900	3.475	CORR only	7.100	Good
N180KDCA.DAT	8.050	8.050	0.800	8.050	LMS & CORR	8.050	Fair to good
N180LCCA.DAT	7.175	7.125	0.925	7.150	LMS & CORR	7.150	Good
N180LDCA.DAT	7.000	6.950	2.300	6.975	LMS & CORR	7.300	Fair
N180MCCA.DAT	7.350	7.325	0.900	7.325	LMS & CORR	7.325	Good
N180MDCA.DAT	10.000	3.300	2.225	3.300	CORR only	10.000	Fair to good
N180NCCA.DAT	7.275	7.225	0.900	7.250	LMS & CORR	7.250	Good
N180NDCA.DAT	6.850	3.325	2.250	6.850	LMS only	7.000	Fair
N180PCCA.DAT	7.100	3.475	0.875	7.100	LMS only	7.100	Good
N180PDCA.DAT	10.000	3.300	2.175	3.300	CORR only	10.000	Fair to good
N180QCCA.DAT	7.350	7.325	0.875	7.325	LMS & CORR	7.325	Good
N180RCCA.DAT	8.350	1.675	3.975	1.675	CORR only	8.350	Fair to good
N180S1.DAT	4.300	1.625	3.950	4.300	LMS only	8.500	Fair to good
N180S10.DAT	6.750	3.325	2.600	6.750	LMS only	6.750	Good to excellent
N180S11.DAT	0.725	7.750	2.725	0.725	LMS only	7.750	Good
N180S12.DAT	7.150	7.200	2.650	7.175	LMS & CORR	7.175	Good
N180S13.DAT	6.675	6.675	0.775	6.675	LMS & CORR	6.675	Good
N180S14.DAT	0.700	7.575	0.700	0.700	LMS & MN/SL	7.575	Fair
N180S2.DAT	6.900	6.900	2.475	6.900	LMS & CORR	6.900	Fair to good
N180S3.DAT	7.050	7.075	0.925	7.050	LMS & CORR	7.050	Fair to good
N180S4.DAT	0.800	1.575	0.800	0.800	LMS & MN/SL	8.300	Fair
N180S5.DAT	8.250	1.650	3.875	1.650	CORR only	8.250	Fair to good
N180S6.DAT	9.375	9.425	3.975	9.400	LMS & CORR	9.400	Good
N180S7.DAT	6.775	3.325	2.425	3.325	CORR only	6.775	Good
N180S8.DAT	7.425	7.450	2.650	7.425	LMS & CORR	7.425	Good
N180S9.DAT	6.650	3.300	0.875	6.650	LMS only	6.650	Good to excellent
N180SC1.DAT	0.000	1.700	0.000	0.000	LMS & MN/SL	8.700	Fair (shape)

TABLE 5 (Continued)

Results of the 12 September 1996 Night Test

FILENAME	LMS	CORR	MN/SL	DECL	METHOD	VISUAL	COMMENT
N180SC10.DAT	0.000	4.625	0.000	0.000	LMS & MN/SL	7.800	Fair (shape)
N180SC2.DAT	0.175	9.375	0.200	0.175	LMS & MN/SL	9.375	Fair (shape)
N180SC3.DAT	0.000	8.925	0.000	0.000	LMS & MN/SL	8.925	Good (shape)
N180SC4.DAT	0.000	1.700	0.000	0.000	LMS & MN/SL	8.500	Fair (shape)
N180SC5.DAT	0.000	1.675	0.000	0.000	LMS & MN/SL	8.300	Fair (shape)
N180SC6.DAT	0.000	4.750	0.000	0.000	LMS & MN/SL	7.800	Fair (shape)
N180SC7.DAT	0.000	1.675	0.000	0.000	LMS & MN/SL	8.300	Fair (shape)
N180SC8.DAT	0.000	1.650	0.000	0.000	LMS & MN/SL	8.000	Fair (shape)
N180SC9.DAT	0.000	1.675	0.000	0.000	LMS & MN/SL	8.200	Fair (shape)
N180SCCA.DAT	8.550	1.700	3.975	8.550	LMS only	8.550	Good
N180TCCA.DAT	8.650	1.700	0.850	8.650	LMS only	8.750	Good
N180UCCA.DAT	8.750	1.700	0.800	8.750	LMS only	8.750	Good to excellent

The main bridge was moved north to the southwestern sector of the 0.5-mm crude oil target. Oil did not entirely cover the target pool.

N105ACCA.DAT – The algorithm result of 0.500 mm, shown in Figure 151, is a good match to the measured data.

N105BCCA.DAT – The algorithm result of 0.5.25 mm, shown in Figure 152, is a good match to the measured data.

N105CCCA.DAT – The algorithm result of 0.525 mm, shown in Figure 153, is a good-to-excellent match to the measured data.

The radiometer position was shifted east, and the main bridge was moved north to measure a different area of the oil target.

N105DCCA.DAT – The algorithm result of 0.500 mm, shown in Figure 154, is a good match to the measured data.

N105ECCA.DAT – The algorithm result of 0.875 mm, shown in Figure 155, is a fair-to-good match to the measured data.

N105FCCA.DAT – The algorithm result of 0.875 mm, shown in Figure 156, is a fair-to-good match to the measured data.

N105GCCA.DAT – The algorithm result of 0.850 mm, shown in Figure 157, is a fair-to-good match to the measured data.

The main bridge was moved north to the 0.5-mm uniform diesel oil target. Most of the oil was located in the southeastern sector of the target. The following data sets were collected in this sector.

N105ADCA.DAT – The algorithm result of 0.675 mm, shown in Figure 158, is a good match to the measured data.

N105BDCA.DAT – The algorithm estimate of 0.550 mm, shown in Figure 159, is a fair match to the measured data. The measured data curve appears flatter (less slope) than the estimate; however the mean value of the estimated curve seems to be a fair match to the measured data.

N105CDCA.DAT – The algorithm estimate of 0.575 mm, shown in Figure 160, is a good-to-excellent match to the measured data.

N105DDCA.DAT – The algorithm estimate of 0.600 mm, shown in Figure 161, is a good-to-excellent match to the measured data set.

The radiometer position was shifted to measure the southwestern sector of the oil target pool. Visually, there seemed to be little-to-no oil coverage in this sector.

N105EDCA.DAT – The algorithm estimate of 0.000 mm, shown in Figure 162, is a good-to-excellent match to the measured data.

N105FDCA.DAT – The algorithm estimate of 0.000 mm, shown in Figure 163, is a good-to-excellent match to the measured data Note the slight sinusoidal shape of the measured data curve.

N105GDCA.DAT – The algorithm estimate of 0.275 mm, shown in Figure 164, is a good-to-excellent match to the measured data.

The main bridge was moved south and the radiometer shifted west to collect data from the south side of the 1-mm crude oil target. Oil did not completely cover the surface of the target pool.

N110ACCA.DAT – The algorithm estimate of 1.400 mm, shown in Figure 165, is a fair match to the measured data.

N110BCCA.DAT – The algorithm estimate of 1.475 mm, shown in Figure 166, is a good match to the measured data.

N110CCCA.DAT – The algorithm estimate of 1.400 mm, shown in Figure 167, is a good match to the measured data.

N110DCCA.DAT – The algorithm estimate of 1.450 mm, shown in Figure 168, is a good match to the measured data.

The radiometer position was shifted to collect data from the east side of the target pool. Visually, it appeared that the thickest oil was in this sector.

N110ECCA.DAT – The algorithm estimate of 2.125 mm, shown in Figure 169, is a fair match to the measured data.

N110FCCA.DAT – The algorithm estimate of 2.250 mm, shown in Figure 170, is a fair match to the measured data.

N110GCCA.DAT – The algorithm estimate of 2.200 mm, shown in Figure 171, is a fair-to-good match to the measured data.

The main bridge was moved 2 to 3 ft north, and the radiometer shifted 2 to 3 ft west to measure an area in the oil target between and slightly north of the positions measured for N110(A–D)CCA.DAT and N110(E–G)CCA.DAT.

N110HCCA.DAT – The algorithm estimate of 1.475 mm, shown in Figure 172, is a fair match to the measured data.

N110JCCA.DAT – The algorithm estimate of 1.475 mm, shown in Figure 173, is a fair match to the measured data.

N110KCCA.DAT – The algorithm estimate of 1.525 mm, shown in Figure 174, is a fair match to the measured data which exhibit a steeper slope and higher temperatures.

N110LCCA.DAT – The algorithm estimate of 1.550 mm, shown in Figure 175, is a fair match to the measured data.

The main bridge was moved north the to 1-mm diesel oil target. The radiometer was positioned to collect data from the southeast sector of the target pool. Light rain was beginning to fall.

N110ADCA.DAT – The algorithm estimate of 0.700 mm, shown in Figure 176, is a fair match to the measured data set. Note its sinusoidal appearance.

N110BDCA.DAT – The algorithm estimate of 0.775 mm, shown in Figure 177, is a fair match to the measured data set. Note its sinusoidal appearance.

N110CDCA.DAT – The algorithm estimate of 0.700 mm, shown in Figure 178, is a fair-to-good match to the measured data set. Note its sinusoidal appearance.

N110DDCA.DAT – The algorithm estimate of 0.725 mm, shown in Figure 179, is a fair-to-good match to the measured data.

The main bridge was moved north and the radiometer position shifted slightly west to collect data from the center of the northern sector of the target pool. Visually, there was little-to-no oil in this sector. The rain continued, increasing in magnitude to moderate.

N110EDCA.DAT – The algorithm estimate of 0.375 mm, shown in Figure 180, is a fair match to the measured data.

N110FDCA.DAT – The algorithm estimate of 0.400 mm, shown in Figure 181, is a fair-to-good match to the measured data.

N110GDCA.DAT – The algorithm estimate of 0.350 mm, shown in Figure 182, is a fair-to-good match to the measured data.

N110HDCA.DAT – The algorithm estimate of 0.325 mm, shown in Figure 183, is a fair-to-good match to the measured data.

The main bridge was moved north to the 2-mm crude oil target. The surface of the target appeared to have uniform oil coverage. Data sets were collected from the southern sector of the oil target. Rain continued. (The file names for the 2-mm crude and diesel oils are slightly different than those conventionally used during this collection.)

N120ADCA.DAT – The algorithm estimate of 2.325 mm, shown in Figure 184, is an excellent match to the measured data.

N120BDCA.DAT – The algorithm estimate of 2.425 mm, shown in Figure 185, is an excellent match to the measured data.

N120CDCA.DAT – The algorithm estimate of 2.225 mm, shown in Figure 186, is an excellent match to the measured data.

N120DDCA.DAT – The algorithm estimate of 2.125 mm, shown in Figure 187, is an excellent match to the measured data.

The bridge was moved north to collect data from the center of the target pool. Rain continued.

N120EDCA.DAT – The algorithm estimate of 1.975 mm, shown in Figure 188, is a good-to-excellent match to the measured data.

N120FDCA.DAT – The algorithm estimate of 1.975 mm, shown in Figure 189, is a good-to-excellent match to the measured data.

N120GDCA.DAT – The algorithm estimate of 1.875 mm, shown in Figure 190, is a good-to-excellent match to the measured data.

The main bridge was moved north to collect data from the northernmost sector of the target pool. Rain continued.

N120HDCA.DAT – The algorithm estimate of 1.525 mm, shown in Figure 191, is a fair match to the measured data.

N120JDCA.DAT – The algorithm estimate of 1.575 mm, shown in Figure 192, is a fair match to the measured data.

N120KDCA.DAT – The algorithm estimate of 1.575 mm, shown in Figure 193, is a fair match to the measured data.

N120LDCA.DAT – The algorithm estimate of 1.475 mm, shown in Figure 194, is a poor-to-fair match to the measured data.

The main bridge was moved north to the southernmost sector of the 2-mm diesel oil target. Rain conditions had decreased to light.

N120ADDA.DAT – The algorithm estimate of 3.400 mm, shown in Figure 195, is an excellent match to the measured data.

N120BDDA.DAT – The algorithm estimate of 3.350 mm, shown in Figure 196, is an excellent match to the measured data.

N120CDDA.DAT – The algorithm estimate of 3.425 mm, shown in Figure 197, is an excellent match to the measured data.

N120DDDA.DAT – The algorithm estimate of 0.550 mm, shown in Figure 198, is a good-to-excellent match to the measured data. If the measured data curve had less sinusoidal response, a 3.3 to 3.5 mm estimate would have been a better choice.

The radiometer position was shifted east to collect measurements from the thickest area of the oil target. Rain continued.

N120EDDA.DAT – The algorithm estimate of 3.850 mm, shown in Figure 199, is a good match to the measured data. The measured data curve exhibits an inflection point near 38 GHz, which might indicate oil thicknesses closer to 4 mm.

N120FDDA.DAT – The algorithm estimate of 3.825 mm, shown in Figure 200, is a good match to the measured data. The measured data curve exhibits inflection points near 39 and 29 GHz, which might indicate oil thicknesses closer to 4 mm.

N120GDDA.DAT – The algorithm estimate of 3.850 mm, shown in Figure 201, is a good-to-excellent match to the measured data.

N120HDDA.DAT – The algorithm estimate of 3.925 mm, shown in Figure 202, is a fair match to the measured data. The measured data curve exhibits an inflection point near 37 GHz, which might indicate oil thicknesses closer to 4.1 mm.

The main bridge was moved north and the radiometer position shifted west to collect data from an area that appeared to be thinner than the previous collection area. Rain continued.

N120JDDA.DAT – The algorithm estimate of 0.700 mm, shown in Figure 203, is a good-to-excellent match to the measured data.

N120KDDA.DAT – The algorithm estimate of 0.550 mm, shown in Figure 204, is a good-to-excellent match to the measured data.

N120LDDA.DAT – The algorithm estimate of 0.450 mm, shown in Figure 205, is an excellent match to the measured data.

The main bridge was moved north to collect data over the 3-mm crude oil target. Light rain continued.

N130ACCA.DAT – The algorithm estimate of 3.750 mm, shown in Figure 206, is a good match to the measured data based on curve shape.

N130BCCA.DAT – The algorithm estimate of 3.750 mm, shown in Figure 207, is a good match to the measured data based on curve shape.

N130CCCA.DAT – The algorithm estimate of 3.650 mm, shown in Figure 208, is a good match to the measured data based on curve shape.

N130DCCA.DAT – The algorithm estimate of 3.825 mm, shown in Figure 209, is a good match to the measured data based on curve shape.

The main bridge was moved 2 to 3 ft north to collect data from a different area in the target pool. Light rain continued.

N130ECCA.DAT – The algorithm estimate of 3.200 mm, shown in Figure 210, is a good match to the measured data based on curve shape.

N130FCCA.DAT – The algorithm estimate of 3.100 mm, shown in Figure 211, is an excellent match to the measured data.

N130GCCA.DAT – The algorithm estimate of 3.175 mm, shown in Figure 212, is an excellent match to the measured data.

N130HCCA.DAT – The algorithm estimate of 3.200 mm, shown in Figure 213, is an excellent match to the measured data.

The main bridge was moved north to the 3-mm diesel oil target. Data sets were collected from the southeast sector, which contained thicker oil. Light rain continued.

N130ADCA.DAT – The algorithm estimate of 4.350 mm, shown in Figure 214, is a good-to-excellent match to the measured data.

N130BDCA.DAT – The algorithm estimate of 0.800 mm, shown in Figure 215, is a good match to the measured data.

N130CDCA.DAT – The algorithm estimate of 7.800 mm is a poor match to the measured data. A better estimate based on the measured data curve shape is 4.550 mm, shown in Figure 216.

N130DDCA.DAT – The algorithm estimate of 4.450 mm, shown in Figure 217, is a good match to the measured data.

The main bridge was moved north to collect data from the northeastern sector of the target pool. The following data sets were collected over a discolored area in the target. Light rain continued.

N130EDCA.DAT – The algorithm estimate of 0.875 mm, shown in Figure 218, is a good match to the measured data.

N130FDCA.DAT – The algorithm estimate of 0.875 mm, shown in Figure 219, is a fair match to the measured data based on the mean value of the measured data curve. Note its sinusoidal shape.

N130GDCA.DAT – The algorithm estimate of 0.900 mm, shown in Figure 220, is a good-to-excellent match to the measured data.

N130HDCA.DAT – The algorithm estimate of 2.850 mm, shown in Figure 221, is a fair-to-good match to the measured data.

The radiometer position was shifted to collect data over the northwestern sector of the target pool where the oil appeared thin. (The following results indicate that the oil was thicker than anticipated.) Light rain continued.

N130JDCA.DAT – The algorithm estimate of 0.750 mm, shown in Figure 222, is a fair match to the measured data based on the mean values of the curves. Note the sinusoidal variation in the measured data curve.

N130KDCA.DAT – The algorithm estimate of 3.250 mm, shown in Figure 223, is a good-to-excellent match to the measured data based on curve shape.

N130LDCA.DAT – The algorithm estimate of 3.425 mm, shown in Figure 224, is a good-to-excellent match to the measured data based on curve shape.

N130MDCA.DAT – The algorithm estimate of 3.550 mm, shown in Figure 225, is an excellent match to the measured data.

N130NDCA.DAT – The algorithm estimate of 3.600 mm, shown in Figure 226, is an excellent match to the measured data.

The main bridge was moved north to the 8-mm crude oil target. Data sets were collected from the southeast sector. Light rain continued. The measured thickness seemed to fluctuate based on operator observation of the laptop display. The operator attempted to capture a variety of thicknesses from this part of the target pool.

N180ACCA.DAT – The algorithm estimate of 9.375 mm, shown in Figure 227, is a good-to-excellent match to the measured data based on curve shape.

N180BCCA.DAT – The algorithm estimate of 8.575 mm, shown in Figure 228, is a good-to-excellent match to the measured data.

N180CCCA.DAT – The algorithm estimate of 8.900 mm, shown in Figure 229, is a good match to the measured data.

N180DCCA.DAT – The algorithm estimate of 8.300 mm, shown in Figure 230, is a fair-to-good match to the measured data.

N180ECCA.DAT – The algorithm estimate of 10.000 mm, shown in Figure 231, is a fair-to-good match to the measured data based on the curve shape of the estimated and the actual measured data points (not the smoothed curve).

N180FCCA.DAT – The algorithm estimate of 8.925 mm, shown in Figure 232, is a good match to the measured data based on curve shape.

The main bridge moved north and the radiometer position was shifted west to collect data from the northwest sector of the target pool. Light rain continued.

N180GCCA.DAT – The algorithm estimate of 7.300 mm, shown in Figure 233, is a good match to the measured data based on curve shape.

N180HCCA.DAT – The algorithm estimate of 3.400 mm is a poor match to the measured data. The LMS-only result of 6.950 mm, shown in Figure 234, is a good-to-excellent match to the measured data.

N180JCCA.DAT – The algorithm estimate of 7.150 mm, shown in Figure 235, is a fair-to-good match to the measured data.

N180KCCA.DAT – The algorithm estimate of 3.475 mm is a poor match to the measured data. The LMS-only result of 7.100 mm, shown in Figure 236, is a good match to the measured data.

N180LCCA.DAT – The algorithm estimate of 7.150 mm, shown in Figure 237, is a good match to the measured data.

The radiometer position was shifted east to collect data from the northeast sector of the target pool. Light rain continued.

N180MCCA.DAT – The algorithm estimate of 7.325 mm, shown in Figure 238, is a good match to the measured data.

N180NCCA.DAT – The algorithm estimate of 7.250 mm, shown in Figure 239, is a good match to the measured data.

N180PCCA.DAT – The algorithm estimate of 7.100 mm, shown in Figure 240, is a good match to the measured data.

N180QCCA.DAT – The algorithm estimate of 7.325 mm, shown in Figure 241, is a good match to the measured data.

The main bridge was moved south and the radiometer position shifted to measure the southwestern sector of the target pool. Light rain continued.

N180RCCA.DAT – The algorithm estimate of 1.675 mm is a poor match to the measured data. An estimate of 8.350 mm, shown in Figure 242, appears to be a better match if the outlying points at 30, 33, and 34 GHz are ignored.

N180SCCA.DAT – The algorithm estimate of 8.550 mm, shown in Figure 243, is a good match to the measured data.

N180TCCA.DAT – The algorithm estimate of 8.650 mm, shown in Figure 244, is a good match to the measured data.

N180UCCA.DAT – The algorithm estimate of 8.750 mm, shown in Figure 245, is a good-to-excellent match to the measured data.

The main bridge was moved north to the 8-mm diesel oil target. Overall, the target was mottled. The radiometer was positioned to collect data from the southeastern sector of the target pool. Light rain continued.

N180ADCA.DAT – The algorithm estimate of 6.95 mm is a fair match to the measured data. A better match, shown in Figure 246, was found using an estimate of 7.200 mm.

N180BDCA.DAT – The algorithm estimate of 7.425 mm, shown in Figure 247, is a good match to the measured data based on curve shape.

N180CDCA.DAT – The algorithm estimate of 10.000 mm, shown in Figure 248, is a good match to the measured data points, if the smoothed curve is ignored.

N180DDCA.DAT – The algorithm estimate of 7.150 mm is a fair match to the measured data. A better match, shown in Figure 249, was found using an estimate of 7.500 mm.

N180EDCA.DAT – The algorithm estimate of 7.425 mm, shown in Figure 250, is a good match to the measured data based on curve shape.

N180FDCA.DAT – The algorithm estimate of 10.000 mm, shown in Figure 251, is a fair-to-good match to the measured data, if the smoothed curve is ignored.

The main bridge was moved north and the radiometer position shifted to collect data from the center of the target pool. This area had a discolored section with a more mottled appearance than the other areas of the target pool. Light rain continued.

N180GDCA.DAT – The algorithm estimate of 3.300 mm is a poor match to the measured data. A 10.000-mm estimate (LMS-only result), shown in Figure 252, is a good match, if the smoothed curve is ignored.

N180HCA.DAT – The algorithm estimate of 3.300 mm is a poor match to the measured data. A 10.000-mm estimate (LMS-only result), shown in Figure 253, is a good match, if the smoothed curve is ignored.

N180JDCA.DAT – The algorithm estimate of 7.200 mm is a fair match to the measured data. A better match is found using an estimate of 7.500 mm, shown in Figure 254.

N180KDCA.DAT – The algorithm estimate of 8.050 mm, shown in Figure 255, is a fair-to-good match to the measured data, if the smoothed curve is ignored.

N180LDCA.DAT – The algorithm estimate of 6.965 mm is a poor match to the measured data. A better shape match is found using an estimate of 7.300 mm, shown in Figure 256.

The radiometer position was shifted west to collect data from the western sector of the target pool. Light rain continued.

N180MDCA.DAT – The algorithm estimate of 3.300 mm is a poor match to the measured data. A 10.000-mm estimate (LMS-only result), shown in Figure 257, provides a better match to the data set, if the smoothed curve is ignored.

N180NDCA.DAT – The algorithm estimate of 6.850 mm is a poor match to the measured data. A better match to the shape of the measured data curve is shown in Figure 258, using an estimate of 7.000 mm, if the smoothed curve is ignored.

N180PDCA.DAT – The algorithm estimate of 3.300 mm is a poor match to the measured data. A 10.000-mm estimate (LMS-only result), shown in Figure 259, provides a better match to the data set, if the smoothed curve is ignored.

The main bridge was moved south to the 3-mm diesel oil target. Fans mounted on the main bridge were turned on, blowing east to west. The following measurements were collected over the center of the target pool where a patch of scummy-looking oil had collected. Rain has stopped.

N130ADFA.DAT – The algorithm estimate of 0.950 mm, shown in Figure 260, is a good match to the measured data.

N130BDFA.DAT – The algorithm estimate of 1.000 mm, shown in Figure 261, is a fair-to-good match to the measured data. Note the presence of the sinusoidal variation.

N130CDFA.DAT – The algorithm estimate of 0.950 mm, shown in Figure 262, is a good-to-excellent match to the measured data.

N130DDFA.DAT – The algorithm estimate of 1.000 mm, shown in Figure 263, is an excellent match to the measured data.

N130EDFA.DAT – The algorithm estimate of 4.100 mm, shown in Figure 264, is a good match to the measured data.

The radiometer position was shifted to a new area in the target pool. The operator noticed that the signature here was somewhat indeterminate, so only one measurement was collected.

N130FDFA.DAT – The algorithm estimate of 0.825 mm, shown in Figure 265, is a fair match to the measured data.

The radiometer position was shifted to collect data from a part of the target pool that had an interesting IR signature.

N130GDFA.DAT – The algorithm estimate of 4.250 mm, shown in Figure 266, is a good-to-excellent match to the measured data.

N130HDFA.DAT – The algorithm estimate of 4.775 mm, shown in Figure 267, is a fair-to-good match to the measured data.

N130JDFA.DAT – The algorithm estimate of 4.375 mm, shown in Figure 268, is an excellent match to the measured data.

N130KDFA.DAT – The algorithm estimate of 3.900 mm, shown in Figure 269, is a good-to-excellent match to the measured data.

The main bridge was moved north to the 8-mm diesel oil target. Fans were turned on, blowing east to west. The radiometer was aimed at an interesting IR signature that rotated clockwise, approximately 1.5 rotations during the measurement period.

N180S1.DAT – The algorithm estimate of 4.300 mm is a poor match to the measured data. If the smoothed curve is ignored, an estimate of 8.500 mm yields a fair-to-good match, shown in Figure 270.

N180S2.DAT – The algorithm estimate of 6.900 mm, shown in Figure 271, is a fair-to-good match to the measured data.

N180S3.DAT – The algorithm estimate of 7.050 mm, shown in Figure 272, is a fair-to-good match to the measured data.

N180S4.DAT – The algorithm estimate of 0.800 mm is a poor match to the measured data. An estimate of 8.300 mm, shown in Figure 273, yields a fair shape match to the measured data points, if the smoothed curve is ignored.

N180S5.DAT – The algorithm estimate of 1.650 mm is a poor match to the measured data. The LMS-only result of 8.250 mm, shown in Figure 274, is a fair-to-good match to the measured data points, if the smoothed curve is ignored.

N180S6.DAT – The algorithm estimate of 9.400 mm, shown in Figure 275, is a good match to the measured data based on curve shape.

N180S7.DAT – The algorithm estimate of 3.325 is a poor match to the measured data. The LMS-only result of 6.775 mm, shown in Figure 276, yields a good match to the measured data points.

N180S8.DAT – The algorithm estimate of 7.425 mm, shown in Figure 277, is a good match to the measured data.

N180S9.DAT – The algorithm estimate of 6.650 mm, shown in Figure 278, is a good-to-excellent match to the measured data.

N180S10.DAT – The algorithm estimate of 6.750 mm, shown in Figure 279, is a good-to-excellent match to the measured data.

N180S11.DAT – The algorithm estimate of 0.725 is a poor match to the measured data. The correlation-only result of 7.750 mm, shown in Figure 280, yields a good shape match to the measured data set.

N180S12.DAT – The algorithm estimate of 7.175 mm, shown in Figure 281, is a good match to the measured data.

N180S13.DAT – The algorithm estimate of 6.675 mm, shown in Figure 282, is a good match to the measured data.

N180S14.DAT – The algorithm estimate of 0.700 mm is a poor match to the measured data. The correlation-only result of 7.575 mm, shown in Figure 283, yields a fair match to the shape of the measured data points.

The main bridge was moved to the 8-mm crude oil target. The wind had greatly increased, driving oil out of this target. The radiometer was positioned to collect data from the southwest sector of the target pool. Fans were turned on, blowing east to west. It is apparent that the radiometer should have been recalibrated prior to the following measurements.

N180SC1.DAT – The algorithm estimate of 0.000 mm is a poor match to the measured data. An estimate of 8.700 mm, shown in Figure 284, results in a fair shape match.

N180SC2.DAT – The algorithm estimate of 0.175 mm is a poor match to the measured data. The correlation-only estimate of 9.375 mm, shown in Figure 285, results in a fair shape match.

N180SC3.DAT – The algorithm estimate of 0.000 mm is a poor match to the measured data. The correlation-only estimate of 8.925 mm, shown in Figure 286, results in a good shape match.

N180SC4.DAT – The algorithm estimate of 0.000 mm is a poor match to the measured data. An estimate of 8.500 mm, shown in Figure 287, results in a fair shape match.

N180SC5.DAT – The algorithm estimate of 0.000 mm is a poor match to the measured data. An estimate of 8.300 mm, shown in Figure 288, results in a fair shape match.

N180SC6.DAT – The algorithm estimate of 0.000 mm is a poor match to the measured data. An estimate of 7.800 mm, shown in Figure 289, results in a fair shape match.

N180SC7.DAT – The algorithm estimate of 0.000 mm is a poor match to the measured data. An estimate of 8.300 mm, shown in Figure 290, results in a fair shape match.

N180SC8.DAT – The algorithm estimate of 0.000 mm is a poor match to the measured data. An estimate of 8.000 mm, shown in Figure 291, results in a fair shape match.

N180SC9.DAT – The algorithm estimate of 0.000 mm is a poor match to the measured data. An estimate of 8.200 mm, shown in Figure 292, results in a fair shape match.

N180SC10.DAT – The algorithm estimate of 0.000 mm is a poor match to the measured data. An estimate of 7.800 mm, shown in Figure 293, results in a fair shape match.

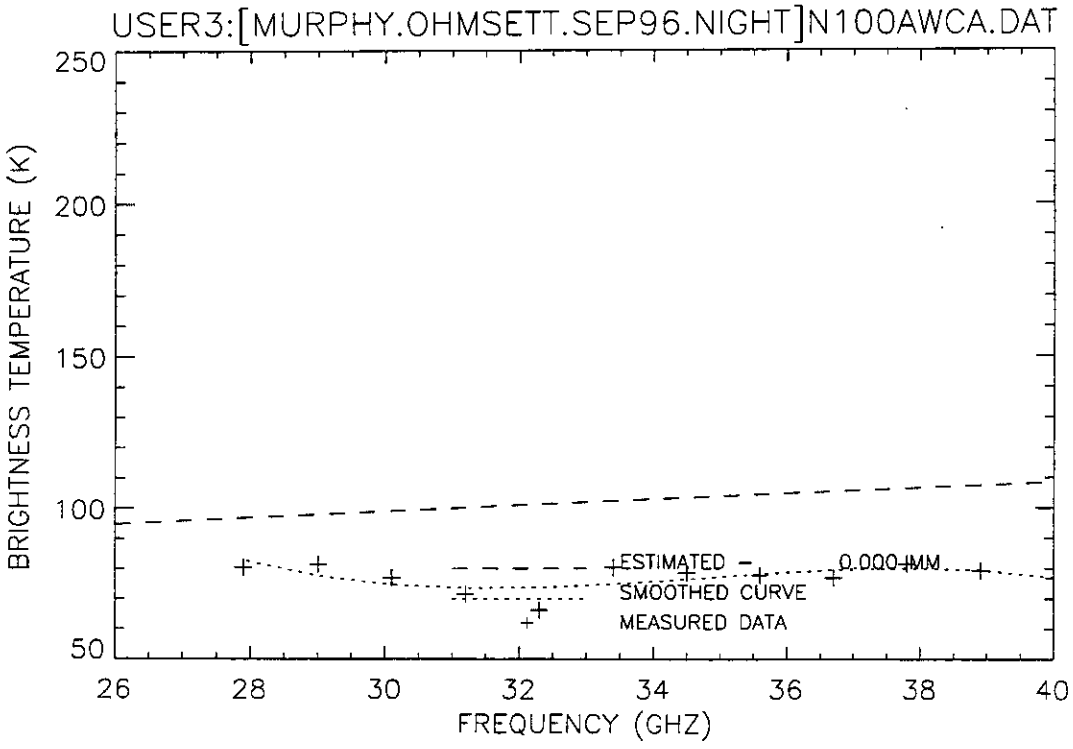

Figure 146. Plot of radiometric brightness temperature versus measurement frequency for water, night test, calm wave conditions, 12 September 1996, sweep A.

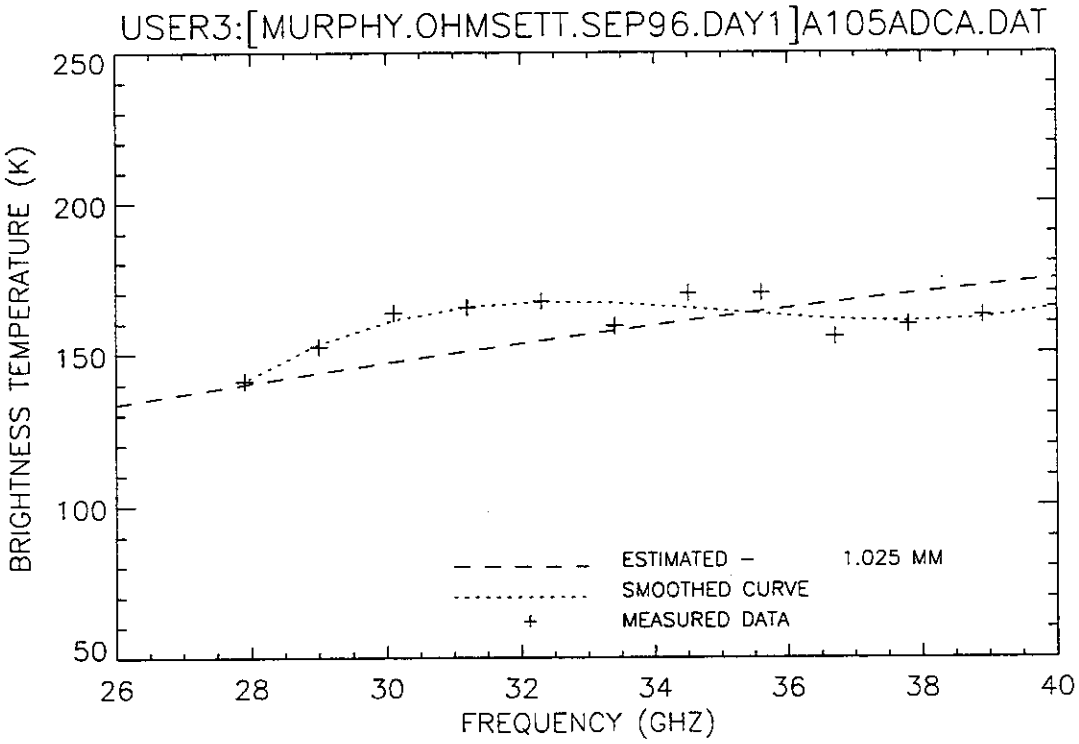

Figure 122. Plot of radiometric brightness temperature versus measurement frequency for 0.5-mm diesel oil, day 1 test, calm wave conditions, 11 September 1996, sweep A.

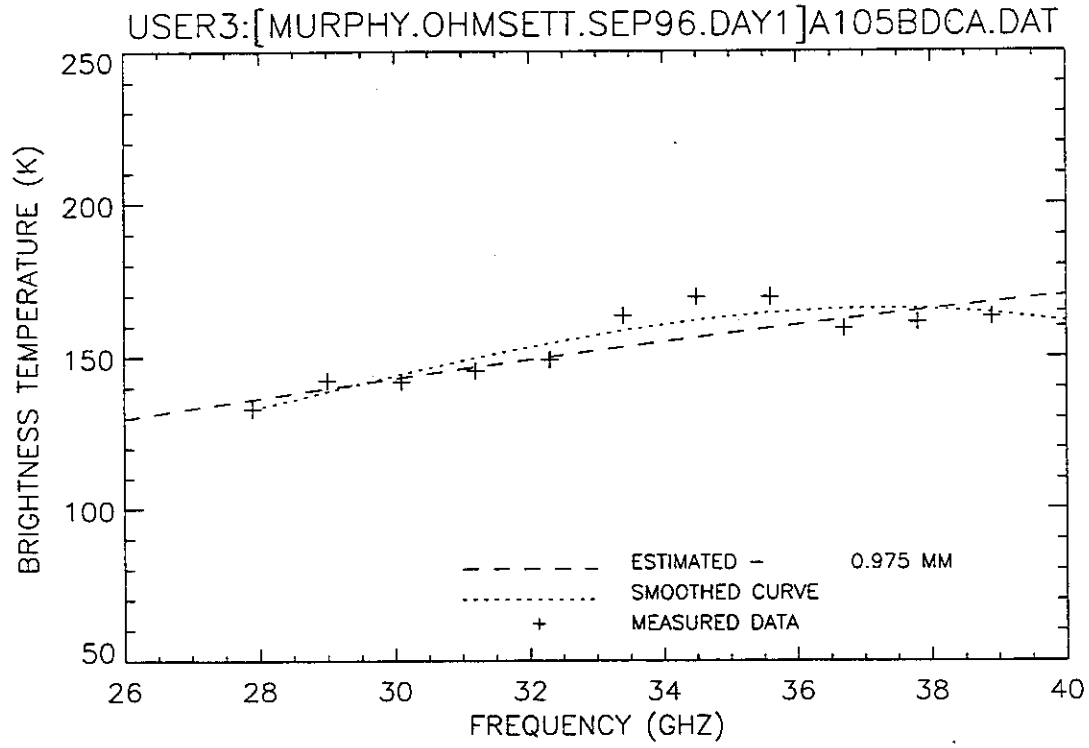

Figure 123. Plot of radiometric brightness temperature versus measurement frequency for 0.5-mm diesel oil, day 1 test, calm wave conditions, 11 September 1996, sweep B.

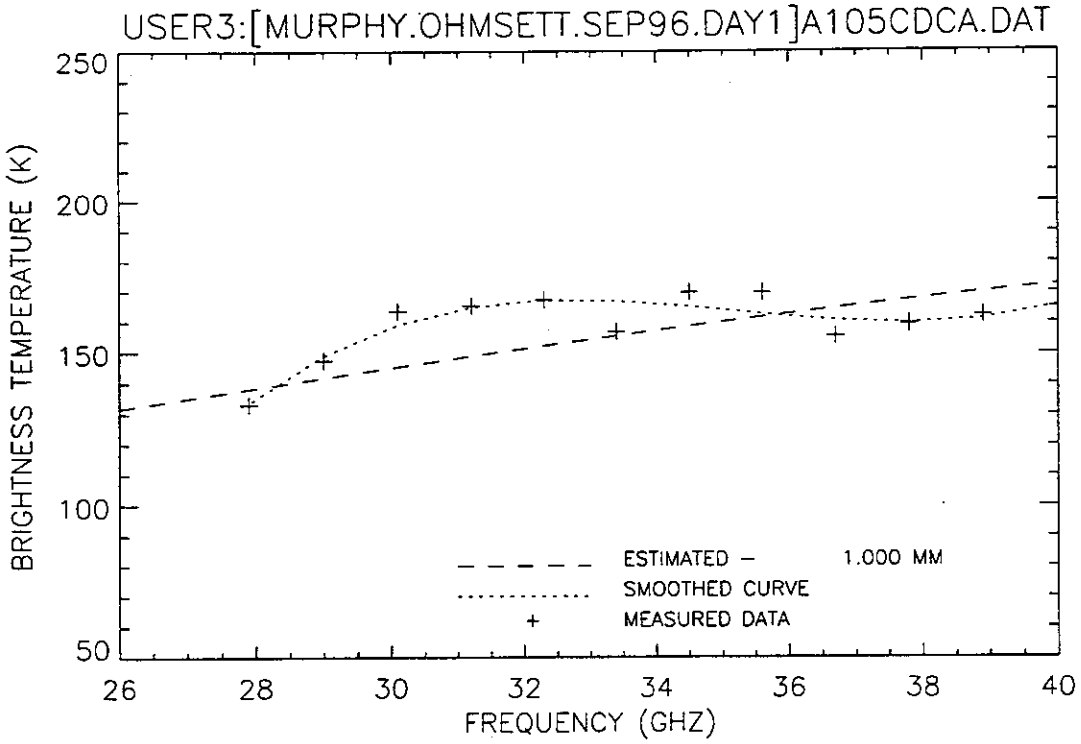

Figure 124. Plot of radiometric brightness temperature versus measurement frequency for 0.5-mm diesel oil, day 1 test, calm wave conditions, 11 September 1996, sweep C.

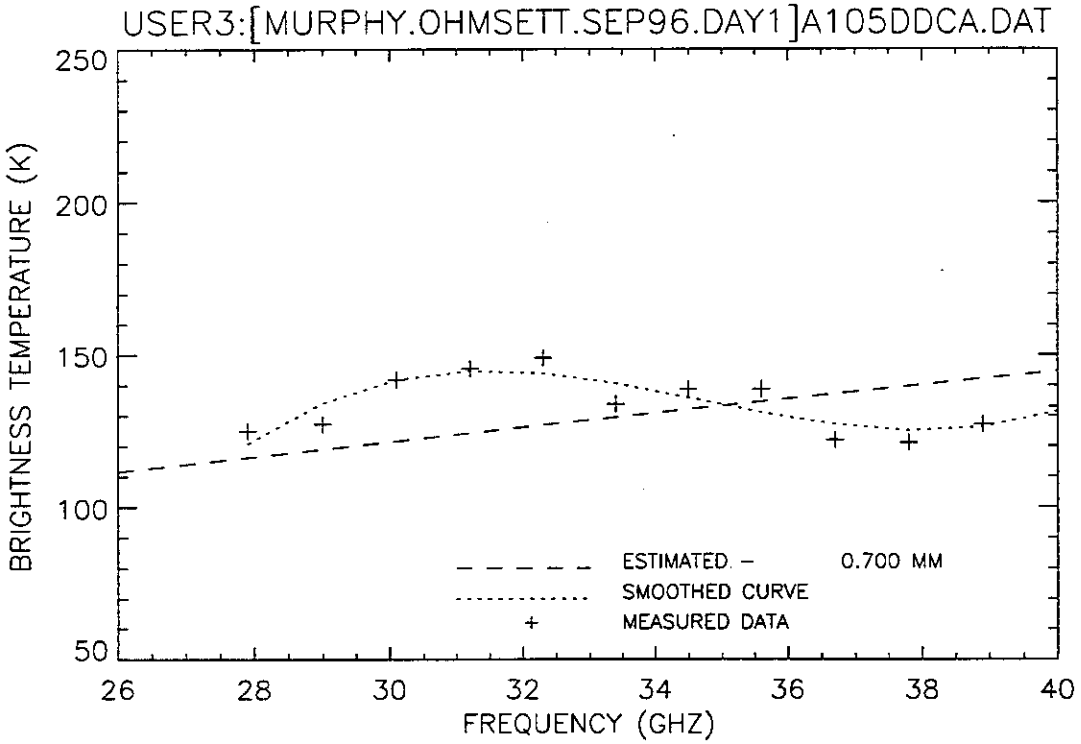

Figure 125. Plot of radiometric brightness temperature versus measurement frequency for 0.5-mm diesel oil, day 1 test, calm wave conditions, 11 September 1996, sweep D.

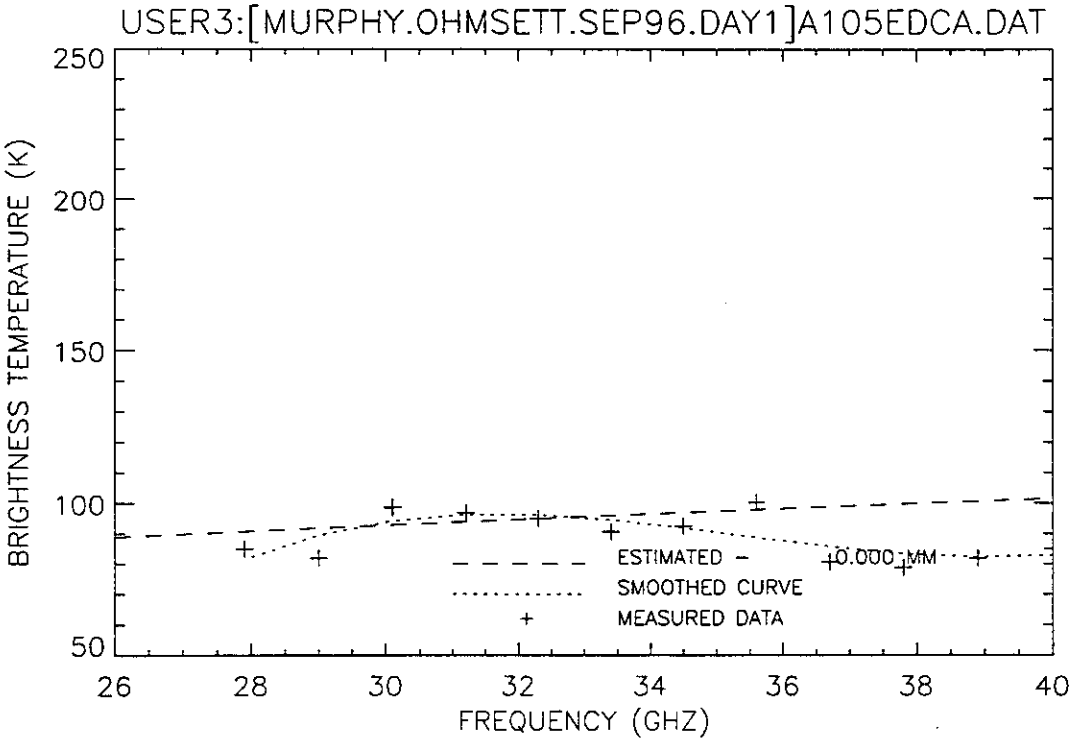

Figure 126. Plot of radiometric brightness temperature versus measurement frequency for 0.5-mm diesel oil, day 1 test, calm wave conditions, 11 September 1996, sweep E.

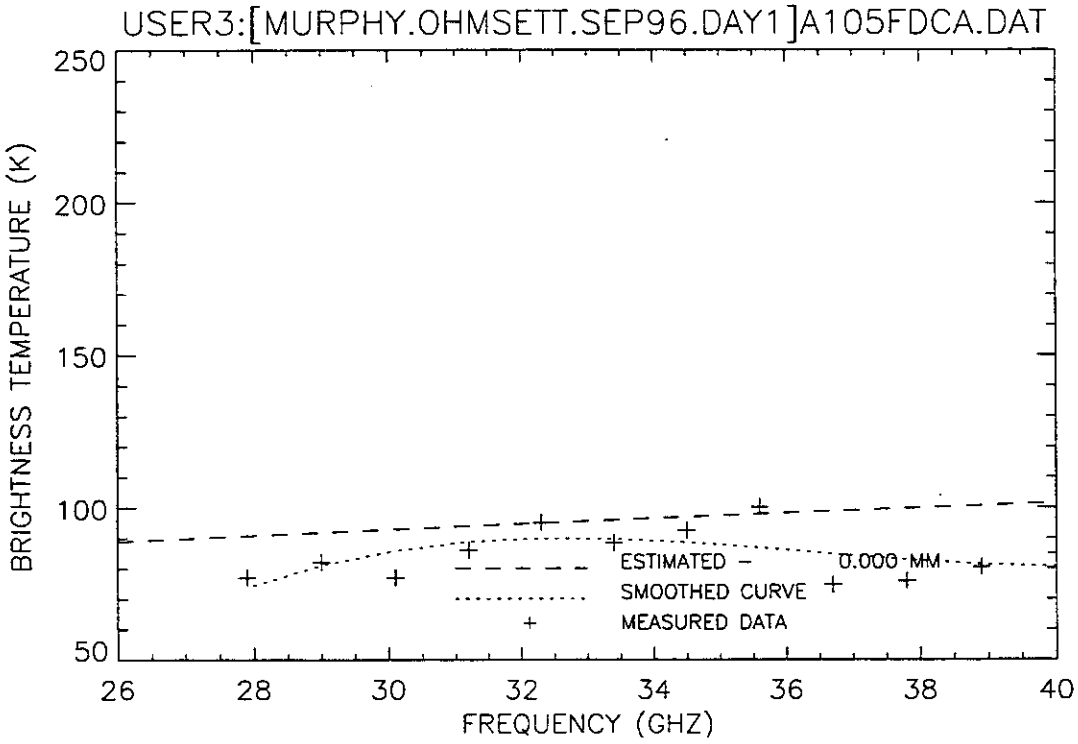

Figure 127. Plot of radiometric brightness temperature versus measurement frequency for 0.5-mm diesel oil, day 1 test, calm wave conditions, 11 September 1996, sweep F.

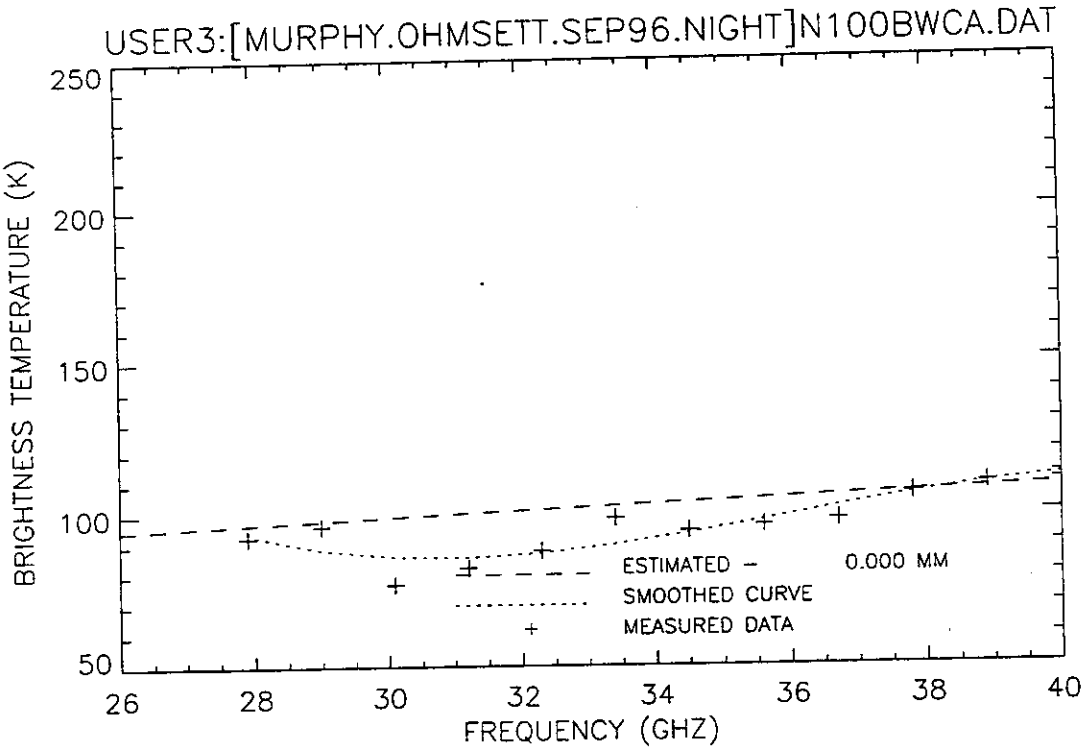

Figure 147. Plot of radiometric brightness temperature versus measurement frequency for water, night test, calm wave conditions, 12 September 1996, sweep B.

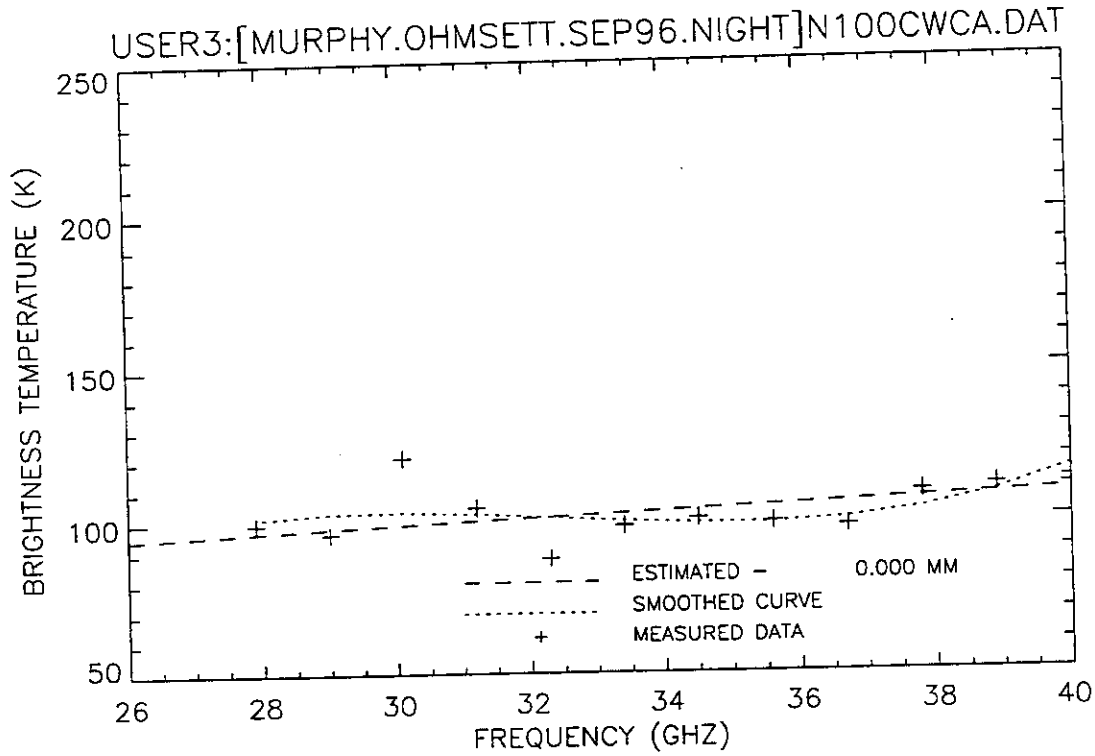

Figure 148. Plot of radiometric brightness temperature versus measurement frequency for water, night test, calm wave conditions, 12 September 1996, sweep C.

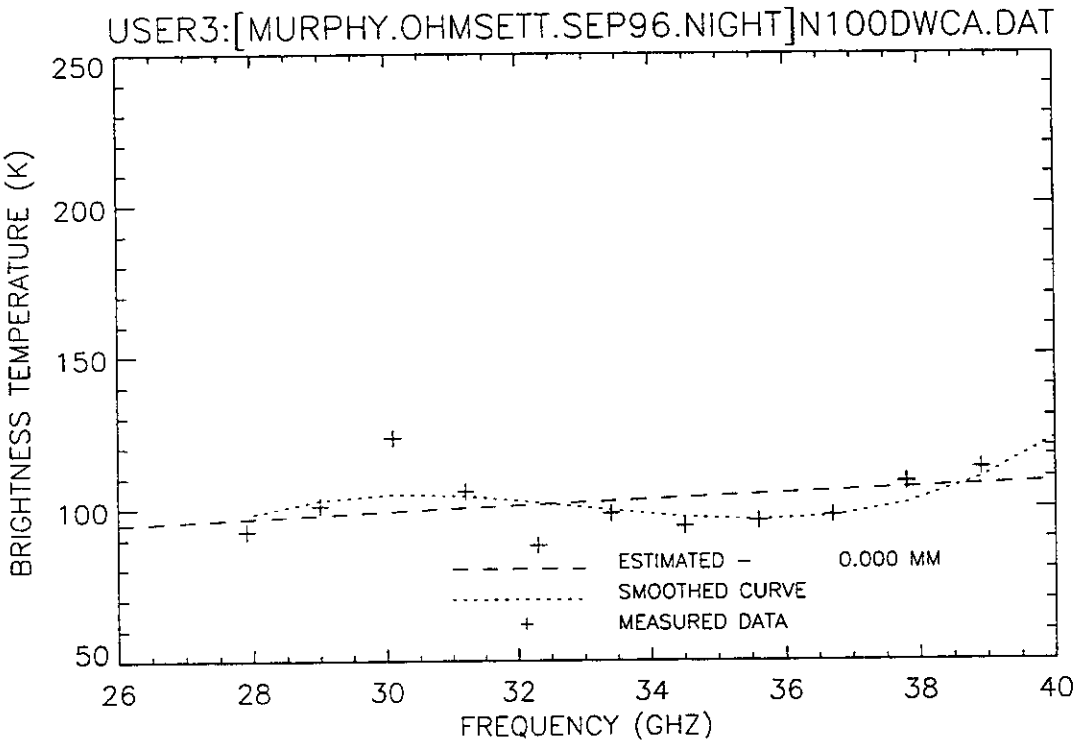

Figure 149. Plot of radiometric brightness temperature versus measurement frequency for water, night test test, calm wave conditions, 12 September 1996, sweep D.

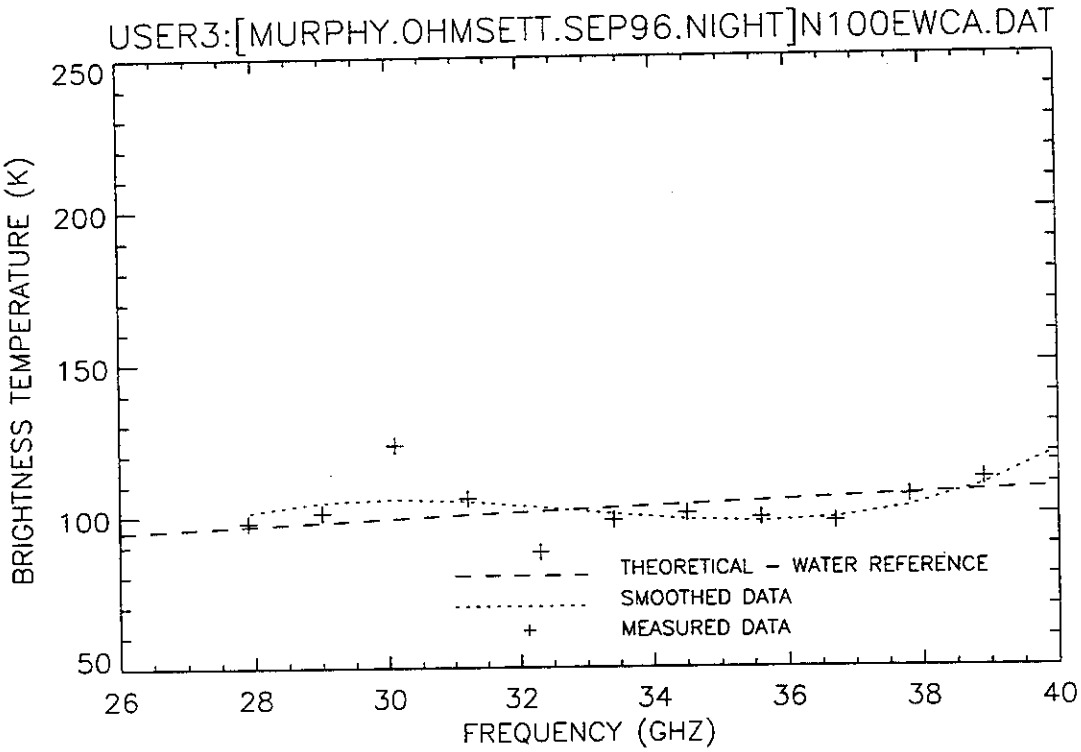

Figure 150. Plot of radiometric brightness temperature versus measurement frequency for water, night test, calm wave conditions, 12 September 1996, sweep E.

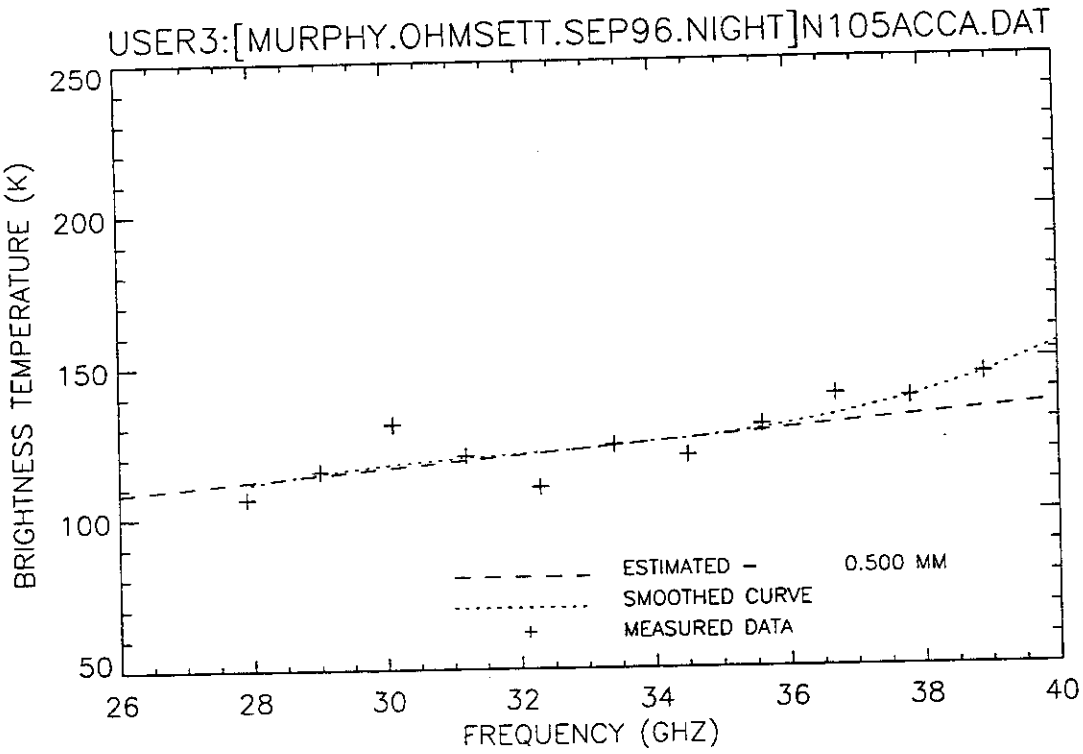

Figure 151. Plot of radiometric brightness temperature versus measurement frequency for 0.5-mm crude oil, night test, calm wave conditions, 12 September 1996, sweep A.

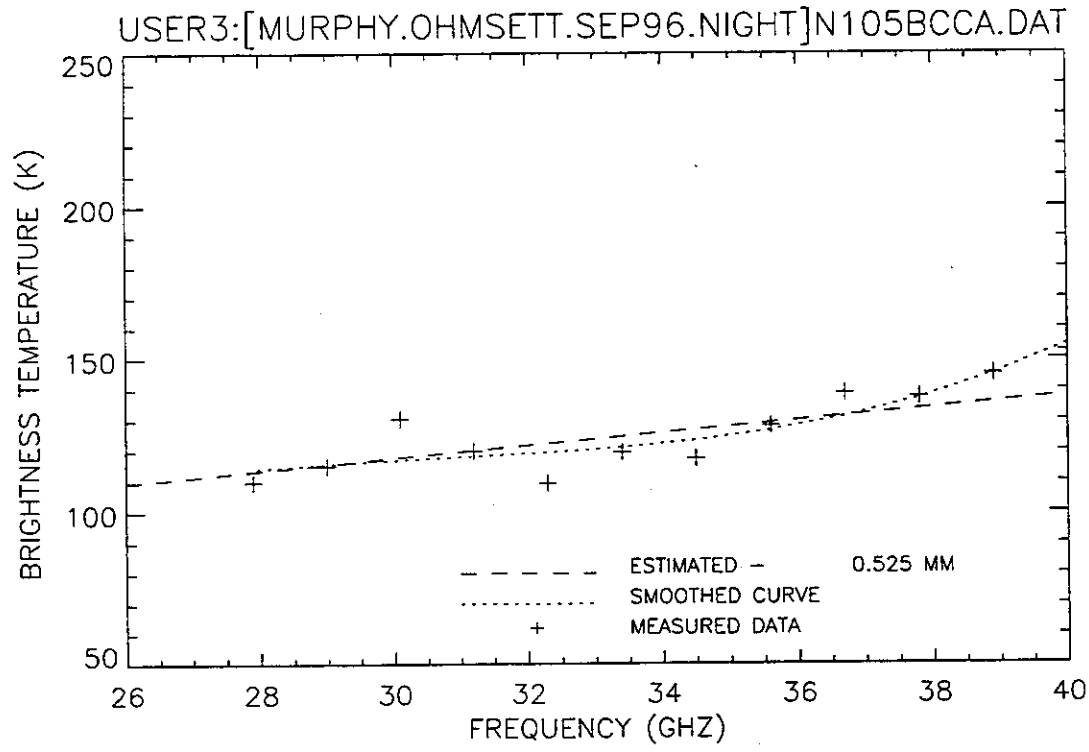

Figure 152. Plot of radiometric brightness temperature versus measurement frequency for 0.5-mm crude oil, night, calm wave conditions, 12 September 1996, sweep B.

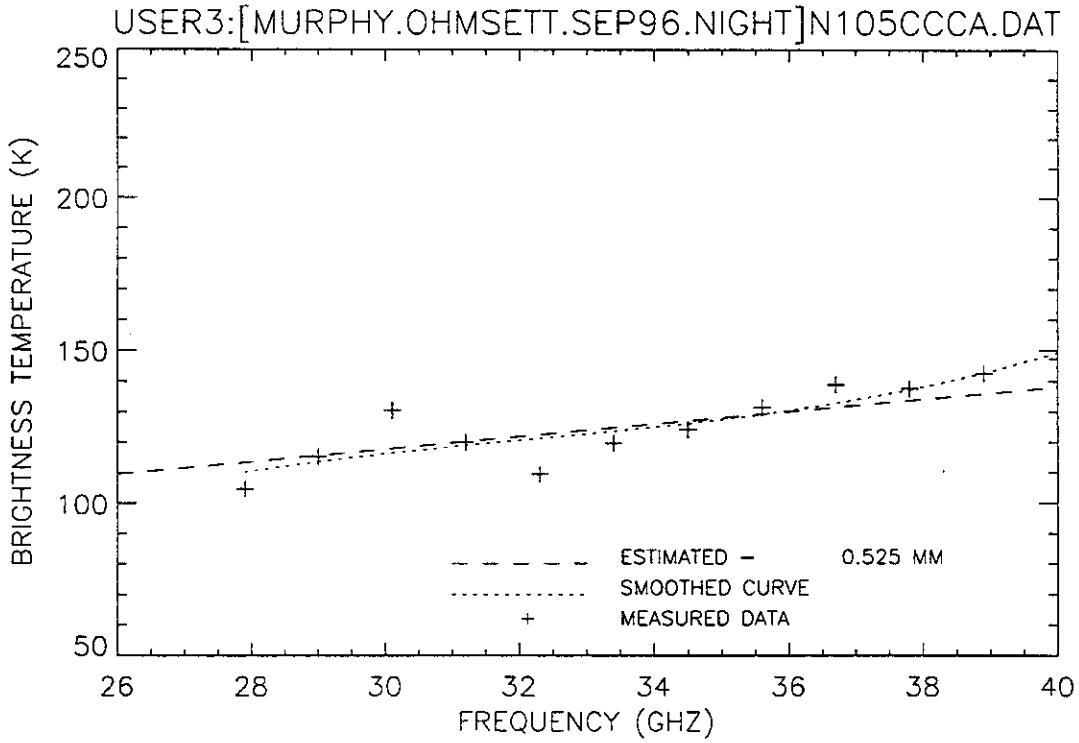

Figure 153. Plot of radiometric brightness temperature versus measurement frequency for 0.5-mm crude oil, night test, calm wave conditions, 12 September 1996, sweep C.

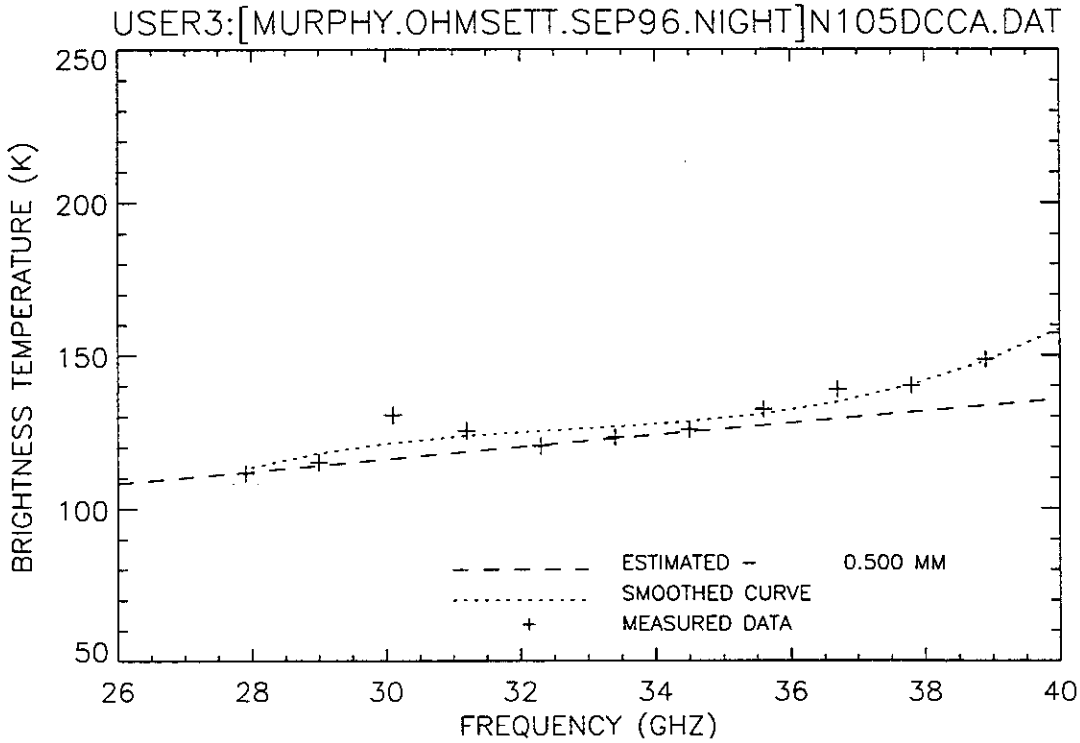

Figure 154. Plot of radiometric brightness temperature versus measurement frequency for 0.5-mm crude oil, night test, calm wave conditions, 12 September 1996, sweep D.

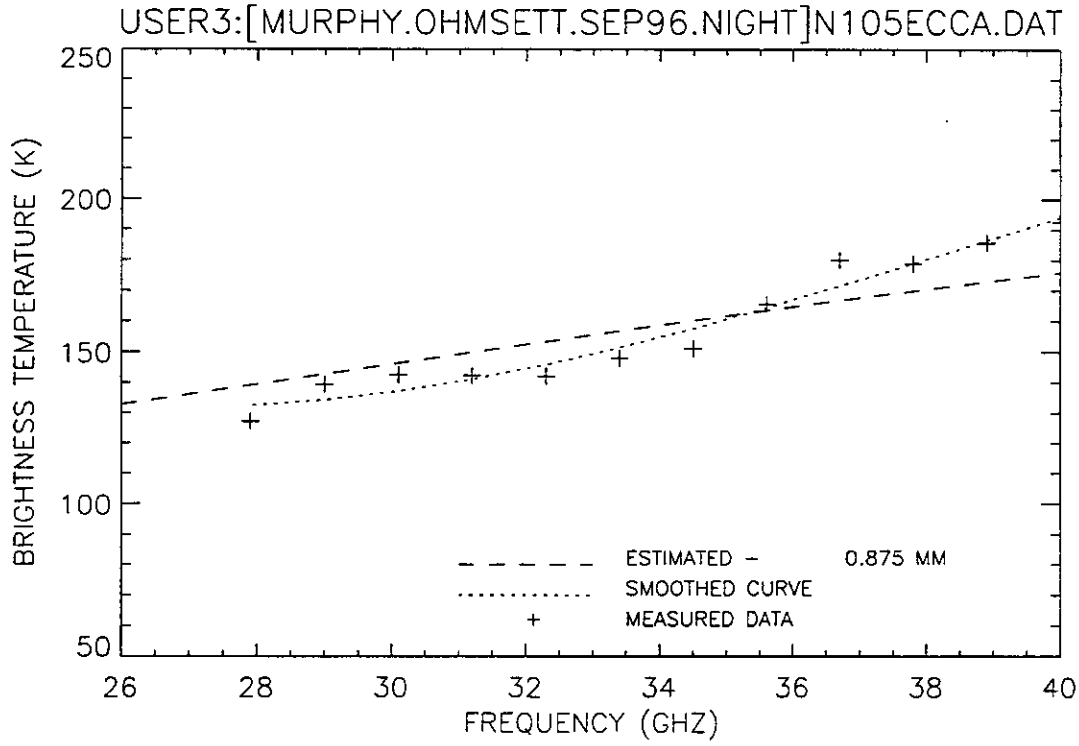

Figure 155. Plot of radiometric brightness temperature versus measurement frequency for 0.5-mm crude oil, night test, calm wave conditions, 12 September 1996, sweep E.

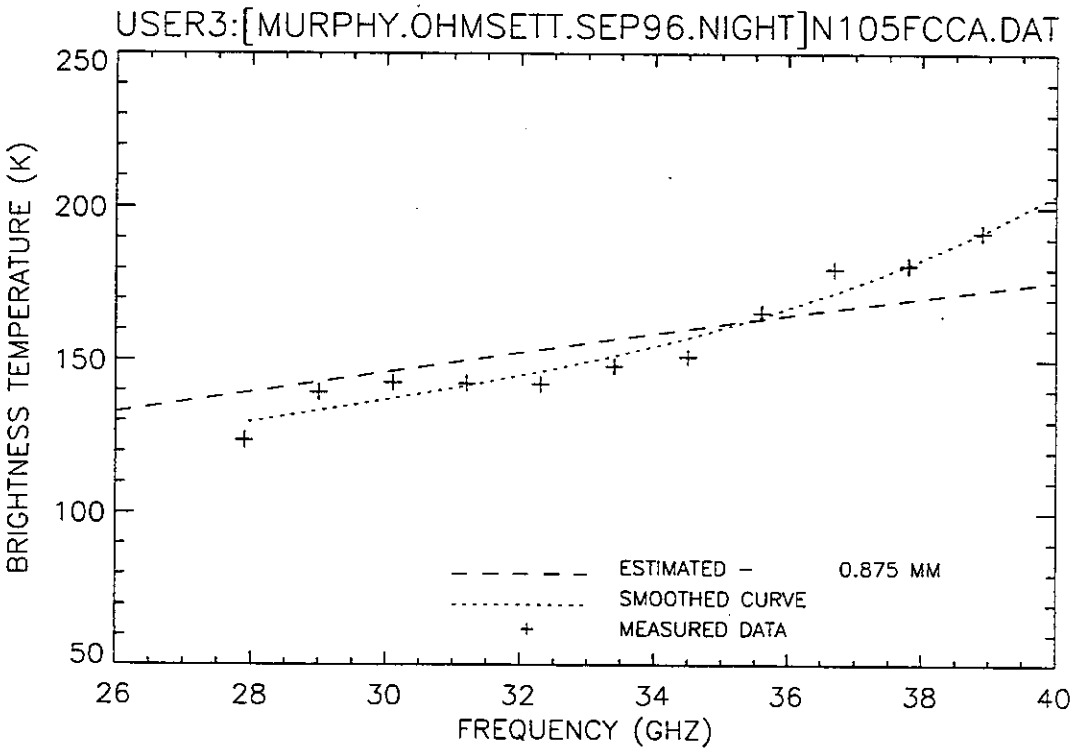

Figure 156. Plot of radiometric brightness temperature versus measurement frequency for 0.5-mm crude oil, night test, calm wave conditions, 12 September 1996, sweep F.

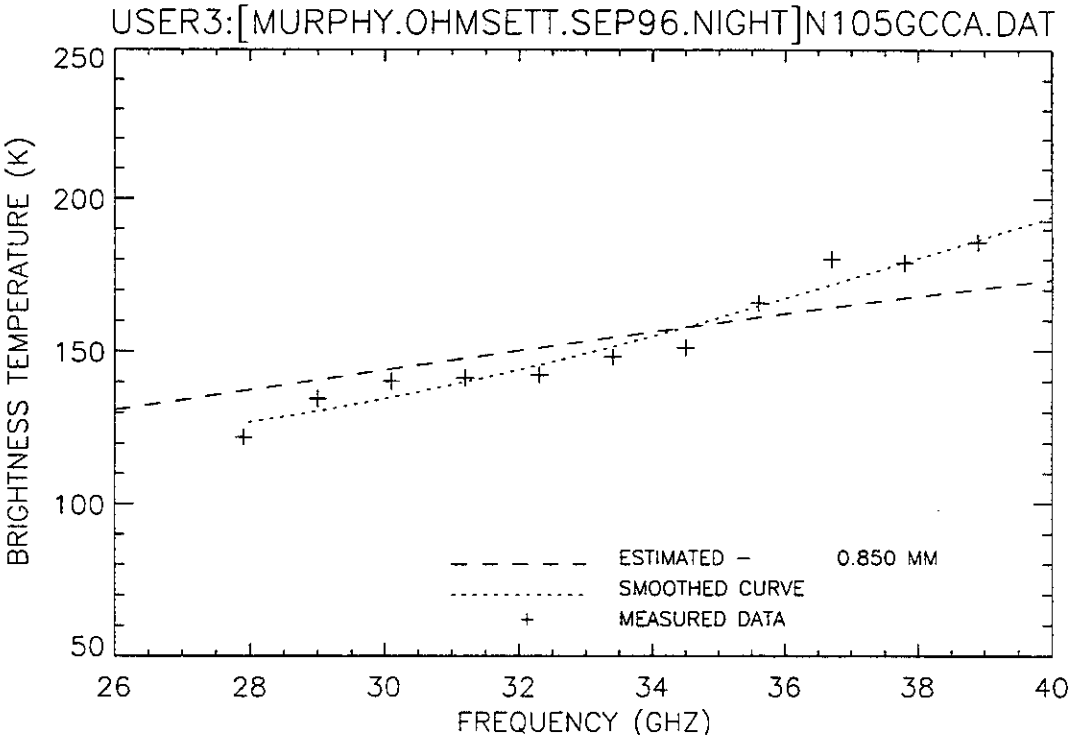

Figure 157. Plot of radiometric brightness temperature versus measurement frequency for 0.5-mm crude oil, night test, calm wave conditions, 12 September 1996, sweep G.

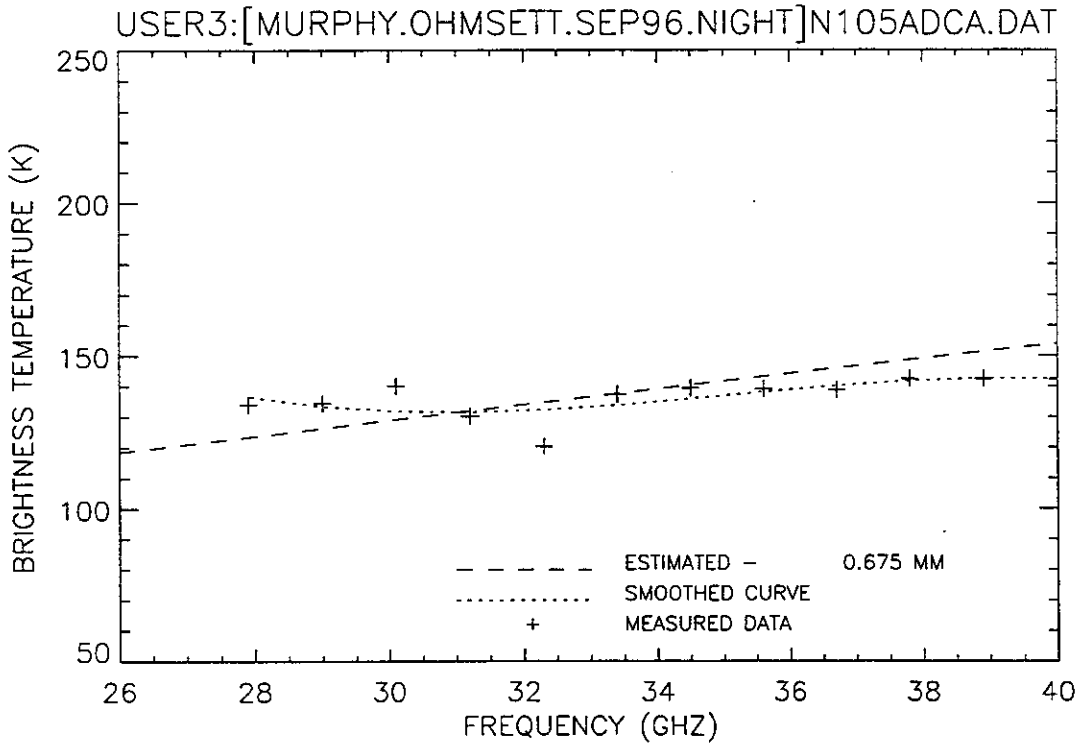

Figure 158. Plot of radiometric brightness temperature versus measurement frequency for 0.5-mm diesel oil, night test, calm wave conditions, 12 September 1996, sweep A.

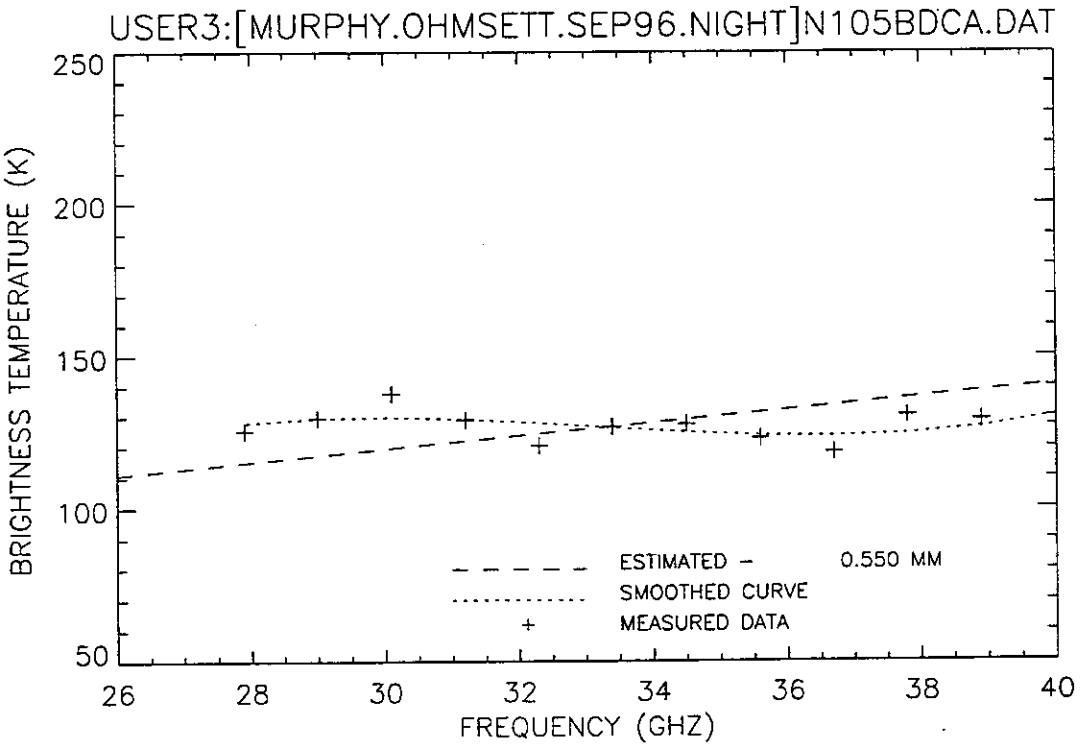

Figure 159. Plot of radiometric brightness temperature versus measurement frequency for 0.5-mm diesel oil, night test, calm wave conditions, 12 September 1996, sweep B.

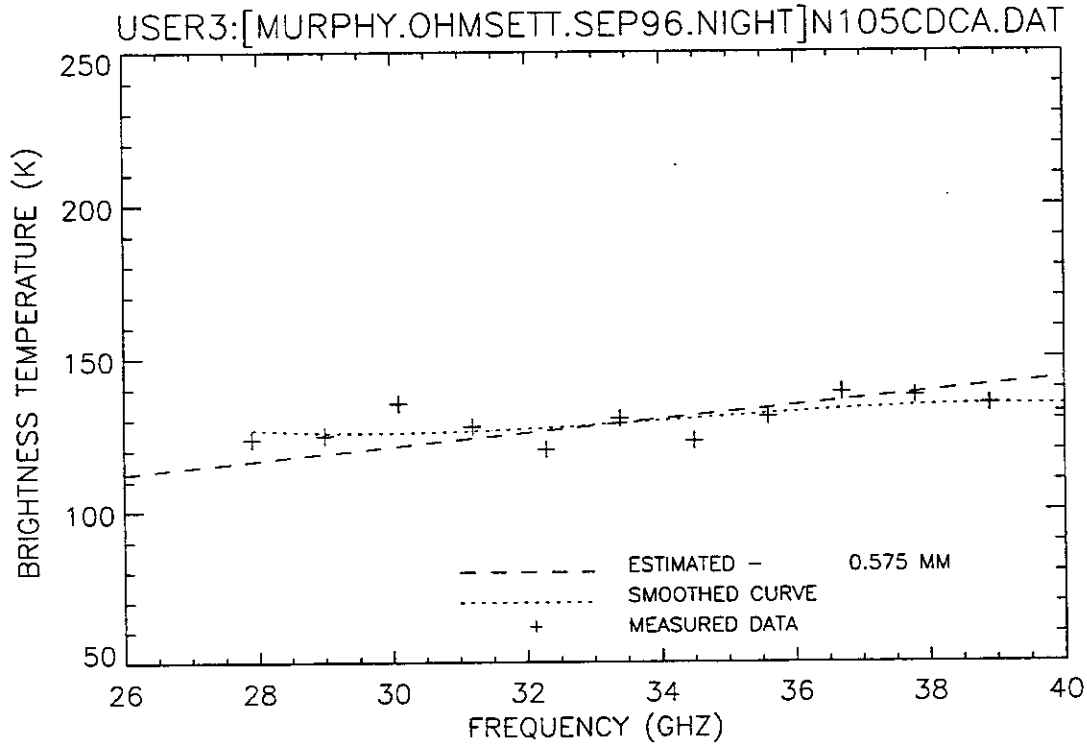

Figure 160. Plot of radiometric brightness temperature versus measurement frequency for 0.5-mm diesel oil, night test, calm wave conditions, 12 September 1996, sweep C.

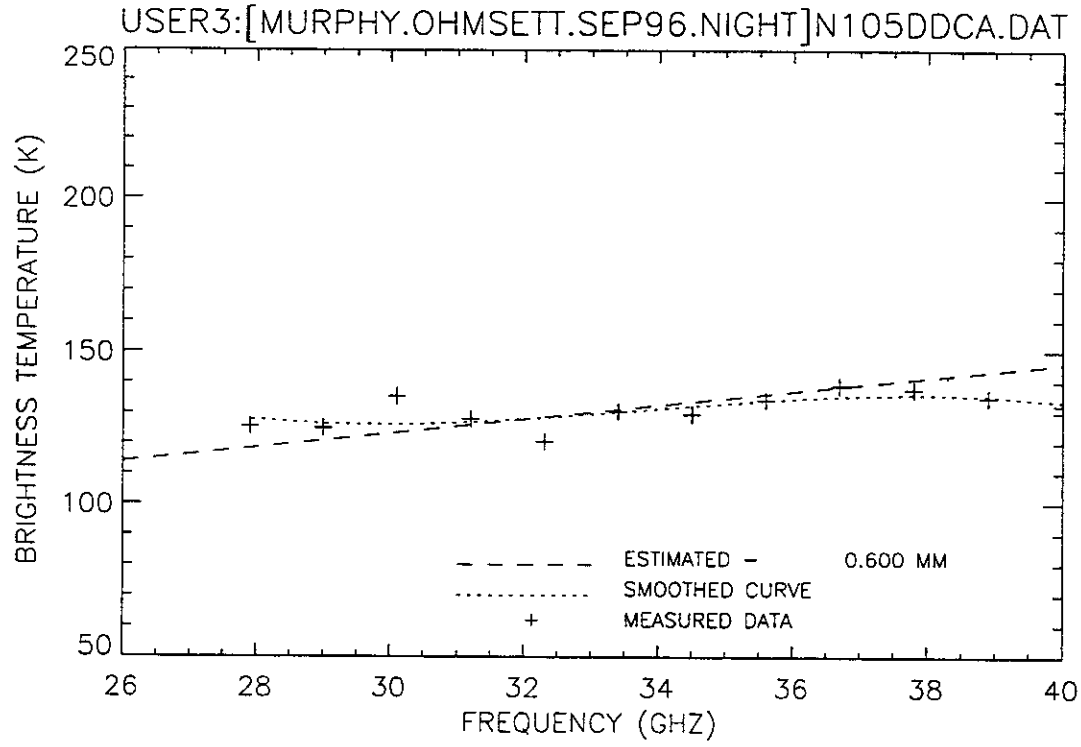

Figure 161. Plot of radiometric brightness temperature versus measurement frequency for 0.5-mm diesel oil, night test, calm wave conditions, 12 September 1996, sweep D.

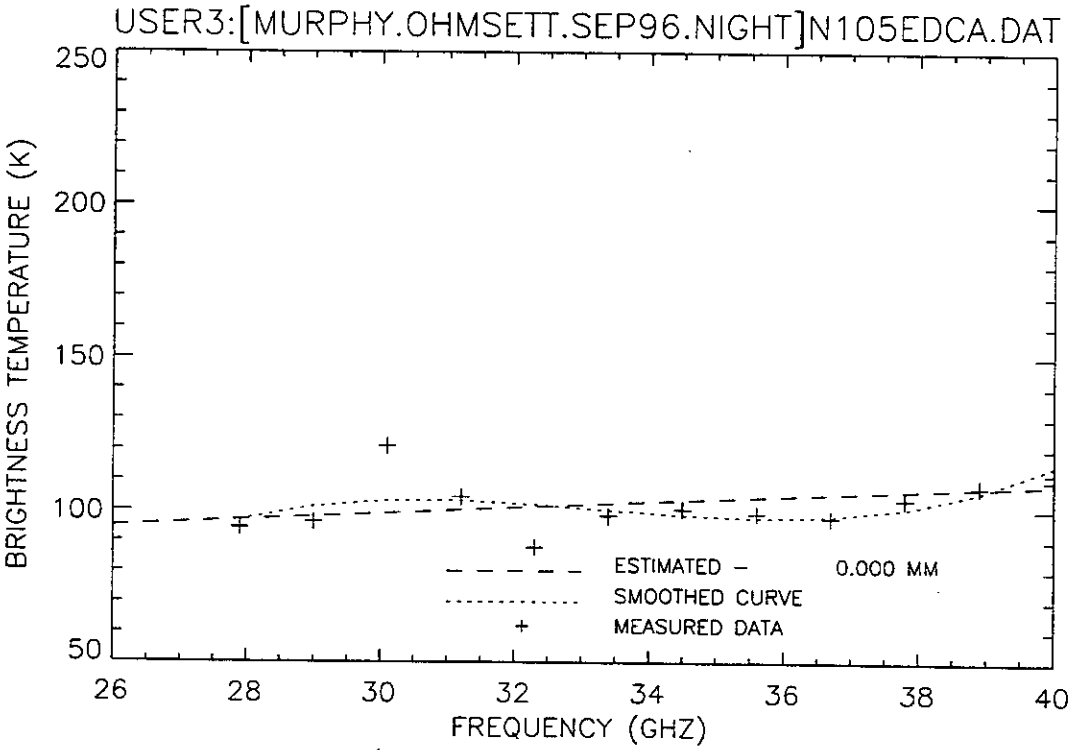

Figure 162. Plot of radiometric brightness temperature versus measurement frequency for 0.5-mm diesel oil, night test, calm wave conditions, 12 September 1996, sweep E.

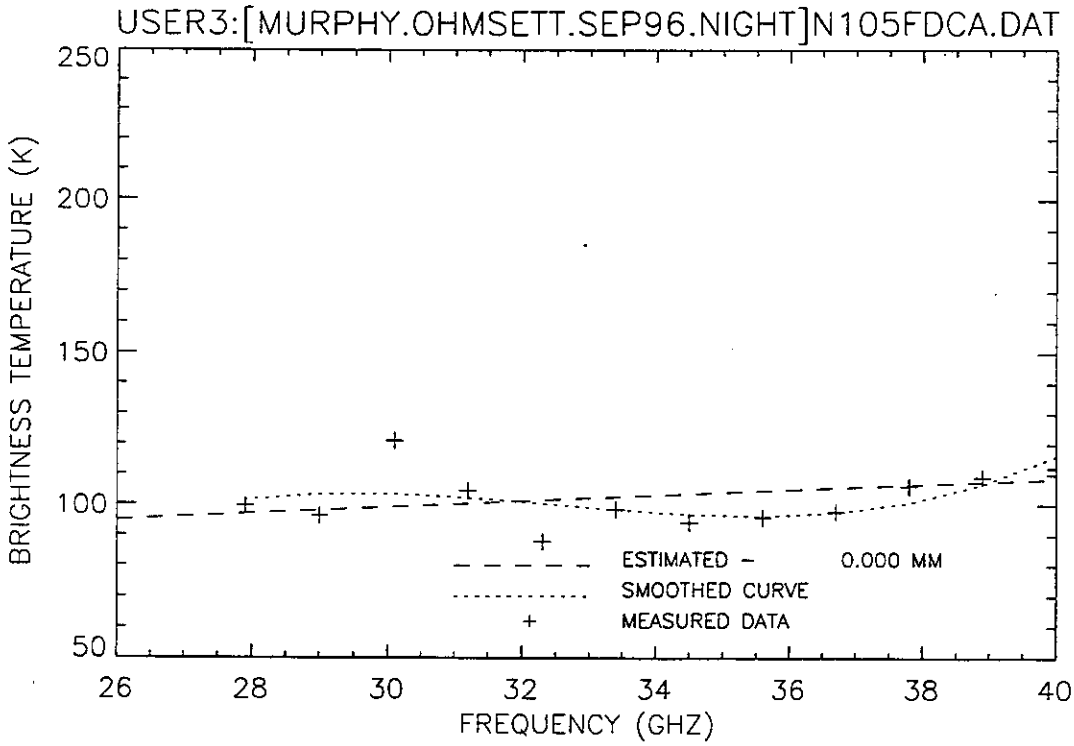

Figure 163. Plot of radiometric brightness temperature versus measurement frequency for 0.5-mm diesel oil, night test, calm wave conditions, 12 September 1996, sweep F.

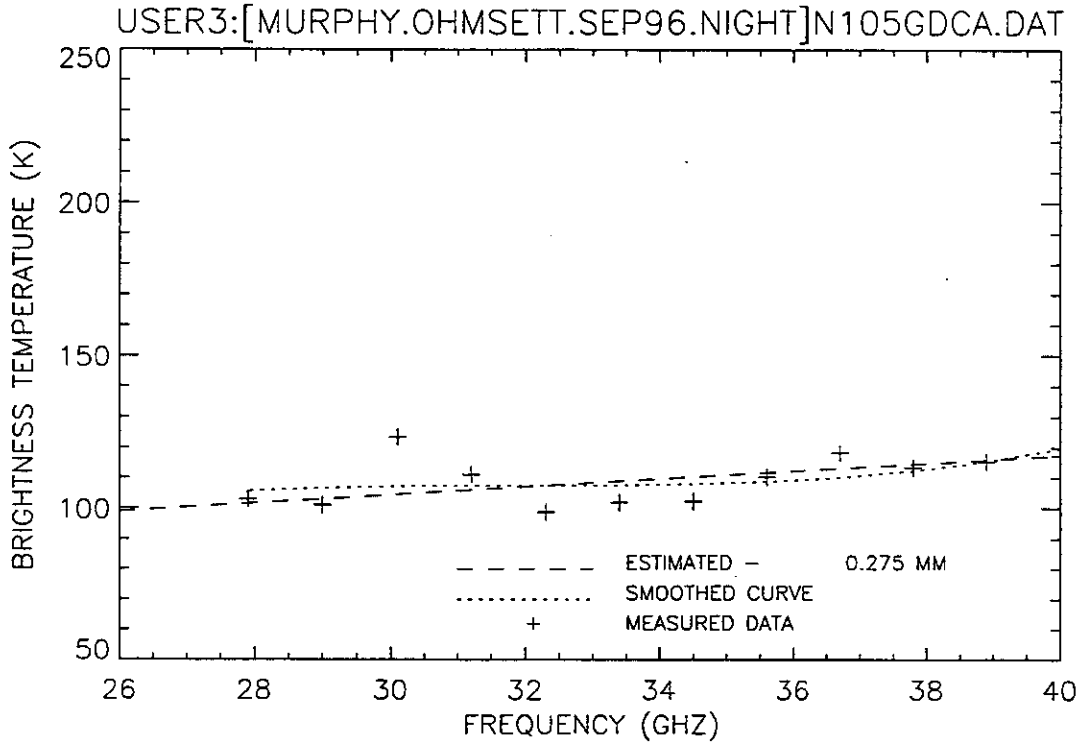

Figure 164. Plot of radiometric brightness temperature versus measurement frequency for 0.5-mm diesel oil, night test, calm wave conditions, 12 September 1996, sweep G.

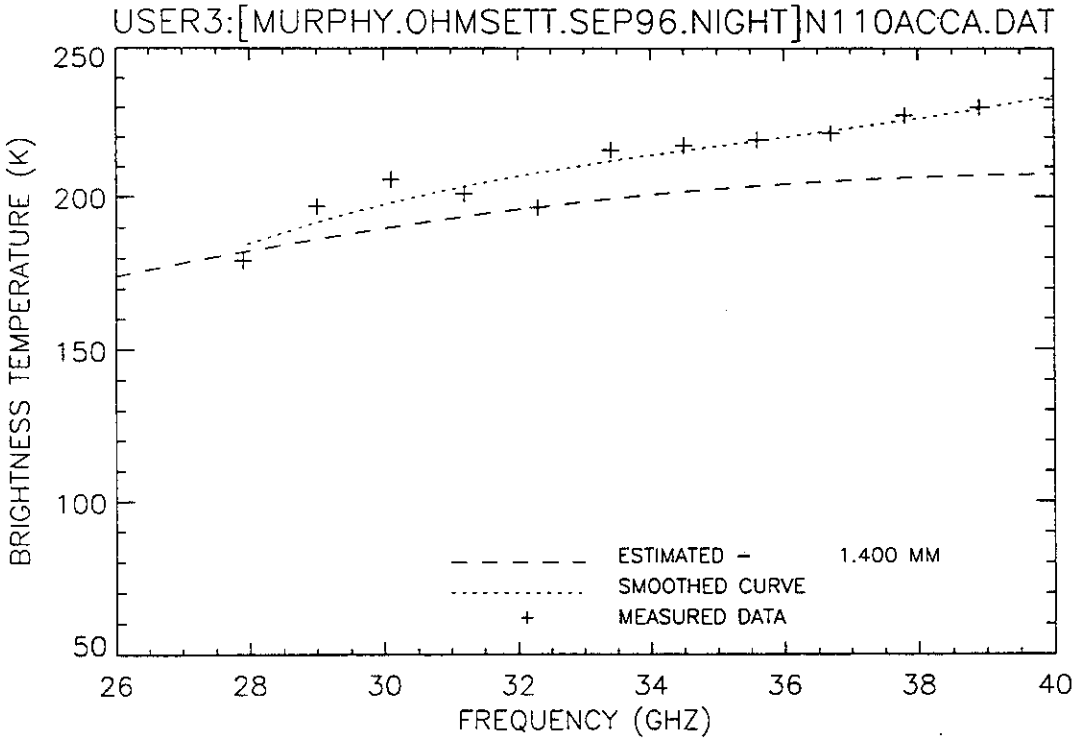

Figure 165. Plot of radiometric brightness temperature versus measurement frequency for 1-mm crude oil, night test, calm wave conditions, 12 September 1996, sweep A.

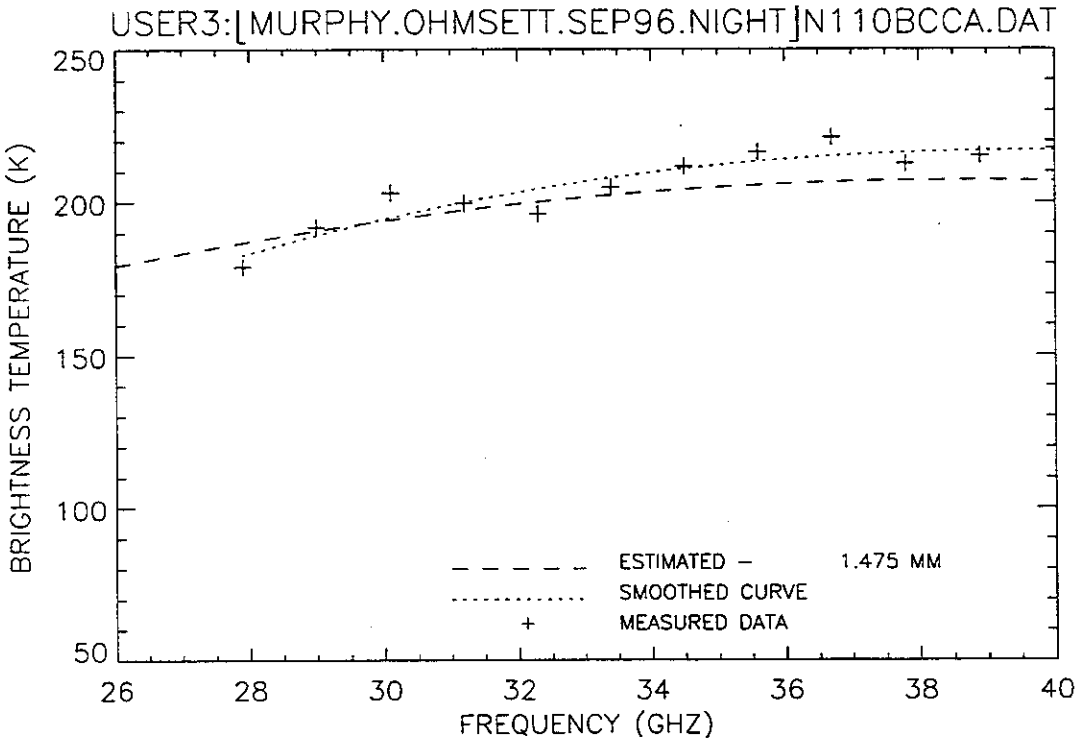

Figure 166. Plot of radiometric brightness temperature versus measurement frequency for 1-mm crude oil, night test, calm wave conditions, 12 September 1996, sweep B.

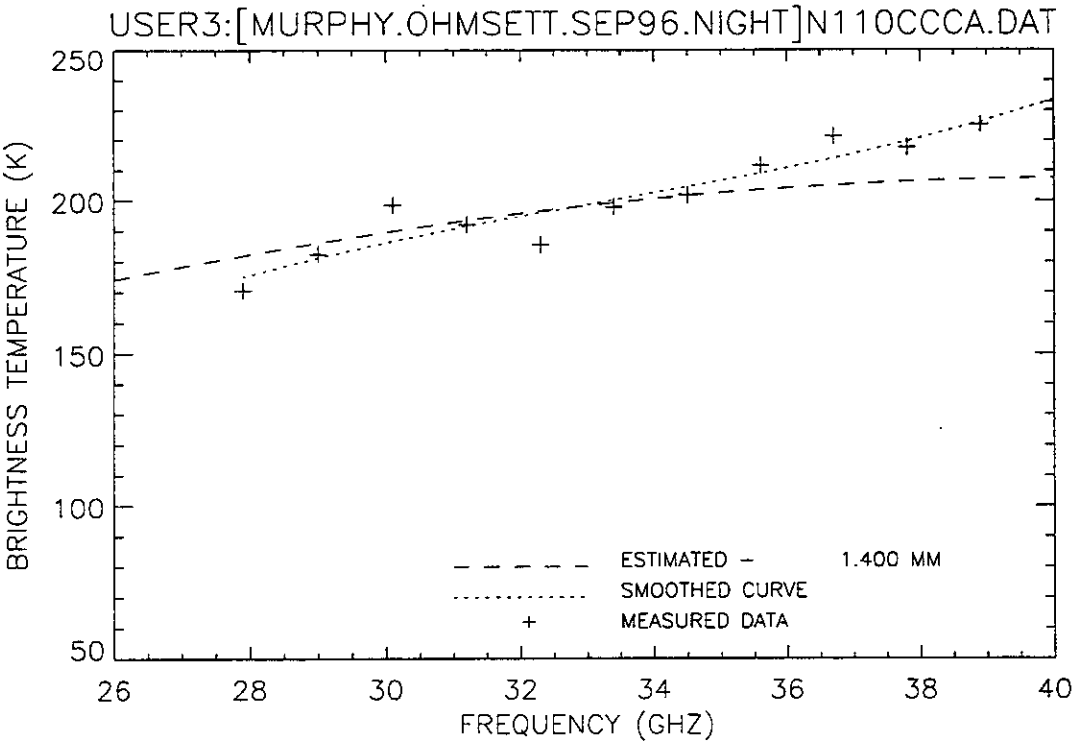

Figure 167. Plot of radiometric brightness temperature versus measurement frequency for 1-mm crude oil, night test, calm wave conditions, 12 September 1996, sweep C.

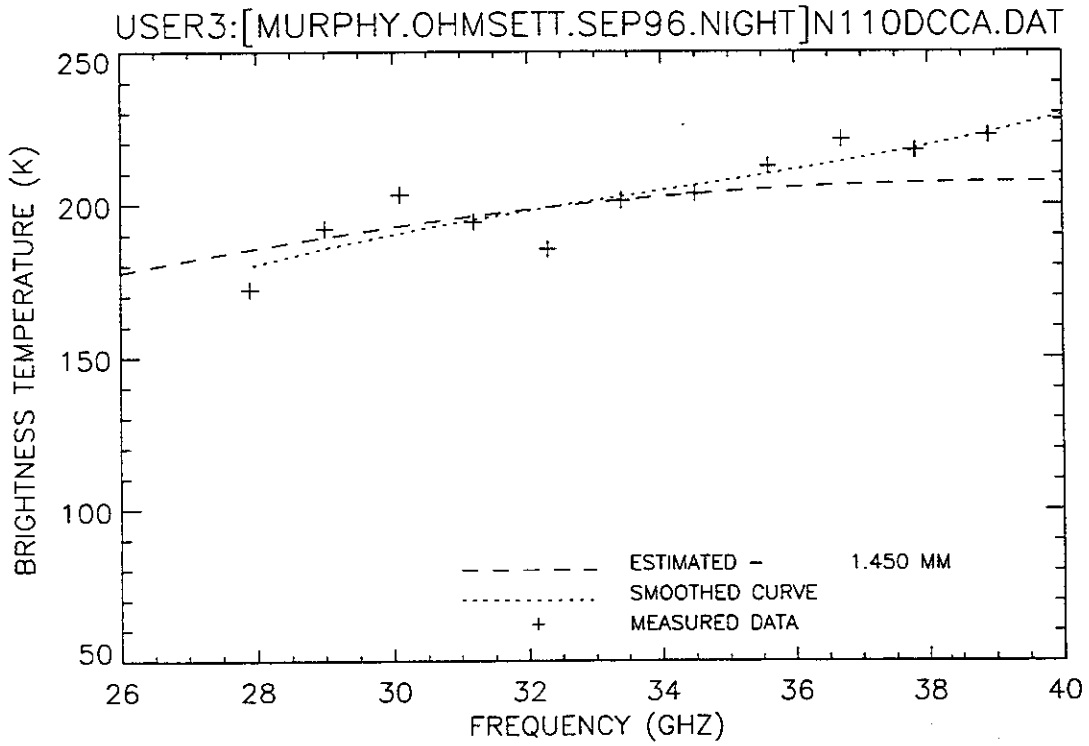

Figure 168. Plot of radiometric brightness temperature versus measurement frequency for 1-mm crude oil, night test, calm wave conditions, 12 September 1996, sweep D.

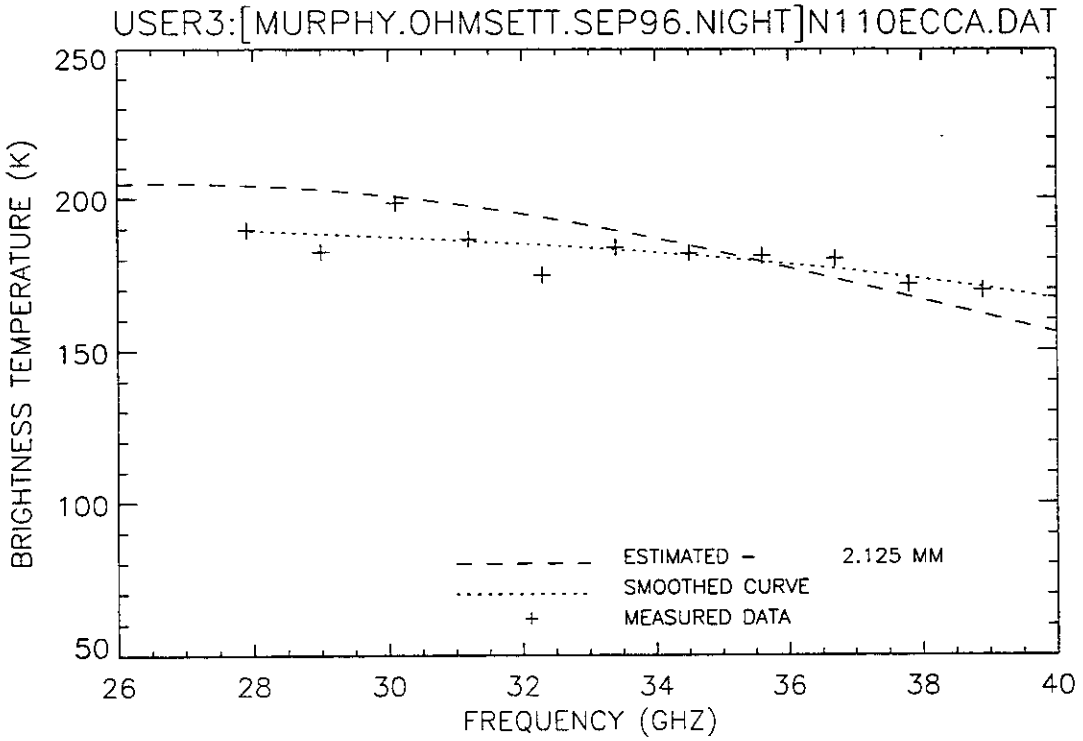

Figure 169. Plot of radiometric brightness temperature versus measurement frequency for 1-mm crude oil, night test, calm wave conditions, 12 September 1996, sweep E.

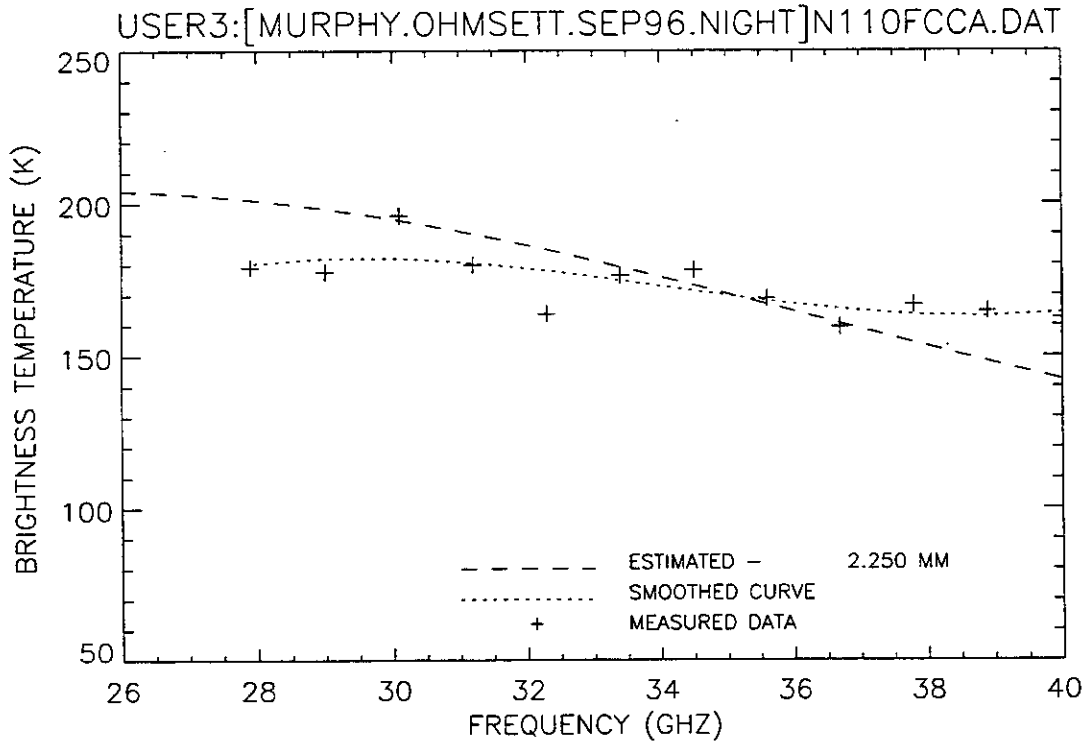

Figure 170. Plot of radiometric brightness temperature versus measurement frequency for 1-mm crude oil, night test, calm wave conditions, 12 September 1996, sweep F.

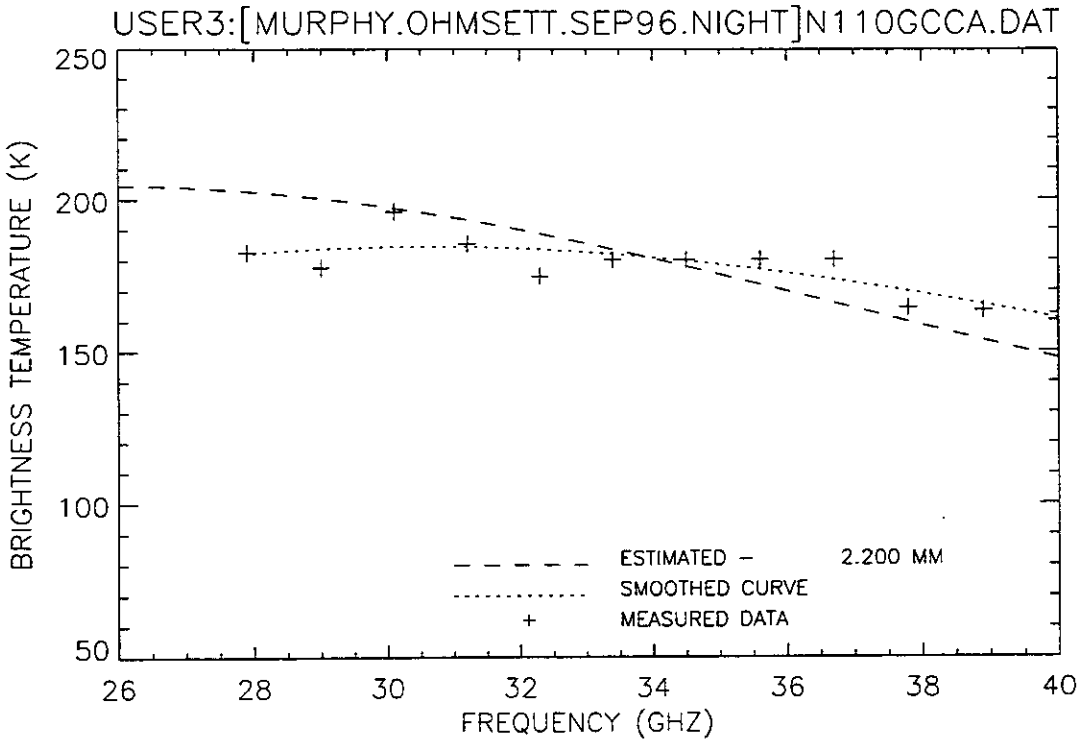

Figure 171. Plot of radiometric brightness temperature versus measurement frequency for 1-mm crude oil, night test, calm wave conditions, 12 September 1996, sweep G.

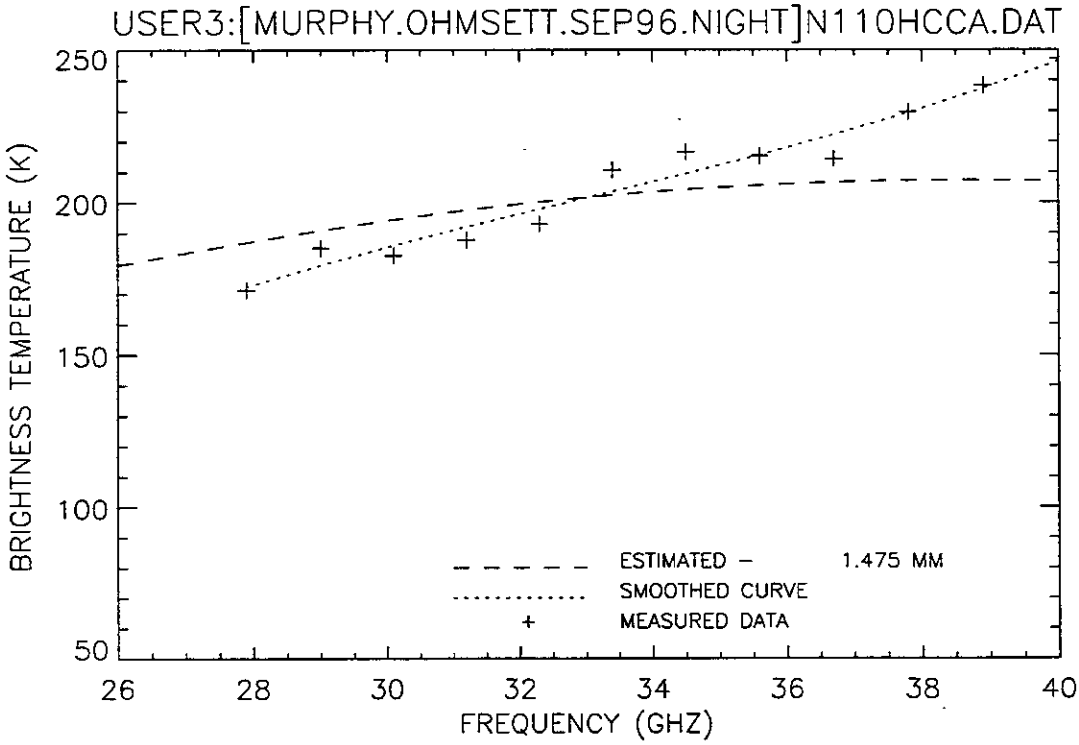

Figure 172. Plot of radiometric brightness temperature versus measurement frequency for 1-mm crude oil, night test, calm wave conditions, 12 September 1996, sweep H.

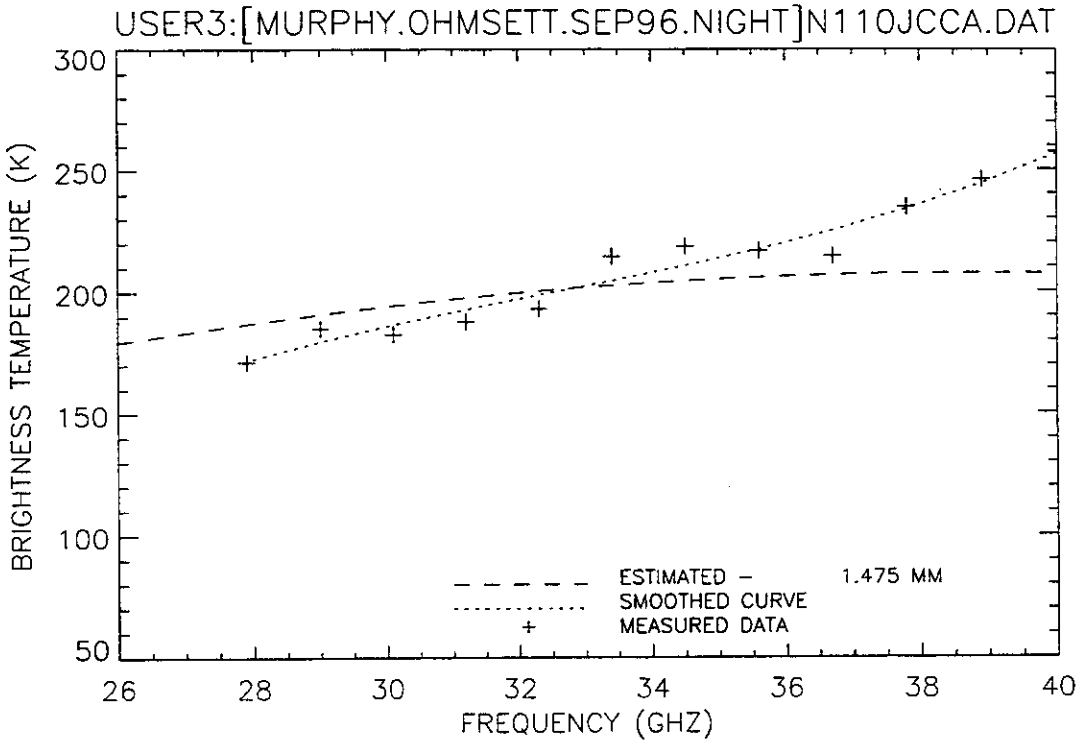

Figure 173. Plot of radiometric brightness temperature versus measurement frequency for 1-mm crude oil, night test, calm wave conditions, 12 September 1996, sweep J.

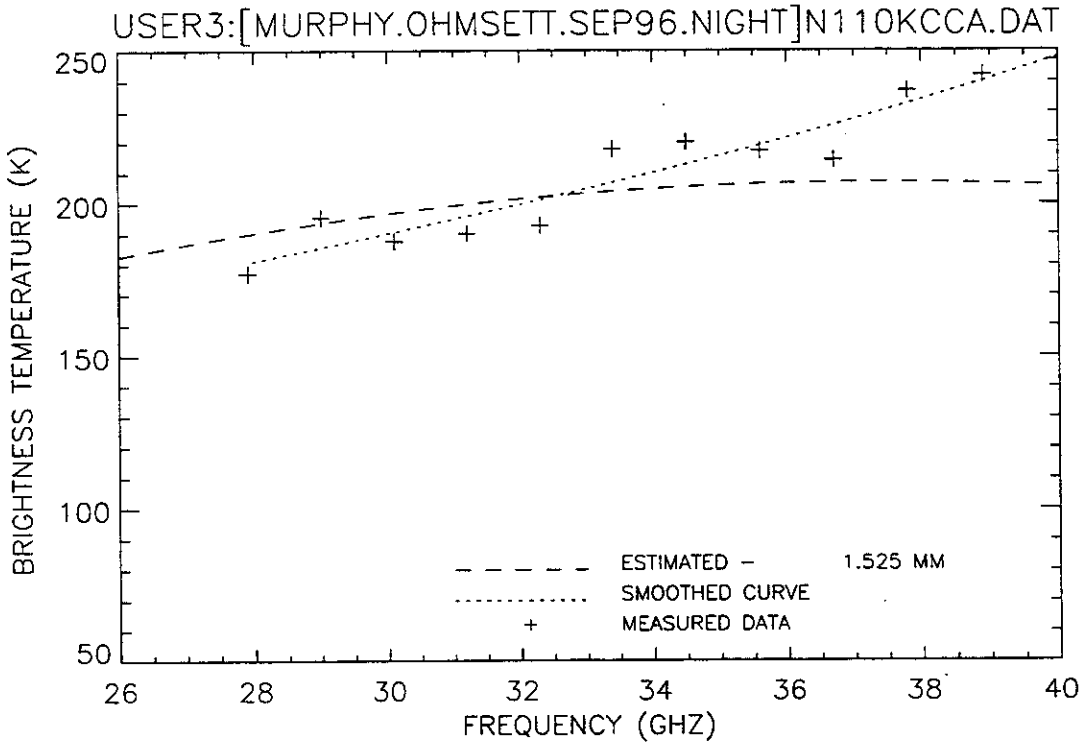

Figure 174. Plot of radiometric brightness temperature versus measurement frequency for 1-mm crude oil, night test, calm wave conditions, 12 September 1996, sweep K.

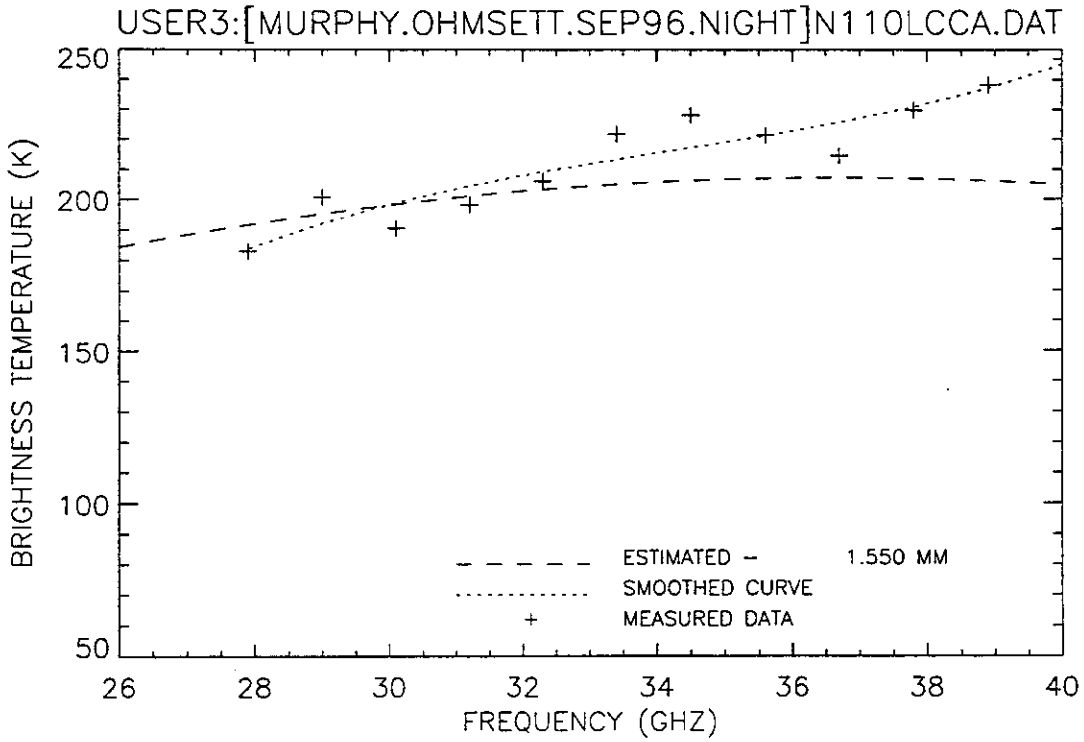

Figure 175. Plot of radiometric brightness temperature versus measurement frequency for 1-mm crude oil, night test, calm wave conditions, 12 September 1996, sweep L.

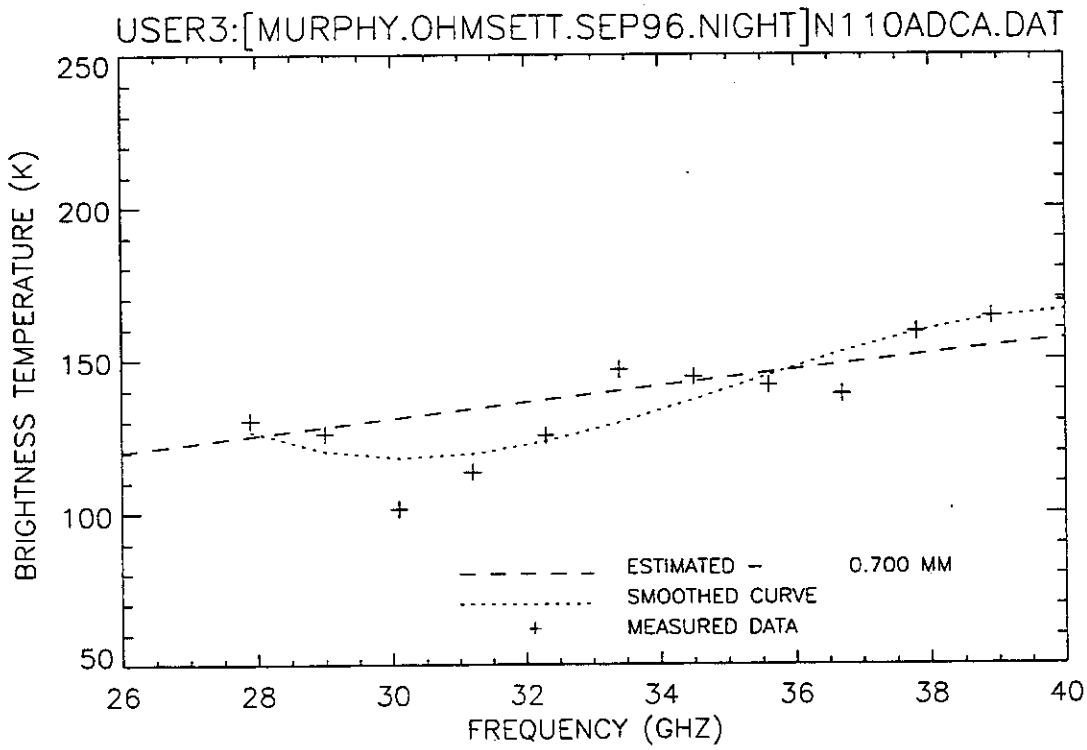

Figure 176. Plot of radiometric brightness temperature versus measurement frequency for 1-mm diesel oil, night test, calm wave conditions, 12 September 1996, sweep A.

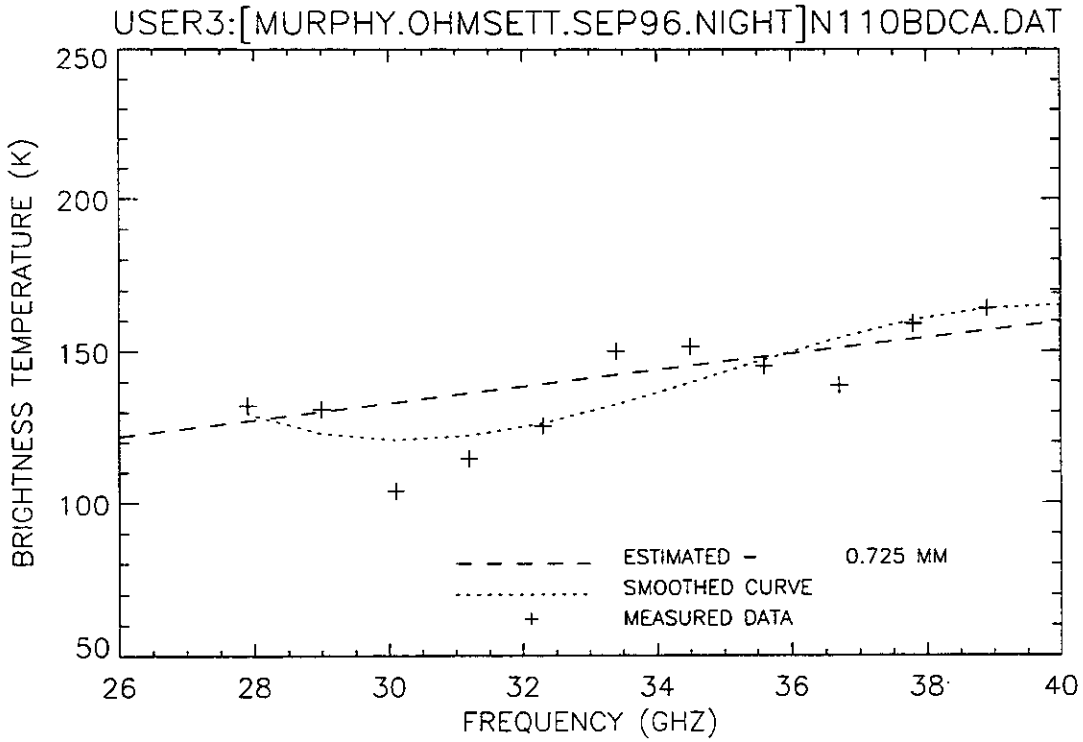

Figure 177. Plot of radiometric brightness temperature versus measurement frequency for 1-mm diesel oil, night test, calm wave conditions, 12 September 1996, sweep B.

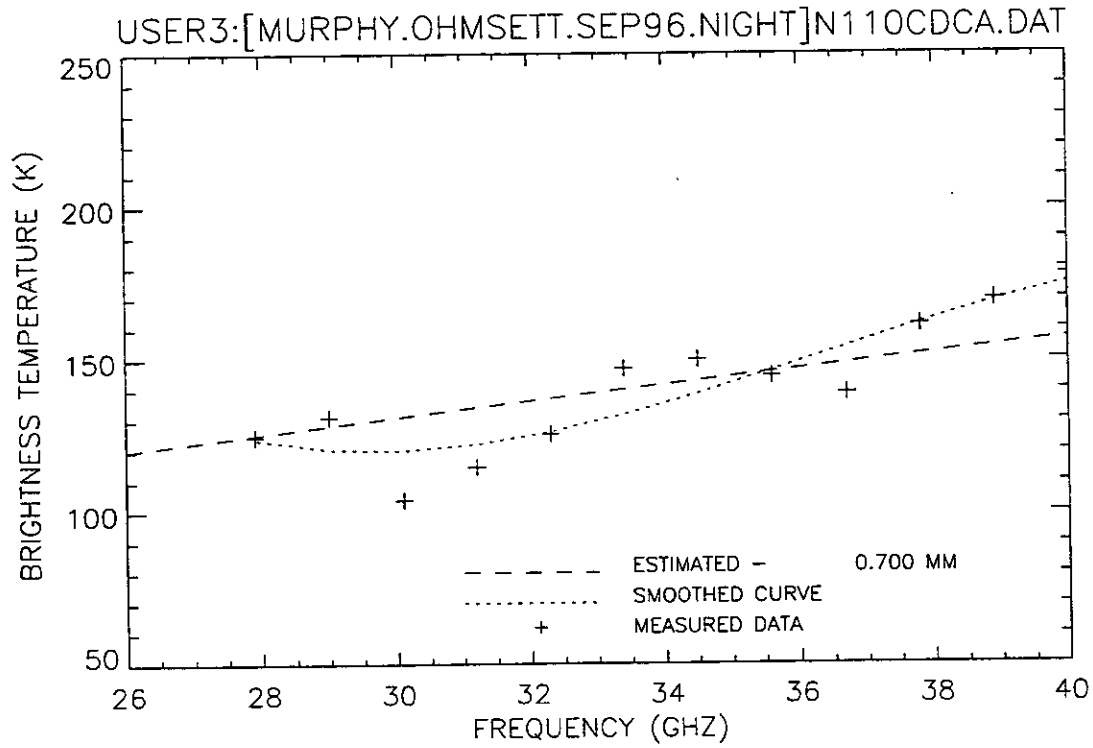

Figure 178. Plot of radiometric brightness temperature versus measurement frequency for 1-mm diesel oil, night test, calm wave conditions, 12 September 1996, sweep C.

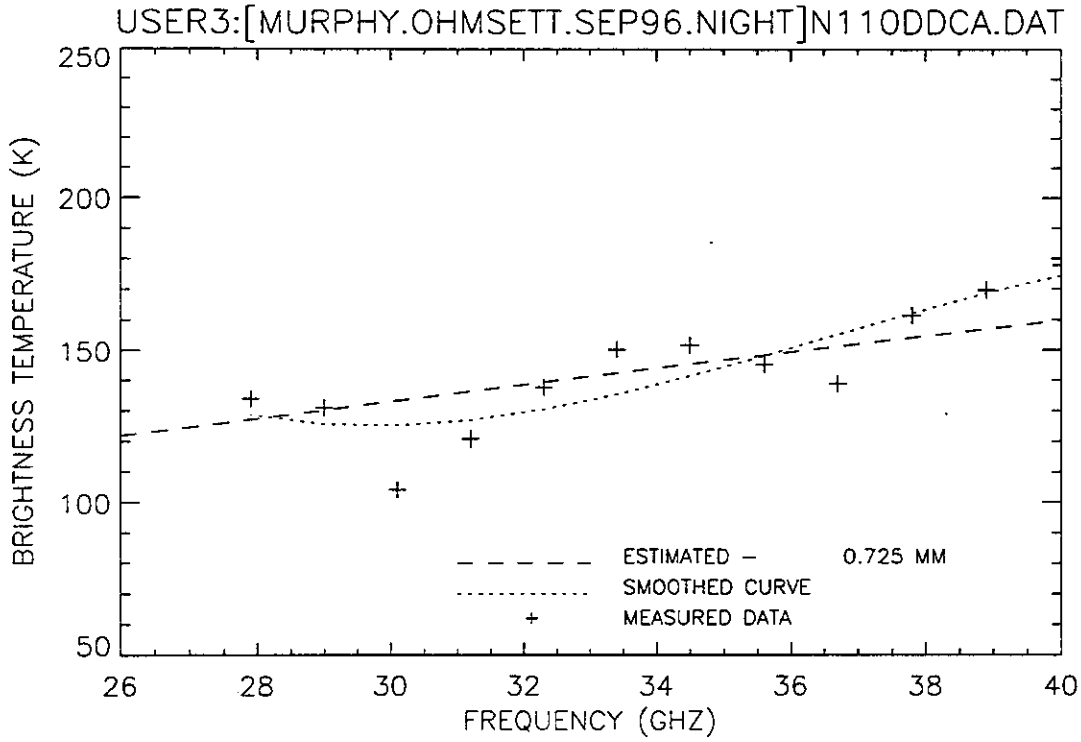

Figure 179. Plot of radiometric brightness temperature versus measurement frequency for 1-mm diesel oil, night test, calm wave conditions, 12 September 1996, sweep D.

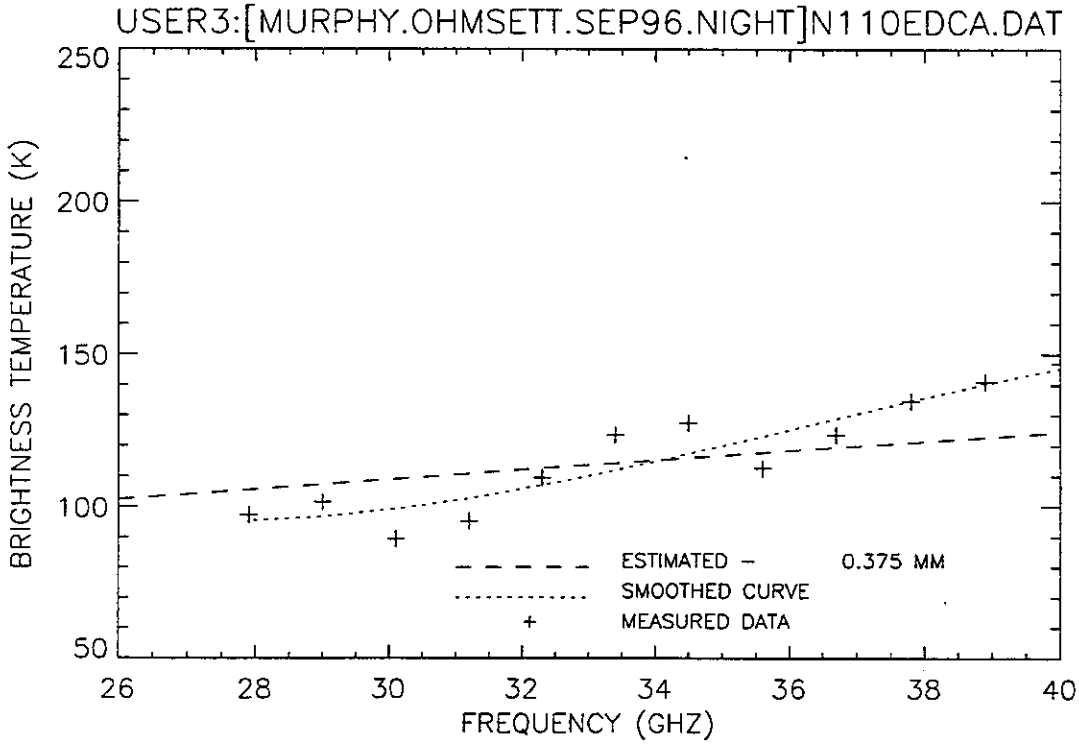

Figure 180. Plot of radiometric brightness temperature versus measurement frequency for 1-mm diesel oil, night test, calm wave conditions, 12 September 1996, sweep E.

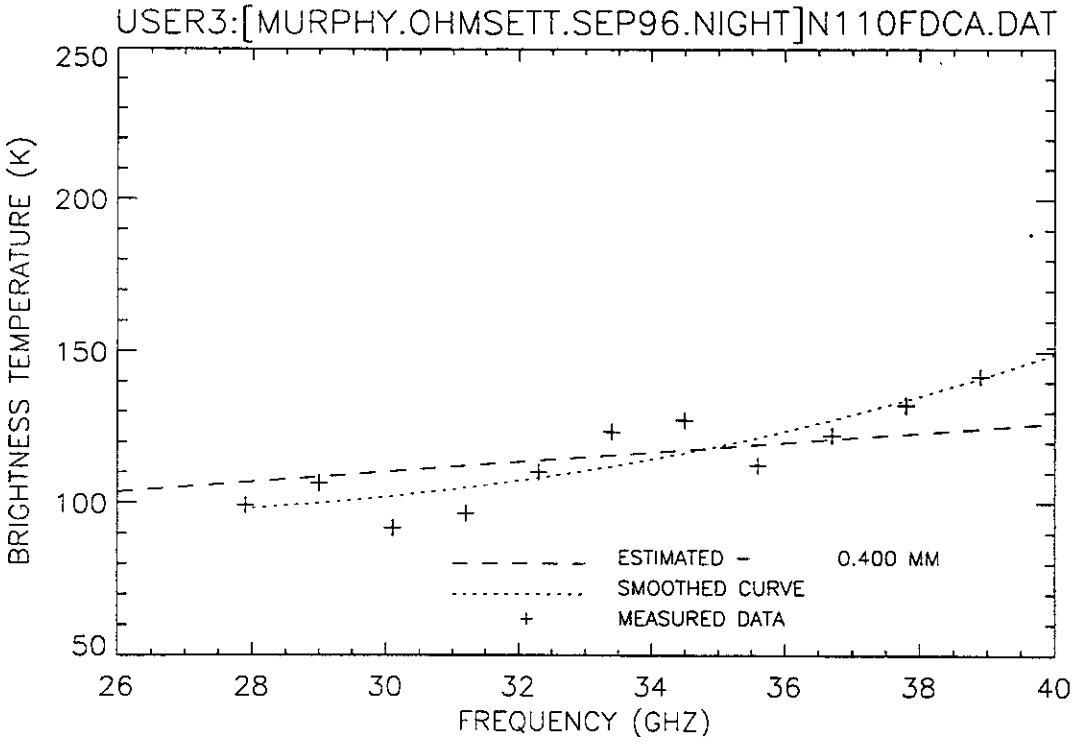

Figure 181. Plot of radiometric brightness temperature versus measurement frequency for 1-mm diesel oil, night test, calm wave conditions, 12 September 1996, sweep F.

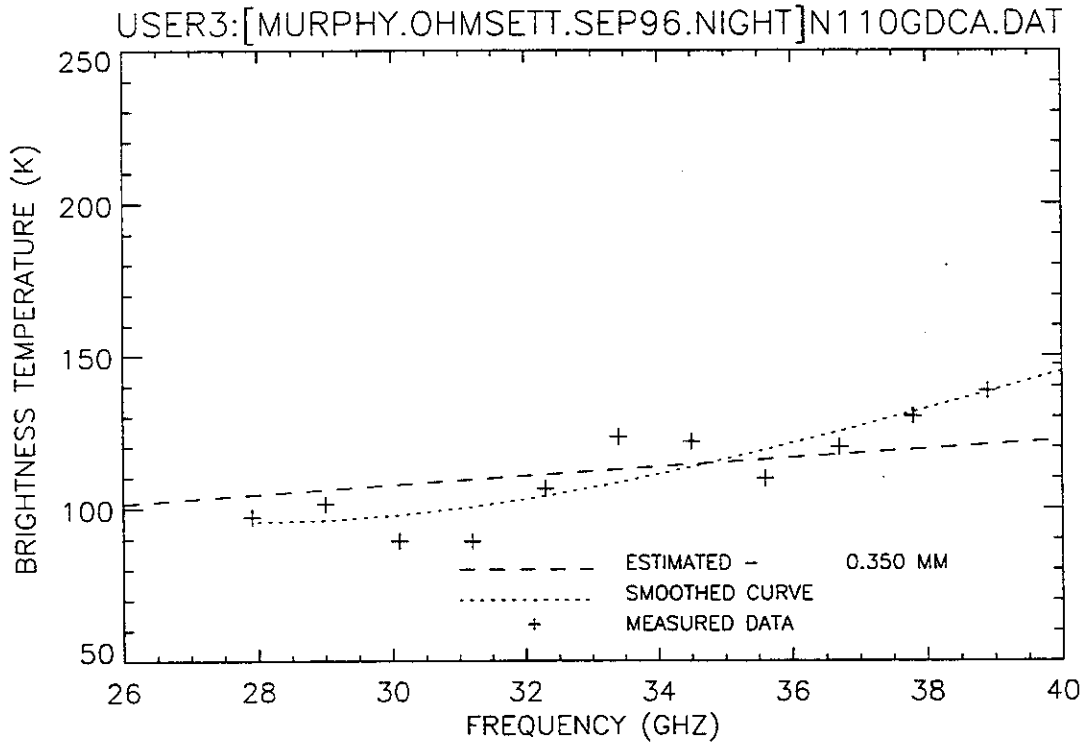

Figure 182. Plot of radiometric brightness temperature versus measurement frequency for 1-mm diesel oil, night test, calm wave conditions, 12 September 1996, sweep G.

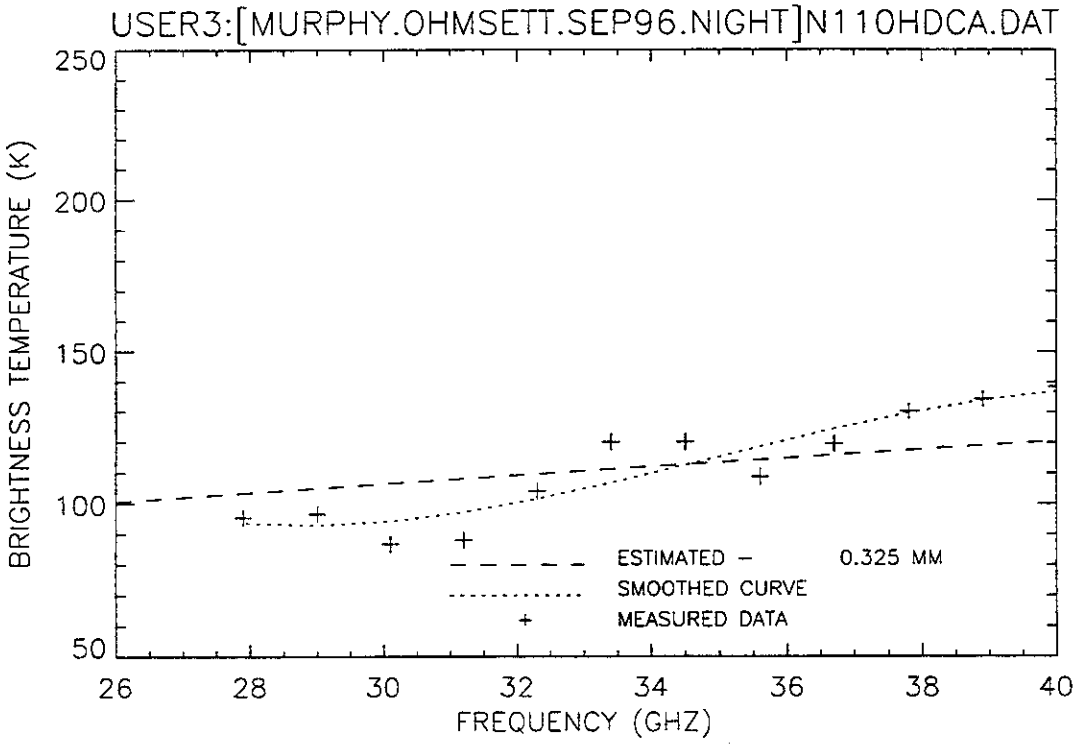

Figure 183. Plot of radiometric brightness temperature versus measurement frequency for 1-mm diesel oil, night test, calm wave conditions, 12 September 1996, sweep H.

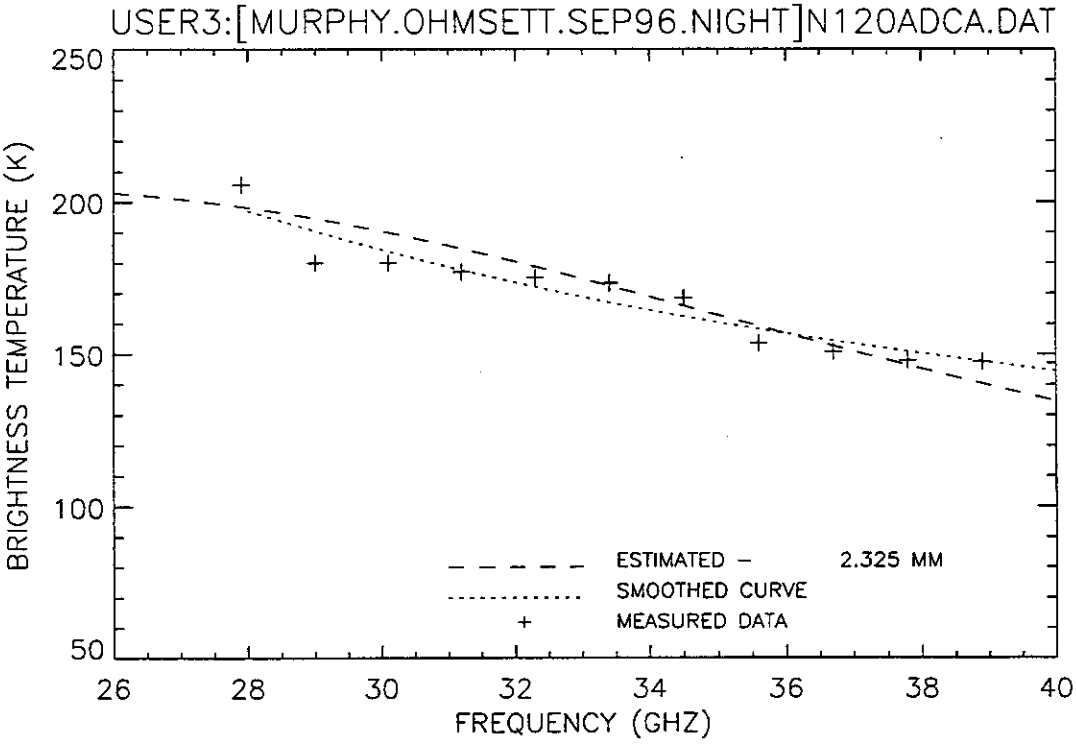

Figure 184. Plot of radiometric brightness temperature versus measurement frequency for 2-mm crude oil, night test, calm wave conditions, 12 September 1996, sweep A.

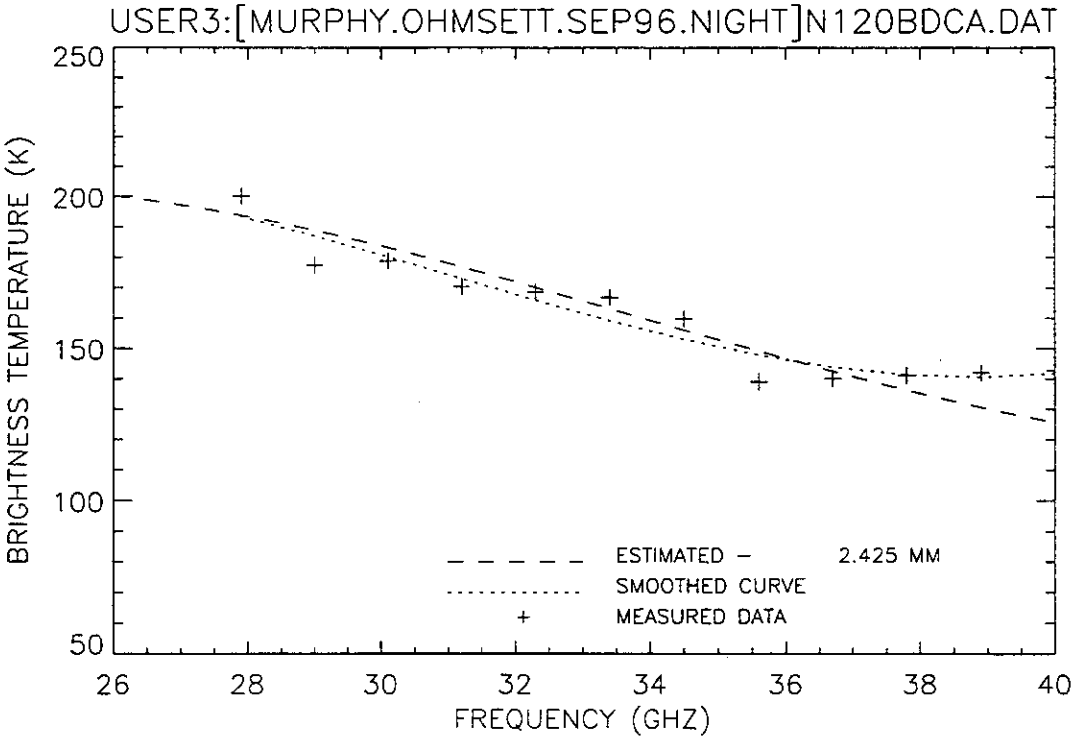

Figure 185. Plot of radiometric brightness temperature versus measurement frequency for 2-mm crude oil, night test, calm wave conditions, 12 September 1996, sweep B.

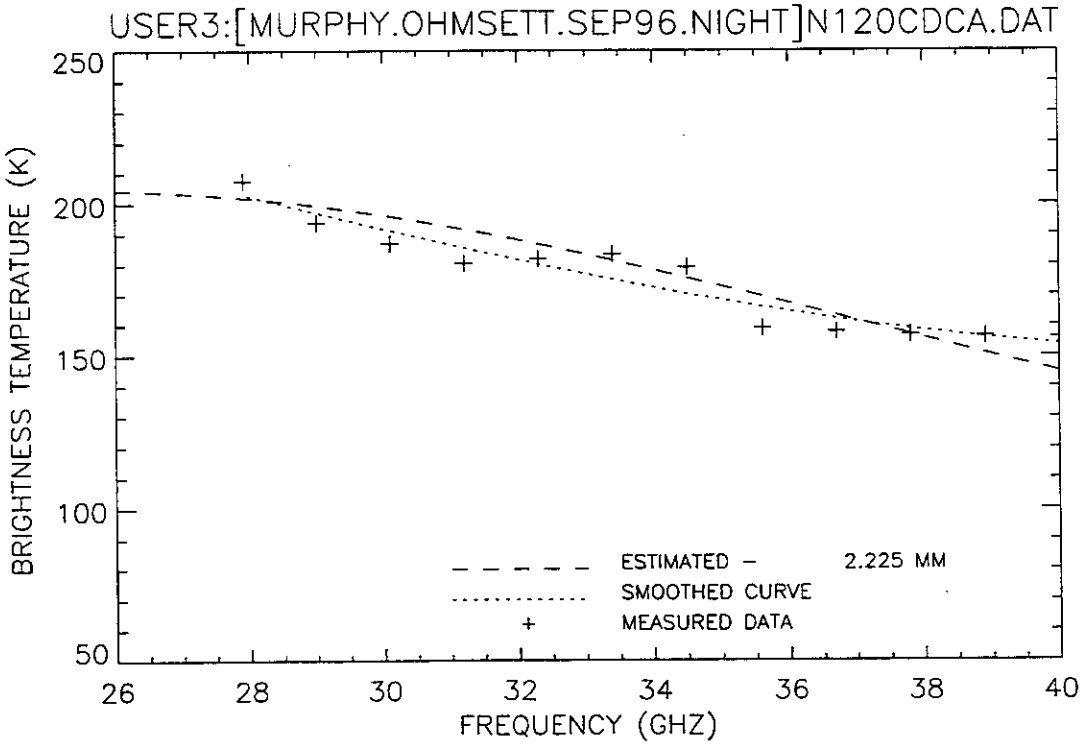

Figure 186. Plot of radiometric brightness temperature versus measurement frequency for 2-mm crude oil, night test, calm wave conditions, 12 September 1996, sweep C.

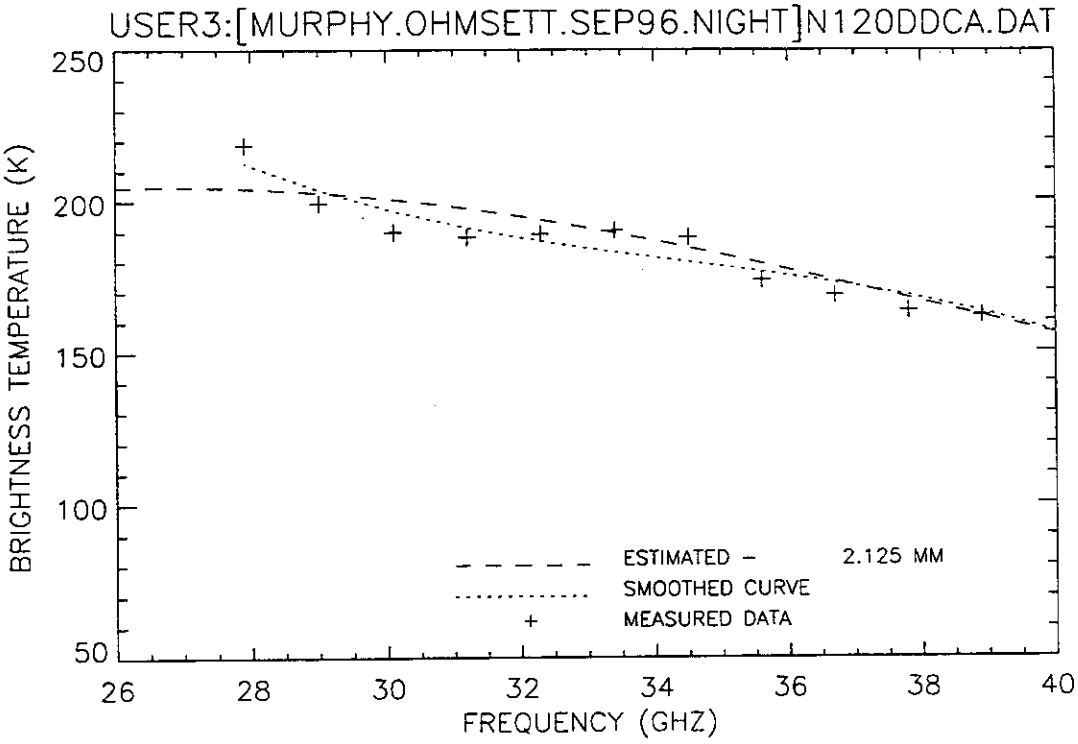

Figure 187. Plot of radiometric brightness temperature versus measurement frequency for 2-mm crude oil, night test, calm wave conditions, 12 September 1996, sweep D.

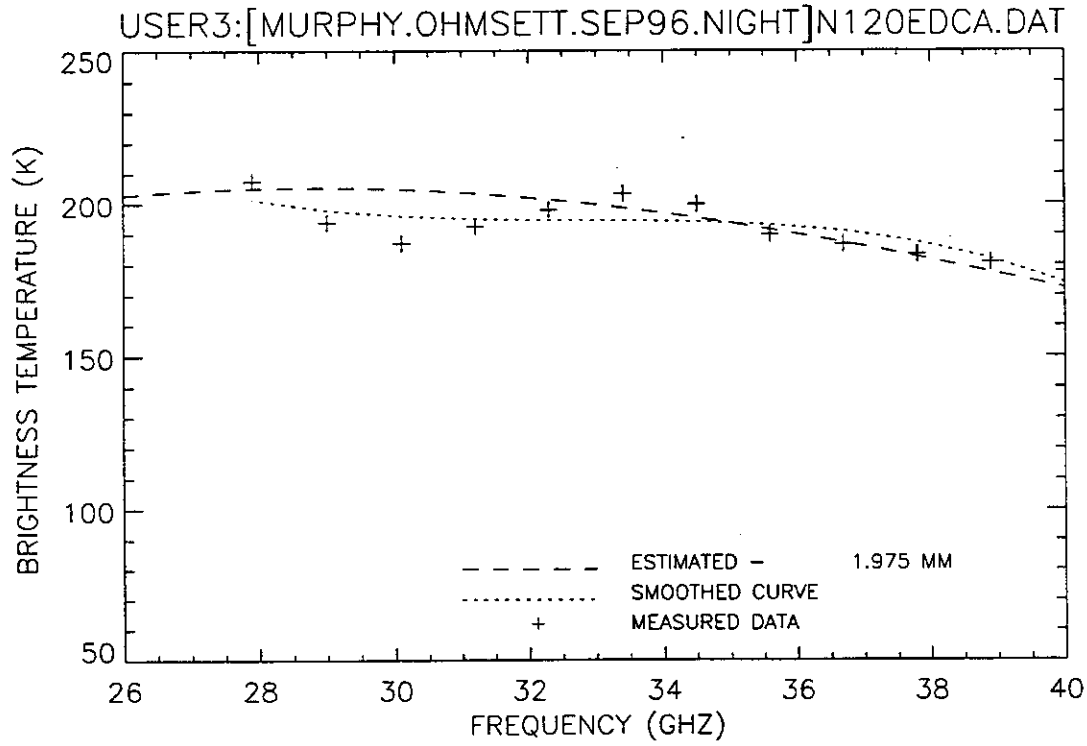

Figure 188. Plot of radiometric brightness temperature versus measurement frequency for 2-mm crude oil, night test, calm wave conditions, 12 September 1996, sweep E.

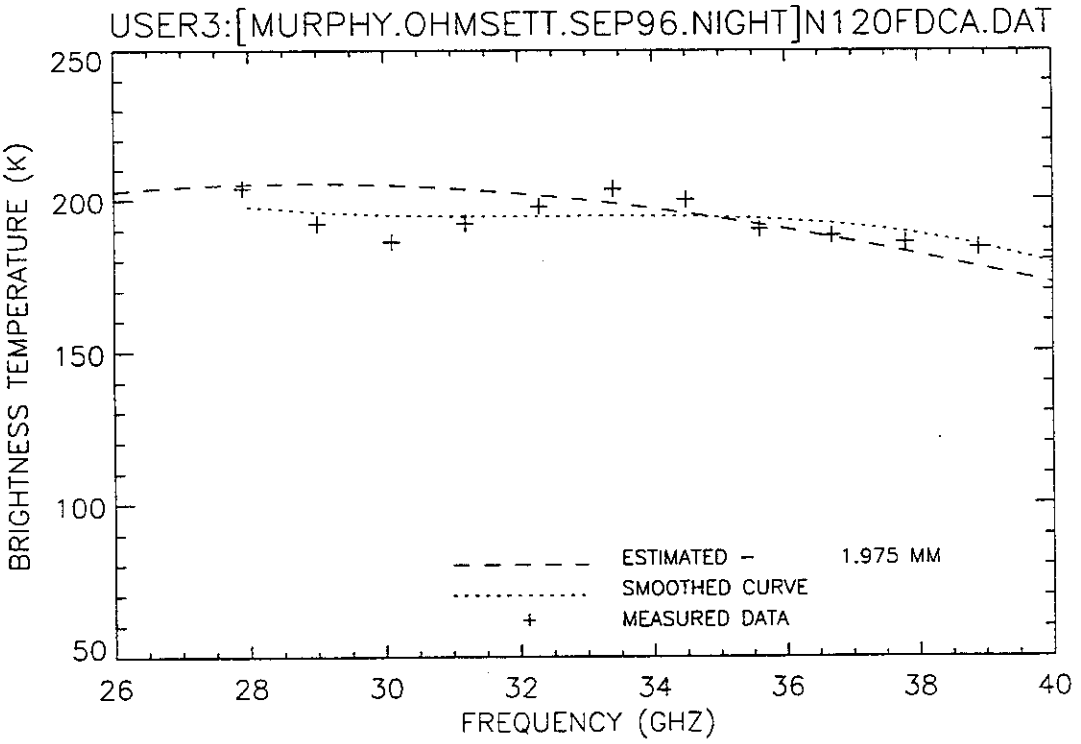

Figure 189. Plot of radiometric brightness temperature versus measurement frequency for 2-mm crude oil, night test, calm wave conditions, 12 September 1996, sweep F.

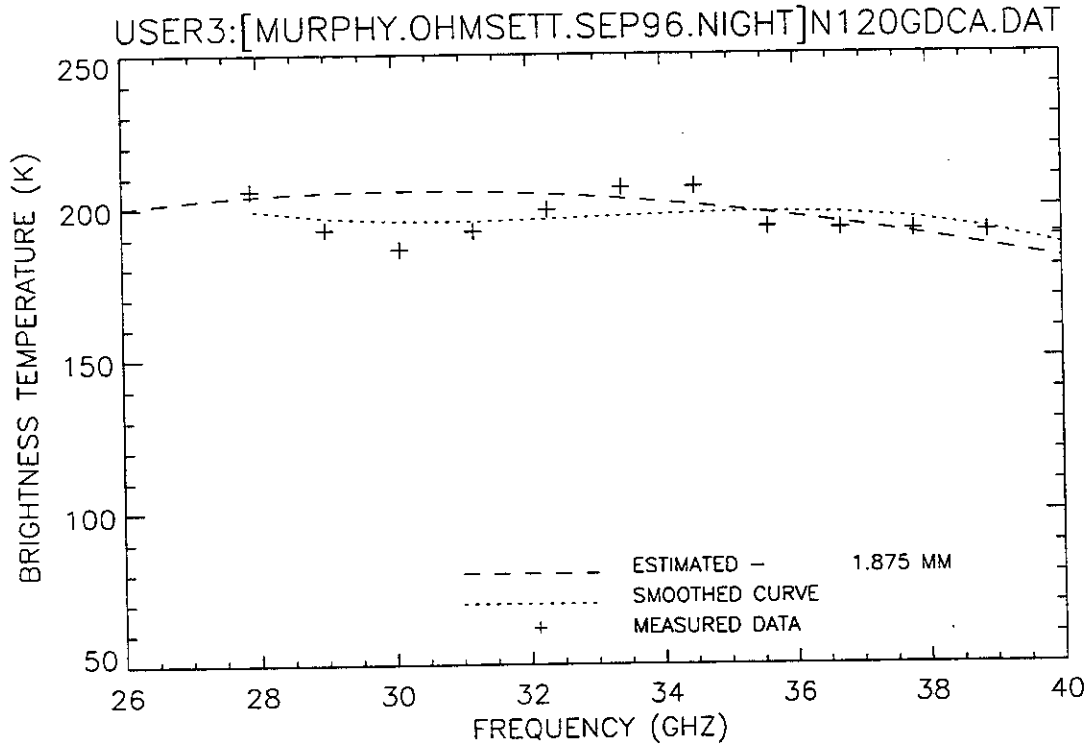

Figure 190. Plot of radiometric brightness temperature versus measurement frequency for 2-mm crude oil, night test, calm wave conditions, 12 September 1996, sweep G.

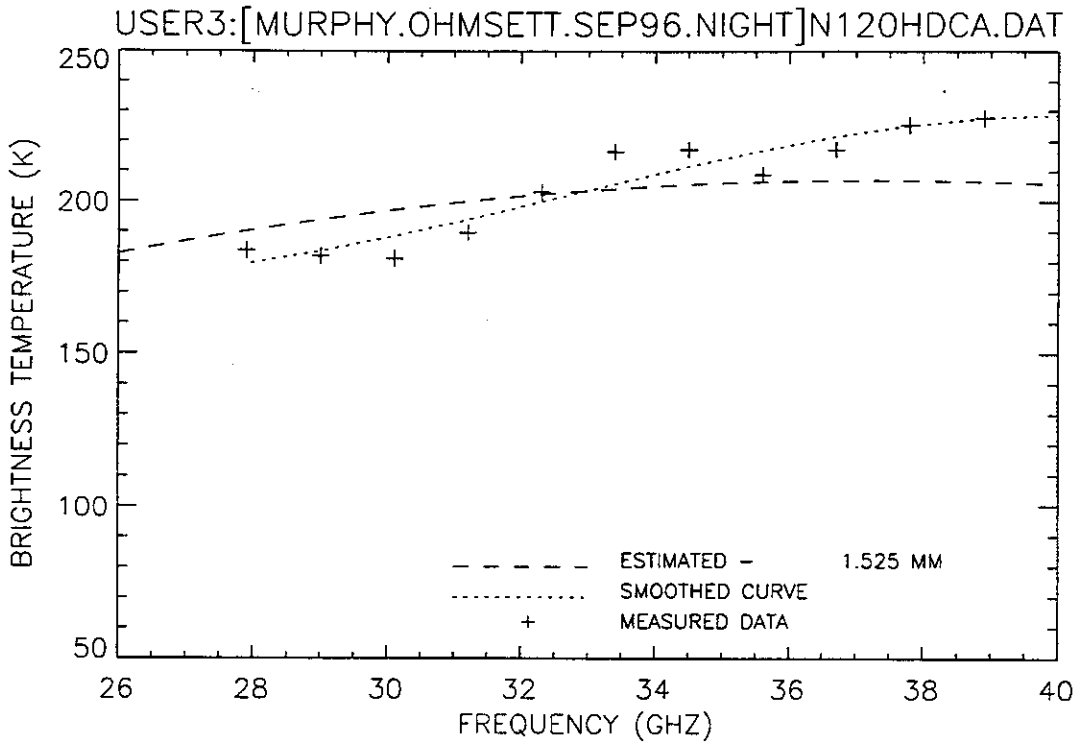

Figure 191. Plot of radiometric brightness temperature versus measurement frequency for 2-mm crude oil, night test, calm wave conditions, 12 September 1996, sweep H.

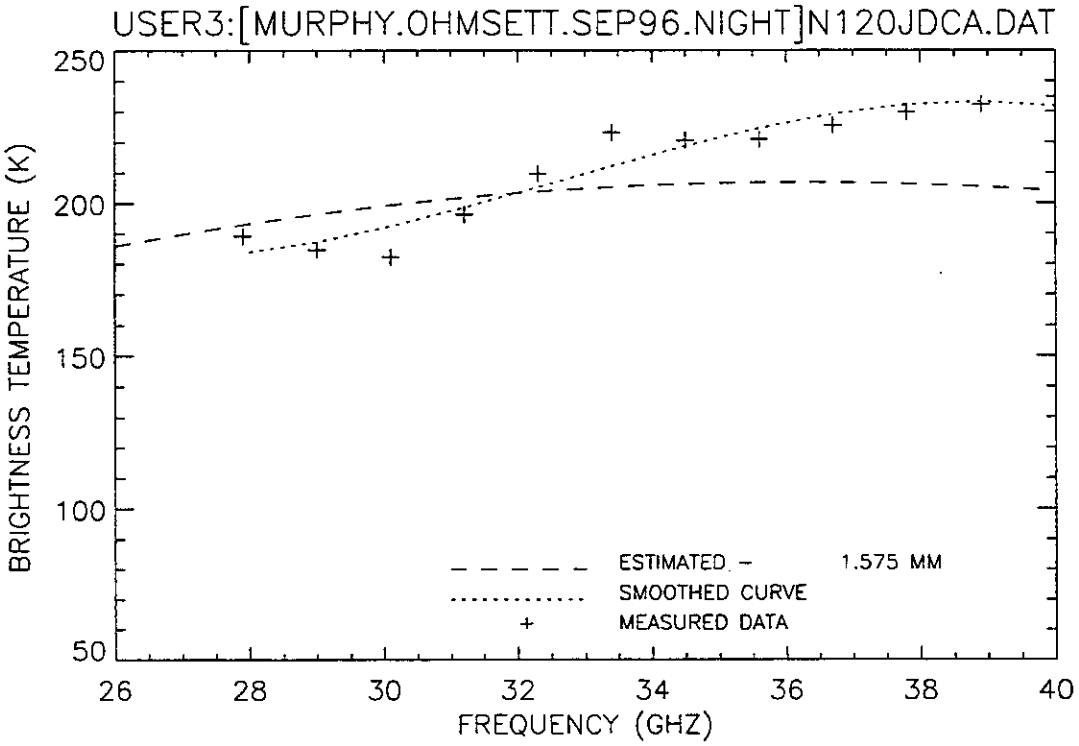

Figure 192. Plot of radiometric brightness temperature versus measurement frequency for 2-mm crude oil, night test, calm wave conditions, 12 September 1996, sweep J.

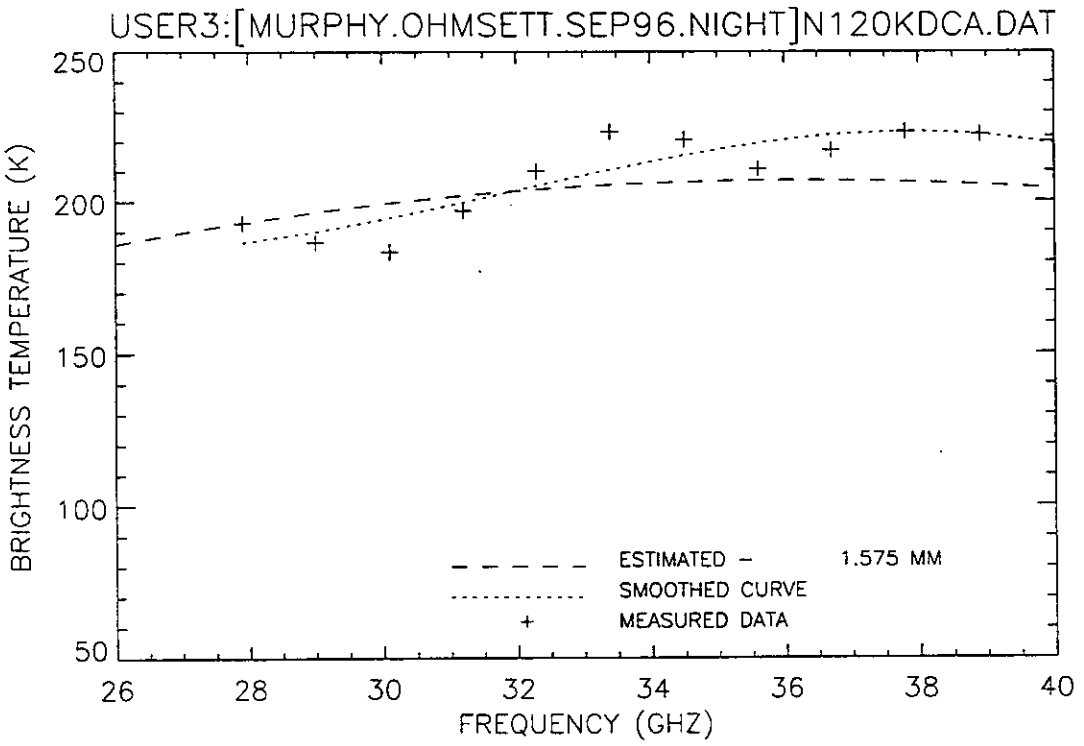

Figure 193. Plot of radiometric brightness temperature versus measurement frequency for 2-mm crude oil, night test, calm wave conditions, 12 September 1996, sweep K.

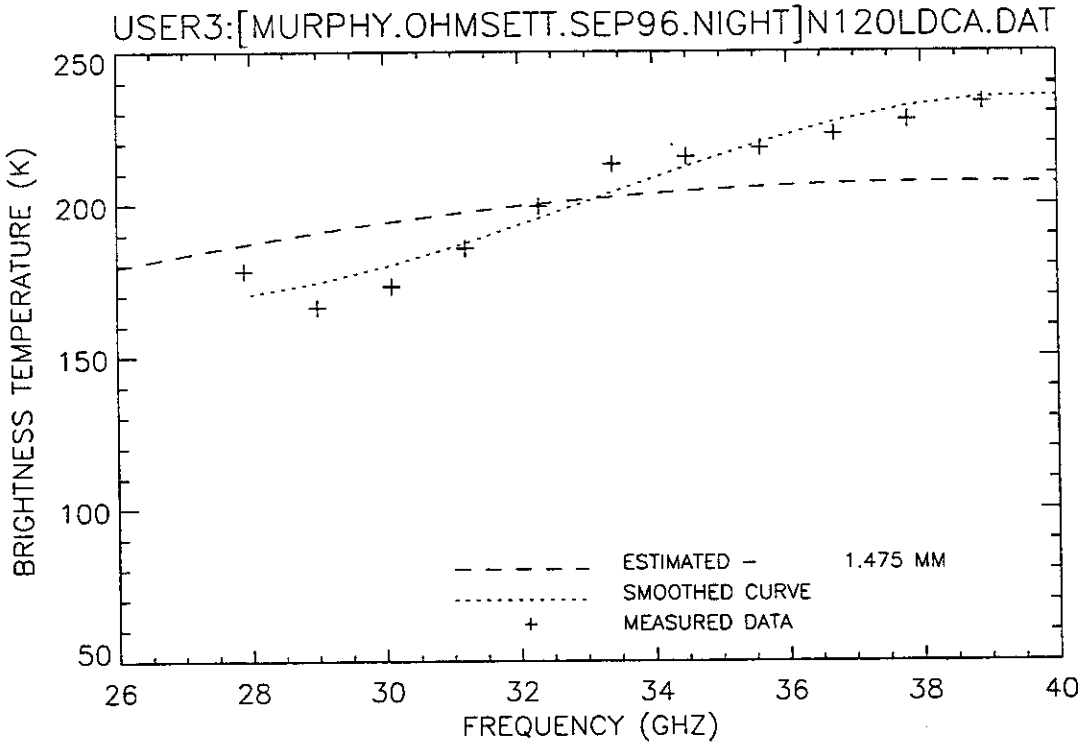

Figure 194. Plot of radiometric brightness temperature versus measurement frequency for 2-mm crude oil, night test, calm wave conditions, 12 September 1996, sweep L.

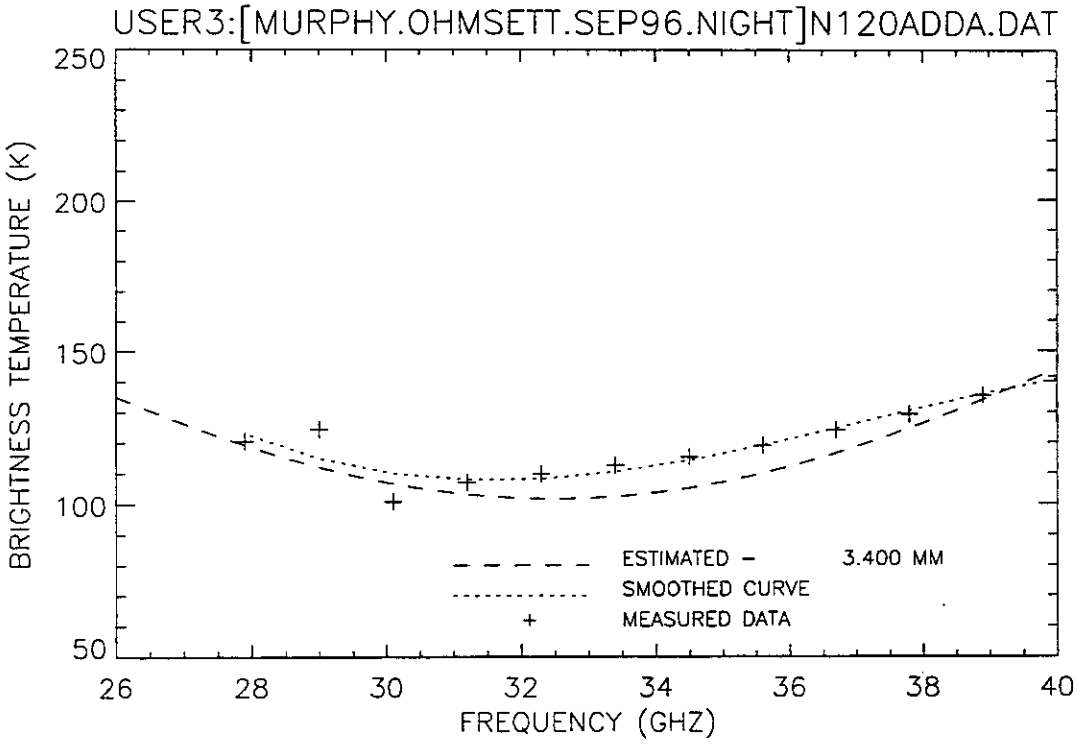

Figure 195. Plot of radiometric brightness temperature versus measurement frequency for 2-mm diesel oil, night test, calm wave conditions, 12 September 1996, sweep A.

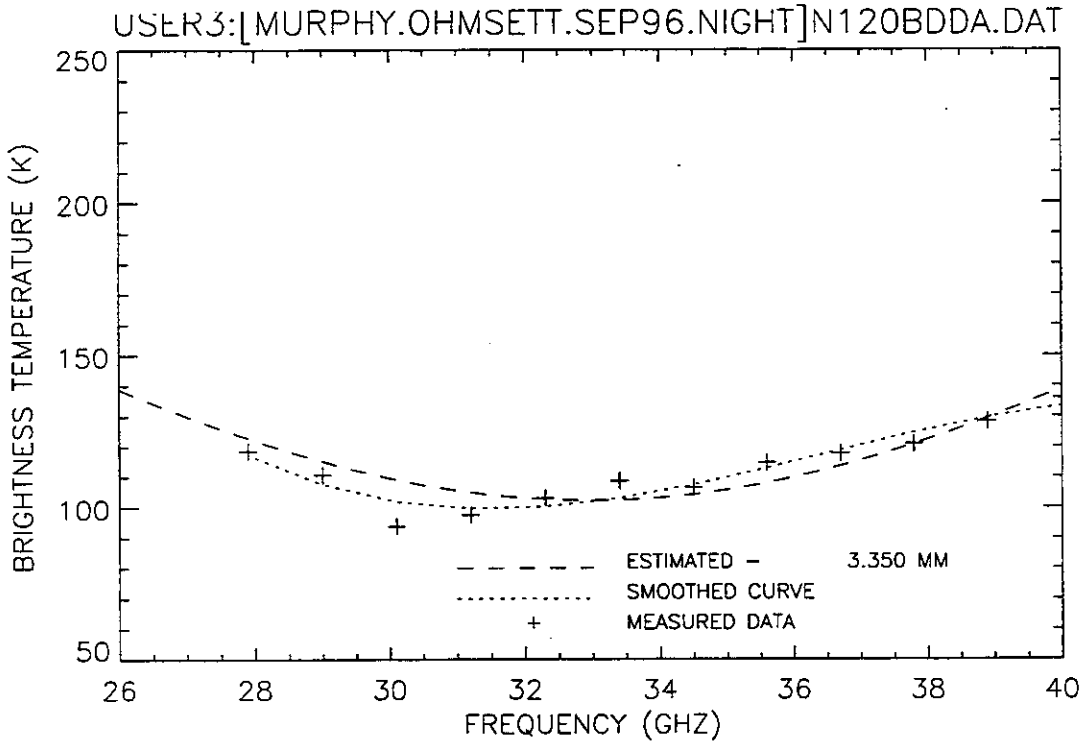

Figure 196. Plot of radiometric brightness temperature versus measurement frequency for 2-mm diesel oil, night test, calm wave conditions, 12 September 1996, sweep B.

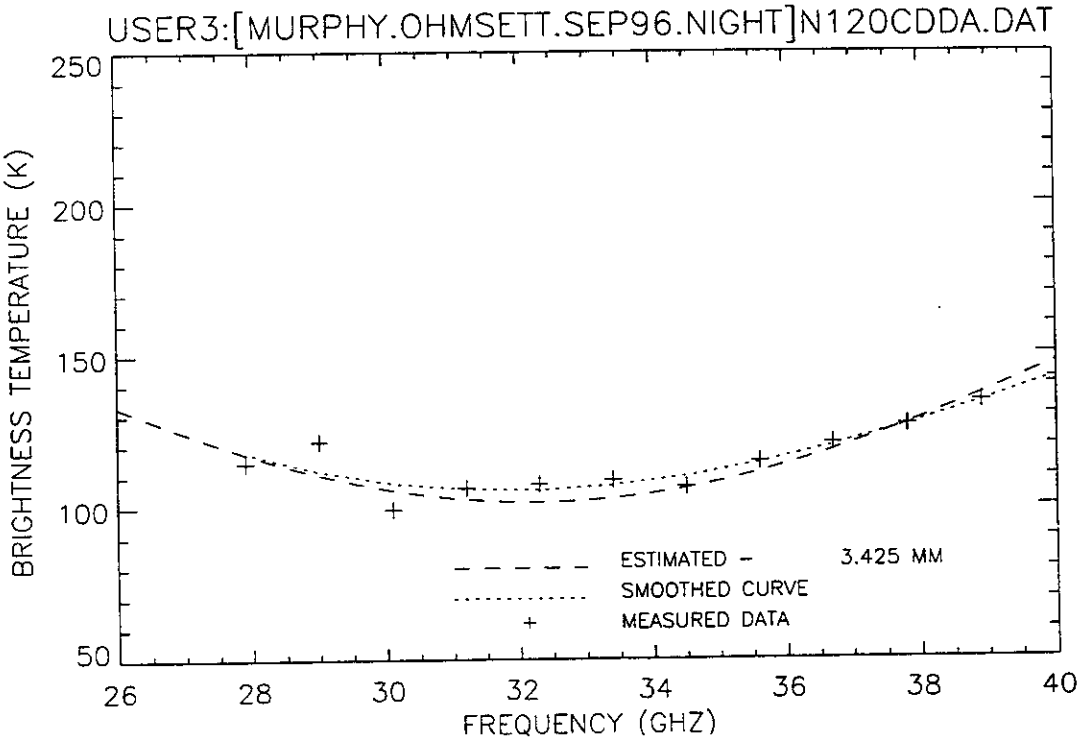

Figure 197. Plot of radiometric brightness temperature versus measurement frequency for 2-mm diesel oil, night test, calm wave conditions, 12 September 1996, sweep C.

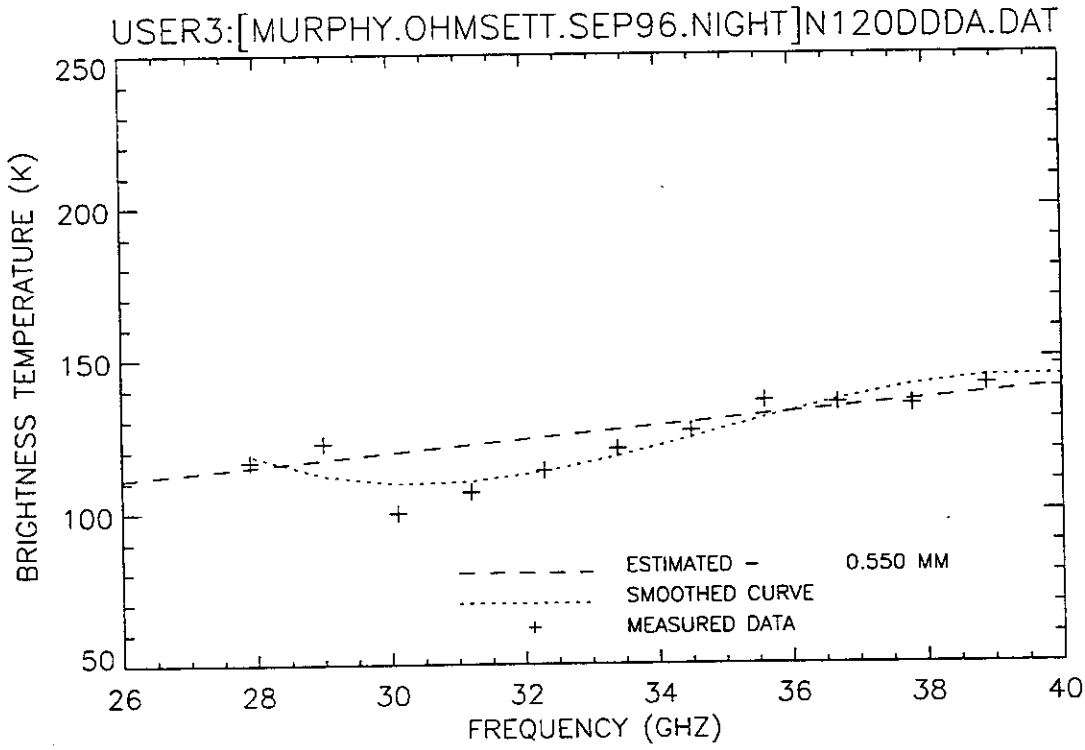

Figure 198. Plot of radiometric brightness temperature versus measurement frequency for 2-mm diesel oil, night test, calm wave conditions, 12 September 1996, sweep D.

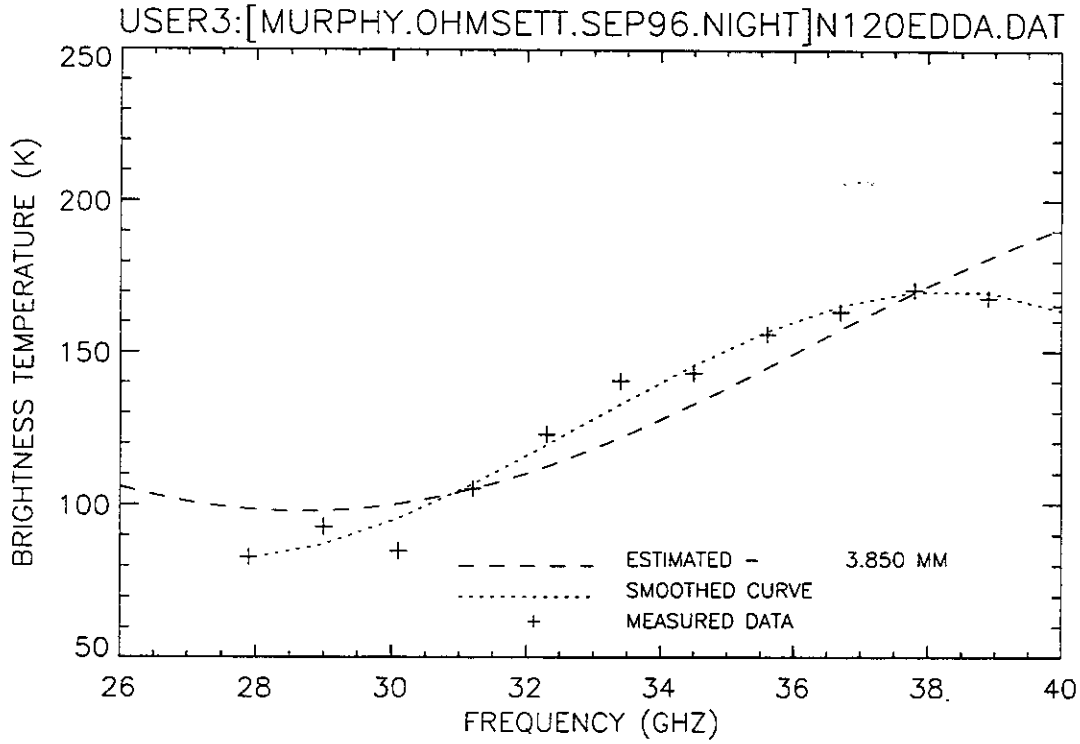

Figure 199. Plot of radiometric brightness temperature versus measurement frequency for 2-mm diesel oil, night test, calm wave conditions, 12 September 1996, sweep E.

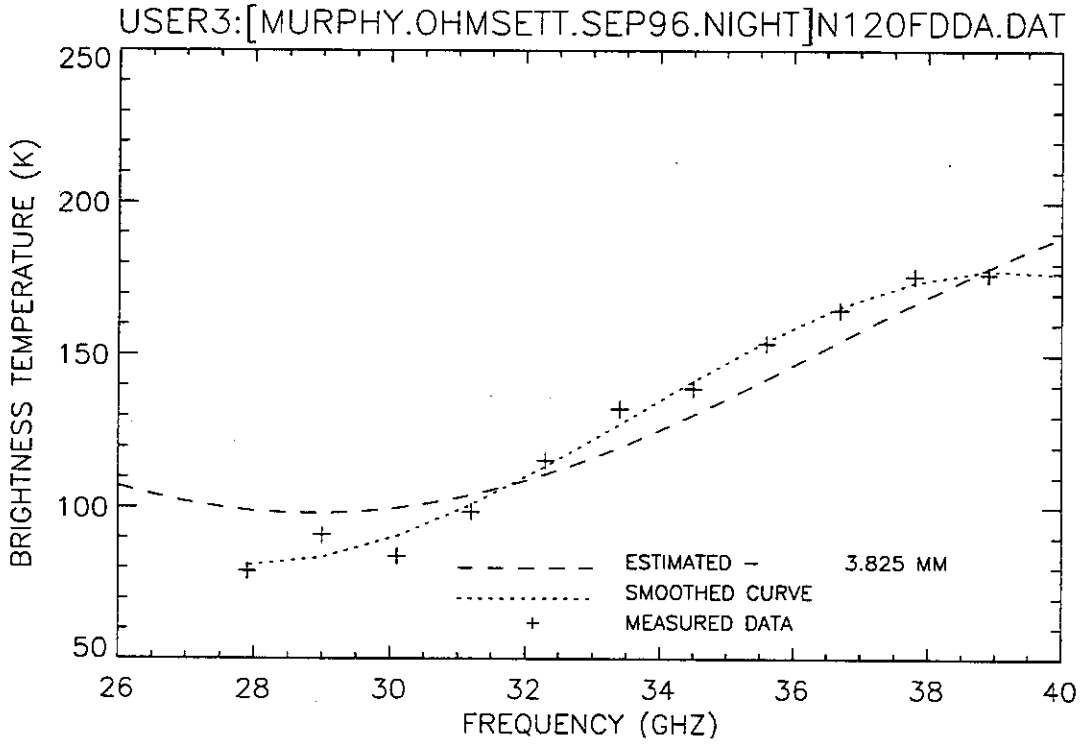

Figure 200. Plot of radiometric brightness temperature versus measurement frequency for 2-mm diesel oil, night test, calm wave conditions, 12 September 1996, sweep F.

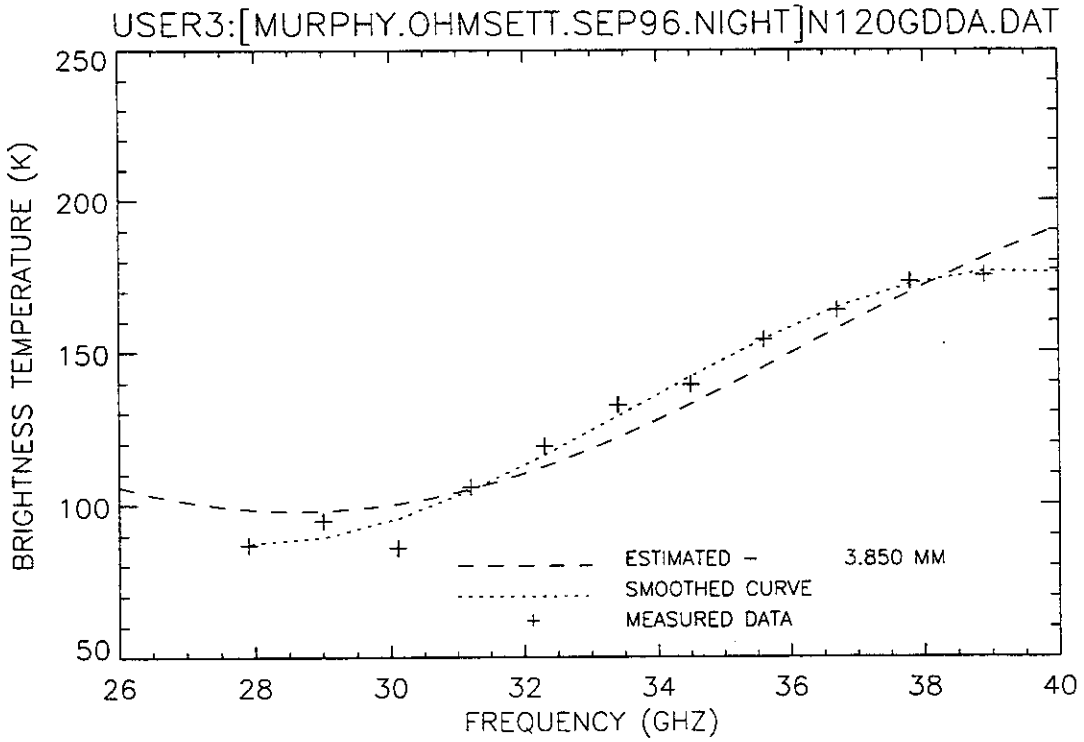

Figure 201. Plot of radiometric brightness temperature versus measurement frequency for 2-mm diesel oil, night test, calm wave conditions, 12 September 1996, sweep G.

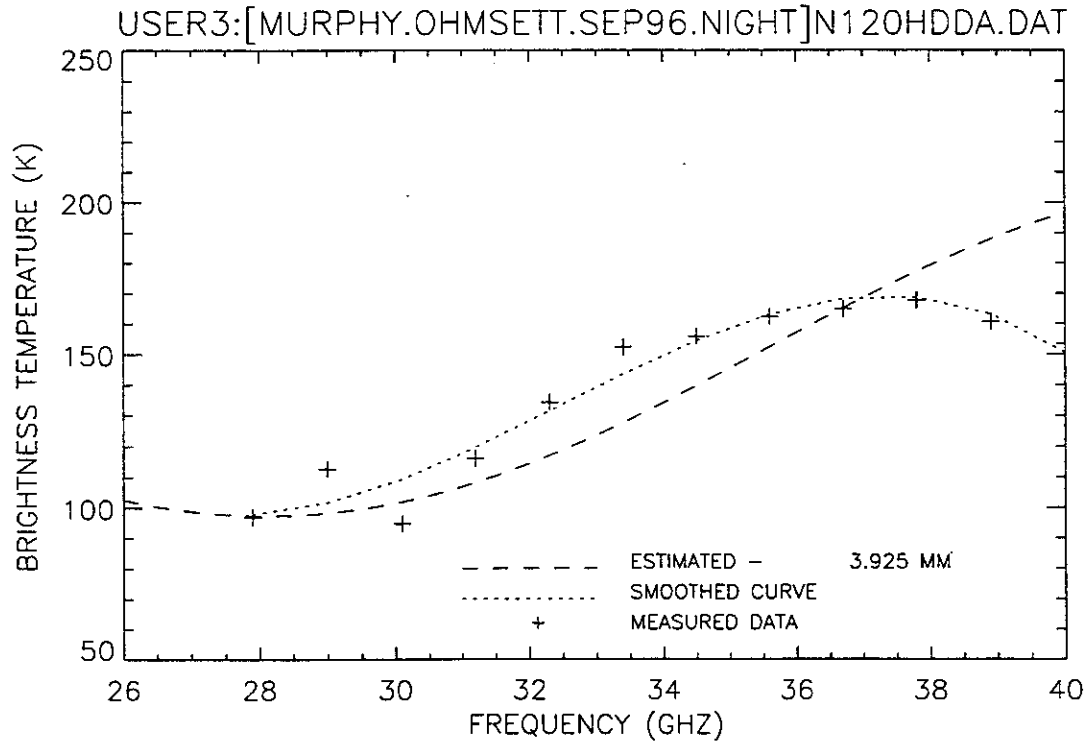

Figure 202. Plot of radiometric brightness temperature versus measurement frequency for 2-mm diesel oil, night test, calm wave conditions, 12 September 1996, sweep H.

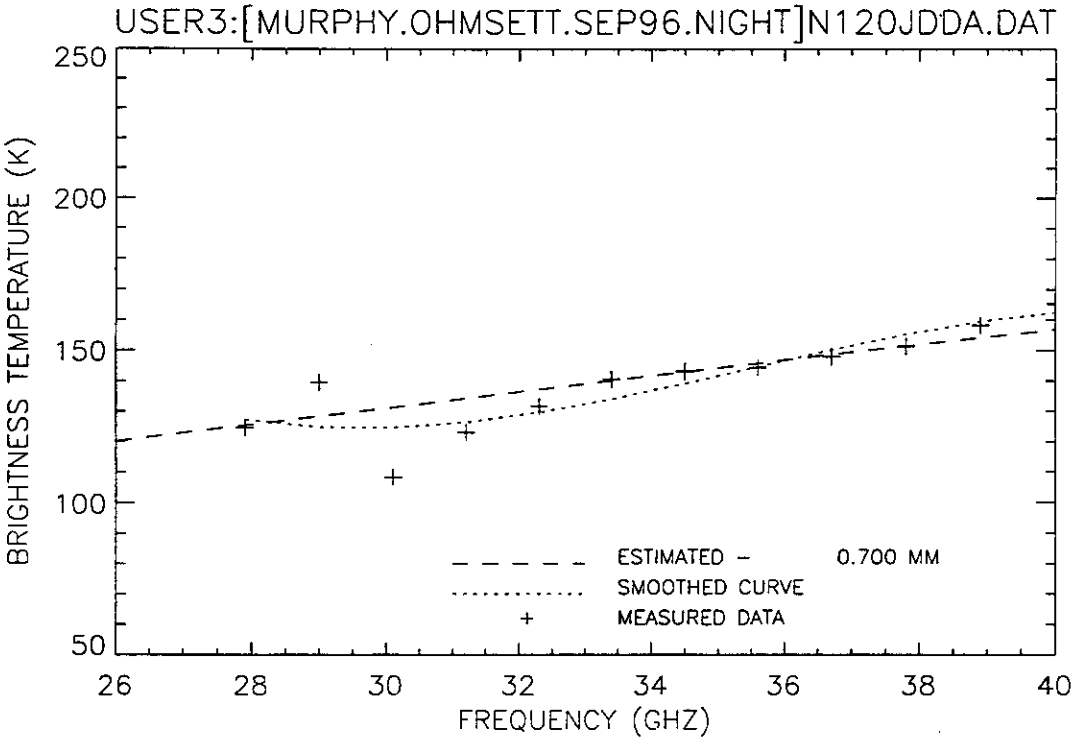

Figure 203. Plot of radiometric brightness temperature versus measurement frequency for 2-mm diesel oil, night test, calm wave conditions, 12 September 1996, sweep J.

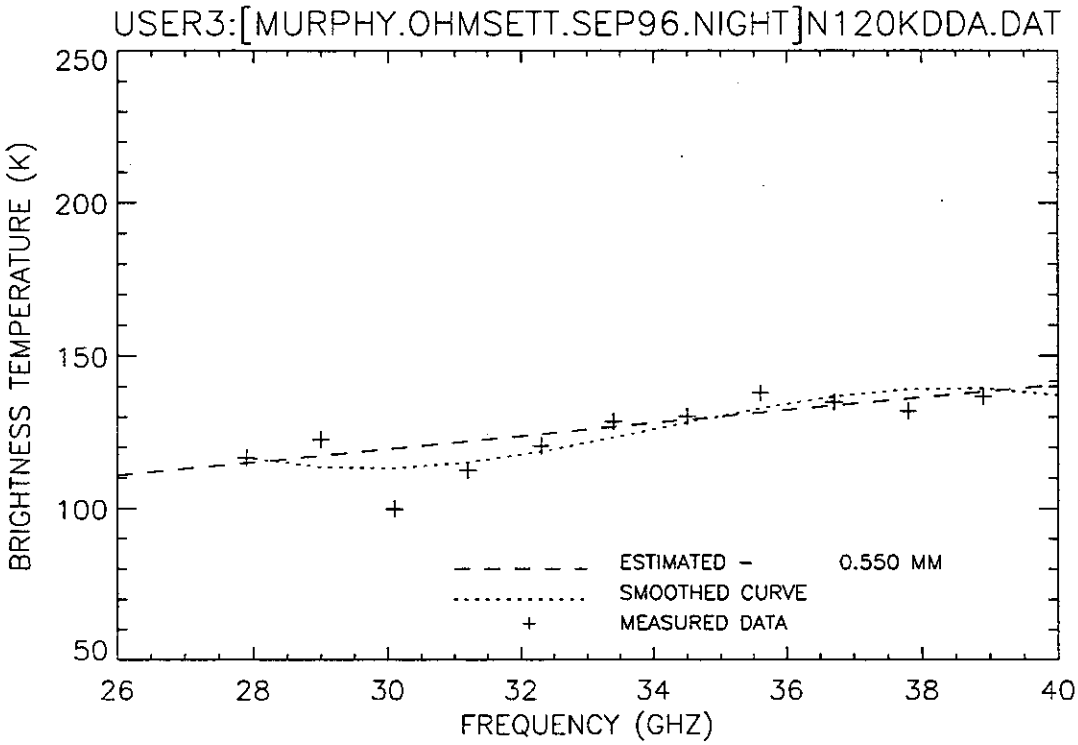

Figure 204. Plot of radiometric brightness temperature versus measurement frequency for 2-mm diesel oil, night test, calm wave conditions, 12 September 1996, sweep K.

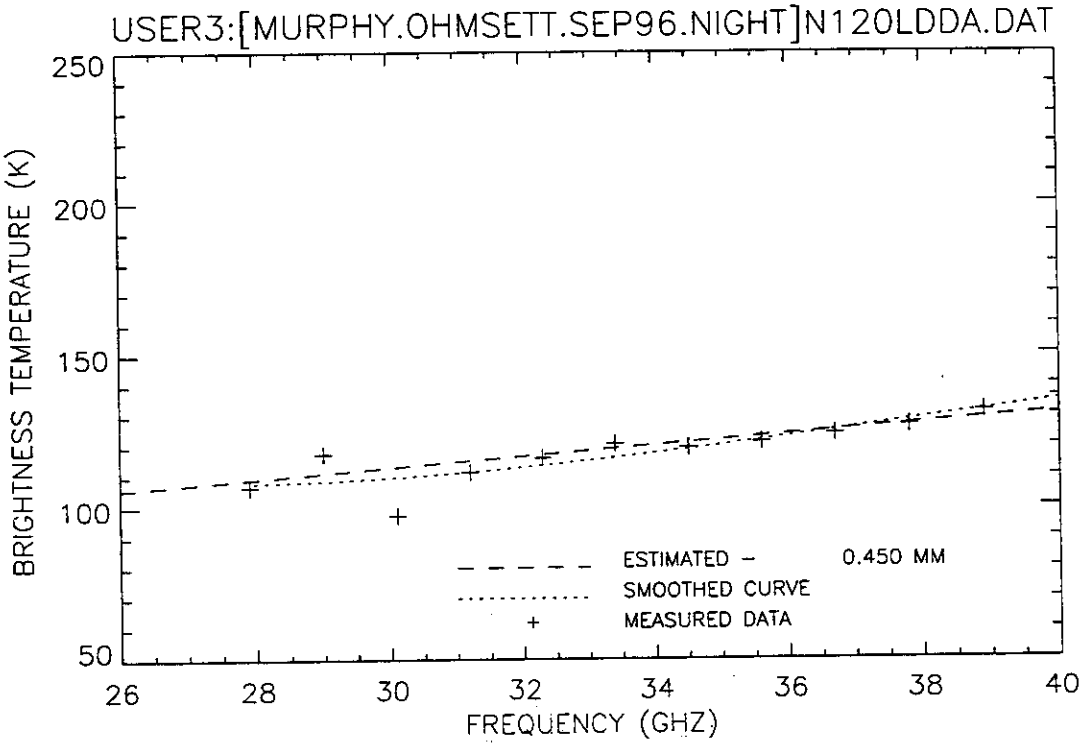

Figure 205. Plot of radiometric brightness temperature versus measurement frequency for 2-mm diesel oil, night test, calm wave conditions, 12 September 1996, sweep L.

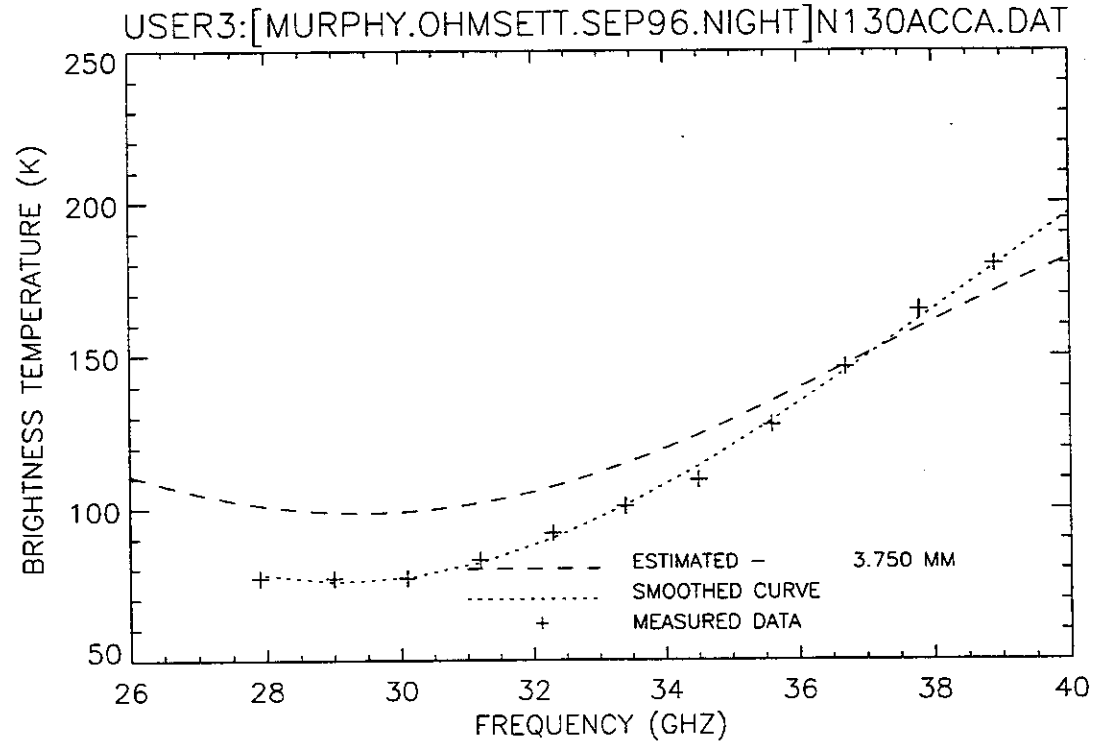

Figure 206. Plot of radiometric brightness temperature versus measurement frequency for 3-mm crude oil, night test, calm wave conditions, 12 September 1996, sweep A.

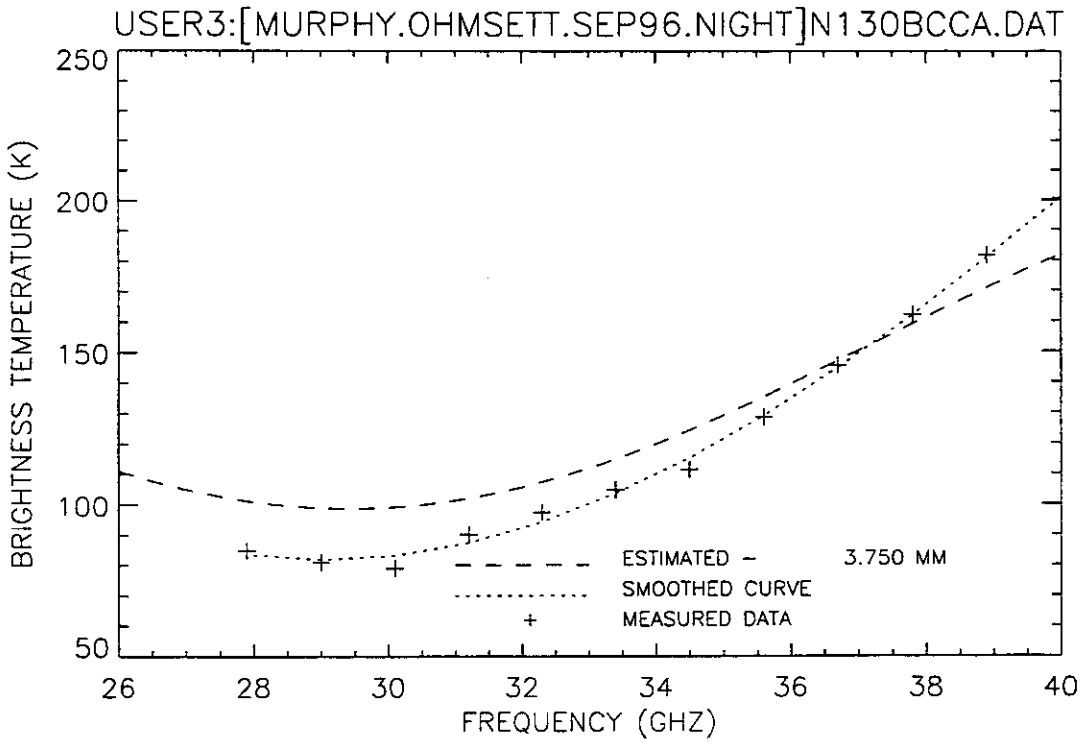

Figure 207. Plot of radiometric brightness temperature versus measurement frequency for 3-mm crude oil, night test, calm wave conditions, 12 September 1996, sweep B.

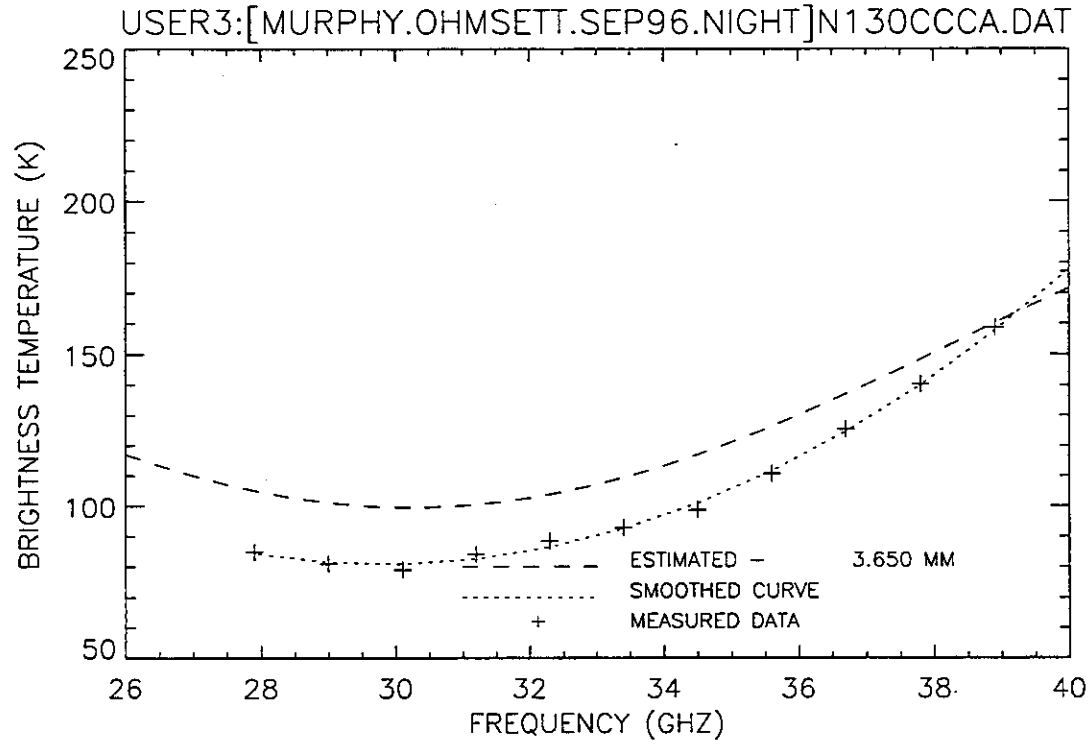

Figure 208. Plot of radiometric brightness temperature versus measurement frequency for 3-mm crude oil, night test, calm wave conditions, 12 September 1996, sweep C.

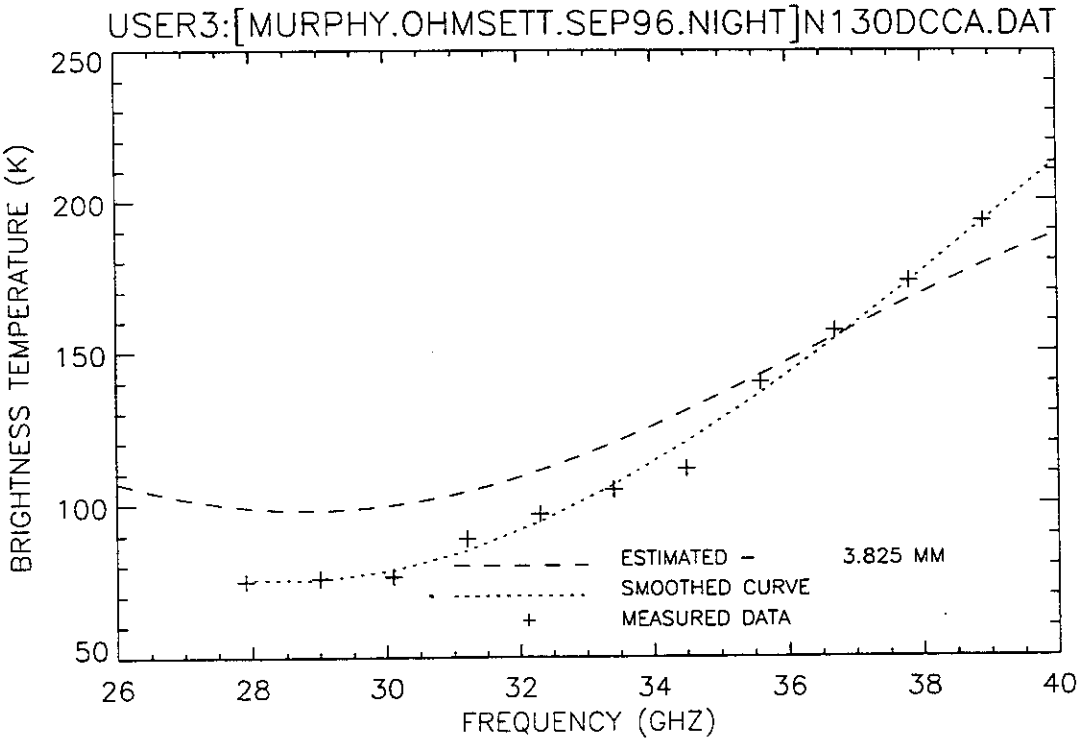

Figure 209. Plot of radiometric brightness temperature versus measurement frequency for 3-mm crude oil, night test, calm wave conditions, 12 September 1996, sweep D.

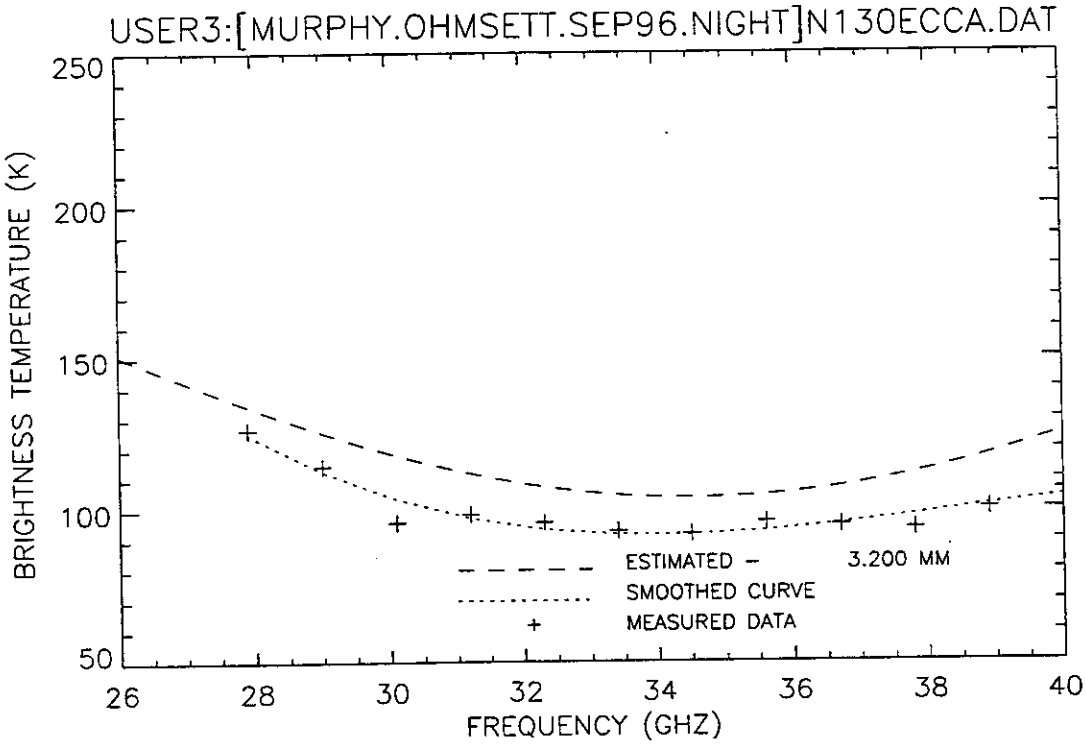

Figure 210. Plot of radiometric brightness temperature versus measurement frequency for 3-mm crude oil, night test, calm wave conditions, 12 September 1996, sweep E.

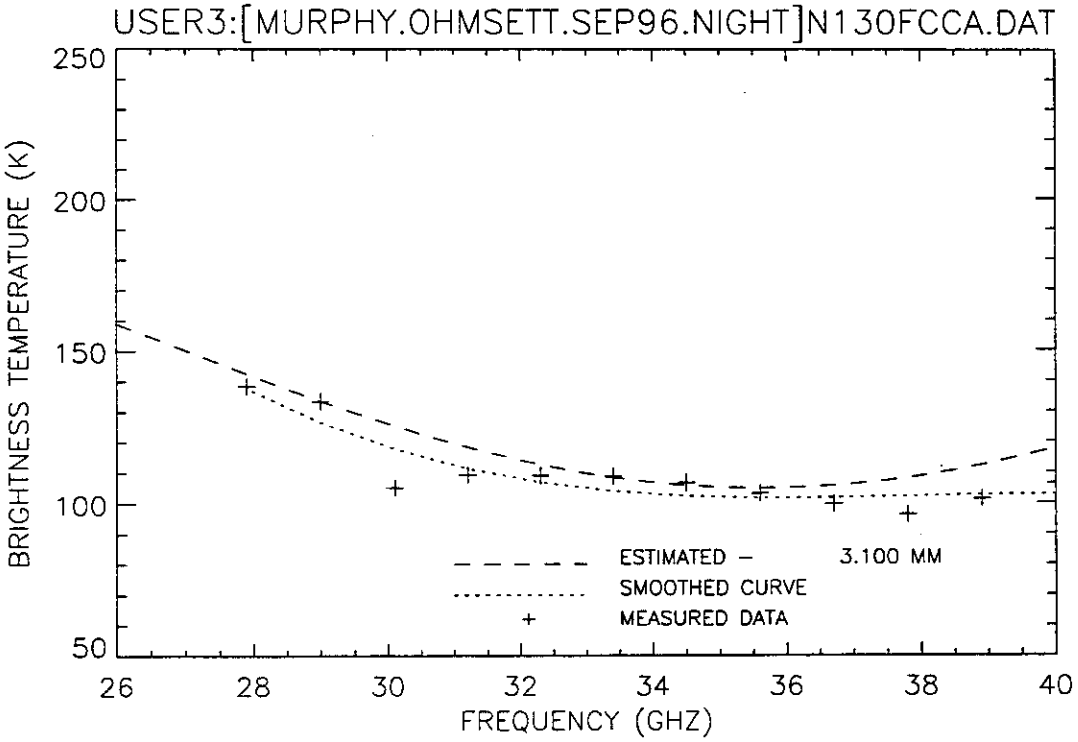

Figure 211. Plot of radiometric brightness temperature versus measurement frequency for 3-mm crude oil, night test, calm wave conditions, 12 September 1996, sweep F.

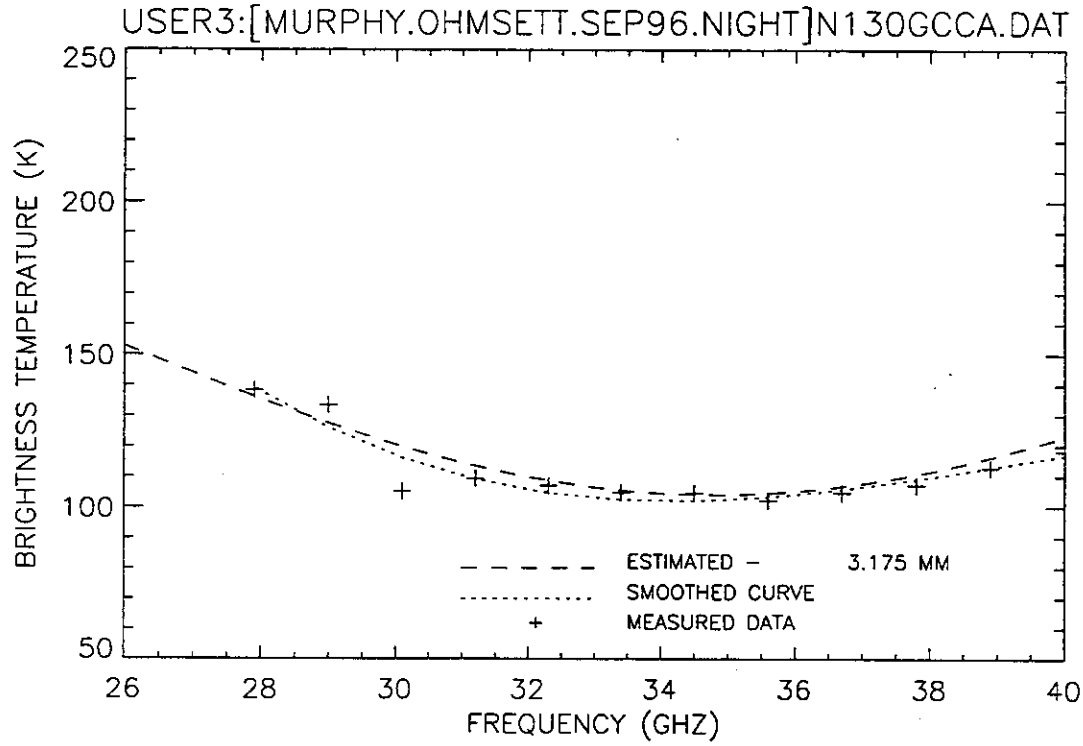

Figure 212. Plot of radiometric brightness temperature versus measurement frequency for 3-mm crude oil, night test, calm wave conditions, 12 September 1996, sweep G.

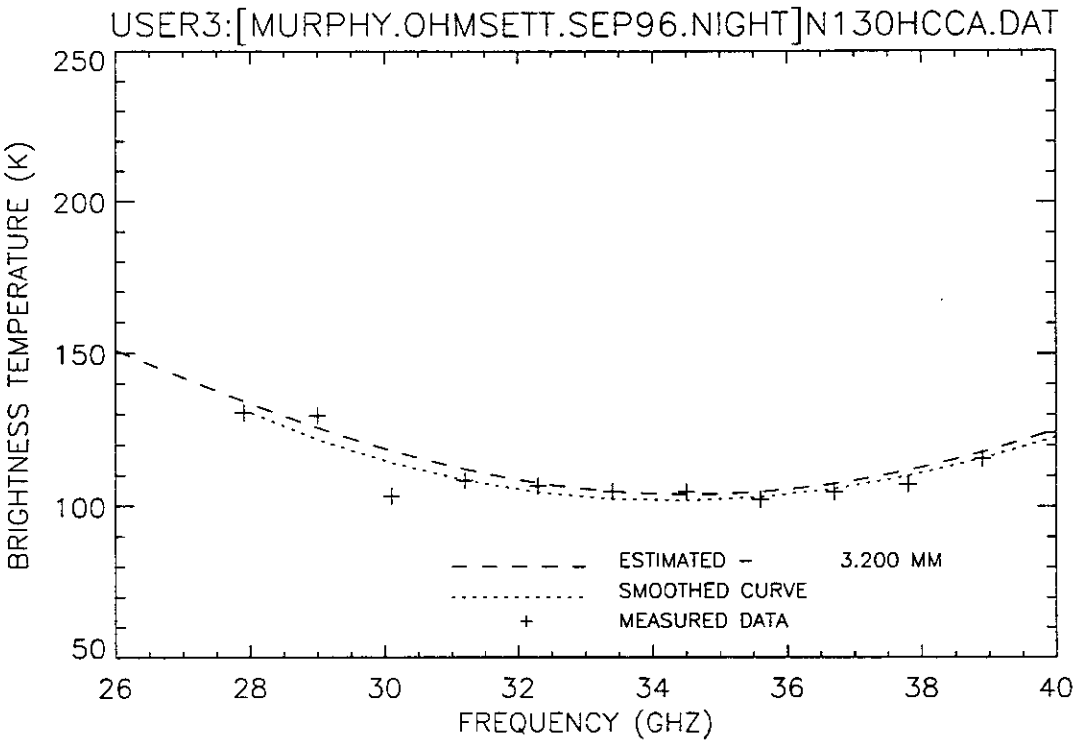

Figure 213. Plot of radiometric brightness temperature versus measurement frequency for 3-mm crude oil, night test, calm wave conditions, 12 September 1996, sweep H.

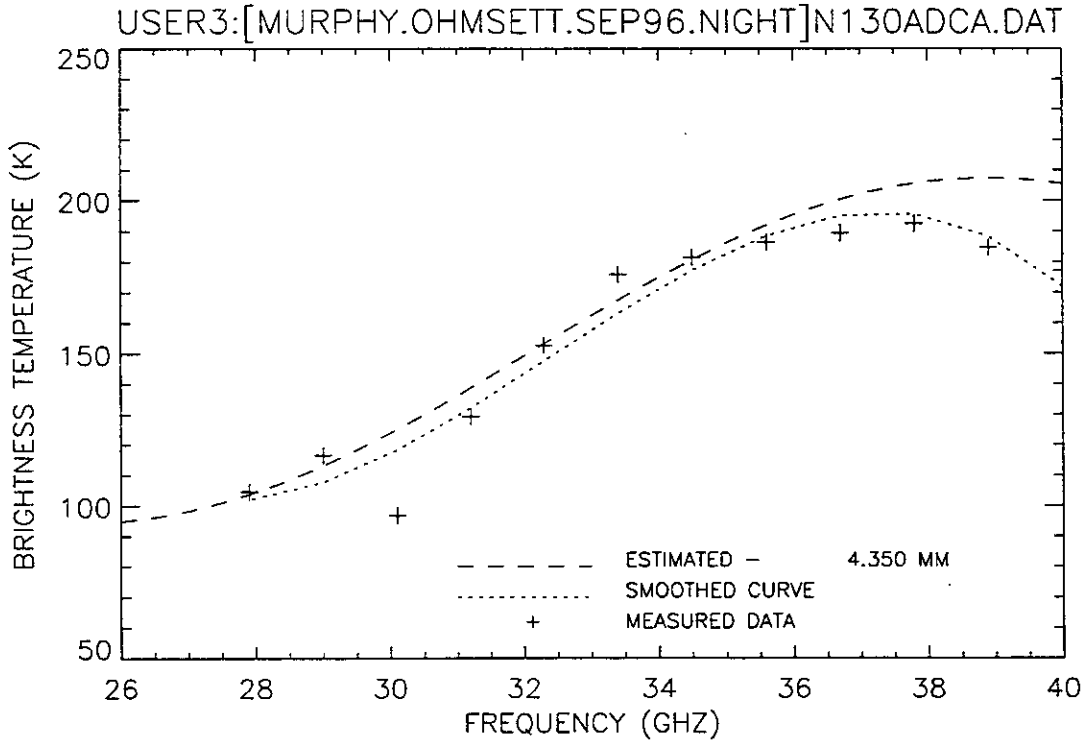

Figure 214. Plot of radiometric brightness temperature versus measurement frequency for 3-mm diesel oil, night test, calm wave conditions, 12 September 1996, sweep A.

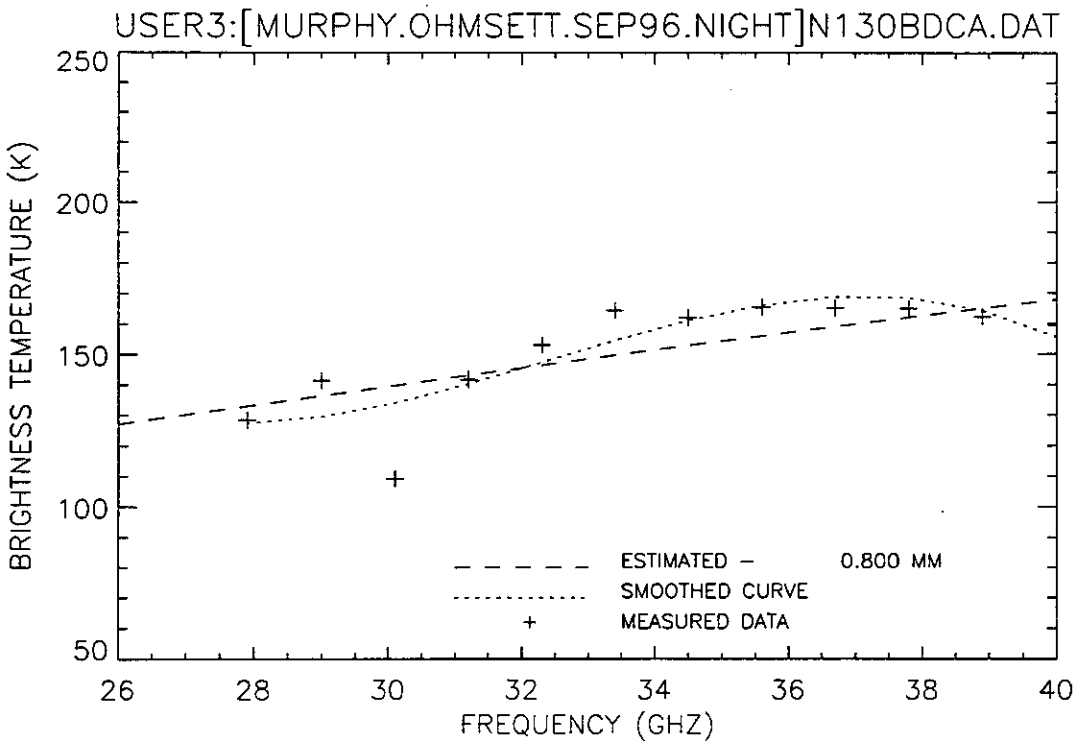

Figure 215. Plot of radiometric brightness temperature versus measurement frequency for 3-mm diesel oil, night test, calm wave conditions, 12 September 1996, sweep B.

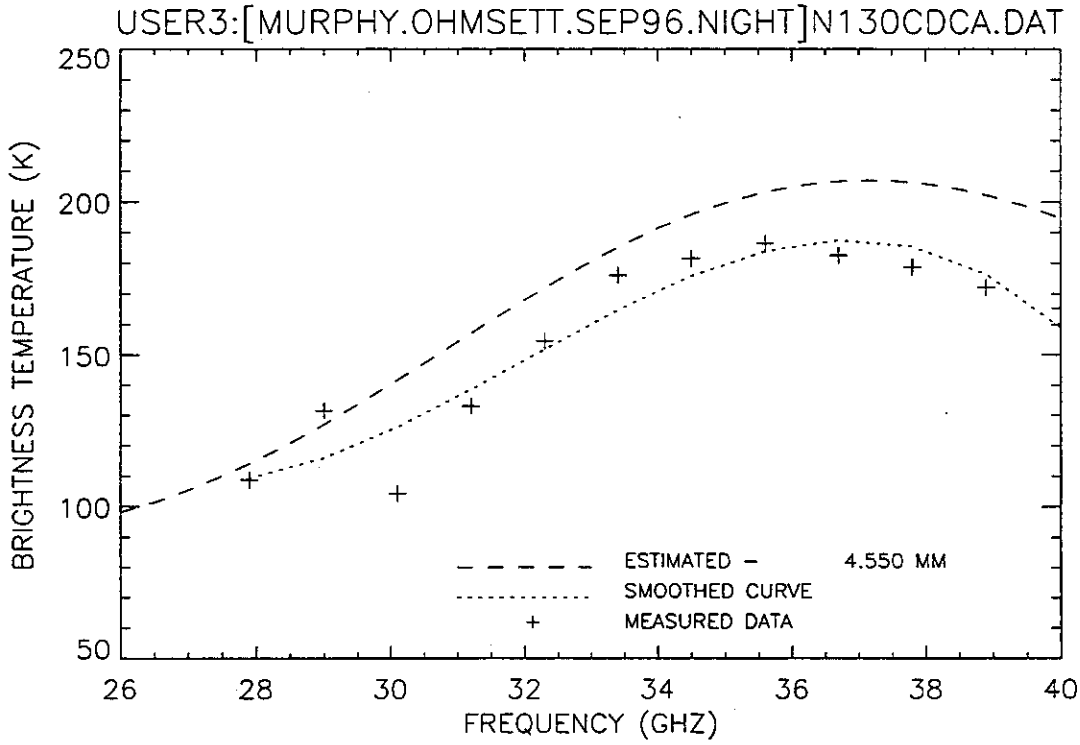

Figure 216. Plot of radiometric brightness temperature versus measurement frequency for 3-mm diesel oil, night test, calm wave conditions, 12 September 1996, sweep C.

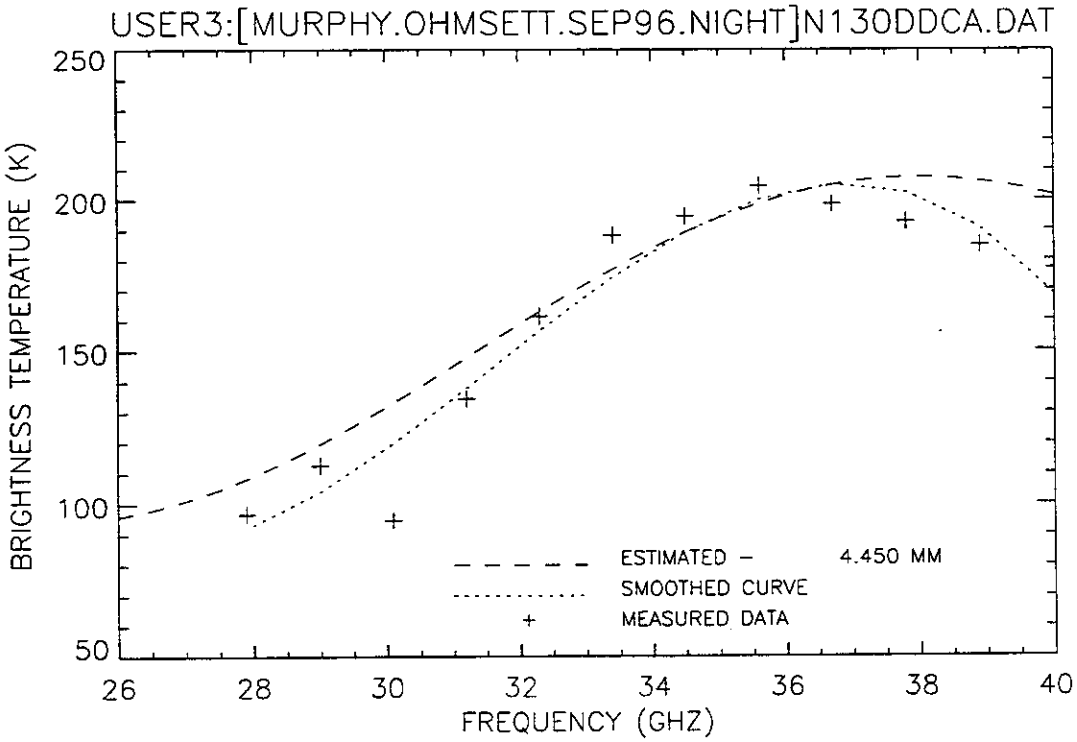

Figure 217. Plot of radiometric brightness temperature versus measurement frequency for 3-mm diesel oil, night test, calm wave conditions, 12 September 1996, sweep D.

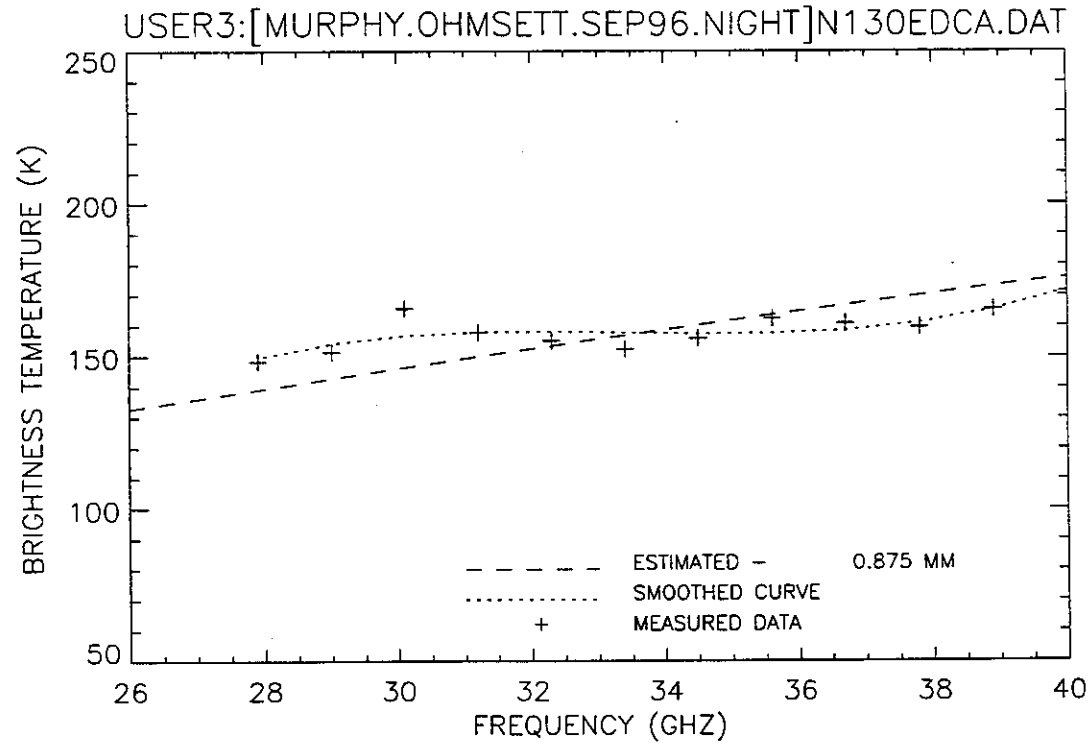

Figure 218. Plot of radiometric brightness temperature versus measurement frequency for 3-mm diesel oil, night test, calm wave conditions, 12 September 1996, sweep E.

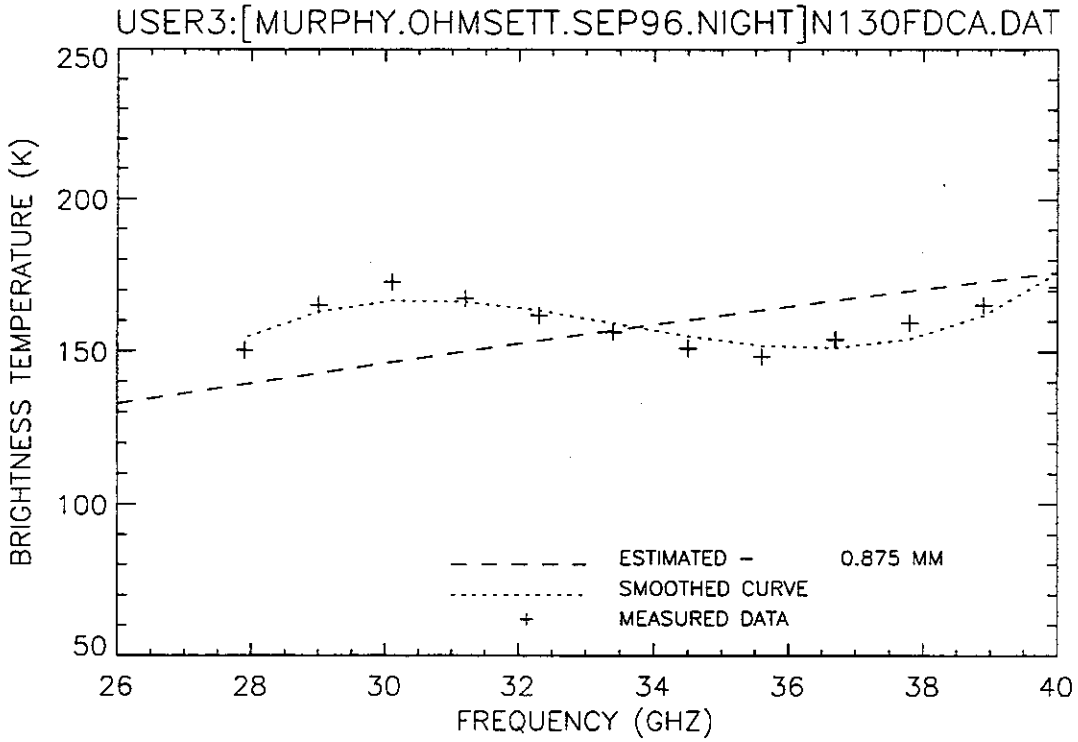

Figure 219. Plot of radiometric brightness temperature versus measurement frequency for 3-mm diesel oil, night test, calm wave conditions, 12 September 1996, sweep F.

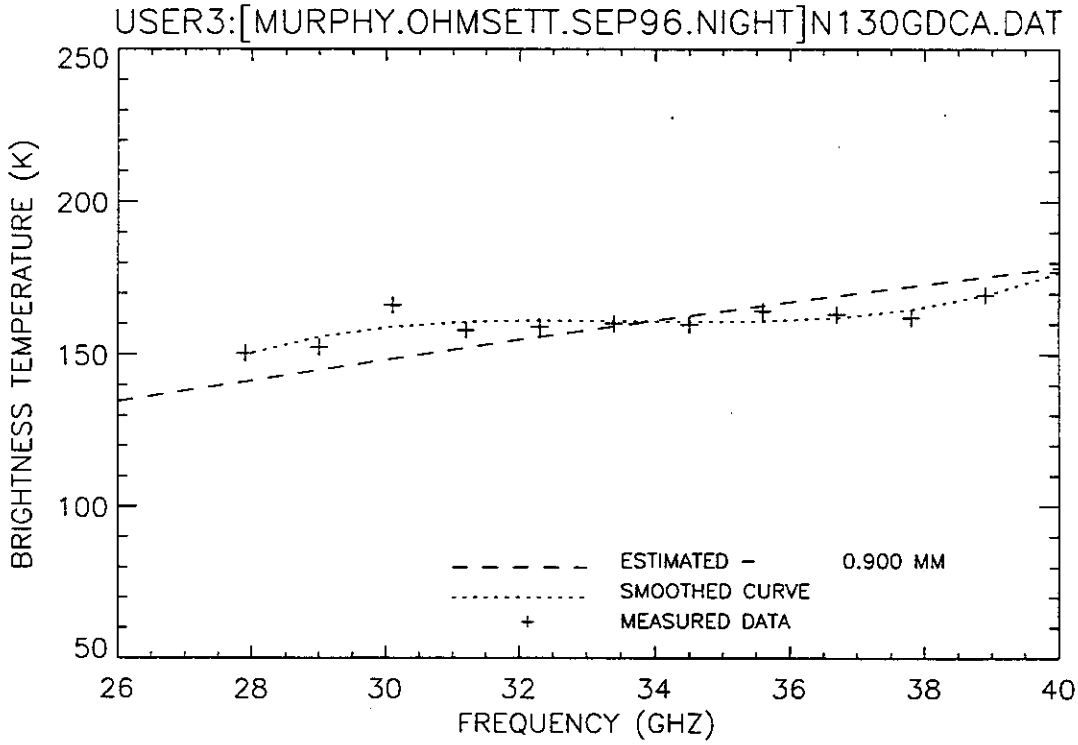

Figure 220. Plot of radiometric brightness temperature versus measurement frequency for 3-mm diesel oil, night test, calm wave conditions, 12 September 1996, sweep G.

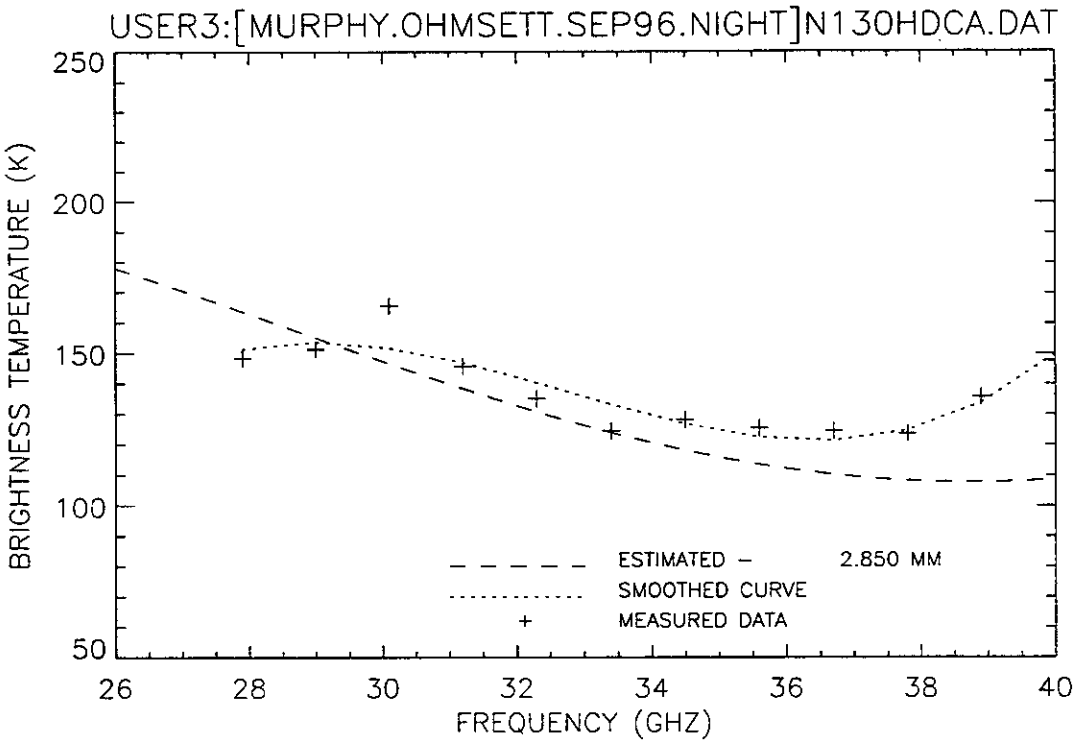

Figure 221. Plot of radiometric brightness temperature versus measurement frequency for 3-mm diesel oil, night test, calm wave conditions, 12 September 1996, sweep H.

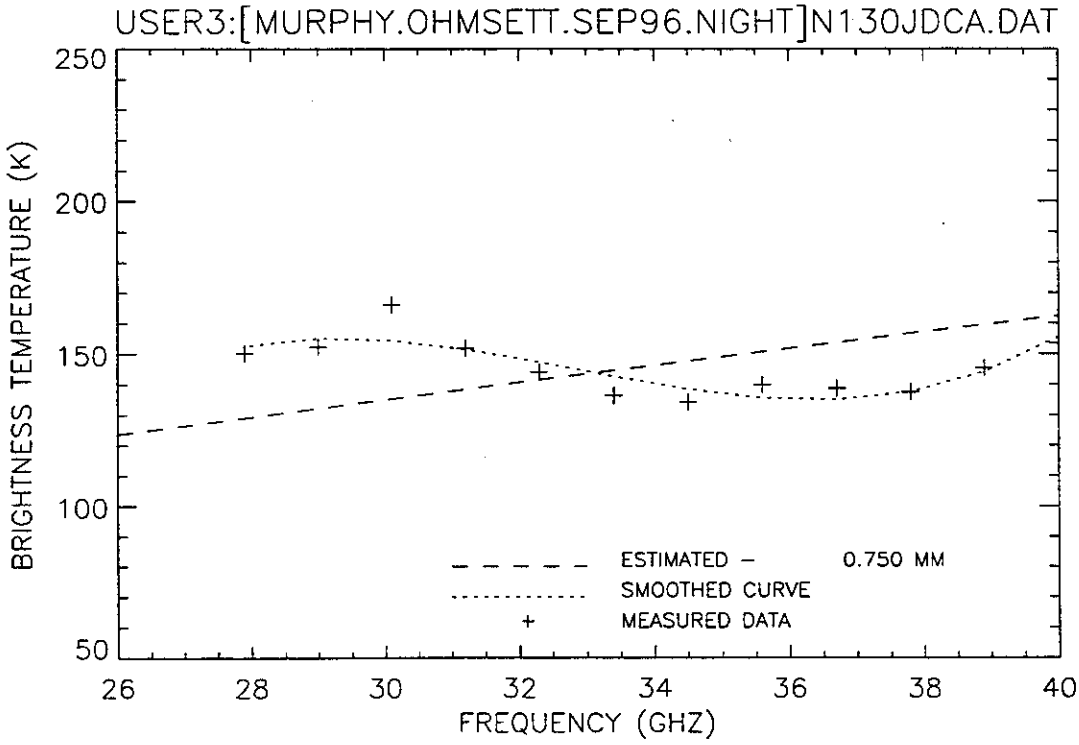

Figure 222. Plot of radiometric brightness temperature versus measurement frequency for 3-mm diesel oil, night test, calm wave conditions, 12 September 1996, sweep J.

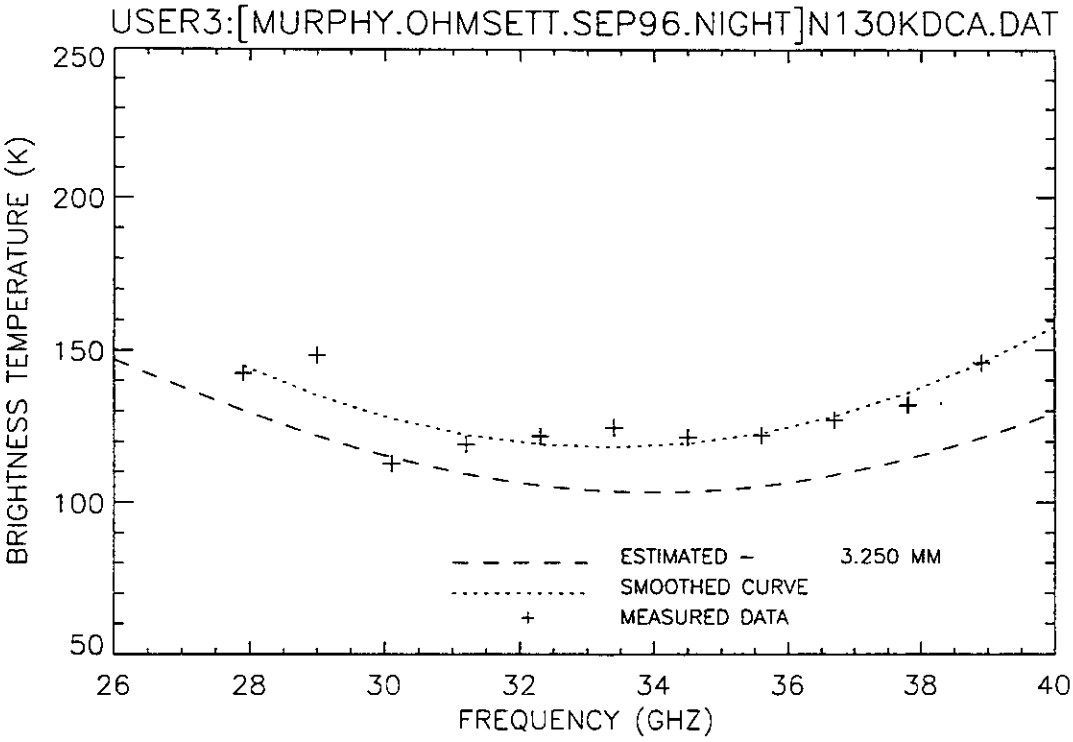

Figure 223. Plot of radiometric brightness temperature versus measurement frequency for 3-mm diesel oil, night test, calm wave conditions, 12 September 1996, sweep K.

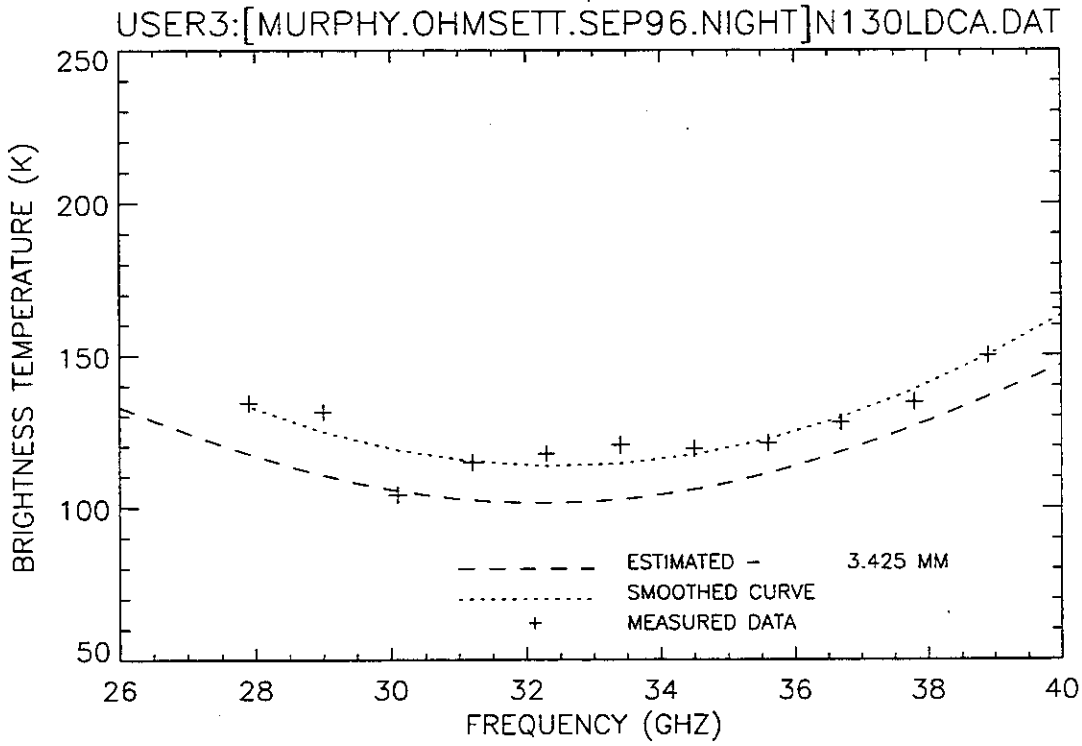

Figure 224. Plot of radiometric brightness temperature versus measurement frequency for 3-mm diesel oil, night test, calm wave conditions, 12 September 1996, sweep L.

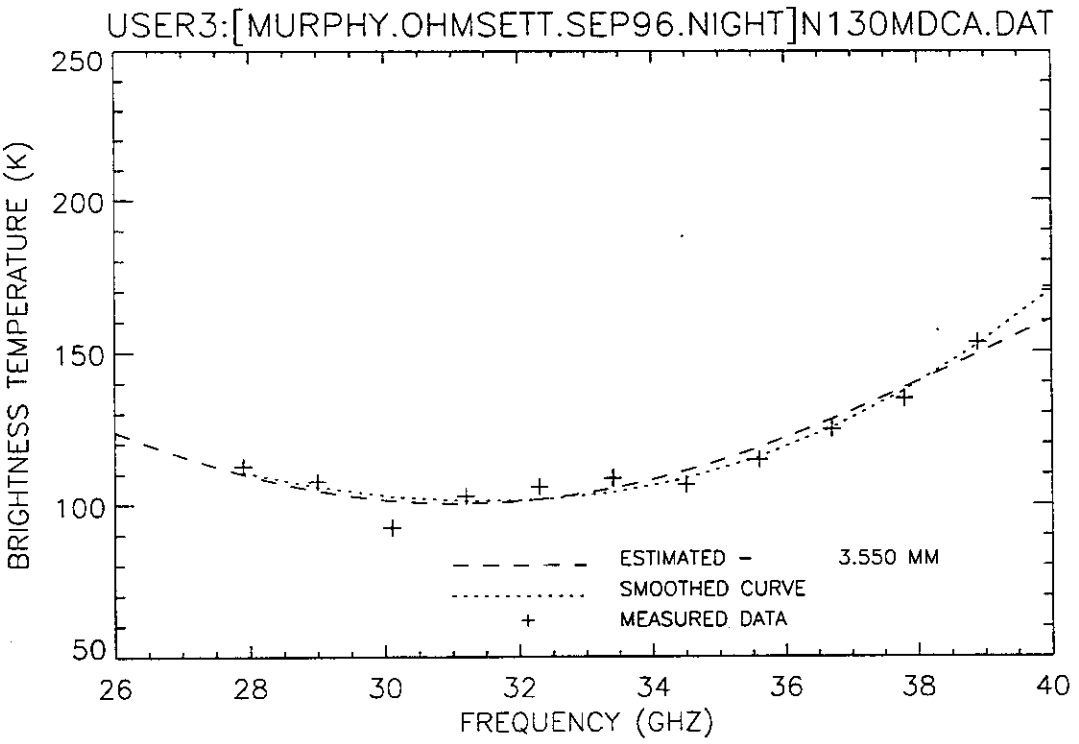

Figure 225. Plot of radiometric brightness temperature versus measurement frequency for 3-mm diesel oil, night test, calm wave conditions, 12 September 1996, sweep M.

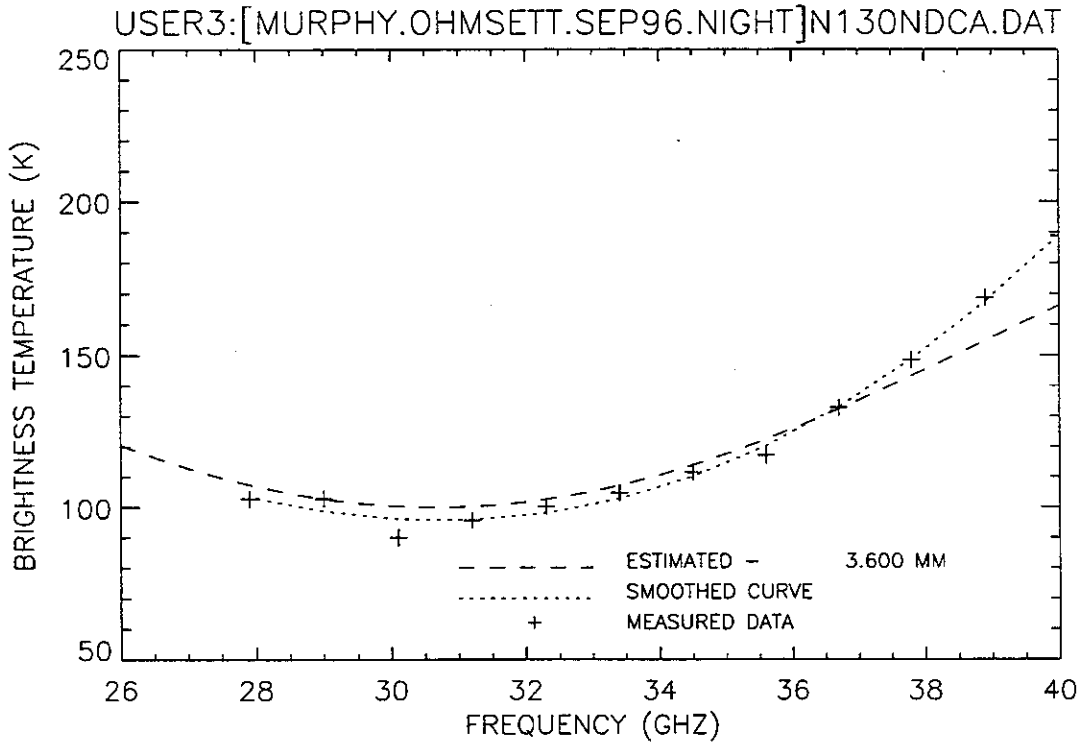

Figure 226. Plot of radiometric brightness temperature versus measurement frequency for 3-mm diesel oil, night test, calm wave conditions, 12 September 1996, sweep N.

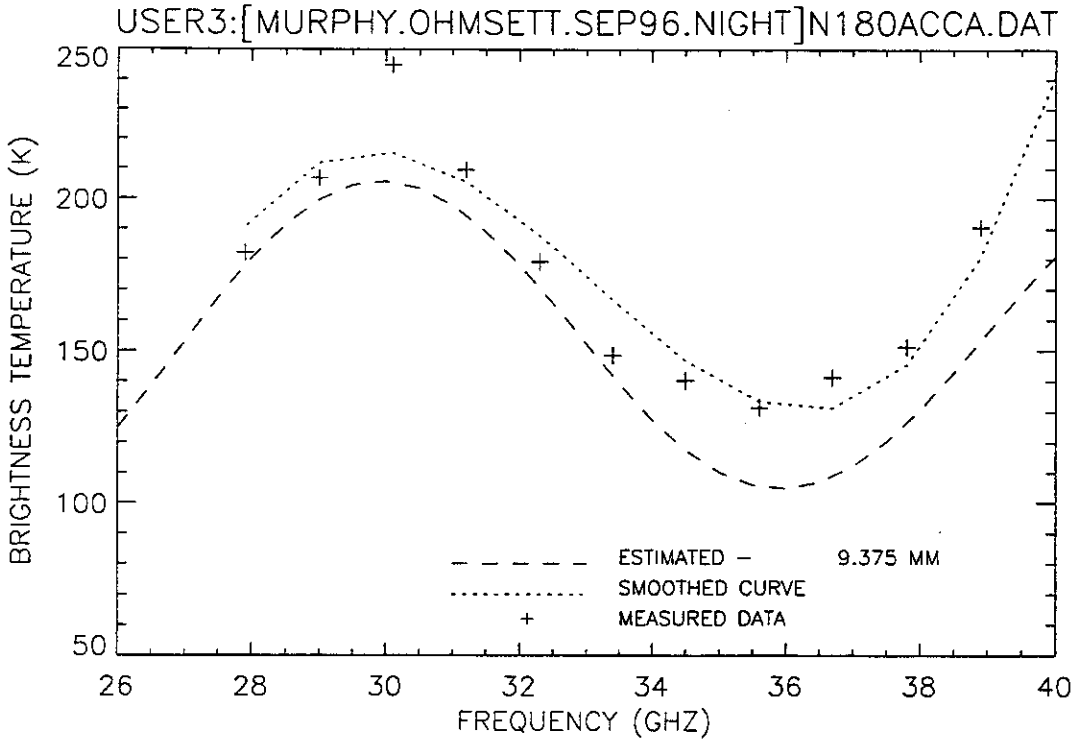

Figure 227. Plot of radiometric brightness temperature versus measurement frequency for 8-mm crude oil, night test, calm wave conditions, 12 September 1996, sweep A.

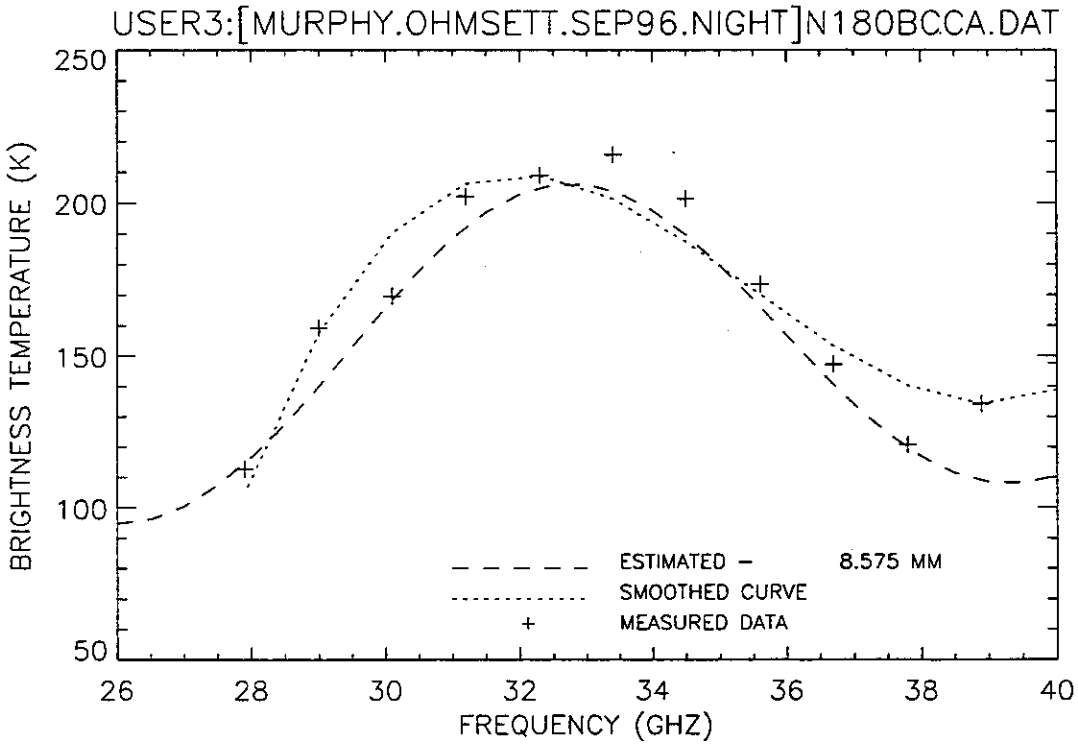

Figure 228. Plot of radiometric brightness temperature versus measurement frequency for 8-mm crude oil, night test, calm wave conditions, 12 September 1996, sweep B.

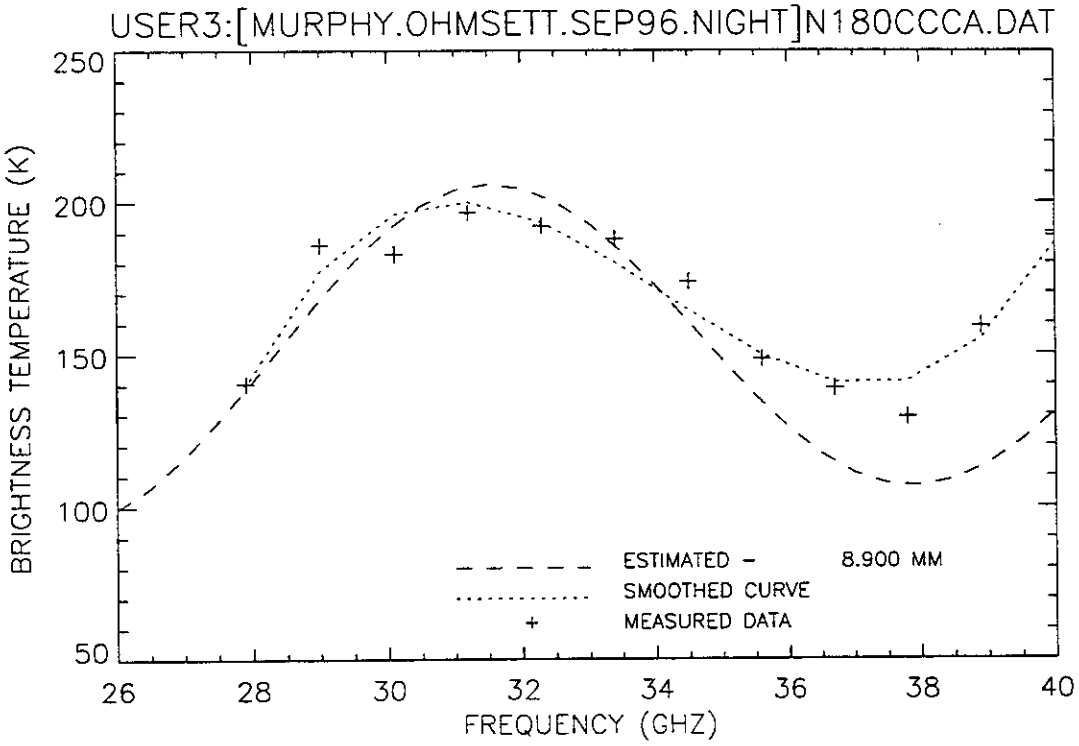

Figure 229. Plot of radiometric brightness temperature versus measurement frequency for 8-mm crude oil, night test, calm wave conditions, 12 September 1996, sweep C.

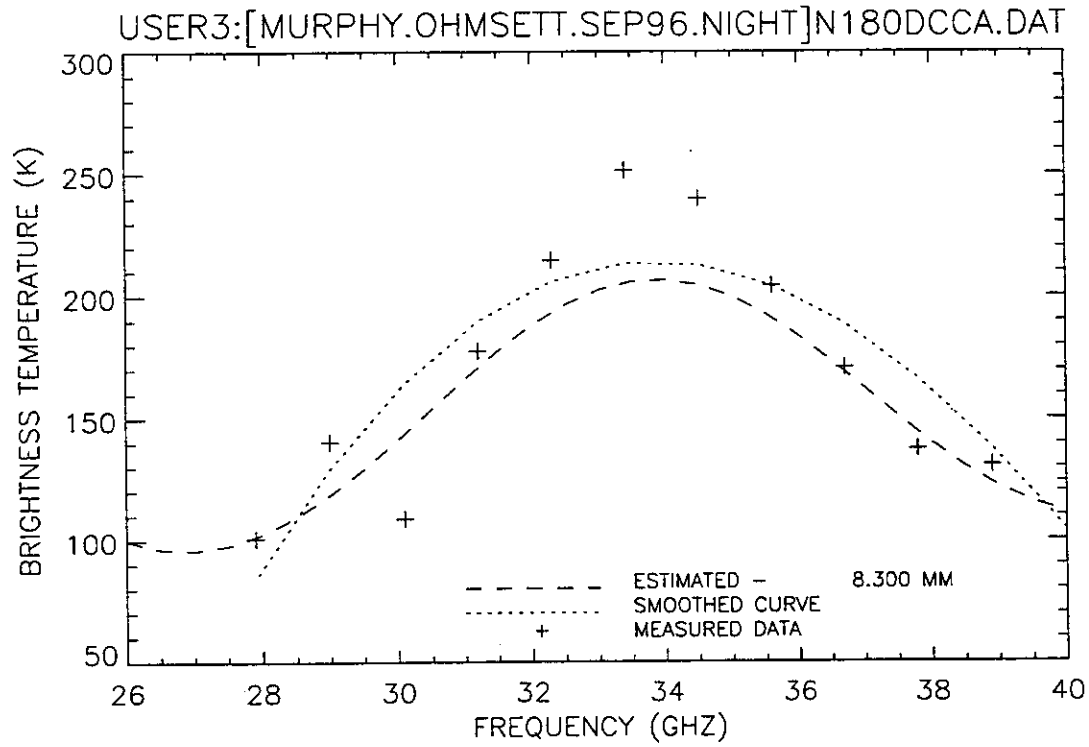

Figure 230. Plot of radiometric brightness temperature versus measurement frequency for 8-mm crude oil, night test, calm wave conditions, 12 September 1996, sweep D.

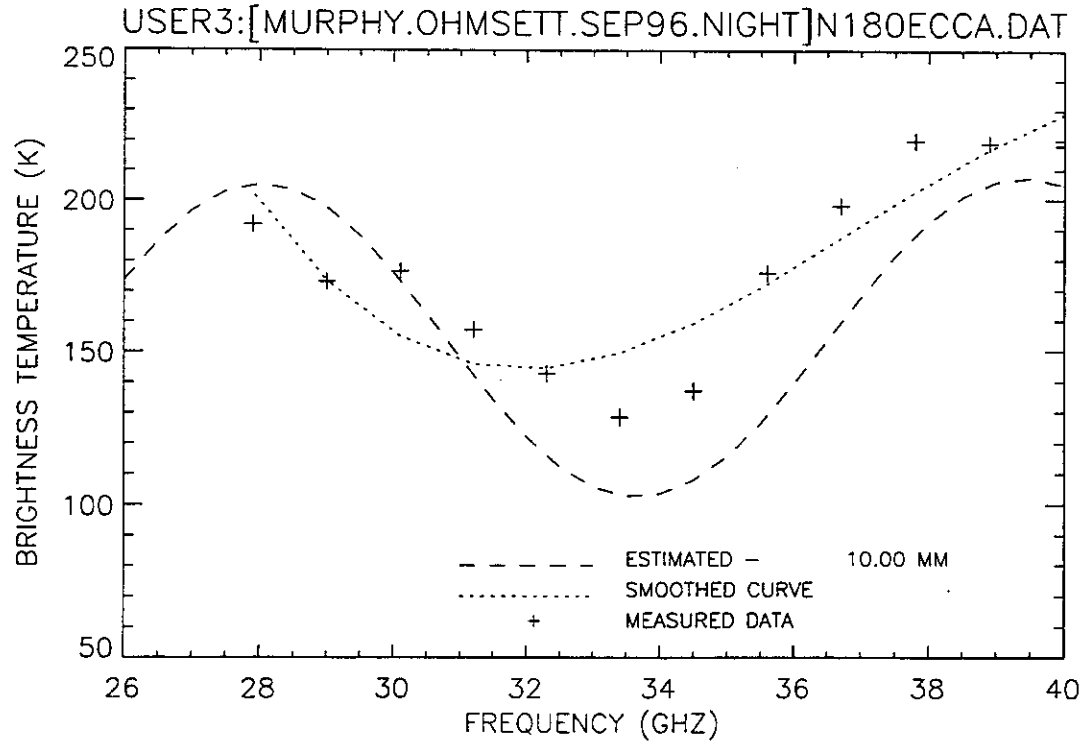

Figure 231. Plot of radiometric brightness temperature versus measurement frequency for 8-mm crude oil, night test, calm wave conditions, 12 September 1996, sweep E.

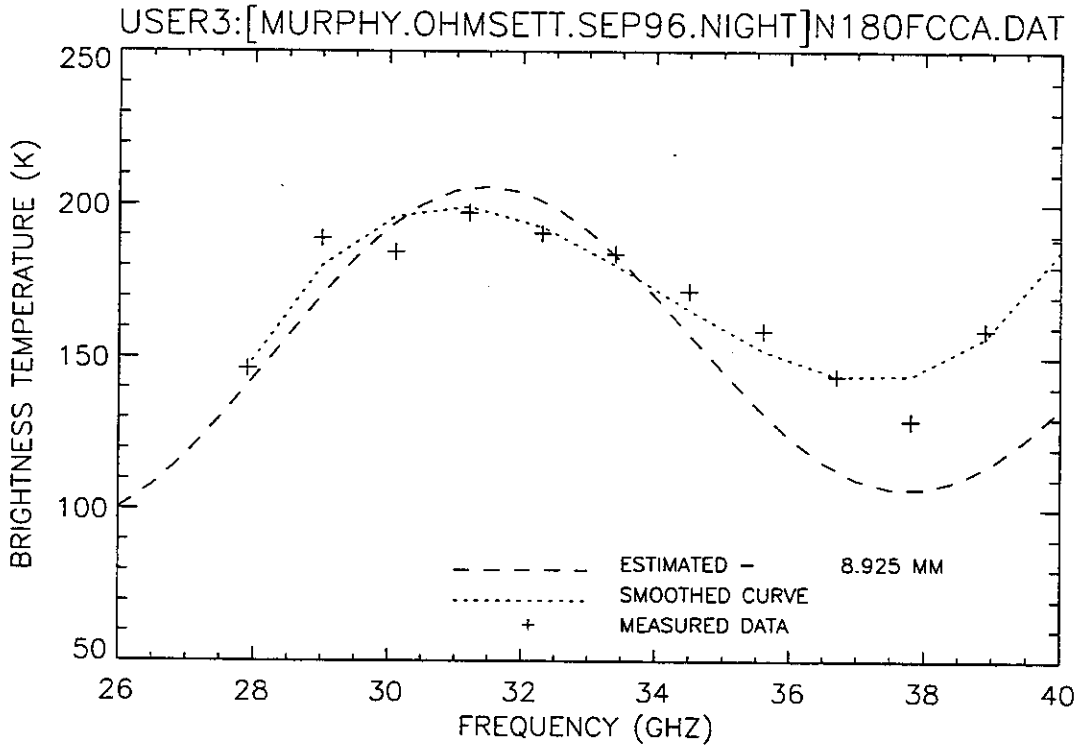

Figure 232. Plot of radiometric brightness temperature versus measurement frequency for 8-mm crude oil, night test, calm wave conditions, 12 September 1996, sweep F.

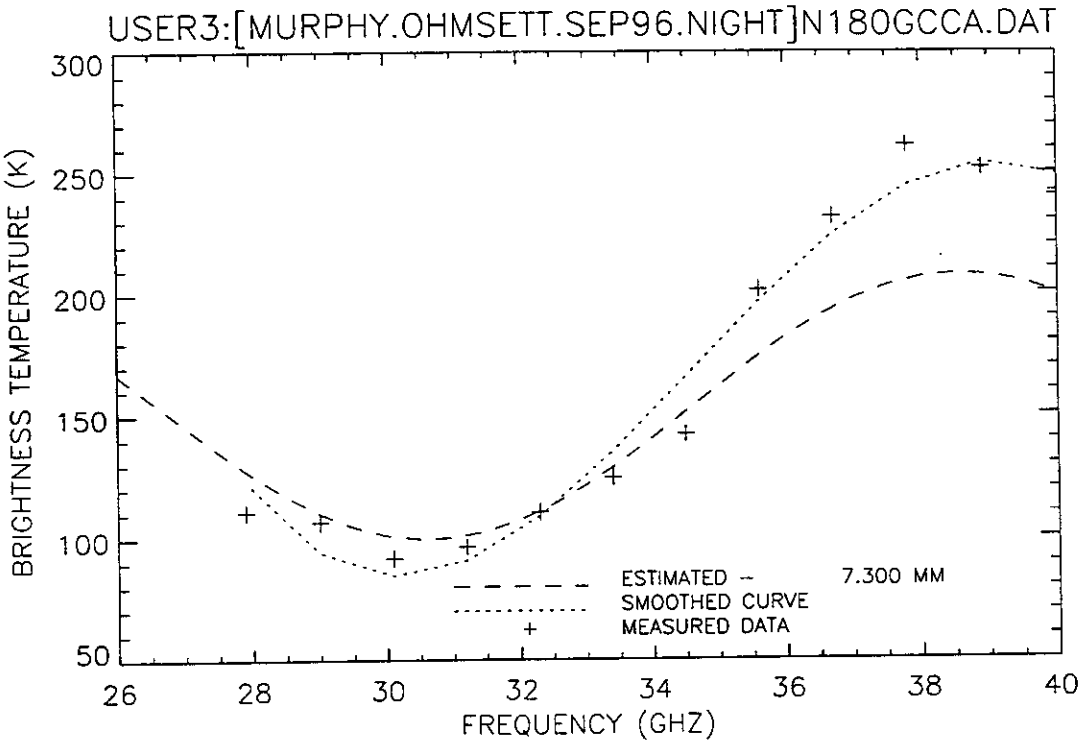

Figure 233. Plot of radiometric brightness temperature versus measurement frequency for 8-mm crude oil, night test, calm wave conditions, 12 September 1996, sweep G.

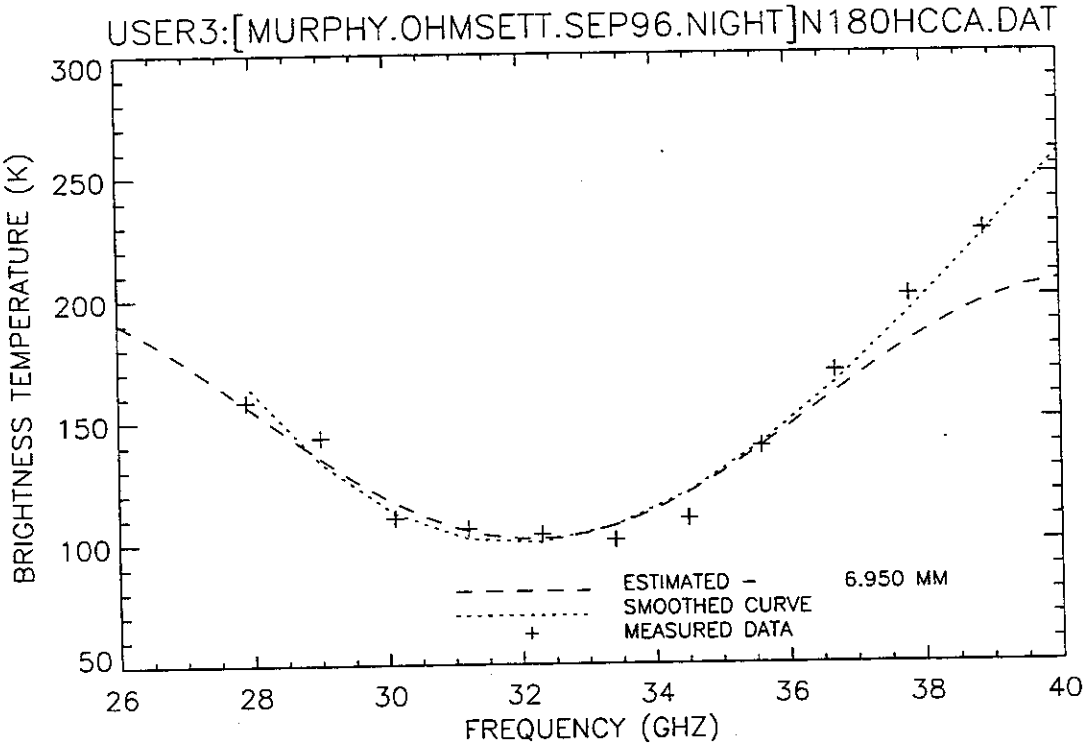

Figure 234. Plot of radiometric brightness temperature versus measurement frequency for 8-mm crude oil, night test, calm wave conditions, 12 September 1996, sweep H.

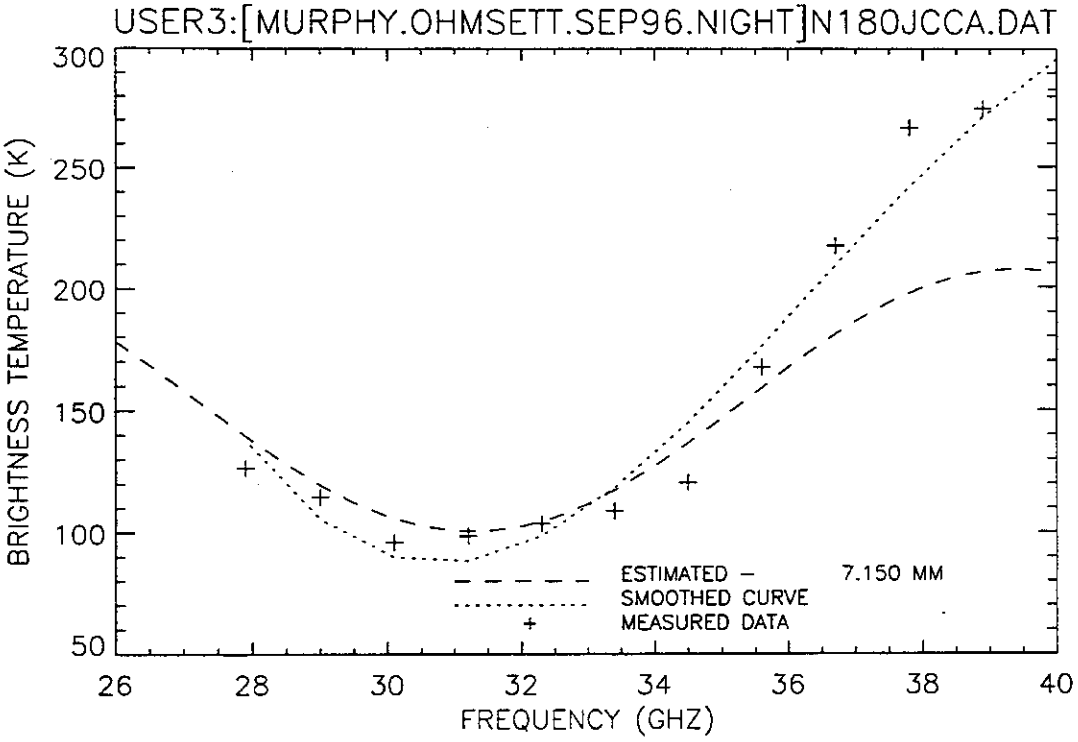

Figure 235. Plot of radiometric brightness temperature versus measurement frequency for 8-mm crude oil, night test, calm wave conditions, 12 September 1996, sweep J.

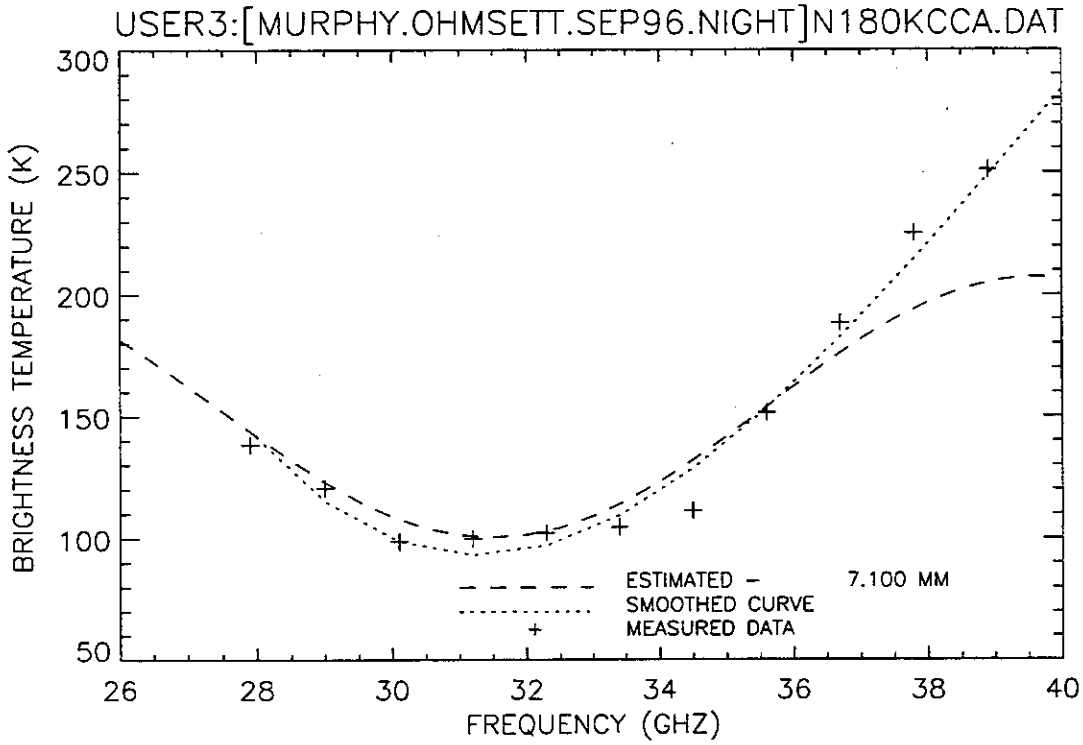

Figure 236. Plot of radiometric brightness temperature versus measurement frequency for 8-mm crude oil, night test, calm wave conditions, 12 September 1996, sweep K.

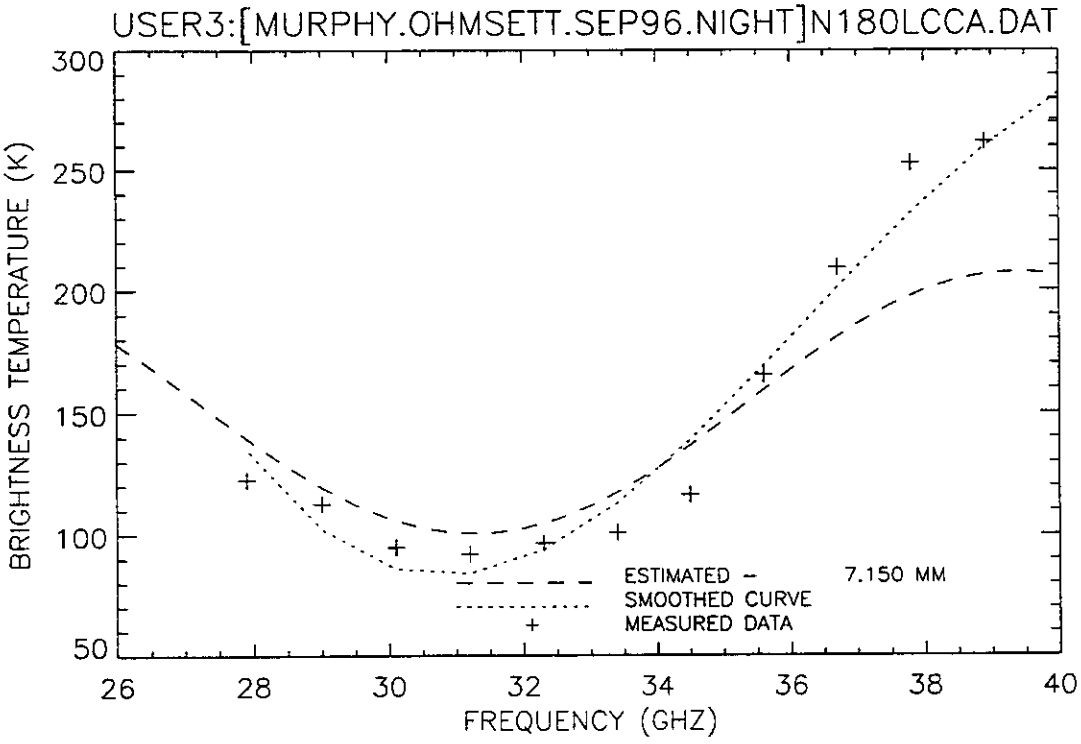

Figure 237. Plot of radiometric brightness temperature versus measurement frequency for 8-mm crude oil, night test, calm wave conditions, 12 September 1996, sweep L.

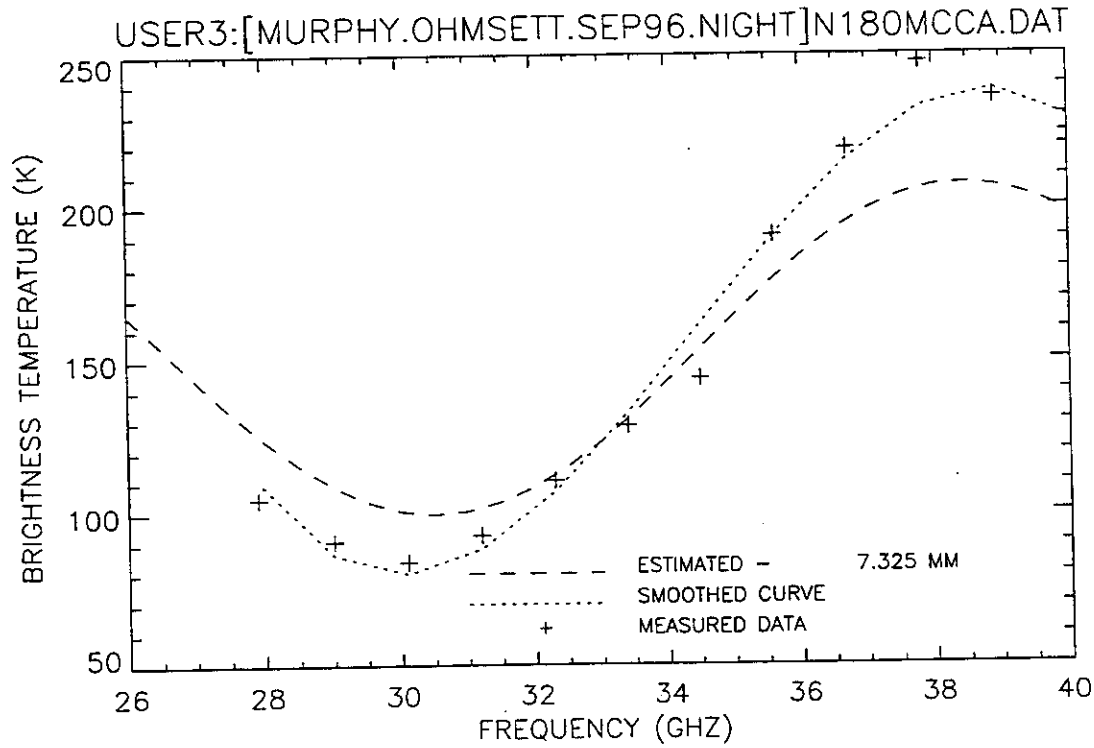

Figure 238. Plot of radiometric brightness temperature versus measurement frequency for 8-mm crude oil, night test, calm wave conditions, 12 September 1996, sweep M.

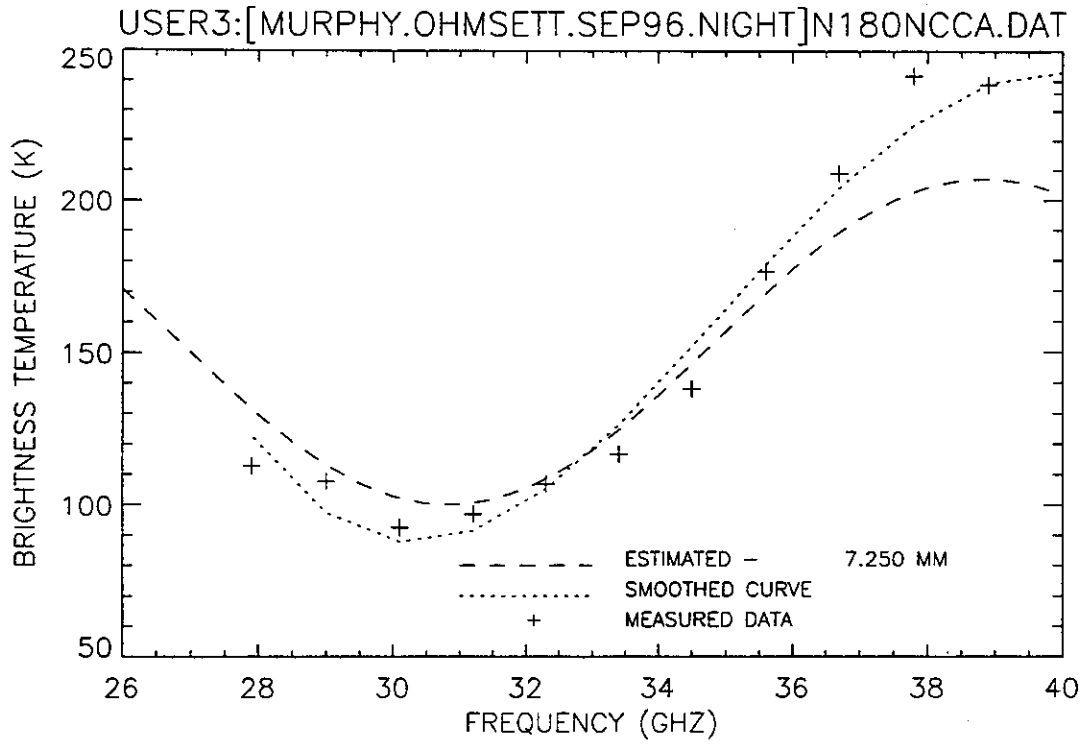

Figure 239. Plot of radiometric brightness temperature versus measurement frequency for 8-mm crude oil, night test, calm wave conditions, 12 September 1996, sweep N.

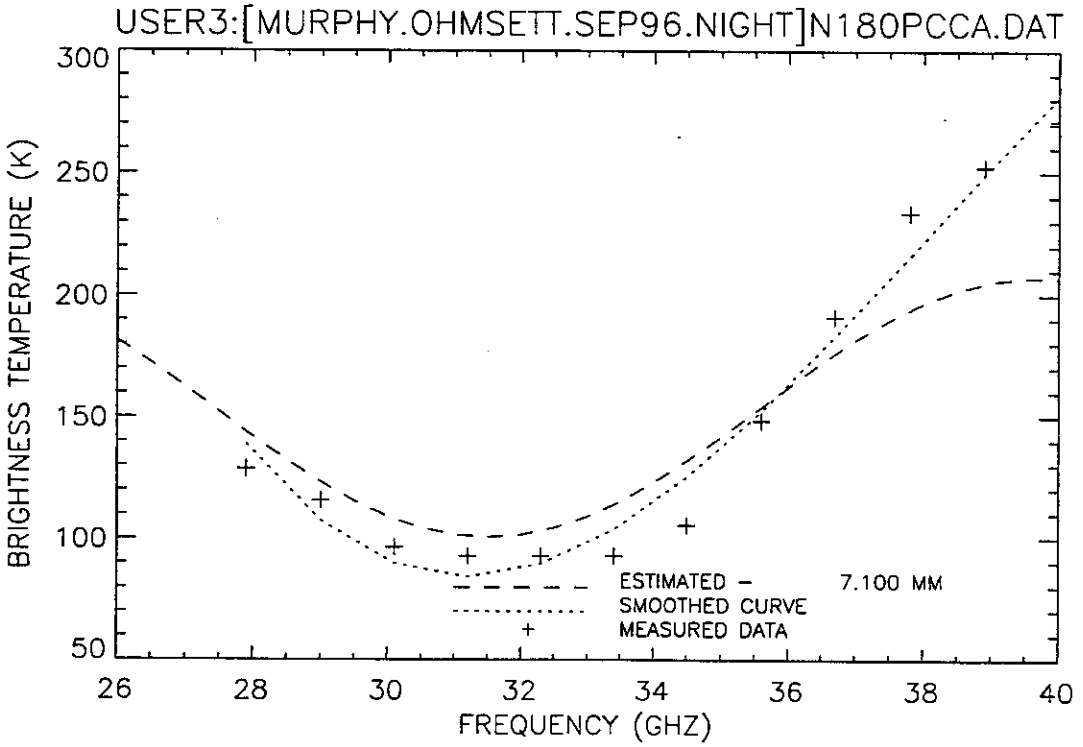

Figure 240. Plot of radiometric brightness temperature versus measurement frequency for 8-mm crude oil, night test, calm wave conditions, 12 September 1996, sweep P.

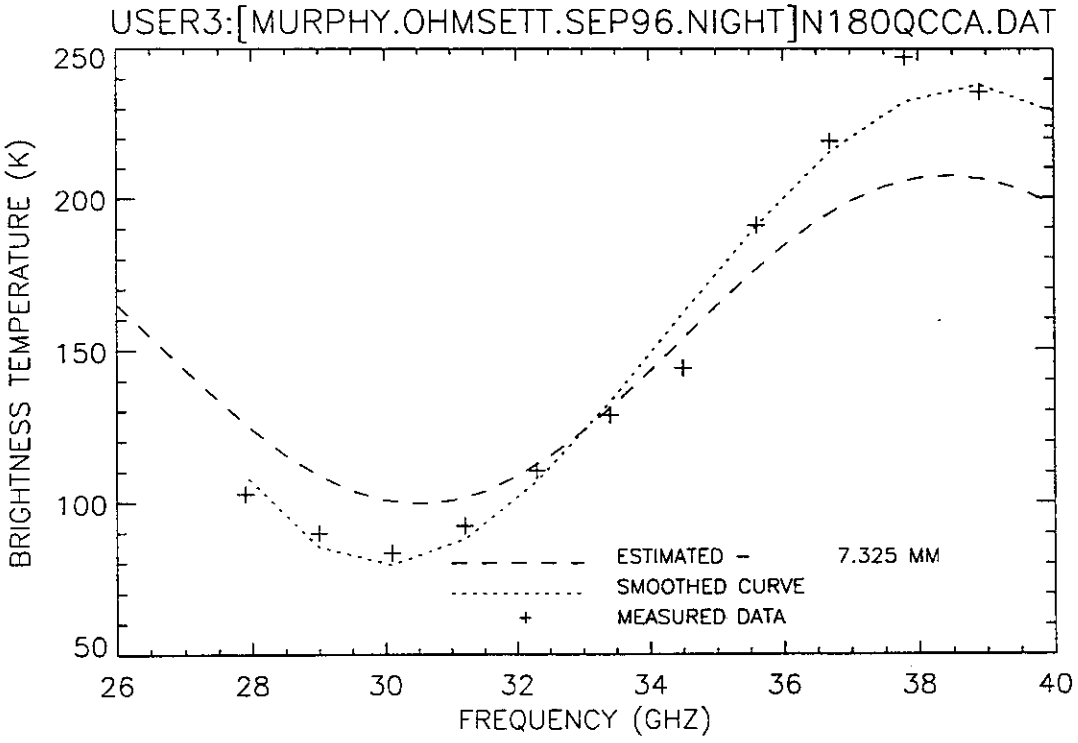

Figure 241. Plot of radiometric brightness temperature versus measurement frequency for 8-mm crude oil, night test, calm wave conditions, 12 September 1996, sweep Q.

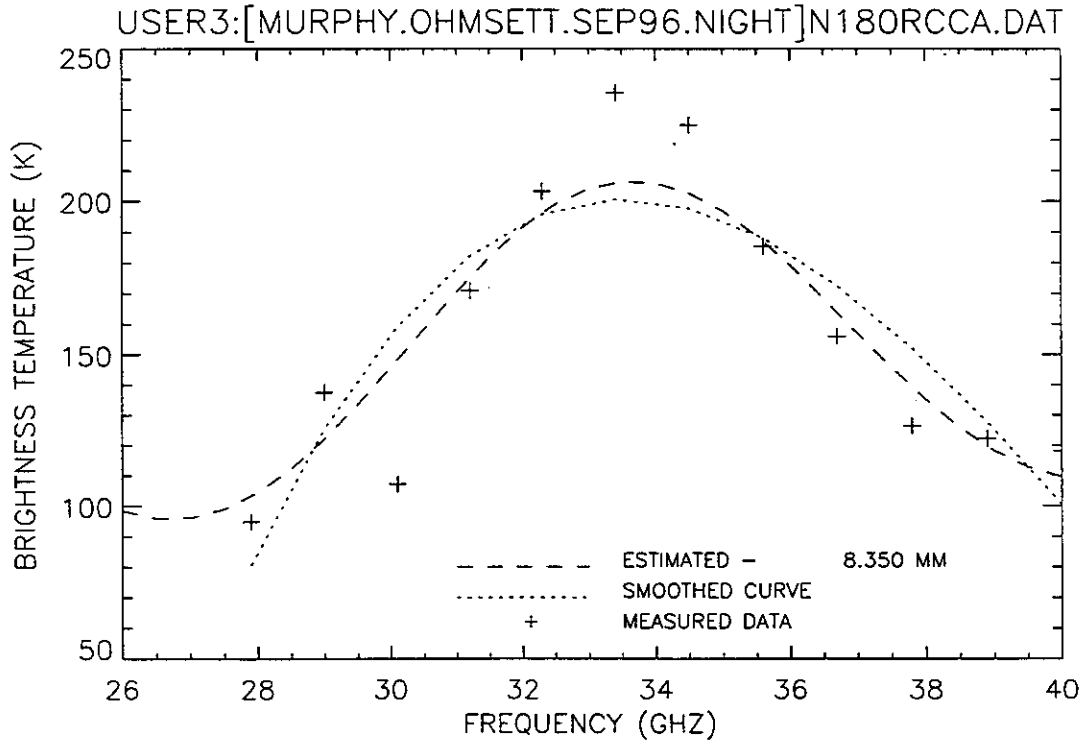

Figure 242. Plot of radiometric brightness temperature versus measurement frequency for 8-mm crude oil, night test, calm wave conditions, 12 September 1996, sweep R.

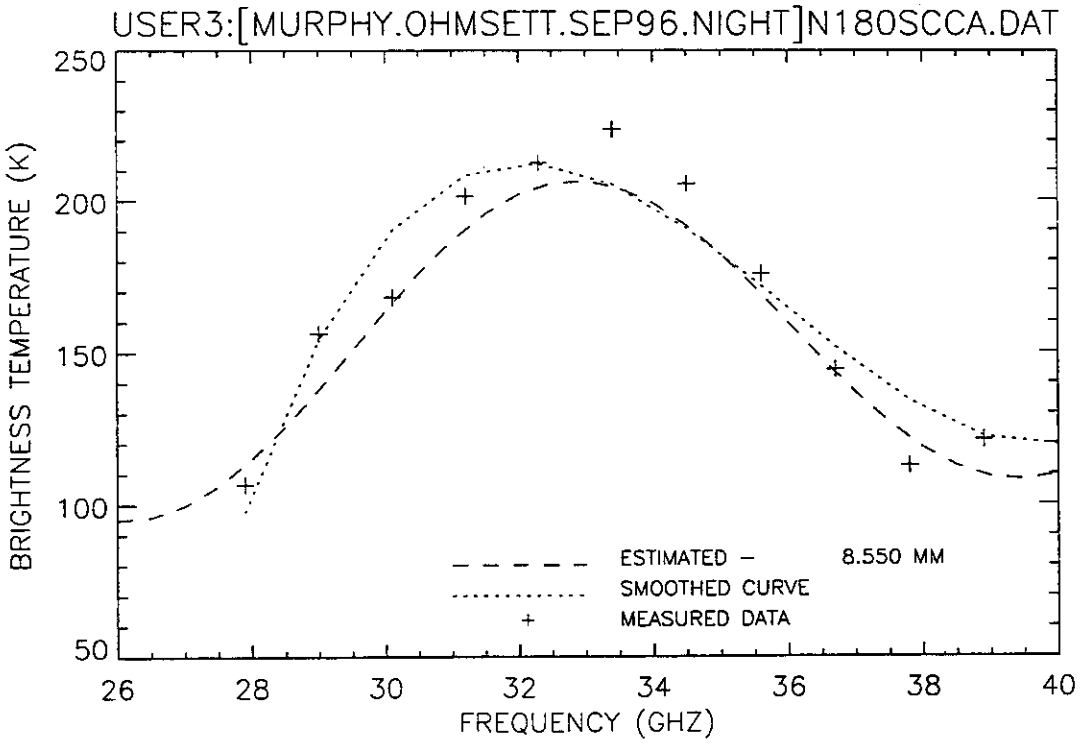

Figure 243. Plot of radiometric brightness temperature versus measurement frequency for 8-mm crude oil, night test, calm wave conditions, 12 September 1996, sweep S.

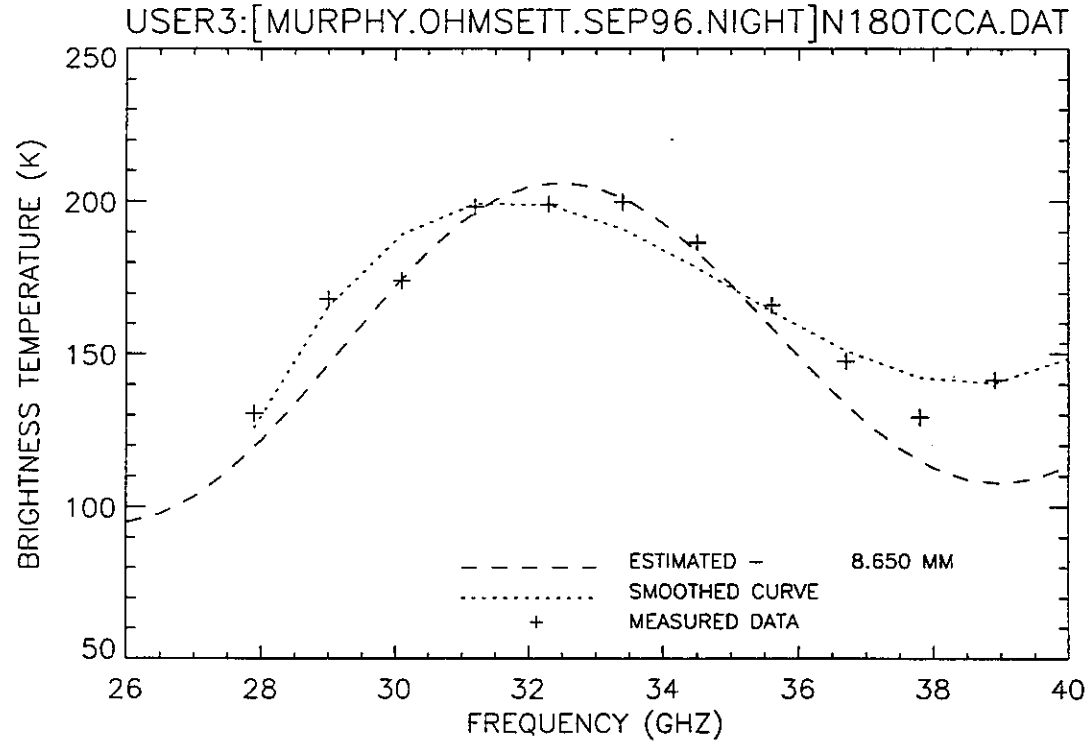

Figure 244. Plot of radiometric brightness temperature versus measurement frequency for 8-mm crude oil, night test, calm wave conditions, 12 September 1996, sweep T.

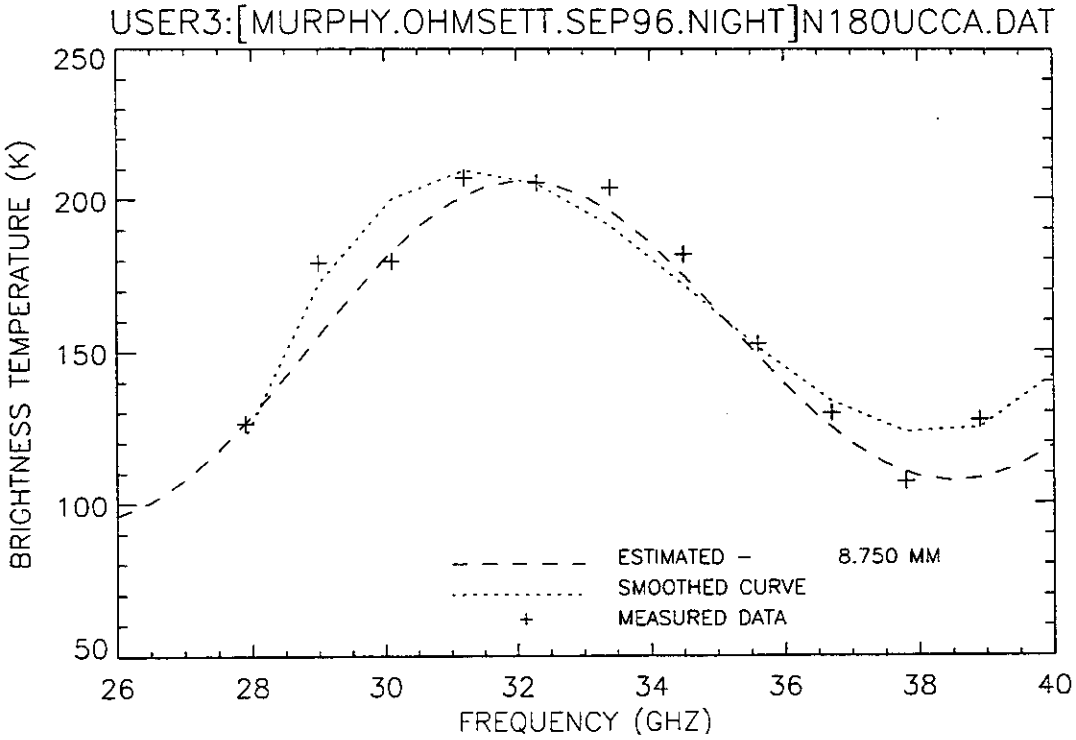

Figure 245. Plot of radiometric brightness temperature versus measurement frequency for 8-mm crude oil, night test, calm wave conditions, 12 September 1996, sweep U.

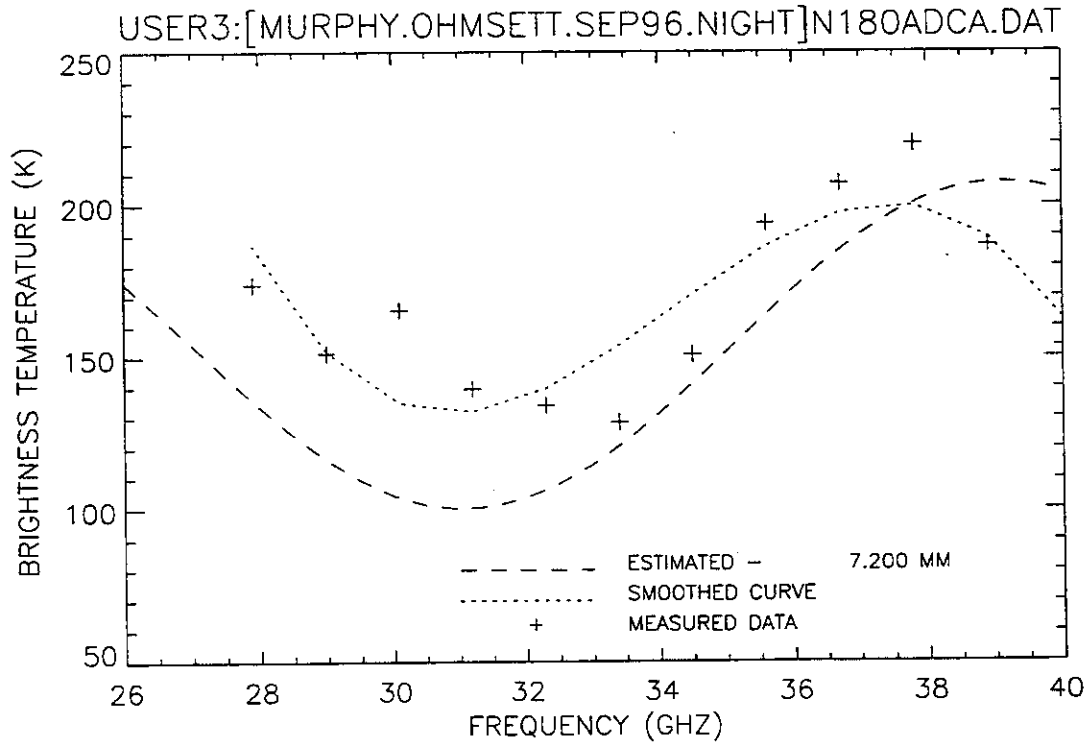

Figure 246. Plot of radiometric brightness temperature versus measurement frequency for 8-mm diesel oil, night test, calm wave conditions, 12 September 1996, sweep A.

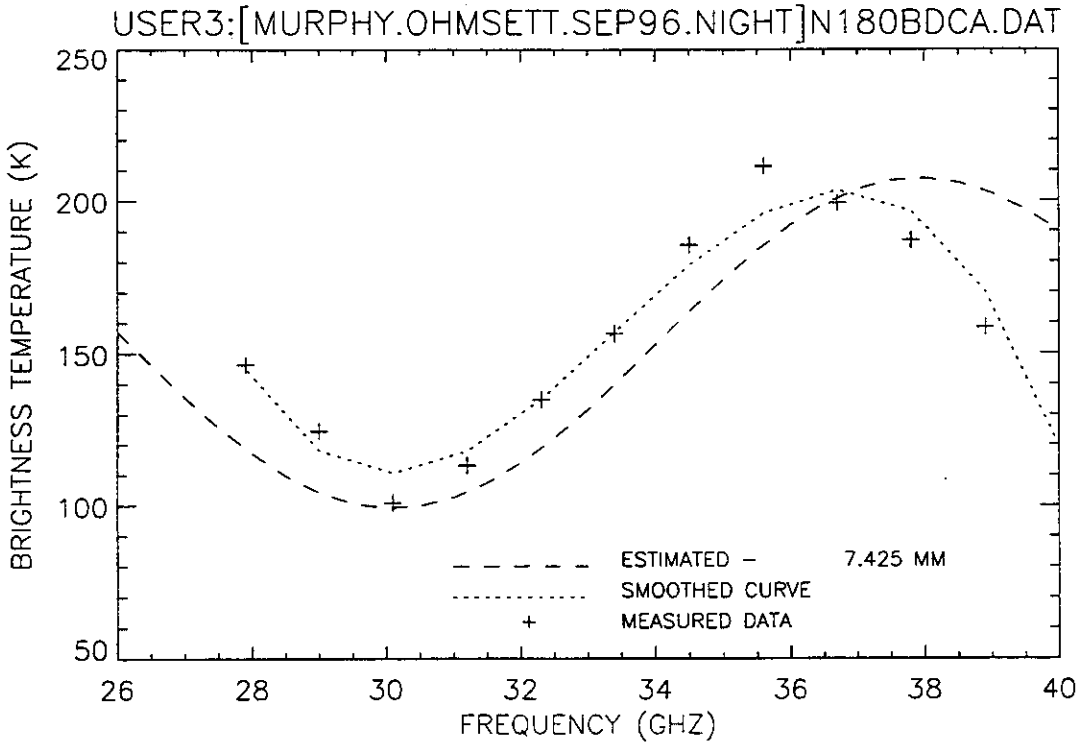

Figure 247. Plot of radiometric brightness temperature versus measurement frequency for 8-mm diesel oil, night test, calm wave conditions, 12 September 1996, sweep B.

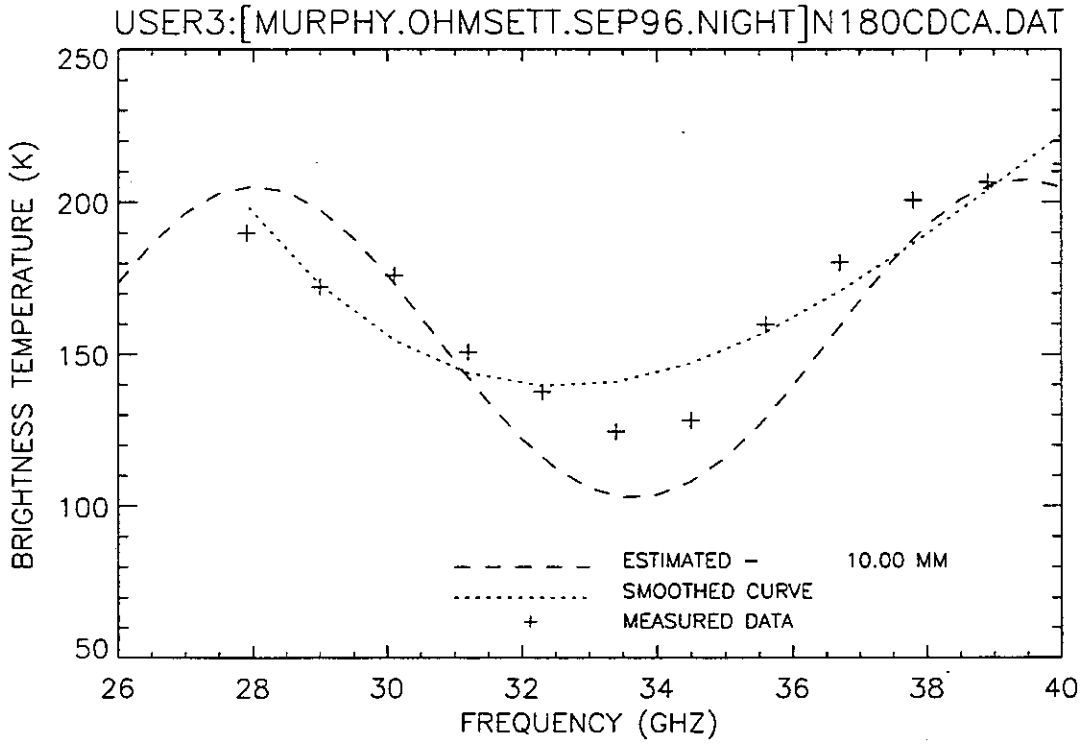

Figure 248. Plot of radiometric brightness temperature versus measurement frequency for 8-mm diesel oil, night test, calm wave conditions, 12 September 1996, sweep C.

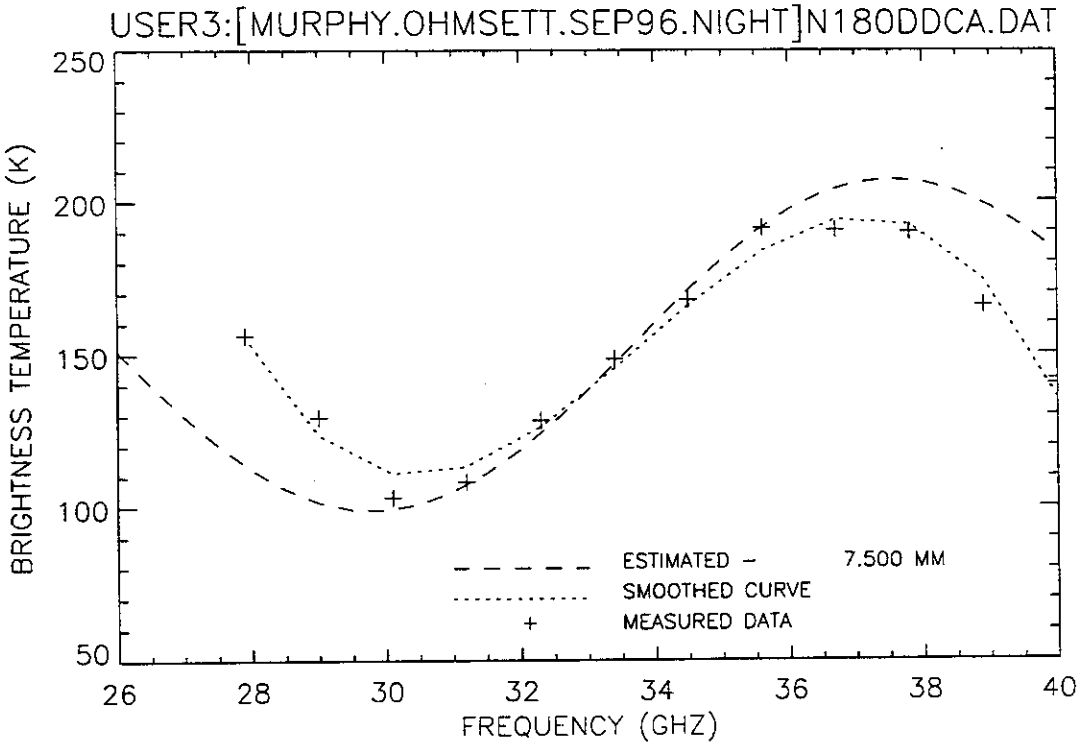

Figure 249. Plot of radiometric brightness temperature versus measurement frequency for 8-mm diesel oil, night test, calm wave conditions, 12 September 1996, sweep D.

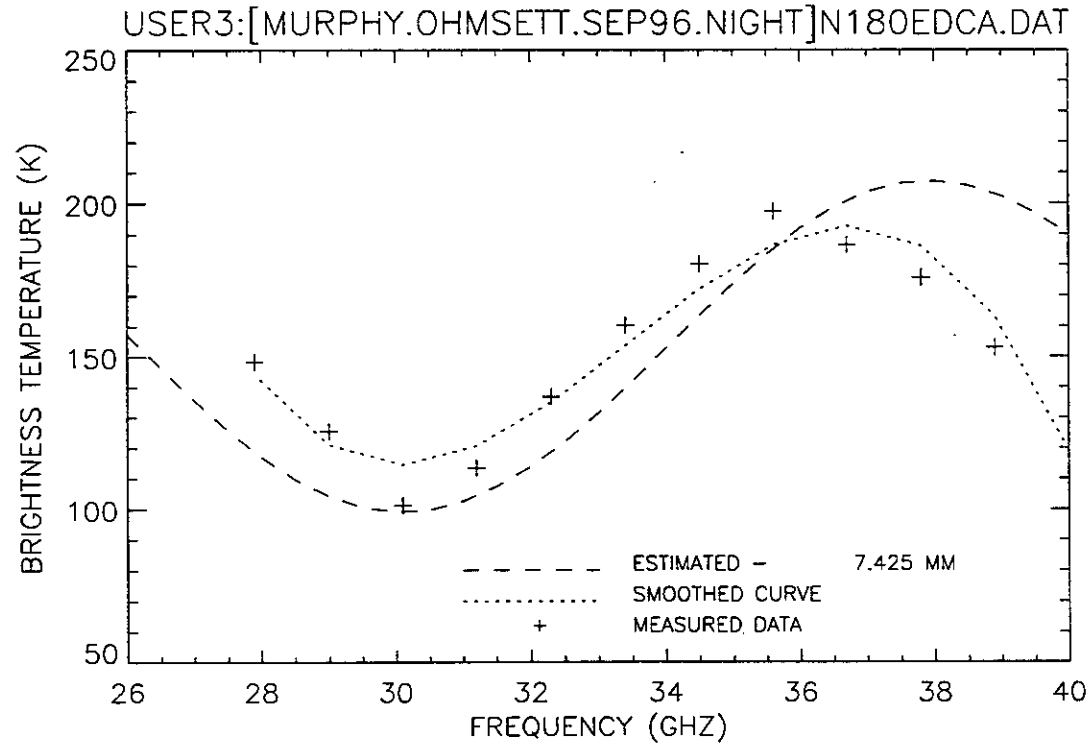

Figure 250. Plot of radiometric brightness temperature versus measurement frequency for 8-mm diesel oil, night test, calm wave conditions, 12 September 1996, sweep E.

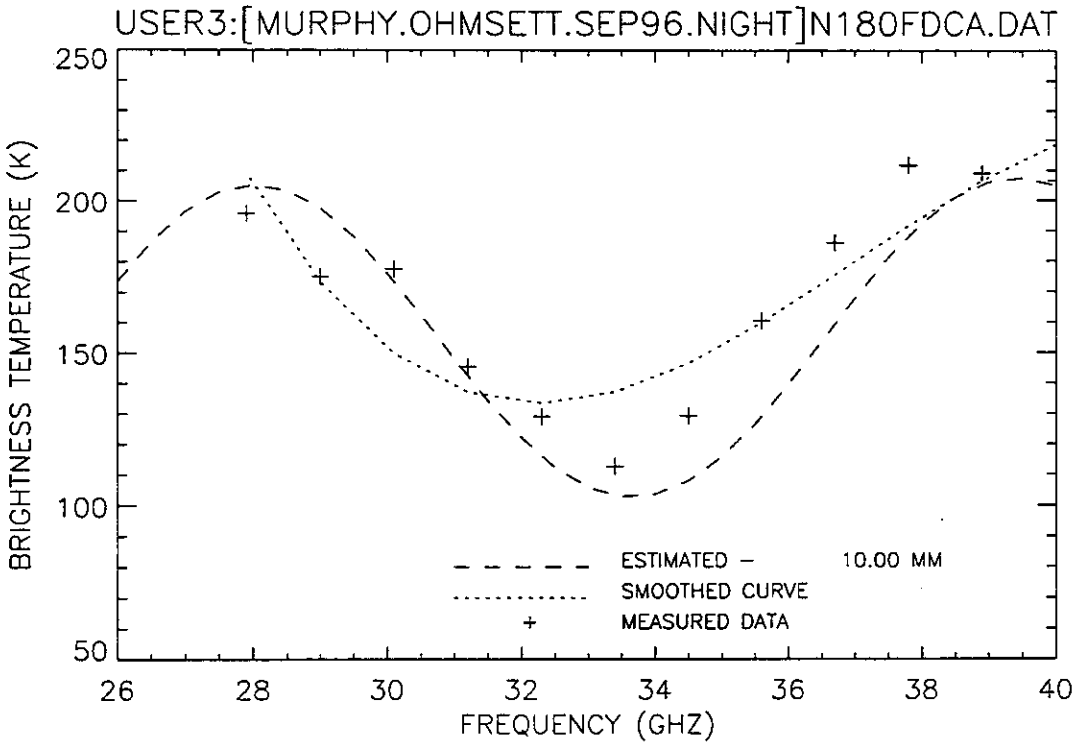

Figure 251. Plot of radiometric brightness temperature versus measurement frequency for 8-mm diesel oil, night test, calm wave conditions, 12 September 1996, sweep F.

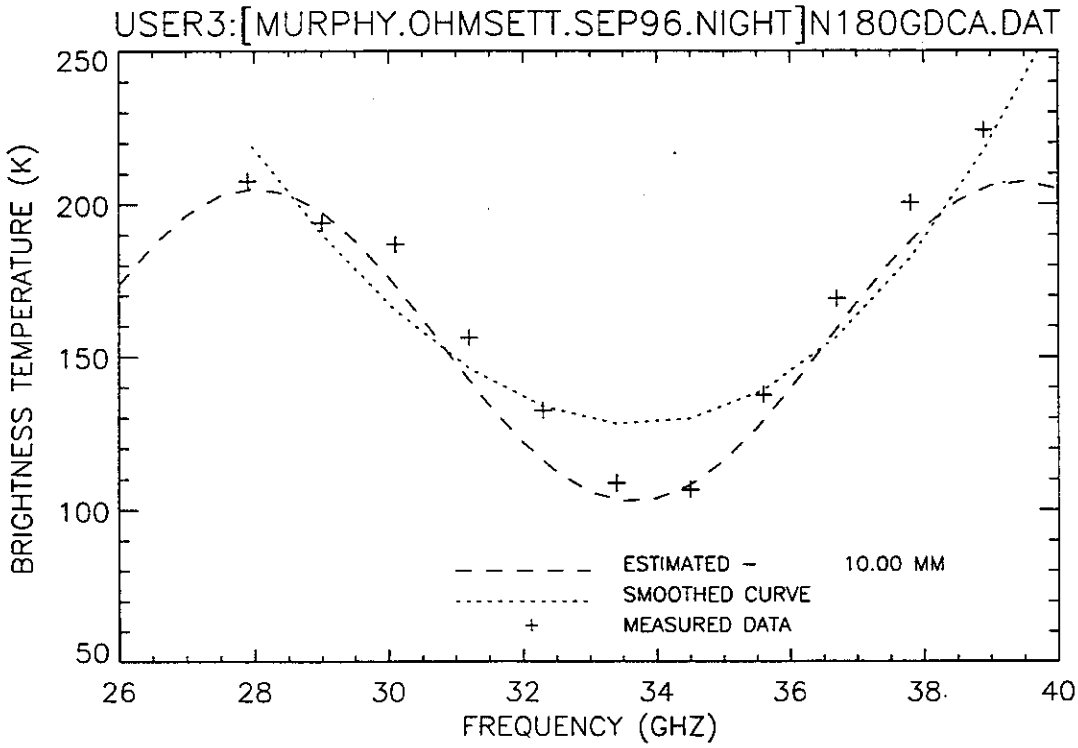

Figure 252. Plot of radiometric brightness temperature versus measurement frequency for 8-mm diesel oil, night test, calm wave conditions, 12 September 1996, sweep G.

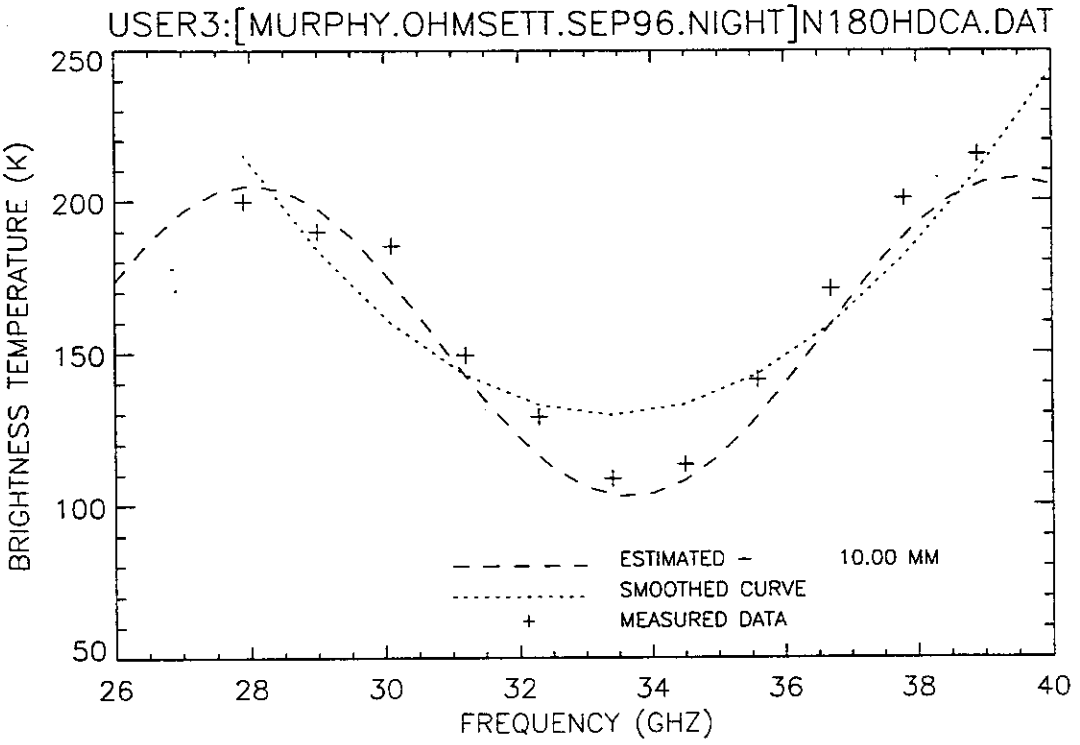

Figure 253. Plot of radiometric brightness temperature versus measurement frequency for 8-mm diesel oil, night test, calm wave conditions, 12 September 1996, sweep H.

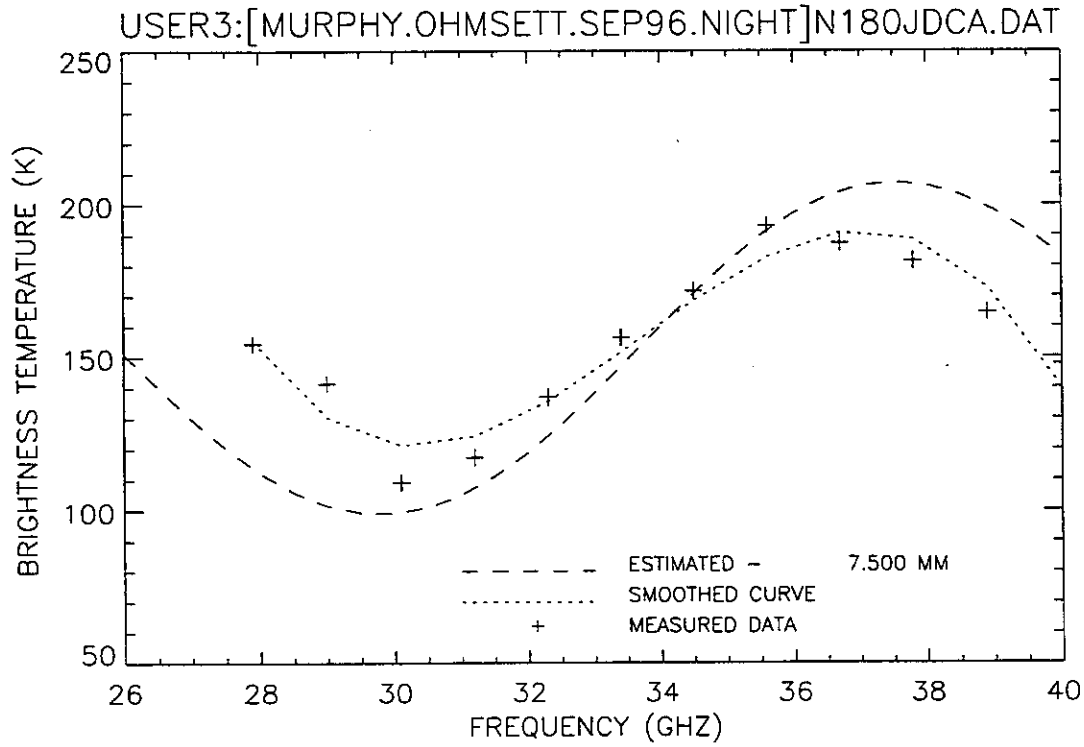

Figure 254. Plot of radiometric brightness temperature versus measurement frequency for 8-mm diesel oil, night test, calm wave conditions, 12 September 1996, sweep J.

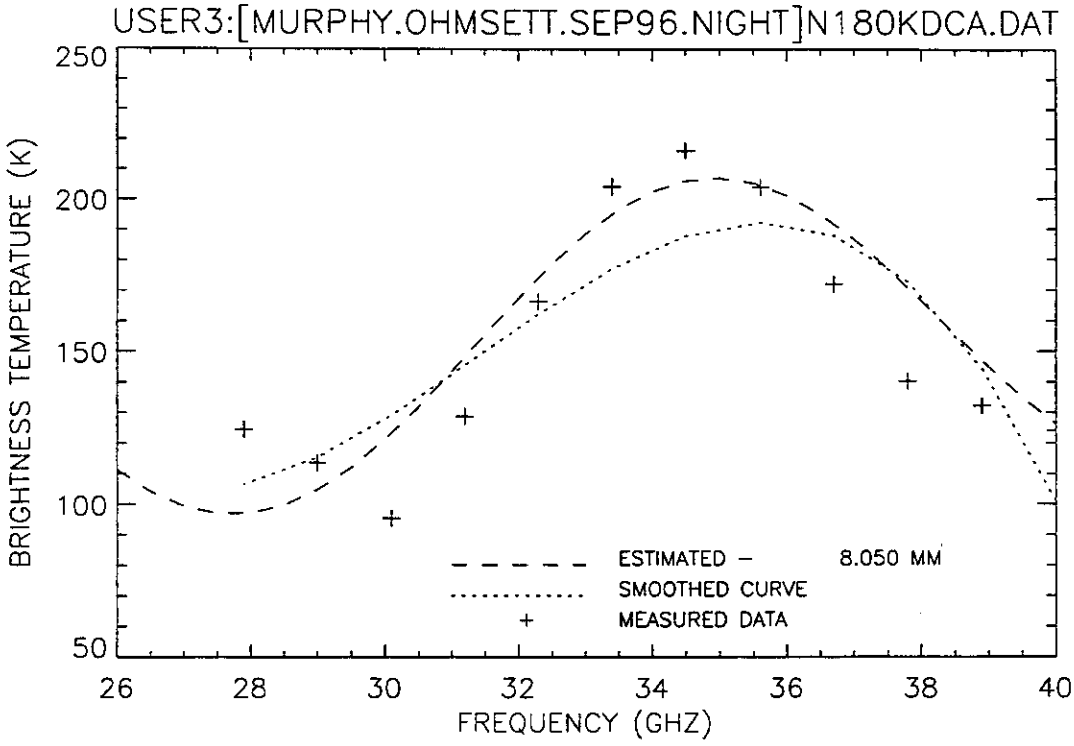

Figure 255. Plot of radiometric brightness temperature versus measurement frequency for 8-mm diesel oil, night test, calm wave conditions, 12 September 1996, sweep K.

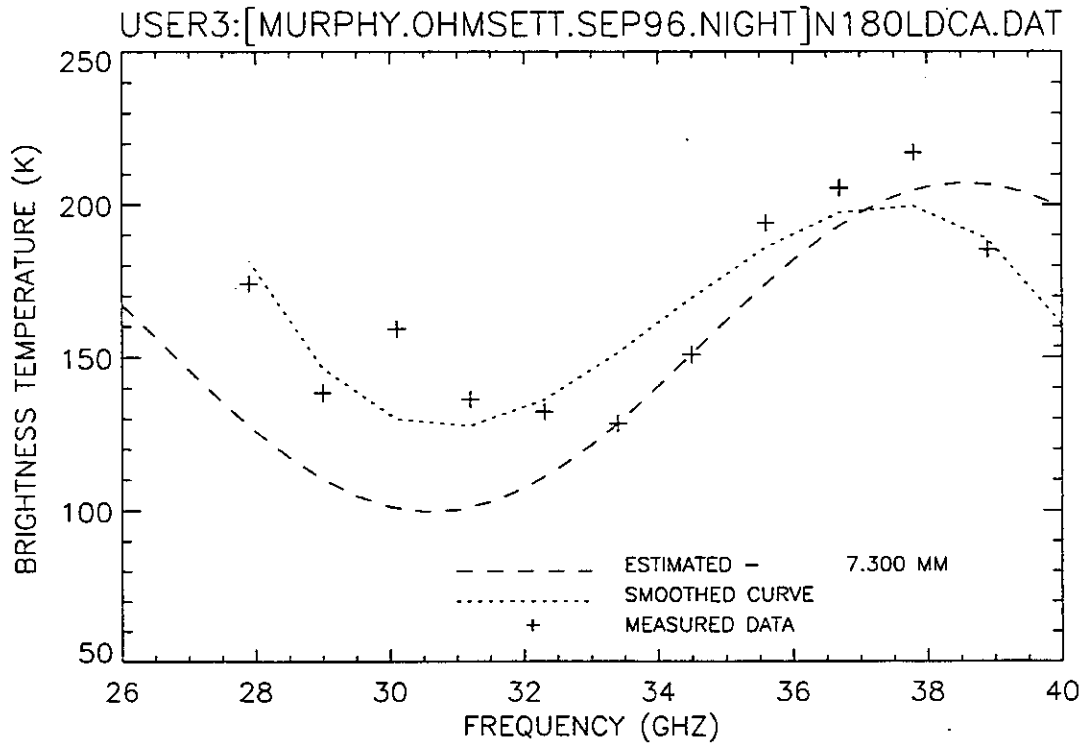

Figure 256. Plot of radiometric brightness temperature versus measurement frequency for 8-mm diesel oil, night test, calm wave conditions, 12 September 1996, sweep L.

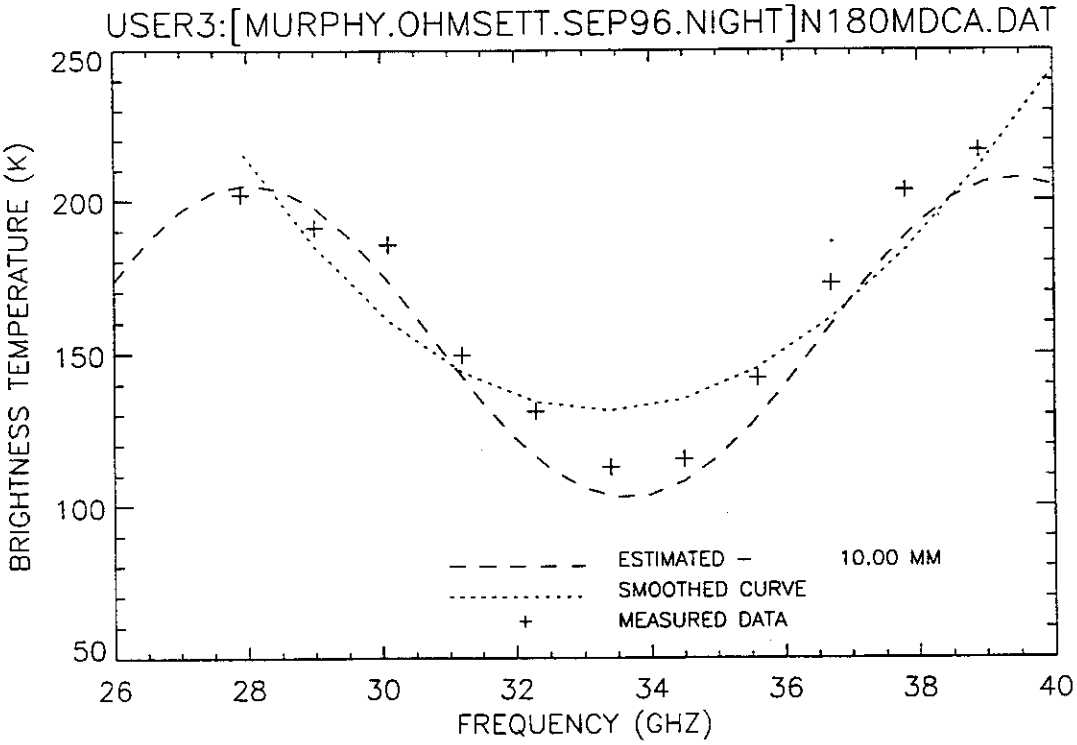

Figure 257. Plot of radiometric brightness temperature versus measurement frequency for 8-mm diesel oil, night test, calm wave conditions, 12 September 1996, sweep M.

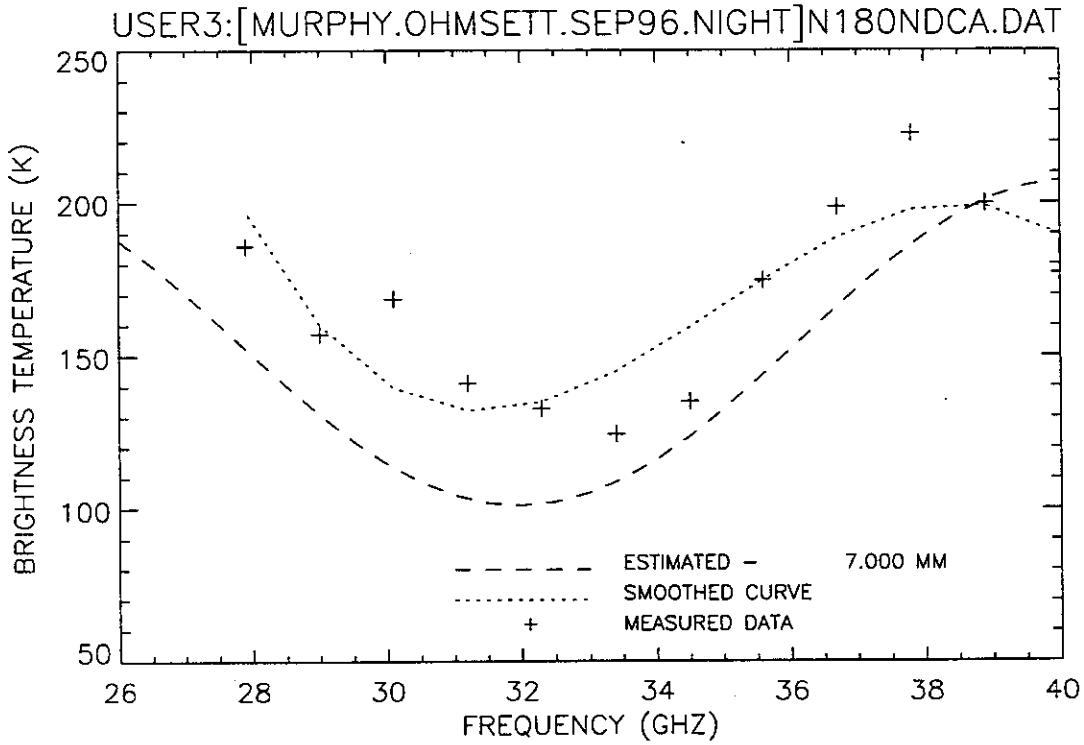

Figure 258. Plot of radiometric brightness temperature versus measurement frequency for 8-mm diesel oil, night test, calm wave conditions, 12 September 1996, sweep N.

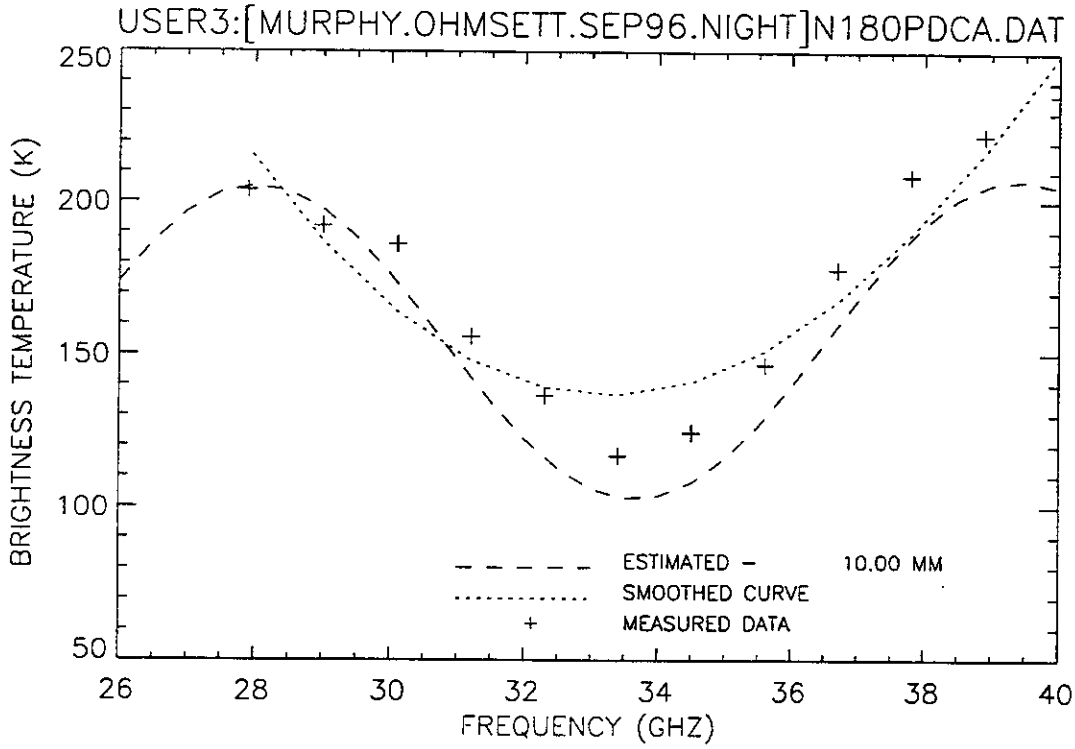

Figure 259. Plot of radiometric brightness temperature versus measurement frequency for 8-mm diesel oil, night test, calm wave conditions, 12 September 1996, sweep P.

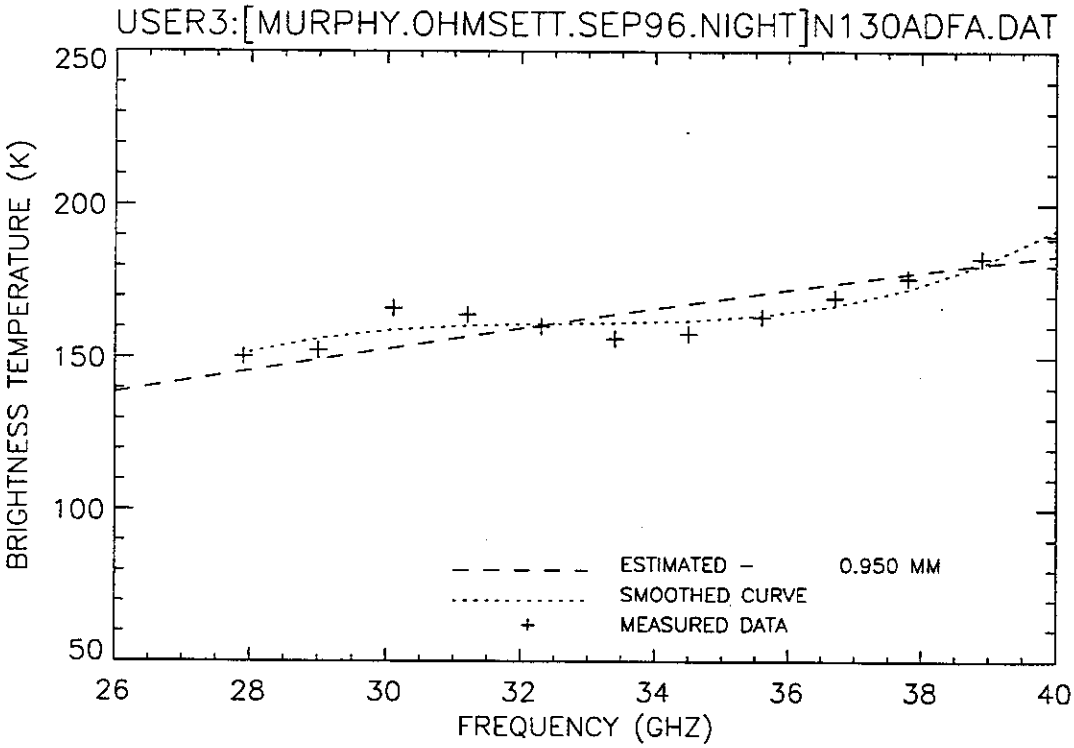

Figure 260. Plot of radiometric brightness temperature versus measurement frequency for 3-mm diesel oil, night test, fans on, calm wave conditions, 12 September 1996, sweep A.

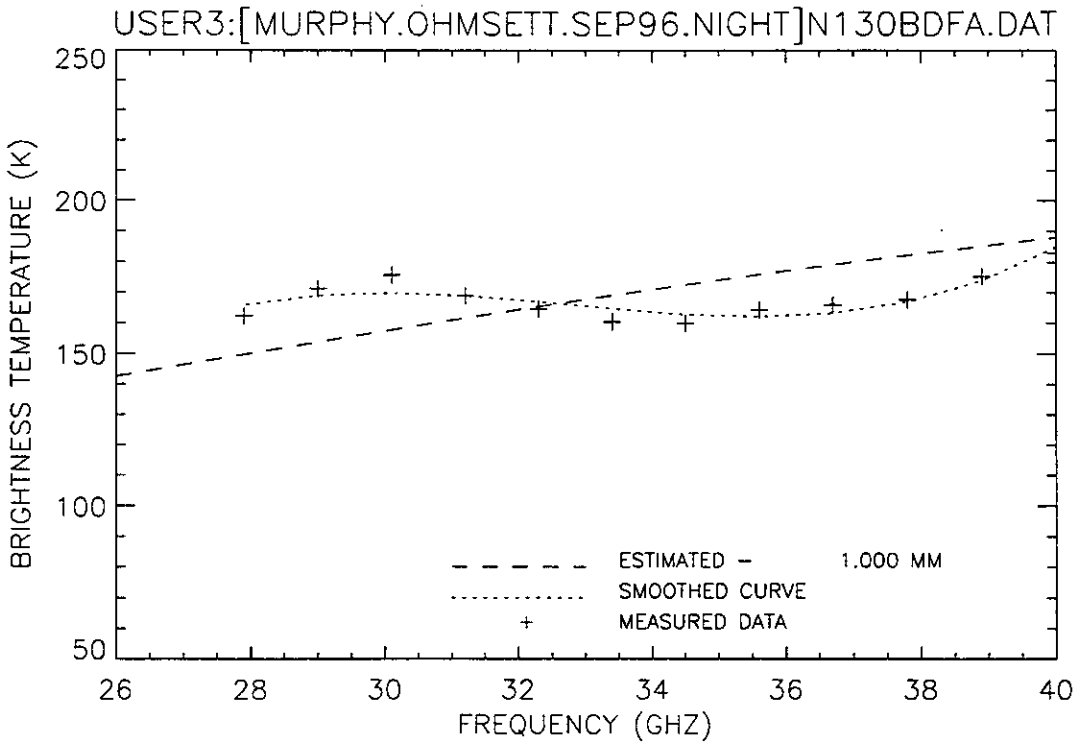

Figure 261. Plot of radiometric brightness temperature versus measurement frequency for 3-mm diesel oil, night test, fans on, calm wave conditions, 12 September 1996, sweep B.

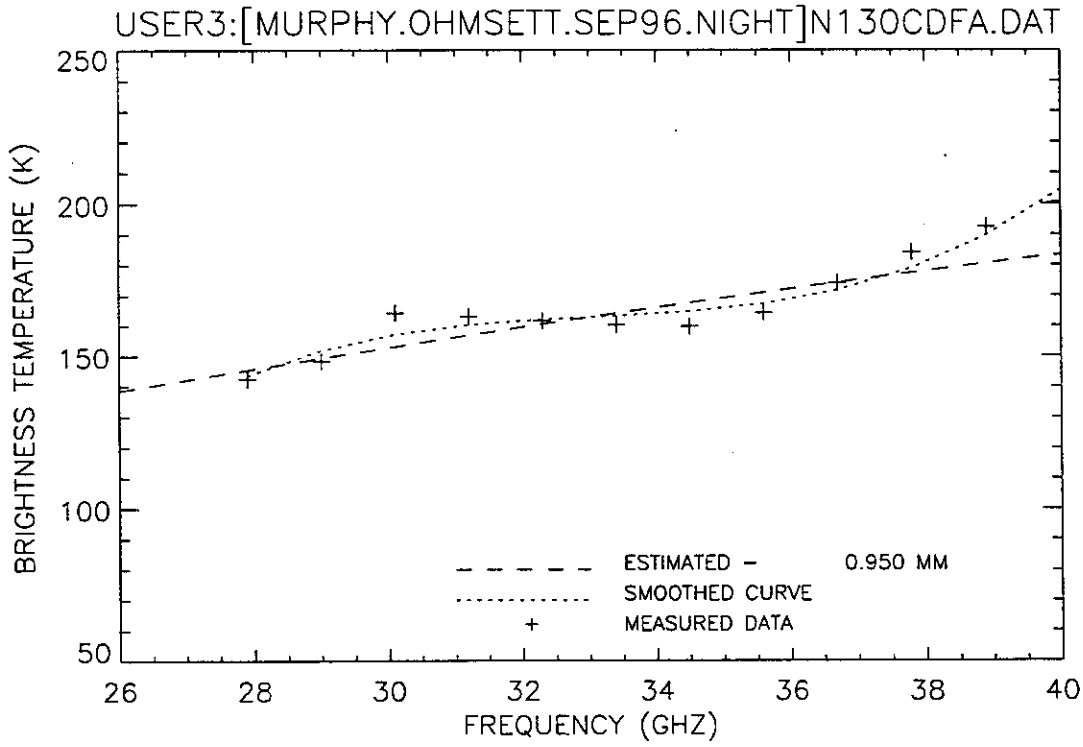

Figure 262. Plot of radiometric brightness temperature versus measurement frequency for 3-mm diesel oil, night test, fans on, calm wave conditions, 12 September 1996, sweep C.

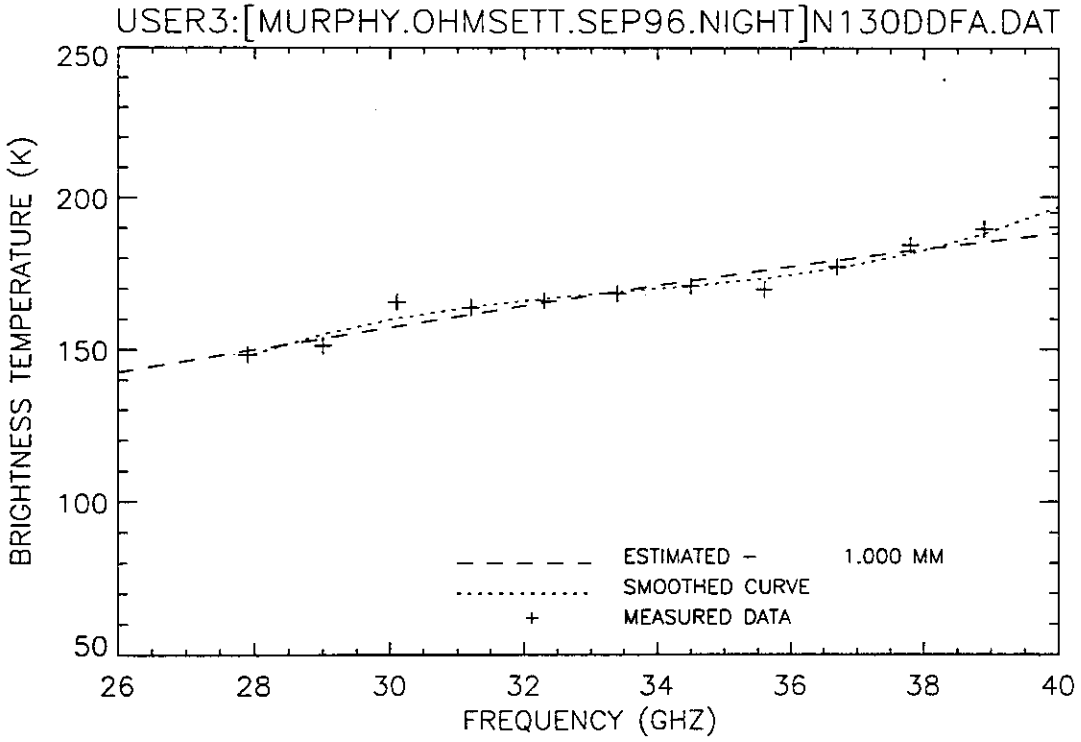

Figure 263. Plot of radiometric brightness temperature versus measurement frequency for 3-mm diesel oil, night test, fans on, calm wave conditions, 12 September 1996, sweep D.

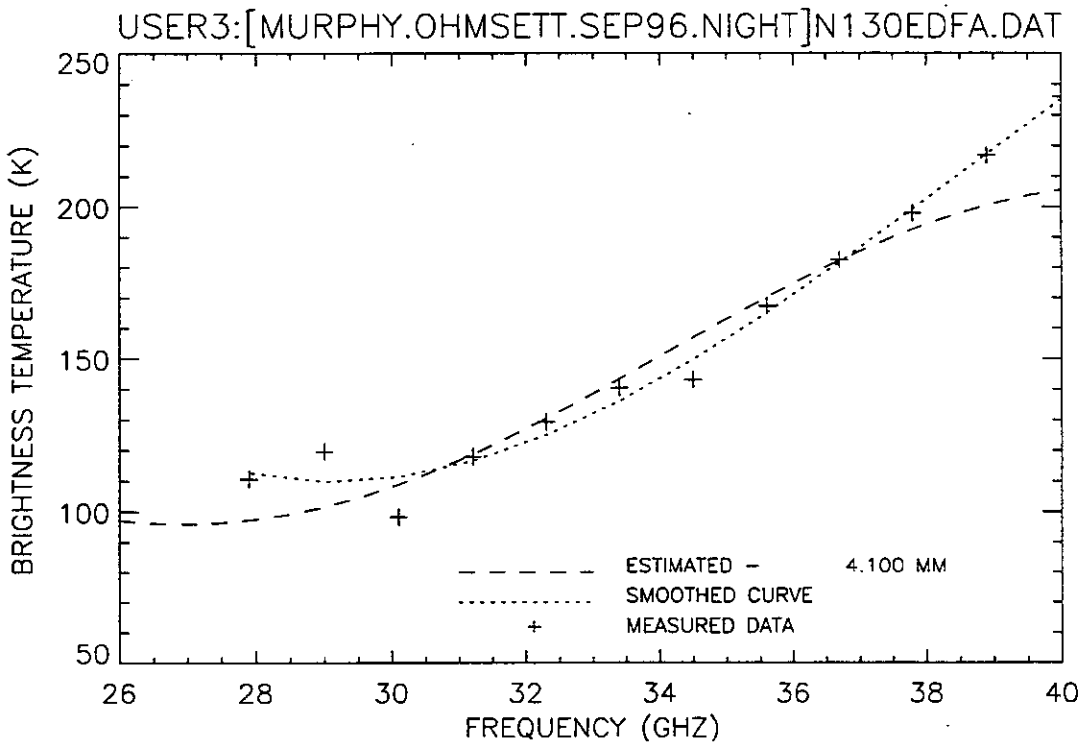

Figure 264. Plot of radiometric brightness temperature versus measurement frequency for 3-mm diesel oil, night test, fans on, calm wave conditions, 12 September 1996, sweep E.

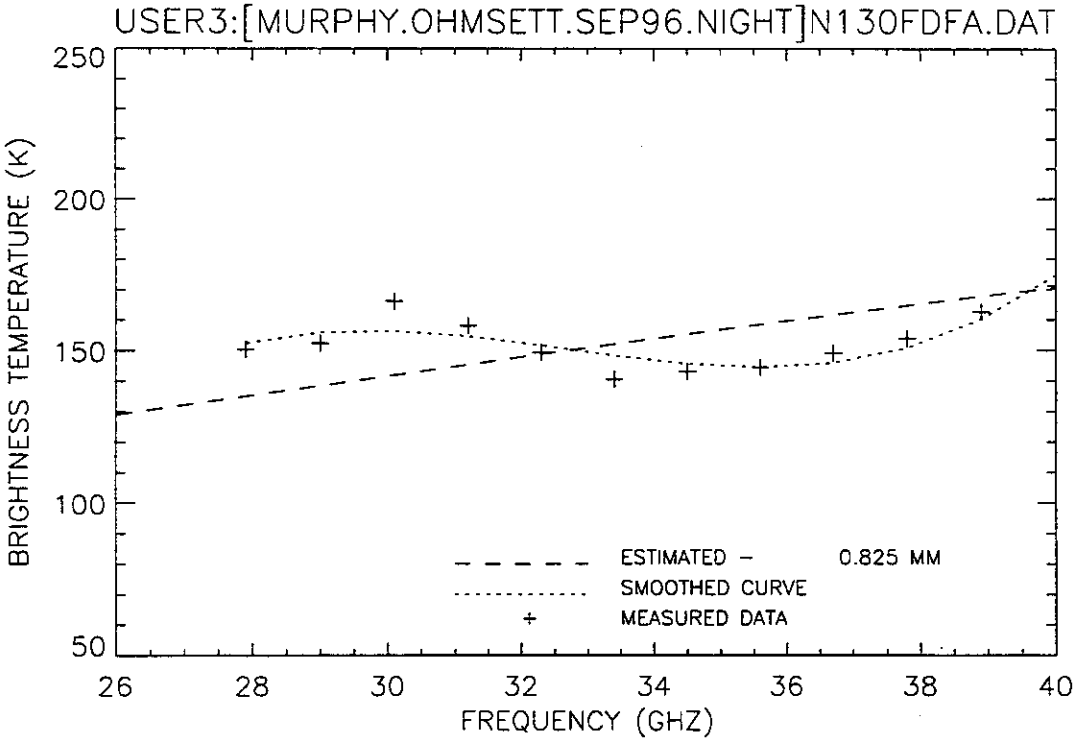

Figure 265. Plot of radiometric brightness temperature versus measurement frequency for 3-mm diesel oil, night test, fans on, calm wave conditions, 12 September 1996, sweep F.

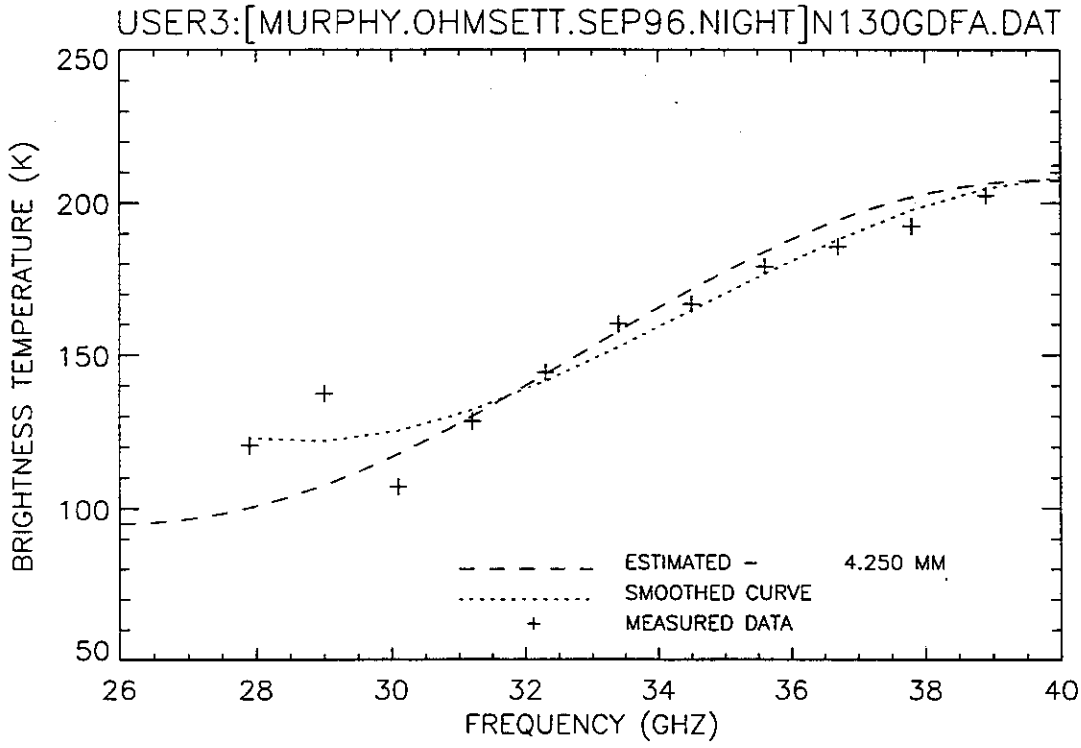

Figure 266. Plot of radiometric brightness temperature versus measurement frequency for 3-mm diesel oil, night test, fans on, calm wave conditions, 12 September 1996, sweep G.

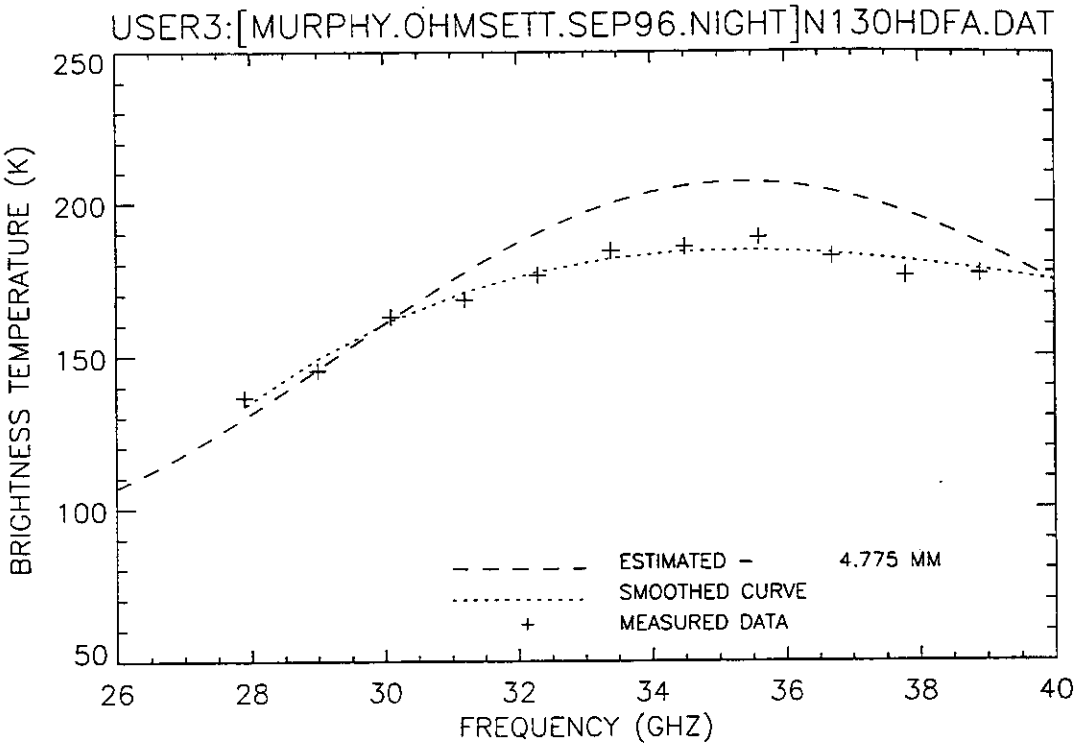

Figure 267. Plot of radiometric brightness temperature versus measurement frequency for 3-mm diesel oil, night test, fans on, calm wave conditions, 12 September 1996, sweep H.

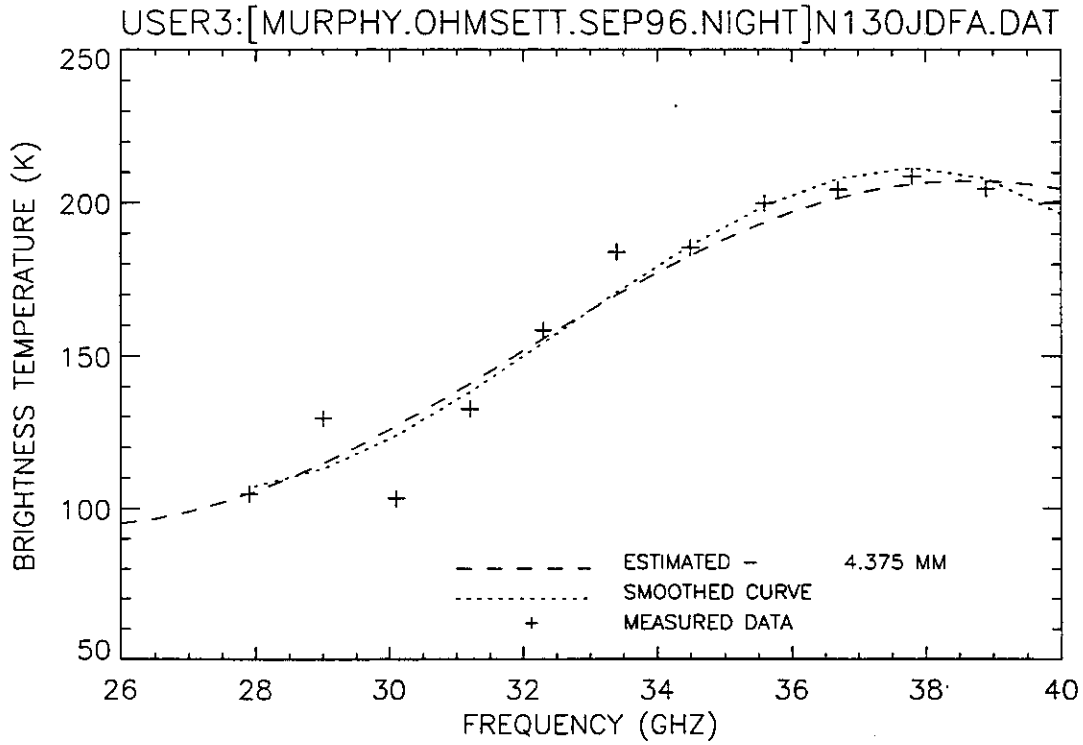

Figure 268. Plot of radiometric brightness temperature versus measurement frequency for 3-mm diesel oil, night test, fans on, calm wave conditions, 12 September 1996, sweep J.

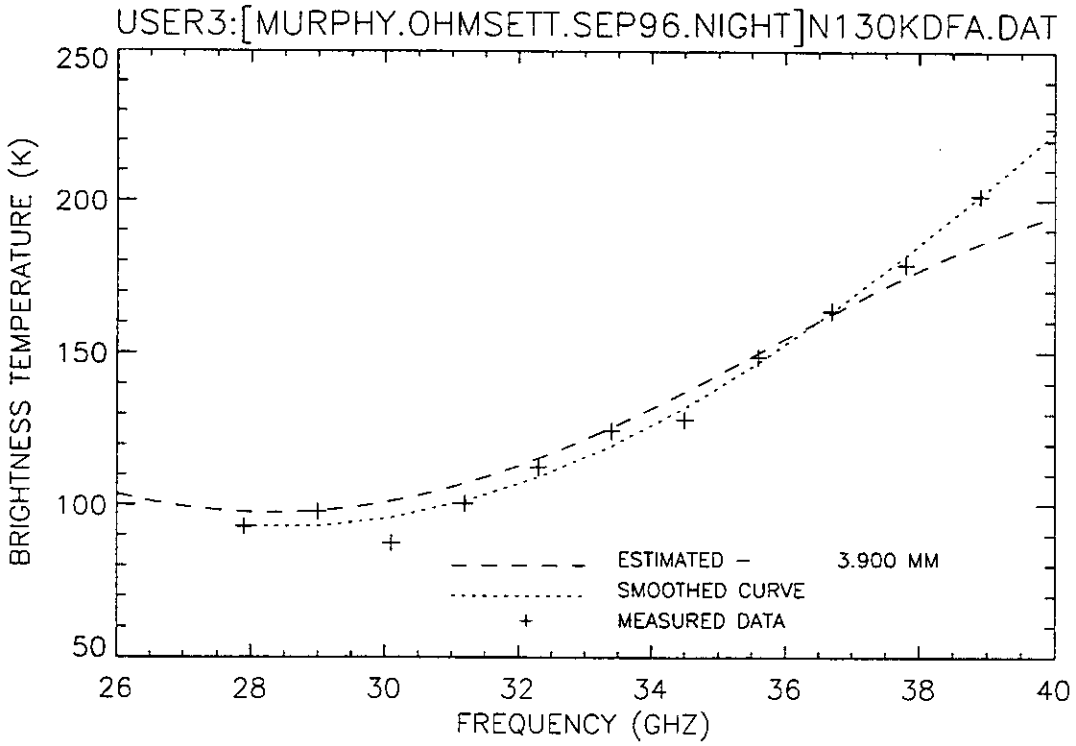

Figure 269. Plot of radiometric brightness temperature versus measurement frequency for 3-mm diesel oil, night test, fans on, calm wave conditions, 12 September 1996, sweep K.

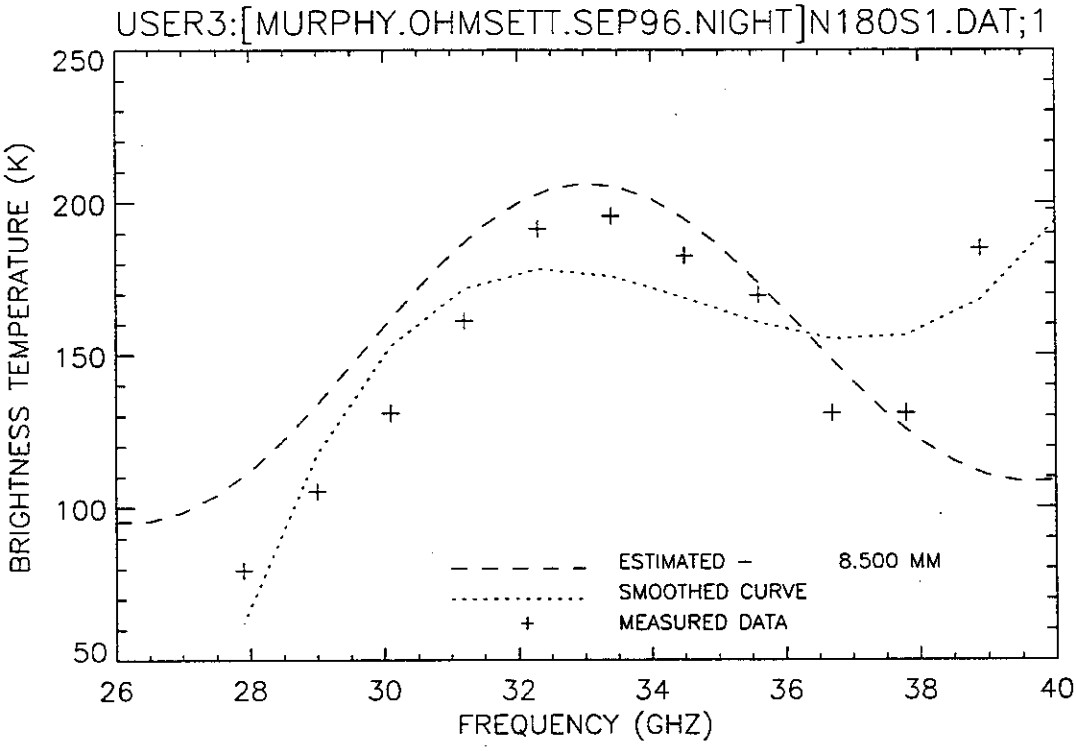

Figure 270. Plot of radiometric brightness temperature versus measurement frequency for 8-mm diesel oil, night test, fans on, calm wave conditions, 12 September 1996, sweep 1.

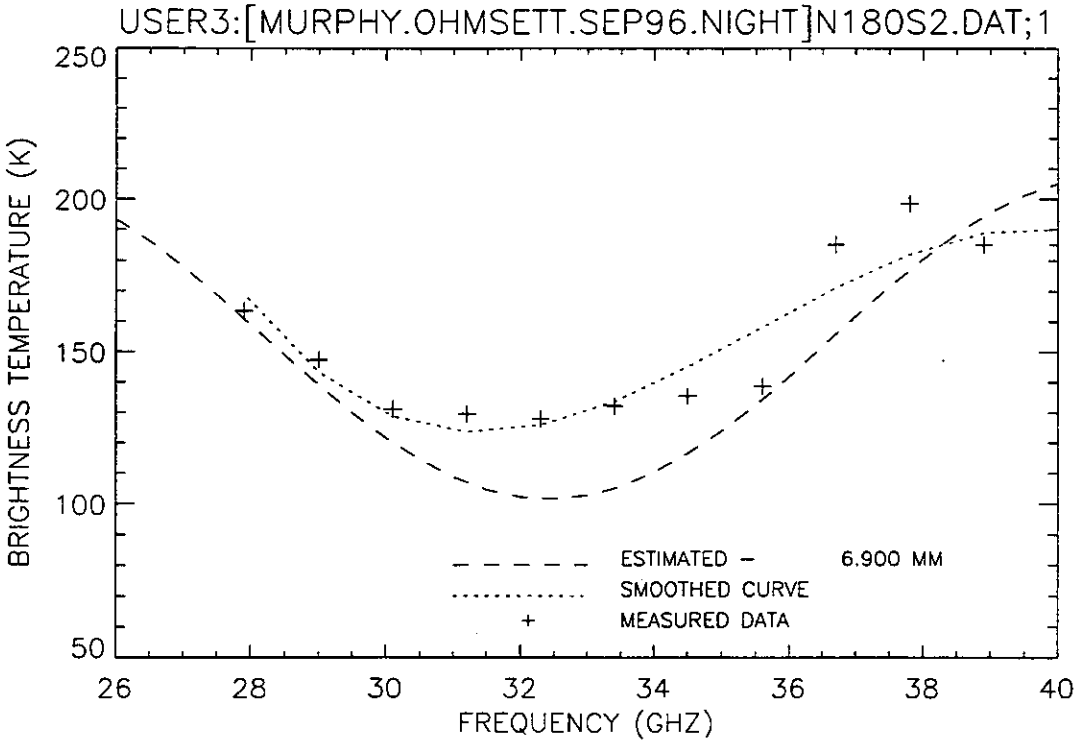

Figure 271. Plot of radiometric brightness temperature versus measurement frequency for 8-mm diesel oil, night test, fans on, calm wave conditions, 12 September 1996, sweep 2.

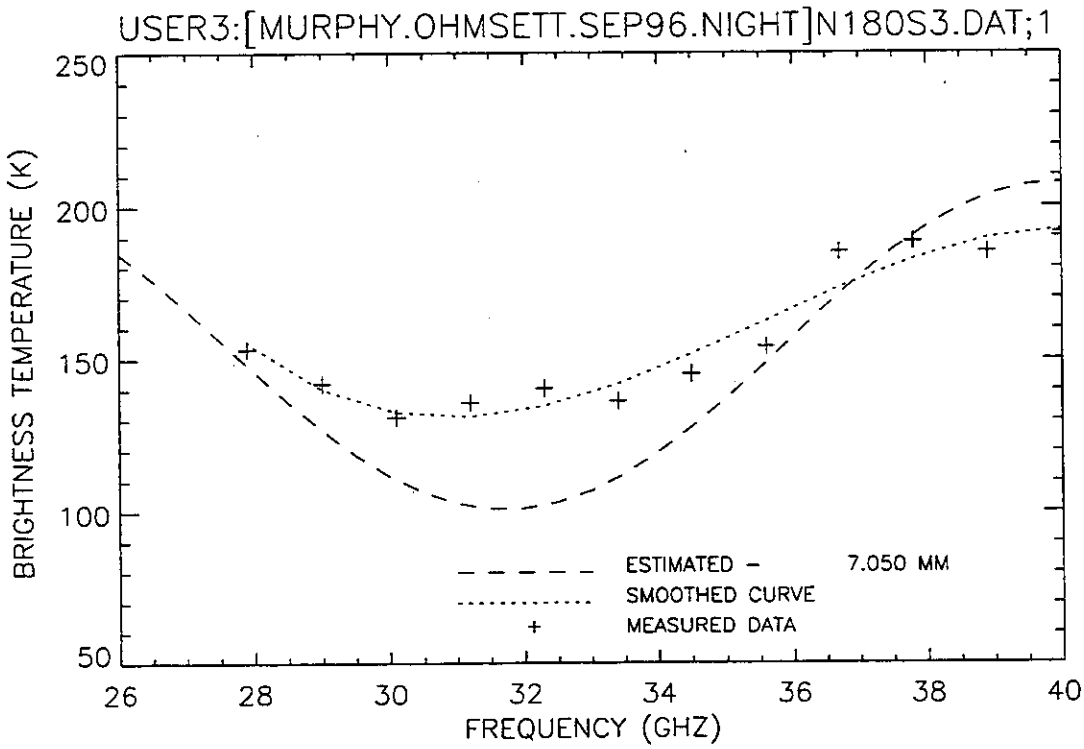

Figure 272. Plot of radiometric brightness temperature versus measurement frequency for 8-mm diesel oil, night test, fans on, calm wave conditions, 12 September 1996, sweep 3.

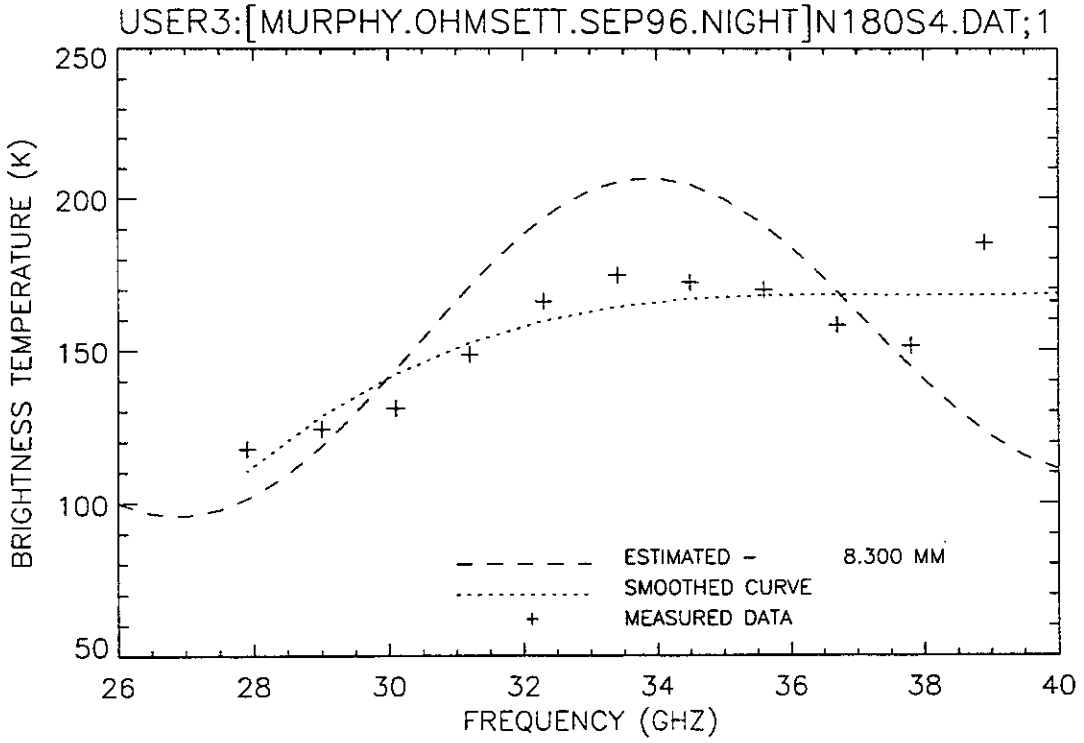

Figure 273. Plot of radiometric brightness temperature versus measurement frequency for 8-mm diesel oil, night test, fans on, calm wave conditions, 12 September 1996, sweep 4.

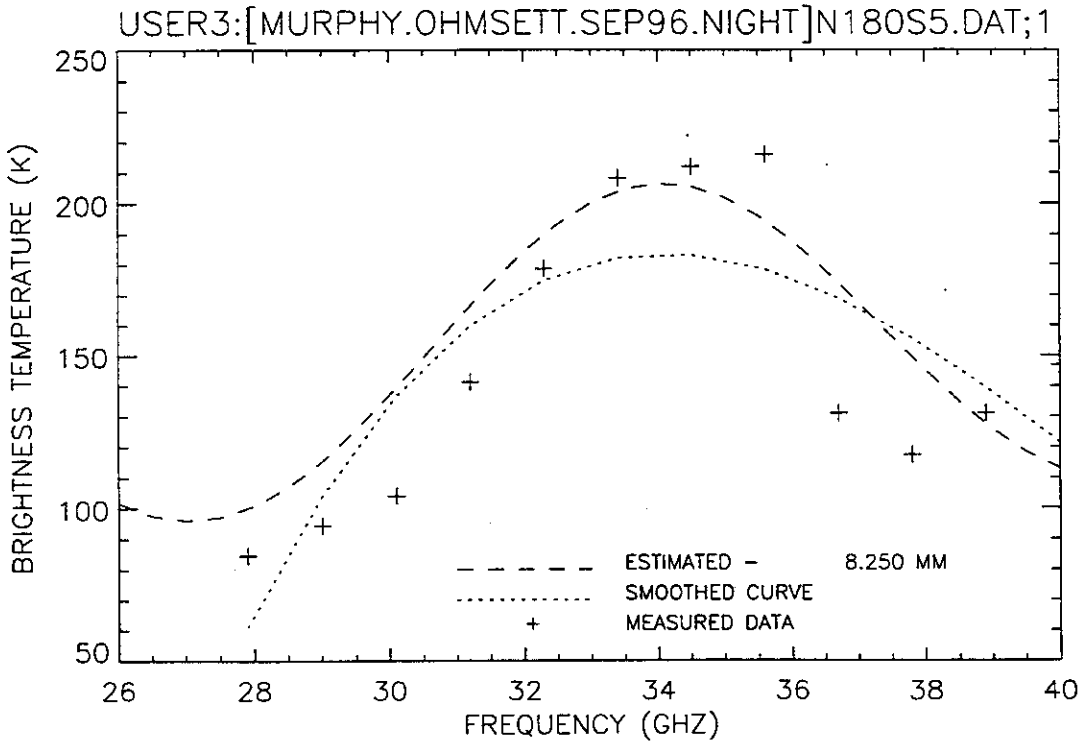

Figure 274. Plot of radiometric brightness temperature versus measurement frequency for 8-mm diesel oil, night test, fans on, calm wave conditions, 12 September 1996, sweep 5.

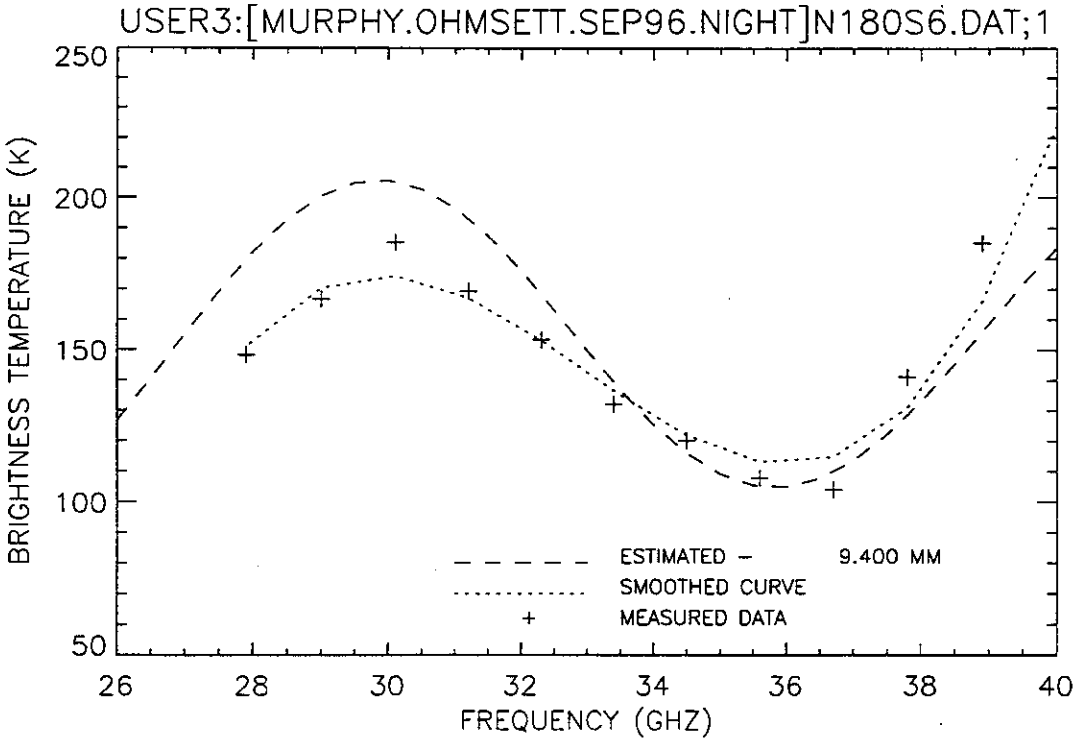

Figure 275. Plot of radiometric brightness temperature versus measurement frequency for 8-mm diesel oil, night test, fans on, calm wave conditions, 12 September 1996, sweep 6.

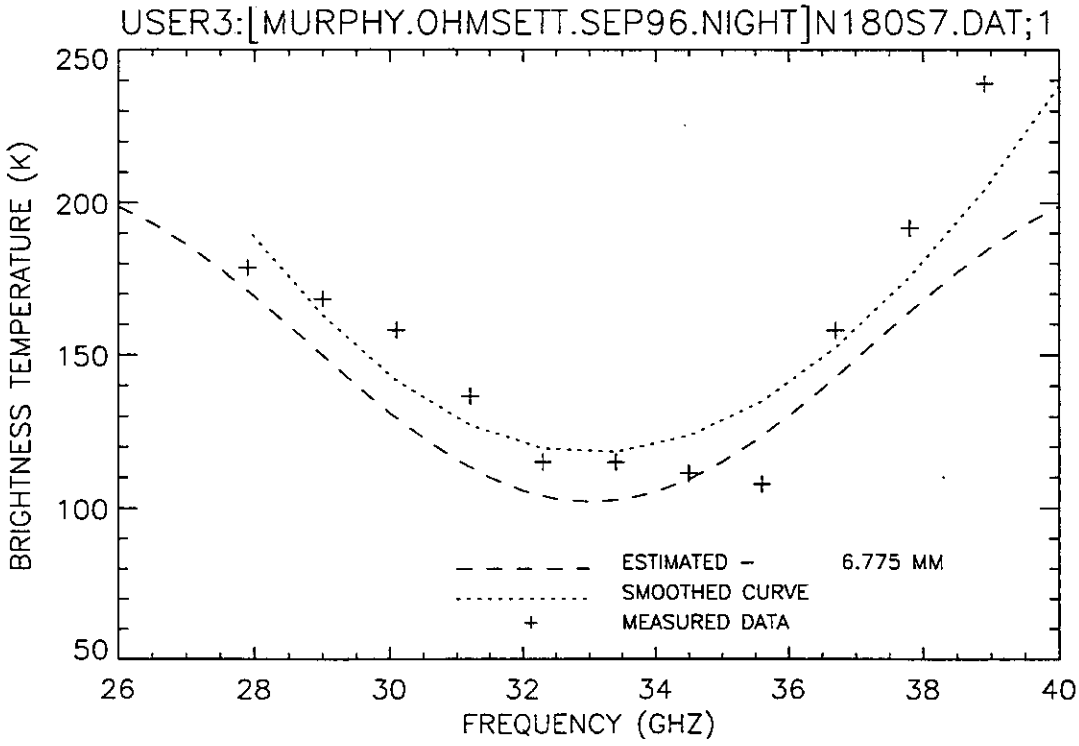

Figure 276. Plot of radiometric brightness temperature versus measurement frequency for 8-mm diesel oil, night test, fans on, calm wave conditions, 12 September 1996, sweep 7.

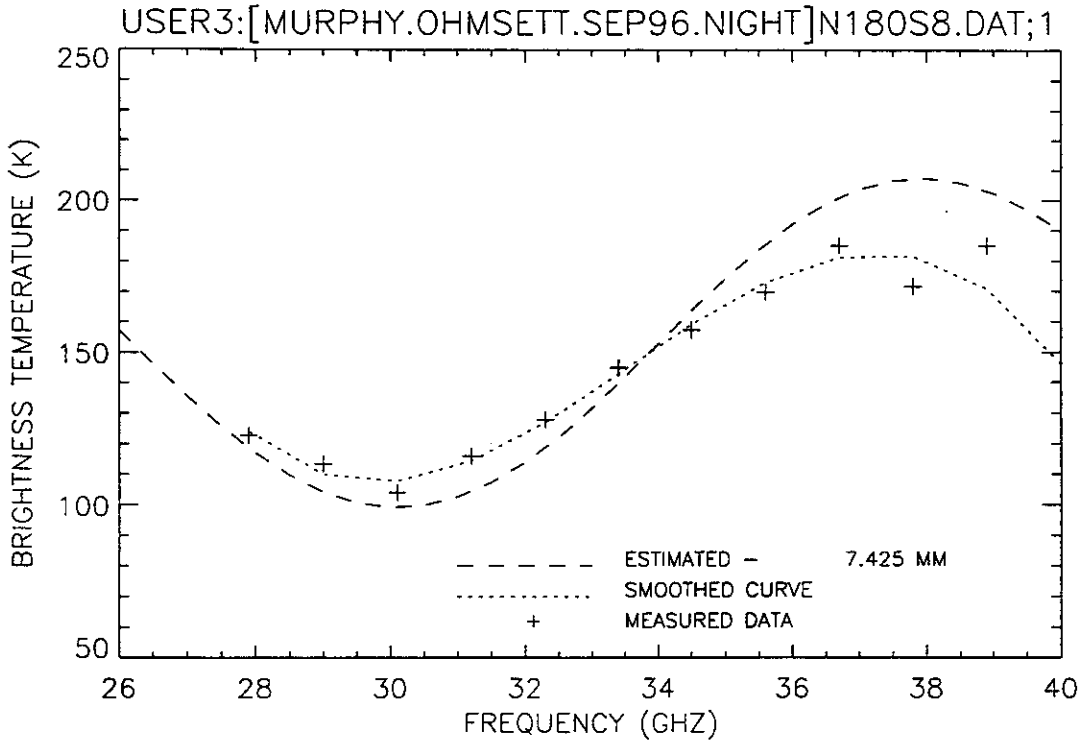

Figure 277. Plot of radiometric brightness temperature versus measurement frequency for 8-mm diesel oil, night test, fans on, calm wave conditions, 12 September 1996, sweep 8.

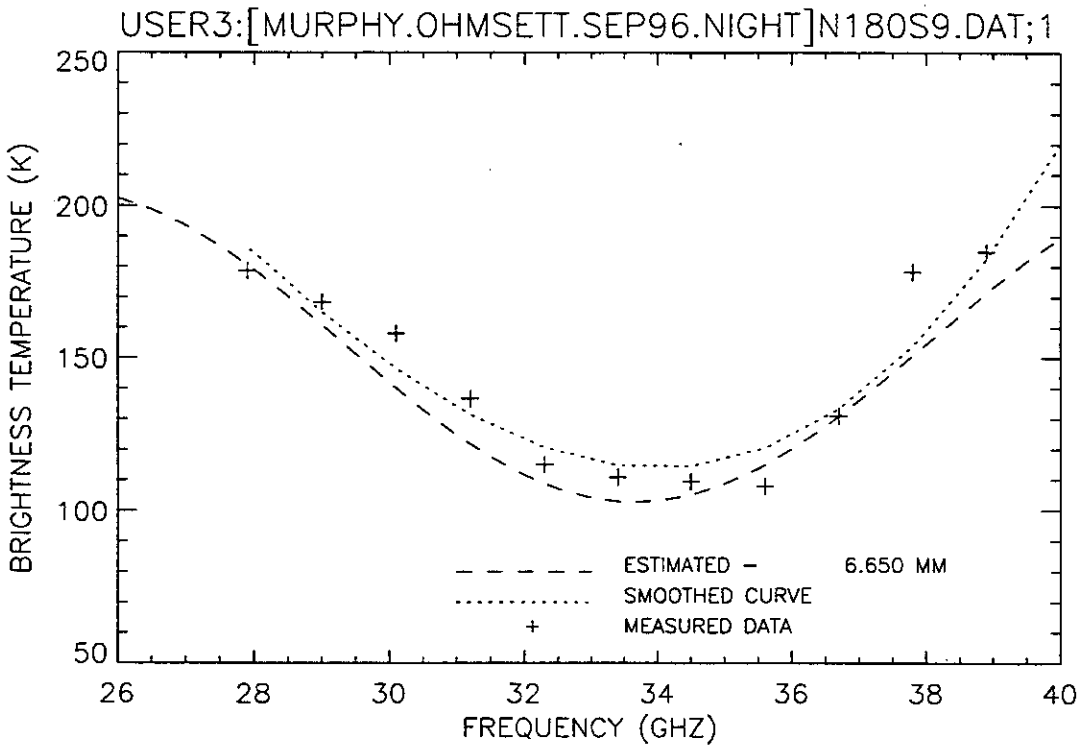

Figure 278. Plot of radiometric brightness temperature versus measurement frequency for 8-mm diesel oil, night test, fans on, calm wave conditions, 12 September 1996, sweep 9.

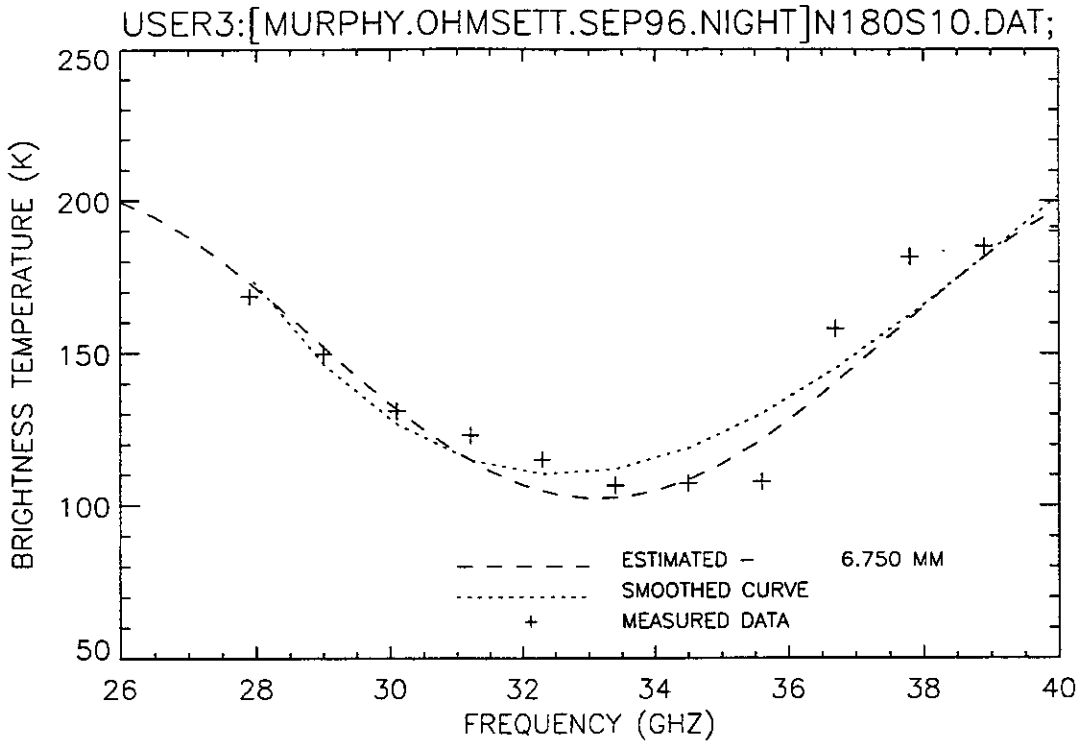

Figure 279. Plot of radiometric brightness temperature versus measurement frequency for 8-mm diesel oil, night test, fans on, calm wave conditions, 12 September 1996, sweep 10.

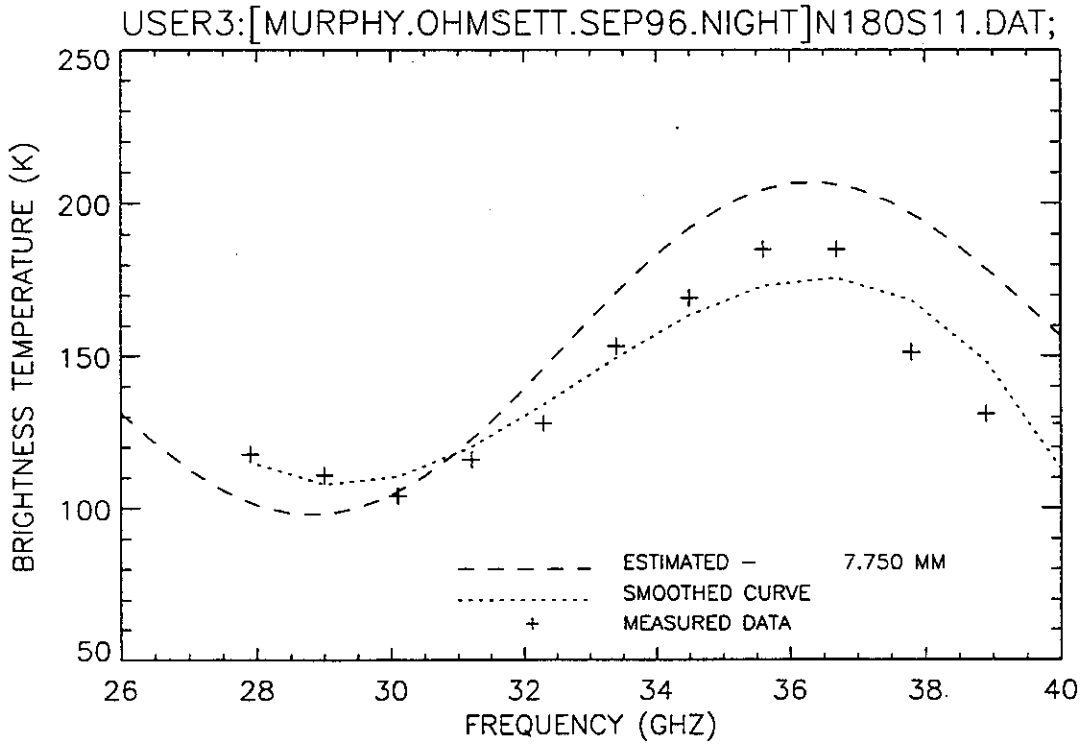

Figure 280. Plot of radiometric brightness temperature versus measurement frequency for 8-mm diesel oil, night test, fans on, calm wave conditions, 12 September 1996, sweep 11.

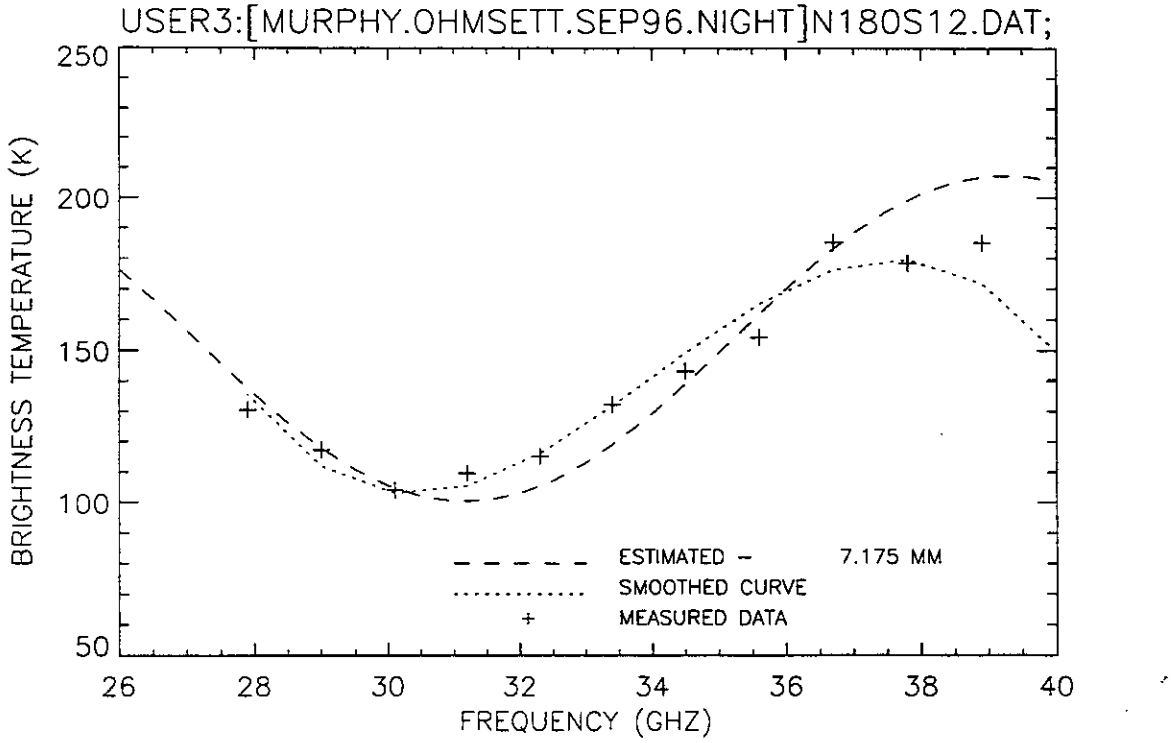

Figure 281. Plot of radiometric brightness temperature versus measurement frequency for 8-mm diesel oil, night test, fans on, calm wave conditions, 12 September 1996, sweep 12.

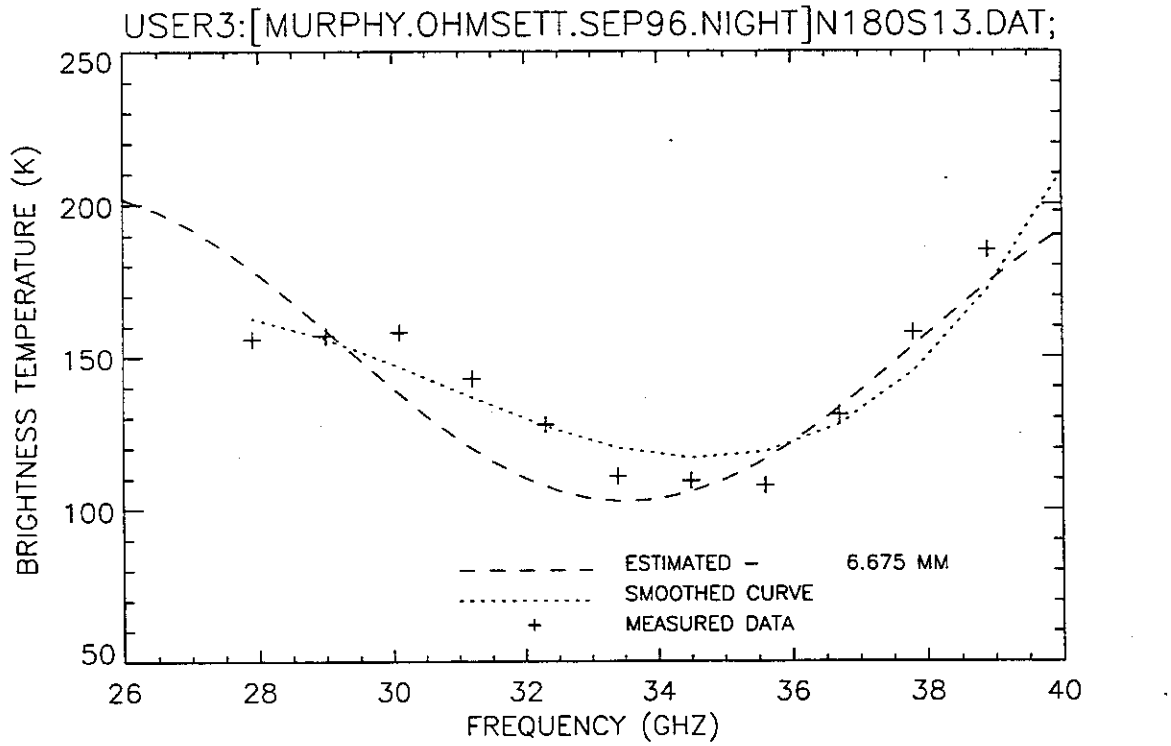

Figure 282. Plot of radiometric brightness temperature versus measurement frequency for 8-mm diesel oil, night test, fans on, calm wave conditions, 12 September 1996, sweep 13.

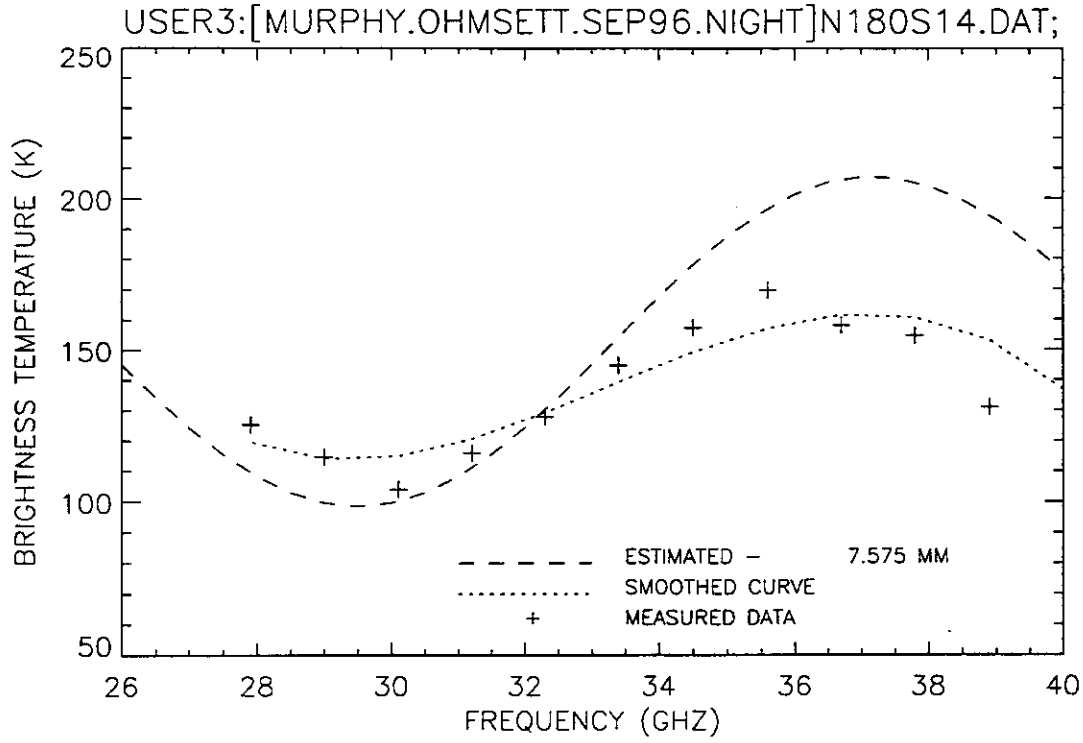

Figure 283. Plot of radiometric brightness temperature versus measurement frequency for 8-mm diesel oil, night test, fans on, calm wave conditions, 12 September 1996, sweep 14.

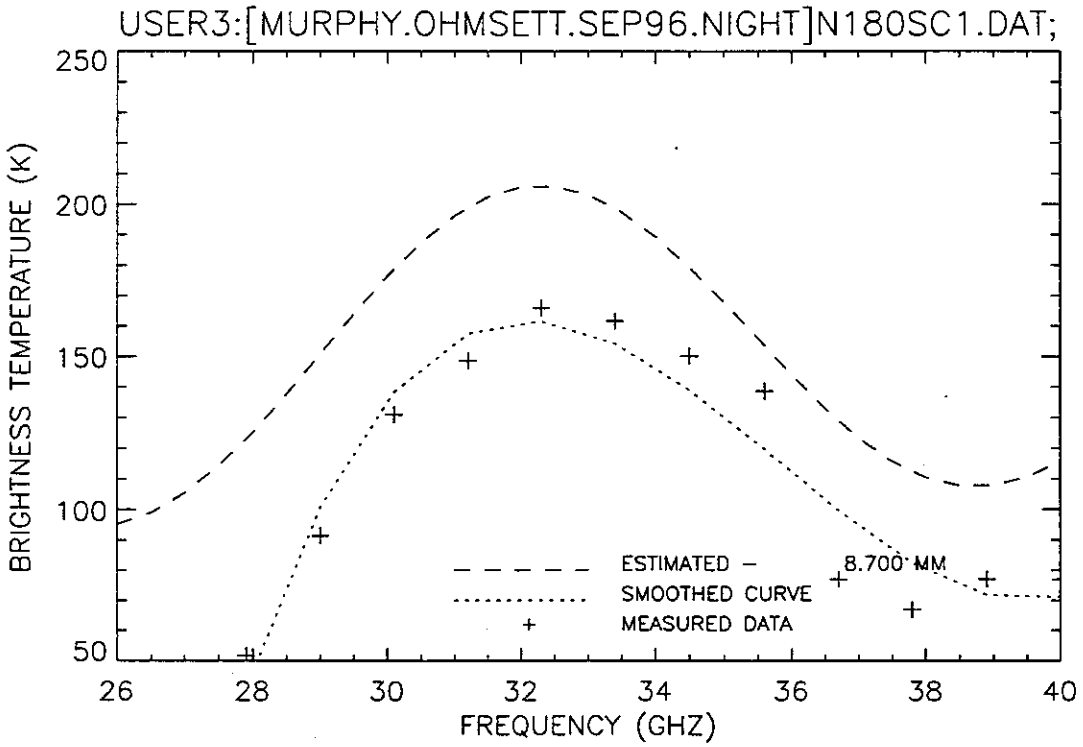

Figure 284. Plot of radiometric brightness temperature versus measurement frequency for 8-mm crude oil, night test, fans on, calm wave conditions, 12 September 1996, sweep 1.

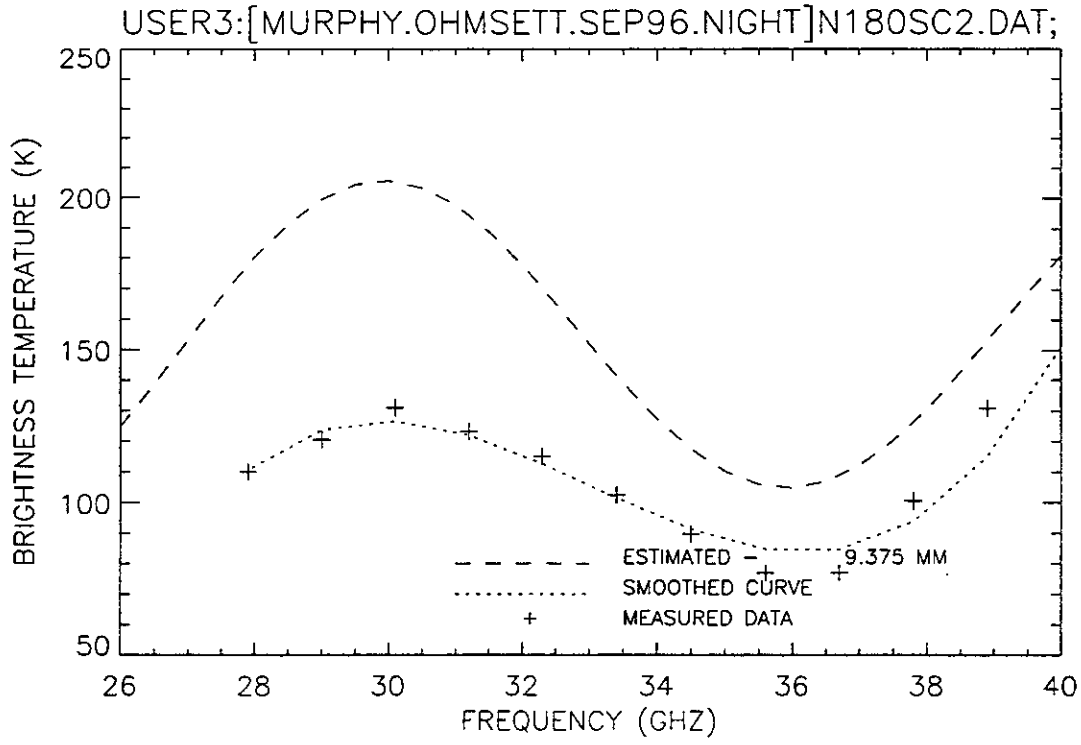

Figure 285. Plot of radiometric brightness temperature versus measurement frequency for 8-mm crude oil, night test, fans on, calm wave conditions, 12 September 1996, sweep 2.

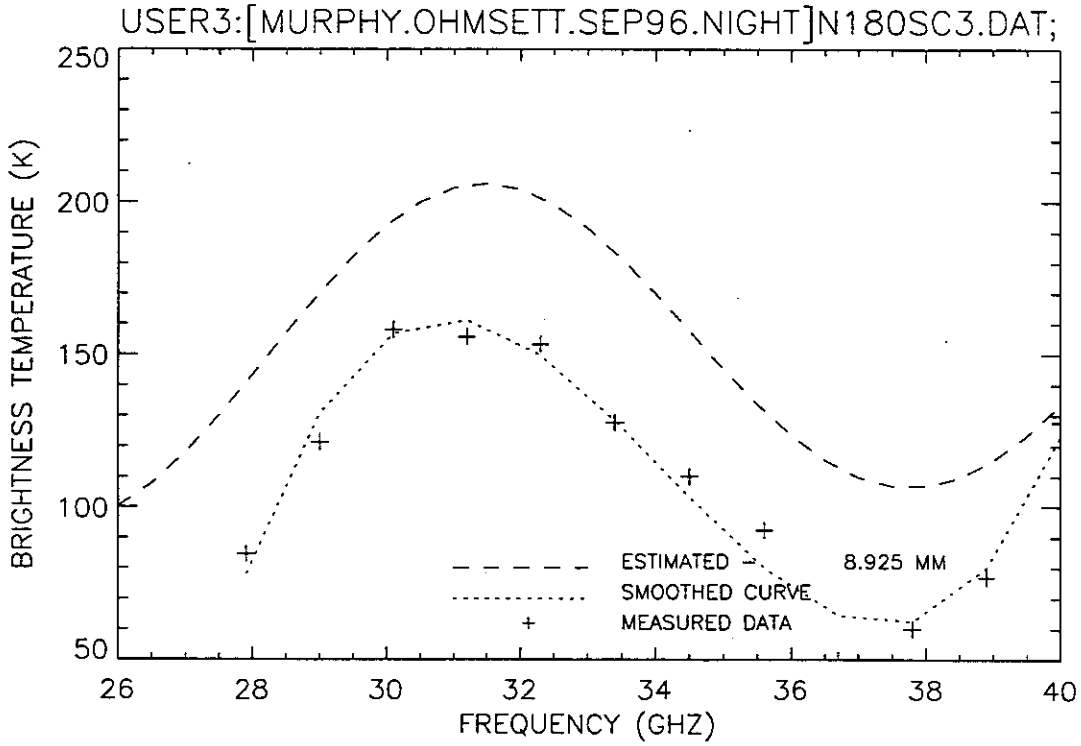

Figure 286. Plot of radiometric brightness temperature versus measurement frequency for 8-mm crude oil, night test, fans on, calm wave conditions, 12 September 1996, sweep 3.

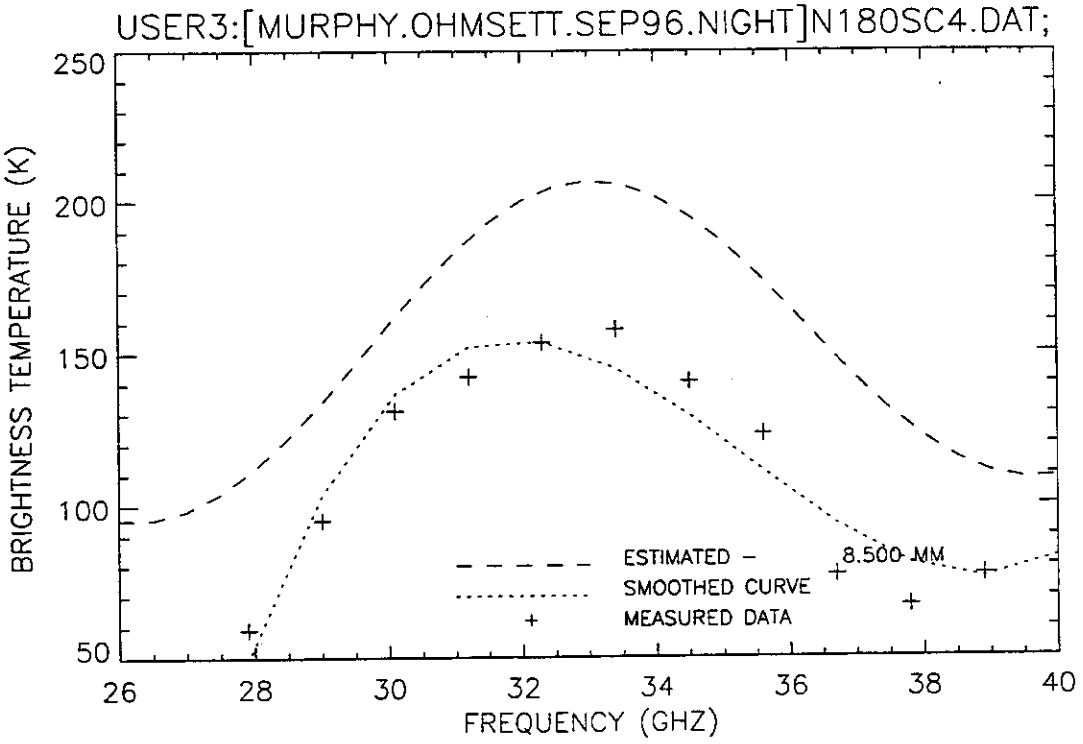

Figure 287. Plot of radiometric brightness temperature versus measurement frequency for 8-mm crude oil, night test, fans on, calm wave conditions, 12 September 1996, sweep 4.

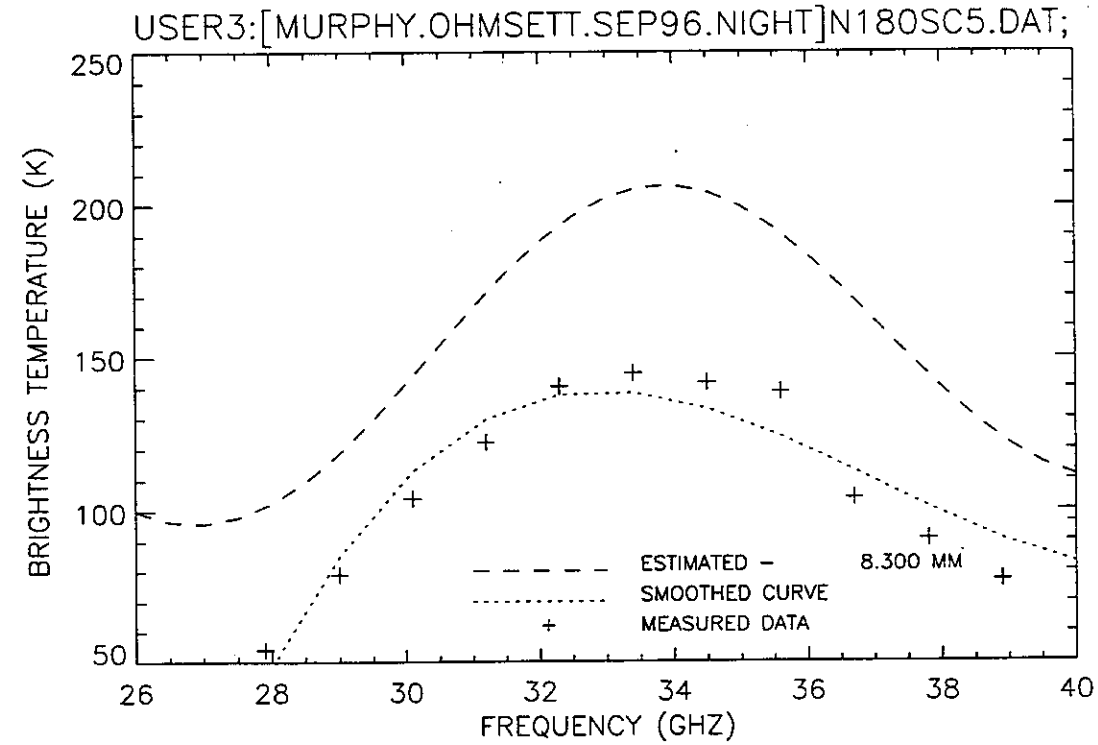

Figure 288. Plot of radiometric brightness temperature versus measurement frequency for 8-mm crude oil, night test, fans on, calm wave conditions, 12 September 1996, sweep 5.

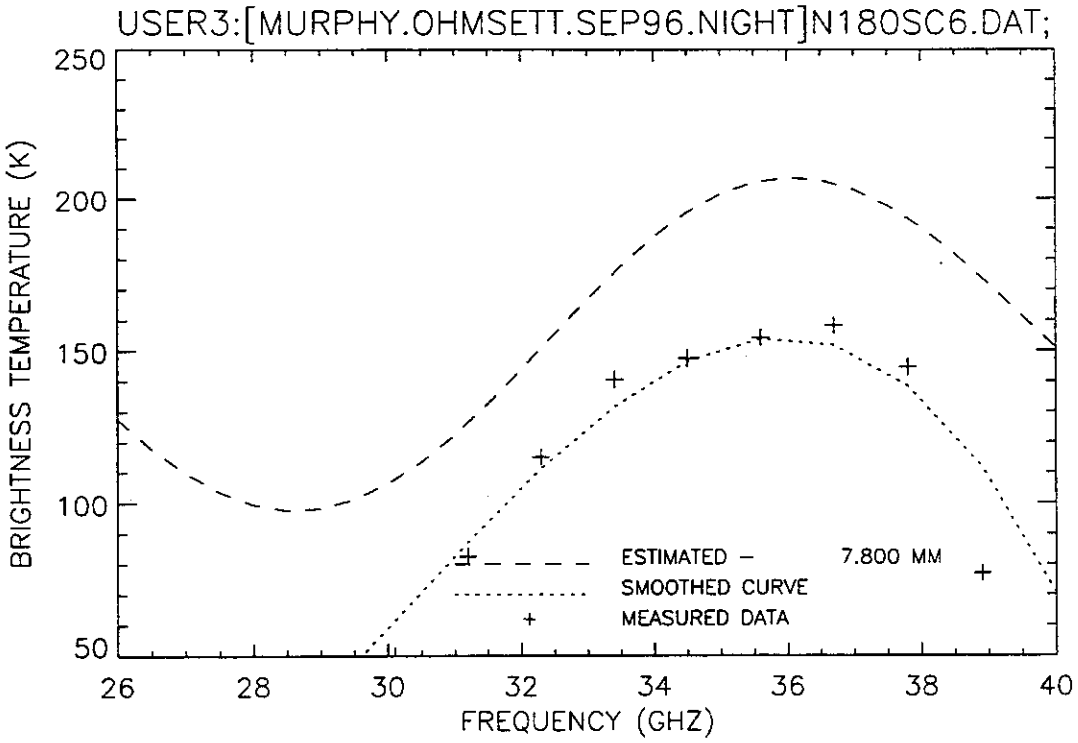

Figure 289. Plot of radiometric brightness temperature versus measurement frequency for 8-mm crude oil, night test, fans on, calm wave conditions, 12 September 1996, sweep 6.

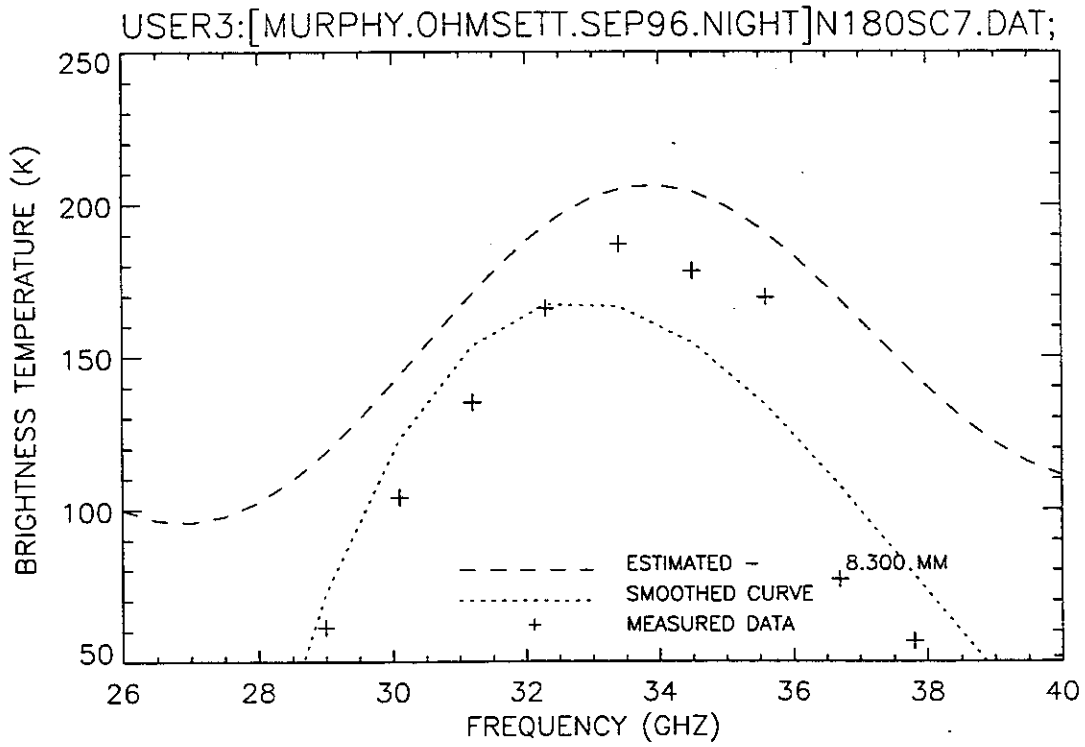

Figure 290. Plot of radiometric brightness temperature versus measurement frequency for 8-mm crude oil, night test, fans on, calm wave conditions, 12 September 1996, sweep 7.

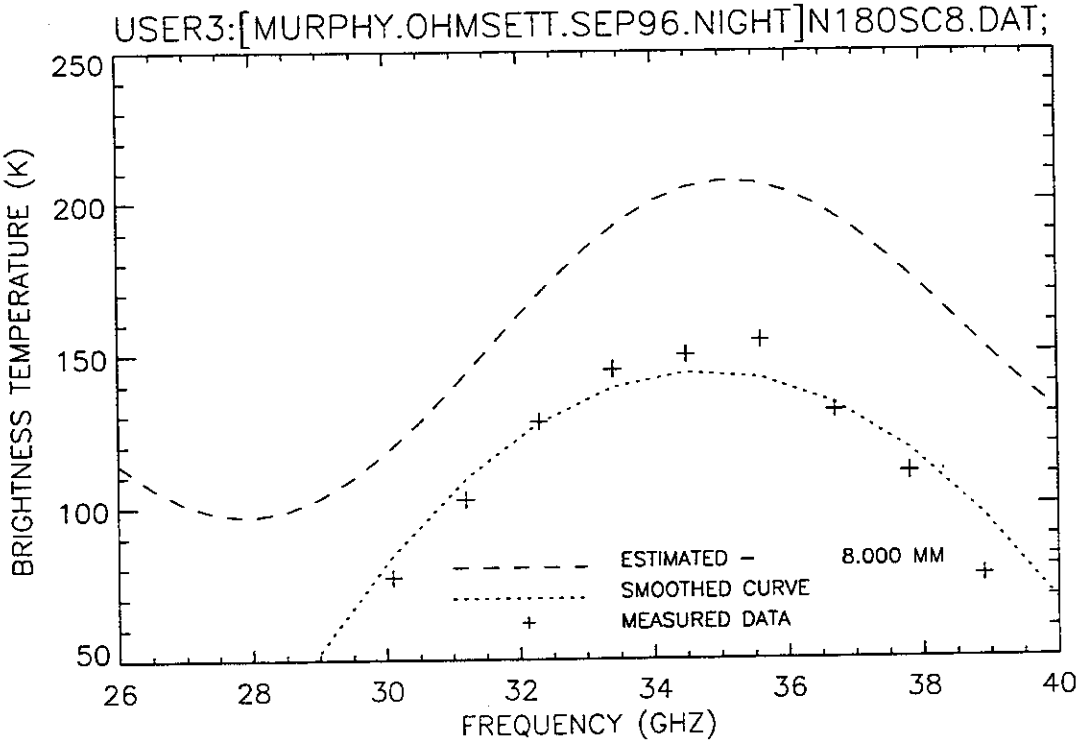

Figure 291. Plot of radiometric brightness temperature versus measurement frequency for 8-mm crude oil, night test, fans on, calm wave conditions, 12 September 1996, sweep 8.

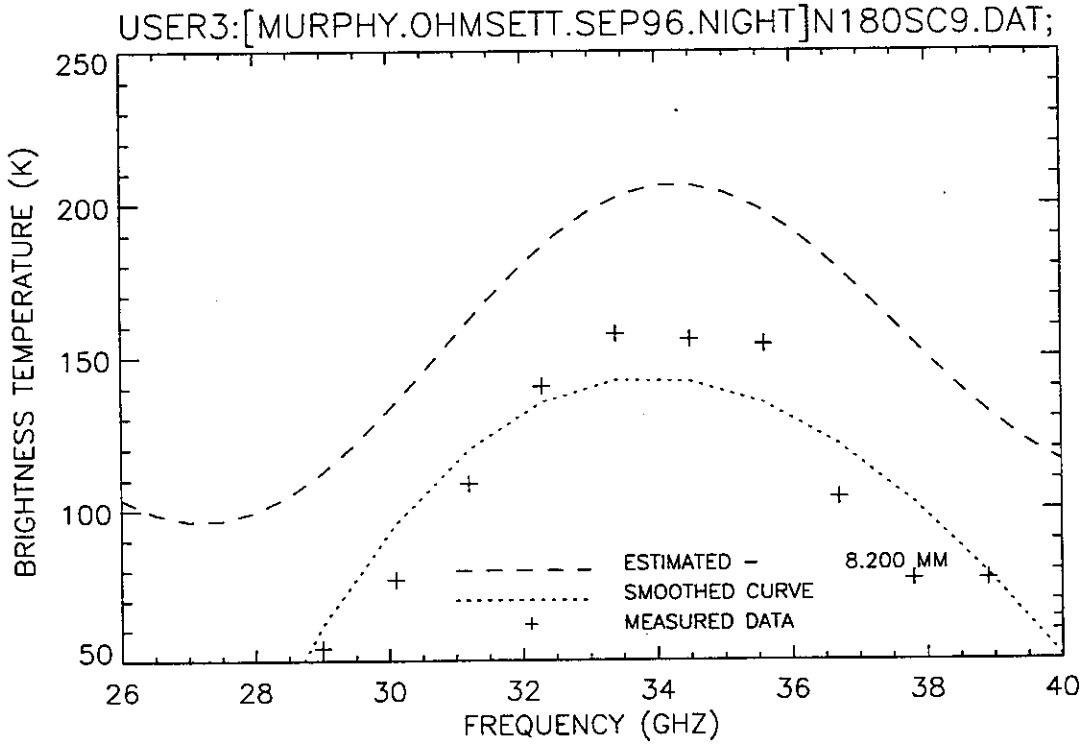

Figure 292. Plot of radiometric brightness temperature versus measurement frequency for 8-mm crude oil, night test, fans on, calm wave conditions, 12 September 1996, sweep 9.

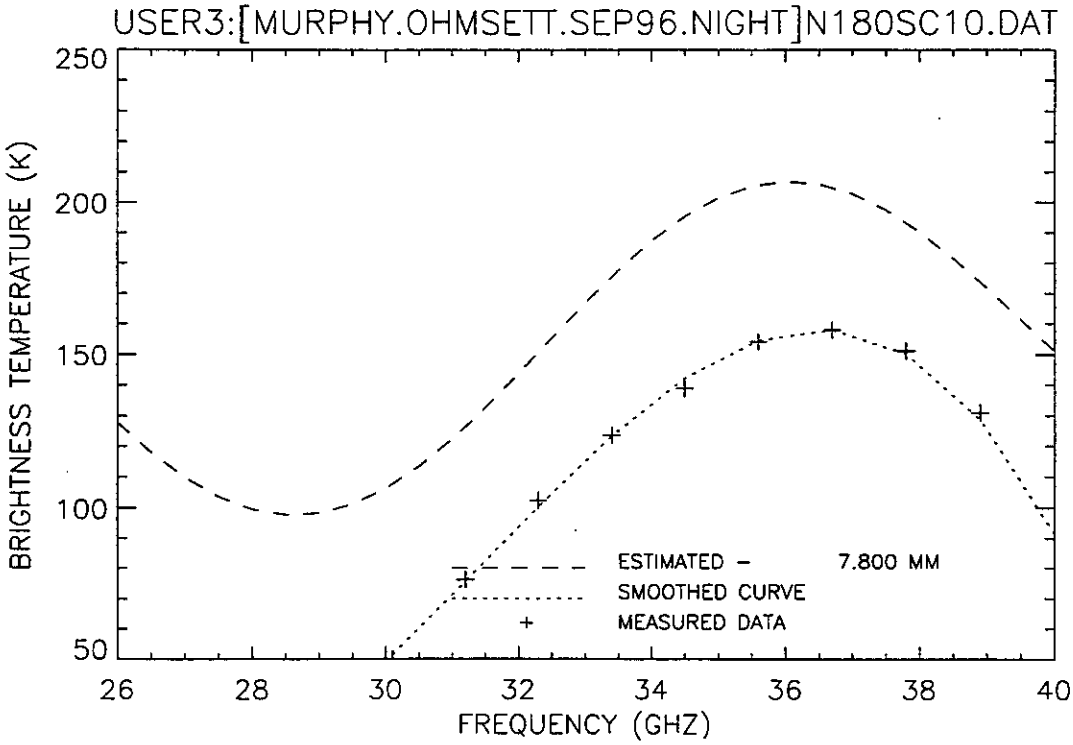

Figure 293. Plot of radiometric brightness temperature versus measurement frequency for 8-mm crude oil, night test, fans on, calm wave conditions, 12 September 1996, sweep 10.

6. Day 2 Test
Diesel and Crude Oil, Wave and Chop Conditions

The day 2 measurements were performed using the same oil targets used for the night measurements. Rain had subsided but wind conditions had increased. The wind was forming ripples on all the target pools in the calm wave condition. Because of inclement weather, data collection was not performed on all the pools under wave and chop conditions. It was felt that if meaningful data could be collected from a selected number of targets under wave and chop conditions, the increase in Ka-band multichannel radiometer over FSR performance could be shown.

The background water temperature reference for all the 8- and 3-mm collections was adjusted because the analysis indicated that the instrument gain had drifted substantially between the 3- and 2-mm collections.

Tables 6 and 7 summarize the results of the postcollection data analysis for the wave and chop conditions, respectively. The shaded blocks indicate algorithm results (LMS, CORR, MN/SL) that are close to or match the analyst's (visual) oil estimate. A comment is provided referring to the fit of the visual (analyst's choice) to the actual data.

The main bridge was positioned over the center of the water target pool at the southern end of the OHMSETT tank. A thin oil sheen was visible. This measurement was collected before the wave generator was started.

D200AWCA.DAT – The algorithm estimate of 0.000 mm, shown in Figure 294, is a fair match to the measured data. Based on using a water reference data set collected later in the day, some slight gain drift was observed.

The wave generator was started using a stroke of 1.5 in. and a frequency of 18 cycles/min; this corresponded to the wave 1 condition used during the October 1994 test. The wave condition was allowed to reach steady state before measurements were collected. As the waves reached steady state, the main bridge was moved north to the 8-mm diesel oil target. Data sets were collected from a position slightly south of the center of the target.

D280ADW2.DAT – The algorithm estimate of 0.800 mm, shown in Figure 295, is a fair match to the measured data.

TABLE 6

Results of the 12 September 1996 Day 2 Test

FILENAME	LMS	CORR	MN/SL	DECL	METHOD	VISUAL	COMMENT
D200AWCA.DAT	0.000	1.425	0.000	0.000	LMS & MN/SL	0.000	Fair
D200ADW2.DAT	3.725	1.225	0.000	3.725	LMS Only	0.000	Poor to fair
D200BDW2.DAT	0.150	0.525	0.000	0.075	LMS & MN/SL	0.075	Fair to good
D200CDW2.DAT	0.270	4.250	0.150	0.200	LMS & MN/SL	0.200	Fair
D200DDW2.DAT							Water reference
D220ACW2.DAT	2.300	2.525	2.250	2.275	LMS & MN/SL	2.275	Good
D220BCW2.DAT	2.300	2.625	2.250	2.275	LMS & MN/SL	2.275	Good
D220CCW2.DAT	2.075	2.075	2.050	2.075	LMS & CORR	2.075	Excellent
D220DCW2.DAT	4.500	3.975	1.225	4.500	LMS only	3.975	Good (shape)
D220ECW2.DAT	1.075	4.050	1.100	1.075	LMS & MN/SL	1.075	Good
D220FCW2.DAT	3.975	4.025	3.950	3.950	LMS & MN/SL	3.950	Good to excellent
D220GCW2.DAT	4.125	0.500	0.800	4.125	LMS only	4.125	Good
D220HCW2.DAT	3.600	3.875	0.250	3.600	LMS only	3.600	Good
New reference temperature assumed							
D230ACW2.DAT	3.475	3.425	0.200	3.450	LMS & CORR	3.450	Fair
D230ADW2.DAT	4.400	4.300	0.975	4.350	LMS & CORR	4.350	Good to excellent
D230BCW2.DAT	4.425	3.400	0.000	3.400	LMS & CORR	3.400	Good (shape)
D230BDW2.DAT	4.125	3.950	3.975	3.950	CORR & MN/SL	3.950	Fair (gain adjusted to 150%)
D230CCW2.DAT	3.225	3.125	0.000	3.175	LMS & CORR	3.175	Good (shape)
D230CDW2.DAT	3.975	3.775	3.900	3.925	CORR & MN/SL	3.925	Fair to good (gain adjusted to 150%)
D230DCW2.DAT	2.70	2.900	2.700	2.700	LMS & MN/SL	2.700	Good
D230DDW2.DAT	4.275	4.075	0.900	4.175	LMS & CORR	4.175	Fair to good (gain adjusted to 150%)
D230ECW2.DAT	0.675	7.150	0.675	0.675	LMS & MN/SL	0.675	Fair to good
D230EDW2.DAT	9.225	9.225	0.875	9.225	LMS & CORR	9.225	Fair to good
D230FDW2.DAT	4.775	1.725	1.025	4.775	LMS only	4.775	Good to excellent
D230GDW2.DAT	4.275	1.275	0.850	4.275	LMS only	4.275	Good
D230HDW2.DAT	4.025	4.075	0.750	4.050	LMS & CORR	4.050	Good
D230JDW2.DAT	2.475	6.075	2.475	2.475	LMS & MN/SL	2.475	Fair
D280ACW2.DAT	6.750	3.275	2.875	6.750	LMS only	6.750	Good (shape)
D280ADW2.DAT	0.800	3.650	0.800	0.800	LMS & MN/SL	0.800	Fair
D280BCW2.DAT	7.075	7.100	0.625	7.075	LMS & CORR	7.075	Good (shape)
D280BDW2.DAT	7.000	6.975	2.500	6.975	LMS & CORR	6.975	Good
D280CCW2.DAT	7.250	7.250	0.725	7.250	LMS & CORR	7.250	Good
D280CDW2.DAT	0.825	1.500	0.800	0.800	LMS & MN/SL	0.800	Poor to fair
D280DCW2.DAT	4.000	3.900	0.725	3.950	LMS & CORR	3.950	Good to excellent
D280DDW2.DAT	0.900	7.475	0.900	0.900	LMS & MN/SL	7.475	Fair to good (shape)
D280ECW2.DAT	6.975	3.425	0.750	6.975	LMS only	6.975	Fair to good
D280EDW2.DAT	7.025	7.000	2.450	7.000	LMS & CORR	7.000	Good
D280FCW2.DAT	7.375	7.375	0.750	7.375	LMS & CORR	7.375	Good
D280FDW2.DAT	7.050	7.050	2.450	7.050	LMS & CORR	7.050	Fair to good

TABLE 6 (Continued)

Results of the 12 September 1996 Day 2 Test

FILENAME	LMS	CORR	MN/SL	DECL	METHOD	VISUAL	COMMENT
D280GCW2.DAT	6.725	3.275	2.900	3.275	CORR only	6.725	Fair to good (shape)
D280GDW2.DAT	1.025	7.425	1.025	1.025	LMS & MN/SL	7.425	Good (shape)
D280HCW2.DAT	6.725	3.275	2.775	6.725	LMS only	6.725	Good
D280HDW2.DAT	6.900	3.300	2.175	6.900	LMS only	6.900	Fair (shape)
D280JDW2.DAT	6.900	3.300	2.175	6.900	LMS only	6.900	Fair (shape)
D280KDW2.DAT	1.125	7.225	1.125	1.125	LMS & MN/SL	1.125	Poor to fair
D280LDW2.DAT	10.000	3.325	2.200	10.000	LMS only	10.000	Fair to good
D280MDW2.DAT	7.175	7.125	2.300	7.150	LMS & CORR	7.150	Good (shape)
D280NDW2.DAT	10.000	3.325	1.175	10.000	LMS only	10.000	Fair (shape)

D280BDW2.DAT – The algorithm estimate of 6.975 mm, shown in Figure 296, is a good match to the measured data.

D280CDW2.DAT – The algorithm estimate of 0.800 mm, shown in Figure 297, is a poor-to-fair match to the measured data.

D280DDW2.DAT – The algorithm estimate of 0.900 mm is a poor match to the measured data. If the correlation-only estimate of 7.475 mm is used, a fair-to-good match to the shape of the measured data is observed, shown in Figure 298.

D2800EDW2.DAT – The algorithm estimate of 7.000 mm, shown in Figure 299, is a good match to the measured data.

D280FDW2.DAT – The algorithm estimate of 7.050 mm, shown in Figure 300, is a fair-to-good match to the measured data.

Wave conditions were increased to wave 2, using a stroke of 1.5 in. and a frequency of 30 cycles/min. The test tank was allowed to reach steady state before measurements continued. Measurements were collected from the same target area.

D280GDW2.DAT – The algorithm estimate of 1.025 mm is a poor match to the shape of the measured data. The correlation-only estimate of 7.425 mm, shown in Figure 301, results in a good shape match.

D280HDW2.DAT – The algorithm estimate of 6.900 mm, shown in Figure 302, is a fair match to the shape of the measured data.

D280JDW2.DAT – The algorithm estimate of 6.900 mm, shown in Figure 303, is a fair match to the shape of the measured data.

D280KDW2.DAT – The algorithm estimate of 1.125 mm, shown in Figure 304, is a poor-to-fair match to the measured data.

D280LDW2.DAT – The algorithm estimate of 10.000 mm, shown in Figure 305, is a fair-to-good match to the measured data, if the smoothed curve is ignored.

D280MDW2.DAT – The algorithm estimate of 7.150 mm, shown in Figure 306, is a good match to the shape of the measured data.

D280NDW2.DAT – The algorithm estimate of 10.000 mm, shown in Figure 307, is a fair match to the shape of the measured data, if the smoothed curve is ignored.

The main bridge was moved to the center of the 8-mm crude oil target; wave 2 conditions were still present in the tank. Because of the windy conditions, oil was escaping from the containment boom.

D280ACW2.DAT – The algorithm estimate of 6.750 mm, shown in Figure 308, is a good match to the shape of the measured data.

D280BCW2.DAT – The algorithm estimate of 7.075 mm, shown in Figure 309, is a good match to the shape of the measured data.

D280CCW2.DAT – The algorithm estimate of 7.250 mm, shown in Figure 310, is a good match to the measured data.

D280DCW2.DAT – The algorithm estimate of 3.950 mm, shown in Figure 311, is a good-to-excellent match to the measured data.

D280ECW2.DAT – The algorithm estimate of 6.975 mm, shown in Figure 312, is a fair-to-good match to the measured data.

D280FCW2.DAT – The algorithm estimate of 7.375 mm, shown in Figure 313, is a good match to the measured data.

D280GCW2.DAT – The algorithm estimate of 3.275 mm is a poor match to the measured data. The LMS-only estimate of 6.725 mm, shown in Figure 314, results in a fair-to-good shape match.

D280HCW2.DAT – The algorithm estimate of 6.725 mm, shown in Figure 315, is a good match to the measured data.

The main bridge was moved to the center of the 3-mm diesel oil target; wave 2 conditions were present. The target had a dividing line of scummy-looking oil; the following measurements were approximately 1 ft south of this dividing line.

D230ADW2.DAT – The algorithm estimate of 4.350 mm, shown in Figure 316, is a good-to-excellent match to the measured data.

D230BDW2.DAT – The algorithm estimate of 3.950 mm is a fair match to the shape of the measured data curve, if the amplitude of the theoretical estimate is increased to 150% of normal, shown in Figure 317.

D230CDW2.DAT – The algorithm estimate of 3.925 mm is a fair-to-good match to the measured data curve, if the amplitude of the theoretical estimate is increased to 150% of normal, shown in Figure 318.

D230DDW2.DAT – The algorithm estimate of 4.175 mm is a fair-to-good match to the measured data curve, if the amplitude of the theoretical estimate is increased to 150% of normal, shown in Figure 319.

The main bridge was moved south and the radiometer position shifted west to collect data from the southwestern sector of the target. This area had the thickest oil because of wind conditions.

D230EDW2.DAT – The algorithm estimate of 9.225 mm, shown in Figure 320, is a fair-to-good match to the measured data.

D230FDW2.DAT – The algorithm estimate of 4.775 mm, shown in Figure 321, is a good-to-excellent match to the measured data.

D230GDW2.DAT – The algorithm estimate of 4.275 mm, shown in Figure 322, is a good match to the measured data.

D230HDW2.DAT – The algorithm estimate of 4.050 mm, shown in Figure 323, is a good match to the measured data.

D230JDW2.DAT – The algorithm estimate of 2.475 mm, shown in Figure 324, is a fair match to the measured data.

The main bridge was positioned over the center of the 3-mm crude oil target with the radiometer shifted west; wave 2 conditions were present in the test tank.

D230ACW2.DAT – The algorithm estimate of 3.450 mm, shown in Figure 325, is a fair match to the shape of the measured data.

D230BCW2.DAT – The algorithm estimate of 3.400 mm, shown in Figure 326, is a good match to the shape of the measured data.

D230CCW2.DAT – The algorithm estimate of 3.175 mm, shown in Figure 327, is a good match to the shape of the measured data.

D230DCW2.DAT – The algorithm estimate of 2.700 mm, shown in Figure 328, is a good match to the measured data.

D230ECW2.DAT – The algorithm estimate of 0.675 mm, shown in Figure 329, is a fair-to-good match to the measured data.

The main bridge was positioned over the 2-mm crude oil target with the radiometer position shifted slightly east of center. Wave 2 conditions were present in the test tank. The target had a dividing line of scummy-looking oil mixed with water. Measurements were collected midway between this dividing line and the southern edge of the target.

D220ACW2.DAT – The algorithm estimate of 2.275 mm, shown in Figure 330, is a good match to the measured data.

D220BCW2.DAT – The algorithm estimate of 2.275 mm, shown in Figure 331, is a good match to the measured data.

D220CCW2.DAT – The algorithm estimate of 2.075 mm, shown in Figure 332, is an excellent match to the measured data.

D220DCW2.DAT – The algorithm estimate of 4.500 mm is a poor match to the measured data. The correlation-only estimate of 3.975 mm, shown in Figure 333, produces a good shape match.

The main bridge was moved north and the radiometer repositioned to measure slightly west of center. The following measurements contained approximately 50% antenna beam fill of oil and 50% beam fill of water. Wave 2 conditions were present in the test tank.

D230ECW2.DAT – The algorithm estimate of 1.075 mm, shown in Figure 334, is a good match to the measured data.

D230FCW2.DAT – The algorithm estimate of 3.950 mm, shown in Figure 335, is an excellent match to the measured data.

D230GCW2.DAT – The algorithm estimate of 4.125 mm, shown in Figure 336, is a good match to the measured data.

D230HCW2.DAT – The algorithm estimate of 4.125 mm, shown in Figure 337, is a good match to the measured data.

The main bridge was positioned over the center of the water target pool. Wave 2 conditions were present. A slight oil sheen was observed in this target.

D200ADW2.DAT – The algorithm estimate of 0.000 mm, shown in Figure 338, is a poor-to-fair match to the measured data.

D200BDW2.DAT – The algorithm estimate of 0.075 mm, shown in Figure 339, is a fair-to-good match to the measured data.

D200CDW2.DAT – The algorithm estimate of 0.200 mm, shown in Figure 340, is a fair match to the measured data.

D200DDW2.DAT – This data set, shown in Figure 341, was used as the water background reference.

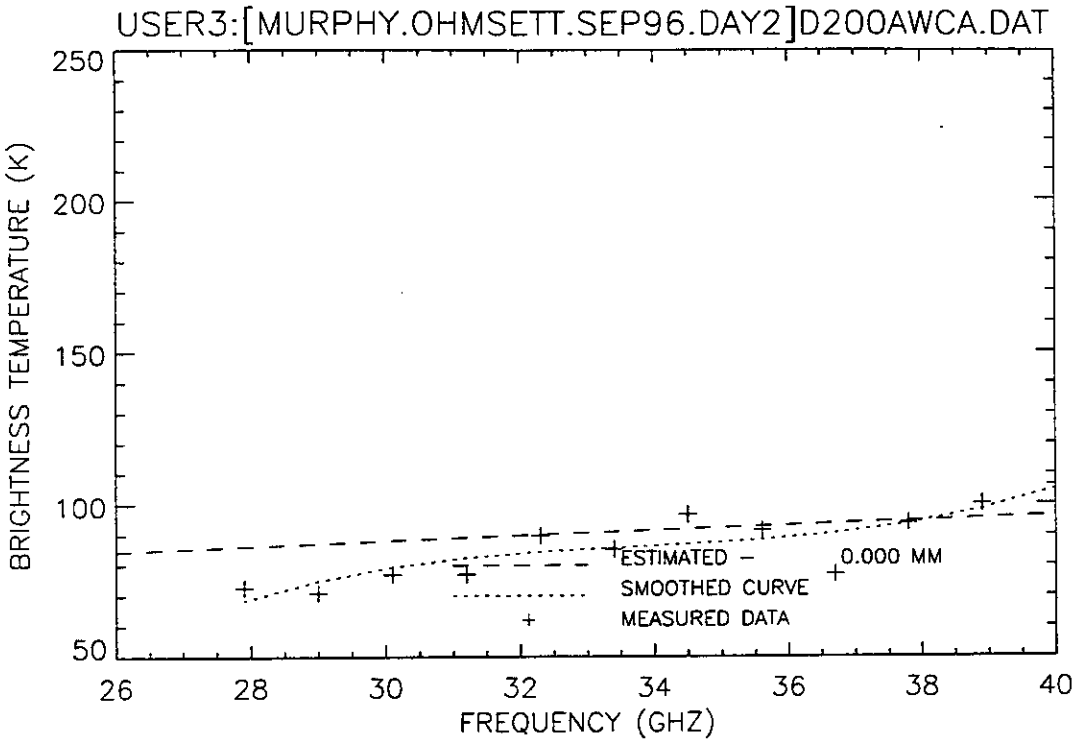

Figure 294. Plot of radiometric brightness temperature versus measurement frequency for water, day 2 test, calm wave conditions, 12 September 1996.

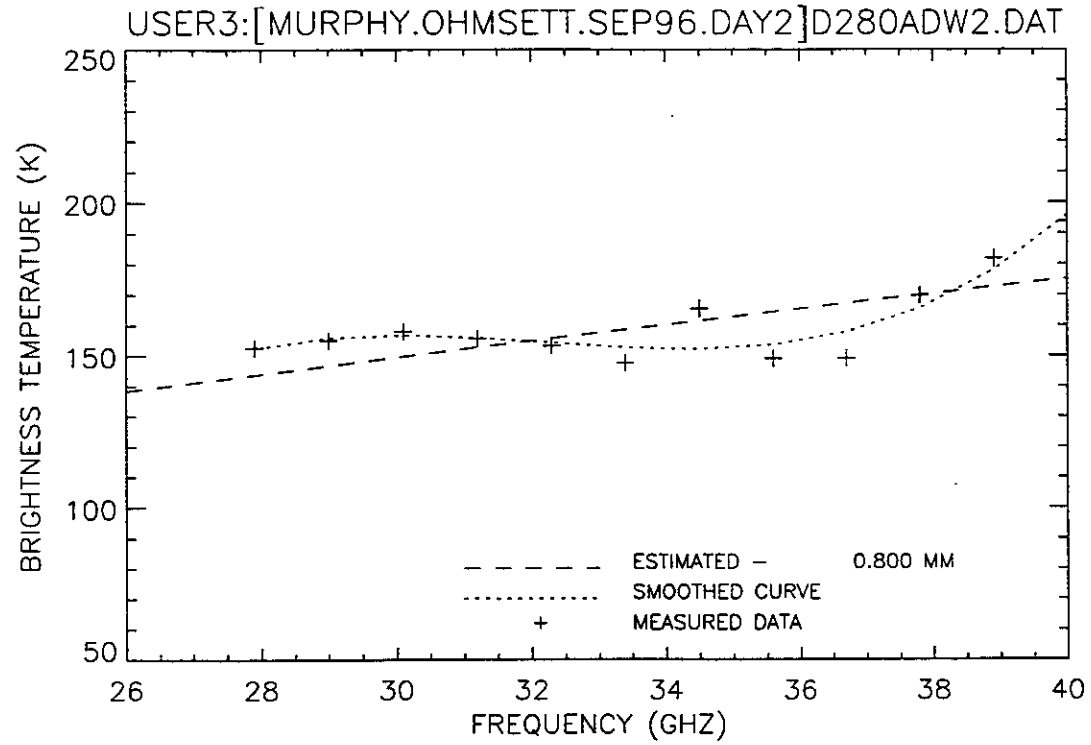

Figure 295. Plot of radiometric brightness temperature versus measurement frequency for 8-mm diesel oil, day 2 test, wave condition 1, 12 September 1996, sweep A.

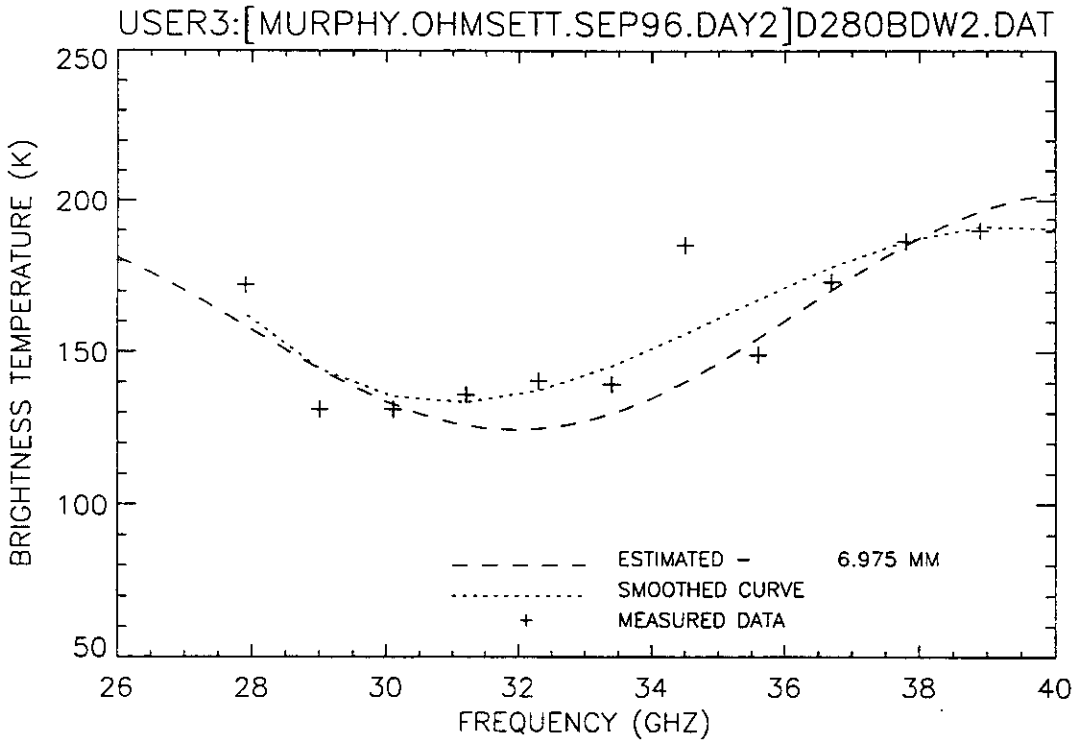

Figure 296. Plot of radiometric brightness temperature versus measurement frequency for 8-mm diesel oil, day 2 test, wave condition 1, 12 September 1996, sweep B.

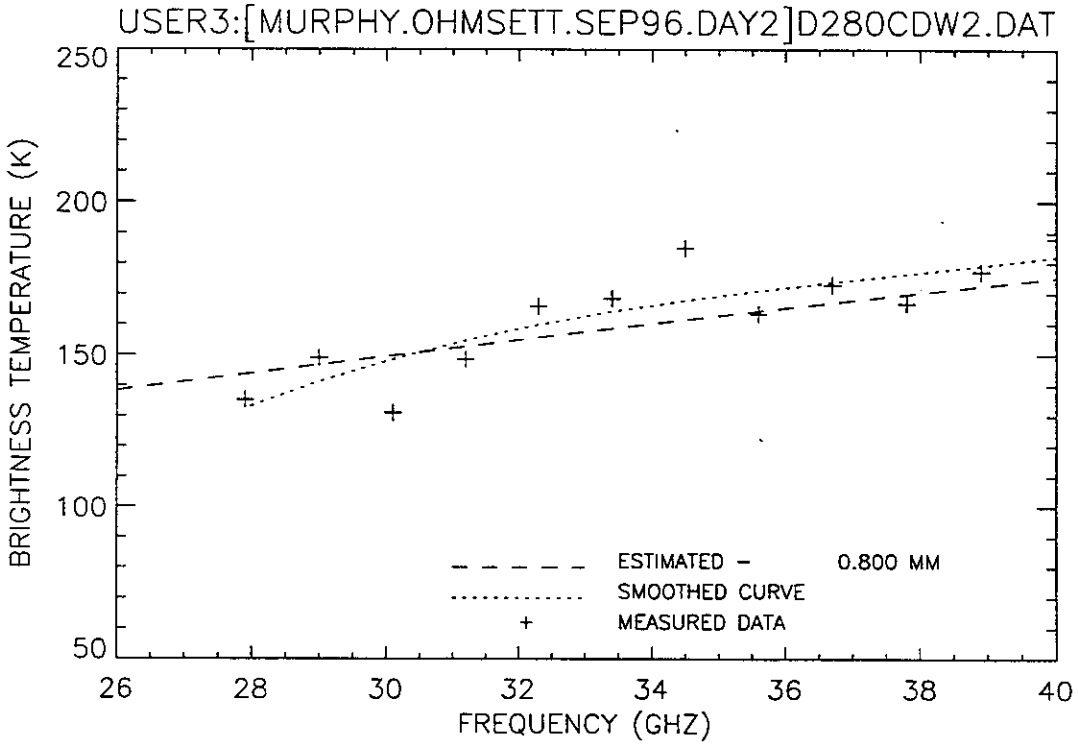

Figure 297. Plot of radiometric brightness temperature versus measurement frequency for 8-mm diesel oil, day 2 test, wave condition 1, 12 September 1996, sweep C.

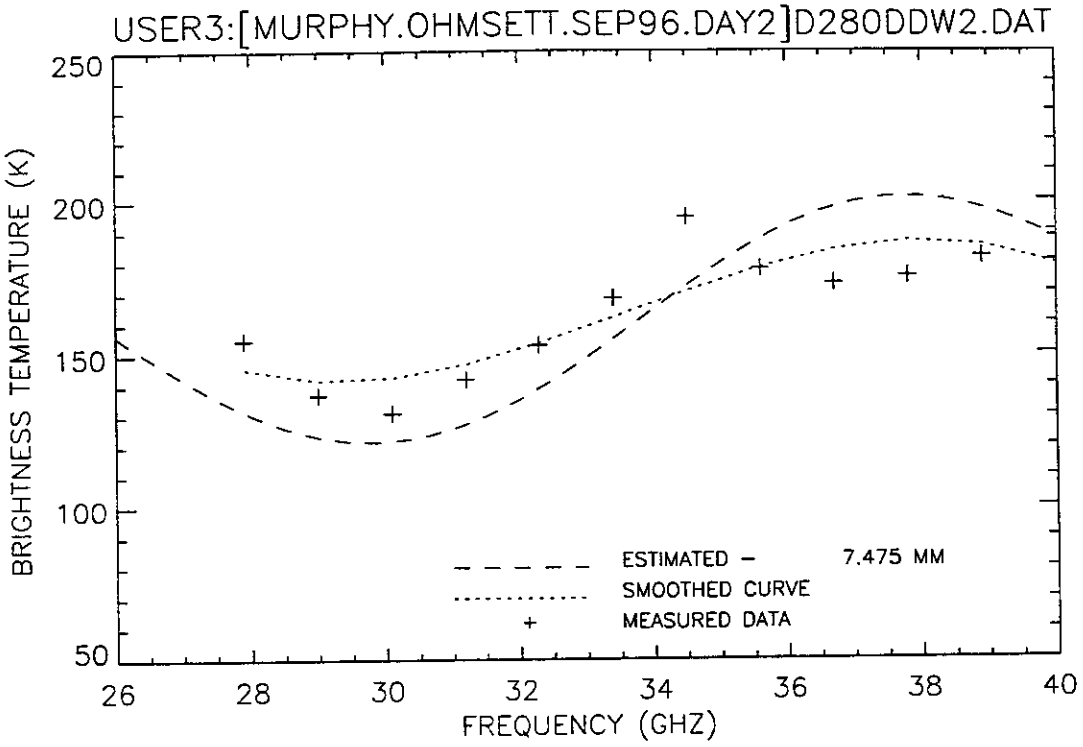

Figure 298. Plot of radiometric brightness temperature versus measurement frequency for 8-mm diesel oil, day 2 test, wave condition 1, 12 September 1996, sweep D.

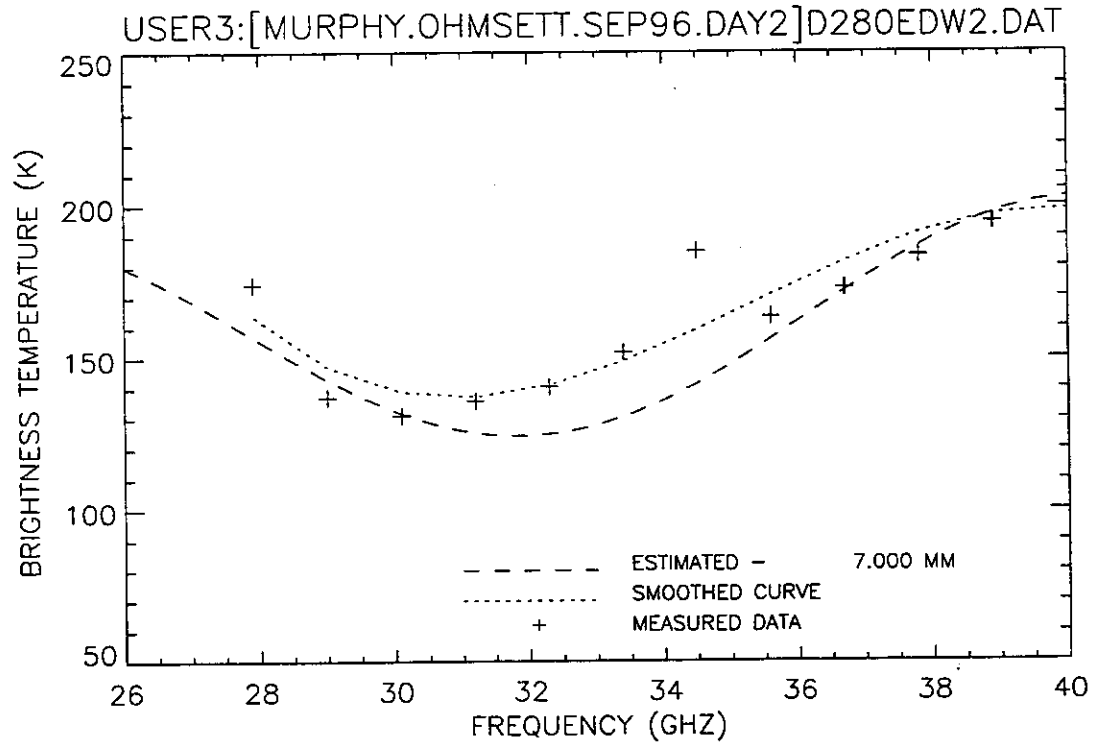

Figure 299. Plot of radiometric brightness temperature versus measurement frequency for 8-mm diesel oil, day 2 test, wave condition 1, 12 September 1996, sweep E.

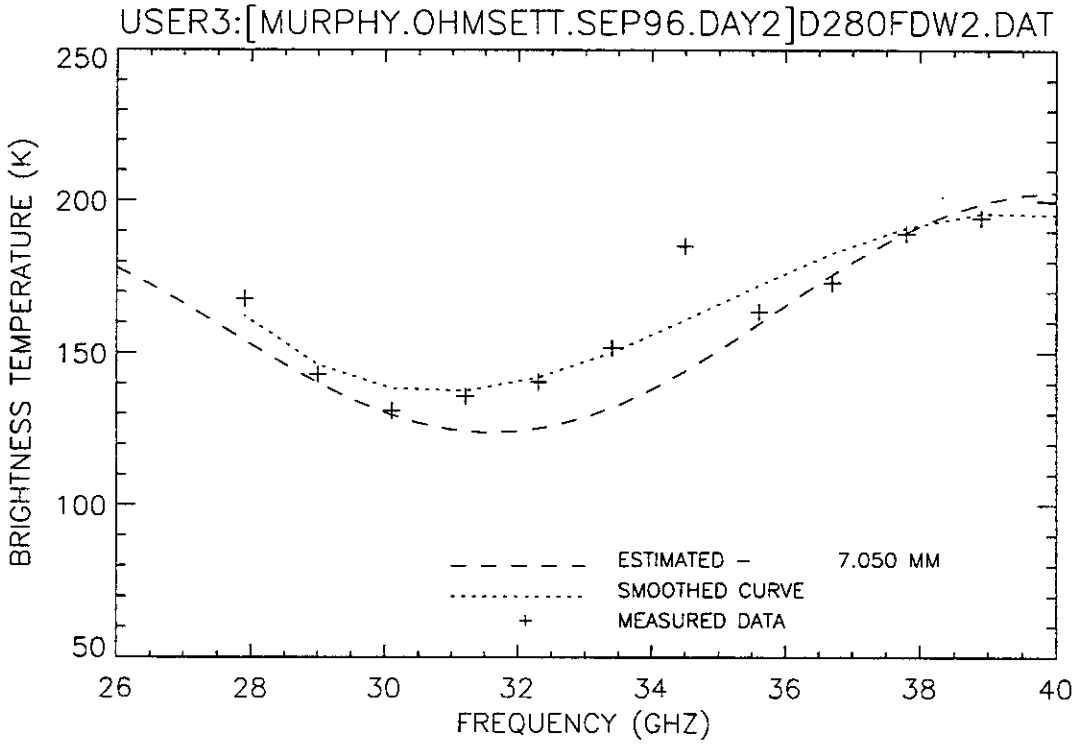

Figure 300. Plot of radiometric brightness temperature versus measurement frequency for 8-mm diesel oil, day 2 test, wave condition 1, 12 September 1996, sweep F.

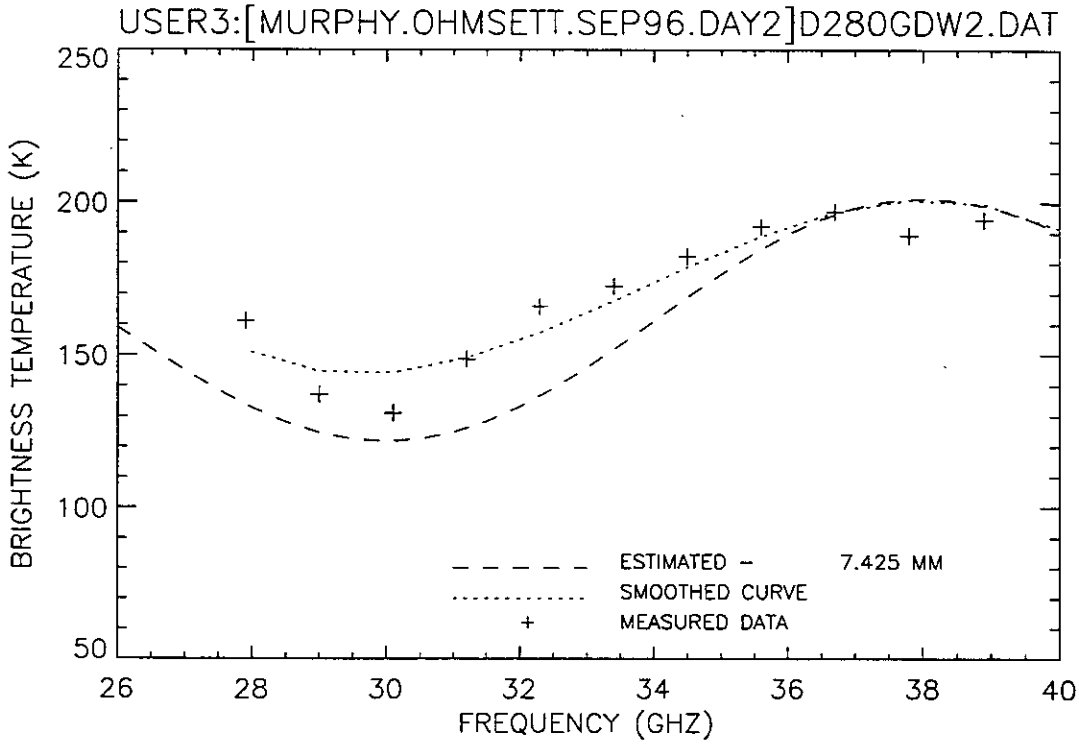

Figure 301. Plot of radiometric brightness temperature versus measurement frequency for 8-mm diesel oil, day 2 test, wave condition 2, 12 September 1996, sweep G.

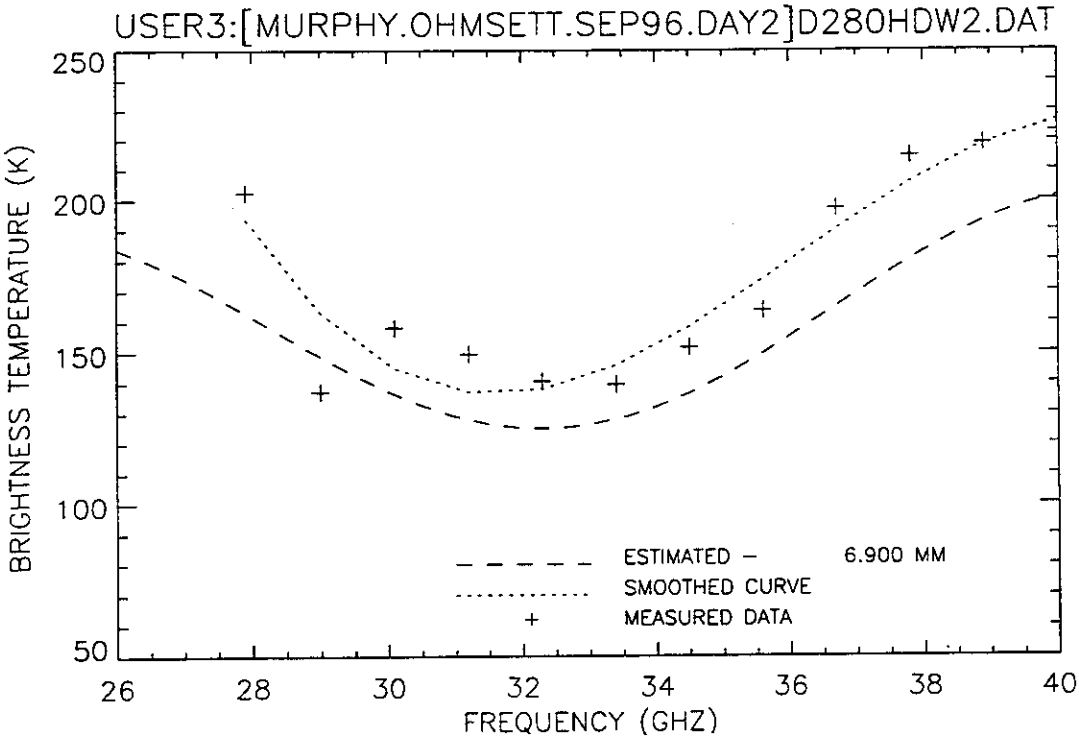

Figure 302. Plot of radiometric brightness temperature versus measurement frequency for 8-mm diesel oil, day 2 test, wave condition 2, 12 September 1996, sweep H.

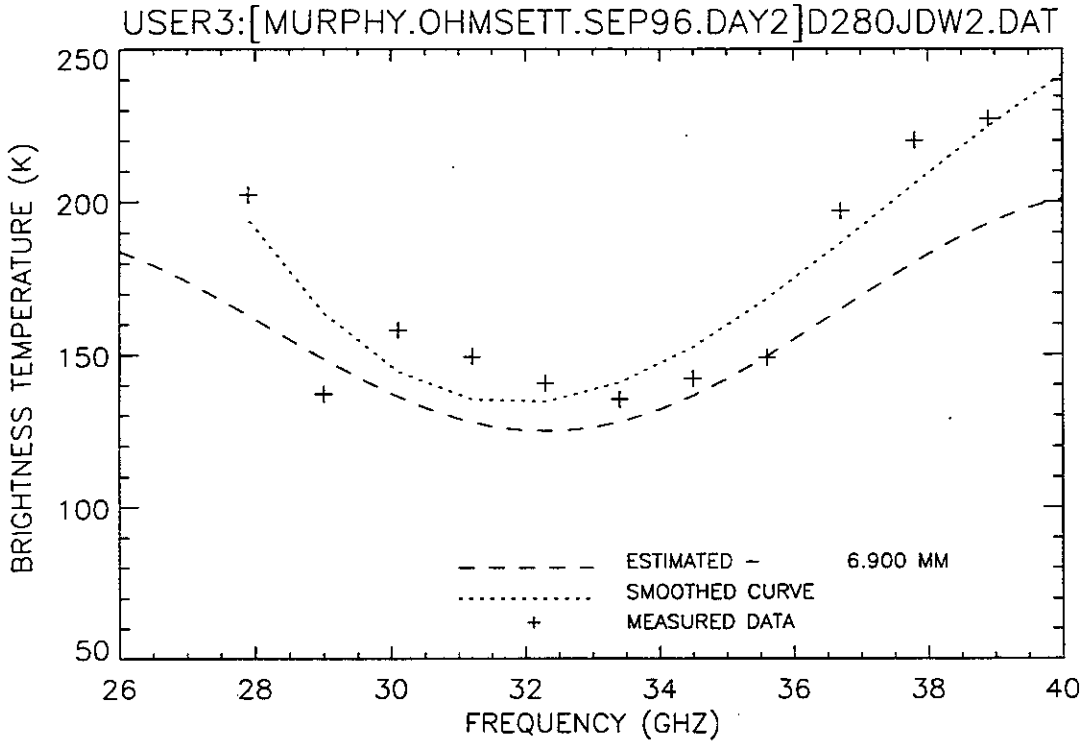

Figure 303. Plot of radiometric brightness temperature versus measurement frequency for 8-mm diesel oil, day 2 test, wave condition 2, 12 September 1996, sweep J.

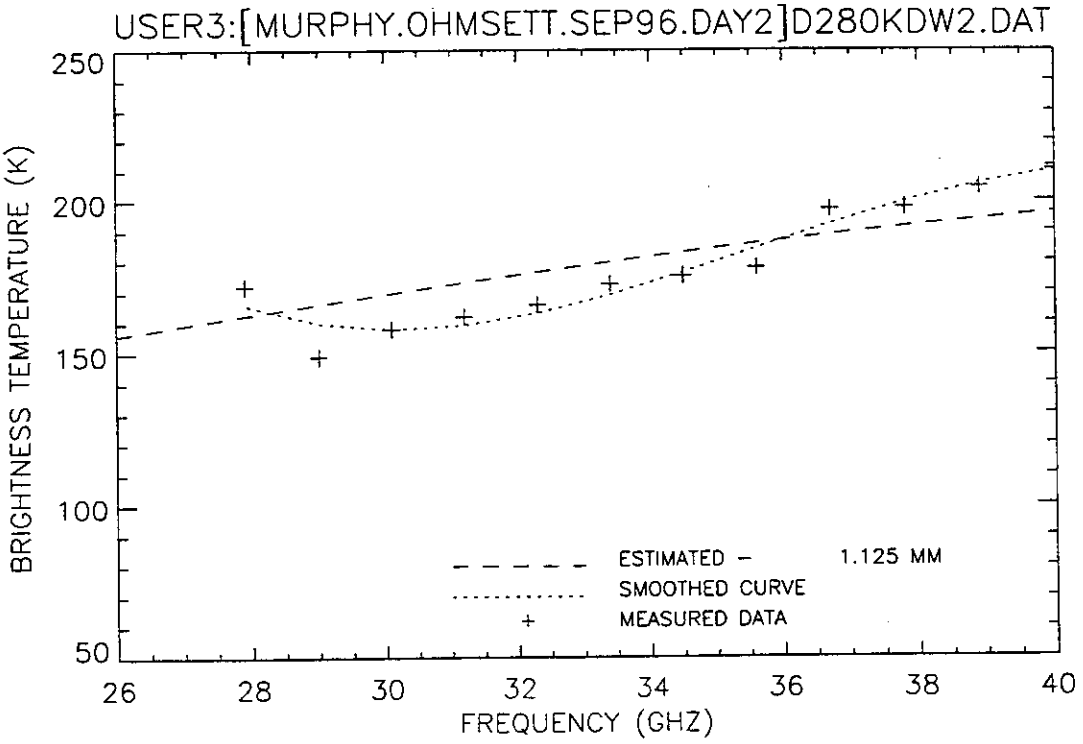

Figure 304. Plot of radiometric brightness temperature versus measurement frequency for 8-mm diesel oil, day 2 test, wave condition 2, 12 September 1996, sweep K.

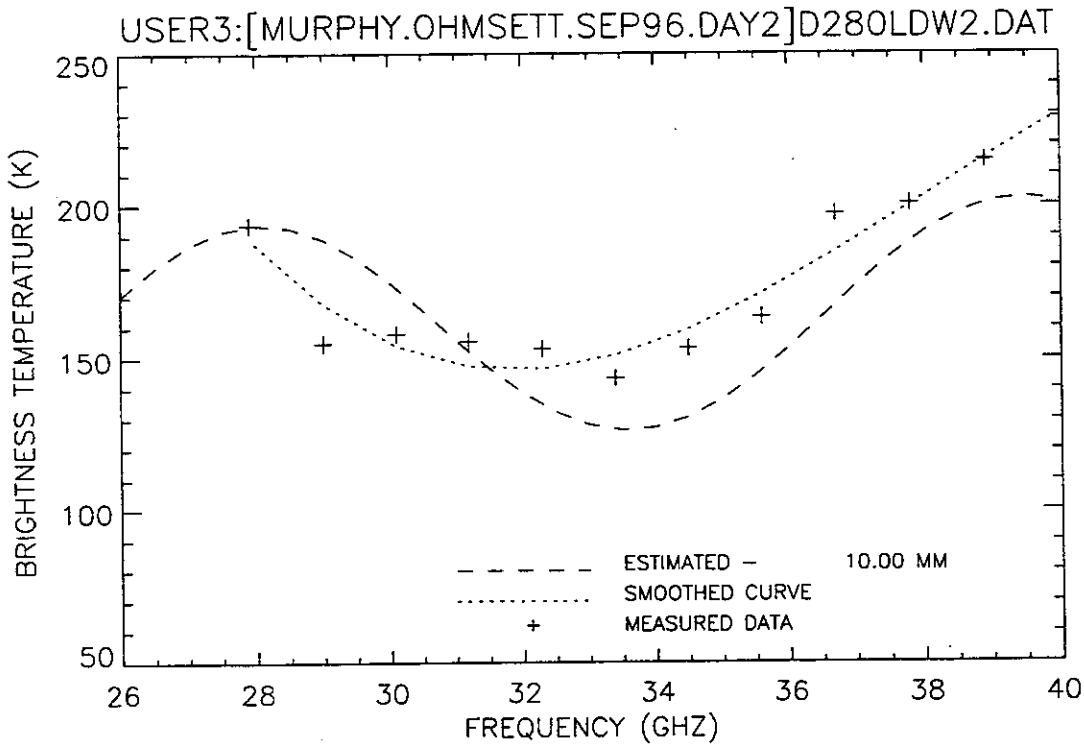

Figure 305. Plot of radiometric brightness temperature versus measurement frequency for 8-mm diesel oil, day 2 test, wave condition 2, 12 September 1996, sweep L.

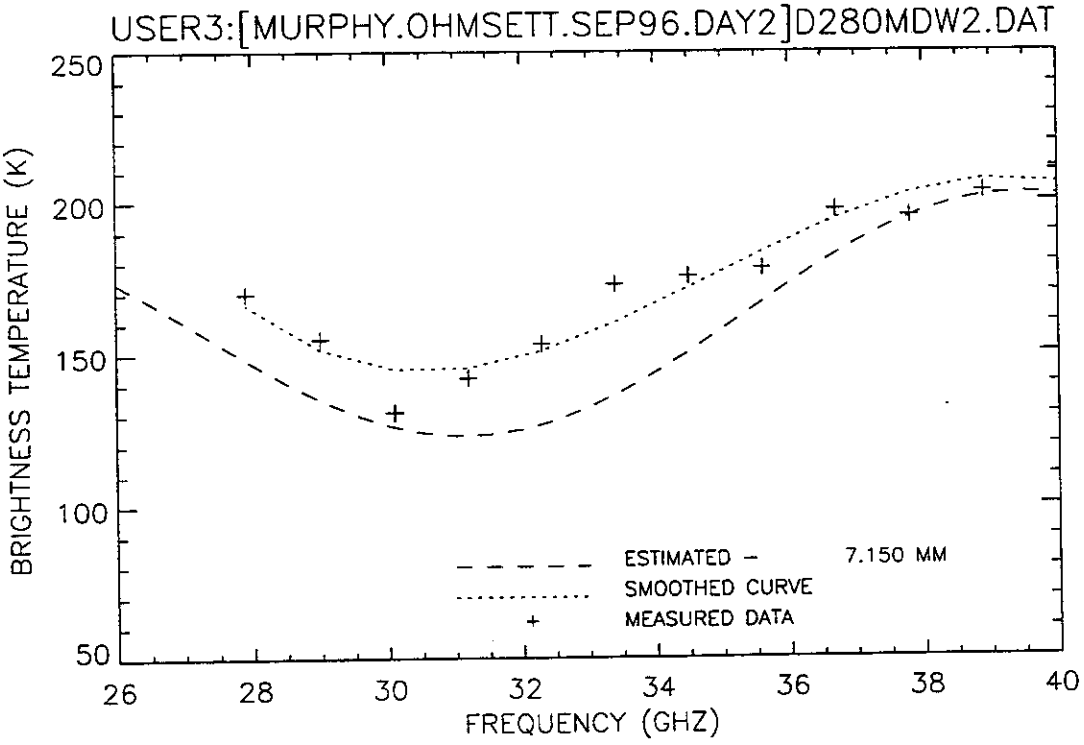

Figure 306. Plot of radiometric brightness temperature versus measurement frequency for 8-mm diesel oil, day 2 test, wave condition 2, 12 September 1996, sweep M.

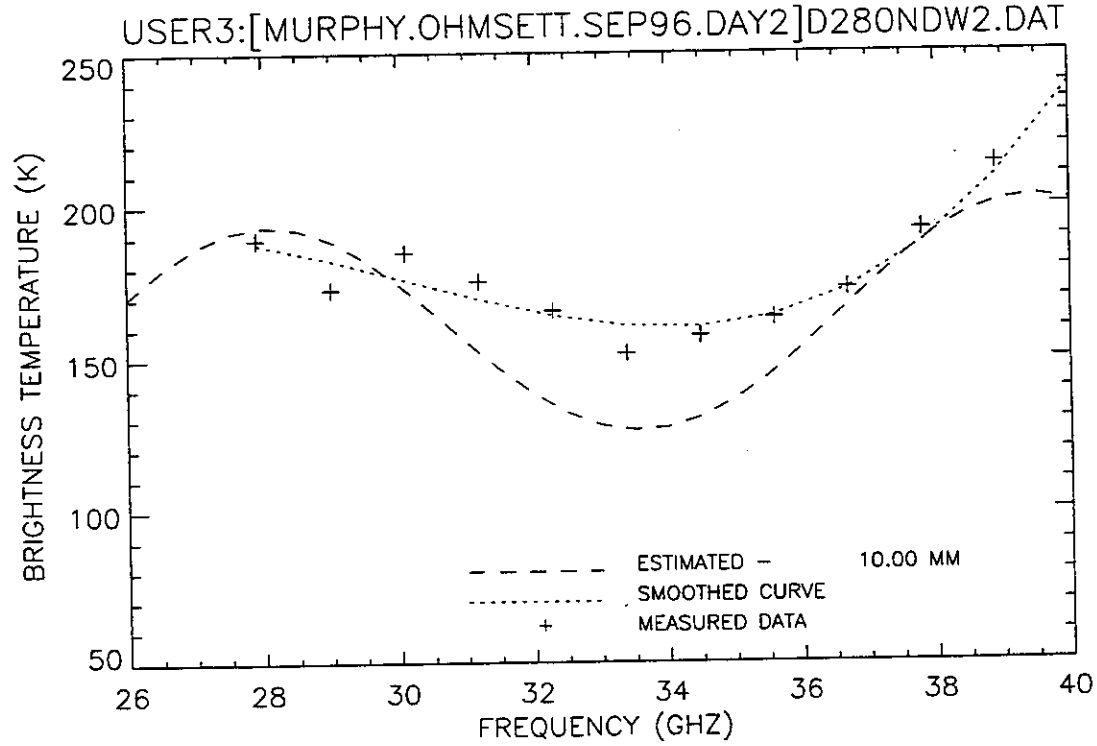

Figure 307. Plot of radiometric brightness temperature versus measurement frequency for 8-mm diesel oil, day 2 test, wave condition 2, 12 September 1996, sweep N.

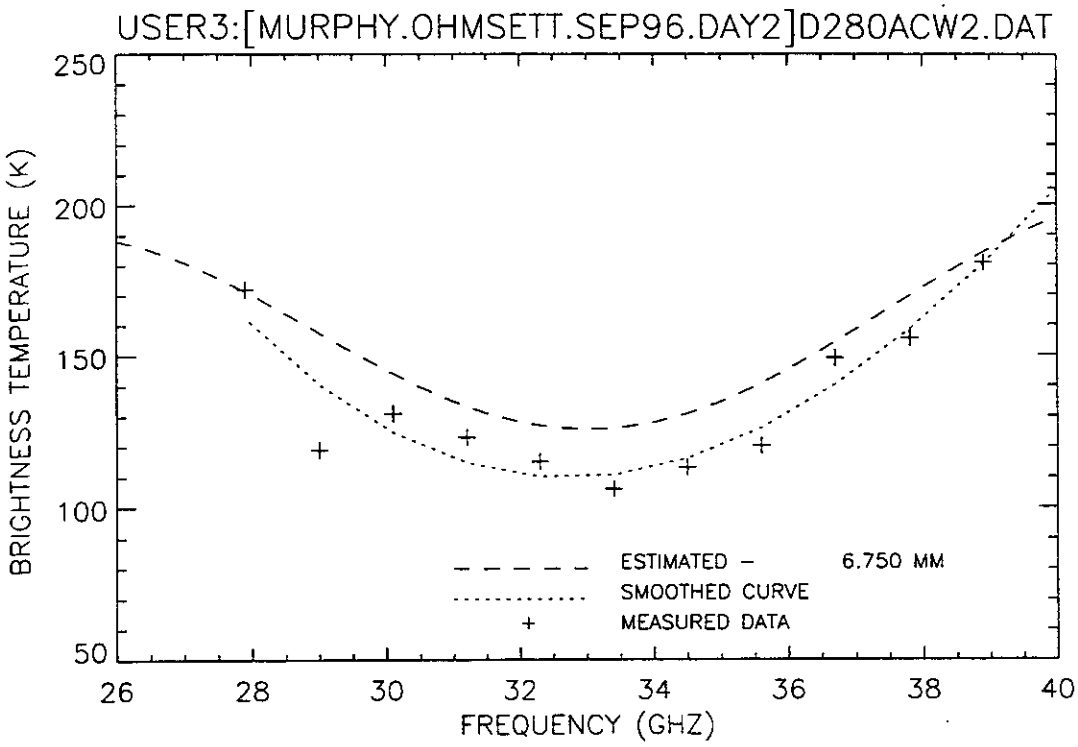

Figure 308. Plot of radiometric brightness temperature versus measurement frequency for 8-mm crude oil, day 2 test, wave condition 2, 12 September 1996, sweep A.

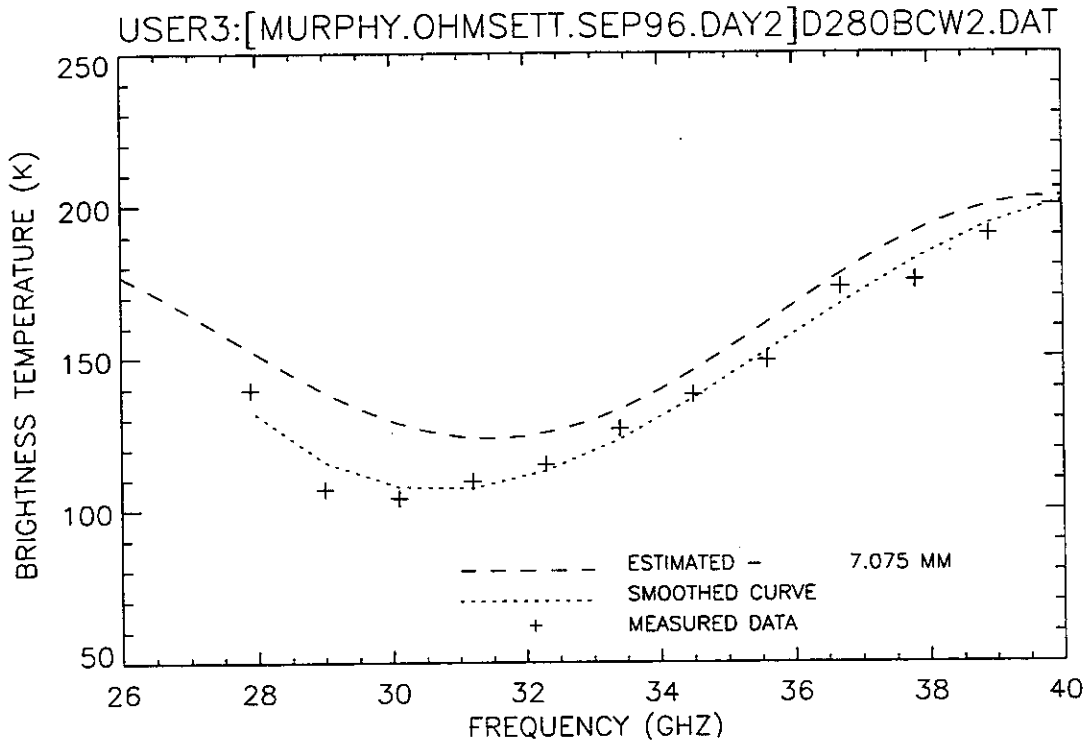

Figure 309. Plot of radiometric brightness temperature versus measurement frequency for 8-mm crude oil, day 2 test, wave condition 2, 12 September 1996, sweep B.

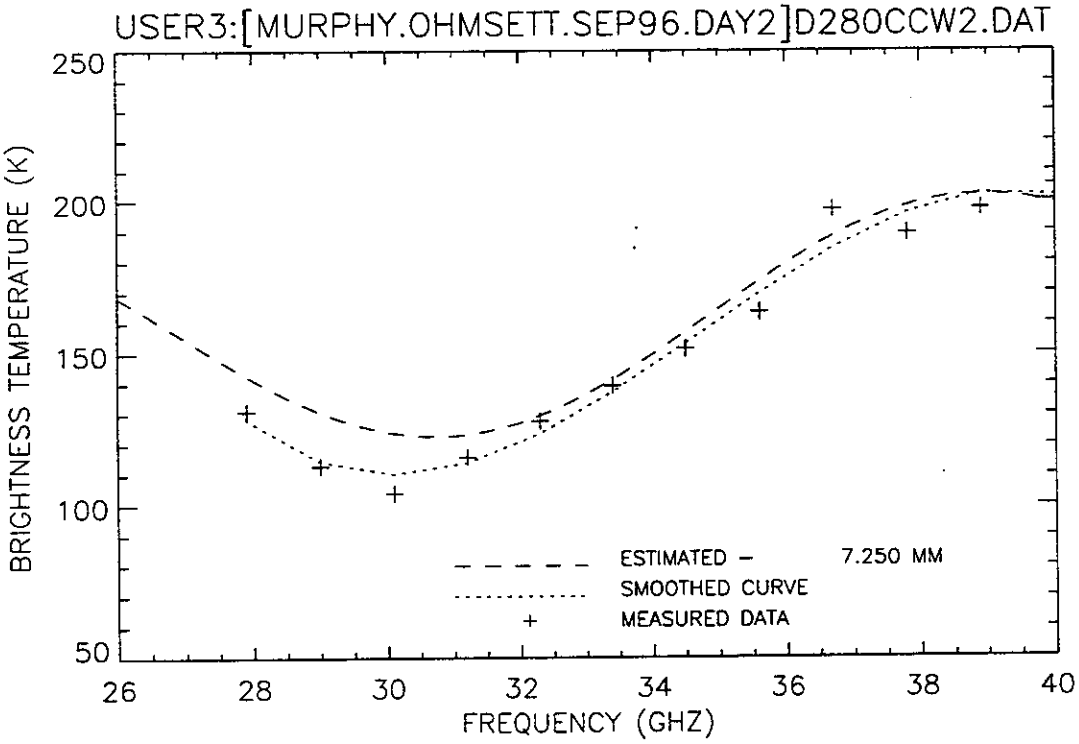

Figure 310. Plot of radiometric brightness temperature versus measurement frequency for 8-mm crude oil, day 2 test, wave condition 2, 12 September 1996, sweep C.

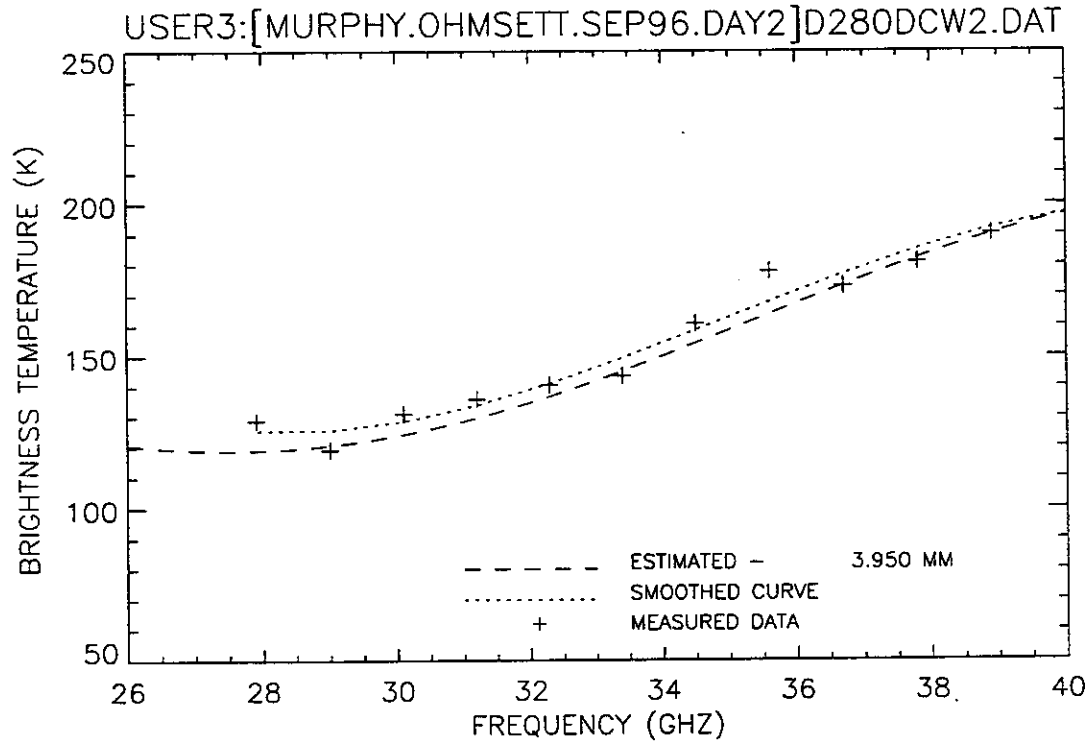

Figure 311. Plot of radiometric brightness temperature versus measurement frequency for 8-mm crude oil, day 2 test, wave condition 2, 12 September 1996, sweep D.

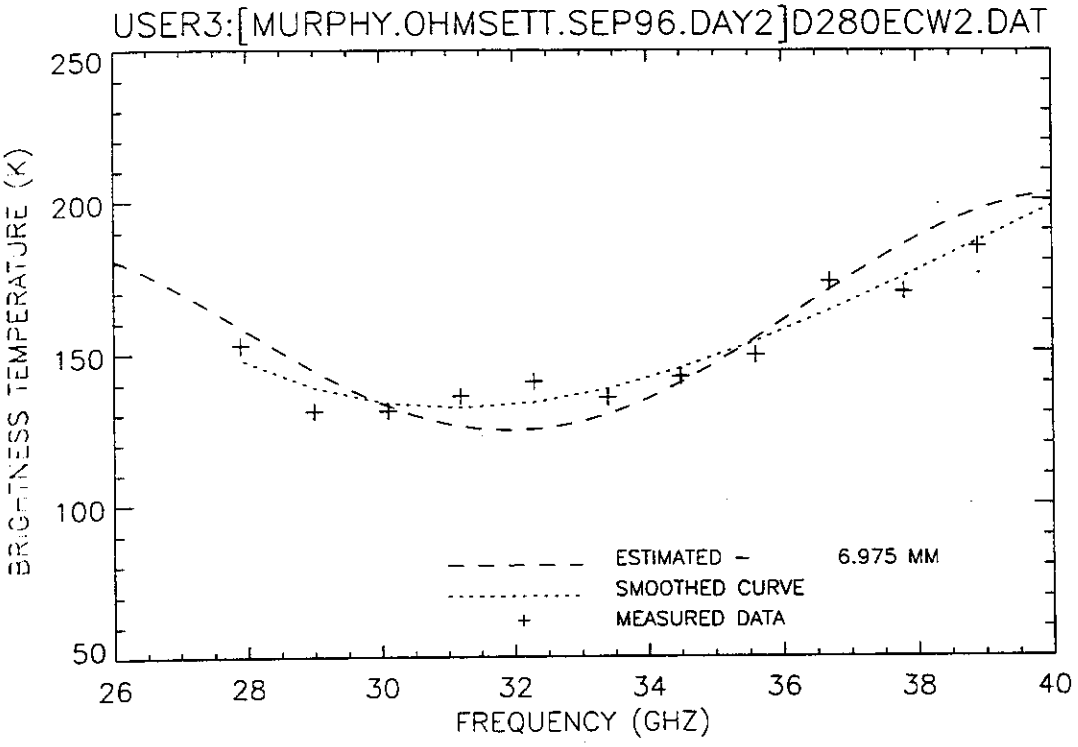

Figure 312. Plot of radiometric brightness temperature versus measurement frequency for 8-mm crude oil, day 2 test, wave condition 2, 12 September 1996, sweep E.

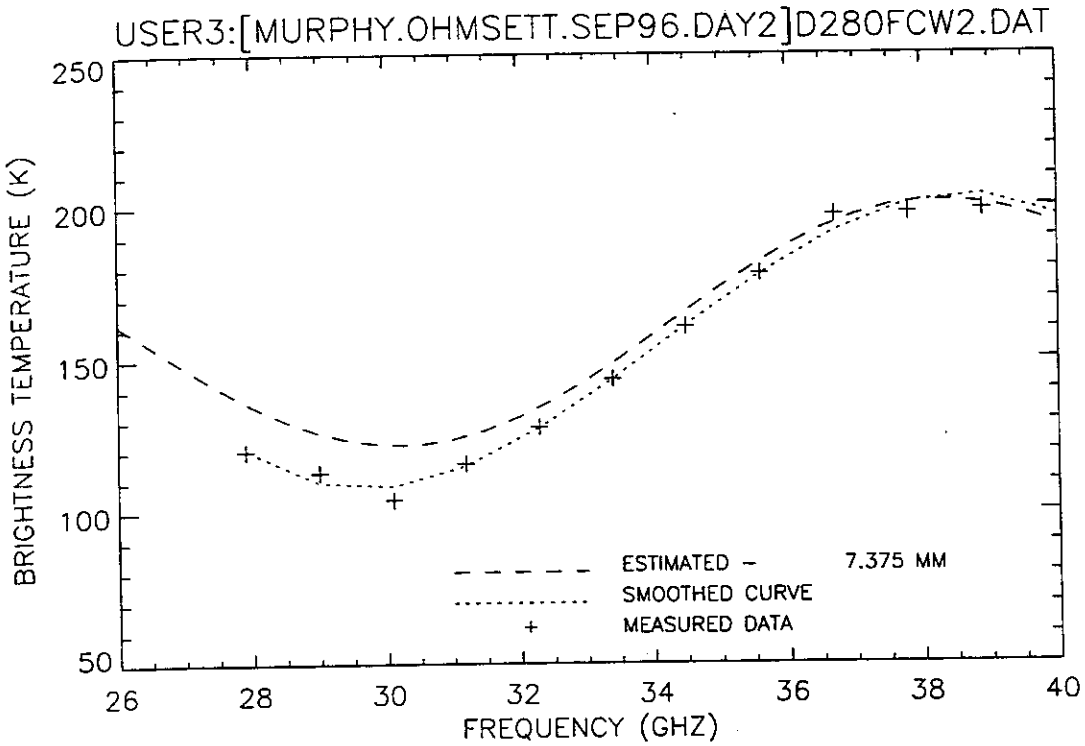

Figure 313. Plot of radiometric brightness temperature versus measurement frequency for 8-mm crude oil, day 2 test, wave condition 2, 12 September 1996, sweep F.

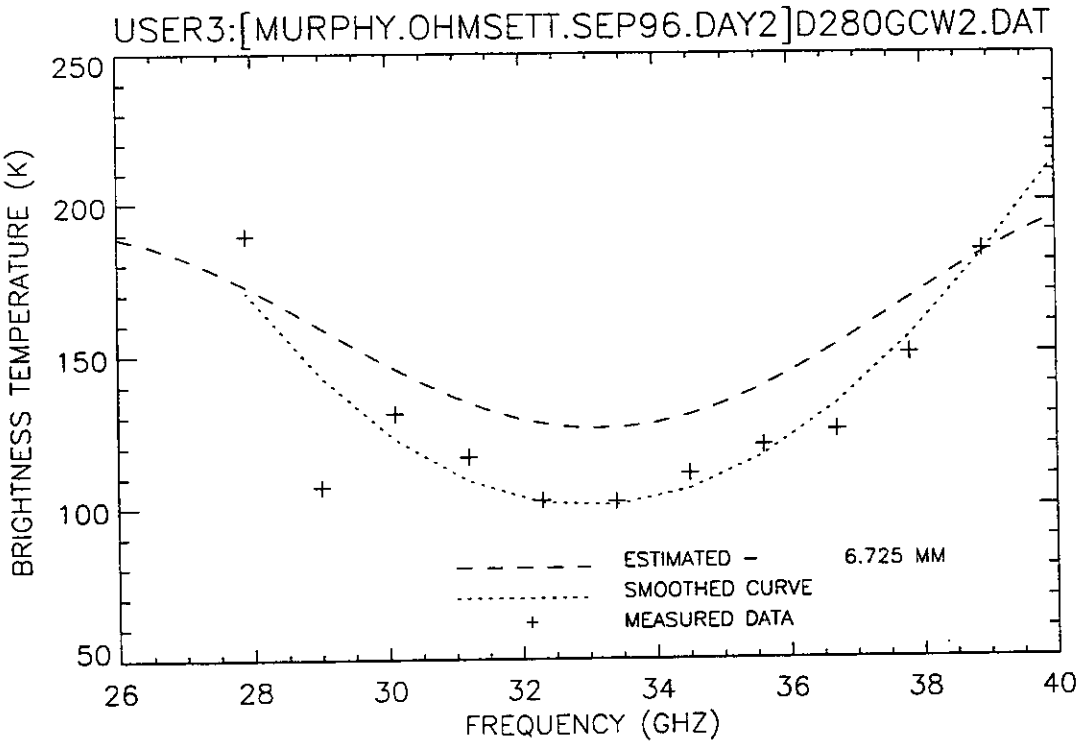

Figure 314. Plot of radiometric brightness temperature versus measurement frequency for 8-mm crude oil, day 2 test, wave condition 2, 12 September 1996, sweep G.

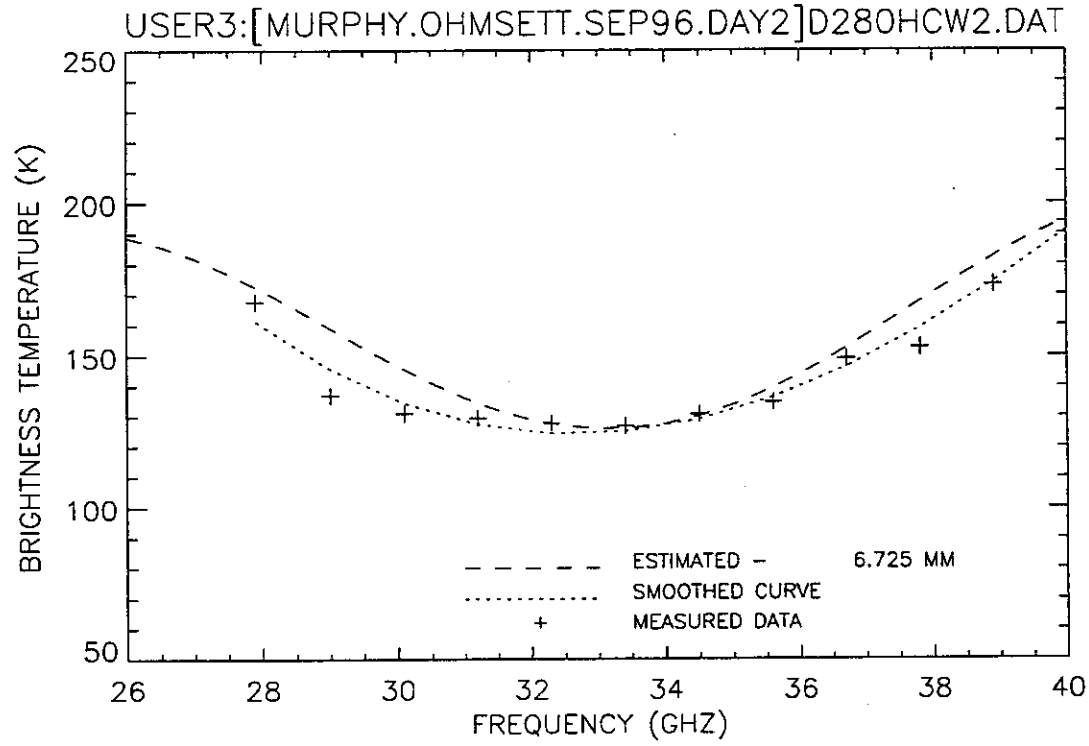

Figure 315. Plot of radiometric brightness temperature versus measurement frequency for 8-mm crude oil, day 2 test, wave condition 2, 12 September 1996, sweep H.

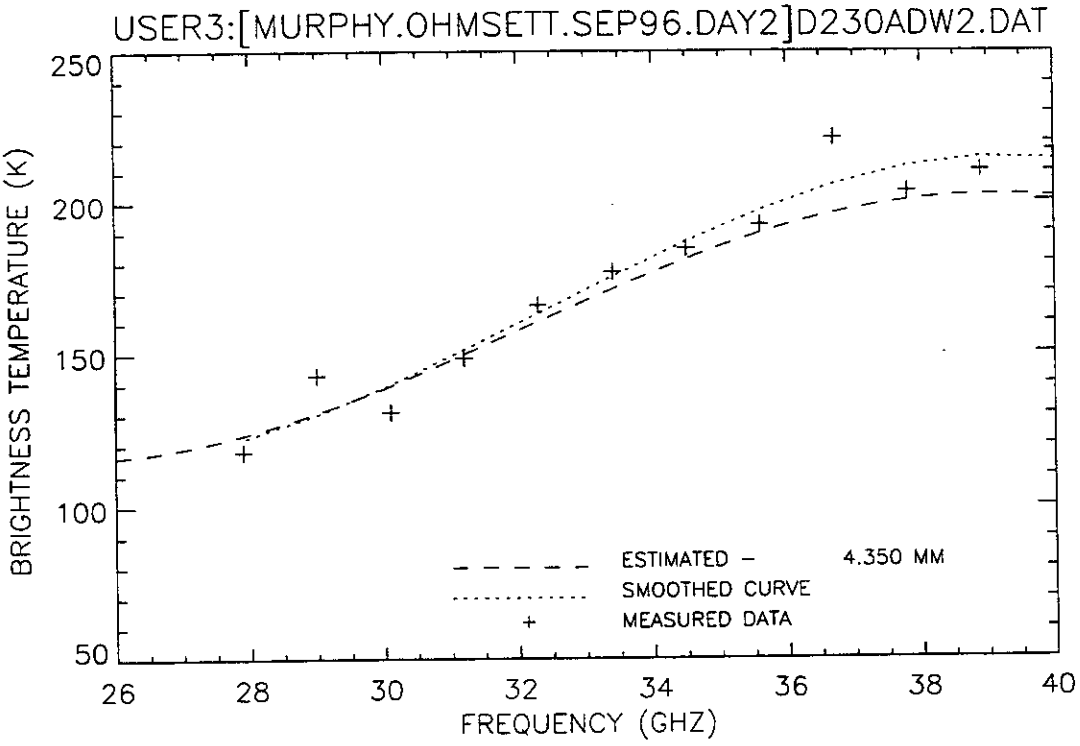

Figure 316. Plot of radiometric brightness temperature versus measurement frequency for 3-mm diesel oil, day 2 test, wave condition 2, 12 September 1996, sweep A.

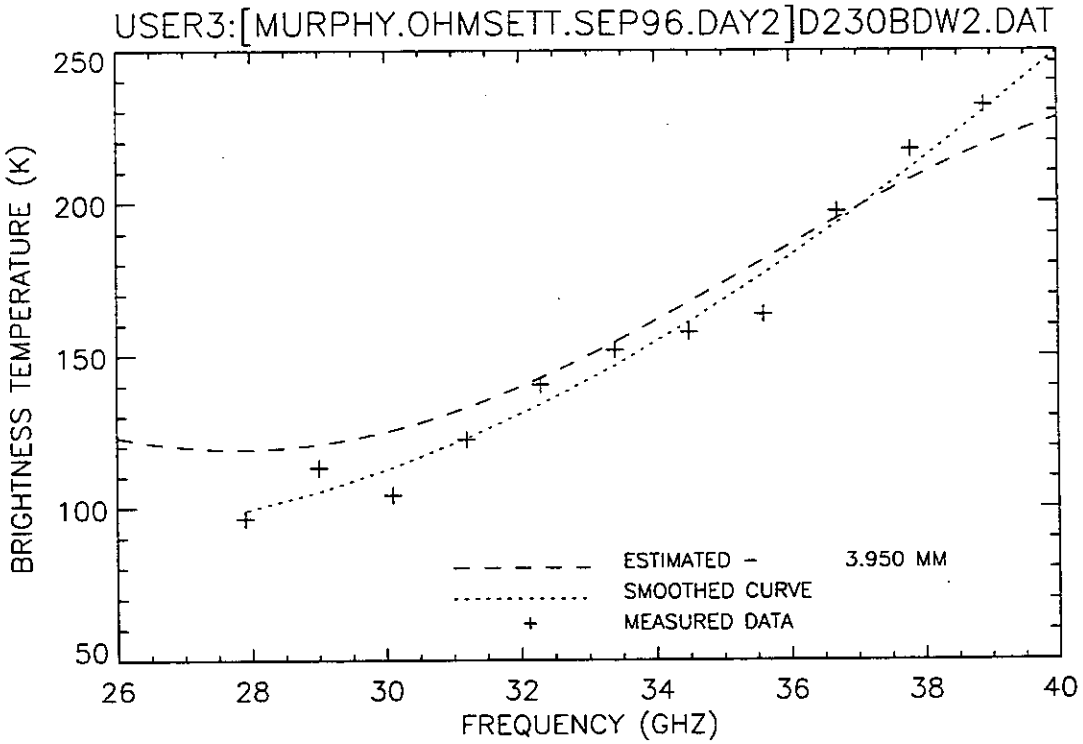

Figure 317. Plot of radiometric brightness temperature versus measurement frequency for 3-mm diesel oil, day 2 test, wave condition 2, 12 September 1996, sweep B.

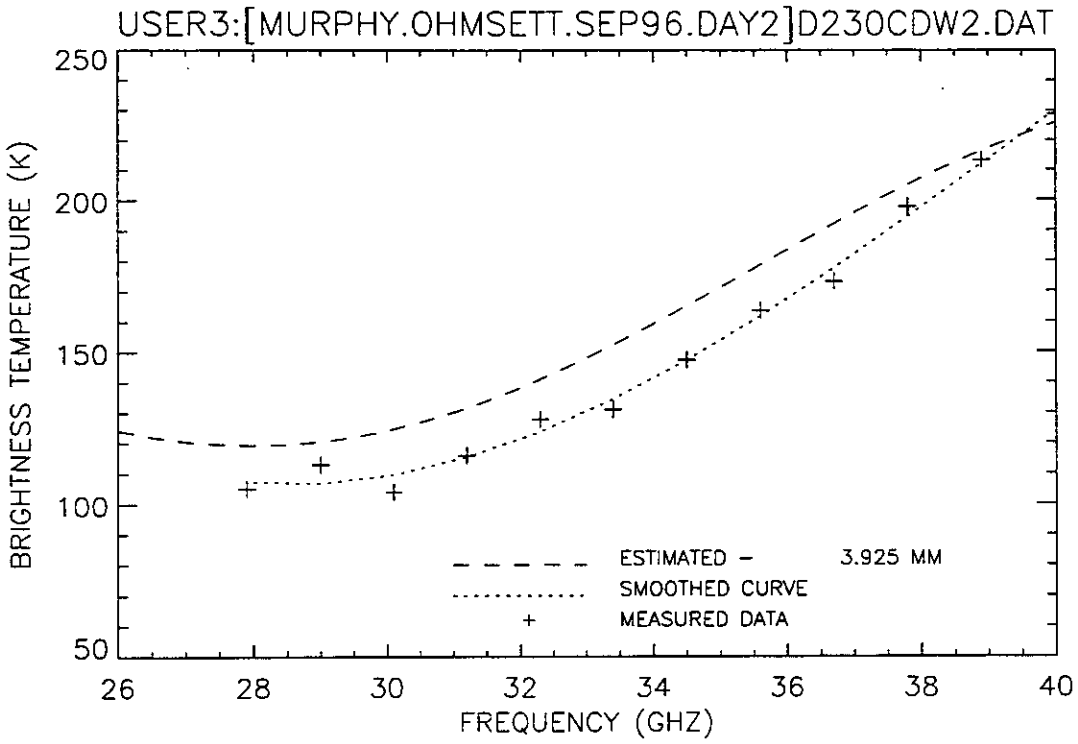

Figure 318. Plot of radiometric brightness temperature versus measurement frequency for 3-mm diesel oil, day 2 test, wave condition 2, 12 September 1996, sweep C.

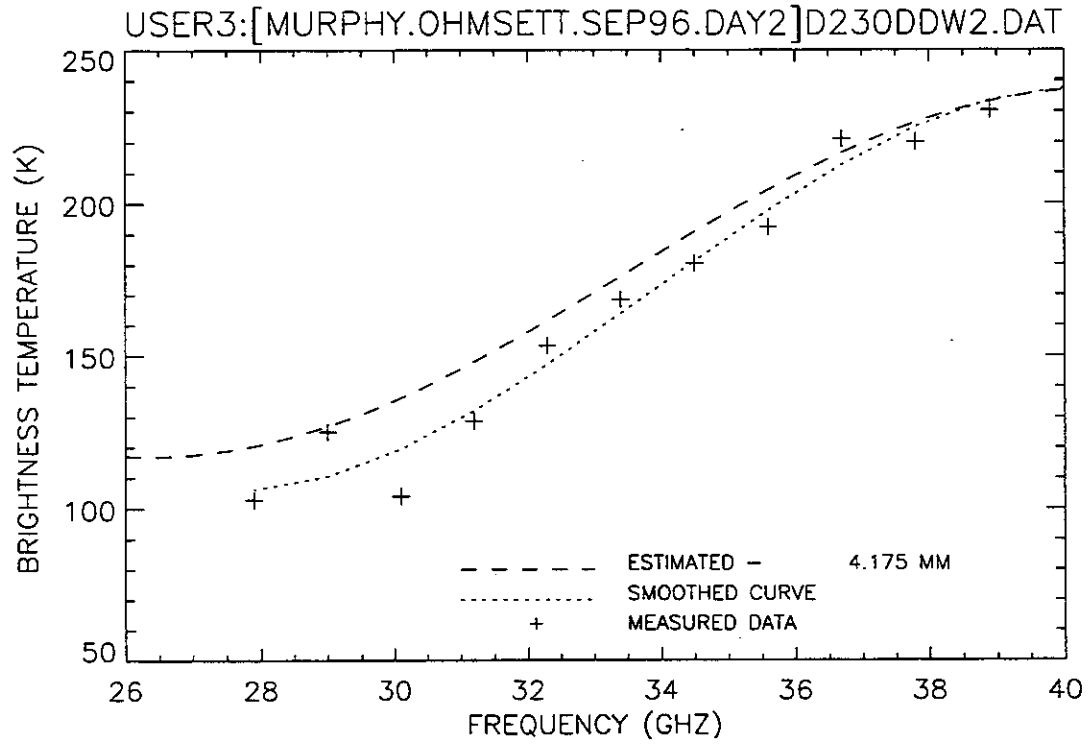

Figure 319. Plot of radiometric brightness temperature versus measurement frequency for 3-mm diesel oil, day 2 test, wave condition 2, 12 September 1996, sweep D.

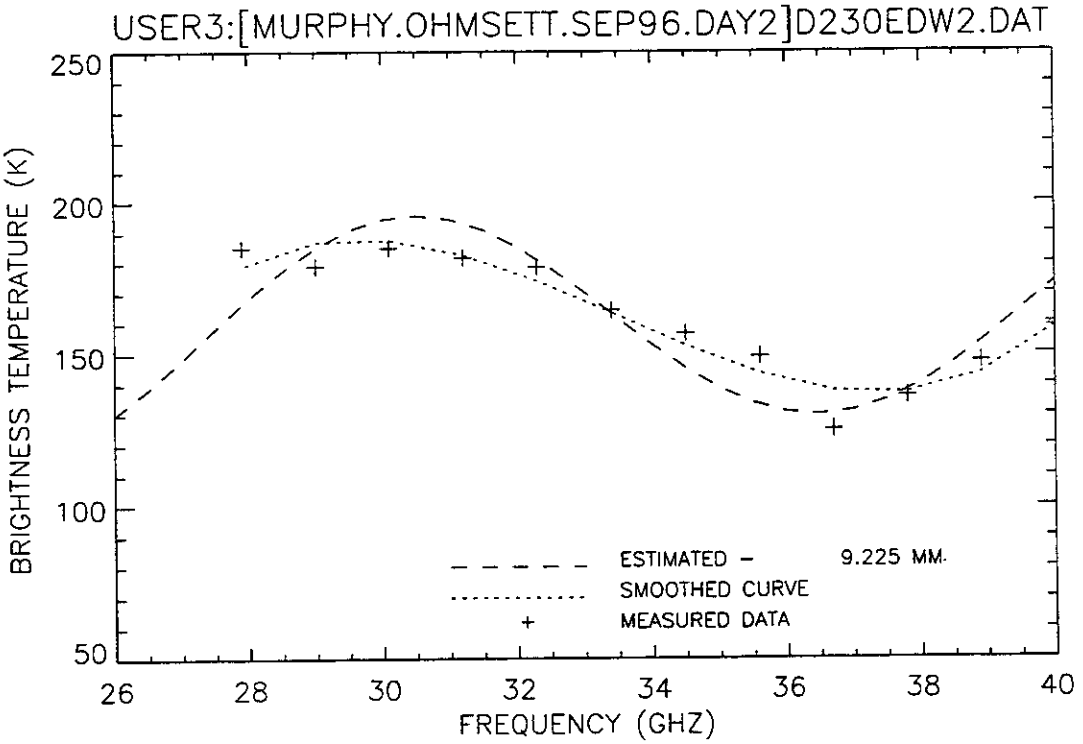

Figure 320. Plot of radiometric brightness temperature versus measurement frequency for 3-mm diesel oil, day 2 test, wave condition 2, 12 September 1996, sweep E.

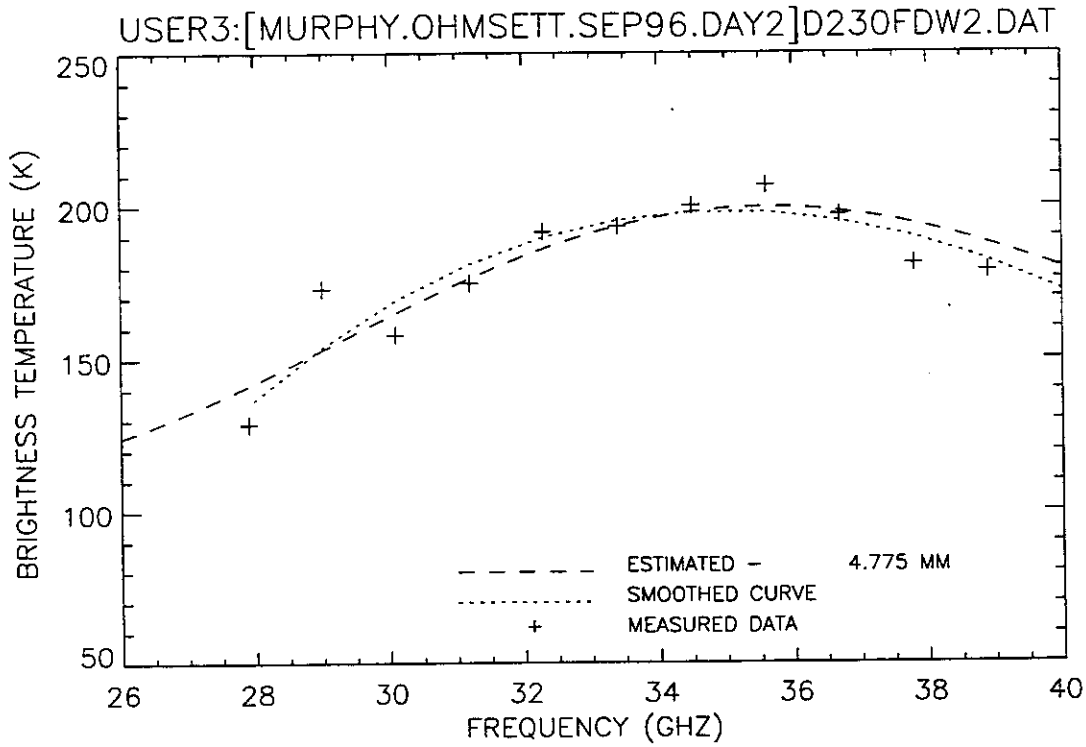

Figure 321. Plot of radiometric brightness temperature versus measurement frequency for 3-mm diesel oil, day 2 test, wave condition 2, 12 September 1996, sweep F.

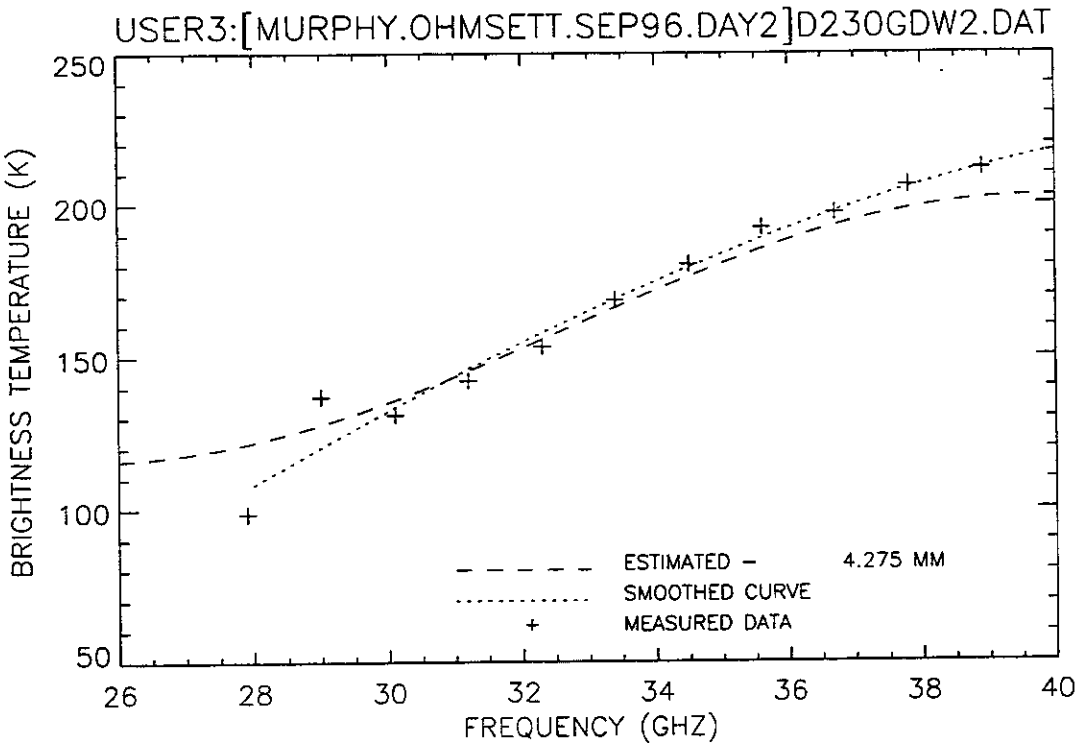

Figure 322. Plot of radiometric brightness temperature versus measurement frequency for 3-mm diesel oil, day 2 test, wave condition 2, 12 September 1996, sweep G.

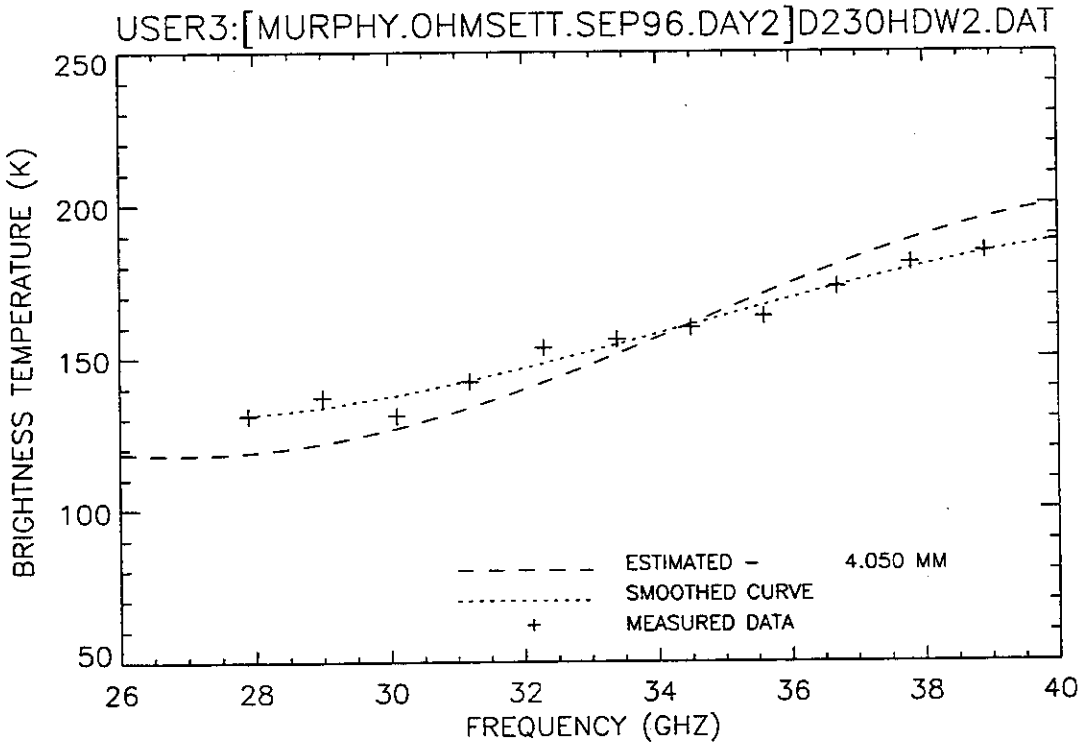

Figure 323. Plot of radiometric brightness temperature versus measurement frequency for 3-mm diesel oil, day 2 test, wave condition 2, 12 September 1996, sweep H.

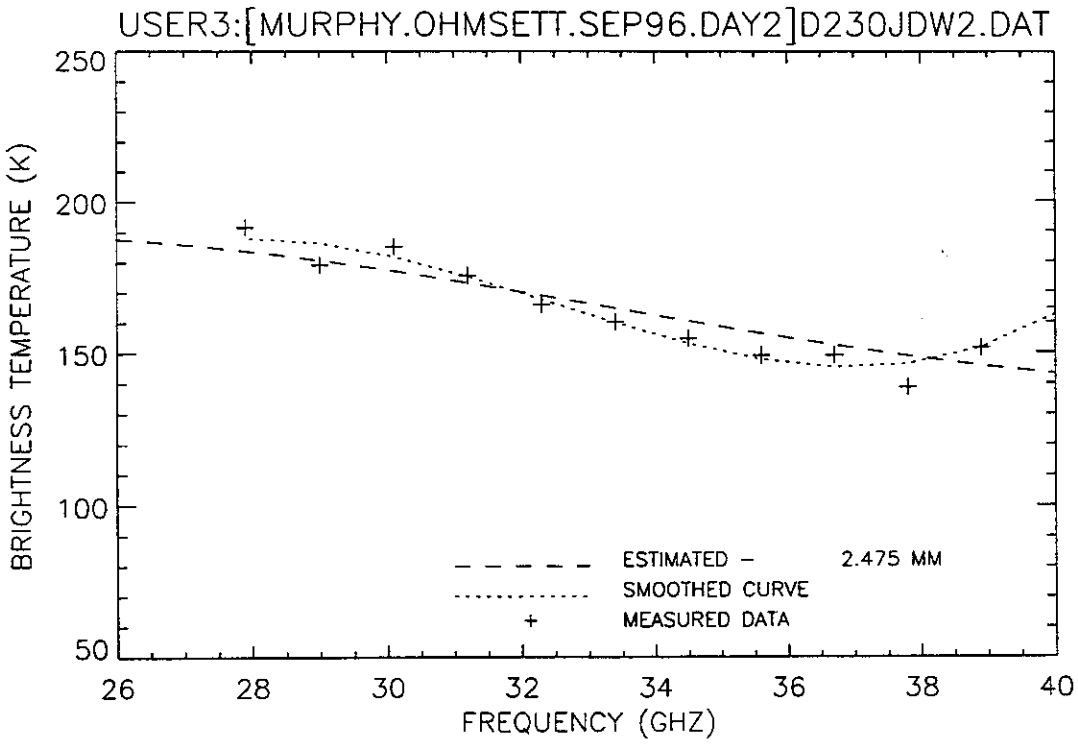

Figure 324. Plot of radiometric brightness temperature versus measurement frequency for 3-mm diesel oil, day 2 test, wave condition 2, 12 September 1996, sweep J.

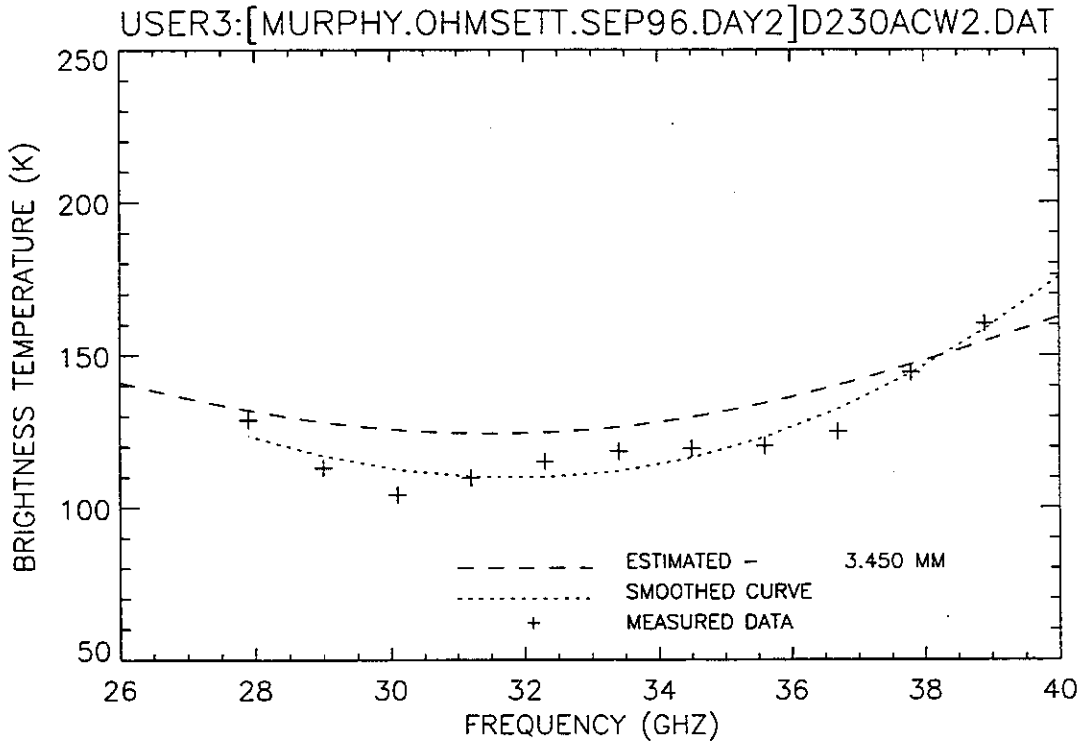

Figure 325. Plot of radiometric brightness temperature versus measurement frequency for 3-mm crude oil, day 2 test, wave condition 2, 12 September 1996, sweep A.

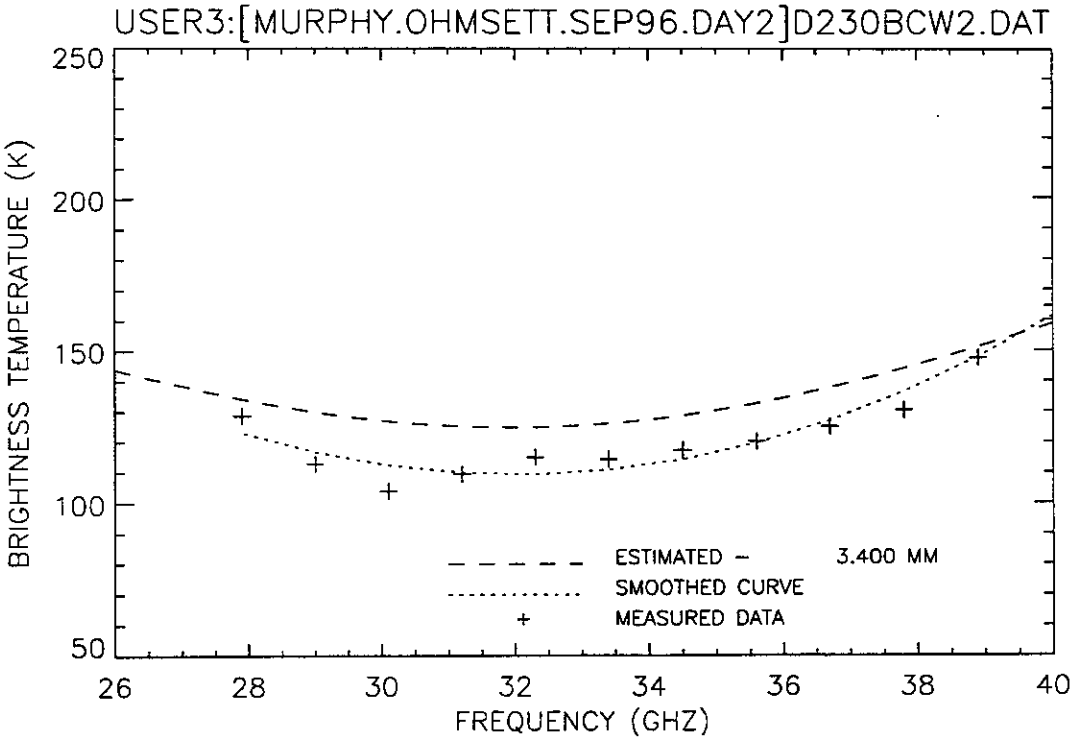

Figure 326. Plot of radiometric brightness temperature versus measurement frequency for 3-mm crude oil, day 2 test, wave condition 2, 12 September 1996, sweep B.

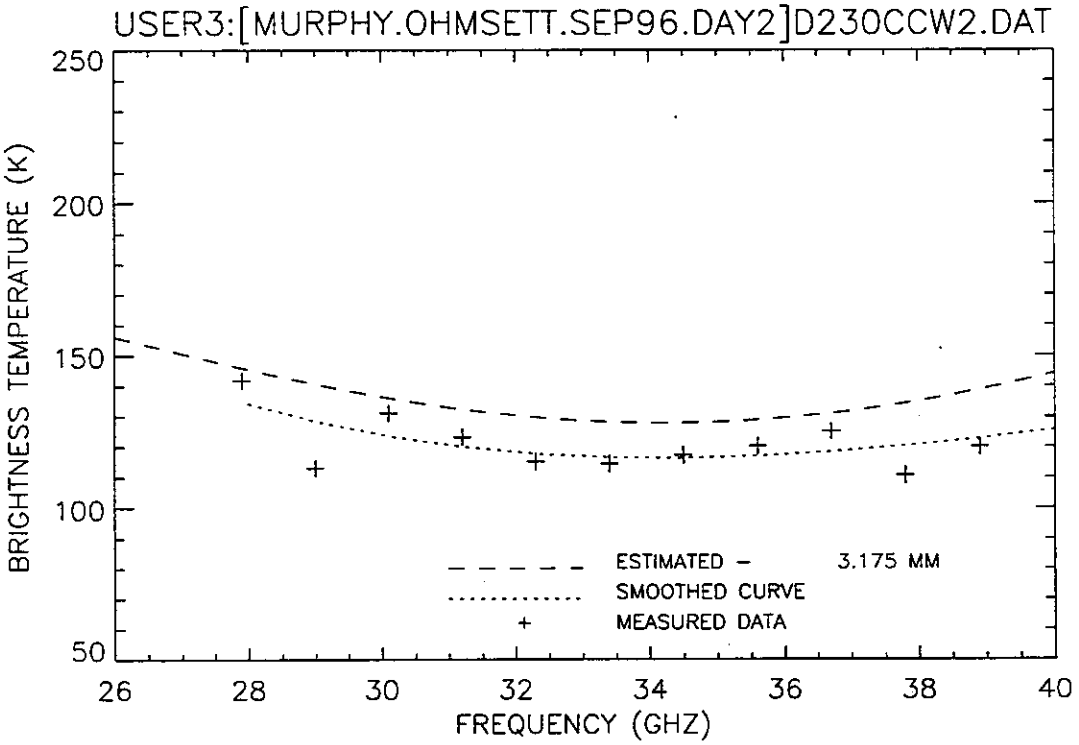

Figure 327. Plot of radiometric brightness temperature versus measurement frequency for 3-mm crude oil, day 2 test, wave condition 2, 12 September 1996, sweep C.

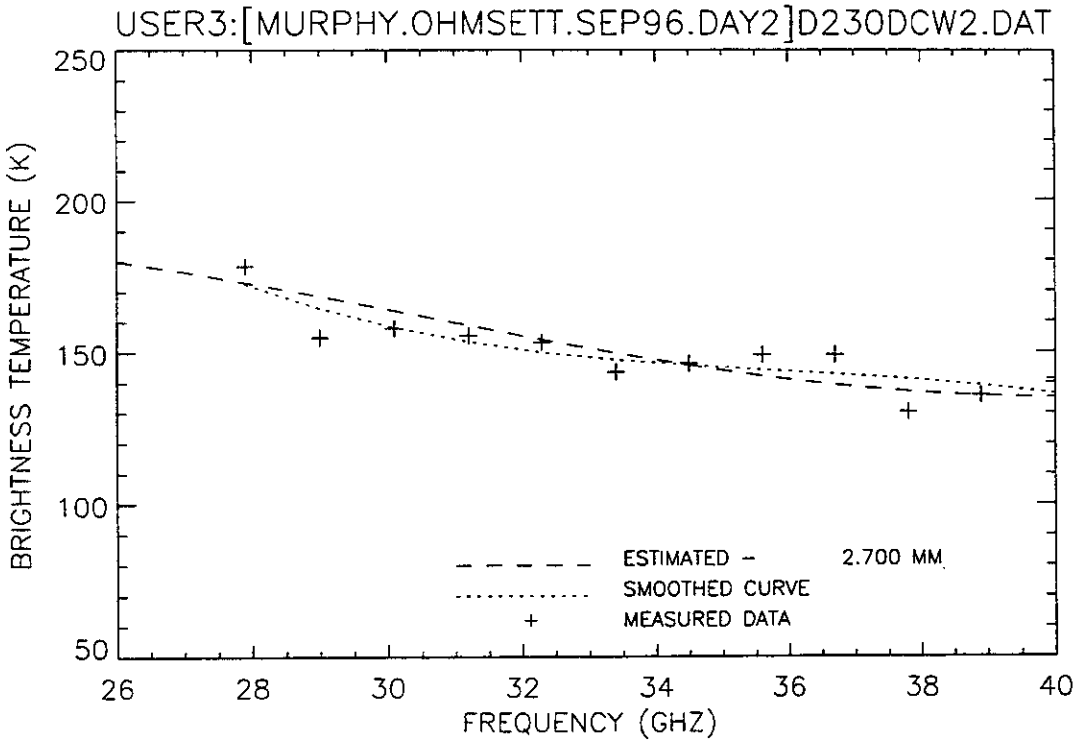

Figure 328. Plot of radiometric brightness temperature versus measurement frequency for 3-mm crude oil, day 2 test, wave condition 2, 12 September 1996, sweep D.

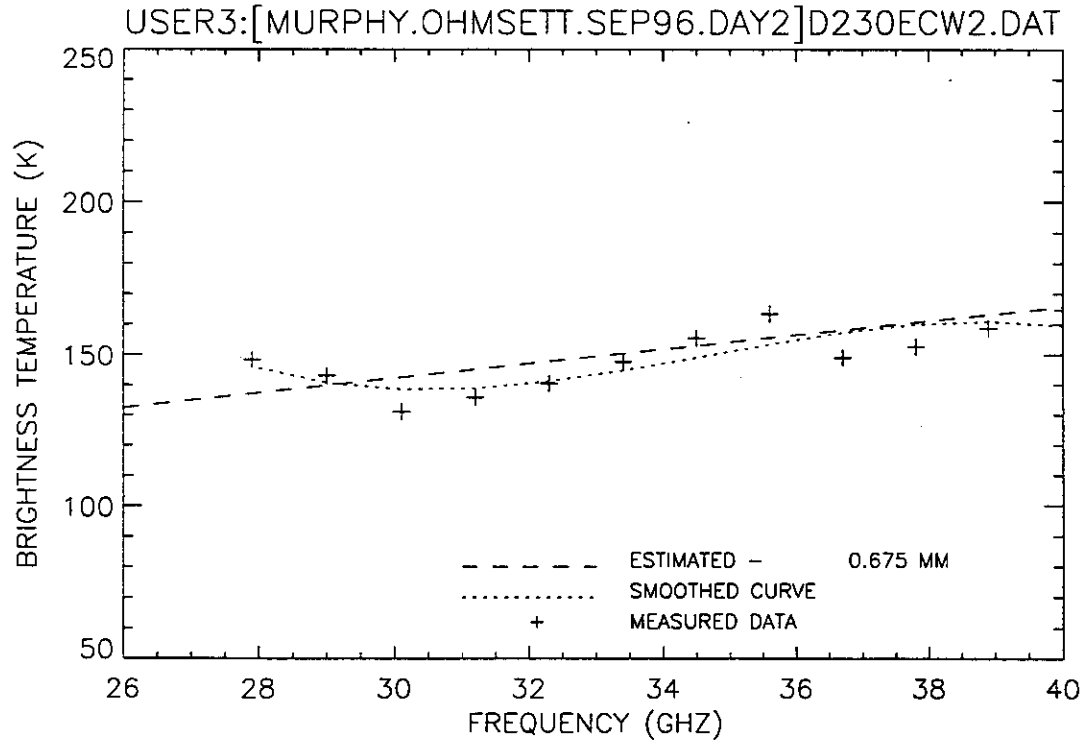

Figure 329. Plot of radiometric brightness temperature versus measurement frequency for 3-mm crude oil, day 2 test, wave condition 2, 12 September 1996, sweep E.

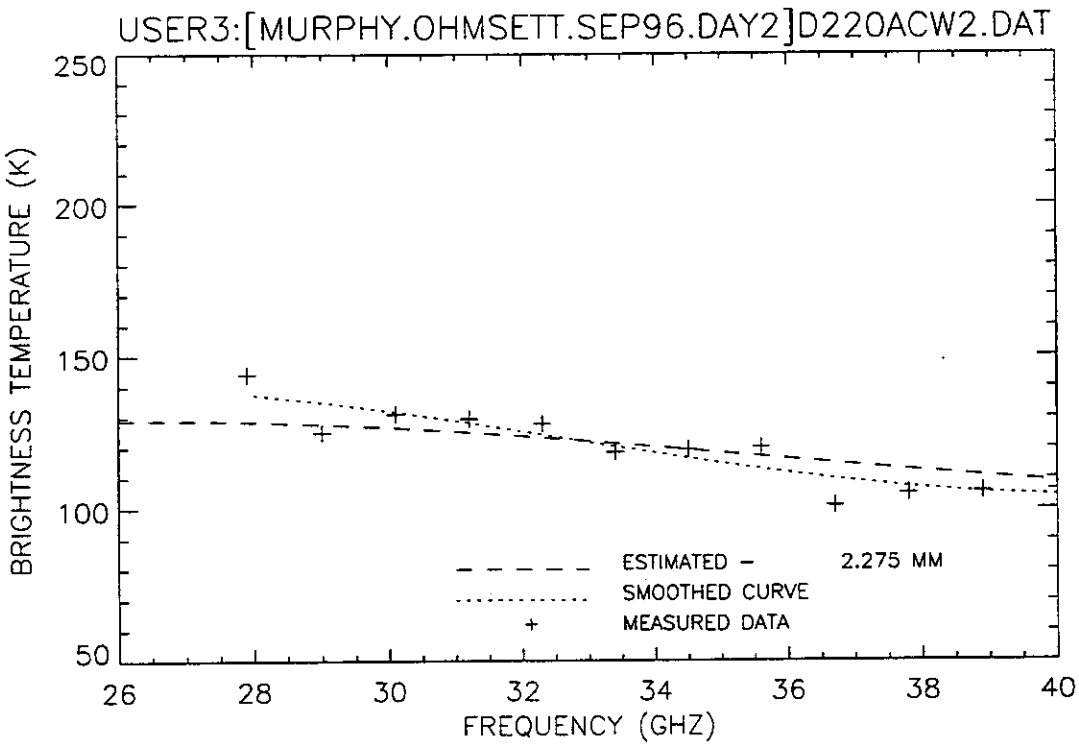

Figure 330. Plot of radiometric brightness temperature versus measurement frequency for 2-mm crude oil, day 2 test, wave condition 2, 12 September 1996, sweep A.

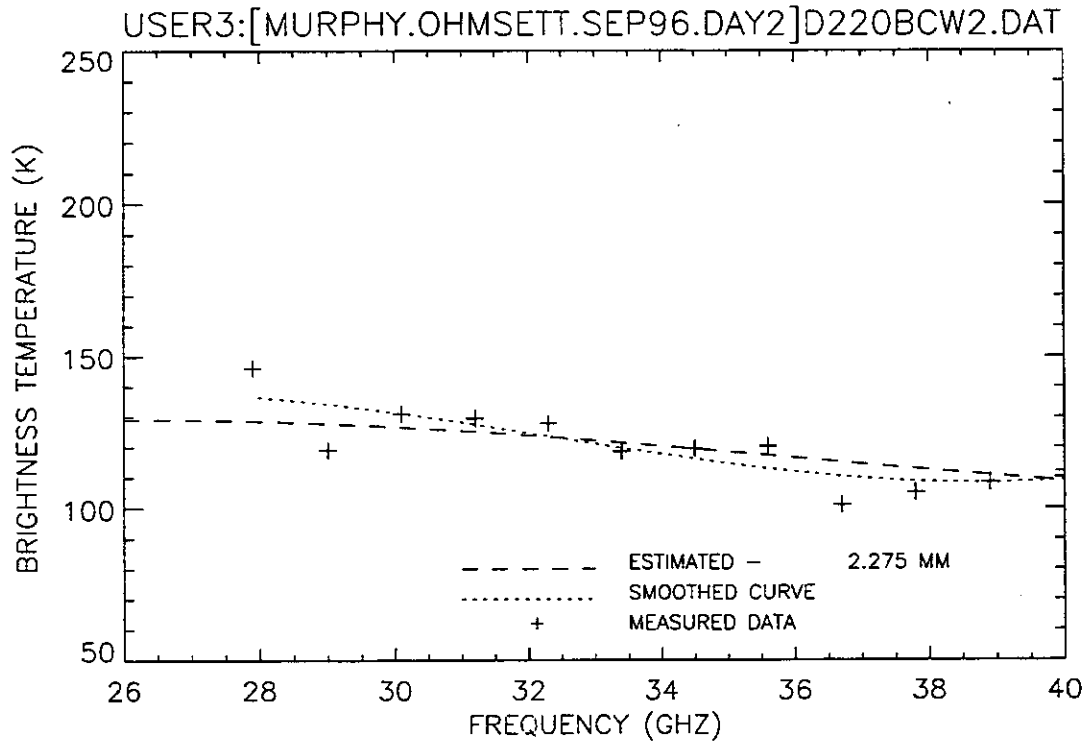

Figure 331. Plot of radiometric brightness temperature versus measurement frequency for 2-mm crude oil, day 2 test, wave condition 2, 12 September 1996, sweep B.

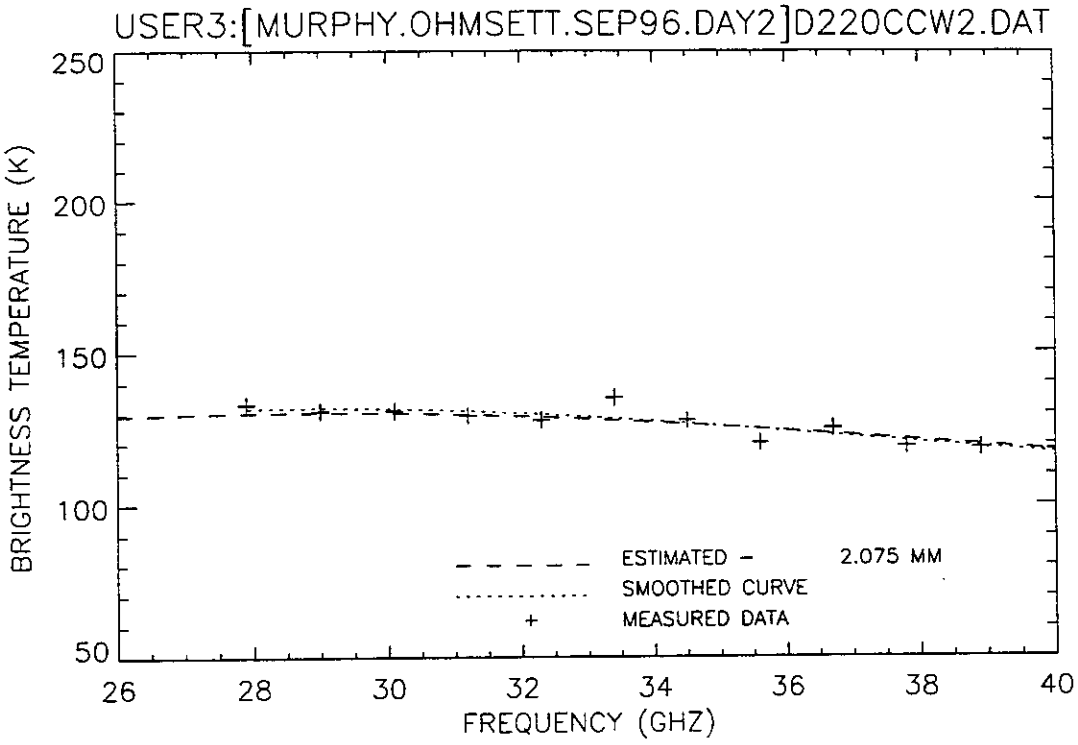

Figure 332. Plot of radiometric brightness temperature versus measurement frequency for 2-mm crude oil, day 2 test, wave condition 2, 12 September 1996, sweep C.

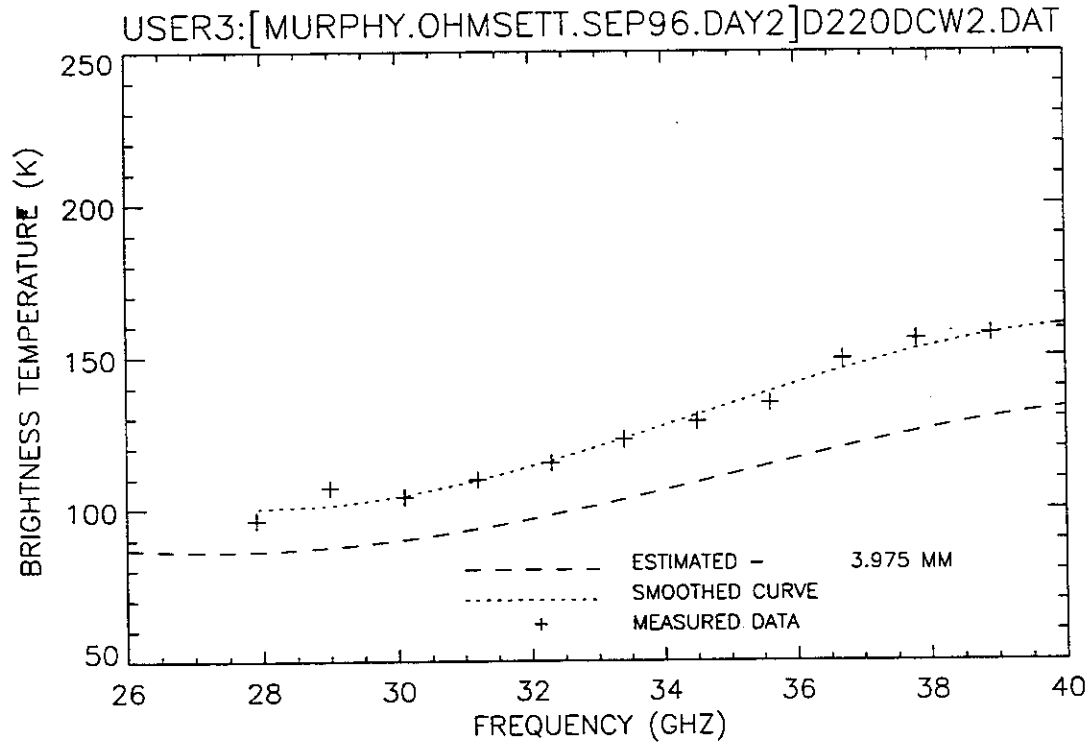

Figure 333. Plot of radiometric brightness temperature versus measurement frequency for 2-mm crude oil, day 2 test, wave condition 2, 12 September 1996, sweep D.

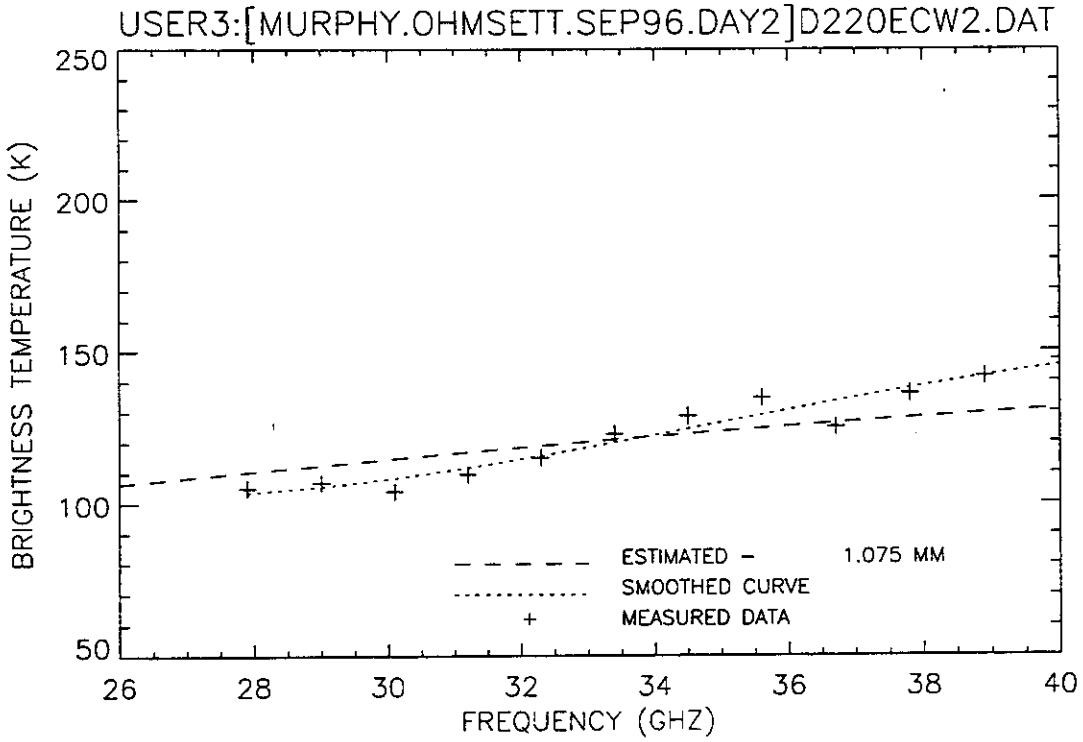

Figure 334. Plot of radiometric brightness temperature versus measurement frequency for 2-mm crude oil, day 2 test, wave condition 2, 12 September 1996, sweep E.

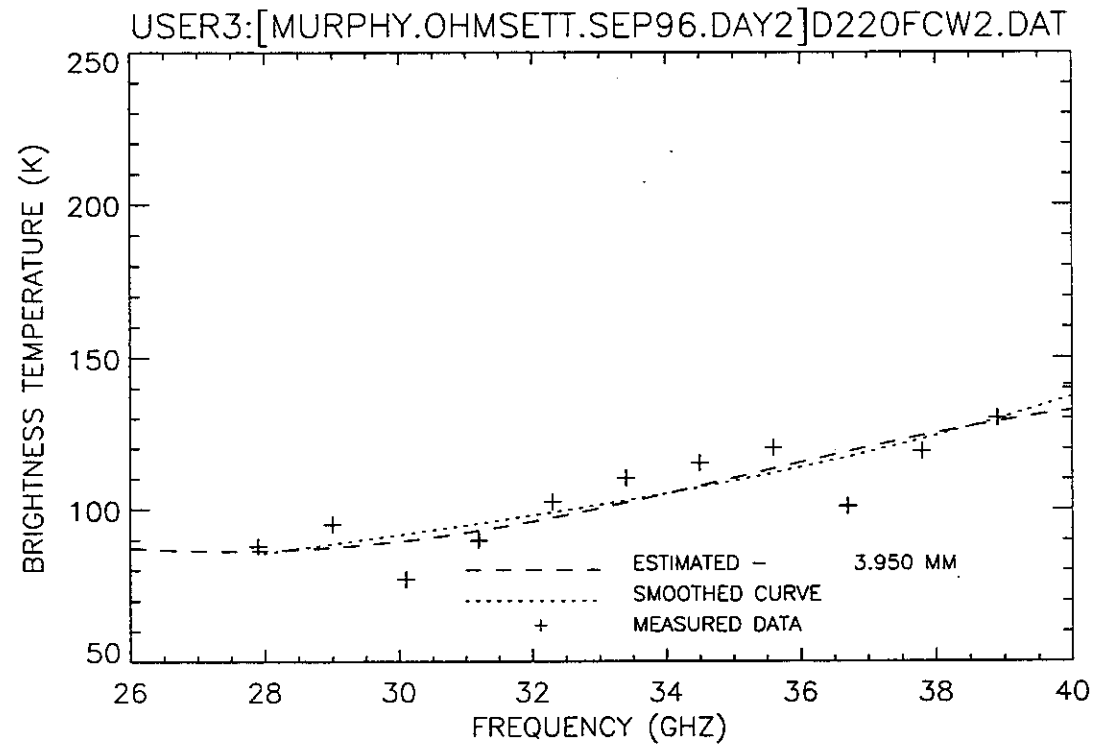

Figure 335. Plot of radiometric brightness temperature versus measurement frequency for 2-mm crude oil, day 2 test, wave condition 2, 12 September 1996, sweep F.

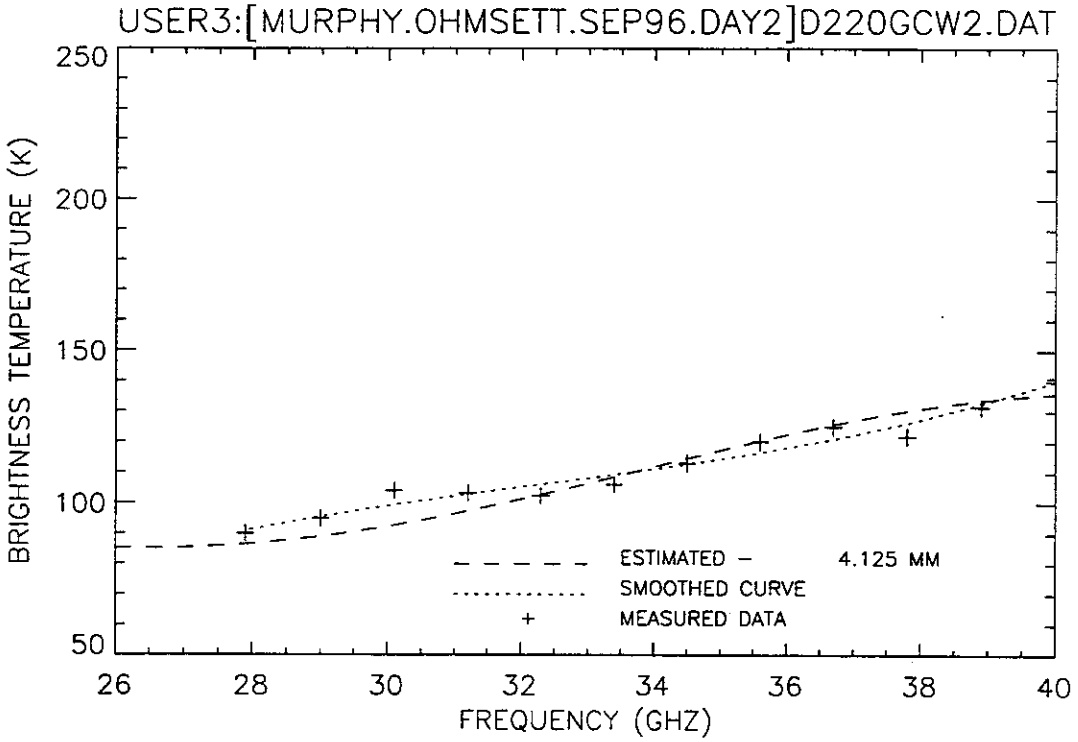

Figure 336. Plot of radiometric brightness temperature versus measurement frequency for 2-mm crude oil, day 2 test, wave condition 2, 12 September 1996, sweep G.

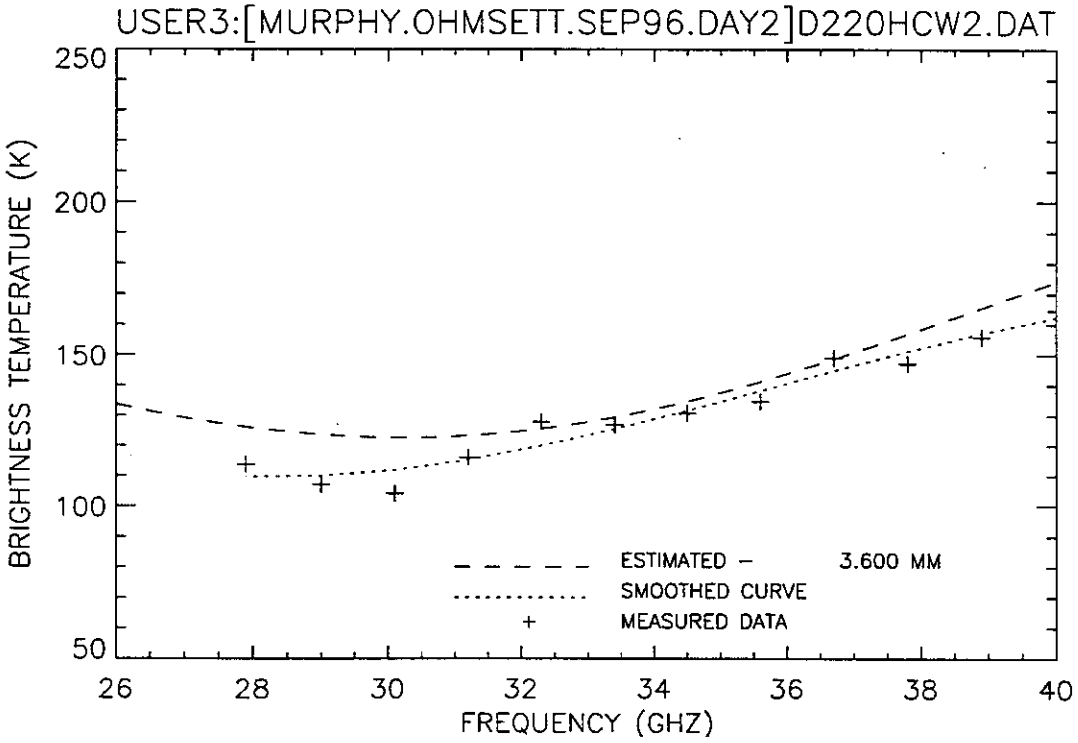

Figure 337. Plot of radiometric brightness temperature versus measurement frequency for 2-mm crude oil, day 2 test, wave condition 2, 12 September 1996, sweep H.

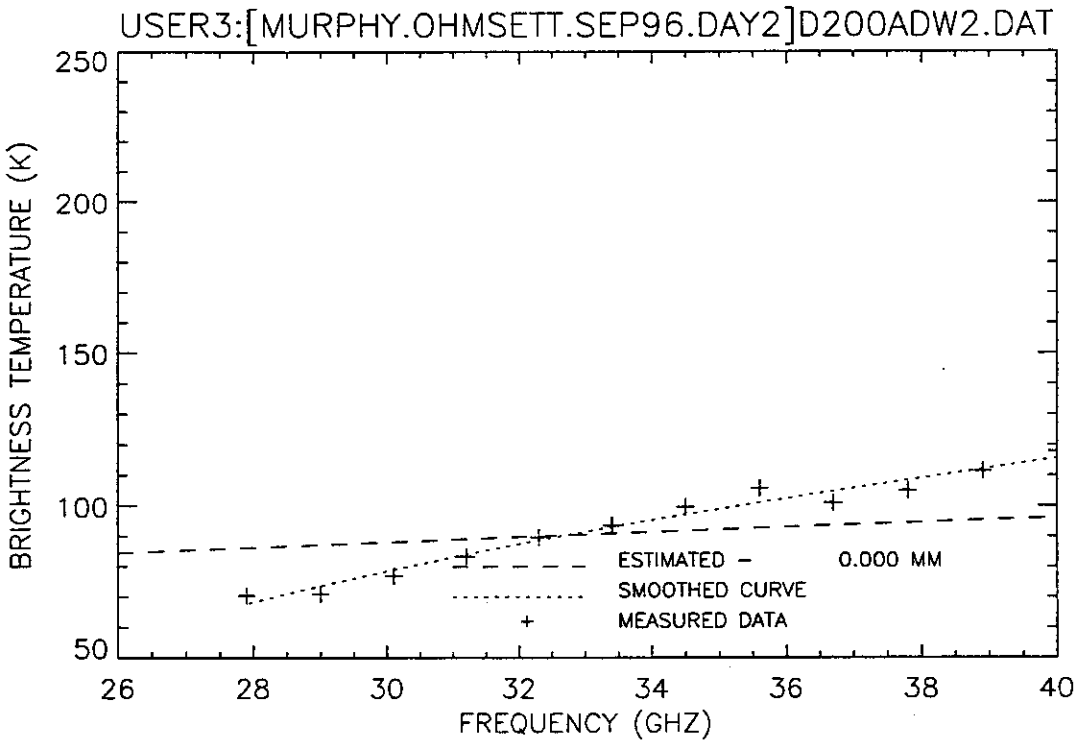

Figure 338. Plot of radiometric brightness temperature versus measurement frequency for water, day 2 test, wave condition 2, 12 September 1996, sweep A.

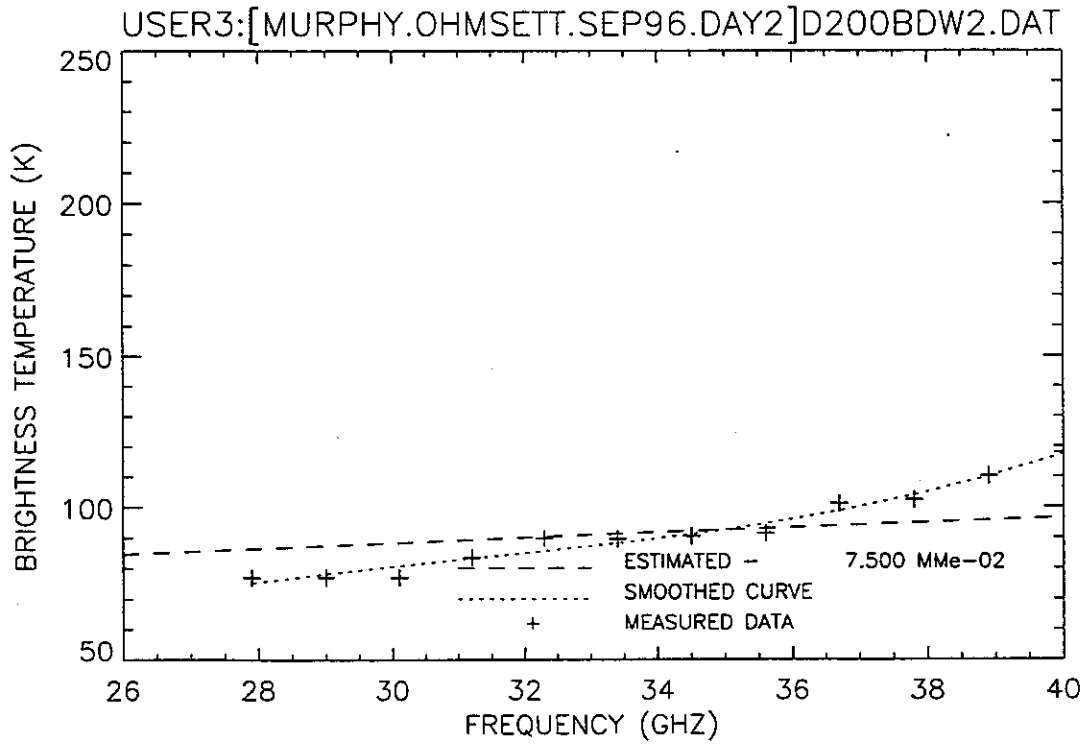

Figure 339. Plot of radiometric brightness temperature versus measurement frequency for water, day 2 test, wave condition 2, 12 September 1996, sweep B.

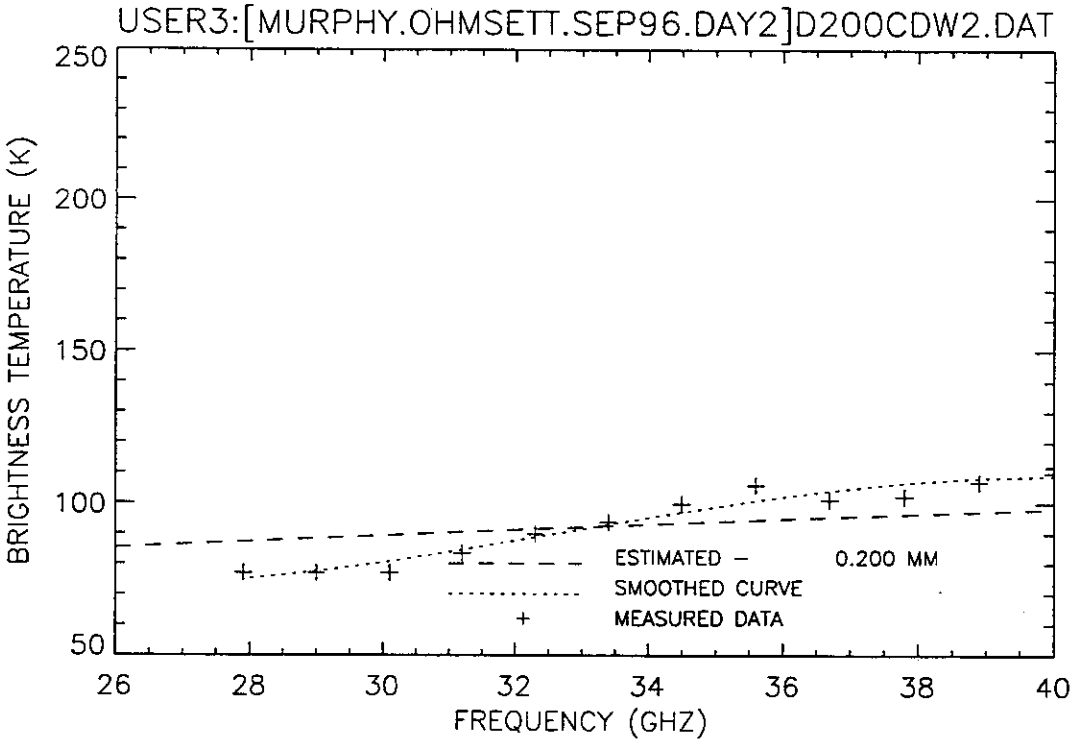

Figure 340. Plot of radiometric brightness temperature versus measurement frequency for water, day 2 test, wave condition 2, 12 September 1996, sweep C.

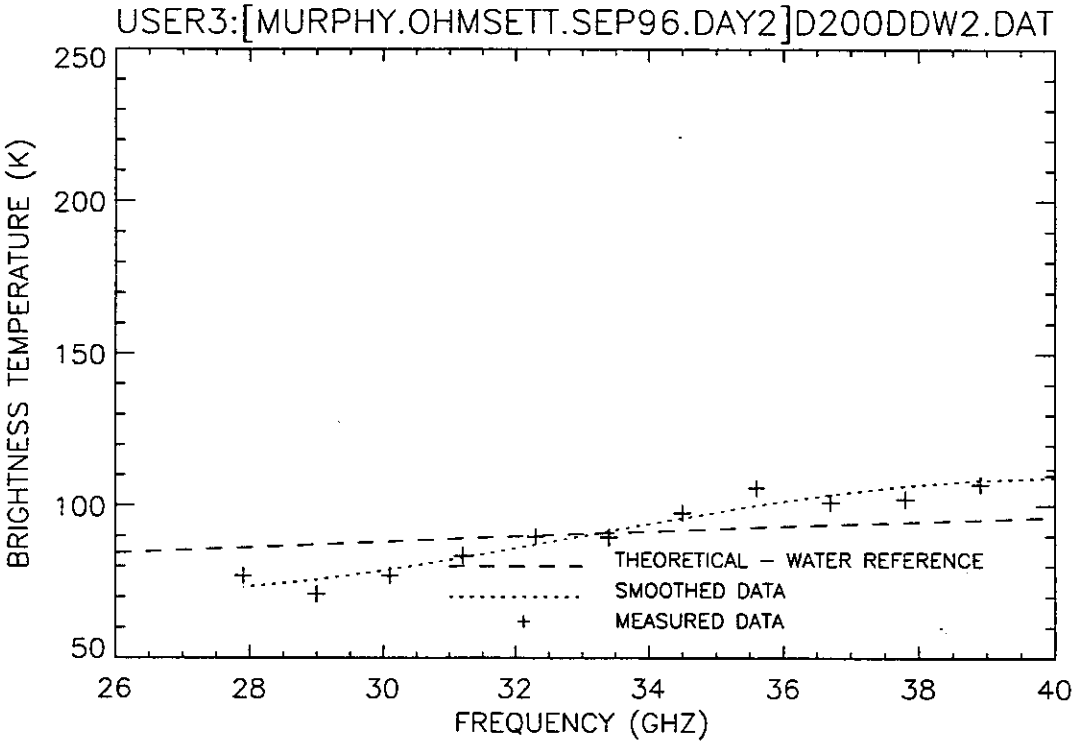

Figure 341. Plot of radiometric brightness temperature versus measurement frequency for water, day 2 test, wave condition 2, 12 September 1996, sweep D.

The wave generator was reset to produce chop condition 1, using a stroke of 1.5 in. and a frequency of 30 cycles/min. The main bridge was positioned over the 8-mm diesel oil target. The following measurements were collected as the chop condition built up to steady state. The reference temperature was adjusted during the postcollection analysis; additionally, the gain factor of the theoretical predictions was decreased by 50% based on the observation that the peak-to-trough amplitude was lower than expected.

Table 7 contains the results of the following chop condition data analysis.

D8A.DAT – The algorithm estimate of 6.975 mm, shown in Figure 342, is a good-to-excellent match to the measured data.

D8B.DAT – The algorithm estimate of 6.675 mm, shown in Figure 343, is a good-to-excellent match to the measured data.

D8C.DAT – The algorithm estimate of 6.850 mm, shown in Figure 344, is a good match to the measured data.

D8D.DAT – The algorithm estimate of 7.275 mm, shown in Figure 345, is a good match to the measured data.

D8E.DAT – The algorithm estimate of 7.150 mm, shown in Figure 346, is a good-to-excellent match to the measured data.

D8F.DAT – The algorithm estimate of 6.950 mm is a fair match to the measured data. A thicker estimate of 7.200 mm with a slightly different gain factor (75%), shown in Figure 347, produces a good shape match.

D8G.DAT – The algorithm estimate of 7.150 mm, shown in Figure 348, is a good match to the measured data.

D8H.DAT – The algorithm estimate of 4.050 mm is a poor match to the measured data. An estimate of 8.000 mm, shown in Figure 349, produces a fair match to the measured data, if the smoothed curve is ignored.

The chop condition had reached steady state. The aimpoint on the oil target remained unchanged.

D8J.DAT – The algorithm estimate of 6.925 mm, shown in Figure 350, is a good-to-excellent match to the measured data.

D8K.DAT – The algorithm estimate of 6.900 mm is a fair match to the measured data. If a slightly thinner estimate is chosen, namely 6.700 mm shown in Figure 351, the shape of the theoretical prediction more closely matches the measured data.

D8L.DAT – The algorithm estimate of 6.875 mm is a fair match to the measured data. If a slightly thicker estimate is chosen, namely 7.200 mm shown in Figure 352, the shape of the theoretical prediction more closely matches the measured data.

The wave generator was reset to produce the chop 2 condition, using a stroke of 1.5 in. and a frequency of 40 cycles/min. After the chop condition reached steady state, measurements continued. The radiometer position was shifted to collect measurements slightly east of center.

The water background reference temperature was adjusted for this analysis to account for a change in the radiometer gain characteristics. The gain factor was reset for unity (100%) unless specified otherwise.

D280ADC2.DAT – The algorithm estimate of 1.050 mm, shown in Figure 353, is a good match to the measured data.

D280BDC2.DAT – The algorithm estimate of 1.100 mm, shown in Figure 354, is a good match to the measured data.

D280CDC2.DAT – The algorithm estimate of 0.950 mm is a poor match to the measured data, which seem to indicate a thicker oil film. The 8.500-mm estimate, shown in Figure 355, is a poor-to-fair match to the data points between 30 and 37 GHz when using a 50% reduction in the amplitude of the theoretical response.

Water and air bubbles were forming on the oil target surface.

D280DDC2.DAT – The algorithm estimate of 0.875 mm is a poor match to the measured data, which seem to indicate a thicker oil film. The 8.500-mm estimate, shown in Figure 356, is a poor-to-fair match to the data points between 30 and 37 GHz when using a 50% reduction in the amplitude of the theoretical response.

TABLE 7

Results of the 12 September 1996 Day 2 Test

FILENAME	LMS	CORR	MN/SL	DECL	METHOD	VISUAL	COMMENT
D200AWC2.DAT	0.000	3.200	0.000	0.000	LMS & MN/SL	0.000	Poor
D200BWC2.DAT	0.000	3.325	0.000	0.000	LMS & MN/SL	0.000	Poor
D200CWC2.DAT	0.000	3.100	0.000	0.000	LMS & MN/SL	0.000	Poor
D200DWC2.DAT	0.000	3.150	0.000	0.000	LMS & MN/SL	0.000	Poor
D200EWC2.DAT	3.675	3.750	3.600	3.700	LMS & CORR	3.700	Good
D200FWC2.DAT	3.725	7.225	0.520	3.725	LMS only	3.725	Good
D200GWC2.DAT							Water reference
New water reference assumed							
D280ACC2.DAT	6.375	6.350	0.825	6.350	LMS & CORR	6.350	Fair
D280ADC2.DAT	1.050	7.175	1.050	1.050	LMS & MN/SL	1.050	Good
D280BCC2.DAT	3.175	6.650	0.600	3.175	LMS only	3.175	Good
D280BDC2.DAT	1.100	1.525	1.100	1.100	LMS & MN/SL	1.100	Good
D280CCC2.DAT	0.825	9.625	0.850	0.825	LMS & MN/SL	9.625	Fair (shape – gain adjusted down by 50%)
D280CDC2.DAT	0.950	3.525	0.950	0.950	LMS & MN/SL	8.500	Poor to fair (shape between 30 and 37 GHz – gain adjusted down by 50%)
D280DCC2.DAT	0.700	9.600	0.725	0.700	LMS & MN/SL	9.600	Good (shape – gain adjusted down by 50%)
D280DDC2.DAT	0.875	7.150	0.875	0.875	LMS & MN/SL	8.500	Poor to fair (shape between 30 and 37 GHz – gain adjusted down by 50%)
D280ECC2.DAT	0.675	9.250	0.700	0.675	LMS & MN/SL	9.250	Good (shape – gain adjusted down by 50%)
D280EDC2.DAT	0.750	3.350	0.775	0.750	LMS & MN/SL	8.500	Poor to fair (shape between 30 and 37 GHz – gain adjusted down by 50%)
D280FCC2.DAT	0.625	9.450	0.650	0.625	LMS & MN/SL	9.450	Good (shape – gain adjusted down by 50%)
D280FDC2.DAT	0.600	0.525	0.600	0.600	LMS & MN/SL	0.600	Good
D280GCC2.DAT	0.700	6.975	2.750	0.700	LMS only	6.950	Good (shape – gain adjusted down by 50%)

TABLE 7 (Continued)

Results of the 12 September 1996 Day 2 Test

FILENAME	LMS	CORR	MN/SL	DECL	METHOD	VISUAL	COMMENT
D280HCC2.DAT	0.825	7.100	0.825	0.825	LMS & MN/SL	7.100	Poor to fair (shape – gain adjusted down by 50%)
D280JCC2.DAT	0.825	3.375	0.850	0.825	LMS & MN/SL	8.500	Poor to fair (shape between 30 and 37 GHz – gain adjusted down by 50%)
D8A.DAT	7.000	6.950	2.600	6.975	LMS & CORR	6.975	Good to excellent, gain adjusted down by 50%
D8B.DAT	6.675	3.225	0.800	6.675	LMS only	6.675	Good to excellent, gain adjusted down by 50%
D8C.DAT	6.875	6.850	2.625	6.850	LMS & CORR	6.850	Good, gain adjusted down by 50%
D8D.DAT	7.250	7.300	0.850	7.275	LMS & CORR	7.275	Good, gain adjusted down by 50%
D8E.DAT	7.125	7.200	0.750	7.150	LMS & CORR	7.150	Good to excellent, gain adjusted down by 50%
D8F.DAT	7.000	6.925	2.750	6.950	LMS & CORR	7.200	Good (shape), gain adjusted to 75%
D8G.DAT	6.750	3.150	2.375	6.750	LMS only	6.750	Good, gain adjusted down by 50%
D8H.DAT	4.150	1.700	3.975	4.050	LMS & MN/SL	8.000	Fair, gain adjusted down by 50%
D8J.DAT	6.950	6.925	2.600	6.925	LMS & CORR	6.925	Good to excellent, gain adjusted down by 50%
D8K.DAT	6.900	3.275	1.000	6.900	LMS only	6.700	Good (shape), gain adjusted down by 50%
D8L.DAT	6.900	6.850	2.650	6.875	LMS & CORR	7.200	Good (shape), gain adjusted down by 50%

D280EDC2.DAT – The algorithm estimate of 0.750 mm is a poor match to the measured data, which seem to indicate a thicker oil film. The 8.500-mm estimate, shown in Figure 357, is a poor-to-fair match to the data points between 30 and 37 GHz when using a 50% reduction in the amplitude of the theoretical response.

D280FDC2.DAT – The algorithm estimate of 0.600 mm, shown in Figure 358, is a good match to the measured data.

The main bridge was moved to collect data from the center of the 8-mm crude oil target. The radiometer position was shifted slightly west of center. Chop 2 conditions were present in the test tank. Oil continued to escape from the containment boom.

D280ACC2.DAT – The algorithm estimate of 6.350 mm, shown in Figure 359, is a fair match to the measured data.

D280BCC2.DAT – The algorithm estimate of 3.175 mm, shown in Figure 360, is a good match to the measured data.

D280CCC2.DAT – The algorithm estimate of 0.825 mm is a poor match to the measured data, which seem to indicate a thicker oil film. The correlation-only estimate of 9.625 mm, shown in Figure 361, results in a fair match to the shape of the measured data (if the smoothed curve is ignored) when using a 50% reduction in the amplitude of the theoretical response.

D280DCC2.DAT – The algorithm estimate of 0.700 mm is a poor match to the measured data, which seem to indicate a thicker oil film. The correlation-only estimate of 9.600 mm, shown in Figure 362, results in a fair match to the shape of the measured data (if the smoothed curve is ignored) when using a 50% reduction in the amplitude of the theoretical response.

D280ECC2.DAT – The algorithm estimate of 0.675 mm is a poor match to the measured data, which seem to indicate a thicker oil film. The correlation-only estimate of 9.250 mm, shown in Figure 363, results in a good match to the shape of the measured data when using a 50% reduction in the amplitude of the theoretical response.

The next data set was collected as a wave passed through the target pool.

D280FCC2.DAT – The algorithm estimate of 0.625 mm is a poor match to the measured data, which seems to indicate a thicker oil film. The correlation-only estimate of 9.450 mm, shown in Figure 364, results in a good match to the shape of the measured data when using a 50% reduction in the amplitude of the theoretical response.

D280GCC2.DAT – The algorithm estimate of 0.700 mm is a poor match to the measured data, which seem to indicate a thicker oil film. The correlation-only estimate of 6.950 mm, shown in Figure 365, results in a good match to the shape of the measured data when using a 50% reduction in the amplitude of the theoretical response.

The next data set was collected as a wave passed through the target pool.

D280HCC2.DAT – The algorithm estimate of 0.825 mm is a poor match to the measured data, which seem to indicate a thicker oil film. The correlation-only estimate of 7.100 mm results, shown in Figure 366, in a poor-to-fair match to the shape of the measured data when using a 50% reduction in the amplitude of the theoretical response.

D280JCC2.DAT – The algorithm estimate of 0.825 mm is a poor match to the measured data, which seem to indicate a thicker oil film. The 8.500-mm estimate, shown in Figure 367, is a poor-to-fair match to the data points between 30 and 37 GHz when using a 50% reduction in the amplitude of the theoretical response.

The main bridge was moved to the water-only target pool. A slight oil sheen was visible. Chop 2 conditions were present. The radiometer collected all the data sets from the center of the target. The operator noted that the brightness temperatures were lower than expected, indicating that the gain of the radiometer had drifted. No recalibration was performed.

D200AWC2.DAT – The algorithm estimate of 0.000 mm, shown in Figure 368, is a poor match to the measured data. Most of the data points are below 50 K.

D200BWC2.DAT – The algorithm estimate of 0.000 mm, shown in Figure 369, is a poor match to the measured data. Most of the data points are below 50 K.

D200CWC2.DAT – The algorithm estimate of 0.000 mm, shown in Figure 370, is a poor match to the measured data. Most of the data points are below 50 K.

D200DWC2.DAT – The algorithm estimate of 0.000 mm, shown in Figure 371, is a poor match to the measured data. Most of the data points are below 50 K.

The radiometer was recalibrated using the hot and cold loads. Measurements continued over the same aimpoint in the target pool. Chop 2 conditions were present.

D200EWC2.DAT – The algorithm estimate of 3.700 mm, shown in Figure 372, is a good match to the measured data.

D200FWC2.DAT – The algorithm estimate of 3.725 mm, shown in Figure 373, is a good match to the measured data.

D200GWC2.DAT – This data set, shown in Figure 374, was chosen as the background water reference.

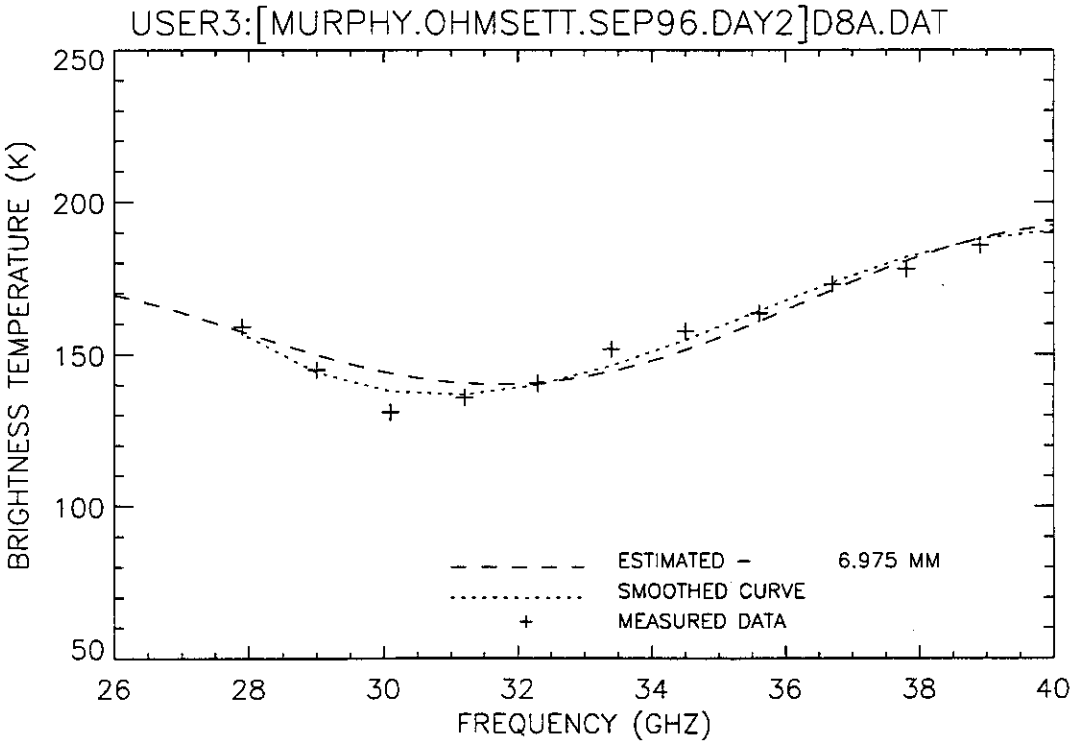

Figure 342. Plot of radiometric brightness temperature versus measurement frequency for 8-mm diesel oil, day 2 test, chop condition building, 12 September 1996, sweep A.

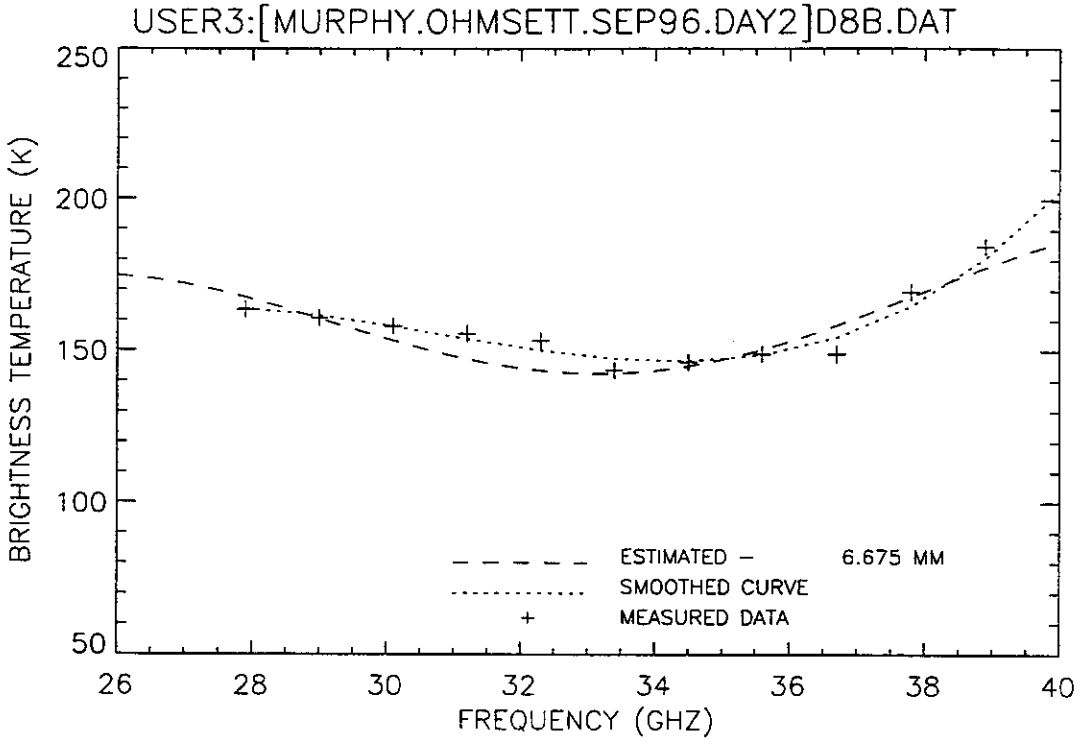

Figure 343. Plot of radiometric brightness temperature versus measurement frequency for 8-mm diesel oil, day 2 test, chop condition building, 12 September 1996, sweep B.

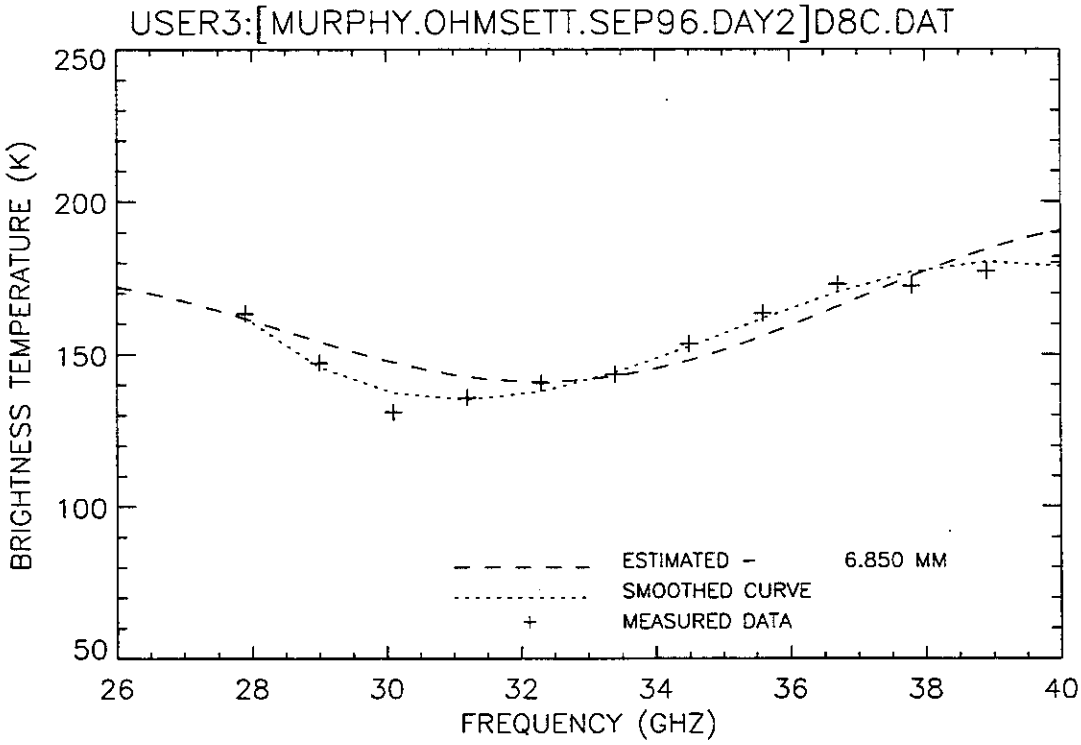

Figure 344. Plot of radiometric brightness temperature versus measurement frequency for 8-mm diesel oil, day 2 test, chop condition building, 12 September 1996, sweep C.

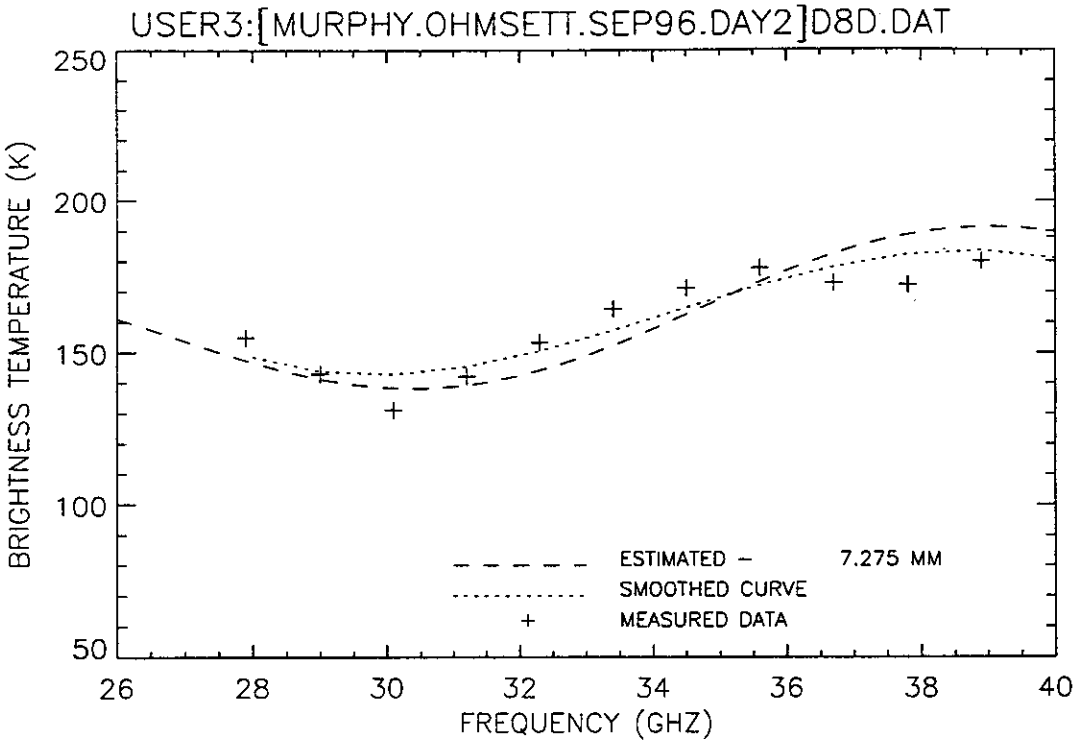

Figure 345. Plot of radiometric brightness temperature versus measurement frequency for 8-mm diesel oil, day 2 test, chop condition building, 12 September 1996, sweep D.

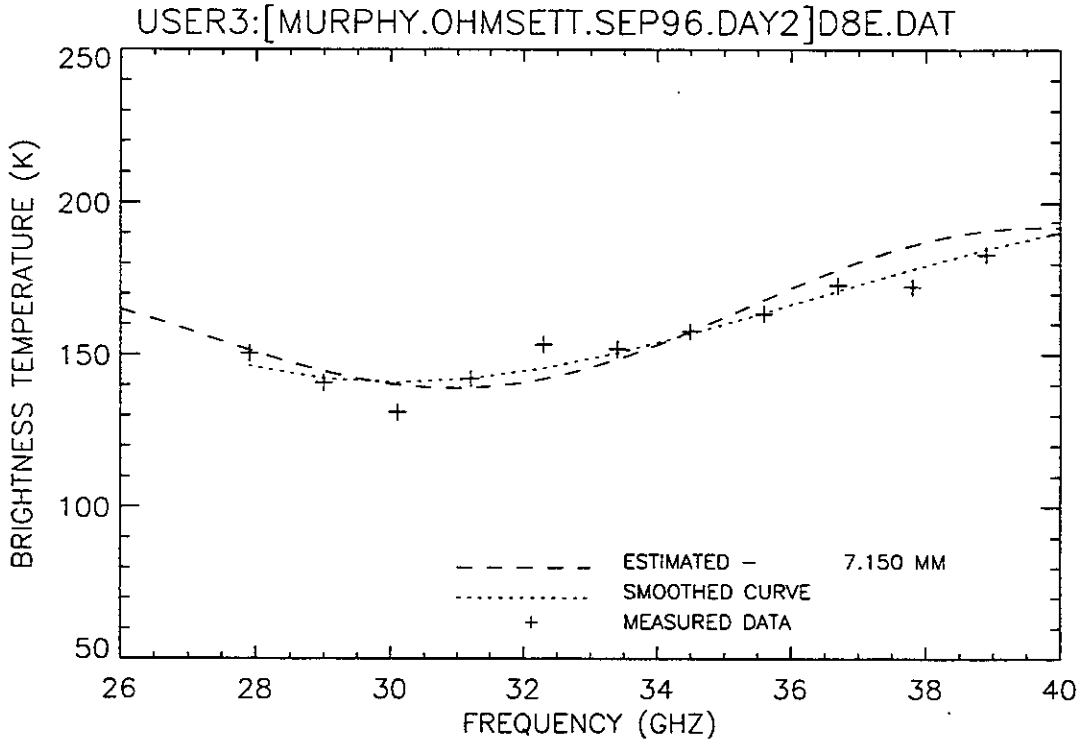

Figure 346. Plot of radiometric brightness temperature versus measurement frequency for 8-mm diesel oil, day 2 test, chop condition building, 12 September 1996, sweep E.

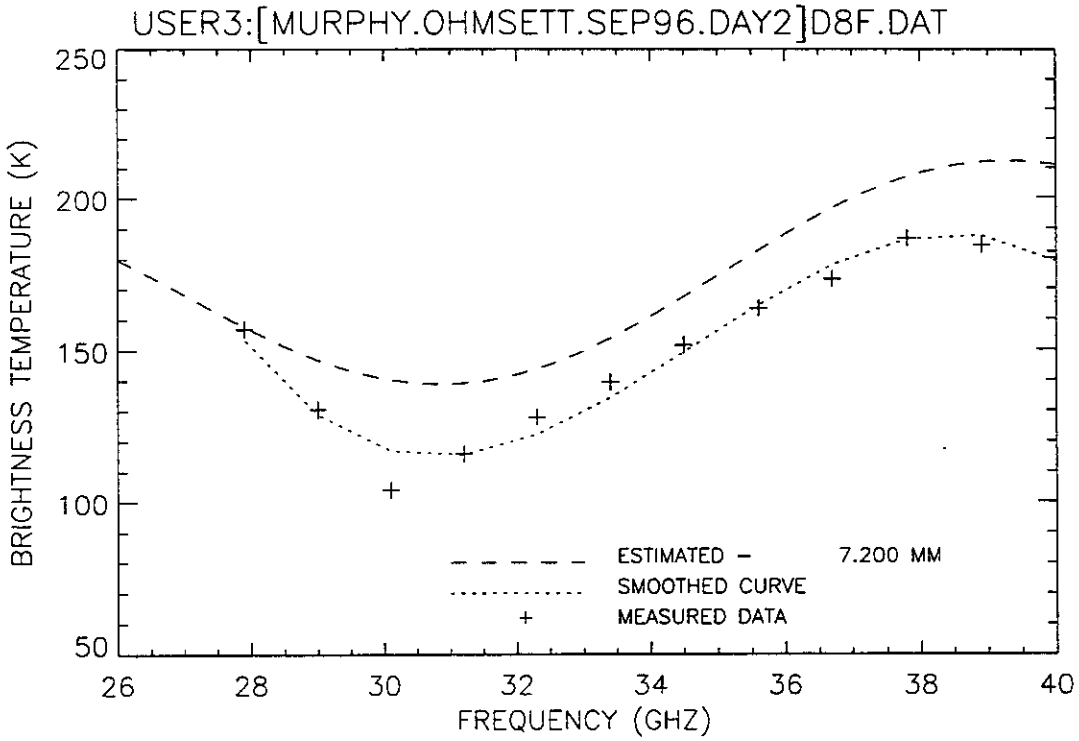

Figure 347. Plot of radiometric brightness temperature versus measurement frequency for 8-mm diesel oil, day 2 test, chop condition building, 12 September 1996, sweep F.

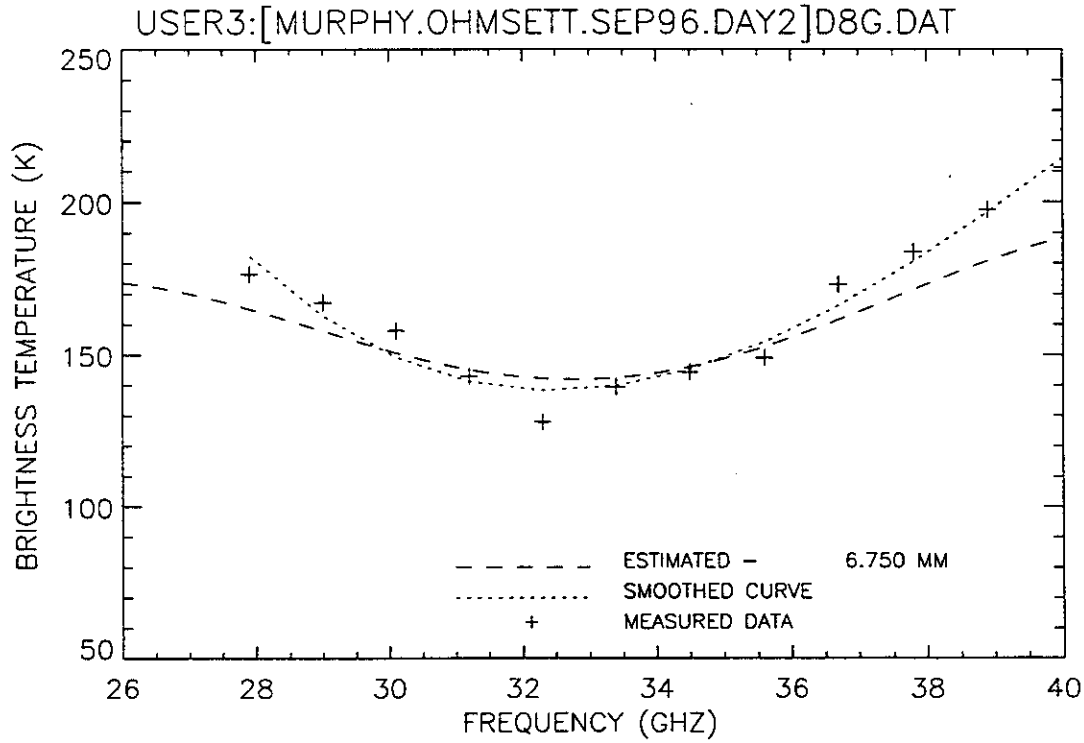

Figure 348. Plot of radiometric brightness temperature versus measurement frequency for 8-mm diesel oil, day 2 test, chop condition building, 12 September 1996, sweep G.

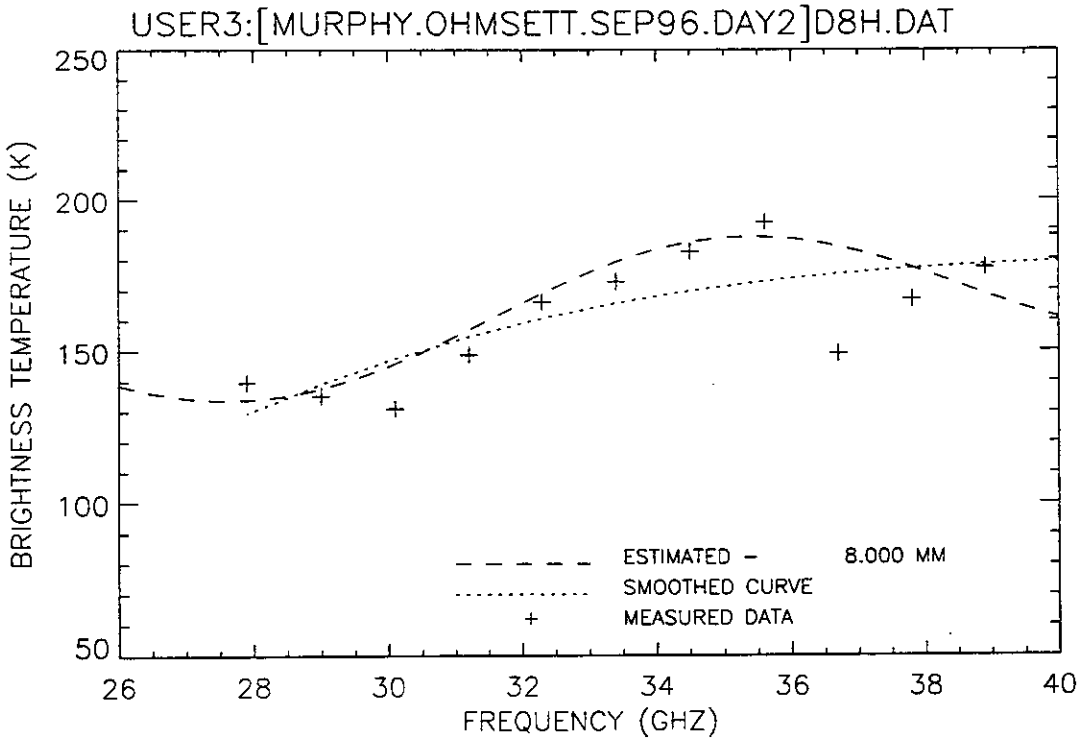

Figure 349. Plot of radiometric brightness temperature versus measurement frequency for 8-mm diesel oil, day 2 test, chop condition building, 12 September 1996, sweep H.

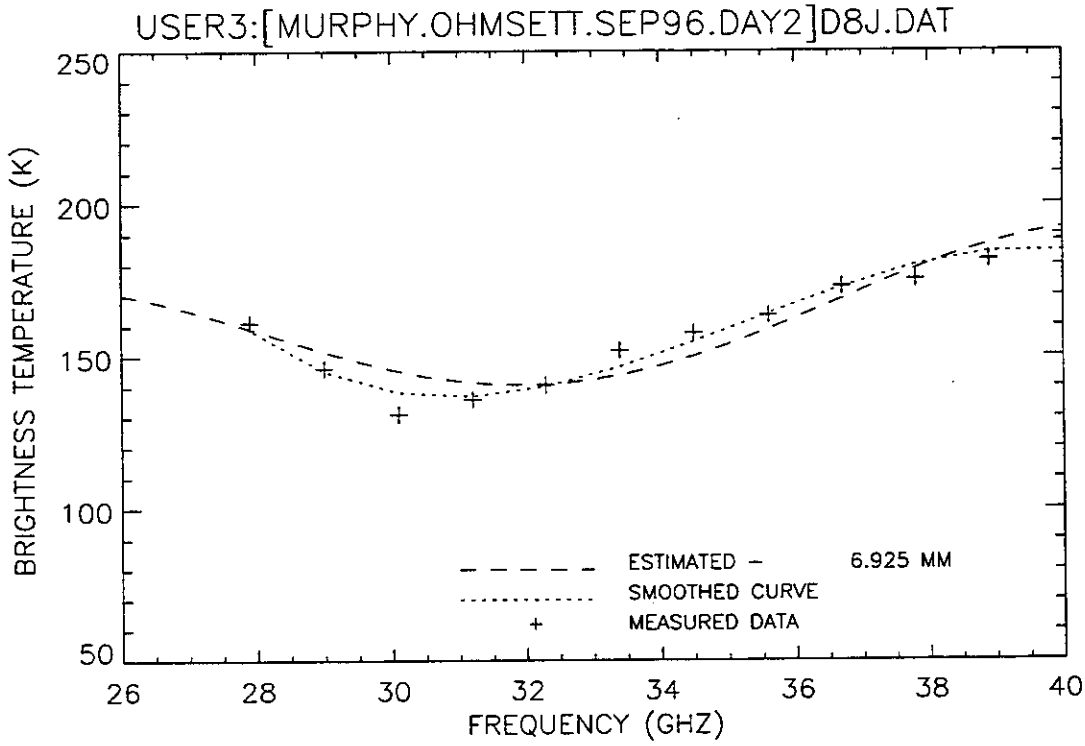

Figure 350. Plot of radiometric brightness temperature versus measurement frequency for 8-mm diesel oil, day 2 test, chop condition 1, 12 September 1996, sweep J.

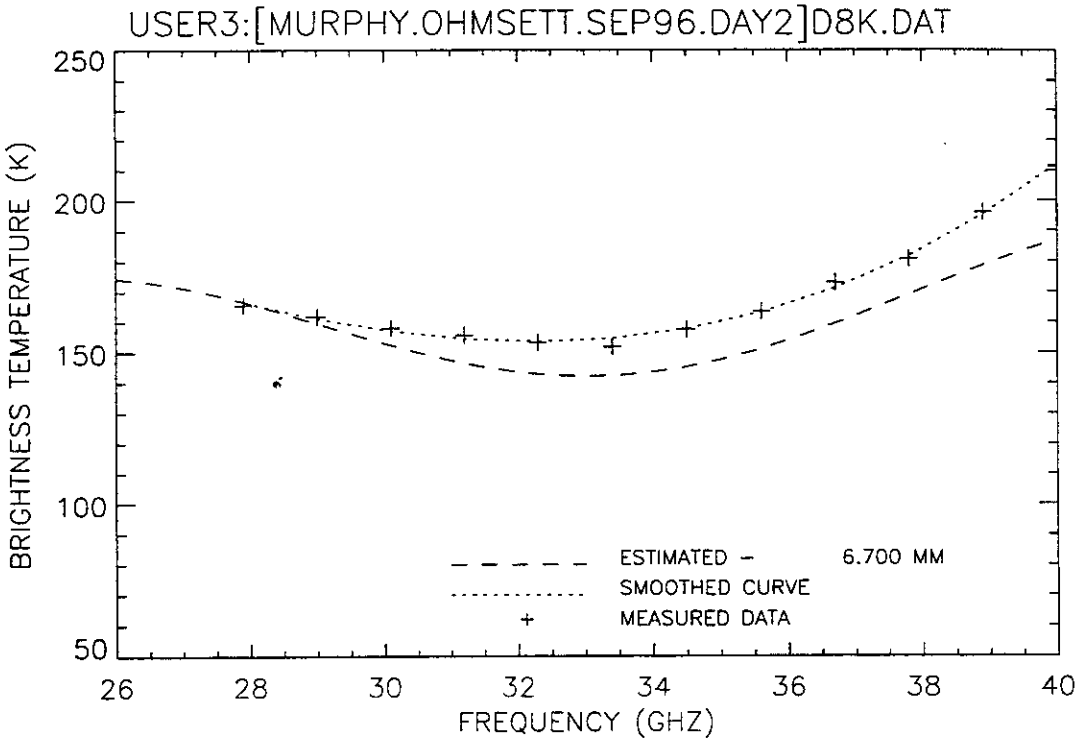

Figure 351. Plot of radiometric brightness temperature versus measurement frequency for 8-mm diesel oil, day 2 test, chop condition 1, 12 September 1996, sweep K.

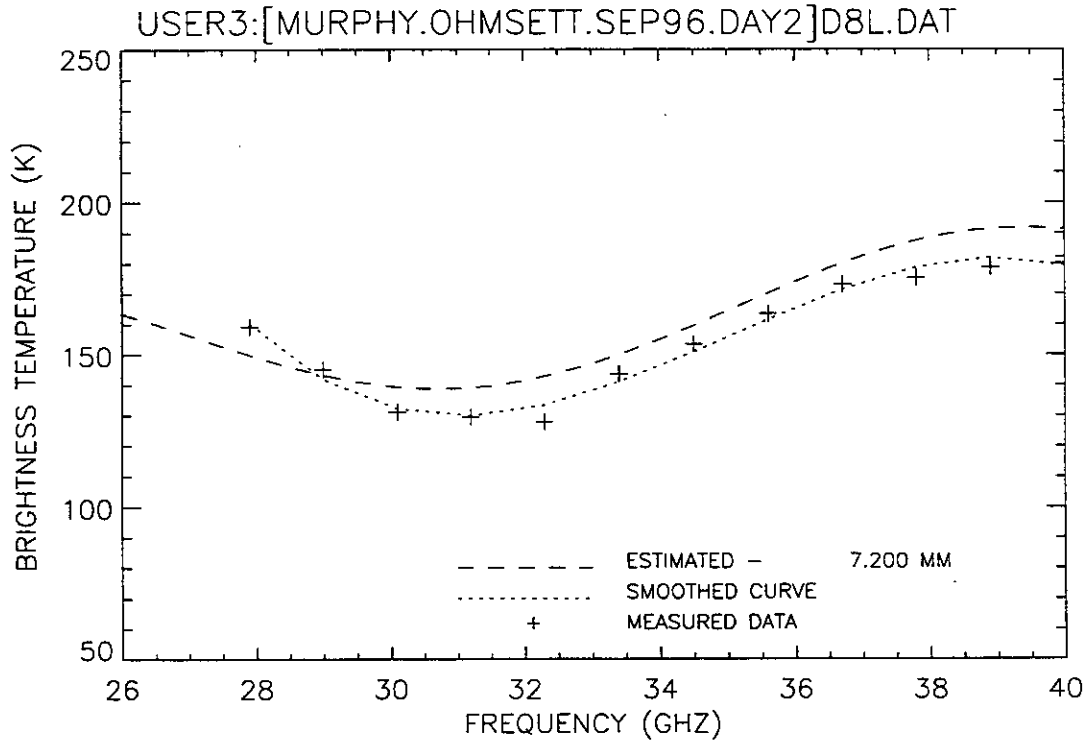

Figure 352. Plot of radiometric brightness temperature versus measurement frequency for 8-mm diesel oil, day 2 test, chop condition 1, 12 September 1996, sweep L.

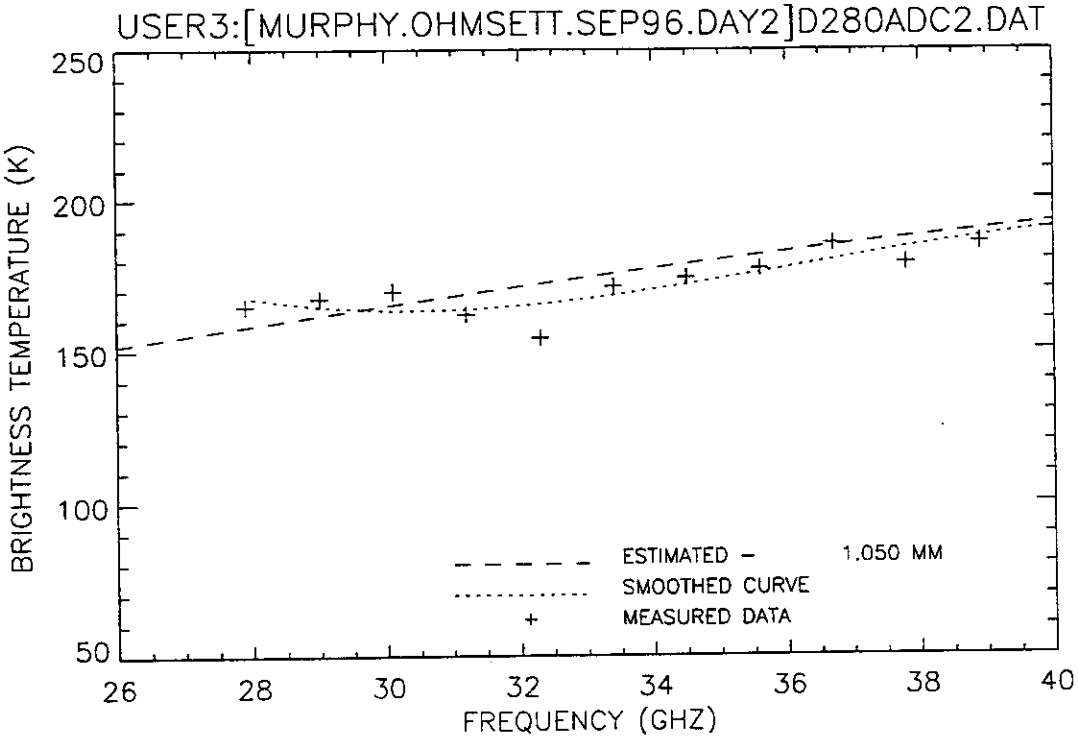

Figure 353. Plot of radiometric brightness temperature versus measurement frequency for 8-mm diesel oil, day 2 test, chop condition 2, 12 September 1996, sweep A.

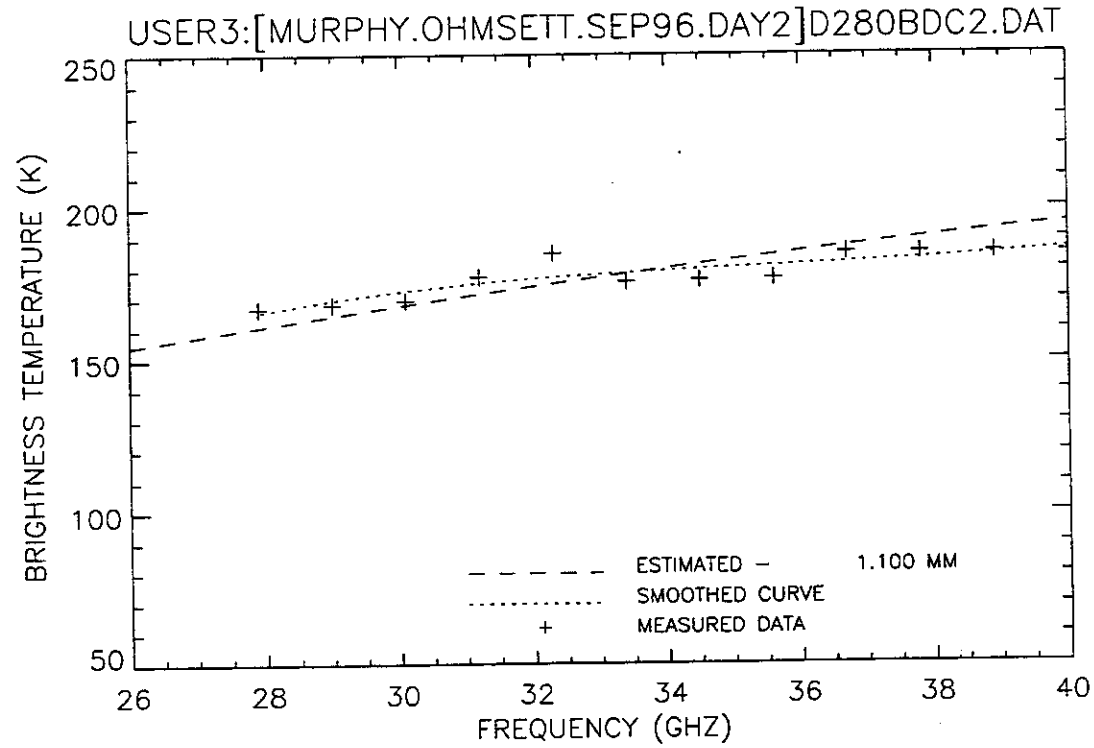

Figure 354. Plot of radiometric brightness temperature versus measurement frequency for 8-mm diesel oil, day 2 test, chop condition 2, 12 September 1996, sweep B.

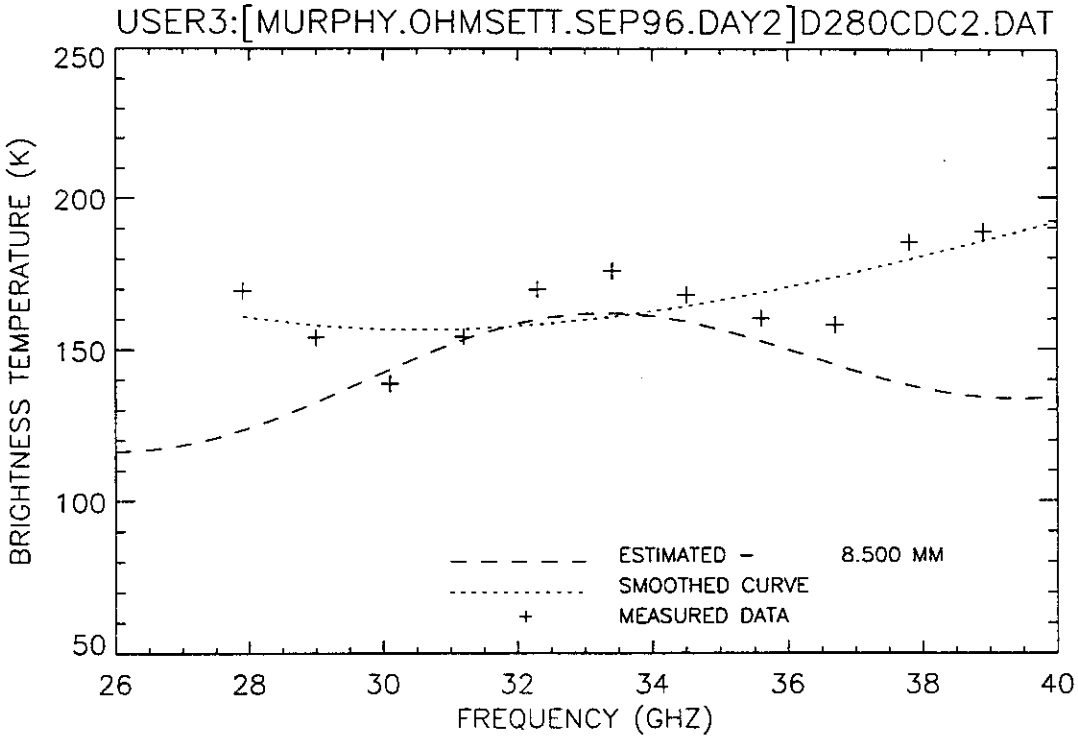

Figure 355. Plot of radiometric brightness temperature versus measurement frequency for 8-mm diesel oil, day 2 test, chop condition 2, 12 September 1996, sweep C.

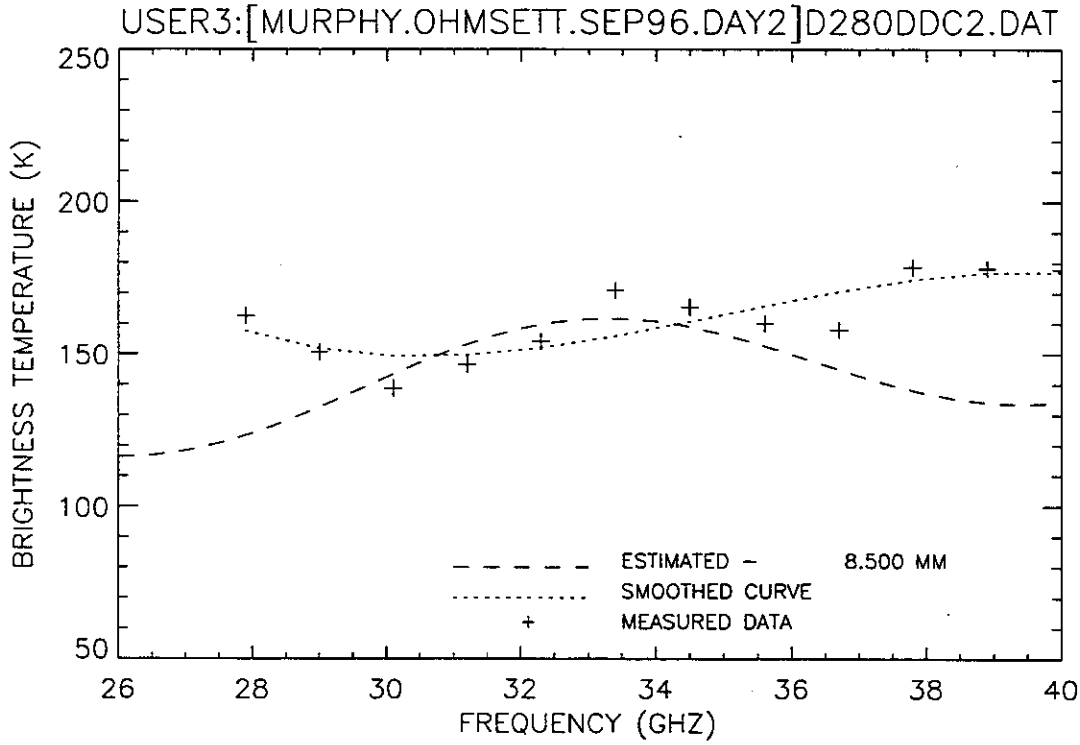

Figure 356. Plot of radiometric brightness temperature versus measurement frequency for 8-mm diesel oil, day 2 test, chop condition 2, 12 September 1996, sweep D.

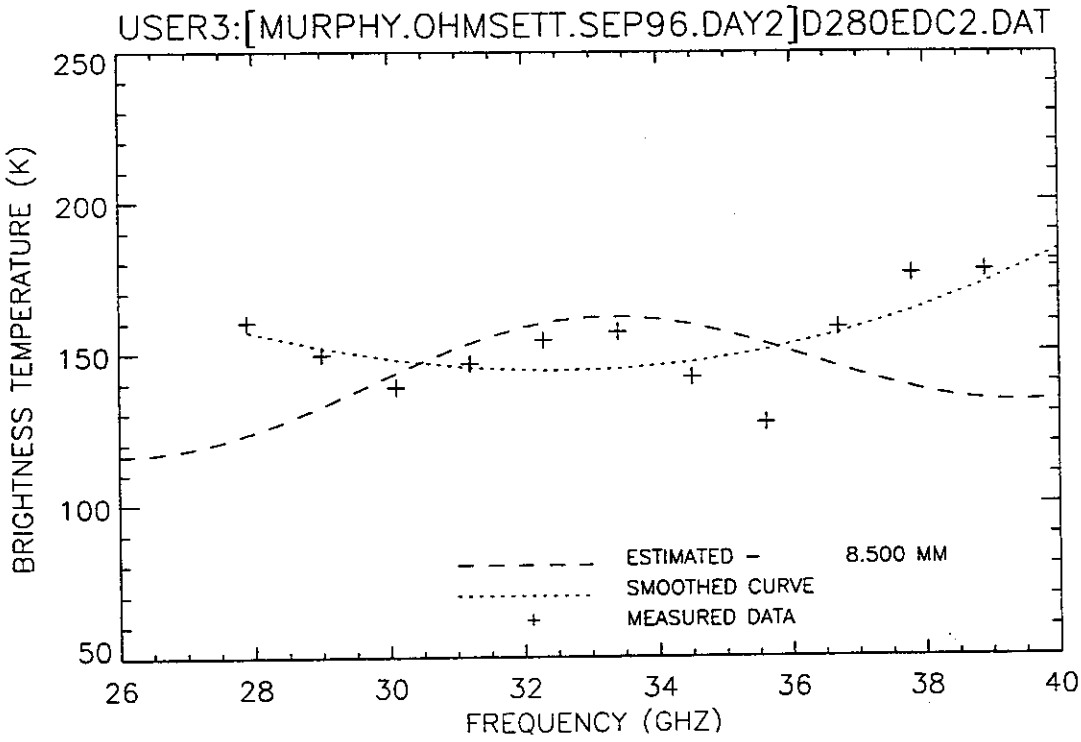

Figure 357. Plot of radiometric brightness temperature versus measurement frequency for 8-mm diesel oil, day 2 test, chop condition 2, 12 September 1996, sweep E.

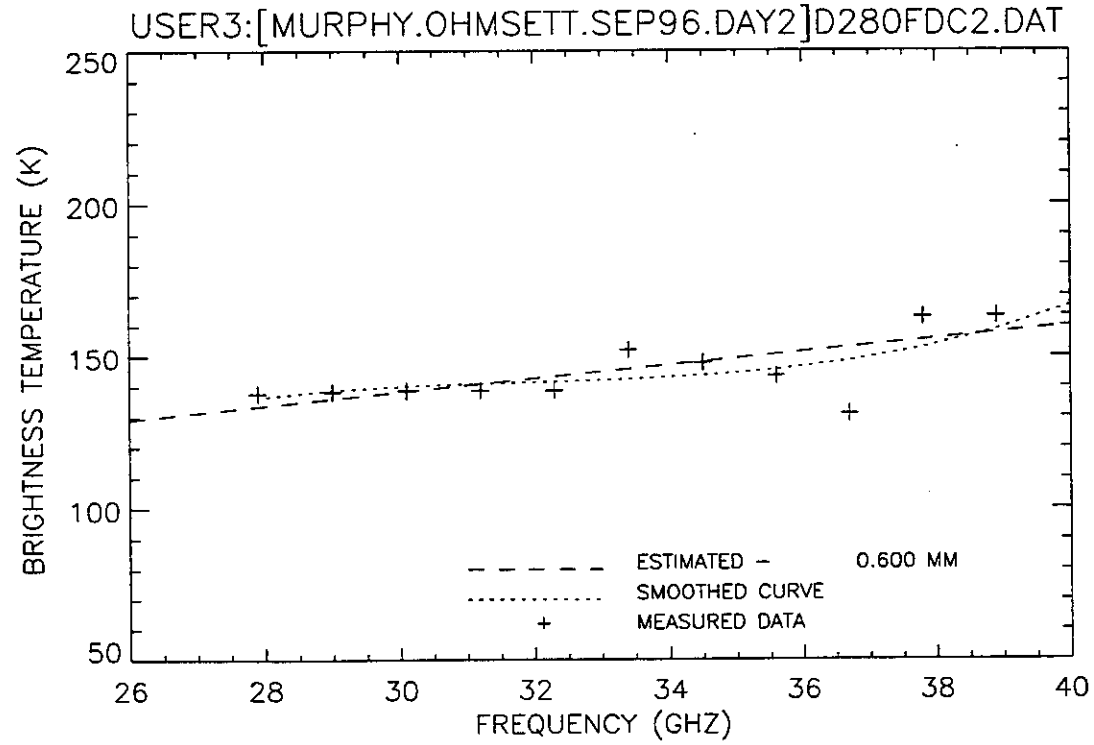

Figure 358. Plot of radiometric brightness temperature versus measurement frequency for 8-mm diesel oil, day 2 test, chop condition 2, 12 September 1996, sweep F.

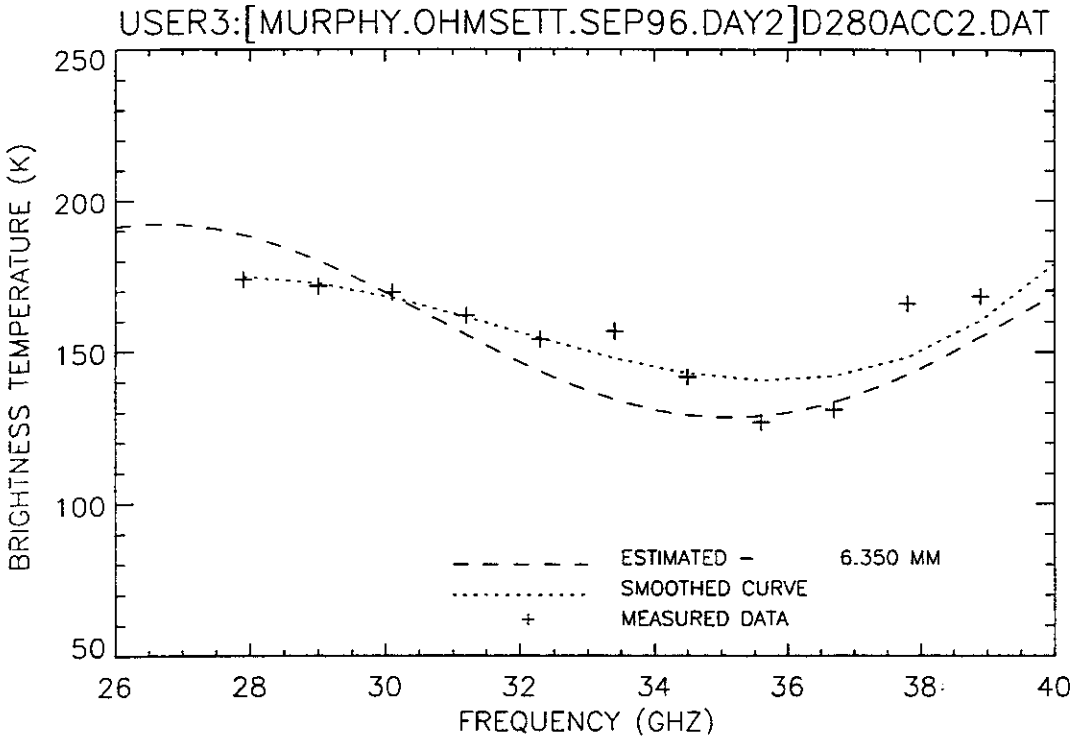

Figure 359. Plot of radiometric brightness temperature versus measurement frequency for 8-mm crude oil, day 2 test, chop condition 2, 12 September 1996, sweep A.

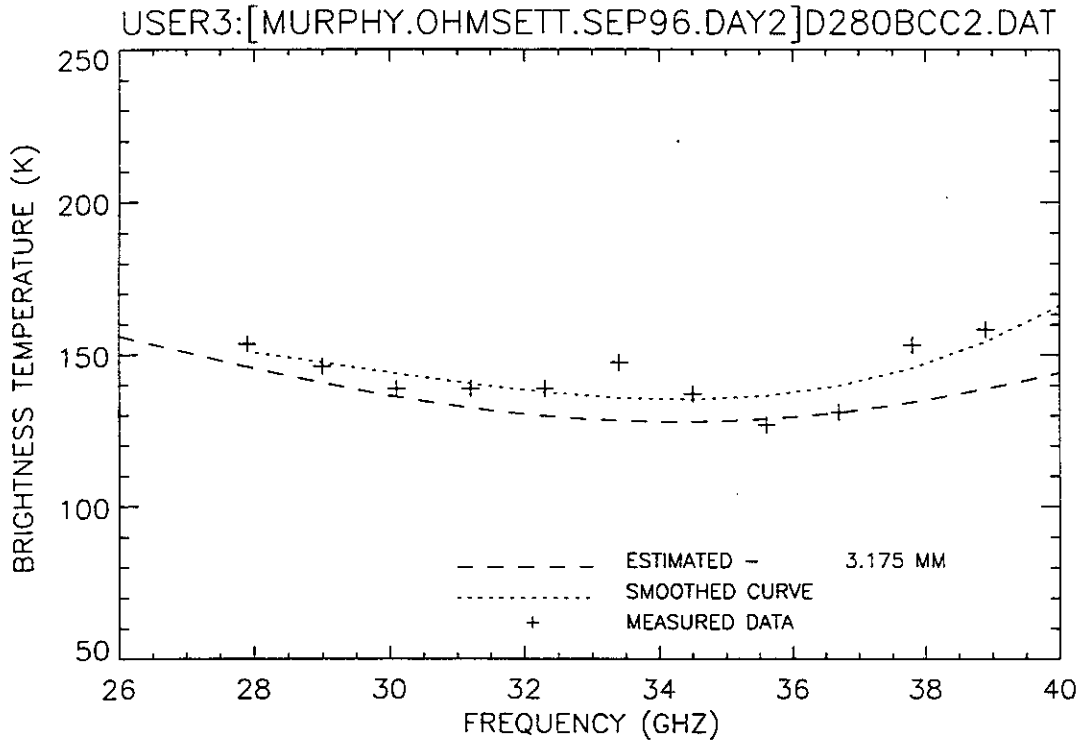

Figure 360. Plot of radiometric brightness temperature versus measurement frequency, for 8-mm crude oil, day 2 test, chop condition 2, 12 September 1996, sweep B.

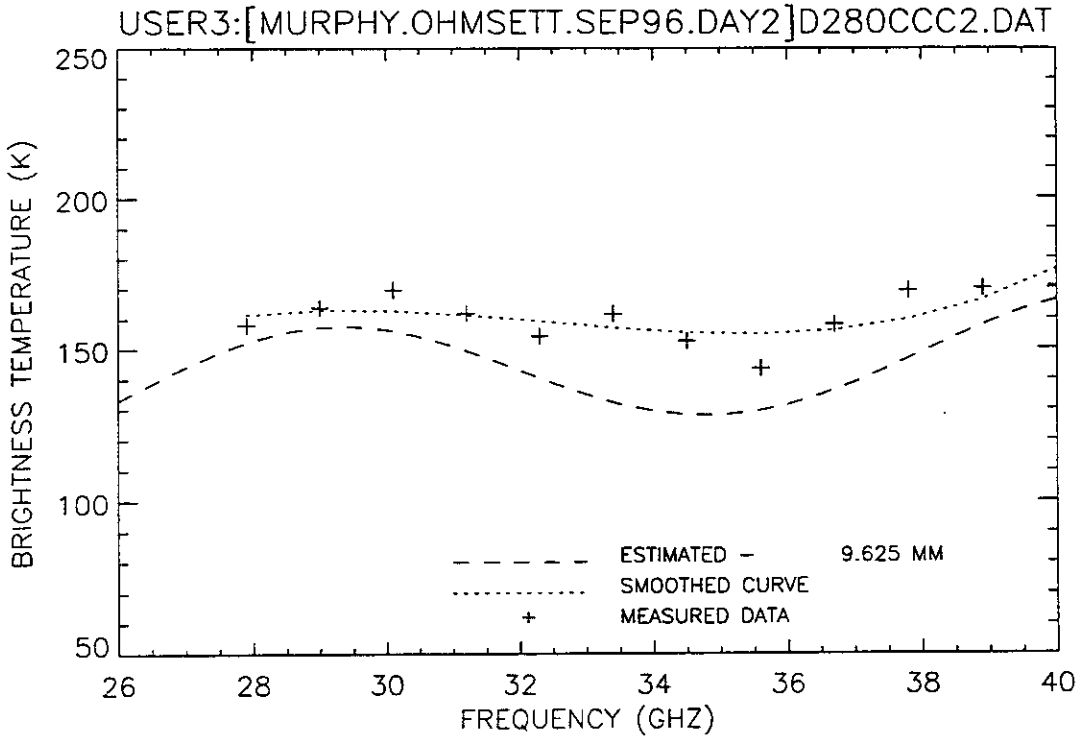

Figure 361. Plot of radiometric brightness temperature versus measurement frequency for 8-mm crude oil, day 2 test, chop condition 2, 12 September 1996, sweep C.

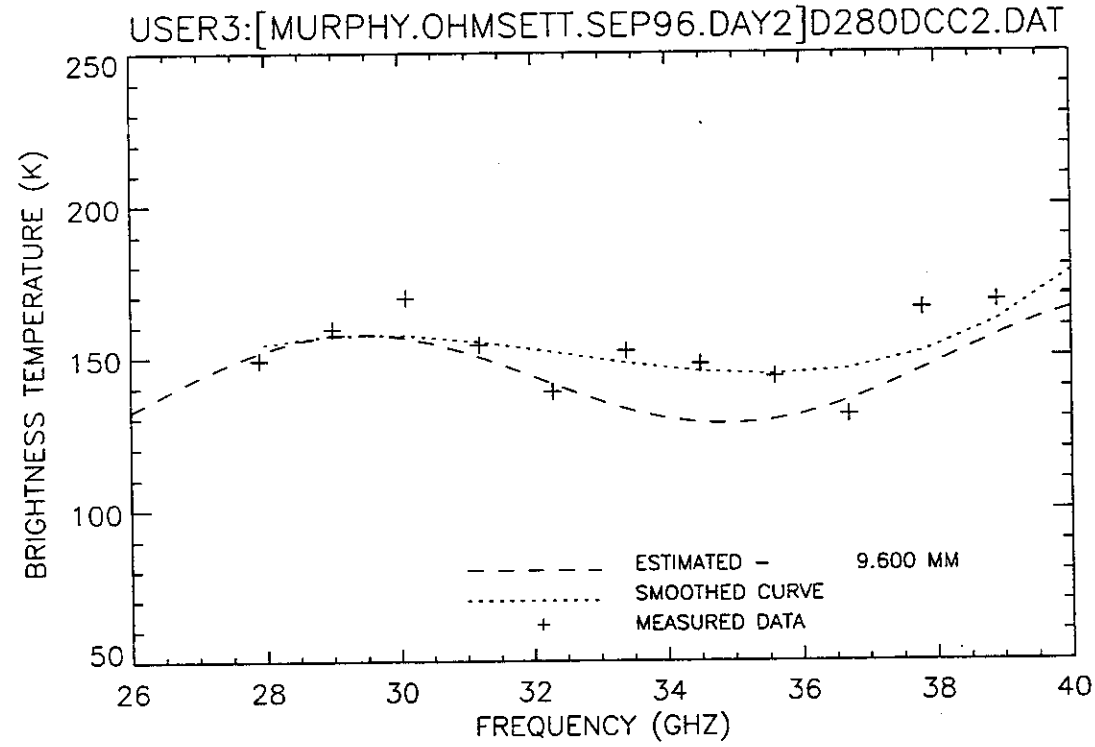

Figure 362. Plot of radiometric brightness temperature versus measurement frequency for 8-mm crude oil, day 2 test, chop condition 2, 12 September 1996, sweep D.

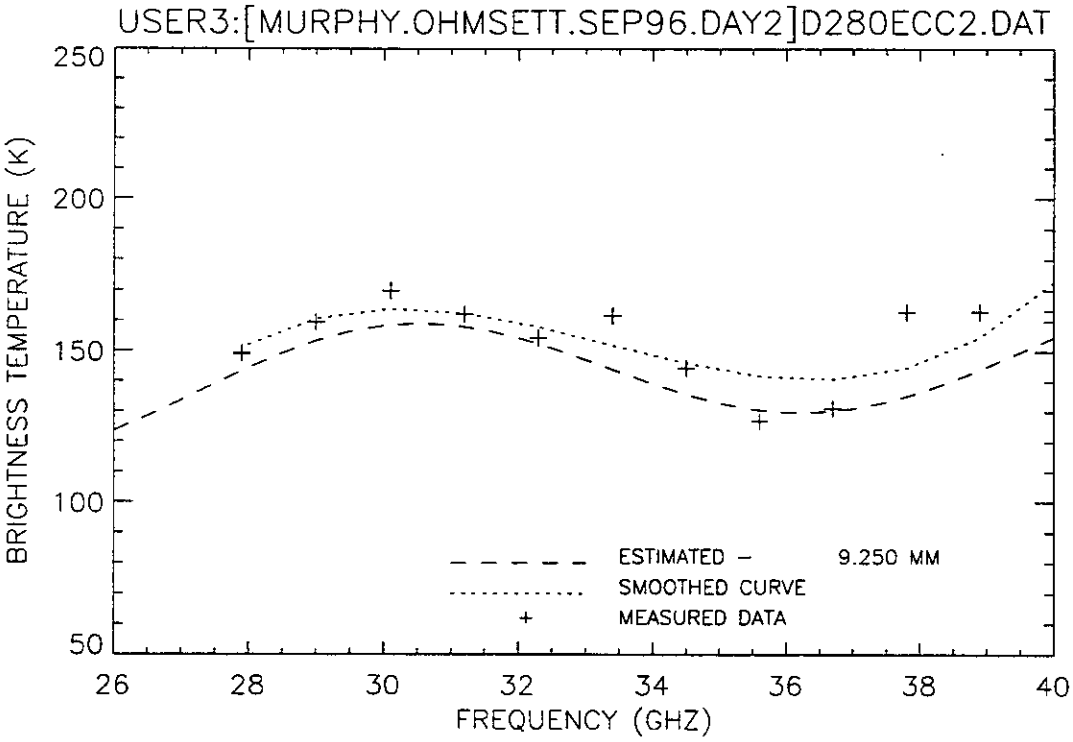

Figure 363. Plot of radiometric brightness temperature versus measurement frequency for 8-mm crude oil, day 2 test, chop condition 2, 12 September 1996, sweep E.

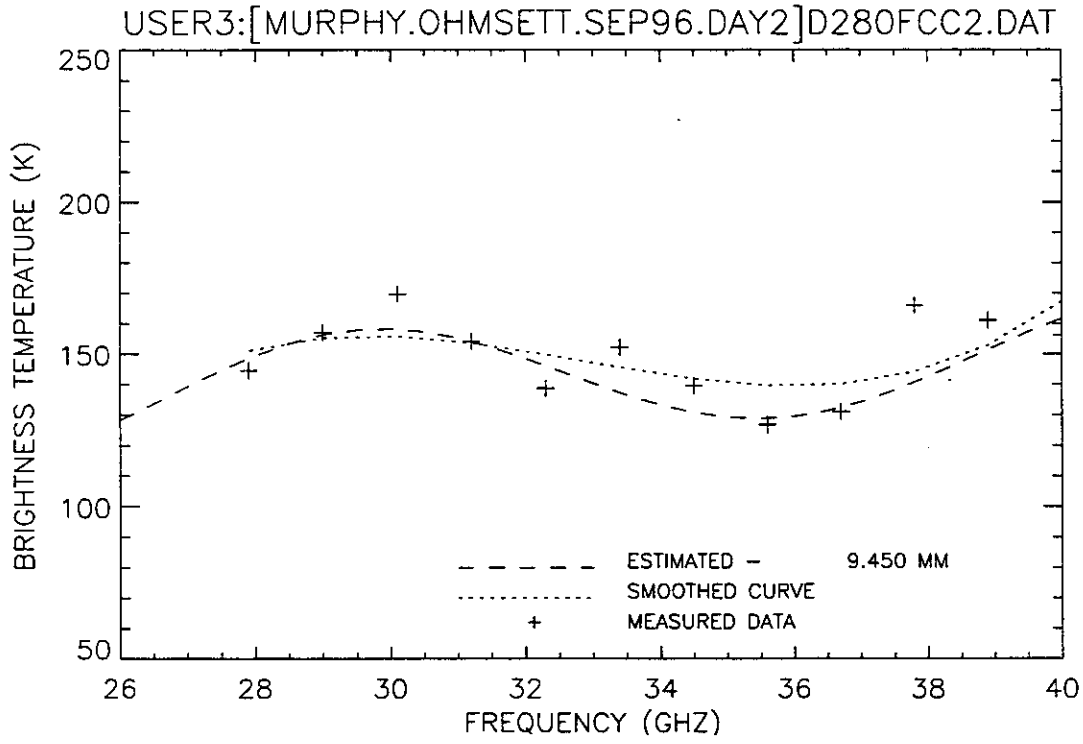

Figure 364. Plot of radiometric brightness temperature versus measurement frequency for 8-mm crude oil, day 2 test, chop condition 2, 12 September 1996, sweep F.

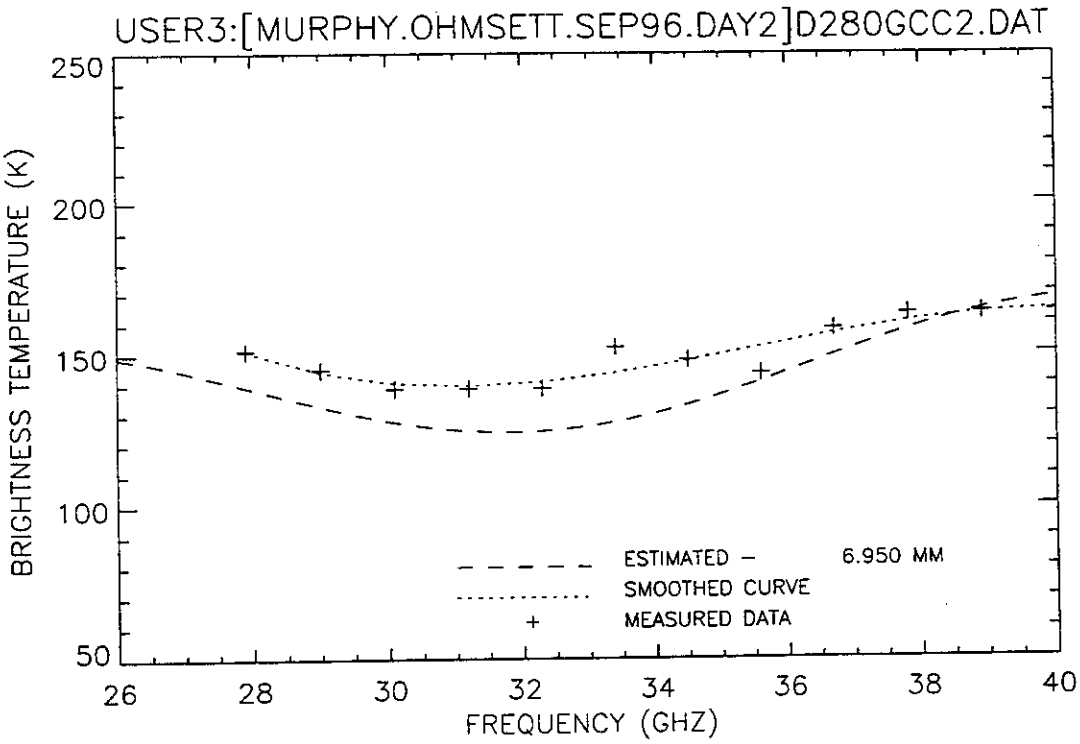

Figure 365. Plot of radiometric brightness temperature versus measurement frequency for 8-mm crude oil, day 2 test, chop condition 2, 12 September 1996, sweep G.

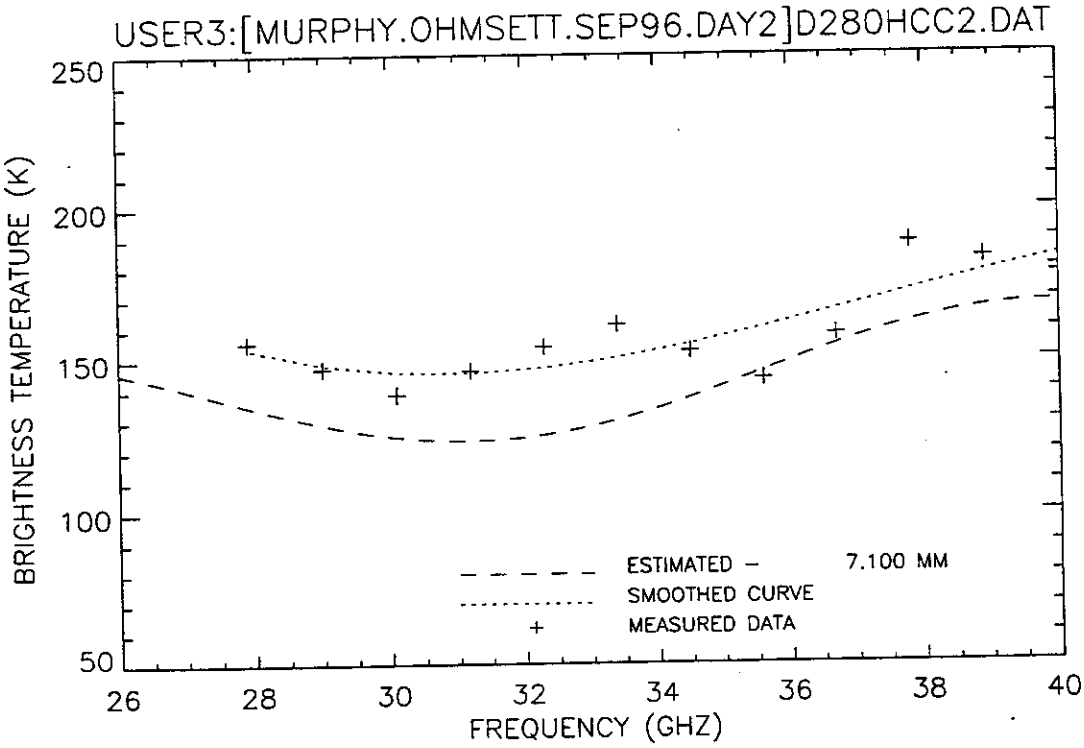

Figure 366. Plot of radiometric brightness temperature versus measurement frequency for 8-mm crude oil, day 2 test, chop condition 2, 12 September 1996, sweep H.

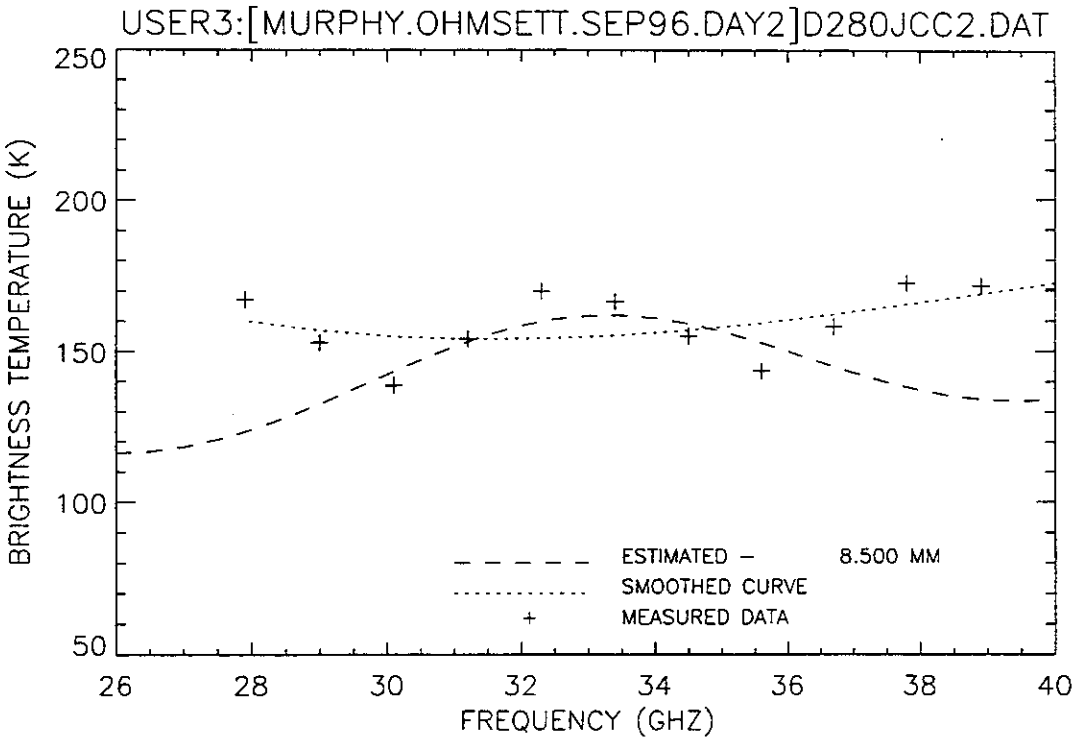

Figure 367. Plot of radiometric brightness temperature versus measurement frequency for 8-mm crude oil, day 2 test, chop condition 2, 12 September 1996, sweep J.

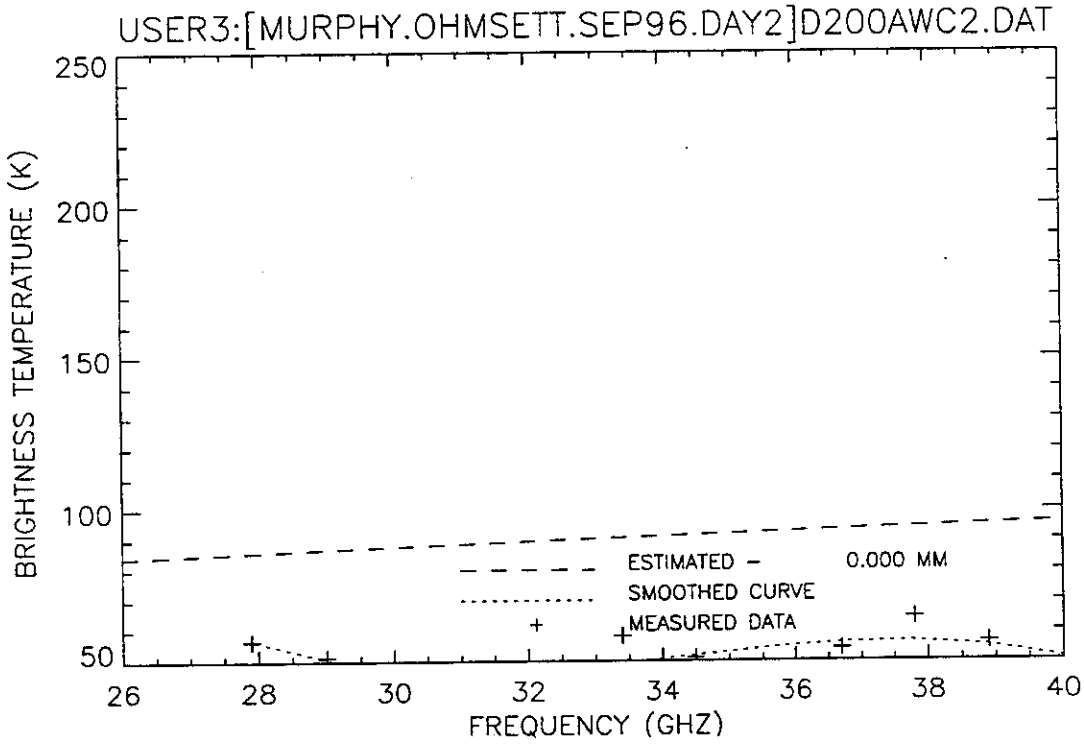

Figure 368. Plot of radiometric brightness temperature versus measurement frequency for water, day 2 test, chop condition 2, 12 September 1996, sweep A.

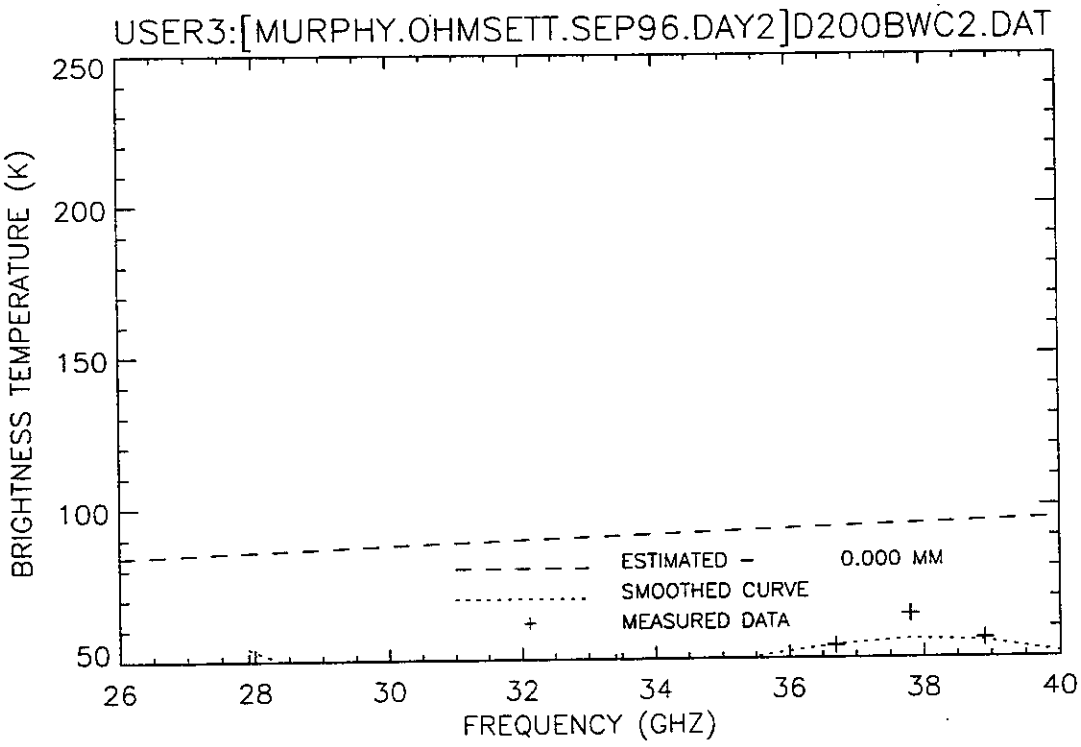

Figure 369. Plot of radiometric brightness temperature versus measurement frequency for water, day 2 test, chop condition 2, 12 September 1996, sweep B.

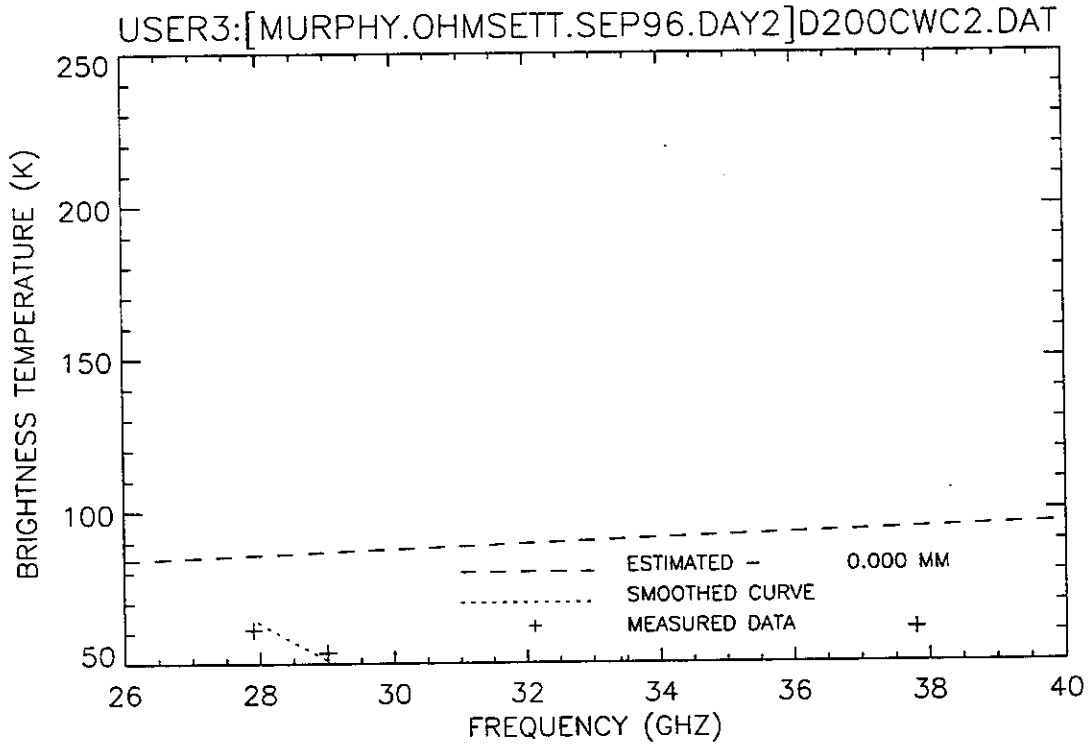

Figure 370. Plot of radiometric brightness temperature versus measurement frequency for water, day 2 test, chop condition 2, 12 September 1996, sweep C.

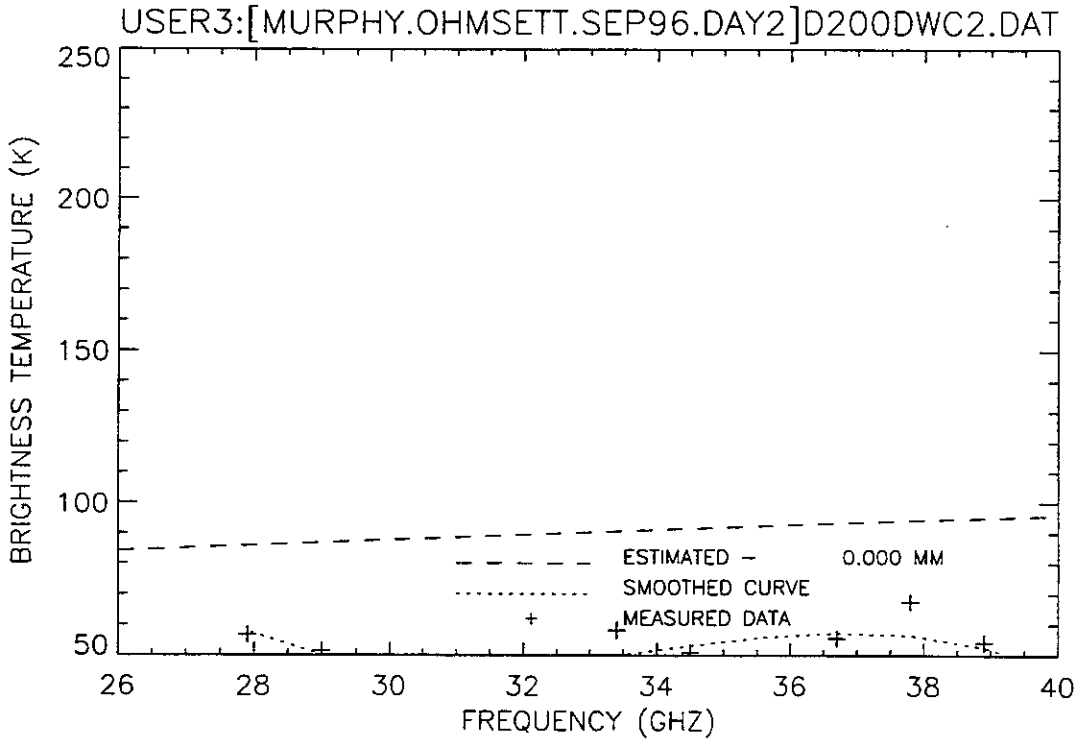

Figure 371. Plot of radiometric brightness temperature versus measurement frequency for water, day 2 test, chop condition 2, 12 September 1996, sweep D.

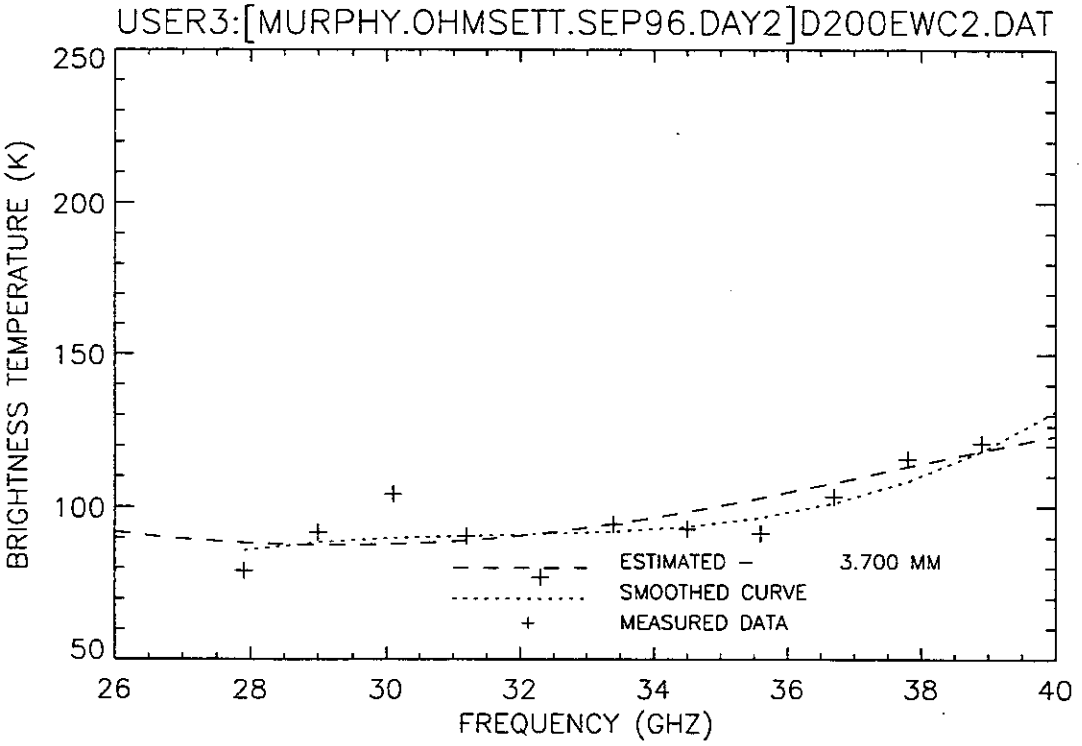

Figure 372. Plot of radiometric brightness temperature versus measurement frequency for water, day 2 test, chop condition 2, 12 September 1996, sweep E.

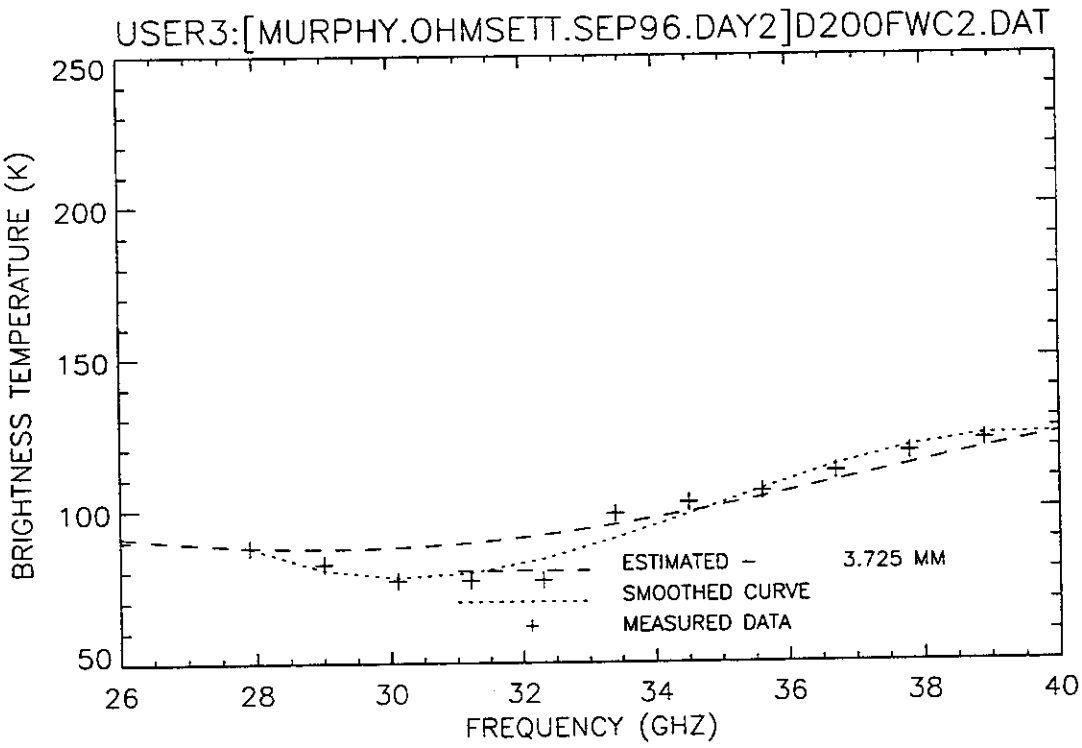

Figure 373. Plot of radiometric brightness temperature versus measurement frequency for water, day 2 test, chop condition 2, 12 September 1996, sweep F.

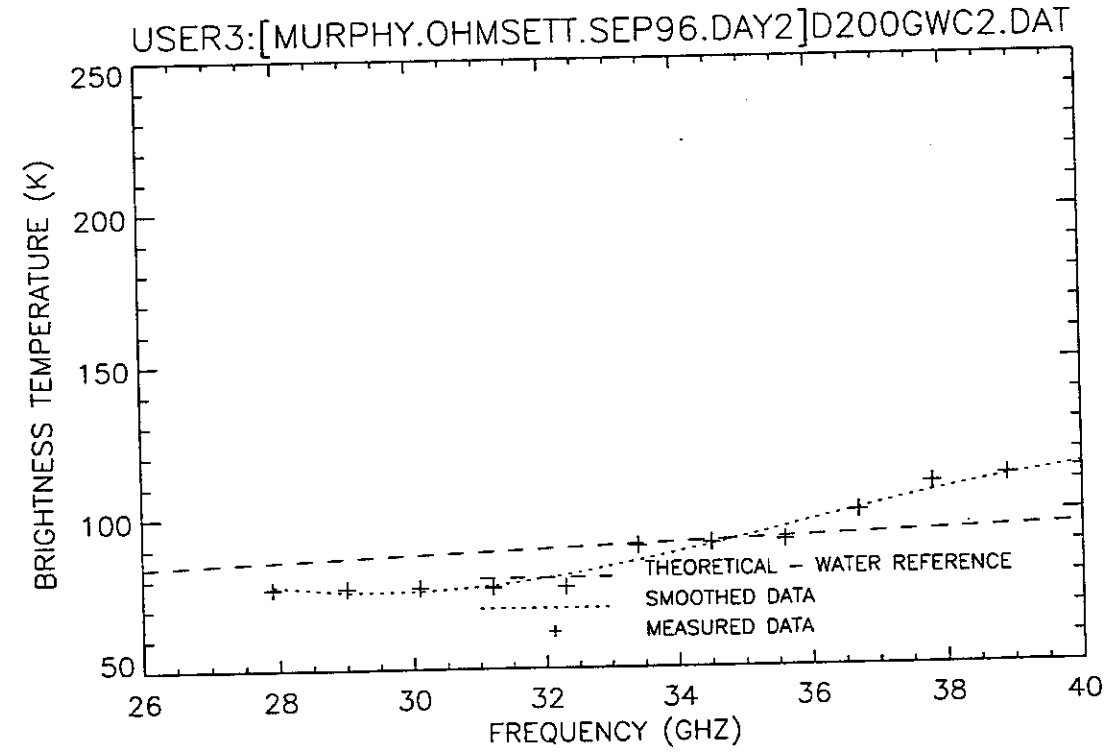

Figure 374. Plot of radiometric brightness temperature versus measurement frequency for. water, day 2 test, chop condition 2, 12 September 1996, sweep G.